Marina Barroso Pereira Pinheiro

Interactions of Rifabutin and Novel Analogs for Tuberculosis with Membranes: Implications for Mechanism of Action and Drug Development

Tese do 3º Ciclo de Estudos Conducente ao Grau de Doutoramento em Ciências Farmacêuticas na Especialidade de Química Farmacêutica e Medicinal

Trabalho realizado sob a orientação do Professor Doutor José Luís Costa Lima e co-orientação de Professora Doutora Maria de La Salette Reis e Doutora Marlene Susana Dionísio Lúcio

Setembro de 2013

É autorizada a reprodução integral desta tese apenas para efeitos de investigação, mediante declaração escrita do interessado, que a tal se compromete.

Assinatura do autor,

“Somewhere, something incredible is waiting to be known.”
(Carl Sagan)

Às quatro pessoas que preenchem a minha vida,

Fernando Dinis,

Maria da Conceição,

Ana Rita,

Pedro Daniel.

Agradecimentos

Durante todo o meu percurso de formação pessoal/académico, foram inúmeras as pessoas e instituições que contribuiram de uma forma muito significativa para o seu desenvolvimento. Será de todo impossível nomear a sua totalidade. Não poderei deixar de expressar, no entanto, os meus sinceros agradecimentos a todos aqueles que foram imprescindíveis durante a minha formação em contexto do doutoramento e que foram fundamentais para o maior desafio académico que enfrentei:

Ao Professor Doutor José Luís Costa Lima, agradeço a oportunidade que me concedeu de integrar o seu grupo de investigação no antigo Departamento de Química-Física e mais recentemente denominado por Química Aplicada. Destaco o seu sentido de humor inigualável que juntamente com o seu carácter de líder, enriqueceram e tornaram o meu percurso durante o doutoramento, uma agradável "Aventura".

À Professsora Doutora Salette Reis, agradeço a importância central que teve no desenvolvimento desta tese. Agredeço por me ter aceite como sua aluna de doutoramento. Destaco o seu rigor pedagógico e científico, o seu carácter dinâmico, a sua disponibilidade, bem como pela exímia orientação durante todas as etapas do meu doutoramento. Agradeço a amizade bem como a importância que as suas palavras de motivação que surgiram sempre de forma perpicaz, contribuiram para a minha formação. Agradeço ainda as oportunidades que me concedeu e que permitiram obter uma maior transversalidade.

À Doutora Marlene Lúcio, agradeço a orientação durante a fase inicial e crítica da tese. Agradeço as dicussões construtivas que derivam do seu espírito crítico, imaginação, originalidade e de trabalho exemplares. Agradeço ainda a amizade, o apoio e a partilha de ideias.

A todos os restantes Professores do Departamento de Química Aplicada, agradeço a simpatia demonstrada.

Al Profesor Dr. Luis Camacho, por haberme permitido llevar a cabo mis estudios en monocapas en el Departamento de Química Física y Termodinámica Aplicada de la Universidad de Córdoba, con un alto rigor científico, gracias a la dirección con la que ha contado.

Al Dr. Juan Giner-Casares, quiero agradecer por haberme brindado su tiempo y sus

conocimientos muy importante para la concreción de este trabajo.

Al Profesor María Teresa Romero y Profesor Marta Morales, a Carlos Rubia-Payá, Luisa Carmona, Cristina Roldan, Eugenio Jimenez-Millan todo su apoyo, afecto y paciencia. Muchas gracias para todas las demás personas en el departamento.

I am very grateful to Professor Gerald Brezesinsky for his scientific advice, knowledge and many insightful suggestions. I also have to thank the oportunity to learn different tecnhiques in the Deutsches Elektronen-Synchrotron in Hamburg and Max Planck Institute.

Agradeço a todas as pessoas talentosas com quem trabalhei ao longo dos últimos anos, nomeadamente Mariana Arêde, Marta Oliveira, Carla Castro, Mariana Fernandes, Ricardo Ribeiro, Ana Sofia Silva, Sílvia Pisco e Fernanda Andrade.

Agradeço a todas as pessoas do laboratório que são para mim bem mais do que colegas de laboratório. À Cláudia Pinho por todo o apoio, amizade e carinho desde o primeiro dia que nos conhecemos. À Sofia Rodrigues por toda a sua dimensão humoral que tanto me anima, pela cumplicidade e amizade. À Catarina Pereira-Leite pela amizade, apoio e empatia.

A todas as pessoas do laboratório que é impossível mencionar, pois iria correr risco de omissão. Desde os “meninos e meninas da investigação”, e em especial à Rosa Couto, Miriam Machado, Catarina Moura e Joana Queiróz, bem como aos alunos de mestrado e de doutoramento até aos investigadores auxiliares e pós-docs. Não esquecendo nunca a Patrícia Monteiro, Manuela Barros e Vera Abreu pela amizade e pela capacidade de trabalho exemplares. Agradeço ainda a todos os elementos do grande grupo de investigação denominado “Bando dos Lipossomas” e agora também das “Nanopartículas Lípidicas”, em especial à Ana Rute Neves e à Catarina Alves.

A todas aquelas pessoas que conheci no contexto da investigação e que apesar de irem-e-virem deixaram saudades. De entre estas pessoas não poderei deixar de referir a Adriana Lima e a Olinda Lima.

Às minhas colegas e amigas de curso Sónia Barroso, Marina Marques e Salomé Teles. Agradeço-vos os tempos na antiga Faculdade de Farmácia em que tivemos tão bons momentos, que recordo com nostalgia.

Agradeço à minha amiga Liliana Rodrigues, pelas novas conversas “psicológicas” e pela sua capacidade de reforço positivo e motivacional.

Ao meu grande amigo Joel Alves. Desde sempre partilhamos, entre outras, a mesma paixão pela investigação. Agradeço-te todo o apoio e influência que és para mim desde sempre.

Às minhas ilustres e distintas amigas Catarina Proença, Isabel Pires, Inês Cruz, Paula Grohmann. E a todos os restantes da grande Carlos Amarante, agradeço-vos a todos a paciência comigo, inclusivamente para conversas sobre “beam”, “ångström”, “shutter”, entre outros termos menos utilizados recorrentemente.

Aos meus queridos pais Fernando Dinis Pereira Pinheiro e Maria da Conceição Barroso Pereira Pinheiro. Agradeço-vos por me terem proporcionado todas as condições para que isto se tornasse possível, muito mais do que o apoio, um incentivo permanente.

À minha irmã e melhor amiga Ana Rita Pinheiro, agradeço toda o apoio, incentivo cumplicidade e paciência ao longo destes anos.

Desejo agradecer a toda a minha restante família e desta forma desculpabilizar-me pelas minhas ausências sucessivas.

Ao ser humano que eu mais admiro, Pedro Bastos. Agradeço-te infinitamente e sem ti esta tese não seria possível. Obrigada por teres estado comigo nos exepcionais e nos menos bons momentos, sempre com as mais assertivas e sábias palavras, que significa(s)m na minha vida paixão, alento e inspiração.

Agradeço ainda à Fundação para a Ciência e Tecnologia (FCT) pelo suporte financeiro e pela bolsa de Doutoramento que me concedeu com referência SFRH/BD/63318/2009 no âmbito do QREN-POPH-Tipologia 4.1 – Formação Avançada, comparticipado pelo Fundo Social Europeu e por fundos nacionais do MCTES.

FCT Fundação para a Ciência e a Tecnologia
MINISTÉRIO DA EDUCAÇÃO E CIÊNCIA

UNIÃO EUROPEIA
Fundo Social Europeu

QREN QUADRO DE REFERÊNCIA ESTRATÉGICO NACIONAL
PORTUGAL 2007.2013

POPH
PROGRAMA OPERACIONAL POTENCIAL HUMANO

Resumo

A tuberculose (TB) é uma doença infeciosa com uma elevada incidência e prevalência em todo o mundo, especialmente nos países subdesenvolvidos. A TB é causada pela bactéria, *Mycobacterium tuberculosis* (MTb), sendo a segunda doença infeciosa mais prevalente da humanidade, logo a seguir à infeção pelo vírus da imunodeficiência humana (VIH). Progressos significativos têm sido alcançados ao longo dos últimos anos, no que concerne à redução da incidência, prevalência e número de mortes associada à doença, sendo objetivo da Organização Mundial de Saúde (OMS) erradicar a TB até 2050. No entanto, a emergência de estirpes multirresistentes ao arsenal terapêutico existente, pode colocar em causa este ambicioso mas factível objetivo da OMS. De acordo com o que foi referido sobre a persistência, número de mortes associado à TB bem como a emergência de estirpes multirresistentes, torna-se imperativo que surjam novos fármacos mais eficazes no combate a esta doença. A abordagem mais imediata consiste na alteração da estrutura química dos antibióticos já existentes e o melhoramento das suas propriedades farmacocinéticas e farmacodinâmicas. Nesse sentido, nesta tese foram estudados novos análogos sintéticos da rifabutina (RFB), nomeadamente a *N'*-acetil-rifabutina (RFB2) e a *N'*-butanoil-rifabutina (RFB3). A RFB foi um dos últimos antibióticos para o tratamento da TB a ser introduzido no mercado, em 1992, sendo a sua extrema eficácia em grande parte devido às suas características anfifílicas e capacidade de atravessar membranas biológicas. Os testes *in vitro* e *in vivo* demonstraram que a RFB2 constitui um candidato promissor e com potencial para chegar ao mercado. A RFB3 é um composto de síntese intermediário entre a RFB2 e outro derivado (com um grupo acilo maior, nomeadamente o undecanoilo) que também demonstrou ser promissor, mas que por uma questão de reduzida solubilidade em soluções aquososas, não foi estudado durante esta tese. A RFB para que exerça a sua ação farmacológica necessita atravessar as membranas das mucosas gastrointestinais, membranas plasmáticas e a membrana bacteriana de forma a alcançar a RNA polimerase, situada no interior da célula bacteriana. Assim, após uma administração por via oral, este antibiótico percorre uma trajetória extremamente complexa que envolve membranas biológicas, alcançando locais de difícil acesso onde a bactéria se encontra alojada, como se verifica no caso da TB pulmonar, em que a bactéria se localiza marioritariamente no interior dos macrófagos alveolares, encontrando-se estes por vezes envolvidos em estruturas como os granulomas.

A primeira abordagem no estudo de interação fármaco-membrana foi a determinação do coeficiente de partição lípido/água por espectrofotometria derivativa de

ultravioleta-visível (UV/Vis) com modelos de surfactante pulmonar e de membrana plasmática eucarionte e procarionte. A previsão da localização da RFB e análogos a nível da bicamada dos modelos membranares foi efetuada por estudos de desativação de fluorescência. Através dos estudos de anisotropia de fluorescência em estado estacionário, espectroscopia de correlação fotónica e de difração de raios-X foi possível estudar a influência dos compostos antimicobacterianos a nível das propriedades biofísicas dos modelos membranares. Para além dos modelos tridimensionais em bicamada, foram também utilizados modelos bidimensionais em monocamada para mimetizar as membranas biológicas. As isotérmicas de Langmuir aplicadas a estes modelos permitiram o estudo da influência dos compostos antimicobacterianos nas propriedades das monocamadas, como a pressão lateral, área de superfície, efeitos a nível das transições, pressão de colapso e compressibilidade. Adicionalmente, foi possível a visualização das monocamadas por microscopia do ângulo de Brewster, permintindo o estudo da influência dos compostos nas monocamadas em termos de alteração da fluidez e influência sobre o tamanho e formato dos domínios lipídicos. A espectroscopia de absorção-reflexão de infravermelhos permitiu o estudo da influência da RFB e análogos na estrutura dos modelos membranares utilizados. A espectroscopia de reflexão UV-Vis permitiu a confirmação da presença do fármaco a nível da interface e da variação da sua concentração com a compressão/descompressão da monocamada. Foram ainda aplicados estudos de simulação computacional de forma a confirmar a hipótese inicialmente colocada de que uma forte ligação ocorre entre o fármaco e a região polar dos fosfolípidos do surfactante pulmonar.

Os resultados obtidos permitiram inferir que a RFB e análogos interagem com as membranas eucariontes e procariontes de forma diferencial. Assim, estes compostos antimicobacterianos possuem uma maior partilha para os modelos membranares procariontes e alteram as suas propriedades biofísicas de uma forma mais pronunciada. A interação com o surfactante pulmonar ocorre através da formação de um complexo de inclusão entre a RFB e os grupos polar dos fosfolipídios, o que poderá justificar a acumulação deste fármaco a nível do pulmão. Os análogos da RFB interagem com as membranas plasmáticas eucariontes de forma mais marcada do que a RFB. Assim, os análogos da RFB deverão possuir uma maior biodisponibilidade, o que poderá eventualmente permitir reduzir o número de tomas, mas também ser responsável por efeitos secundários mais pronunciados, sendo por isso necessário estudos futuros para assegurar que estas novas moléculas promissoras possam chegar ao mercado.

Palavras-chave: biofísica, interações fármaco-membrana; modelos membranares; rifabutina; tuberculose.

Abstract

Tuberculosis (TB) is an infectious disease with a high worldwide incidence and prevalence, especially in the developing countries. TB is caused by the bacterium MTb, being the second most common infectious disease affecting the humankind, after the human immunodeficiency virus (HIV) infection. Significant progresses over the last years have been made to reduce the incidence, prevalence and number of deaths caused by the disease, being the main goal of the World Health Organization (WHO) the eradication of TB until 2050. Nevertheless, the emergence of multidrug resistant (MDR) strains may undermine the ambitious but praticable objective of the WHO. Therefore, and according the above-mentioned concerns about TB persistence, mortality and emergence of MDR strains, new and more effective drugs are urgently needed. The most obvious approach is the alteration of the chemical structure of old antibiotic families and their improvement in terms of their pharmacokinetics and pharmacodynamics properties. In this context, two novel synthetized rifabutin (RFB) analogs were studied in this thesis, namely, *N'*-acetyl-rifabutin (RFB2) and *N'*-butanoyl-rifabutin (RFB3). RFB was one of the last antibiotics introduced in the market for the treatment of TB (in 1992), being extremely efficient, in part due to its amphiphilic properties and ability to cross the biologic membranes. RFB2 was tested *in vitro* and *in vivo* and demonstrated to be a promising candidate with potential to reach the market. RFB3 is an intermediate synthetic compound between RFB2 and other analog (with a higher acyl group, undecanoyl), which was demonstrated to be a promise compound but which was abandoned since it has a poor solubility in aqueous solutions. In order to exert its pharmacological effect and reach the intracellular RNA polymerase, RFB needs to cross the biological membranes, including gastrointestinal tract, plasmatic human and bacterial membranes. Thus, after the oral intake, RFB follows a complex course, in order to reach the sites where the bacterium is located, sometimes places of difficult access as in the case of the pulmonary TB, where the bacteria is located inside the alveolar macrophages (AMs), which in some cases are inside the granulomas.

The first approach to the study of the drug-membrane interactions was the determination of the partition coefficient lipid/water by UV/Vis derivative spectrophotometry, using eukaryotic plasma and pulmonary surfactant (PS) membrane models, and prokaryotic plasma membrane models. The prevision of the location of RFB and analogs within the lipid bilayer of the membrane models was assessed using fluorescence quenching. The steady-state anisotropy, dynamic light scattering and x-ray diffraction studies allowed to study the influence of the antimycobacterial compounds on

the biophysical parameters of the membrane models. Besides the three-dimensional (i.e. bilayers), two-dimensional (i.e. Langmuir monolayers) models were used to mimic the biological membranes. The Langmuir isotherms applied to the mentioned membrane models allowed to study the influence of the antimycobacterial compounds on the monolayers properties, such as the lateral pressure, surface area, transitions, collapse pressure and compressibility. Additionally, the visualization of the monolayers was possible by the Brewster angle microscopy (BAM), which allowed to study the influence of the antimycobacterial compounds in the fluidity of the monolayers as well as in the shape/size of the lipid domains of the monolayers. The infrared absorption-reflection spectroscopy (IRRAS) allowed the study of the influence of RFB and analogs on the structure of the chosen membrane models. The UV-Vis reflection spectroscopy permitted the confirmation of the drug's presence at the air-water interface and the variation of its concentration with the monolayer compression/decompression. Computational simulation studies were also applied and corroborate the initial hypothesis of a strong binding between the drug and the polar head groups of the phospholipids of the PS.

The results obtained allowed to infer that RFB and its analogs interact by a differential way with the eukaryotic and prokaryotic membranes. Thus, these compounds possess a higher partition to the prokaryotic membrane models, having a more pronounced effect on its biophysical properties. The interaction with the PS occurs with the formation of an inclusion complex between RFB and the polar groups of the phospholipids, which may be related with the drug's accumulation in the lungs. The analogs of RFB interact with the eukaryotic plasma membranes more markedly than RFB. Thus, the analogs seem to have a higher bioavailability, which may allow a dosage reduction, although probably with more pronounced side effects, being further studies needed to ensure that these novel promising molecules may reach the market.

Keywords: biophysics, drug-membrane interactions; membrane models; rifabutin; tuberculosis.

Index

INDEX OF FIGURES

CHAPTER IV

1. Liposomes as drug delivery systems for the treatment of TB.

2. Molecular interaction of Rifabutin on model lung surfactant monolayers.

3. Interplay of mycolic acids, antimycobacterial compounds and pulmonary surfactant membrane: a biophysical approach to disease.

6. Effects of a novel antimycobacterial compound on the biophysical properties of a pulmonary surfactant model membrane.

7. Evaluation of the structure-activity relationship of rifabutin and analogs: a drug-membrane study.

8. The influence of Rifabutin on Human and Bacterial Membrane Models: Implications for its Mechanism of Action.

9. Interactions of *N'*-acetyl-rifabutin and *N'*-butanoyl-rifabutin with lipid bilayers: A synchrotron X-ray study.

Index of Tables

CHAPTER IV

1. Liposomes as drug delivery systems for the treatment of TB.

3. Interplay of mycolic acids, antimycobacterial compounds and pulmonary surfactant membrane: a biophysical approach to disease.

4. Differential interactions of rifabutin with human and bacterial membranes: implication for its therapeutic and toxic effects.

5. Drug-membrane interaction studies applied to *N'*-acetyl-rifabutin.

6. Effects of a novel antimycobacterial compound on the biophysical properties of a pulmonary surfactant model membrane

7. Evaluation of the structure-activity relationship of rifabutin and analogs: a drug-membrane study

8. The influence of Rifabutin on Human and Bacterial Membrane Models: Implications for its Mechanism of Action.

9. Interactions of *N'*-acetyl-rifabutin and *N'*-butanoyl-rifabutin with lipid bilayers: A synchrotron X-ray study

Abbreviations

AFM	Atomic force microscopy
AMs	Alveolar macrophages
APLT	Aminophospholipid translocase
ATP	Adenosine triphosphate
BAM	Brewster angle microscopy
BCG	Bacille-Calmette-Guérin
CAMPs	Cationic antimicrobial peptides
CHOL	Cholesterol
CL	Cardiolipin
DCs	Dendritic cells
DMPC	1,2-dimyristoyl-sn-glycero-3-phosphocholine
DPH	1,6-diphenylhexatriene
DPH-PA	Propionic acid-1,6-diphenylhexatriene
DPPC	1,2-dipalmitoyl-sn-glycero-3-phosphocholine
ER	Endoplasmic reticulum
EPC	Egg-phosphocholine
G	Gaseous
GIXD	Grazing incidence X-ray diffraction
GPI	Glycosylphosphatidylinositol
HIV	Human immunodeficiency virus
IL	Interleukin
IRRAS	Infrared absorption-reflection spectroscopy
LAM	Lipoarabinomannan
LBs	Lamellar bodies
LC	Liquid-condensed

LE	Liquid-expanded
LED	Fluorescent light-emitting diode
LPS	Lipopolysaccharides
LTA	Lipoteichoic acid
LUVs	Large unilamellar vesicles
MAs	Mycolic acids
MDR	Multidrug resistant
MLVs	Multilamellar vesicles
MTb	*Mycobacterium tuberculosis*
NK	Natural killer
OMS	Organização Mundial de Saúde
PC	Phosphatidylcholine
PE	Phosphatidylethanolamine
PG	Phosphatidylglycerol
PI	Phosphatidylinositol
PIM	Phosphatidylinositol mannosides
PM-IRRAS	Polarization-modulation infrared absorption-reflection spectroscopy
PS	Pulmonary surfactant
Pser	Phosphatidylserine
RFB	Rifabutin (en) Rifabutina (pt)
RFB2	*N'*-acetyl-rifabutin (en) *N'*-acetil-rifabutina (pt)
RFB3	*N'*-butanoyl-rifabutin (en) *N'*-butanoil-rifabutina (pt)
RIF	Rifampicin
RNS	Reactive nitrogen species
ROS	Reactive oxygen species

S	Solid
SAXS	Small-angle X-ray scattering
SSM	Sputum smear microscopy
SUVs	Small unilamellar vesicles
TB	Tuberculosis (en) Tuberculose (pt)
TDM	Trehalose 6,6′-dimycolate Cord factor
TNF-α	Tumor necrosis factor alpha
ULVs	Unilamellar vesicles
UV-Vis	Ultraviolet-visible spectroscopy (en) Ultravioleta-visível (pt)
VIH	Vírus da imunodeficiência humana
XDR	Extensively Drug-Resistant
WAXS	Wide-angle X-ray scattering
WHO	World Health Organization

Symbols

A	Area per lipid molecule
A_{min}	Limiting area per lipid molecule
B	Cooperativity
C_s^{-1}	Elastic modulus
D	Derivative intensity
d-spacing	Repeat distance
f_i	Fractional contribution of component i to the total lifetime
$FWHM$	Full width at half maximum
G	Anisotropy instrumental correction factor
H_I	Normal hexagonal phases
H_{II}	Inverted hexagonal phases
I	Fluorescence intensity
K_D	Stern-Volmer constant for dynamic quenching
K_p	Partition coefficient
K_q	Bimolecular quenching constant
K_S	Stern-Volmer constant for static quenching
K_{SV}	Stern-Volmer constant
$[L]$	Lipid concentration
L_α	Liquid-crystalline (monolayers) or fluid phase (bilayers)
L_β	Untilted solid-crystalline (monolayers) or gel phase (bilayers)
$L_{\beta'}$	Tilted solid-crystalline (monolayers) or gel phase (bilayers)
L_c	Crystalline phase
L_o	Liquid-ordered phase
Log D	Logarithm of partition coefficient
Log P	Logarithm of distribution coefficient
m_ω	Demodulation ratio

$P_{\beta'}$	Rippled phase
pKa	Logarithmic acid dissociation constant
$[Q]_m$	Membrane's drug concentration
R	Reflectivity
r_∞	Limiting value of anisotropy
r_{ss}	Steady-state fluorescence anisotropy
T	Temperature
T_m	Main phase transition temperature
V_{app}	Apparent volume of the *sphere of action*
V_m	Lipid molar volume
π	Surface pressure
Θ	Angle of incidence in X-ray diffraction studies
λ	Wavelength
ξ	Correlation length
τ	Fluorescence lifetime
Φ	Phase angle
χ^2	Reduced chi squared

Chapter I

Introduction

1. Observations Beyond the Thesis

TB is still a major infectious disease that affects the humankind. The emergence of multidrug resistant strains is one of the main concerns associated with the TB management. In this regard, new antibiotic molecules are needed, being the re-engineering of old drug families molecules the most immediate way to their obtention. Nevertheless, the drug's mechanism of action must be fully understood since the design of drugs taking in consideration solely the pharmacologic target is not a guaranty of success. The ryfamicins, which inhibit the bacterial RNA polymerase include among others, RFB and rifampicin (RIF). The ryfamicins are a very successful class of drugs in the TB treatment, being RIF a first-line drug commonly used throughout the entire TB treatment. RFB, which was one of the last antibiotics to TB treatment brought to the market, is generally used as a second-line drug. Nevertheless, RFB is at least as effective and safe as RIF, presenting however a much higher financial cost associated. RFB is used as a first choice in cases where resistance to the RIF occurs, as well in the case of co-infected HIV/TB patients, since it is less prone to interact with the enzymes that metabolize the antiretroviral drugs. The accepted mechanism of action of RFB involves the binding to the β-subunit of the RNA polymerase, causing the inhibition of the RNA transcription and consequently the inhibition of the bacterial protein synthesis. The binding constant for prokaryotic RNA polymerases is 10000-fold higher than those for eukaryotic enzymes, which in part might explain the higher selectivity of this drug to the bacteria. However, a lack of correlation exists between the RFB inhibitory activity on the RNA polymerase and the antibiotic efficacy. In fact, the drug's penetration through the bacteria cells explains the higher activity against Gram-positive compared to the Gram-negative despite the quite similar RNA polymerase inhibitory activities. Therefore, the efficiency of the interactions of the antibiotics with the membranes constitutes one of the most important pharmacological features, playing an essential role on its biological activity, and should be accounted in order to understand their full mechanism of action. RFB has an intracellular target, and hence it must pass across phospholipid bilayers to reach the RNA polymerase and elicit its pharmacological effect. Since RFB has a high lipophilicity, the passive diffusion is probably the most relevant process of the RFB's permeation through the membranes. The plasma concentrations achieved by RFB do not reflect the much

higher concentrations that can be reached in target organs and infected cells. In fact, RFB penetrates well into infected cells (i.e. macrophages) and in organs as the lungs the concentrations are at levels six times higher compared with the plasma concentrations. On the other hand, RFB, despite being well-tolerated, presents some of the side effects including uveitis, rash, nausea, vomiting, neutropenia, anemia, discoloration of the skin and body fluids (tears, saliva, urine and perspiration) and, rarely, clinically important impairment of the liver function. Indeed, the mentioned side effects seem to be related with the RFB tropism and affinity to the membranes, including the ability to reach to specialized membranes of the human body (e.g. epiretinal, stractum corneum membranes) and the capacity to diffuse through the human body, crossing several biological membranes, promoting the discoloration of body fluids (e.g. tears, perspiration, urine and saliva). In addition, the lipids of the MTb (i.e. mycolic acids (MAs) and cord factor (TDM)) are recognized to be responsible for the impairment and dysfunction of the PS membrane. Moreover, the mentioned lipids change the compressibility of the PS causing an impairment of its normal function and thus it is appealable to study the effect of drugs on the PS membrane models and understand if the drugs have any protective effect.

In this thesis, RFB was used as the lead compound for the new promising molecules against TB. Therefore, studies of the RFB2 and RFB3-membrane interactions are needed, since antibiotic–membrane interactions play a crucial role for the understanding of the drugs bioavailability, the drugs entrance into the cellular compartments, and the drugs-induced toxicity. In addition, a relationship between the chemical structure of the molecules and the corresponding effect in the plasma membrane will be useful. The founded correlation will give useful indications for understanding the influence of different structural interdependencies between antimycobacterial compound's chemical composition and antimycobacterial compound's expected effects, which ultimately may permit the development of more effective and less toxic anti-TB drugs. Moreover, the knowledge about drug-membrane biophysical interactions is of utmost importance for the rational development of new drugs as well as for the development of lipid-based nano-carriers (e.g. lipid nanoparticles and liposomes) as drug delivery systems for these antimycobacterial compounds.

2. Objectives of The thesis

Three main objectives are undertaken in this thesis, being interlinked:

- The first objective is to get a more complete picture about the mechanism of action of RFB. Nowadays, the mechanism of action of RFB and several other drugs is viewed as the binding to a specific target (e.g. enzyme, receptor). Notwithstanding, since the oral intake of RFB, the primary barriers that the drug encountered by the drug are in fact the biological membranes. In addition, to reach the RNA polymerase RFB has to cross trough several different types of membranes. The idea beyond the selective binding to the bacterial RNA polymerase is highly simplistic and has several weak points. Thus, the question related with the higher efficacy in Gram-positive than in Gram-negative, despite the similar binding activity to the RNA polymerase remains unsolved. Moreover, it is well known that part of the success of RFB is due to its bioaccumulation in the lungs and in the infected cells, being the mechanism beneath this an open question. In addition, the toxic effects of this drug are not fully understood and do not seem to be related with the binding to the RNA polymerase that also exist in the human cells.

- The second objective is devoted to the study of RFB2 and RFB3-membrane interactions in order to appreciate if the RFB analogs have favorable pharmacokinetic properties to reach the market. In this regard, a relationship between the chemical structure of the antimycobacterial compounds and their activity on the membranes was also established. This may be useful to the design of more effective drugs with less side effects, since a rational drug design will certainly benefit of the knowledge beyond the interactions with the membranes at the molecule level.

- The third objective is to get a higher knowledge regarding the MTb infection and the TB disease. In this context, for the first time a biophysical approach applied to TB was developed, which may contribute to a higher knowledge related with the MTb infection and TB disease. Despite a physiopatologic effect, the lipids present in the MTb cell wall seem to be related with the bacteria access to the target (i.e. AMs). Moreover, the effect of the drug at the PS level in the presence of MTb lipids was also studied in order to understand the putative protective effect of the drug, from the effects of the lipids present in the MTb cell wall, at the PS membrane.

3. Structure of the Thesis

This thesis is divided into five chapters:

Chapter I: Introduction. This chapter includes the introduction of the thesis, which comprises the motivation and the main objectives. Moreover, it covers a general description of the other chapters, namely their organization and structure.

Chapter II: Theoretical Background. A full description of the theoretical concepts approached in this thesis is provided in this chapter. Therefore, the concepts considered essential to understand the results and the conclusions are scrutinized, including predominatly two main fields, the TB and the biomembranes. Thus, the chapter starts with the description of the infectious disease TB, the epidemiology and etiology of TB, how the transmission occurs, the physiopathology concepts, the main clinical manifestations of the disease, the diagnosis methods, the vaccines and the treatment for TB. In the treatment are included the chemotherapy and the drugs with interest for TB, including RFB and its analogs. Moreover, the concepts regarding the biological cell membranes are addressed, including their function, structure, the molecular composition of the eukaryotic, prokaryotic plasma membranes and PS, as well as the lamellar phase transition of the membrane models used to mimic the former membranes.

Chapter III: Methods to Evaluate the Antimycobacterial Compounds-Membrane Interactions. In this chapter, the biophysical techniques used during this thesis are presented. The methods applied to the drug-membrane interaction studies were: UV-Vis Derivate Spectrophotometry to calculate the partition coefficient of the antimycobacterial compounds; Fluorescence Quenching to study the location of the antimycobacterial compounds within the lipid bilayers of the membrane models; Steady-state Anisotropy, X-ray studies and Dynamic Light Scattering to study the influence of the antimycobacterial compounds on the biophysical parameters of the membrane models. Moreover, Langmuir Isotherms, Brewster Angle Microscopy, Polarization Modulation Infrared Reflection-Absorption Spectroscopy, Reflection UV-Vis Spectroscopy and Computational Simulations were carried out in the monolayers as membrane model systems in order to understand the influence of RFB and analogs on the structure and lipid organization.

Chapter IV: Progress Beyond the State-of-the Art. This chapter is focused exclusively in the manuscripts that this thesis originated, namely:

1 – Liposomes as drug delivery systems for the treatment of TB.
Pinheiro M, Lúcio M, Lima J, Reis S. Nanomedicine. 2011; 6(8):1413-28. doi:10.2217/nnm.11.122.

2 – Molecular interaction of Rifabutin on model lung surfactant monolayers.
Pinheiro M, Lúcio M, Reis S, Lima JLFC, Caio JM, Moiteiro C, et al. The Journal of Physical Chemistry B. 2012;116(38):11635–45. doi: 10.1021/jp303725j.

3 – Interplay of mycolic acids, antimycobacterial compounds and pulmonary surfactant membrane: a biophysical approach to disease.
Pinheiro M, Giner-Casares J, Lúcio L, Caio J, Moiteiro C, Lima L, et al. BBA:Biomembranes. 2013;1828:896–905. doi: 10.1016/j.bbamem.2012.09.015.

4 – Differential interactions of rifabutin with human and bacterial membranes: implication for its therapeutic and toxic effects.
Pinheiro M, Arêde M, Nunes C, Caio JM, Moiteiro C, Lúcio M, et al. Journal of Medicinal Chemistry. 2013;56(2):417–26. doi: 10.1021/jm301116j.

5 – Drug-membrane interaction studies applied to *N'*-acetyl-rifabutin.
Pinheiro M, Arêde M, Caio JM, Moiteiro C, Lúcio M, Reis S. European Journal of Pharmaceutics and Biopharmaceutics. 2013; doi: 10.1016/j.ejpb.2013.02.015.

6 – Effects of a novel antimycobacterial compound on the biophysical properties of a pulmonary surfactant model membrane.
Pinheiro M, Arêde M, Giner-Casares JJ, Nunes C, Caio JM, Moiteiro C, et al. International Journal of Pharmaceutics. 2013; 450(1-2):268-77. doi: 10.1016/j.ijpharm.2013.03.062.

7 – Evaluation of the structure-activity relationship of rifabutin and analogs: a drug-membrane study.
Pinheiro M, Leite-Leite P, Arêde M, Nunes C, Caio JM, Moiteiro C, et al. ChemPhysChem. 2013; doi: 10.1002/cphc.201300262.

8 – The Influence of Rifabutin on Human and Bacterial Membrane Models: Implications for Its Mechanism of Action.

Pinheiro M, Nunes C, Caio JM, Moiteiro C, Lúcio M, Brezesinski G, et al. The Journal of Physical Chemistry B. 2013; 117(20):6187-93. doi: 10.1021/jp403073v.

9 – Interactions of *N′*-acetyl-rifabutin and *N′*-butanoyl-rifabutin with lipid bilayers: A synchrotron X-ray study.

Pinheiro M, Nunes C, Caio JM, Moiteiro C, Brezesinski G, Reis S. International Journal of Pharmaceutics. 2013; 10;453(2):560-8; doi: 10.1016/j.ijpharm.2013.06.018.

Chapter V: Conclusions. In this chapter, the main concluding remarks based on the findings of the studies presented in this thesis are described. Furthermore, the limitations of the experimental studies and future perspectives for further research are also presented.

CHAPTER II

Theoretical Background

1. Tuberculosis

"If the importance of a disease for mankind is measured by the number of fatalities it causes, then tuberculosis must be considered much more important than those most feared infectious diseases, plague, cholera and the like. One in seven of all human beings dies from tuberculosis. If one only considers the productive middle-age groups, tuberculosis carries away one third, and often more." [1]

Robert Koch
(lecture on the evening of March 24 in 1882, about his discovery of *Mycobacterium tuberculosis*)

Tuberculosis (TB) is an ancient disease, first described by Hippocrates (400 B.C.) in his works ‘‘Of the Epidemics’’ and posterior documented by Claudius Galen during the Roman Empire period [2]. The etiologic agent of TB, *Mycobacterium tuberculosis* (MTb) (Figure 1) was first described by Robert Koch in 1882 [3]. In fact, TB is a disease rich in paradoxes, being one of the first diseases for which the causative agent was identified (i.e. MTb), and one of the earliest for which a vaccine and a diagnostic method were developed. Anti-TB drugs effective against MTb are also available for more than a half century [4]. Despite the above-mentioned, TB is still a leading cause of death among infectious diseases [5]. During the Industrial Revolution, TB reached epidemic levels in Europe, being responsible for one in four deaths from the sixteenth to eighteenth centuries [2]. Nowadays, TB is still a major worldwide health concern, being the cause of a serious health condition among millions of people every year, ranking as the second leading cause of death from an infectious disease worldwide, after the human immunodeficiency virus [6-8]. Indeed, somewhere in the world almost 20 people develop TB and four people die from the disease each minute [9].

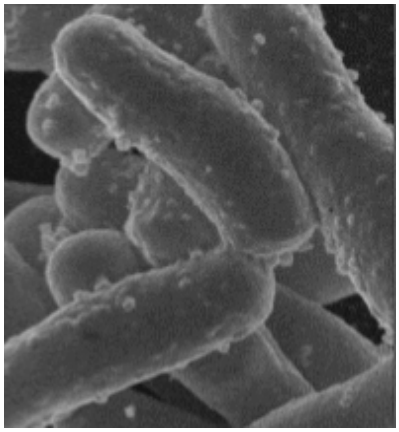

Figure 1. Scanning electron microscope image of MTb. Adapted from [10].

1.1. Epidemiology

MTb infection currently affects around a third of the world's population (approximately 2 billion of people). With such a reservoir, the control of TB seems to be a difficult task to achieve [11]. In most cases, the bacterium and the host establish an equilibrium, and thus infected individuals can remain asymptomatic for several decades, if not for their entire lifetime. However, about one-tenth of the infected individuals develop the disease [12]. Besides representing a severe health problem in developing countries, TB has become a renewed threat in the Western world since the mid 1980's. In view of this situation, in 1993 the WHO declared TB as a global public health emergency [13]. Geographically, TB has more prevalence in Asia and Africa [7],[14]. In fact, countries as India and China account together for almost 40% of the world's TB cases. About 60% of cases are in the South-East Asia and Western Pacific regions. The African Region has 24% of the world's cases, and the highest rates of cases and deaths per capita. In Europe there is an enormous disparity in the rates of TB between the western and eastern, being the rates of disease different between urban and non-urban settings [15]. In the particular case of Portugal, which is one of the most concerning in Europe, the incidence in 2012 was of 2480 new cases, resulting in 117 deaths [16].

Worldwide, 3.7% of the new cases and 20% of the previously treated cases were estimated to have multidrug-resistant TB (MDR-TB). According to the WHO, 8.7 million cases of active TB emerge annually, resulting in 1.4 million deaths in 2011. Figure 2 shows the regional incidences of TB. From the 8.7 million people who developed TB worldwide, 13% were HIV-positive. Globally in 2011, there were an estimated 630 000 cases of MDR-TB. In addition, there were an estimated 0.5 million cases and 64 000

deaths among children in the same year. The number of notifications, which are mandatory, to the national TB control programs are roughly two thirds of the estimated total, being therefore major efforts needed to ensure that all the cases are notified to the regulatory authorities [7].

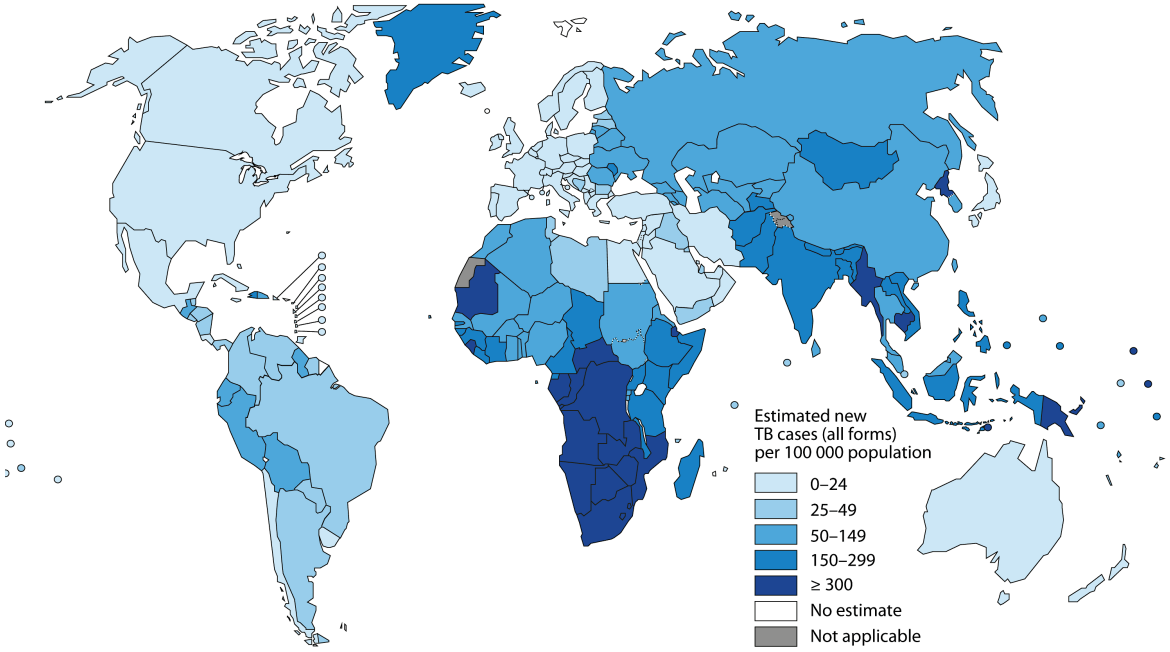

Figure 2. Estimated TB incidence rates, 2011. Adapted from [7].

Progress towards a decrease in the TB burden has been made in the absolute TB cases and deaths. Thus, new cases of TB have been declining for several years and the mortality rate has decreased 41% since 1990 [13]. Notwithstanding, the significant progress that has been made to reduce the global impact of TB, the emergence of MDR-TB (resistant to at least two main first-line anti-TB drugs, isoniazid and RIF) and extensively drug-resistant (XDR) (resistant to three or more second-line anti-TB drugs) threatens these advancements [17-18].

The major goal of the WHO is to eradicate TB as a public health problem until 2050 by reaching a global incidence of the disease to less than one case per million population [13]. This although possible, constitutes an ambitious goal to approach. To be achieved, this goal requires intensified efforts and more effective and affordable new technologies to prevent both infection and disease, and quick mechanisms to allow their worldwide introduction [19].

1.2. Etiology

The *Mycobacterium tuberculosis* complex comprises closely related species, which are the cause of TB in human and other animals including, MTb, *Mycobacterium bovis*, *Mycobacterium africanum*, *Mycobacterium microti* and *Mycobacterium canetti* [20-21]. In humans, TB is primarily caused by MTb and *Mycobacterium africanum*, being the former species restricted to the West Africa. Both species are obligate human pathogens with limited survival outside of the human body and with no known animal reservoir. *Mycobacterium bovis* is a cattle pathogen, which may also affect the human. Nevertheless, *Mycobacterium bovis* infections in humans decreased markedly due to the introduction of milk pasteurization and meat-control practices [22]. *Mycobacterium microti* causes TB in small rodents like voles and its importance for TB in humans remained unclear. *Mycobacterium canetti* can also cause TB in humans, but only a restricted number of strains have been isolated so far [20].

With the evolution of science and most specifically genetics, the point of view that TB had its origin in nonhuman animals has markedly changed. Actually, the most probable scenario strongly suggests that humans were responsible for the TB in the other animals and that TB seems to have its origin in Africa following the out-of-Africa migrations of modern humans [22-23].

1.3. Transmission

TB infection is usually initiated by the entry of MTb in the respiratory system through aerosol droplets (Figure 3). Thus, people with active TB can infect many others by coughing, sneezing, spitting, or speaking [24].

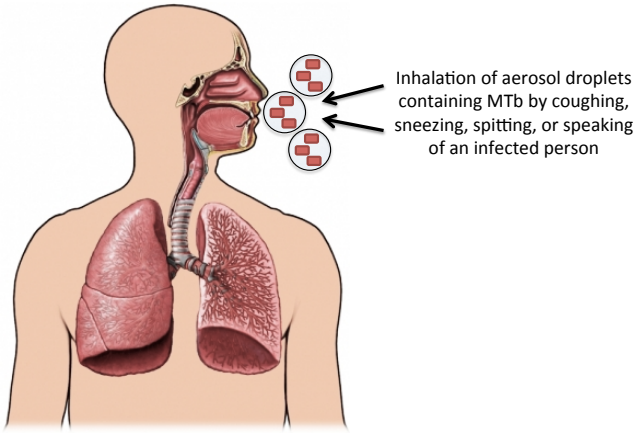

Figure 3. TB transmission.

The association of TB with HIV infection has significantly exacerbated the situation in developed and developing nations [25]. HIV infection is the highest risk factor identified, so far, for the progression of latent tuberculosis to an active disease state, with co-infected people having a higher 5-15% risk of early development of active TB [26]. TB represents a major cause of death in HIV co-infected individuals [27-29]. Other conditions can also impair the human host defense, increasing the risk of TB reactivation, including other co-infections (helminths, non-tuberculous mycobacteria, virus) and comorbidities as type-2 diabetes. Latent MTb infection may also be reactivated following treatment with biological therapy, such as the tumor necrosis factor alpha (TNF-α)/interleukin (IL) 12/IL-23 blockers, commonly used in inflammatory diseases such as rheumatoid arthritis, Crohn's disease, psoriasis and others [30-32]. Additionally, poverty, malnutrition and indoor air pollution constitute etiological risk factors that affect the TB incidence and the treatment outcomes [31].

1.4. Physiopathology

In the lungs the facultative intracellular parasite MTb is non-specifically phagocytized, mainly by the alveolar macrophages (AMs), within which is able to survive and multiply [33-34]. Other phagocytic cells such as the local dendritic cells (DCs) and interstitial macrophages may also participate in the uptake of the MTb bacilli. In addition, the bacilli can even enter through the bronchial epithelium [30]. Besides, the MTb places itself nearby the PS, which may suffer dysfunction when the lipids, of the extremely rich in lipids mycobacteria cell wall, are present at the air/water interface [35]. The main lipids implied in this pulmonary surfactant negative effect seem to be the MAs and TDM [35-37]. In comparison with other microorganisms, MTb has an unusual ability to delay the adaptive immune response for 2-3 weeks in humans and experimental animals (Figure 4) [38]. The MTb-infected cells fail to migrate from the infected lung focus to the local draining lymph nodes, where the T-cell are located. This delay allows the production of a significant mass of the bacilli before the adaptive immunity can develop sufficiently to control the infection [30].

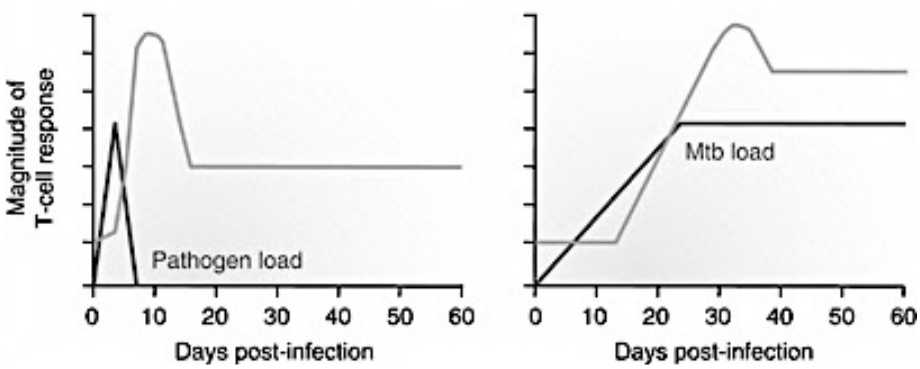

Figure 4. Delayed onset of adaptive immunity in TB (Right) compared with other infectious (Left). Adapted from [38].

Nevertheless, in most people the infection does not constitute a healthy problem because MTb have developed an extraordinary ability to live in balance with immune responses [39]. In fact, MTb has the extreme capacity to infect its host for decades without causing clinical disease. The reactivation only occurs in clinical situations where the immunity of the host is compromised [9]. The granuloma is the structure developed by the host in order to contain the infection and eliminate the disease, being produced after immune signal events. Thus, the infected AMs release cytokines to recruit different populations of cells, including macrophages to the infected site. In addition, dendritic cells present antigens to T cells in the lymph nodes, in which a T-cell response can subsequently be developed. The MTb persist in a latent state within the granuloma, often for decades, surrounded the infected cells (i.e. macrophages) by T cells, B cells, DCs, neutrophils, natural killer (NK) cells and fibroblasts (Figure 5) [40] that with their death cause the formation of a necrotic zone in the center of the granuloma, which eventually disintegrates, releasing the bacteria into the lung, and hence into the environment [9],[41].

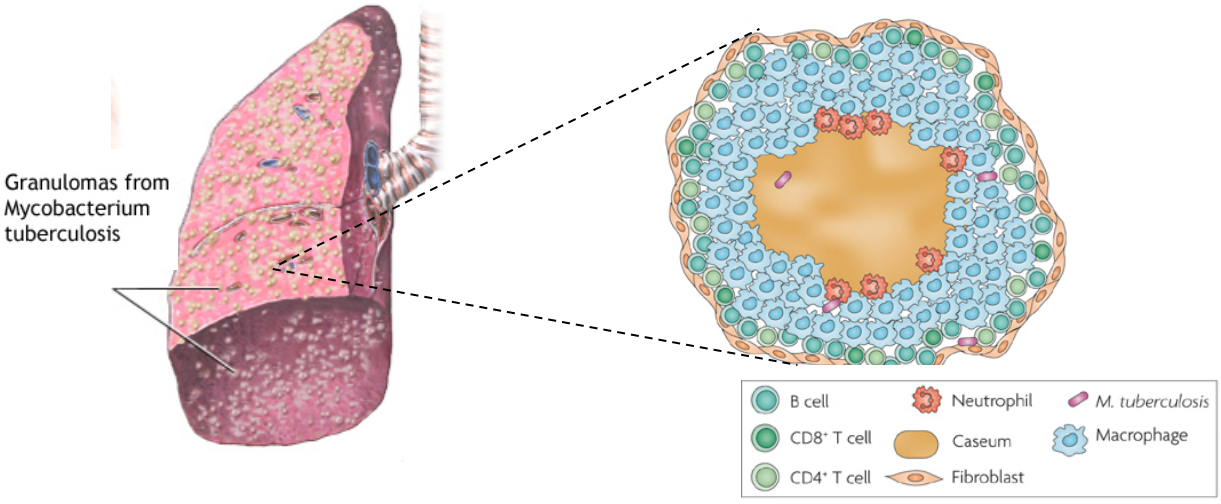

Figure 5. Schematic representation of TB granulomas. Adapted from [42].

The MTb are ingested by the macrophages, being phagocytized. The phagocytosis involves membrane invaginations, which leads to the phagosome formation. Inside the phagosome, a hostile environment is created to the MTb. In fact, the bacillus is exposed to an acidic pH, reactive oxygen and nitrogen species (ROS and RNS), hydrolytic enzymes, and cationic antimicrobial peptides (CAMPs). The final steps of the bacterial destruction and clearance require the fusion between the phagosome and the lysosome [43]. Nevertheless, MTb is shielded from the environment by a robust cell wall, protecting and allowing the adaptation of MTb to the intracellular environment of macrophages and their survival even under drastic conditions. MTb is a bacillus shielded by a unique waxy cell wall composed of abundant glycolipids, mycolic acids (MAs), cord factor (TDM), peptidoglycans, and other carbohydrate, lipid, and protein molecules [44]. The mycobacterial cell wall differs from that of most other bacteria and forms a diffusion barrier, which is 100 to 1000-fold less permeable to hydrophilic molecules than that of *Escherichia coli* [45-46]. The success of MTb as a pathogen can be attributed to its extraordinary stealth and capacity to adapt to environmental changes throughout the course of infection. These changes include: nutrient deprivation, hypoxia, various exogenous stress conditions and, in the case of the pathogenic species, the intraphagosomal environment. Moreover, due to the highly hydrophobic waxy cell wall, bacilli are resistant to the digestion by liposomal enzymes and also resistant to the killing effects of macrophages [47]. Knowledge of the physiology of the MTb during this later stage has been limited by the slow growth exhibited by the bacterium in the laboratory [48]. In addition, although the exact nature of the carbon sources used during the infection remains unknown, MTb has been shown to metabolize host-derived cholesterol (CHOL) and triacylglycerol from the host cell and store the products in the form of intracellular lipid droplets [43].

In the human host, the MTb is able to persist in a dormant state, causing latent TB without clinical disease (Figure 6). The bacterium enters into a nonreplicating stage with low-to-absent metabolic activity. A stimulus, as for example anti-TB drug treatment or immunosuppression of the host, may lead to the bacilli recover and grow to high abundance causing reactivation of TB. Nevertheless, MTb in a dormant and in a replicative stage seem to coexist and their balance will determinate the latent or the active TB [43].

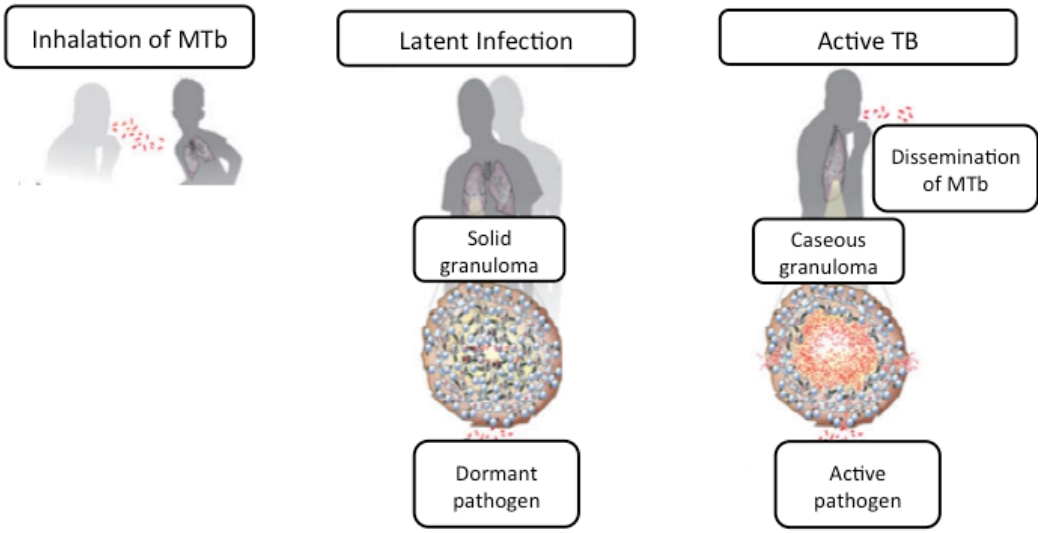

Figure 6. Schematic representations of the major steps from infection to disease in TB. Adapted from [49].

Less than 10% of the infected individuals develop active TB (Figure 6). In the active disease, the number of pathogen increases exponentially by killing host cells and, by spreading through lymphatic circulation to regional lymph nodes in the lungs (3 to 8 weeks after infection). A recent report showed that mycobacteria generates cell-to-cell heterogeneity by an asymmetric division and growing mother cell gives rise to daughter cells that differ in elongation rate and size (Figure 7). The resulting subpopulations of cells demonstrate different susceptibility to the antibiotics [50]. Later on, dissemination of the bacilli from the infected lungs to distant highly irrigated organs (e.g. central nervous system, spongy bone, liver, kidneys and genitalia) takes place (3 months after infection). At this stage, acute TB meningitis or disseminated TB can sometimes result in death. Finally, extrapulmonary manifestations (e.g. lesion in bones and joints) can appear [33]. In contrast with the pulmonary TB, the extrapulmonary TB is generally non-infectious [22].

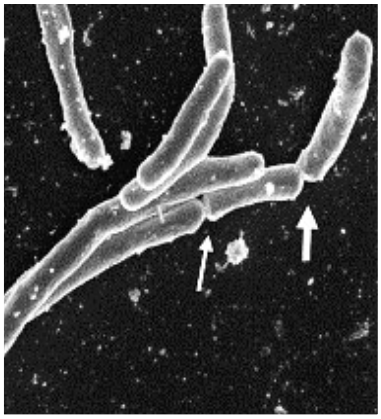

Figure 7. Scanning electron microscope image of MTb showing the asymmetrical cell division. Arrows represent the asymmetrical cell division. Adapted from [10].

1.5. Clinical Manifestations

The incubation of the MTb in the lungs corresponds to the primary pulmonary TB. In this stage when the symptoms appear are generally limited to a mild fever [51]. Nevertheless, the majority of people remain asymptomatic. In a later stage of reactivation of TB the symptoms include, fever, cough, weight loss, fatigue, night sweats. Other symptoms as chest pain, dyspnea and hemoptysis may also occur, being although much less frequent [51-52]. Clinically, pulmonary TB is characterized by widespread lung damage in the form of areas of pulmonary atelectasis, fibrosis and scarring [53] resulting in decreased pulmonary compliance and impaired gas exchange. A similar clinical manifestation is observed in disorders related with pulmonary surfactant (PS) dysfunction [44],[47]. In the case of the extrapulmonary TB, the symptoms are strongly dependent of the organ system affected. For instance, in the skeletal TB the symptoms are general absent and when appear are restricted to a localized pain over the affected site. In the tuberculous pericarditis the symptoms are unspecific, including dyspnea, cough, orthopnea, edema. When the lymphatic and hematogenous are affected (miliary TB), systemic symptoms as fever, weight loss and night sweats are common. Septic shock and acute respiratory distress syndrome may also occur [51].

1.6. Diagnosis

Currently, conventional methods to identify MTb include microscopy, culture, radiography and serologic studies (Table 1) [54].

Table 1. Key Features of Tests for TB. Adapted from [51].

Test	Advantages	Disadvantages
Smear microscopy	Ease, speed, and cost-effectiveness of the technique Quantitative estimate of the number of bacilli Usefulness in determining infectiousness and in monitoring treatment progress	Low sensitivity No capacity to differentiate from nontuberculous mycobacteria
Chest radiography	Ready availability Capacity to differentiate latent infection from active TB	Low sensitivity and specificity Not confirmatory
Tuberculin skin test	High specificity in non–BCG-vaccinated populations Cost-effectiveness	Training required for administration and interpretation Return visit required in 48-72 h for test result Possible booster effect Possible false-positive and false-negative results
Nucleic acid amplification test	High specificity Higher sensitivity than smear microscopy Rapid (1-2 days) diagnosis Capacity to differentiate TB from other mycobacteria	Low sensitivity with smear-negative TB Contamination-prone Technical skill and expertise required Results may remain positive in patients who have completed treatment High cost

The diagnostic method developed by Robert Koch 131 years ago is still used nowadays for the identification of MTb. The former method allows the observation of bacteria in cultures and in host tissues and is based on the adittion of methylene blue and brown counterstaining of the host tissues with vesuvin [43]. The sputum smear microscopy (SSM) diagnosis is one of the most widely used diagnostic tests for the identification of MTb, being simple and fast, however with several limitations (i.e. low sensitivity and the absence of capacity to differentiate from nontuberculous mycobacteria). The Ziehl–Neelsen is a commonly used coloration technique to demonstrate the acid-fast bacilli [55]. Still, this method does not distinguish between TB and nontuberculous strains and the identification of isolates may take a long time (up to 6 to 8 weeks) [54]. In 2009, the WHO recommended the sensitive fluorescent light-emitting diode (LED) microscopy instead of traditional Ziehl–Neelsen associated with optical microscopy. However, only 2% of the worldwide laboratories have LED microscopes [7]. The chest radiography has limited utility as a diagnosis tool for pulmonary TB since it presents poor specificity and reader inconsistency [56-57]. On the other hand, the tuberculin skin test, described by Koch in 1890 was until 2001 the only method capable of diagnosing latent TB [40]. This method measure the immune response against soluble antigens of MTb as a delayed-type hypersensitivity reaction at the site of injection [58].

Fast and highly sensitive diagnostic tests that allow to identify MFR strains are recognized by the WHO to be a crucial key to effectively fight TB [59]. In this context, several diagnostic tests were developed. Xpert® MTb/RIF and Genotype® mtBdRplus are recent molecular assays with high sensitivity and specificity, based on the amplification of the MTb genome as well in the detection of a resistance to the most commonly used anti-TB drugs. Xpert® MTb/RIF assay is a rapid molecular method, within 2 hours, the diagnosis of TB and the simultaneous assessment of RIF resistance, using unprocessed sputum samples or specimens from extrapulmonary sites [57]. The Xpert® MTb/RIF assay was endorsed by the WHO since 2010, being currently adopted by several countries [7]. Genotype® mtBdRplus assay is a fast diagnostic method that can be used from MTb isolates or directly from pulmonary smear-positive clinical specimens. In addition, this method allows to identify resistance to the RIF and isoniazid, by detecting the most common mutations within the hot spot region of the rpoB gene and katG, respectively [60]. Many other novel diagnostic techniques with potential to revolutionize the TB diagnosis are now available. Their introduction in the market has been delayed, in part due to their expensive cost and exclusion of many drugs for the resistance patterns profile [61].

1.7. Vaccines

The only vaccine that exists for TB (i.e. Bacille-Calmette-Guérin, BCG) was developed almost a century ago by Albert Calmette and Camille Guérin of the Pasteur Institute, being part of the expanded program of immunization supported by the WHO since 1974 [62]. BCG consists of an attenuated form of *Mycobacterium bovis* [22],[63]. This vaccine provides limited protection and only during childhood, failing to protect the adult against pulmonary TB. In addition, BCG confers protection for a limited period and no longer than 10 to 20 years. [43]. Currently, there are more than 12 novel vaccines in clinical trials [64] but replacing BCG will not be easy, since it is one of the most widely used vaccines, and despite its limitations, is cheap, safe and well established [4]. The new vaccines aim to replace BCG by improving the recombinant BCG or by introducing genetically attenuated MTb, in order to be safer, more immunogenic, inducer a longer protection time and induce of protection against resistant MTb strains [65-66]. Three recombinant BCG strain constructs were designed to replace the BCG vaccine and have entered clinical trials, namely rBCG30, rBCGΔUreC:Hly and Aeras 422. The first and the second, rBCG30 and rBCGΔUreC:Hly are novel vaccine candidates that have successfully completed Phase I clinical trials. The first one is a BCG strain overexpressing the immunodominant MTb antigen 85B and the second one has the strain deficient in urease (with the consequence of an acidic pH in vaccine-containing phagosomes) and expresses listeriolysin (which enables it to perforate the phagosomal membrane. The third, Aeras 422, which expresses the similar pore-forming bacterial molecule perfringolysin has been discontinued following adverse effects in Phase I trials [67]. The second group includes MVA85A, AdAg85A and AERAS-402. These potential vaccines correspond to viral vectors that express immunodominant MTb antigens for the initiation of strong lymphocyte responses. The first and the second are in phase I and the third is in phase II clinical trials. Others, as Hybrid-1 possesses fusion proteins of immunodominant antigens with the aim to induce strong immune responses [68]. Examples of protein–adjuvant vaccines include M72 in phase I, Hybrid 1 and HyVac4 are currently ongoing Phase I clinical trials. *Mycobacterium vaccae* is an inactivated whole-cell strain of *Mycobacterium vaccae* and was initially developed as a therapeutic TB vaccine candidate, being now considered a prophylactic vaccine [69]. In addition, RUTI® is made of detoxified, fragmented MTb cells, encapsulated in liposomes and it is in Phase I [70].

The objective of the WHO is the licensing and commercialization of at least one new vaccine by 2020 [62]. The introduction of new vaccines in the market is predicted to result in cost savings, as well as a reduction in TB morbidity and TB-related mortality [71].

Additionally, vaccine conceived to be used in subjects infected with MTb will be the future of the research related with vaccines for TB [69],[72].

.

1.8. Treatment

Until the mid 1900's, the only known cure for TB was a regimen of rest, fresh air, sunshine, and a hearty diet [73-74]. The incredible success of MTb as a human pathogen may be in part explained by its ability to avert the early control by T-cells. In fact, this contributes to explain the reason why parenterally administered vaccines have no effect on the replication of MTb in the lungs for 2 weeks after infection [38]. The use of drugs that induce the autophagy (a vital homeostatic process triggered by starvation and other cellular stresses), such as dexamethasone, rapamycin or vitamin D might be used to destroy MTb [75]. However, prolonged or excessive autophagy may caused an increased cell death [76]. Other approaches, such as phage therapy, start to be exploited as an alternative to the conventional chemotherapy. In fact, the phage therapy was a research topic before the discovery of antibiotics, especially in Eastern Europe and the Former Soviet Union and is nowadays gathering the TB researchers attention because of their biological characteristics, which may constitute an advantage in treating MDR-TB [55]. In addition, immunotherapy has a potential role in TB therapy. Thus, immunosuppressive agents could be considered in order to reduce the strong antibacterial immune response in the host [77].

Despite the above-mentioned, the current chemotherapy using antibiotics with activity for the MTb is the most widely form of TB treatment and will be discussed in the next section.

1.8.1. Anti-tuberculosis drugs

Clinical management of TB using antibiotics poses serious questions due to the reduction of the efficacy of chemotherapy. This may be attributed to the degradation of the drug before reaching the target, the low levels of cell permeability to drugs or primary drug resistance. Other reasons for the failure of chemotherapy may be the difficulty in achieving adequately high drug concentrations at the infection site, inadequate penetration into macrophages, and low stability levels in cells [34],[78]. The treatment of TB is also complicated because MTb are intracellular pathogens that reside inside macrophages, and show low metabolism. Therefore, the treatment is made for 6 months or longer with combinations of agents to minimize the emergence of antimicrobial

resistance [70],[79]. The necessity of an extended period of treatment is a direct result of the lifecycle of the bacilli, some of wish may enter into a “dormant” or “persistent” phase after the initial infections [80].

These long treatment schedules are associated with severe toxic side effects, including hepatotoxicity, and result in poor compliance, one of the main reasons for the emergence of MDR strains [81-82].

The most effective pharmacotherapy is comprised of a multi-drug combination of isoniazid, pyrazinamide and RIF. During the initial intensive stage (2 months), these three agents are administered together with ethambutol. The second phase (4 months) comprises exclusively RIF and isoniazid. These four drugs, together with streptomycin, make up the so called first line therapy [8],[83]. Additionally, streptomycin was the first anti-TB drug used in therapy, being used since 1944 [84]. The therapeutic regimen recommended by WHO is highly effective and presents cure rates of around 90% in HIV-negative patients. In the cases of MDR-TB, the treatment currently recommended by the WHO comprises 20 months of treatment with second-line drugs for most patients, and are associated with multiple (and sometimes serious) side-effects and lower cure rates [7].

Isoniazid, a pro-drug, when activated has as main targets the NADH-specific enoyl-acyl carrier protein reductase and β-ketoacyl acyl carrier protein synthase, involved in MAs synthesis. Depletion of MAs results in bacterial killing [85]. RIF, a lipophilic ryfamicin derivative, binds to the β-subunit of RNA polymerase and inhibits RNA transcription and consequently, protein synthesis in MTb. Pyrazinamide, a pro-drug, is highly effective against semidormant bacilli in acidic environment (like macrophages). It is activated by pyrazinamidase to pyrazinoic acid, which by lowering intracellular pH, inactivates a vital fatty acid synthase, targets enzymes participating in the synthesis and polymerization of the cell wall arabinan, and interacts with three homologous, membrane associated arabinosyltransferases. It also affects proteins encoded by isoniazidinducible genes and acyl carrier proteins and other proteins regulating their expression. Streptomycin binds to a ribosomal protein and 16S rRNA causing misreading of mRNA and faulty protein synthesis. This drug may be used as a first-line or second-line drug for treating patients with failing therapy or MDR-TB [86]. The second-line drugs are generally more toxic, more expensive and less active than first-line agents and include drugs like RFB, ethionamide, amikacin, kanamycin A and levofloxacin [33]. Aminoglycosides, kanamycin and amikacin also inhibit protein synthesis (peptide chain elongation). Fluoroquinolones such as levofloxacin inhibit DNA replication by DNA gyrase inactivation and are important second-line drugs for treating MDR-TB. Ethionamide, a structural analog of isoniazid, is used as a second-line drug for MDR-TB and shares the target with isoniazid. Similar to isoniazid, ethionamide is also a pro-drug, however, it is activated by a

monooxygenase [86]. RFB (like RIF binds to β-subunit of RNA polymerase and inhibits RNA transcription and consequently, protein synthesis) has been demonstrated to have activity against *M. avium* complex in both *in vitro* and *in vivo* models [13]. RFB is mostly used in HIV co-infected patients because it has fewer drug interactions with antiretroviral agents than RIF [46].

Currently, there are ten TB drug candidates in clinical trials. The aim is to find compounds that allow the improvement of the compliance to the therapy. Thus, finding effective drugs against resistant strains, with fewer side effects and that allow the reduction of the duration of the treatment [59]. In this context, TMC207, a recently discovered inhibitor of the F0/F1 ATP (adenosine triphosphate) synthase, is active against non-replicating MTb and is in Phase II clinical trials [73]. Others as PA824, and OPC67683 in Phase II clinical trials, and SQ109 and LL-3858 in Phase I trials. However, even for these drugs, with a new mechanism of action, the resistance develops *in vitro* at rates similar or even faster than the existing drugs [73]. On the other side, TMC207 (bedaquiline) already has FDA approval for MDR-TB under the FDA's accelerated approval for orphan drugs, being this drug associated with an increased mortality in the treated group [87-88]. Rifapentine (a ryfamicin with longer half-life than rifampicin) as part of a 4-month regimen for the treatment of drug-susceptible TB is evaluated, being this compound in phase III clinical trials. Others are also in advanced clinical development (phase III trial), such as delamanid (OPC-67683), gatifloxacin and moxifloxacin [7],[89].

Although the development of new anti-TB drugs is an obvious approach to fight TB, mechanisms to improve the efficacy of the existing drugs can represent a faster strategy [90]. In this regard, improvement of the therapeutic index of existing anti-TB drugs should be considered, aiming at the maximization of the drug concentration at infected sites, reduction of toxic effects and reduction of the treatment duration. This may be obtained for instance by the encapsulation of the drugs in nanoparticles and in another hand by the improvement of the pharmacokinetics properties of the existing antibiotics [28].

1.8.1.1. Rifabutin and Analogs

RFB, (Figure 8) discovered in 1980, [91] has a broad spectrum of antimicrobial activity, including activity against mycobacteria, a variety of Gram-positive and to a less extent Gram-negative bacteria, and also protozoans such as *Toxoplasma gondii*. RFB is commonly used to treat *Mycobacterium avium* and MTb. It is also useful in the treatment

of *Helycobacter pylori* infections and specially indicated in the case of eradication failures using other antibiotics [92].

RFB is a ryfamicin derivate and its mechanism of action constists of a specific inhibition of DNA-dependent RNA synthesis in prokaryotes. The binding constants for prokaryotic RNA polymerases are 10.000 fold stronger than eukaryotic RNA polymerase. In addition, a single point mutation in the bacterial RNA polymerase enzyme accounts for the majority of the resistances for RFB. The DNA-dependent RNA polymerase is a complex enzyme with an α_2, β, β' and σ-subunit structure. The binding site for RFB on the RNA polymerase occurs at the β structure, which is encoded by the *rpoB* gene [93-94]. RFB is a inducer of the CYP3A, being also metabolized by these enzymes [95]. Therefore, it is used as an alternative to RIF in subjects coinfected with HIV and MTb [96]. RFB is generally well-tolerated but there are some problematic side effects, which include uveitis, rash, nausea, vomiting, neutropenia, anemia, discoloration of the skin and body fluids (tears, saliva, urine and perspiration), and, rarely, clinically important impairment of the liver function [92].

RFB is listed in the WHO essential medicines. Most of the studies show that its efficacy is higher or even higher than similar drugs as RIF [97]. However, its high cost when compared with other similar drugs (e.g. RIF) makes its choice almost inaccessible in the worldwide TB control programs [98].

RFB is a highly lipid-soluble compound, [97] showing an apparent terminal half-life of 45 h (range 16 to 69 h) [96]. After a single oral dose (usually 300 mg) it shows a great absorption and distribution. The maximum plasma concentration achieved is 0.37–0.9 mg/L [92]. In addition, RFB shows higher penetration in the lungs and infected cells (e.g. macrophages) [97]. The extent of binding to plasma proteins varies between 71% and 94%, being RFB extensively metabolised, specially in the liver [92]. In addition, the log *P* predicted for RFB using MarvinView 5.11.5 from Chemaxon® is 4.53. The RFB molecule contains some groups that can undergo protonation (piperidine nitrogen, pK_a 9.5 and imidazole nitrogen, pK_a 3.5) and deprotonation (naphthol oxygen, pK_a 6.5). At the physiological pH, while zwitterionic species predominate (83.4%), cations make up 16.6% (predicted using MarvinView 5.11.5 from Chemaxon®).

Regarding the concerns about TB, RFB was chosen as the lead compound for new analogs showing to be promising molecules against TB. Herein, *N'*-acetyl-rifabutin (RFB2) and *N'*-butanoyl-rifabutin (RFB3) (Figure 8) were obtained from RFB, using a selective acylation of the secondary amine [80]. In comparison to RFB, RFB2 has an extra acetyl group ($COCH_3$) and has shown better *in vitro* and *in vivo* therapeutic index, thereby being a promising drug for clinical application in TB treatment. RFB3 has a bulkier group

in its constitution, namely butanoyl (COC_3H_7), added with the major goal of improving the pharmacokinetics properties as an anti-TB drug candidate [80].

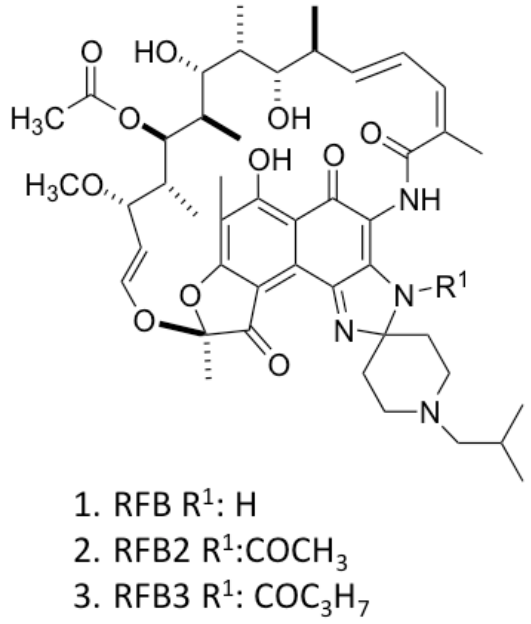

Figure 8. Chemical structure of rifabutin (RFB), *N'*-acetyl-rifabutin (RFB2) and *N'*-butanoyl-rifabutin (RFB3).

Additionally, the predicted log *P* is 5.53 for RFB2 and 5.68 for RFB3 using MarvinView 5.11.5 from Chemaxon®. Therefore, the substitution of a hydrogen atom in the imidazole ring by an acetyl or a butanoyl group leads to an increment of the molecules hydrophobicity. This substitution leads to the reduction of the positively charged molecules.

2. Biological Cell Membranes

"*Cellular organization, far from an afterthought, must have been from the beginning part and parcel of the origin of life. . . Therefore a believable biopoetic scheme is one that creates mounting levels of biological order naturally, by providing the means to convert the flux of energy into the organization of matter. This seems to me inconceivable without compartments*." [99]

Franklin Harold, 1986

Cells are the basic unit of all living organisms, being the membrane lipid bilayer the structure that delimits the surrounding environment that serve as the margin between life and death [100-101]. In fact, all cells have a cell membrane composed of amphiphilic compounds, which results in a closed interior compartment separated from the outside world. The cells are also formed by several internal compartments (i.e. organelles), which are also separated by membranes [102-103]. The cell membranes control the exchange of matter and energy with the extracellular environment or with the cytosol in the case of the internal compartments [102],[104].

Biological membranes composition varies extraordinarily depending of the cell (eukaryotic or prokaryotic) and even within the cell, being their complex organization also dynamic in order to mediate and modulate conformational changes, signaling, trafficking, and recognition [105].

Generally, cell membranes composition consists in a mixture of phospholipids, proteins and other macromolecules, constituting one biological example of a complex and multifunctional self-assembling nanosystem (Figure 9) [102].

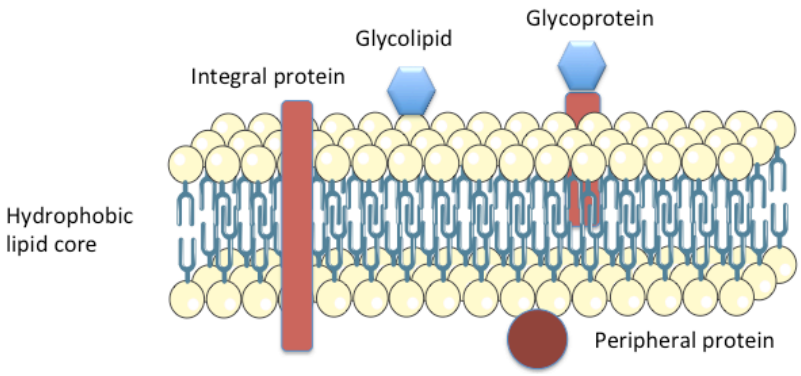

Figure 9. Schematic representation of the basic structure of the cellular membrane. Adapted from [106].

2.1. Membrane Functions

The most basic and important function of biological membranes is to define a boundary, whether between or within cells and the internal compartments (Figure 10). In fact, the membrane provides an internal compartment that allows spatial control of different functions, being its barrier function considered fundamental for the appearance of life on the early Earth [107].

Many cellular processes depend upon the ability of the cell membrane to isolate different areas, while enabling communication and tightly regulated transport within and across membranes [107-108].

Other important functions of the cell membranes include the creation of chemical and electrical gradients, the regulation of the transport of solutes in the inner and outer compartments of the cells, the control of the activity of membrane bound enzymes accommodating them to perform their metabolic functions in a coordinated way, the providing of substrates for metabolism (e.g. arachidonic acid in the prostaglandin synthesis) and the promotion of signal transduction and protein trafficking [109].

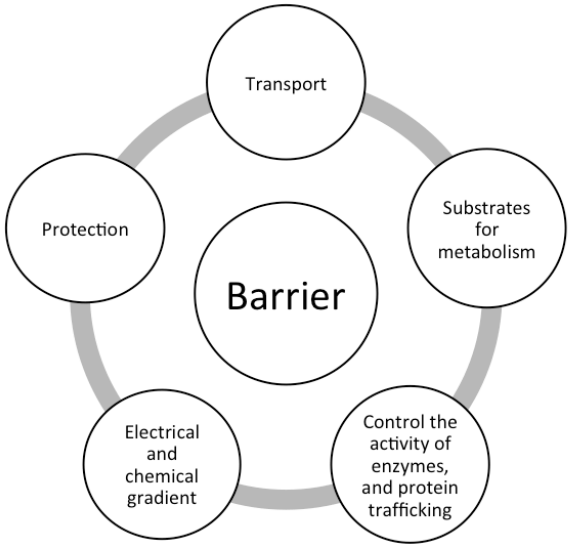

Figure 10. Schematic representation of the membrane functions.

2.2. Membrane Structure

The lipid bilayer was recognized by Gorter and Grendel in 1925 as the basis for cell membrane architecture [110-111]. Indeed, the cell is to the living organism as the lipid bilayer it is to the biological membranes. Proteins were added to the comprehensive picture of membranes, first in 1935 by Danielli and Dawson, and later in 1966 by Robertson's unit membrane model [110]. However, detailed study of the structure of cell membranes began merely four decades ago with the fluid mosaic model proposed by Singer and Nicholson in 1972 [111]. This model hypothesized the membrane as a fluid lipid bilayer with proteins that diffuse freely within the plane of the cell membrane [112]. After that it was discovered the existence of large membrane domains (e.g., basal, lateral and apical membrane regions of glandular, endothelial and epithelial cells) and lateral microdomain structures (e.g., lipid rafts, caveolae, and coated pits) [111]. Lipids rafts are an example of a domain where lipids of a specific chemistry are associated with each other in order to form key platforms for membrane protein sorting and construction of signaling complexes [113]. In addition, the knowledge that the lipids via alterations in the membrane pressure profile may regulate protein and channel function, states the importance of the lipid bilayer in the membranes. For instance, certain drugs (e.g. anesthetics) exert part of their action on membrane proteins and receptors via changes in the pressure profile [110]. Currently, membranes are viewed as a mosaic of different compartments or domains maintained by an active cytoskeleton network (Figure 11) [113-114].

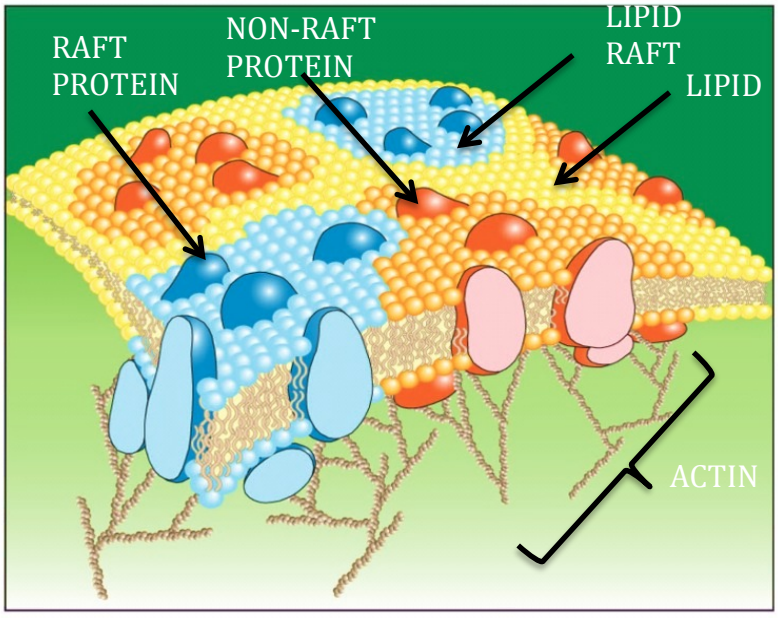

Figure 11. Schematic representation of the modern concept of celular membrane structure. Adapted from [114].

2.3. Membrane Composition

Biological membranes present a substantial variability in their composition and physical properties, depending of the cell (prokaryotic or eukaryotic) and even within the cells (e.g. according to the organelle). Nevertheless, all biological membranes contain lipid bilayers as its basic structural unit [115]. Generally, membranes are formed by lipids, protein and other macromolecules (e.g. carbohydrates) [102]. In addition, cell membranes can be interpreted as a two-phase system consisting of the lipid raft phase, enriched in CHOL, and proteins and saturated lipids, dispersed in a matrix phase [116].

The lipids present in the membranes can be divided into three groups based on their chemical structure: glycerophospholipids (or phospholipids), sphingolipids and sterols (Figure 12) [117].

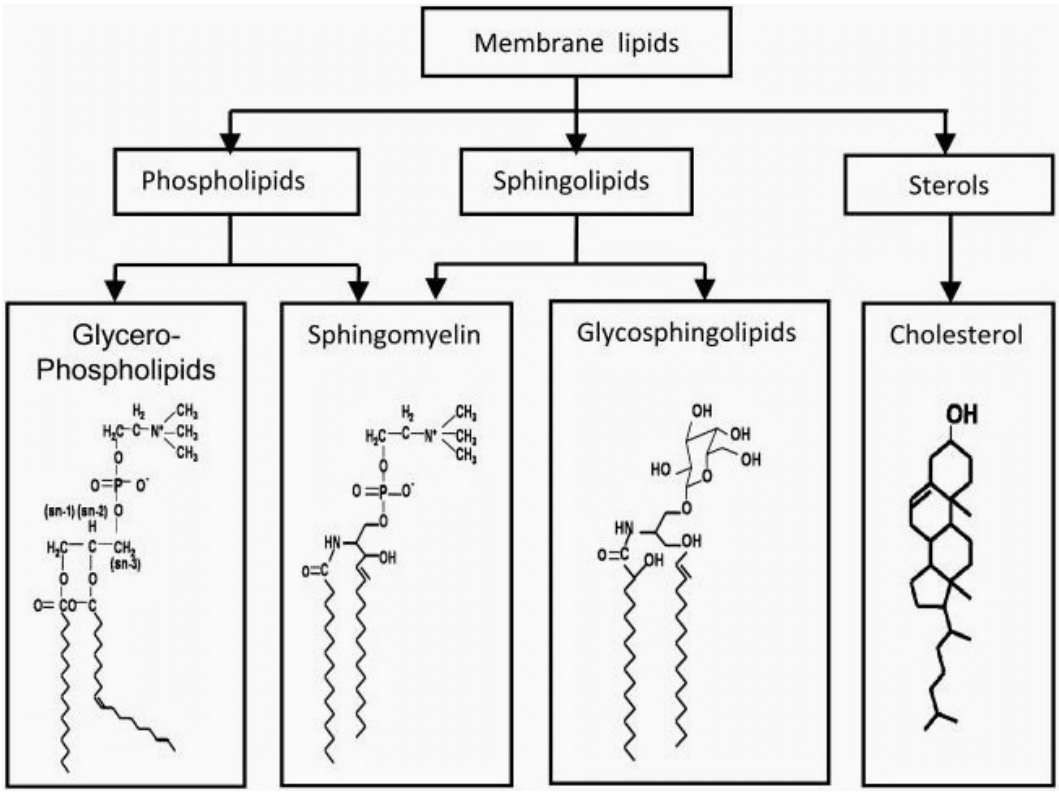

Figure 12. Composition of membrane lipids and their chemical structures. Adapted from [117].

Glycerophospholipids are amphiphilic molecules composed by a hydrophilic head group formed by an alcoholic group, a phosphate and a glycerol molecule. The glycerol molecule connectes the polar head group with two hydrophobic alkyl chains (Figure 13).

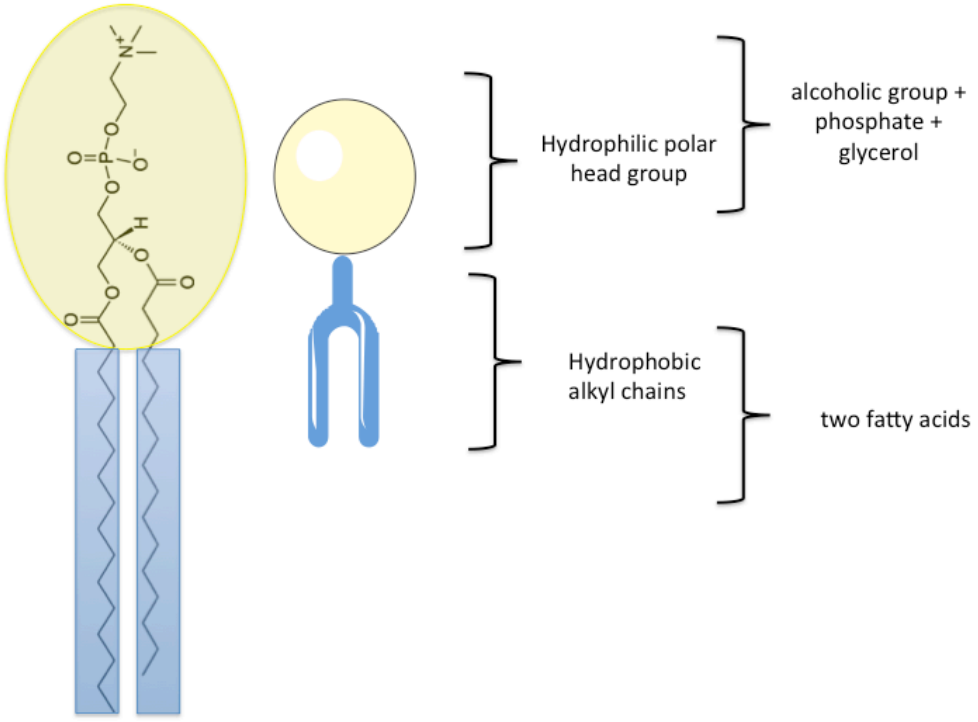

Figure 13. Schematic structure of a glycerophospholipid [118].

The self-assembly of the glycerophospholipids into two-dimensional bilayer sheets, yields to the cell membrane a thickness of approximately 5 nm. The hydrocarbon tails of the glycerophospholipids are hydrophobic, densely packed and therefore shielded from the aqueous moiety [102]. Glycerophospholipids are further divided into different groups based on their hydrophilic head groups. The most common alcohol moieties found in the glycerophospholipids of the membranes are the aminoacid serine, ethanolamine, choline, glycerol, and the inositol (Figure 14) [118].

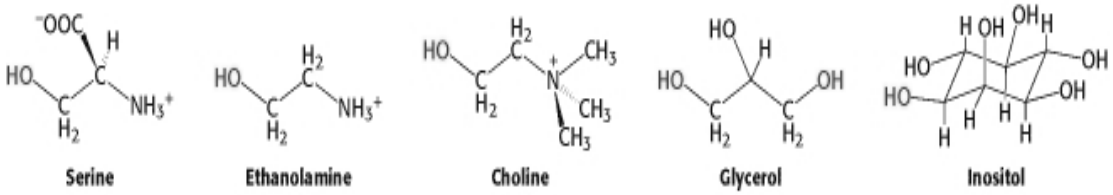

Figure 14. Schematic structure of the most common alcohol groups of the glycerophospholipids. Adapted from [118].

Examples of glycerophospholipids commonly found in biological membranes include, among others, phosphatidylcholine (PC), phosphatidylethanolamine (PE),

phosphatidylserine (PSer), phosphatidylinositol (PI), cardiolipin (CL), and phosphatidylglycerol (PG) (Figure 15).

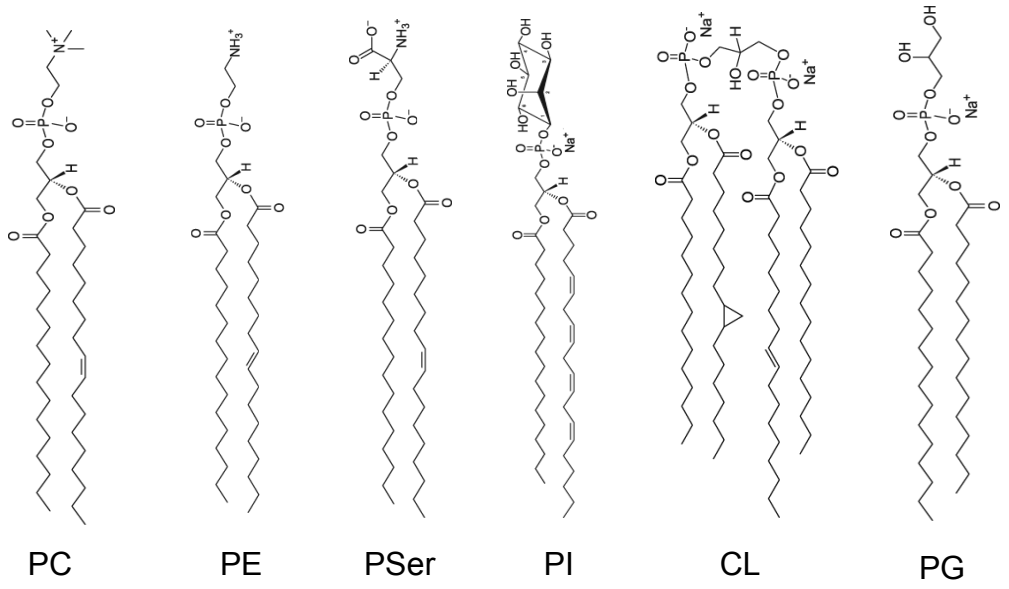

Figure 15. Schematic structure of the most common glycerophospholipids found in membranes.

Regarding the negative charge of the phosphate group, lipids with an alchool group without charge or with zwitterionic charge are negatively charged phospholipids (e.g. PI, CL, PG, PSer). Others are zwitterionic phospholipids (e.g. PC, PE) because of the positively charged alchool group.

The hydrocarbon chains present in the phospholipids can differ in their length or in the number of unsaturated bonds. The most common in natural membranes are the saturated fatty acids, such as the palmitic (C16), stearic (C18), and myristic (C14). From the unsaturated fatty acids, the oleic (C18:1), a stearic acid with one double bond in the middle of the chain, is the most frequent in the membranes. The majority of the natural lipids contain one or more double bonds in *cis* conformation (e.g. higher animals, plants), while a *trans* conformation is found in the Monera kingdom. Generally the number of double bonds increases with the length of the hydrocarbon chain, being more frequent to find an even number of carbons in the hydrophobic chains of each phospholipid, than an odd number, which are found in rare cases [119].

Sphingolipids are phospholipids that have a sphingosine, an amino alcohol as a backbone, which contains a long, unsaturated hydrocarbon chain, conferring greater hydrophobicity to the core of the lipid bilayer [120]. The major sphingolipid in mammalian cells is sphingomyelin (SM) [100]. In sphingomyelin, the amino group of the sphingosine is linked to a fatty acid by an amide bond, being the primary hydroxyl group of sphingosine esterified with a phosphoryl choline (Figure 12) [118]. CHOL (Figure 12) is the most representative sterol of the animal eukaryotic membranes. It is a steroid built from a

hydrophilic hydroxyl group, that interacts with the phospholipids' hydrophilic head groups and a bulky steroid group, which interacts with the hydrophobic acyl chains of lipids [111],[121]. CHOL has a "schizophrenic" behaviour in the membranes, decreasing the membrane fluidity in fluid phases and increasing the membrane fluidity in gel phases [122].

The lipid rafts are aggregates of phospholipids, CHOL and glycosphingolipids associated with key biological processes, such as endocytosis, signaling, protein transport, apoptosis, and cytoskeleton organization (Figure 16) [100],[123].

The proteins present in the membranes may be only bounded to the surface or have one region buried within the membrane (Figure 16). Therefore, membrane proteins can be classified into two broad classes, integral (intrinsic) and peripheral (extrinsic), based on the nature of the membrane-protein interactions. The majority of the biological membranes contain both types of membrane proteins. Most integral proteins contain residues with hydrophobic side chains that interact with the hydrocarbon tails of the phospholipids of the membranes. On the other hand, the extrinsic proteins do not interact with the hydrophobic core of the phospholipid bilayer, establishing interactions with the integral membrane proteins or with the phospholipid polar head groups of the membranes. For instance, one of the most important proteins of the eukaryotic plasma membrane includes the cytoskeletal protein spectrin, which lines the intracellular side of the membrane [106]. The plasma membrane contains proteins that act as sensors (e.g. receptors) of external signals, allowing the cell to change its behaviour in response to external signs [106],[124].

Glycoconjugates are carbohydrate molecules bounded to a lipid or protein (Figure 16). These molecules may be classified into four typical family groups: proteoglycans, glycoproteins, glycolipids and glycosylphosphatidylinositol (GPI)-anchored proteins. Glycoconjugates play essential roles in many physiological processes of the membranes, such as cell growth and development, and cell-to-cell interactions and recognition. In adittion, glycosphingolipids and GPI-anchored proteins participate in the production of rafts in the membranes [125-126].

In specialized membranes, ionic channels are also present, being used to generate the ion gradients across the membranes and synthese of energy (e.g. ATP), to drive the transmembrane movement of selected solutes, or, in nerve and muscle cells, to produce and transmit electrical signals [106],[124].

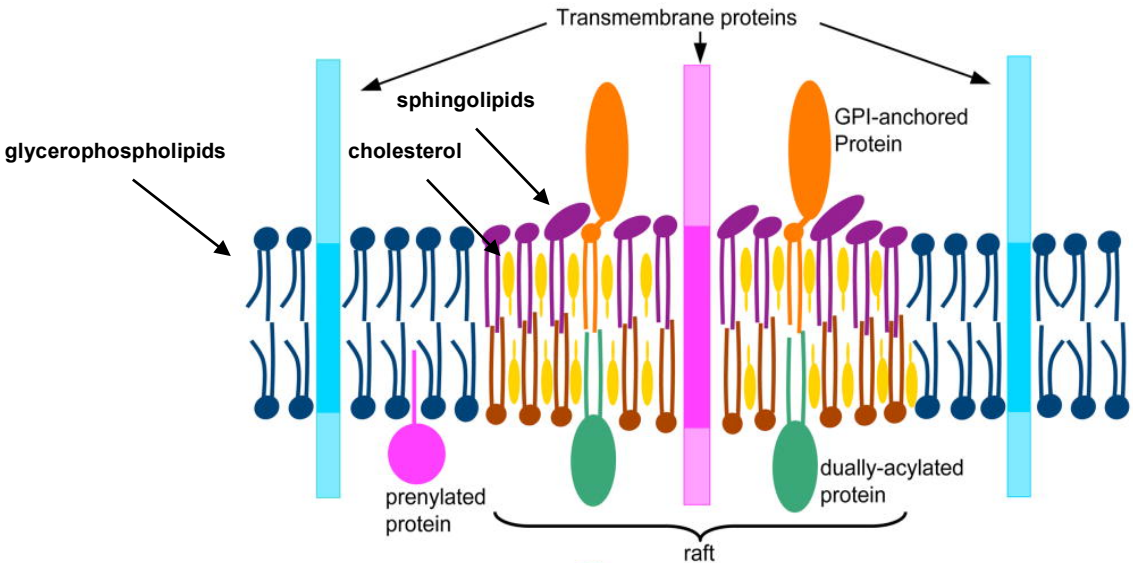

Figure 16. Simplified model of lipid-raft structure in biological membranes. Adapted from [127].

2.3.1. Molecular Composition in Eukaryotic Cell Membranes

The eukaryotic cells exhibit an impressive number of well-defined internal membranes associated with the nucleus and the organelles. There is a remarkable difference concerning the membrane composition between the plasma membranes and that of the various organelles (Figure 17). For instance CHOL, a universal molecule in the membranes of all animals (sitosterol in plants and ergosterol in fungi) in amounts between 20-50% (total lipids) is much less representative in the membranes that outline the organelles, as the mitochondria (less than 5%), Golgi (approximately 8%) and endoplasmic reticulum (roughly 10 %) [119],[128-129]. CHOL is responsible for the regulate of the degree of membrane fluidity–rigidity. In addition, as above-mentioned, CHOL is an important component of the so-called “lipid rafts” [130]. Lipid rafts are also formed by sphingolipids and proteins and are phase-separated micro-domains in biomembranes, forming the rigid and relatively ordered state, generally defined as the liquid ordered (L_o) phase [131-132].

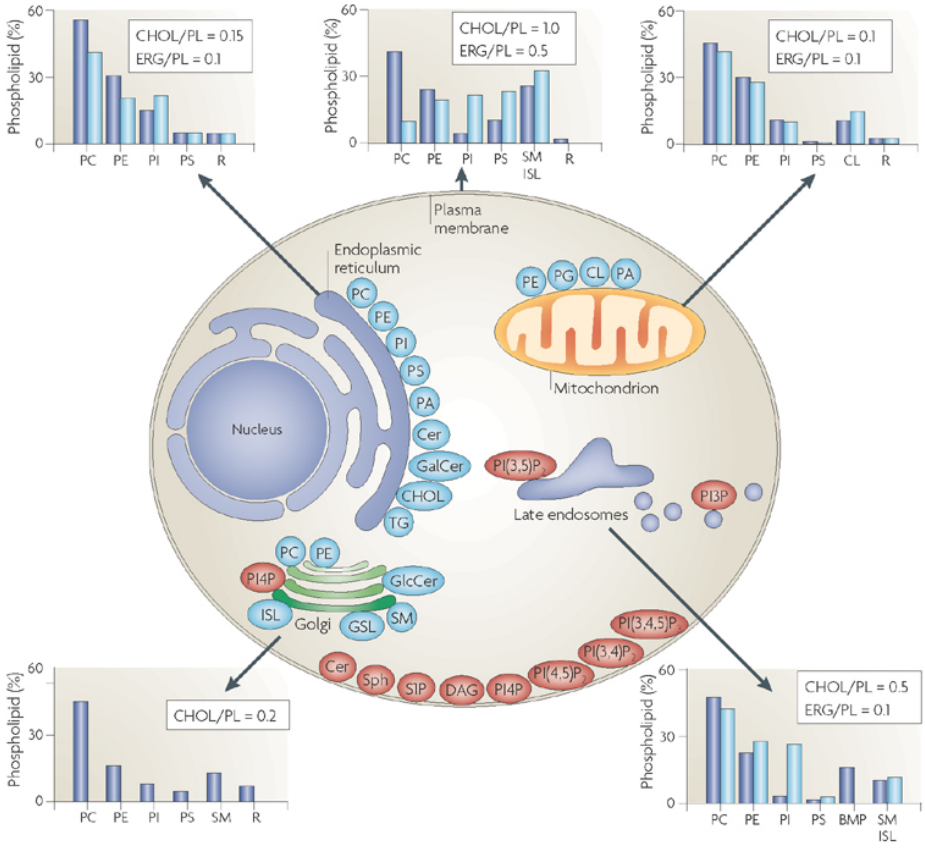

Figure 17. Lipid composition of different membranes varies throughout the eukaryotic cell. The lipid composition (shown in graphs) are expressed as a percentage of the total phospholipids in mammals (blue) and yeast (light blue). Adapted from [100].

There is an asymmetry in the lipid composition of the two monolayers of the bilayer of the plasma membrane [133]. In the outer monolayer, the more prevalent lipids are the PC, SM, CHOL and glycolipids. On the other side, the PSer, PI and PE are the most representative lipids of the inner monolayer. The membranes of the eukaryotic cells are predominantly composed of zwitterionic lipids. The standard membrane lipid is the zwitterionic PC, comprising 50% of the cellular lipids [120]. The amount of the negatively charged lipids present in the eukaryotic membranes is approximately 10%, being the positively charged lipids absent [106],[119],[134].

The phospholipids and the CHOL of the plasma membranes are mainly synthesized on the cytosolic surface of the ER, while PE is also generated by PSer decarboxylation in mitochondria [120]. After the phospholipids production, the protein “flippase” (Figure 18) facilitates the energetically unfavorable movement of a phospholipid’s polar head group through the hydrophobic membrane interior [135]. The mentioned ER flippase does not require metabolic energy, mediating a rapid transverse movement of most of the phospholipids and promoting a symmetrical transbilayer lipid distribution. The asymmetry of the plasma membrane is maintained due to the energy-dependent flippase, the aminophospholipid translocase (APLT) that uses ATP hydrolysis to catalyze a fast, inward translocation of PSer and PE to the cytoplasmic leaflet.

Additionally, the loss of lipid asymmetry as well the exposition of Pser at the cytoplasmic leaflet are signals that trigger cell apoptosis, promoting the engulfment of apoptotic cells by the immune systems cells as the macrophages [135].

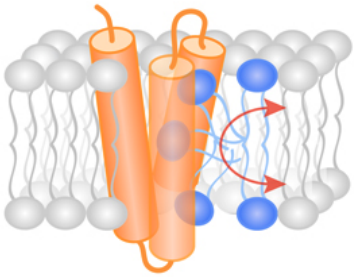

Figure 18. Flippase mechanism. Transmembranar flippase (orange) provides a central hydrophilic path for the transiting headgroup while leaving the hydrophobic chains of the lipid (gray) in the bilayer. Adapted from [136].

2.3.2. Molecular Composition in Prokaryotic Cell Membranes

Normally, the prokaryotic cells only have a plasma membrane and some structured internal membrane systems. The membranes of prokaryotes possesses great differences in comparance to the eukaryotic cell membranes and for instance, the sterols (including CHOL) are universally absent [119],[128] (Figure 19).

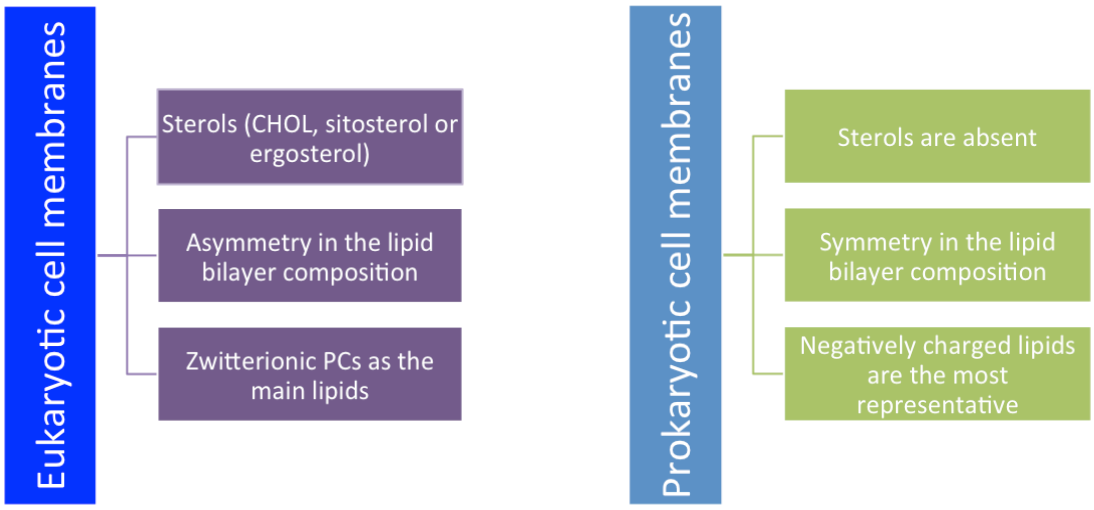

Figure 19. Schematic representation of the main differences between eukaryotic and prokaryotic cell membranes.

Remarkably, the prokaryotic show a greater variety in their membrane composition in comparison to the eukaryotic, being the membrane's composition an important parameter for the species identification (Figure 19) [119].

The glycerophospholipids are the primary building blocks of the bacterial membranes, being the lipids PG, CL, PE and PI the most representative in prokaryotic cell membranes [137],[138]. The lipid synthesis in the bacteria occurs in the cytoplasmic membrane by enzymes that are predominantly integral membrane proteins with the catalytic domain in the cytoplasm [139-140].

The prokaryotes have the ability to modify the biochemical composition and properties of their membranes in order to survive to the hostilities of the environment. One of the mechanism of resistance to the cationic antibiotics is the addition of positively charged amino acids to PG, lowering the net negative charge of their cellular envelope, thereby decreasing the affinity of several antibacterial agents [137].

The domains also exist in the bacterial membranes, being the knowledge about its function and composition very scarce. Contrastingly to the mammalian membranes, lipids as the CHOL and sphingomyelin are not included in the domains composition. On the other hand, lipids (e.g. CL and PE) and proteins seem to compose the bacterial lipid domains [141].

There are major structural and chemical composition differences between Gram-positive and Gram-negative bacteria (Figure 20 and 21). Generally, Gram-negative bacteria contain both anionic and zwitterionic phospholipids, while many Gram-positive bacteria contain predominantly anionic lipids [142]. Thus, Gram-negative bacteria have a highly permeable outer membrane that contains lipopolysaccharides (LPS) on its outer leaflet, with the inner leaflet composed mainly of zwitterionic phospholipids as the PE. Gram-positive bacteria have lipoteichoic acid (LTA) adhered to the cell surface membrane, which contain predominantly PG and CL lipids [141]. Both possess in its constitution a peptidoglycan layer outside of the cell membrane, being thicker in the case of the Gram-positive bacteria [141]. The mycobacterial cell wall is formed by a thick waxy mixture of lipids and polysaccharides, being characterized by the presence of a high content of MAs (Figure 20 and 21). MAs are α-alkyl-β-hydroxyl high molecular weight fatty acids. Each molecule consists of a hydrophobic long saturated 2-alkyl branch and a hydrophilic head group (containing the groups COOH and OH) [143], occuring in the cell wall of MTb as variable mixtures of different classes (α-MA, methoxy-MA and keto-MA) [144-145]. In addition, the major MAs-containing molecule, the glycolipid trehalose 6,6′-dimycolate (TDM, cord factor) has an important role in the physiopathology of the mycobacteria [146]. The mycobacterial plasma membrane appears to be a typical bacterial membrane and resembles a Gram-positive wall. However, some controversy

may be found in the literature related with their classification with the Gram stain [142],[148],[150]. If a Gram stain is performed on *Mycobacterium* species, it stains very weakly Gram-positive or not at all (cells referred to as "ghosts"), being the Ziehl-Neelsen stain a more accurate method for the identification of the *Mycobacterium* species [147]. For the former reason, the *Mycobacterium* species are commonly classified as acid-fast Gram-positive bacteria due to their lack of an outer cell membrane [142],[148-149]. Notwithstanding, the phylogenetic classification of *Mycobacterium* species is controversial because their cell wall has characteristics of both Gram-positive and Gram-negative bacteria [150]. In addition, the most common phospholipids in the mycobacterial plasma bilayer include PI, CL, PG, PSer and PE [151-153]. The PI, a precursor for more complex glycolipids, such as the PI mannosides (PIMs) and lipoarabinomannan (LAM) seems to be a phospholipid with important roles in the structure and physiology of these bacteria as well as during host infection [152-153].

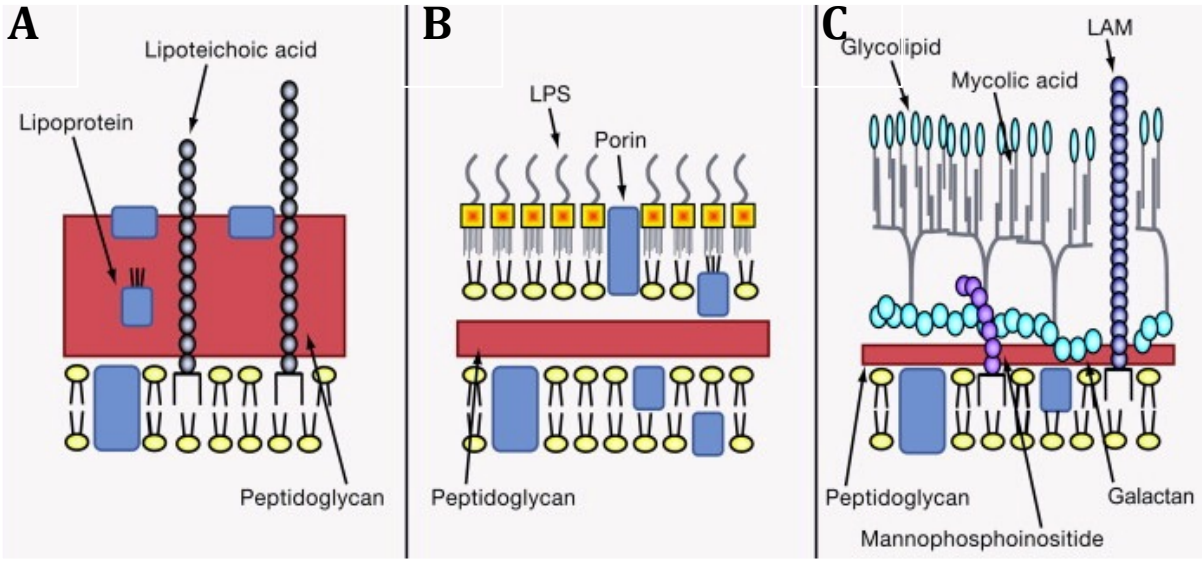

Figure 20. Schematic representation of bacterial cell walls (A - Gram-positive bacteria; B – Gram-negative bacteria; C - Mycobacteria). Adapted from [154]

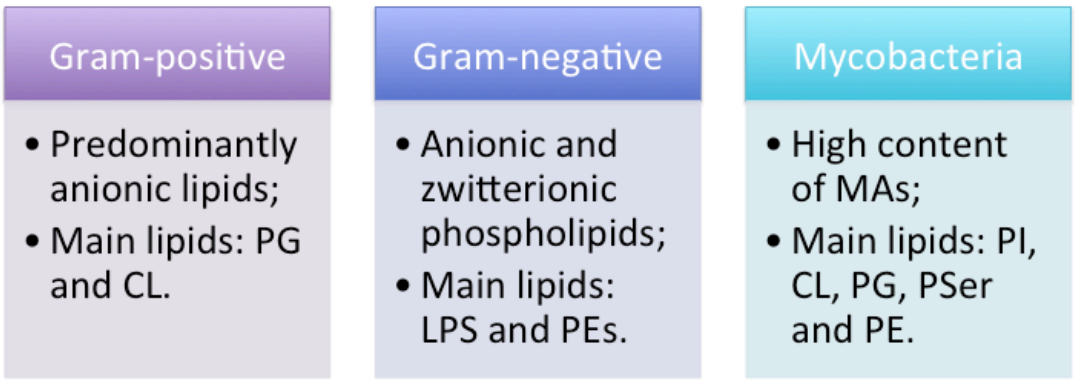

Figure 21. Schematic representation of the differences between Gram-postive, Gram-negative and Mycobacteria cell membranes. Adapted from [154].

2.4. Pulmonary Surfactant Membrane

The first evidences of the existence of a surface material, that eases the lungs´ expansion and stabilizes the terminal airways, emerged in 1920 with the pioneer work of the Danish physician Kurt von Neergard [155]. After that, the PS was remarkably related within neonatal respiratory distress syndrome, allowing the utilization of natural or synthetic surfactant in the clinical practice since 1980 [156-157]. Its use is further indicated in meconium aspiration syndrome, persistent pulmonary hypertension, pulmonary haemorrhage, pneumonia and delivery of drugs directly to the lung, including antibiotics, anti-inflammatory agents and bronchodilators [26],[158].

The PS (Figure 22) is a thin and fluid layer that decreases the surface tension between the gaseous-aqueous interface in the lungs [159].

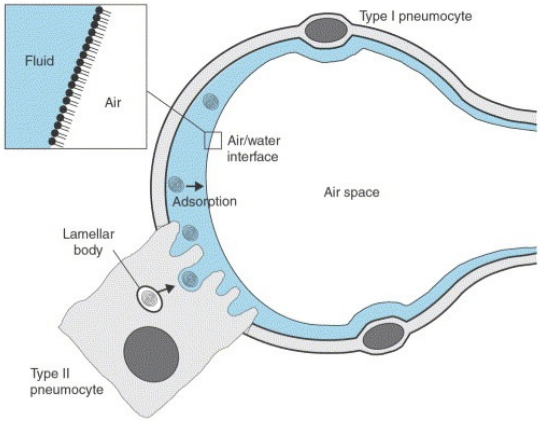

Figure 22. Schematic representation of the PS in an alveolus of the lung. Adapted from [160].

The PS surfactant main role is the reduction of the alveoli surface tension, allowing the reduction of the respiratory work and the prevention of alveoli collapse. Besides this crucial function, it contributes to the small airway permeability and improves the mucocilliary depuration [161-162]. The PS is produced by the ER of the type II alveolar epithelial cells, being stored in lamellar bodies (LBs). Once secreted in response to extracellular signals, the extracellular pool of the phospholipids within LBs transforms into a surfactant film that lines the alveolar surface [163-164]. Additionally, the phospholipid fraction obtained from bronchoalveolar lavage contains a number of different morphological and biochemical forms of surfactant including multilamellar and unilamellar vesicles (Figure 23) [163].

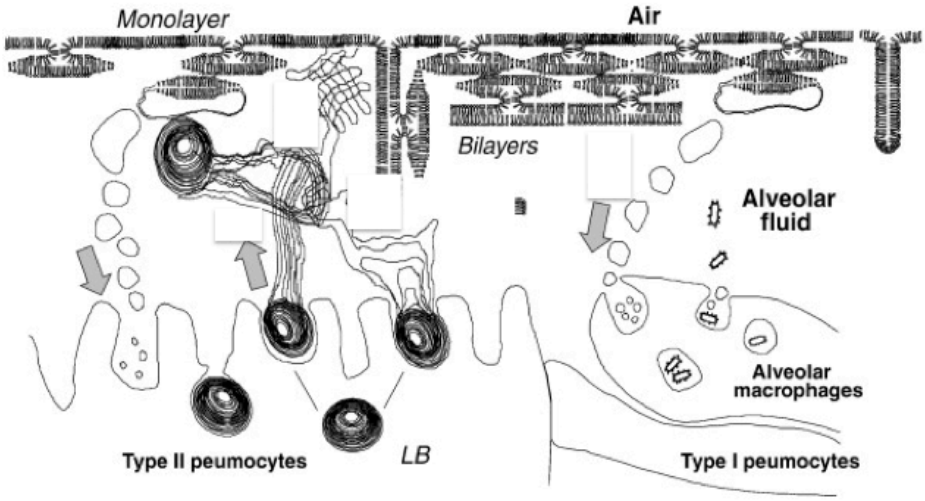

Figure 23. Schematic representation of the PS polymorphism. Adapted from [165].

The PS is composed of: 80% phospholipids, 8% neutral lipids, and 12% proteins, including proteins from plasma and lung tissue, as well as, four surfactant-related proteins (Figure 24) [164],[166]. DPPC (1,2-dipalmitoyl-sn-glycero-3-phosphocholine), the main component of the lung surfactant system is the primary responsible for its unique property of reducing the surface tension to near zero-values. Due to its main transition temperature of approximately 41 ºC, at the body temperature the surfactant exists in the gel phase. This, although adequate to reach a low superficial tension, results in a low capacity for adsorption at the interface. Thus, surfactant lipids such as unsaturated phosphatidylcholines, CHOL and other, help DPPC in this task [35],[167].

Four surfactant proteins have been identified so far (SP-A, SP-B, SP-C, and SP-D), and are classified by their hydrophilicity (SP-A, SP-D) versus hydrophobicity (SP-B, SP-C). These proteins play a key role in the performance of the surfactant surface, as well as in the immunological defense and particle depuration. (89) While the main function of

SP-A and SP-D is to participate in innate pulmonary immune defenses, SP-B and SP-C interact extensively with surfactant phospholipids and increase their ability to efficiently lower surface tension. PS contains a small percentage of neutral lipids that are generally comprised of CHOL, CHOL esters, diglycerides, triglycerides, and free fatty acids whose functions have not been fully characterized but seem to have a part in supporting DPPC adsorption at the interface [168].

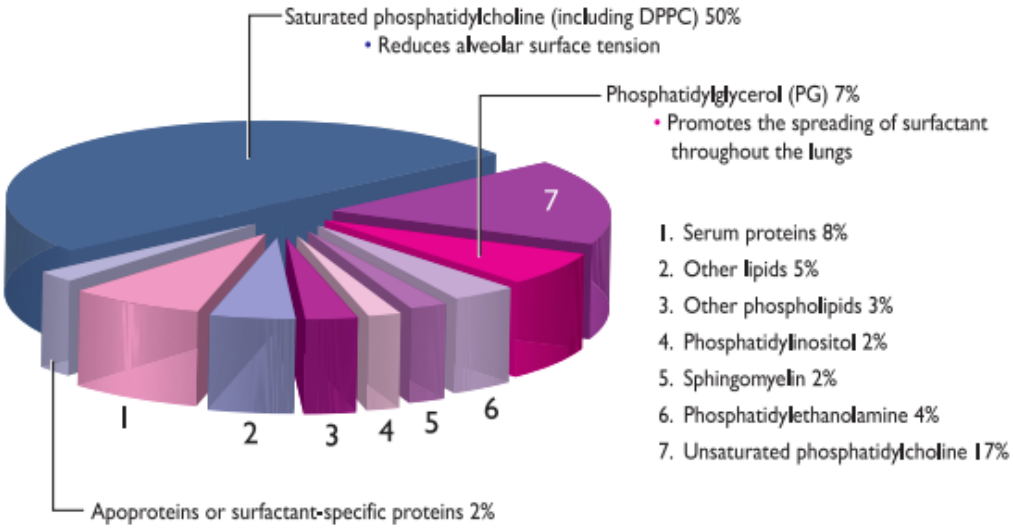

Figure 24. Composition of human PS. Adapted from [169].

2.5. Lamellar Phase Transition

The “hydrophobic effect” of the phospholipids is due to their amphiphilic properties and happens in order to minimize the contact between lipid hydrocarbon tails and the aqueous environment, which results in self-assembled “polymorphs” in the hydrated state. At zero to low hydrations and/or temperatures most of the lipids form crystalline phases (L_c), generally of the lamellar type. In the former phase, phospholipids possess short and long ranges similar to true crystals.The lamellar phase is characterized by one-dimensional stack of lipid bilayers separated by water layers. Each bilayer is formed by two monolayers stacked back-to-back, thus protecting the hydrocarbon chains from the contact with the water [131]. Molecules with cylindrical shapes would predominantly yield lamellar bilayers (Figure 25A), whereas molecules with conical shape would stabilize phases with curvature, such as hexagonal and cubic phases (Figure 25B) [110].

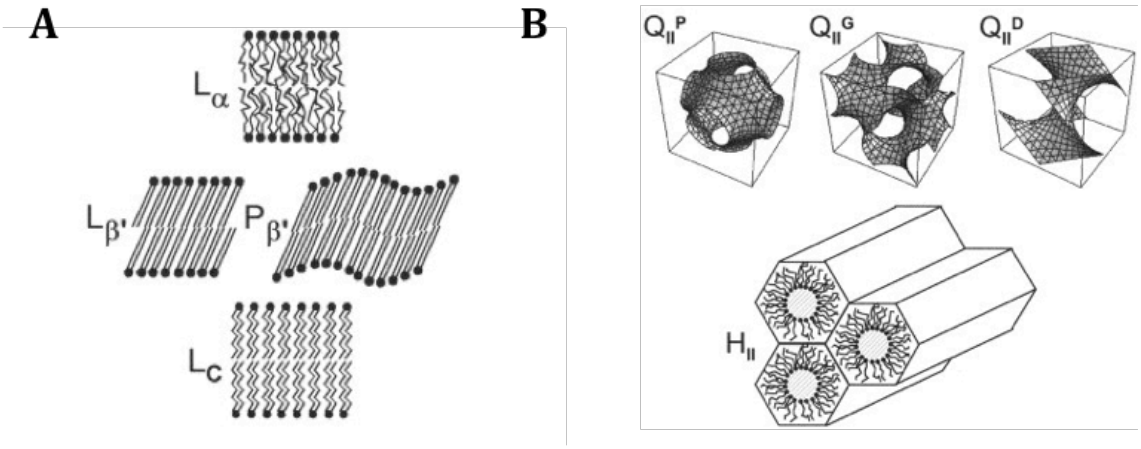

Figure 25. Schematic drawing of lipid-water phases (A – Lamellar phases; B – Isotropic phases (cubic and hexagonal)). Adapted from [170].

Since the early 1980s, it was determined that the geometric shape of the phospholipids determines the "preferred phase" exhibited in aqueous solution (Figure 26) [171].

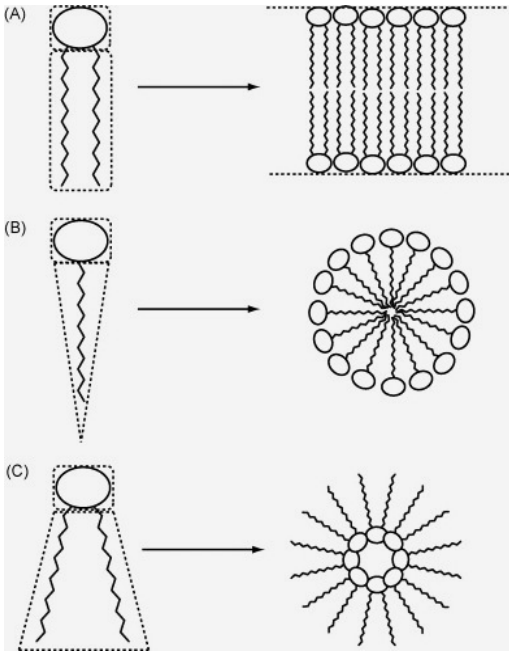

Figure 26. Schematic representation of the phospholipid packing in solutions (A – Lamellar phases and tend to form bilayer structures; B- Cone shaped phospholipids and tend to form micelles or inverted truncated cones; C- Cone shaped phospholipids and tend to form inverted micelles or hexagonal phases. Adapted from [171].

Therefore, the geometry of the phospholipids is cylindric, when the cross-sectional areas of the head groups and acyl chains are the same. When the phospholipid head group area is larger than the acyl chains, the lipid assumes the shape of a cone or a wedge and tends to form normal hexagonal (H_I) phases. On the other hand, if the phospholipid head group is small and the acyl chains are larger, the lipid seems an inverted cone, tending to form inverted hexagonal (H_{II}) phases or inverted micelles [171]. However, the morphology of the phospholipids will be dependent of several other factors such as the degree of hydration of the phospholipid head groups, the pressure and the temperature [172]. Some of the phospholipids, as the PCs and PGs, generally form bilayer structures (Figure 25A). Moreover, PE is a class of lipids abundantly found in biological membranes and prone to form an inverted hexagonal phase (H_{II}) (Figure 22B) [173].

In the non-lamellar phases the more common arrangements include the hexagonal and cubic phases. The H_I and H_{II} lipid phases are phases in which the lipids form tubular structures. In the H_I phase, the center of the cylinder is made up of the hydrophobic tails, while in the H_{II} phase the hydrophobic tails face outwards and the core of the tube is comprised of the polar head groups (Figure 25B). The cubic phases are lipid aggregates that form a three-dimensional lattice (Figure 25B) [171].

In the lamellar phases, lipids could be present in three different phases: the gel phases (denoted by L_β, $L_{\beta'}$ or $P_{\beta'}$), the liquid-ordered phase (L_o), and the liquid crystalline or fluid phase (L_α) (Figure 27). In the L_β the hydrocarbon chains are packed into 2D hexagonal lattices in their all-trans conformation. In this phase, the chains are ordered parallel to the normal bilayer. Additionally, when the polar head group area-packing requirement exceeds twice that of the chains (for diacyl lipids), the tilted gel ($L_{\beta'}$) is formed. The lamella of the gel phase may undertake periodic modulation, resulting in a rippled phase ($P_{\beta'}$), which exists in some phospholipids (e.g. PC, PG) and is formed just below the fluid lamellar phase (L_α). The former phase happens upon melting of the crystalline and gel phases where the polar head groups are totally disordered and the the chains are fluid, closely resembling the cell membranes [113],[174]. In addition, the L_α is a perfect example of a liquid-crystalline phase. The sub- pre-, and main phase transition temperatures can thus be ascribed respectively to the $L_C \rightarrow L_{\beta'}$, $L_{\beta'} \rightarrow P_{\beta'}$, and $P_{\beta'} \rightarrow L_\alpha$ phase transitions [172]. The L_o phase is an intermediate phase between the gel and the fluid phases, not only being characterized by a highly lateral mobility of the lipids but also by an ordered structure with extended fatty acids [131],[175].

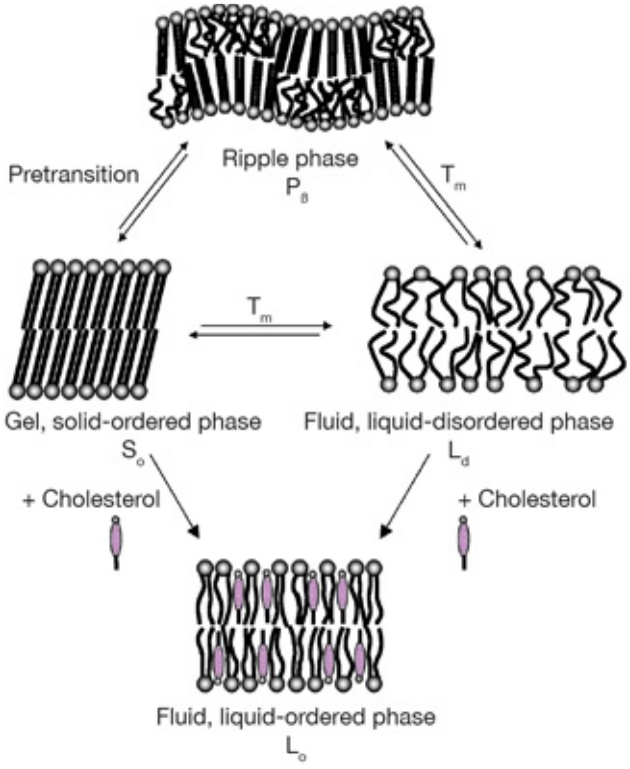

Figure 27. Scheme illustrating the different physical states adopted by a lipid bilayer in aqueous medium. Adapted from [176].

2.6. Membrane Model Systems

In the last years, the knowledge about cell membranes has been tremendous and in part was brought by the development of membrane models systems [177-178]. In fact, the cell membrane is an impressive complex system where every part is connected with each other [179]. Thus, the design of a cell membrane model implies a simplification of the biological membranes. One of the major drawbacks pointed to the actual membrane models systems of the cell plasma membrane is the lack of asymmetry and the absence of proteins in their constitution [180]. However, these issues may be surpassed and for instance the insertion of proteins in the lipid bilayer starts to be common in the design of membrane model systems [181]. Notwithstanding, in the biophysical studies of drug-membrane interactions, of more importance that the imitation of nature is the development of suitable membrane model systems that allow to understand the interactions of the drug at the molecular level. In the biophysical investigations, the use of membrane model systems permit to understand the diffusion of the drugs through the membrane lipids and their distribution, and therefore the prediction of the potential toxicity of the drugs [111]. In recent years, membrane models have also been studied to understand their mechanisms of interaction with peptides and nanocarriers, which can be useful in the design and development of efficient drug delivery systems [182]. The main advantage in the utilization

of the membrane models is the possibility to perform the experimentations under conditions that the cells may not be able to withstand and remain viable. In addition, the usage of membrane models allow to study the drug-membrane lipid bilayer interactions with the head groups of lipids, with hydrophobic alkyl chains, and with both head groups and hydrophobic acyl chains [178]. Independently of the target position (intracellular or located within the membrane), the drug molecules must interact with the membranes before reaching their targets and elicit a pharmacological action; therefore, drug-membrane lipid interactions are inevitable and membranes are not amorphous and unreactive structures [111].

There are two main types of conventional membranes model, an intact vesicle platform (three dimensional membrane models) and a planar lipid arrangement (two dimensional membrane models) [183]. Conventional membrane models systems include Langmuir monolayers, lipid vesicles (or liposomes), micelles and supported lipid bilayers [184-185]. These conventional membrane model systems, sometimes described in the literature as artificial membrane models, offer the possibility of manipulation of the lipid content, salt concentration, pH and other factors in order to mimic the composition, curvature, electrostatic potential or permeability properties of the chosen biological membranes [186].

Alternatively to the conventional, more sophisticated membrane models as sensing platforms consisting in cell-derived membranes and miniaturized lab-on-a-chip architectures are used to study membranes that contain specific receptors for instance [181],[183].

2.6.1. Liposomes

The discovery of liposomes took place in 1965, when Bangham and coworkers showed evidence of the phospholipids self-assembly, with the phospholipid tails orienting towards each other to form one or more bilayers entrapping an aqueous pool, when in an aqueous compartment [187-188]. This discovery confirmed earlier studies that claimed that all plasma and intracellular membranes are based on phospholipid bilayers, and encouraged the use of liposomes as the main model system to study the physicochemical and other properties of biological membranes [189-190]. Liposomes are closed vesicles commonly formed by hydration of a dry phospholipid film above the T_m. In the conventional technique (Figure 28), the lipid vesicles are prepared by dissolving the chosen lipids in organic solvents (a 3:1 mixture of chloroform:methanol), being the solvents evaporated under a vacuum to form thin films of lipids at the bottom of a round-bottom flask. Then, the dried lipid films are rehydrated in the aqueous buffer in order to

form the lipid vesicles. The suspension obtained is vortexed until complete dissolution of the lipid film [111]. The resulting structures are multilamellar vesicles (MLVs), which consist of many concentric bilayers in a single particle. MLVs can be further processed by sonication or by extrusion through a filter to form liposomes with a single membrane bilayer [190-191]. Unilamellar vesicles (ULVs) can be further classified into small unilamellar vesicles (SUVs) and large unilamellar vesicles (LUVs) [36]. Alternatively to the conventional method, novel techniques to prepare liposomes offer advantages, such as the possibility to prepare lipid vesicles without using volatile organic solvents or detergents [192], such as the polyol dilution method [193] and the bubble method [194].

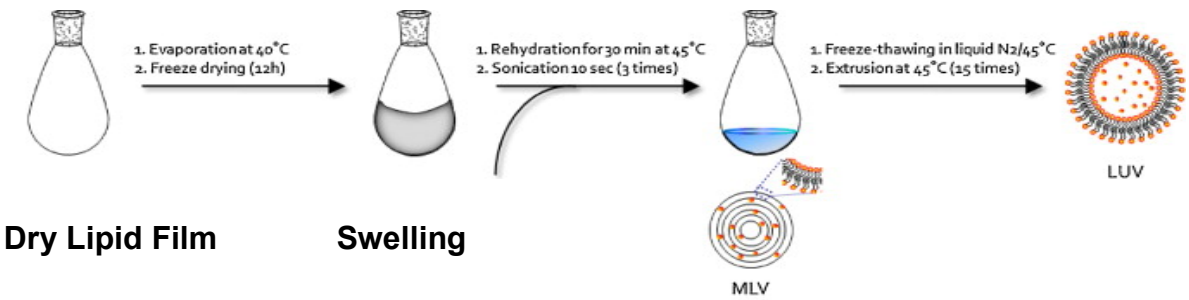

Figure 28. Schematic representation of a conventional method (i.e. lipid film hydration) of liposomes preparation. Adapted from [195].

The liposomes diameter size ranges from 20 nm to several hundreds of nanometers, whereas the thickness of the phospholipid bilayer membrane is approximately 4-7 nm. Their classification is generally based upon their size and number of lipid bilayers (Figure 29). MLVs comprise several lipid bilayers separated by aqueous spaces, and their diameter varies between a few hundred to thousands of nanometers. SUVs show a diameter inferior to 100 nm and LUVs a diameter superior to 100 nm [191],[196].

Additionally, during the last years liposomes have also attracted great interest as efficient carriers for drugs, diagnostics, vaccines, nutrients and other bioactive agents [192].

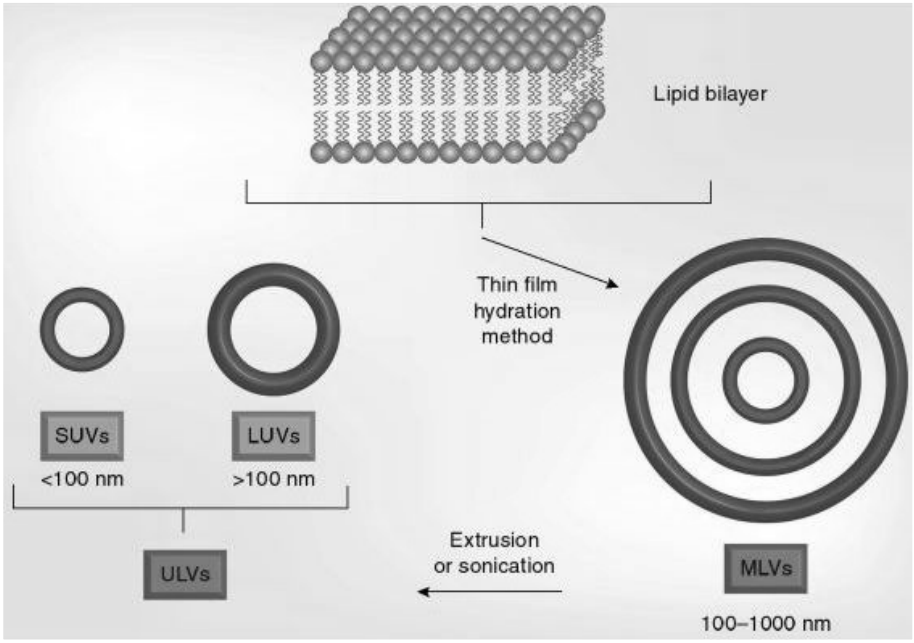

Figure 29. Liposomes of different size and number of lamellae.

2.6.2. Langmuir Monolayers

The history of the monolayers is very old and dates back to the period of the 18th century BC in Babylon, where pouring oil on water or water on oil and observing the subsequent spreading was considered a superstition dedicated to the Gods. Later, the same divination practice was also adopted by the Greeks. The first scientific approach towards to the monolayers was undertaken by Benjamin Franklin in 1744 and thereafter more extensively by Irving Langmuir, which was awarded with the Nobel Prize in 1932 by its contribution in the surface chemistry. Katharine Blodgett also gave a significant contribution to the monolayers film and in 1935 demonstrated the sequential transfer of monolayers onto the solid substrate to form multilayer films, which are nowadays referred to as Langmuir-Blodgett films [197-198].

The preparation of the Langmuir monolayers is quite simple and consists in the spreading of a surfactant (e.g. lipid solution, dissolving the lipid in a organic solvent) and use of a syringe to produce a droplet at the end of the needle that touches on the surface of the aqueous subphase (Figure 30). After approximately 15 min, the solvent evaporates and a monolayer is formed on the surface of the aqueous subphase. The addition of a certain substance (e.g. drug) on the monolayer or in the subphase will be strongly dependent of its solubility in the monolayer and the main purpose of the study. Additionally, the monolayers are produced in a balance, commonly referred to as a Langmuir trough, that consists in a trough usually made up of hydrophobic materials (e.g. Teflon) [198].

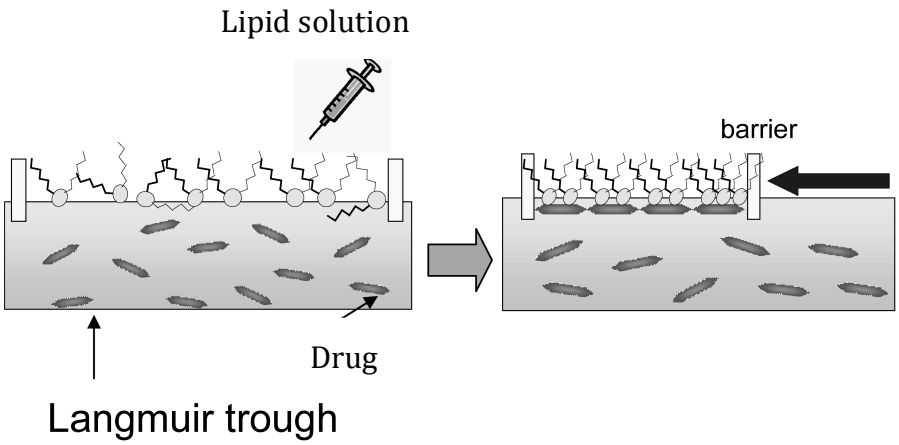

Figure 30. Schematic representation of the Langmuir monolayers preparation. Adapted from [199].

In fact, the Langmuir monolayers are considered the most simple membrane model systems, being basically half a membrane [110]. Although, they are less appropriate to study transmembrane processes, they are most suited to mimic processes at membrane surfaces and are more similar to the rearrangement of several biological membranes (e.g. PS, gastric mucosa) [200-201]. Langmuir monolayers as membrane model systems allow controlling several parameters such as lipid composition, subphase, and temperature. In addition, lipid monolayers are very well-defined, stable and bidimensional systems with planar geometry and for the above-mentioned reasons are frequently used to mimic membranes [111],[202].

2.6.3 Membrane Models Commonly Used to Mimic Eukaryotic, Prokaryotic Cell Membranes and Pulmonary Surfactant

The most common membrane models used to mimic human and bacterial plasma membranes are three-dimensional (i.e. vesicles), being the two-dimensional (i.e. monolayers) also used.

To mimic the human plasma membrane, the PCs are generally present, being the EPC, DMPC and DPPC the main phospholipids used [203]. Lipid mixtures are also used, being the CHOL commonly used associated with the PCs [204]. Phospholipids frequently associated with the PCs include among others, PSer, PG [205].

In order to mimic bacterial membranes, the most frequently used lipids are the PGs [206]. In addition, mixtures are commonly used, being CL and PE recurrently associated with the PGs [207-208].

Generally, the *in vitro* studies use monolayers as the classical model to mimic the PS [209]. In the literature, three-dimensional, namely vesicles are also described to mimic the PS [209-210]. The models generally include DPPC as the main compound present in the PS [210-220]. However, mixtures of DPPC and other lipid surfactants different from the previous are also used [35],[221]. Since DPPC stands for 40-45% of the PS composition, it is used in higher quantities or even as the only component of the PS surfactant model. When present, the other lipid added to DPPC mimics the effect produced by the non-dipalmitoyphosphatidylcholine lipids, aiding in the lipid monolayer fluidity and influencing, *in vivo*, DPPC adsorption at the air/water interface [35],[37],[221]. Natural PS as Curosurf®, Exofurf®, Survanta® or Alveofact® are also used, being derived from animals and therefore more similar to the human PS [209],[215-216],[222].

CHAPTER III

Methods to Evaluate the Antimycobacterial Compounds-Membrane Interactions

"Experiments never deceive. It is our judgment that deceives itself because it expects results which experiments do not give." [223]

Leonardo da Vinci, 15th century

The transport of antibiotics across the the cell membranes is a biological process, often misunderstood because of its complex and dynamic nature [111]. In this regard, model lipid membranes, which mimic many aspects of cell-membrane lipids, allow to account the passive diffusion across the bilayers, which is the most important process of the drug's permeation, specially in the case of drugs with high lipophilicity, such as RFB and analogs [224]. Indeed, drug-lipid membrane interactions allow to predict the pharmacokinetic properties, such as absorption, distribution, transport, accumulation, metabolization, elimination and hence efficacy [111],[225]. In fact, RFB is administrated orally and therefore it must cross biological membranes to be absorbed, distributed, metabolized and eliminated from the body [96]. Thus, understanding the role of these interactions on the pharmacokinetic properties of the antibiotics is critical for the development of more potent antimycobacterial compounds [224]. These interaction studies can be of particular interest when applied to novel potential drugs as in the case of RFB2 and RFB3, in order to predict their pharmacokinetic properties and understand if they have physical chemistry properties that enable them to reach the clinical trials and even further, the market. Moreover, these interaction studies can be used to design and develop efficient drug delivery systems [111].

Several biophysical techniques may be used to assess the interaction between drugs and membrane models. The drug-membrane interactions techniques employed allowed to study the partition of the drug to the membrane models, the location of the drug within the lipid bilayers and the influence of the drug on the biophysical parameters of the membrane models chosen (Figure 31).

In this chapter, the biophysical techniques to assess drug-membrane interaction studies are discussed. The complete description of the experiments, as well as, the main

results and the correlation with the therapeutic and toxic effects are presented with more detail in the several sections of Chapter IV.

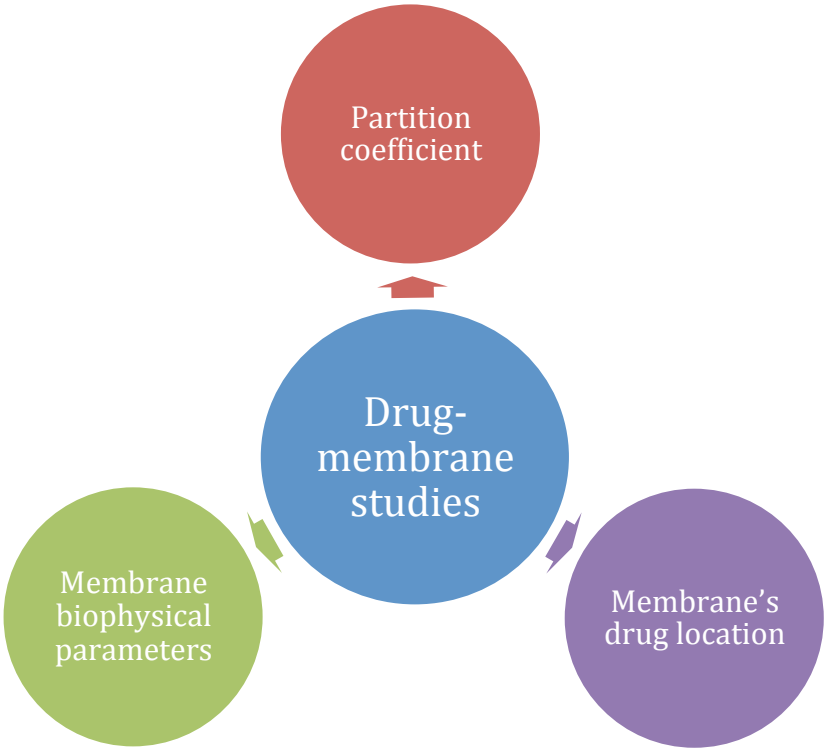

Figure 31. Schematic representation of drug-membrane studies.

1. Drugs Transport Through Cell Membranes and Lipophilicity Measurements

Drugs transport trough the cell membranes (Figure 32) follows the passive diffusion and/or active transport [226]. Passive diffusion may occur through the lipid bilayer (transcellular pathway) or through the water-filled pores or tight junctions (paracellular pathway). The transcellular diffusion is the main route in the case of the lipophilic drugs. The lipophilicity is a complex concept since it covers both nonpolar and polar interactions [227]. The lipophilicity of a drug molecule, expressed in terms of the logarithm of octanol–water partition, coefficient log *P*, or in the case of ionised molecular species, distribution coefficient log *D*, are important molecular descriptors of the pharmacokinetics properties of a drug molecule. Indeed, the lipophilicity affects the absorption, distribution, metabolization and elimination (i.e. pharmacokinetics) of a drug, affecting also their pharmacodynamic and toxicological properties [228].

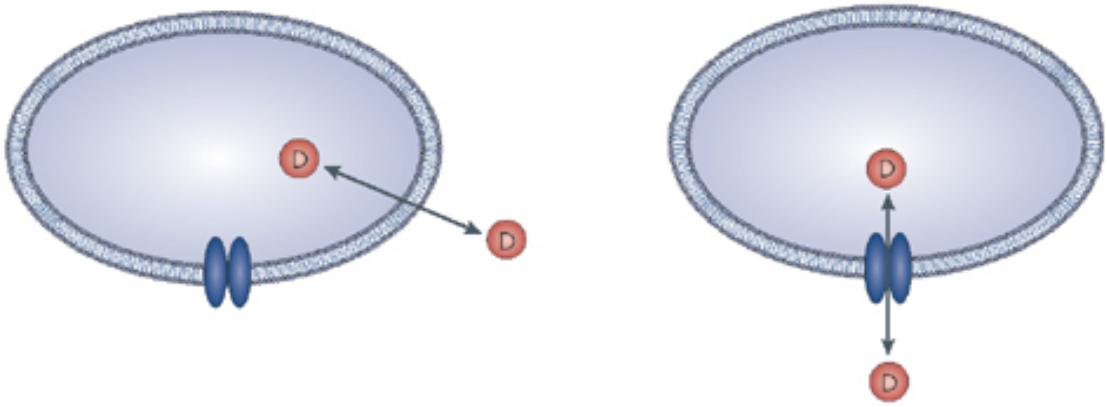

Figure 32. Membrane transport of drugs. Left, the drug (D) partitions into the lipid bilayer of the membrane according the log *P*; Right, the drug transport occurs via carriers that exist in the membranes. Adapted from [229].

Several systems were used since the 20th century to evaluate the lipophilicity of the drug. For instance, oil-water, heptane-water and octanol-water among others. The octanol–water system is the reference system to evaluate the lipophilicity of a drug, being the log *P* a characteristic constant for a chemical substance [227].

To reach the market, a drug molecule should have a log *P* comprised in a certain range [230]. A low lipophilicity is associated with a scarce interaction with the biological membranes and therefore, low absorption and distribution. On the other side, a high lipophilicity is connected with an extensive and unpredictable metabolism, high plasma protein binding or accumulation to tissues. In addition, a preferred log *P* for the penetration through biological barriers is also described for the antimycobacterial compounds as is pointed to be between 1.3 and 4.1 [231]. In the last years, the octanol–water system has received a lot of criticism, regarding its limitation to mimic the biomembranes environment. This system has a hydrophobic chain with a polar head group (hydroxyl), allowing it to account for the hydrophobic and hydrogen bonds interactions. The partition coefficient is related with the neutral monomer species, being the distribution coefficient the resultant of the ratio of the sum of the concentration of all species in octanol to the corresponding concentration sum in water [227].

Therefore, alternatives as the partitioning into liposomes and immobilised artificial membrane chromatography are gaining support. Because of their structural and anisotropic environment similar to the biomembranes, the liposomes constitute a realistic analytical system and can mimic closely the cell membranes, providing additional information to that obtained with the octanol–water system [232]. In addition, their constitution in phospholipids allow accounting for the electrostatic interactions between charged drugs and the polar head groups of the phospholipids. Moreover, the

conformational changes are also accounted and for instance the binding of a cationic molecule to the anionic phosphate anion leads to the repulsion of the positively charged quaternary nitrogen towards the water phase and thus, to a “opening” of the polar region and a penetration of the drug into the hydrophobic tails [227]. The immobilised artificial membrane chromatography consists of monolayers of phospholipids covalently immobilized on a silica surface, thus mimicking the lipid environment on a solid matrix [226],[233].

Several software programs can be used to determinate the log *P* and log *D* of a drug molecule. Nevertheless, their prediction is related to a large error, which is associated with the complexity in the inter- and intramolecular interactions and the conformational effects involved in partitioning process [227].

Active transport of drug molecules through the membrane is outside the scoop of this thesis, being although mentioned due to the contextual reasons. The active transport is especially relevant in the case of hydrophilic drugs, occurring against the gradient of concentrations, and implies their transport by carrier-facilitated transport across the membranes [226].

1.1. Determination of the Partition Coefficient by UV-Vis Derivative Spectrophotometry

The determination of the partition coefficient (*Kp*) of a drug may be determined from the UV-Vis derivative spectrophotometry technique [234-236]. The mentioned technique is based in the interaction of the light (in the range of the UV and Visible, respectively 180-400 and 400-750 nm) with the matter (e.g. lipids suspensions) in order to perform a quantitative measurement, with the ratio providing the partition of a drug between the water and the lipid. It requires the preparation of a series of lipids suspensions (e.g. micelles, liposomes) of increasing lipid concentrations, without (references) and with a fixed concentration of a drug (samples). Furthermore, the absorbance of the samples is measured in the UV-Vis range. In addition, the absorbance A, is defined as the $\log_{10}$ of the ratio of the incident to transmitted light beams and since both incident and transmitted light are measured in watts it is a unit-less quantity [237]. The concentration of the drug tested must be considered regarding its therapeutical relevance and needs to agree with the Beer-Lambert law [237]. Nevertheless, because the *Kp* is a ratio, the concentration of the drug should not change the *Kp* considerably.

The UV-Vis Derivate Spectrophotometry technique is based on the spectral variations presented by the drug in the presence of increasing lipid concentrations [238]. The major drawback of this technique is the strong signal arising from the lipids, which is

caused by the vesicles scattering [239]. This scattering corresponds to the Rayleigh light scattering, being specially pronounced in the UV region [240]. However, this might be overcomed by the subtraction of the lipid blank suspensions (i.e. references) to the samples and the derivation of the data. The use of derivation generally goes to the third or even fourth, being a commitment between the signal and the noise [239-240]. Therefore, derivative spectrophotometry allows to eliminate the effects of the residual background signals without need to prior separation procedures and permit the improvement of the resolution of overlapping spectra by the derivation [241-242]. The presence of the isosbestic points, (i.e. specific wavelength where the samples have the same absorbance) prove two important features, that the residual background signal effects were entirely eliminated and that the drug exists in two states, in the water and lipid bilayer phases [243]. In addition, with increase of the lipid concentrations the absorbance shift for lower or higher wavelength is also indicative of the drug's partition. Therefore, a shift for lower wavelength (hypsochromic shift) is caused by the increase of the polarity in the drug molecules's surrounding. On the other hand, a shift for higher wavelength (batochromic shift) suggests a decrease of the polarity of the drug's surrounding [244].

The *Kp* is generally calculated from the second and third derivative spectra at the wavelengths where the scattering is eliminated, by fitting Equation 1 to the experimental data (D_t versus [L]) using a non-linear least-squares regression method where the adjustable parameter is the partition constant, *Kp* (in molar) [232],[235],[242]:

$$D_T = D_w + \frac{(D_m - D_w)K_p[L]V_m}{1 + K_p[L]V_m} \qquad (1)$$

In this equation, *D* is the second or the third derivative intensity ($D=(d^nAbs)/(d\lambda^n)$) obtained from the absorbance values of the total concentration of the drug (D_T), drug distributed on the lipid membrane phase (D_m), drug distributed in the aqueous phase (D_w), *[L]* is the lipid concentration and V_m is the lipid molar volume [242].

The mathematical treatment of the absorbance data was performed using a developed routine application for Microsoft Excel®, designed as K_p calculator [245], being the K_p represented several times by the log *D* (for ionized drug) or log *P* (for non-ionized drugs), which consists in the ratio between the K_p and the V_m, being an dimensionless unit.

2. Evaluation of Drug's Membrane Location

The knowledge regarding the drug's location within the lipid bilayers may give useful information about their pharmacokinetics properties (e.g. understand if the drug diffuse across the lipid bilayer) and mechanisms of action, since the drug's location may compromise the integrity of the biological membranes, affecting the biophysical parameters and promoting a membrane disturbance or even disruption [224].

The drug's location within the lipid bilayer may be assessed by direct or indirect techniques. The direct techniques comprise among others, X-ray, neutron diffraction, nuclear magnetic resonance (NMR) and infrared spectroscopy (IR) [246]. Indirect techniques generally require the use of fluorescent probes with a well know location with the lipid bilayers. The fluorescence quenching (i.e. deactivation of the probe's fluorescence induced by the drug) is a mean to study the drug relative location within the lipid bilayer, being the quenching much more higher the nearer the drug's location to the probe [247-248].

2.1. Steady-state Fluorescence Quenching

The location of RFB and analogs in the membrane models was studied by fluorescence quenching. The fluorescence quenching is a sensitive method to determine the drug's relative location in the lipid bilayer [249]. The former technique involves the utilization of fluorescent probes. The probes should exhibit a constant fluorescence and must be used in appropriate concentrations in order to not perturb the lipid [250]. Thus, in the experiments included in this thesis the probes chosen, namely, 1,6-diphenylhexatriene (DPH) and propionic acid-1,6-diphenylhexatriene (DPH-PA) (Figure 33), have a negliglbe perturbing effect on the lipid bilayers in the concentrations used (i.e. 1:300 molar ratio probe:lipid) [251].

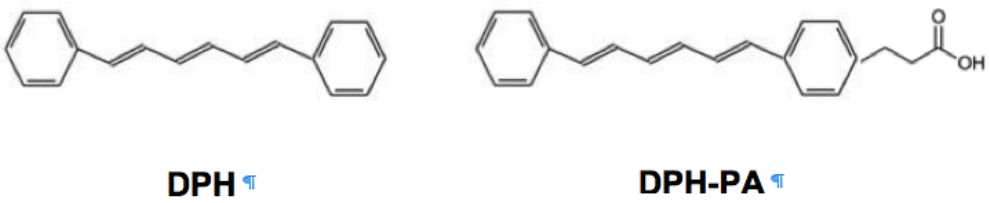

Figure 33. Chemical structures of DPH and DPH-PA. Adapted from [252-253].

DPH is a hydrophobic rod-shaped probe that prefers the hydrophobic acyl chain region of the lipid bilayers [254]. Therefore, it is widely used in experiments to study the membrane fluidity and ordering of the lipid [255]. DPH-PA is a more polar probe than DPH due to the propionic acid group, [256-257] being therefore anchored to the surface of the membrane in the phospholipids polar head groups [258].

The fluorescence quenching of a membrane bond fluorophore provides a measure of its accessibility to the drug (quencher) and can be related with the concentration of the quencher by the Stern-Volmer equation [259]:

$$\frac{I_0}{I} = 1 + K_{SV}[Q]_m \qquad (2)$$

In this equation I_0 and I are the fluorescence intensities in the absence and presence of the quencher, respectively; K_{SV} is the quenching constant, called the Stern–Volmer constant; $[Q]_m$ is the concentration of the quencher that is able to partition the membrane. In fact, the extrinsic fluorophores used in quenching studies are inserted into the lipid bilayer and consequently the accessibility of the drug to the fluorophores should be determined using the fraction of drug molecules that are able to partitioning with the lipid bilayer. The $[Q]_m$ is calculated from the total drug concentration ($[Q]_T$) and from the drug's partition coefficient (K_p), as described by the Equation 3 [249]:

$$[Q]_m = \frac{K_p[Q]_T}{K_p\alpha_m + (1-\alpha_m)} \qquad (3)$$

where α_m is the volume fraction of the membrane phase ($\alpha_m = V_m/V_T$; V_m and V_T represent the volumes of the membrane and water phases, respectively). In addition, the fluorescence intensities should be corrected in order to eliminate the "inner filter effect", using the Equation 4. The former effect happens if the drug absorbs at the wavelength of excitation of the fluorophore, decreasing the effective intensity of the exciting light beam and thus decreasing the measured fluorescence intensity [249].

$$I_{corr} = I\frac{A_Q}{A_F}\frac{1-10^{-A_F}}{1-10^{-A_Q}} \qquad (4)$$

where I_{corr} is the corrected fluorescence intensity, I the experimental fluorescence, A_Q and A_F, the absorbance of the sample in the absence and presence of the quencher [249].

As above-mentioned, the fluorescence quenching study is useful to predict the relative location of the drugs within the lipid membrane. Therefore, the use of different

probes with different membrane locations allows to infer the preferential location of the drug within the lipid bilayer, being the higher K_{SV} value obtained for a certain probe, indicative of a closer proximity of the drug to that probe in comparison to the other. In addition, high K_{SV} values obtained for probes located in the deep regions of the lipid bilayer, suggest the accessibility of the drugs to the hydrocarbon regions and the ability to penetrates the membrane lipid bilayer [249].

2.1.1. Fluorescence Quenching Mechanism

A huge variety of molecular interactions may result in fluorescence quenching, including excited-state reactions, molecular arrangements, energy transfer, ground-state complex formation, and collisional quenching [249]. Fluorescence quenching mechanisms are usually categorized into dynamic and static quenching by different mechanisms (Figure 34) [260]. For both static and dynamic quenching, the quencher and the fluorophore should be in contact. The collisional or dynamic quenching implies the diffusion of the quencher to the fluorophore during the lifetime of the excited state [249]. Upon contact, the fluorophore returns to the ground state, without emission of a photon. On the other hand, the static quenching, the quencher and fluorophore form a complex, being this complex nonfluorescent [249]. When this complex absorbs light, immediately returns to the ground state without emission of a photon [249].

In order to distinguish the fluorescence quenching mechanism, the fluorescence lifetimes is the most appropriate method. In addition, to definitely prove the type of fluorescence quenching, studies at several temperatures must be performed. In the case of dynamic quenching, higher temperatures result in faster diffusion and hence larger amounts of collisional quenching [249]. On the other side, in the case of static quenching higher temperature will result in the dissociation of the weakly bound complexes, and consequently smaller amounts of static quenching (Figure 34) [249].

The Equation 5 describes the mathematical formalism beyond the collisional quenching of fluorescence [249]:

$$\frac{I_0}{I} = 1 + K_D[Q]_m \qquad (5)$$

The K_D corresponds to the dynamic portion of the quenching and is determined by the lifetime measurements. That is, $\tau_0 / \tau = K_D$. The τ_0 is the lifetime of the fluorophore in the absence of the quencher and τ is the lifetime of the fluorophore in the presence of the

quencher. The observation of a linear Stern-Volmer plot does not prove that collisional quenching of fluorescence has occurred since the static quenching also results in Stern-Volmer linear plots [249]. The Equation 6 describes the mathematical formalism beyond the static quenching of fluorescence [249]:

$$\frac{I_0}{I} = 1 + K_S[Q]_m \qquad (6)$$

The K_S corresponds to the static portion of the quenching. In the case of the static quenching the τ_0 / τ =1. Thus, in the static quenching the lifetime remains the same since only the fluorescent molecules are observed and the uncomplexed fluorophores have the unquenched lifetime τ_0 [249].

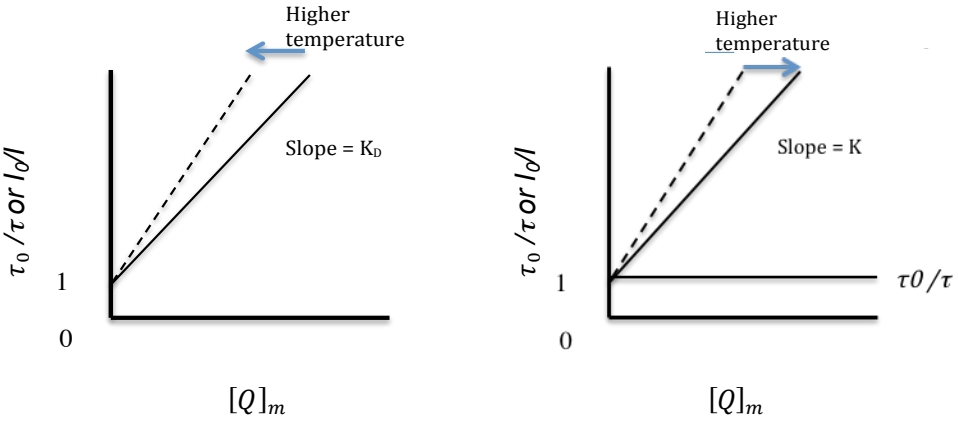

Figure 34. Comparison of dynamic and static quenching. Adapted from [249].

Additionally, the bimolecular quenching constant (K_q) is a fundamental parameter that reflects the efficiency of quenching or the accessibility of the probes to the drug, and is calculated as follows (Equation 7) [249]:

$$K_q = \frac{K_{SV}}{\tau_0} \qquad (7)$$

2.1.2. Deviations from the Linear Stern-Volmer Plots

The linearity of the Stern-Volmer plot indicates that only one type of quenching (i.e. collisional or static) occurs. However, negative and positive deviations from the Stern-Volmer equation are frequently observed [249].

Negative deviations to the Stern-Volmer linearity generally indicate the presence of fractions of fluorophore with different accessibility to the quencher. This occurs commonly in proteins because due to the tryptophan residues, which act as fluorophores and are positioned in distinct environments and consequently have different accessibility to the quencher [249],[261].

Positive deviations from the Stern-Volmer equation are commonly observed when the extent of the quenching is large. The combined static and dynamic quenching may result in an upward curvature to the Stern-Volmer non-linear plot. Indeed, the fluorescence quenching may result from both dynamic and static quenching. In those cases, after the determination of the dynamic component, the static contribution may be found by linearization of the following second order equation (Equation 8) in $[Q]_m$ [249]:

$$\frac{I_0}{I} \times \frac{1}{1+K_D[Q]_m} = 1 + K_S[Q]_m \qquad (8)$$

In addition, the positive deviation of the Stern-Volmer plots can also be interpreted in terms of a “sphere of action” static quenching model [249],[260]. According to this model, instantaneous quenching occurs if the quencher molecules are adjacent to the fluorophore at the moment of excitation. When the fluorophore and the quencher are closer there is a high probability that the quenching will occur before these molecules diffuse apart. As the quencher concentration increases, the probability also increases, because the quencher is within the sphere of action of the fluorophore at the moment of excitation. Therefore, only a certain fraction of the excited fluorophore is quenched by the Stern-Volmer collisional mechanism. Moreover, this model assumes that if the quencher is located inside a spherical volume (V) adjacent to the fluorophore, the probability for the quencher to be inside this volume at the time of excitation depends on the volume itself and on the quencher concentration ($[Q]_m$), as it is described by the modified Stern-Volmer equation (Equation 9) [249-250]:

$$ln\left(\frac{I_0\tau}{I\tau_0}\right) = V[Q]_m \qquad (9)$$

2.2. Time-Resolved Fluorescence Quenching

Time-resolved measurements are widely used in fluorescence spectroscopy to monitor molecular interactions and motions that occur in the picosecond-nanosecond time range, being especially useful in the analysis of the biomolecular structure and dynamics

[262]. Time-resolved fluorescence quenching provides additional information to the steady-state fluorescence. For instance, time-resolved fluorescence quenching allows to distinguish between static and dynamic quenching through the fluorophore lifetime measurements [249]. The lifetimes measurements may be determined using pulse fluorimetry or phase-modulation fluorimetry techniques [223]. Pulse fluorimetry uses a short exciting pulse of light and yields the d-pulse response of the sample, convoluted by the instrument response. The technique used in this work, namely, phase-modulation fluorimetry uses modulated light at variable frequency and provides the harmonic response of the sample, which is the Fourier transform of the d-pulse response [223]. In this technique, a sinusoidally modulated light at high frequency excites the sample. Regarding the existence of a lag time between absorption and emission, the emission is delayed in time relatively to the modulated excitation. The mentioned delay is measured as a phase shift φ_ω between the excitation and emission, where ω is the modulation frequency in radians/s. Additionally, the finite time response of the sample results in demodulation of the emission by a factor m_ω. The finite lifetime of the excited state avoids the emission from exactly following the excitation, which results in a decrease in the peak-to-peak amplitude of the modulated emission, being measured relatively to the modulated excitation (Figure 35) [263].

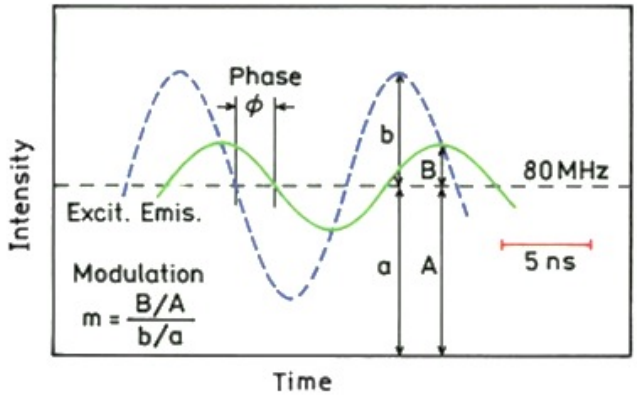

Figure 35. Frequency-domain lifetime measurements. In this example the assumed decay time is 5 ns and the light modulation frequency is 80 MHz. Adapted from [263].

The phase shift and modulation of the emission depend on the relative values of the lifetime and on the light modulation frequency, being the dependence of the phase angle φ and modulation *m* on the light modulation frequency used to determine the intensity decay of the sample. Moreover, the phase angle and modulation are measured over a wide range of frequencies (Figure 36). The frequency response of the sample used in this work was in the 0-200 MHz range. The increment in the light modulation frequency is accompanied by the phase angle rises from 0 to 90º [263].

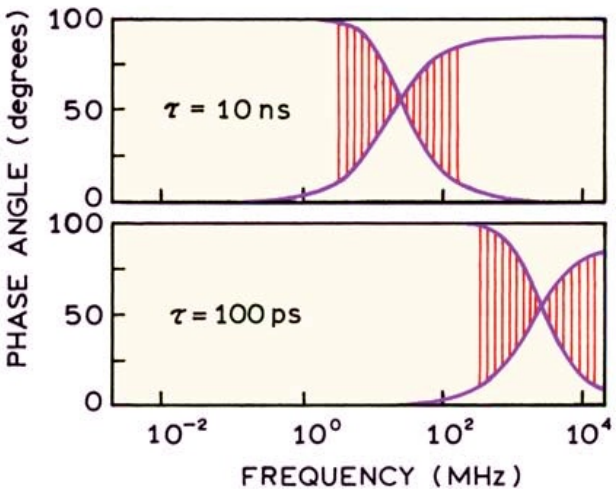

Figure 36. Frequency-domain example. The phase angle increases and the modulation decreases with increasing modulation frequency. Adapted from [263].

The shape of the frequency response is determined by the number of decay times displayed by the sample. In the case of a single exponential decay, the frequency response is simple, being the phase and modulation related to the decay time (τ) by the Equations 10 and 11 [263]:

$$\tan \varphi_\omega = \omega t \qquad (10)$$

$$m_\omega = (1 + \omega^2 \tau^2)^{-1/2} \qquad (11)$$

Nevertheless, the majority of the samples display more than one decay time. In those cases it becomes necessary to measure the phase and modulation values over the widest possible range of modulation frequencies. Therefore, the lifetime of the multi-exponential fluorophores is defined by (Equation 12) [263]:

$$\chi^2 = \frac{1}{\upsilon}\left[\sum_{i=1}^{N} \frac{\left[\Phi(\omega_i) - \Phi_c(\omega_i)\right]^2}{\sigma_\Phi(\omega_i)} + \sum_{i=1}^{N} \frac{\left[M(\omega_i) - M_c(\omega_i)\right]^2}{\sigma_M(\omega_i)}\right] \qquad (12)$$

being *N*, the total number of frequencies. Therefore, the number of data points is twice the number of frequencies, so that the number of degrees of freedom is $u = 2N - p$ (p = number of fitted parameters). The subscript *c* is used to indicate calculated values for assumed values of the fractional contribution of the component *i* to the total lifetime (f_i)

and τ_i. The σ_ϕ and σ_M are, respectively, the uncertainties in the phase and modulation values [263].

Finally, a fitting procedure (nonlinear least-squares) is applied to the data, being obtained a χ^2, that if comprised between 0.8-1.2 is indicative of a good fit [223],[263].

3. Biophysical Modifications of the Membrane

The majority of the drugs are able to directly or indirectly influence the biophysical membrane properties, by means of the interactions with proteins and/or phospholipids [264-265]. A large number of drugs affect the fluidity of the membranes, which is a parameter fundamentally linked to the membrane structure. In fact, the fluidity is a critical property of the membranes that interferes with the activity of the membrane proteins and modulates the membrane permeability [266]. Moreover, changes in the membrane fluidity can affect the receptor and enzyme activity and influence the drugs ability to pass through the membrane, which in turn can affect their efficacy. In fact, the fluidity is closely dependent of the biophysical parameters T_m, phospholipids packing order and cooperativity of the membranes [267].

Several biophysical techniques can be performed in order to obtain a detailed analysis of the complexity of membrane dynamics and thermodynamics in the absence and presence of drug molecules. Thus, in this work, several techniques were employed, providing a detailed and complementary description of the modifications in the membrane biophysical properties caused by RFB and analogs.

It is estimated that more than 150 different methods to study the biophysical parameters of the membrane models exist [267]. For that reason, in this thesis only the carried out methods are going to be described.

3.1. Dynamic Light Scattering

Dynamic light scattering (DLS) exploiting the count rate is a reliable, simple and reproducible technique to determinate the biophysical parameters of the membrane as the T_m and the cooperativity. In addition, despite the T_m, this method also allows the determination of also sub-transitions involving under-phases [267-268]. The alteration in the measured scattering intensity reflects changes in the optical properties of the material. Thus, discontinuity in the mean count rate (average number of photons detected per second) as the temperature changes corresponds to an alteration in the optical properties of the studied material (i.e. transition from the initial state to another one). Data as the

normalized mean count rate versus the temperature after being collected may be fitted using the Equation 13 [267]:

$$r_s = r_{s1} + p_1 T + \frac{r_{s2} - r_{s1} + p_2 T - p_1 T}{1 + 10^{B(1/T - 1/T_m)}} \qquad (13)$$

where r_s is the average count rate, T is the temperature (°C), p_1 and p_2 correspond to the slopes of the straight lines at the beginning and at the end of the plot, and r_{s1} and r_{s2} are the respective count rate intercepting values at the y axis. From the experimental data it is possible to calculate the cooperativity (B) and the midpoint of the phase transition, which corresponds to the T_m. In addition, the T_m may be calculated from the slope and the inflection point of the data fitted to sigmoid curves of count rate (r_s) versus temperature (T) (Figure 37) [232],[250],[267].

The experimental procedure to determine the influence of drugs on the biophysical parameters of the membrane models is very simple and does not require the use of an exogenous probe. Therefore, the effect of a certain concentration of a drug is tested using the three dimensional membrane model with a lipid concentration that allows to obtain a count rate included in the range of the count rate indicated for the equipment [267]. Moreover, parameters as the temperature intervals, number of measurements to be made at each step after equilibration time, temperature range and scan speed should be adjusted to obtain the desired accuracy level [267].

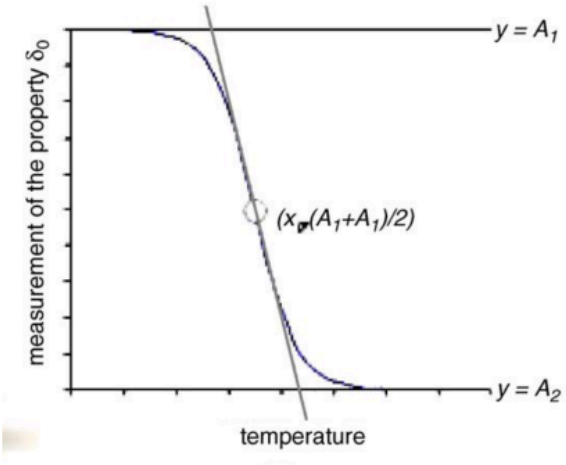

Figure 37. Schematic representation of the process of phase transition as propagation of a physical macroscopic property (δ0) (e.g. count-rate) and corresponding curve as property vs. temperature. Adapted from [267].

3.2. Steady-state Anisotropy

Fluorescence polarization methods, and specifically anisotropy provide useful information on the molecular mobility, fluidity of a medium, lipid's order parameter, and cooperativity [223].

The fluorescence can be considered as the result of three independent sources of light polarized along three perpendicular axis O_x, O_y, O_z, being the I_x, I_y, I_z the intensities of these sources, and the total intensity the sum of all these sources. The values of the intensity components depend on the polarization of the incident light and on the depolarization processes. In addition, the excitation light may be vertically polarized, horizontally polarized or even unpolarized (i.e. natural light) [223]. In the particular case of the steady-state determination the light must be vertically polarized, being the fluorescence intensities measured with the emission polarizer oriented parallel ($I_{\parallel}$) and perpendicular ($I_{\perp}$) to the excitation polarized. The steady-state anisotropy (r_{ss}) is then defined by the following relationship between the relative intensities of fluorescence (Equation 14) [223][249]:

$$r_{ss} = \frac{I_{\parallel} - GI_{\perp}}{I_{\parallel} + 2GI_{\perp}} \qquad (14)$$

being G an instrumental correction factor given by the ratio of the sensitivities of the detection system for vertically and horizontally polarized light (Equation 15) [249]:

$$G = \frac{I_{\perp}}{I_{\parallel}} \qquad (15)$$

The experimental procedure for the steady-state anisotropy is very similar to the former method (DLS), however with an additional requirement, namely an extrinsic fluorophore inserted within the lipid bilayer. In a highly ordered lipid bilayer (i.e. gel phase), the movement of the probe is extremely restricted and a parallel orientation of the fluorophore molecules to the vertical excitation polarizer is induced. Thus, the molecules of the fluorophore emit polarized light since they remain immobile during the lifetime of the excited state. On the other hand, if the environment surrounding the fluorophore is fluid, the free rotation of the fluorophore molecules pushes a random fluorophore orientation, resulting in a decrease in the emission of polarized light. The explanation for this decrease is based on the lack of alignment with the vertical excitation polarizer [249].

From the experimental data obtained it is possible to determine the cooperativity (B) and the T_m, calculated from the slope and the inflection point of the data fitted to

sigmoid curves of steady-state anisotropy (r_s) versus temperature (T) data (Equation 16) [249].

$$r_s = r_{s1} + p_1 T + \frac{r_{s2} - r_{s1} + p_2 T - p_1 T}{1 + 10^{B(1/T - 1/T_m)}} \quad (16)$$

The r_{s1} and r_{s2} are the respective steady-state anisotropy intercepting values at the y axis, T is the temperature (°C) and p_1 and p_2 correspond to the slopes of the straight lines at the beginning and at the end of the plot.

In addition, from the values of anisotropy it is also possible to determine the limiting value of anisotropy (r_∞), which reflects the restriction of movement of the probes. This value is obtained using Equation 17, which is only valid for values of r_{ss} between 0.13 and 0.28 [269]:

$$r_\infty = 4/3 r_{ss} - 0.10 \quad (17)$$

The order parameter can be calculated from the Equation 18:

$$s = \sqrt{r_\infty / r_0} \quad (18)$$

where r_0 (fundamental anisotropy) is the fluorescence anisotropy in the absence of any rotational motion of the probe and r_∞ (limiting anisotropy).

Steady-state fluorescence anisotropy measurements allow the quantification of the fluidity gradient across bilayer structures, which may be used to understand the mechanism of action. In the case of RFB and RFB2 the fluidity seems to be slightly affected in the human membrane model, particularly in comparison in with the bacterial membrane model, which suffers a decrease of the fluidity in the presence of the antimycobacterial compounds. Therefore, the increment of the phospholipid order may be responsible for the impairment and disruption of the bacterial membranes with consequent cell death [270-271].

3.3. X-Ray Scattering

Historically, X-rays were discovery in 1895 by Röntgen (nobel prize in 1901) and so named because of their unknown nature [272]. The X-rays are invisible and possess an extraordinary ability to penetrate through the human body and opaque objects.

Radiographies were then developed, putting a source of X-rays on one side of a certain object and a photographic film on the other [273]. Later in 1992, the exact nature about the X-ray was established with the von Laue's (nobel prize in 1914) discovery that the diffraction caused by a crystal is close related with its structure [273-274].

Currently, the X-ray scattering techniques are applied to several fields, playing a major role in the elucidating of the drugs effects on the structural details of biological membrane models [275]. In fact, X-ray scattering experiments constitute a valuable approach to get an insight into the membrane properties, since it has many advantages as the fact of being non-invasive and label-free [271]. Moreover, these techniques applied in the field of phospholipid membrane models allows to investigate the influence of the drugs on the phase of the lipids [276].

The X-ray scattering measurements are preferentially made on synchrotron and lab-based X-ray sources [276]. These experiments are based on the measurement of the scattered intensity as a function of scattering angle relative to the incident beam. In addition, the scattered intensity is expressed in terms of the scattering vector, q, which represents the modulus of the change in momentum of the scattered radiation (Equation 19) [276]:

$$q = \frac{4\pi sen\theta}{\lambda} \qquad (19)$$

where λ is the wavelength of the scattered radiation and 2θ is the scattering angle relative to the incoming beam. The Braggs peaks exhibit an angular position, which indicates a periodic spacing within the sample, and may be used to measure the periodic spacings within the sample. Additionally, the mentioned distances, d, of the spacing can be calculated using the Bragg equation and the angular position of for example, the first order diffraction peak (Equation 20):

$$n\lambda = 2dsen(\theta) \qquad (20)$$

where n is the order of the reflection and therefore a positive integral number (n = 1 for first order). For the first order scattering peak, the Equation can be simplified and rewritten as (Equation 21) [276]:

$$d = \frac{2\pi}{q} \qquad (21)$$

Samples as the MLVs with lipid bilayers oriented randomly show strong reflections in comparison with unilamellar vesicles. For that reason, MLVs are generally used due to their possession of a positional order. Vesicles with only one lamella, as the LUVs and ULVs do not have a positional order normal to the plane of the bilayer, which results in diffuse peaks and difficult to be analysed [271]. Therefore, the experimental procedures used involved the preparation of MLVs of several phospholipids without and with the tested drug in several concentrations [277].

The scattering data obtained is radially symmetric but may be transformed and plotted as intensity versus the scattering vector, q or the s (lamellar spacing) [276].

Furthermore, X-ray scattering is mainly classified into small-angle X-ray scattering (SAXS) and wide-angle X-ray scattering (WAXS), depending on the scattering angle [278].

3.3.1. Small-Angle X-Ray Scattering

SAXS is nowadays one of the most powerful methods for probing the nanostructures of self-assembled systems [279-280]. With the development of sophisticated third-generation synchrotrons in the late 1980s, SAXS experiments were put into practice with the intention to study the temperature-driven transitions in lyotropic liquid-crystal systems [279].

SAXS corresponds to the X-ray scattering at the small angle (< 2.3º) region, providing information in the size range of nanometers [278]. In the field of phospholipids, SAXS is typically applied to obtain the distances between the lipid bilayer plus water layer (Figure 38).

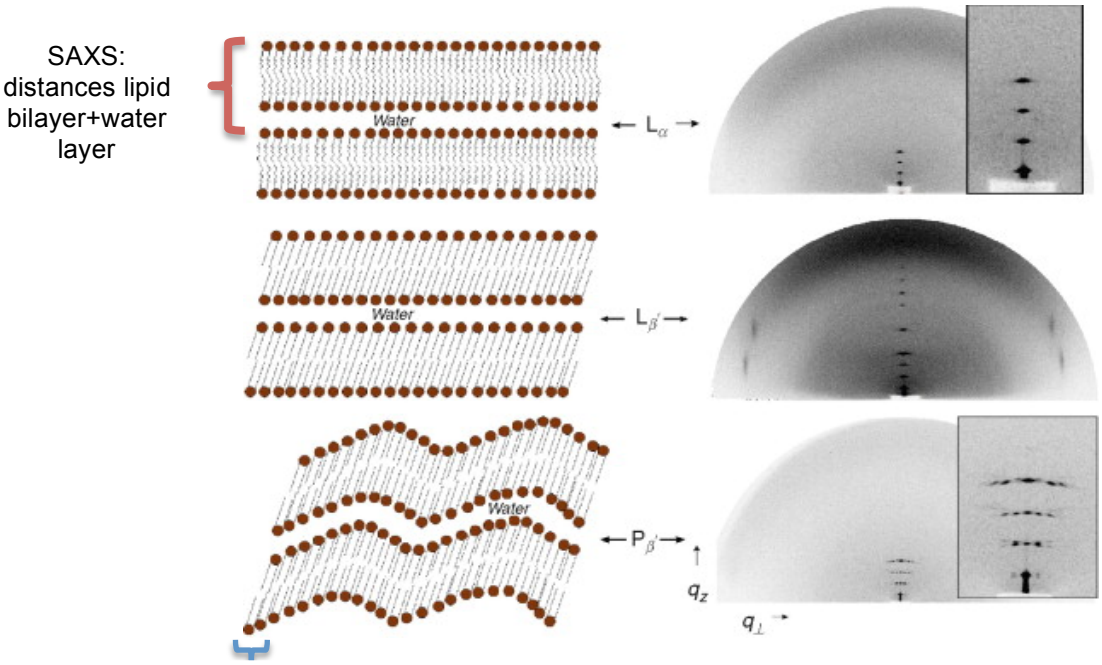

Figure 38. Schematic of the diffraction patterns obtained according different lipid phases and the corresponding distances measured by SAXS and WAXS. Adapted from [281].

In addition, with SAXS measurements it is possible to assign different lipid phases through the relation between the positions of the diffraction peaks: lamellar (1:1/1:2/1:3/1:4/...), cubic (1:1/1:√2/1:√3/1:√4/1:√5/1:√6/1:√8/…), and hexagonal (1:1/1:√3/1:√4/1:√7/...). The Lorentzians fitting is applied to the Bragg peaks in order to obtain the precise position of the peaks and the full width at half maximum (FWHM). The *FWHM* is required to calculate the correlation length (ξ) between the lipid bilayers, through the Equation 22:

$$\xi = \frac{2\pi}{FWHM} \qquad (22)$$

The ξ is a measure of the correlation between the bilayers. If the correlation is high, it indicates that the frequency of appearance of that *d* is also high, i.e., a large number of bilayers present in the same long-range distance, *d* (or thickness) determined by SAXS [282].

3.3.2. Wide-angle X-Ray Scattering

WAXS is used to obtain information on sub-nanometer scale structures, such as the lipid packing [278]. In addition, in order to determinate the short-range distances (*d* <10 Å) a wide-angle detection is required with values of θ of the order of 5 to 180 ° [277]. At temperatures below the chain-melting transition, where the hydrocarbon chains of membrane lipids adopt ordered states, the WAXS measurement result in well-defined Bragg peaks [283]. At temperatures above the T_m the hydrocarbon chains of the phospholipids are melted and therefore a diffuse Bragg peak appears. The Bragg peaks assume different features according to the phospholipids packing. Thus, the packing may be hexagonal or pseudo-hexagonal. In addition, the symmetry of the chain subcell depends on the specific lipid phase (Figure 39). A distorted hexagonal lattice (pseudo-hexagonal), with two nearest neighbours, is found in the $L_{\beta'}$ gel phase. On the other hand, hexagonal lattices, in which a lipid chain has six nearest neighbours, is found in the L_{β} and $P_{\beta'}$ gel phases [284]. The Lorentzians fit is also applied to the Braggs peaks obtained by WAXS measurements, which allows to obtain the *s*, essential to determinate the distances between the polar head groups of the phospholipids (Figure 38). In addition, the *FWHM* is also calculated, allowing to determinate the correlation between the phospholipid head groups. If the correlation is high, it suggests that the frequency of appearance of *d* (distance between the phospholipid head groups, being a measure of the phospholipid packing) is high, and a large number of phospholipids present the same short-range distance, *d* [282].

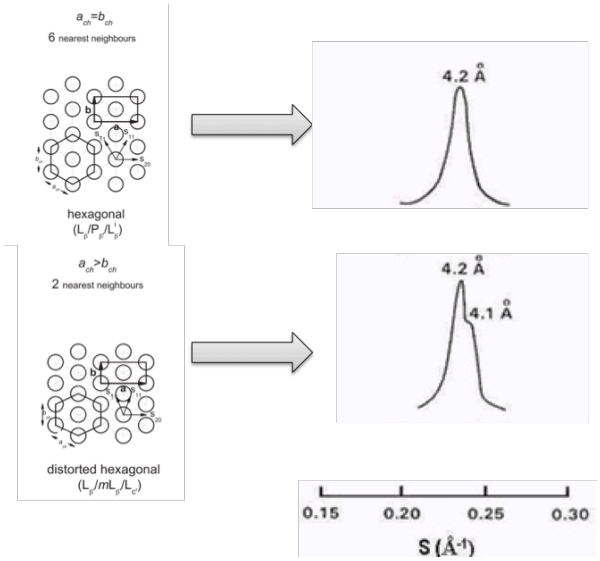

Figure 39. Hydrocarbon chain packing symmetries and the corresponding WAXS patterns. Adapted from [284-285].

4. Surface Pressure-Molecular Area *(π-A)* Isotherms

The surface pressure-molecular *(π-A)* isotherm corresponds to a plot of the surface pressure variation with the area available to each molecule on the aqueous subphase surface. The *π-A* isotherms give valuable information about the influence of the drugs in the monolayers lipid phases and the phase transitions, which are both dependent on the temperature, the pressure, and the pH [286],[287]. Monolayers of various phospholipid compositions at the air–water interface have been intensively used to understand the interactions of the drugs with the alveolar lining layer that exists in the lungs [288]**.** The interactions of the etiologic agent of TB, MTb with the PS were performed at the air-water interface, using monolayers of MAs to mimic the presence of the bacteria in the alveolar lining layer. In addition, the plasma membranes were used to understand the relationship between the structure and effect of RFB and analogs in the biological membranes. The monolayers were prepared as above-mentioned in the theoretical background chapter.

The presence of a monolayer in the air/water interface causes a differential interfacial tension between the surface with the presence of the surfactant (γ_m) and the clean surface (γ_0), being this difference, the surface pressure (π), which can be measured by the Wilhelmy plate technique, Thus, by sliding the barriers across the interface, the monolayer is compressed, which results in an increase of the surface pressure. Knowing the number of molecules present at the interface, the surface pressure can be related to the average area per molecule and the surface pressure isotherms can be plotted until the compression on the monolayer is such that it collapses.

From the Langmuir isotherms it is possible to distinguish various phases of the monolayer (Figure 40). For instance, in the case of the PCs such as DPPC, during compression the monolayer changes from a state where the molecules are far apart and the interactions are practically negligible, “gaseous’ monolayer” (G), to a “liquid-expanded” (LE) and posteriorly to a “liquid-condensed” (LC), distinguishable by the proximity of the surfactant molecules. A small reduction in the area per molecule leads the monolayer to the “solid” (S) state, where the amphiphilic molecules are tightly packed, being the hydrophobic tails aligned in parallel to the interface air/water [289]. Furthermore, with the monolayer compression the collapse is reached (a plateau appears) and a break out of the molecules occurs, which may induce a different rearrangement (e.g. micelles, multilayers). The transitions between the phases are not always distinct and often more than one phase may be present [289-290].

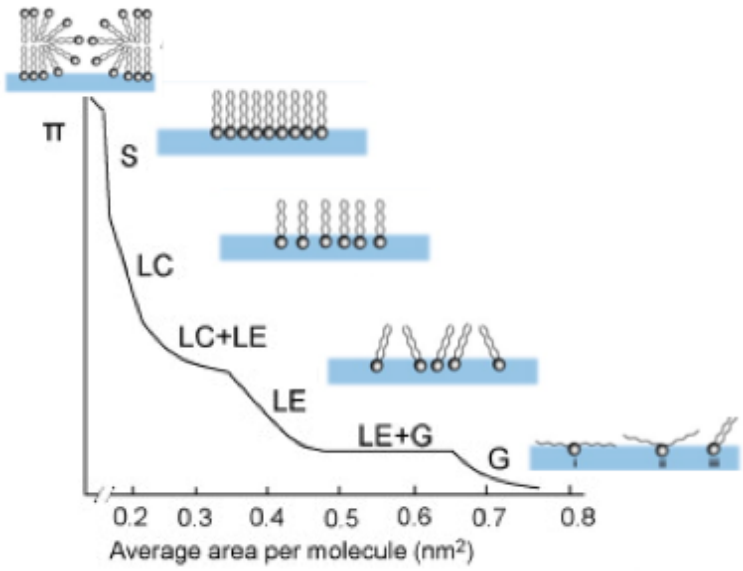

Figure 40. Schematic example of π–A isotherm, exhibiting a variety of phases which can occur. G: gaseous, LE: liquid-expanded, LC: liquid-condensed, and S: solid. Adapted from [197].

Several important parameters can be acquired using the pressure-molecular area (π-A) of the Langmuir isotherms, namely the collapse pressure ($\pi_{collapse}$), the limiting area per lipid molecule in the compressed state (A_{min}), hysteresis, and compressibility [291].

The $\pi_{collapse}$ corresponds to the beginning of a plateau region in the isotherm, where the surface pressure remains constant even with the decrease of the area, and is an indication of the monolayer stability [292].

The A_{min} corresponds to the mean area occupied by one molecule of lipid in the surface layer just before the collapse. It indicates both the molecular packing and the interactions between the monolayer components [293-294].

The hysteresis is generally acquired by consecutive measurements of monolayer compression/decompression isotherms and corresponds to the difference between compression and decompression areas [295-296].

It is well-known that the rheological properties of a monolayer can be obtained on the basis of the compressibility calculation. Indeed, the change of the surface tension with the area in a liquid film can be attributed to its interfacial elasticity. The compressibility of the monolayers can be determined using the Equation 23 and 24 [286],[291]:

$$C_s^{-1} = -A\,(d\pi/dA) \qquad (23)$$

$$K = \frac{1}{Cs-1} \qquad (24)$$

where C_s^{-1} is the elastic modulus, A is the area per lipid molecule, π is the surface pressure, and K is the compressional modulus. The C_s^{-1} describes the relationship between the surface pressure increase and the area per molecule decrease. A higher value of C_s^{-1} (lower of K) is indicative of a less compressible monolayer and therefore a more ordered monolayer.

The isotherms are not always reproducibility, being their shape different from the expected (e.g. phase transitions are not observed, $\pi_{collapse}$ with a different value than the expected). The major sources of experimental errors include, impurities in the monolayer, impurities in the subphase or in the trough, the solubility of the monolayer material, drifts in the surface pressure measuring system, water level alteration caused by evaporation, leakage through the barrier, surface density of monolayer material alteration by spreading of different amounts and/or excess of materials [292].

The application of other techniques to the Langmuir isotherms as the optical microscopy, specially Brewster angle microscopy (BAM), the synchrotron X-ray diffraction at grazing incidence (GIXD) and the infrared reflection-absorption spectroscopy (IRRAS) allowed a detailed characterization of drug-membrane interactions [288].

5. Brewster Angle Microscopy

BAM, a microscopy tool introduced in 1991 [297], permits the morphological observation of the dynamic process of monolayer compression at the air-water interface [296],[298]. The main advantage of BAM is that the morphology of the monolayers at the air/water interface is visualized without the need of probes as it happens in the fluorescence microscopy [299]. Thus, BAM is a powerful technique that allows the visualization of the two-dimensional organization of the monolayers, including the size and shape of the lipid domains [300]. BAM allows the identification of the phase transitions of a monolayer by the appearance of lipid domains. The lipid domains are attributed to the reflection caused by alkyl chains and the polar headgroups [297]. In addition, BAM gives information about the fluidity of the monolayer in relation to the geometry of the domains observed at the air-water interface. Therefore, the contrast in the BAM images results from of the local differences in the monolayer refractivity index, caused by differences in the local molecular density or packing. In the BAM images, the dark background corresponds to the fluid phase and the light gray areas to the condensed domains at the interface [301-302].

BAM is mounted in a trough and is composed by the optical components, namely a laser, the polarizers, lens and a charge-coupled device camera [298]. It also possesses a video camera that allows to record the monolayer by both film and pictures [297].

The BAM angle is determined using the Snell's law (Equation 25):

$$\tan \alpha = \frac{n2}{n1} \qquad (25)$$

where α is the Brewster angle in radians, n_1 the refractive index of air (≈ 1) and n_2 the refractive index of water. Therefore, if a *p*-polarised light impinges at the air–water interface at the Brewster angle (53.1°), no light is reflected from the interface between the two media with different refractive indices (Figure 41). Therefore, at the mentioned angle of incidence, the introduction of a Langmuir monolayer at the air/water interface modifies the Brewster angle conditions, and light is reflected. The BAM images obtained are commonly digitised and filtered in order to reduce diffraction fringes caused by the coherent nature of the laser beam and finally processed to improve their quality [292].

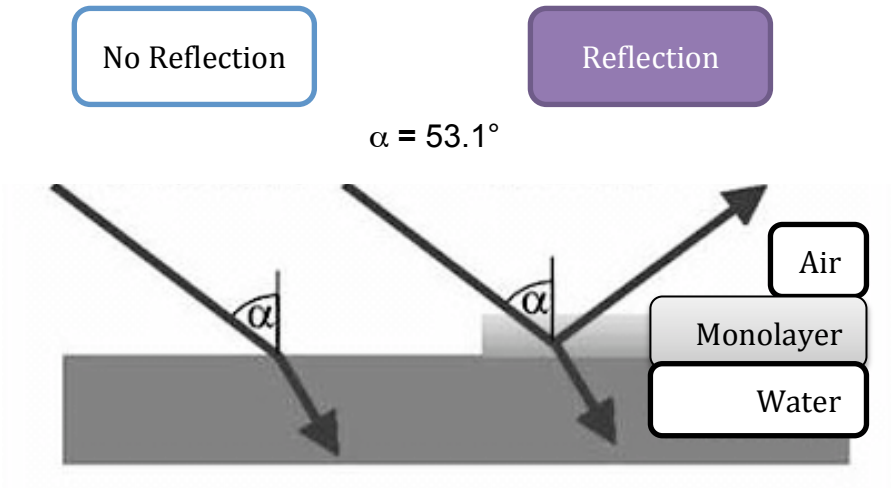

Figure 41. Principle of Brewster Angle Microcopy.

6. Polarization Modulation Infrared Reflection-Absorption Spectroscopy

The first successful application of the IRRAS (infrared reflection absorption spectroscopy technique to the Langmuir monolayers was in 1985 [303]. A major difficulty addressed is the strong signal that arises from the liquid and vapor phases of water, that mask the vibrations of important vibrational groups, as the amide, specially important in the study of proteins and drugs with this chemical group [303]. In this regard, the PM-

IRRAS (polarization modulation infrared reflection absorption spectroscopy) developed by Baldez *et al* was developed [303]. PM-IRRAS is a more sensitive technique due to its combination with a polarization-modulation by means of a photoelastic modulator, which allows to minimize the signal of interferents as the water and carbon oxid [304].

PM-IRRAS is associated with a trough, which must have an adequate size (≥ 6 cm) in order to minimize the meniscus formation. The IRRAS equipment includes an adjustable incident infrared radiation that allows an illumination of the aqueous surface at a wide range of incident angles. The optical path must have a position for a high quality polarizer. Additionally, the entire setup must be enclosed and purged to keep the relative humidity levels low and constant. In addition, the PM-IRRAS uses a polarization modulation technique [303]. This technique is based in the mid-infrared radiation on the monolayers films, being a minor fraction (6%) of the light reflected from the molecular constituents of the surface. The data is generally presented as plots of reflectance–absorbance versus wavenumber. The reflectance-absorbance is defined by the Equation 26 [305]:

$$-\log_{10}(R/R_o) \qquad (26)$$

where R is the reflectivity of the film-covered surface and R_o is the reflectivity of the aqueous subphase. In addition, the incident light in a well-defined polarization state, either parallel (p-polarized) or perpendicular (s-polarized) to the plane of incidence, impinges onto the surface air-water at a previous defined angle of incidence, being the reflected light detected at an angle equal to the angle of incidence [305], which in the experiments of this thesis was set up to 80°.

IRRAS constitute a powerful *in situ* technique to study the interactions of drugs with lipids and proteins at the air-water interface, providing information concerning the changes in the molecular structure and orientation of the monolayer constituents caused by the studied drugs [305-306]. This versatile technique has a broad of application fields, including the determination of the ordered state of the monolayer, which includes the study of the lipid chain conformation and tilt as well as the study of the secondary structure of the proteins [305].

IRRAS measurements provide frequencies and intensities of molecular vibrations. Each chemical group possesses a certain frequency of vibration and for that reason may be identified and characterized (Table 2). Additionally, the frequency of the vibration of some groups is sensitive to the hydration (e.g. phosphate and carbonyl), the conformational order (e.g. methylene) as well as the secondary structure of the proteins (e.g. amide) [305]. The study of the phosphate (PO_2^-) and carbonyl (C=O) groups allows

to understand the interactions of a drug with the polar regions of the monolayer films. The PO_2^- symmetric stretch arises at ~ 1090 cm^{-1}, and is not sensitive to the hydration of the monolayer. The spectral region of 1190-1300 cm^{-1} contains the asymmetric PO_2^- stretching vibration, which is sensitive to the phosphate group hydration (i.e., H-bond formation). A lower wavenumber comprised in this range is indicative of a high hydration degree, being a higher wavenumber indicative of a less hydrated monolayer [305]. The same is also true for the carbonyl group (C=O) comprised in the range of 1710-1740 cm^{-1} [305]. Therefore, a wavenumber near 1740 cm^{-1} corresponds to unhydrated C=0 bonds and 1720 cm^{-1} arising from hydrated C=O bonds [305]. The decrease in the vibrational frequencies of the methylene group (CH_2) is an indication of the increase of the conformational order of the acyl chains present in the monolayer. Therefore, the decrease in the asymmetric CH_2 stretching frequency from approximately 2922.5 to 2917 cm^{-1} with the monolayer compression provides information about the formation of all-trans conformation (characteristic of condensed monolayers) and the loss of gauche conformers (characteristic of expanded monolayers) [305],[307],[308]. The amide I band can give information concerning the secondary structure of the proteins and according to the band position allows the identification of β-turns (1662–1682 cm^{-1}), α-helices (1645–1662 cm^{-1}), and β-sheets (1613–1637 cm^{-1}). If the band appears as two components: one at the β-sheet position and another as a shoulder at 1682–1710 cm^{-1} it is indicative of an antiparallel β-sheet. The parallel β-sheet is predicted to a have higher frequency for the lower component [309-312]. The disorder of the random coils (unstructured) occurs at the same wavenumbers as of the α-helices (1637–1650 cm^{-1}), originating from the former broader and less intense bands compared to the α-helices [310-311],[313]. The amide II (1520-1560 cm^{-1}) is also sensitive to the secondary structure of the proteins, being although less used or used as complementary information since it is less sensitive than the amide I [305]. Other chemical groups may be identified, being the above-mentioned groups the most common and the ones characterized during this thesis. In addition, the positive or negative sign of the bands indicates the orientation of the chemical groups, perpendicular or parallel, respectively with respect to the air/solution interface [314]. Additionally, the existence of identical or nearly identical chemical groups in the drug, lipid or protein may be overcomed by the use of isotope labels [305].

Table 2. Infrared vibration modes used for analysis of IRRAS spectra.

Vibration Mode	Wavenumber (cm^{-1})	Comments
CH_2 symmetric strech	2849-2854	Qualitive indicator of the conformational order
CH_2 asymmetric strech	2916-2924	Qualitive indicator of the conformational order
PO_2^- symmetric strech	~ 1090	
PO_2^- asymmetric strech	1220-1250	Frequency is sensitive to the hydration
C=O (ester) strech	1710-1740	Frequency is sensitive to the hydration
Amide I	1610-1690	Frequency is sensitive to secondary structure
Amide II	1520-1560	Frequency is sensitive to secondary structure

7. UV-Vis Reflection Spectroscopy

The UV-Vis (in the range of 250-700 nm) spectroscopy is an important tool to be applied to the monolayers when the studied drug is a chromophore and absorbs in the UV and/or visible radiation [315]. This technique permits to identify the presence of the drug in the monolayer and its amount during the monolayer compression, because the water subphase does not absorb in this spectral region and therefore does not interfere with the spectral analysis of the monolayer studied [316]. At normal incidence, the reflection increment from the air-water interface due to the presence of a Langmuir film can be given by the Equation 27 [292]:

$$\Delta R = A\,(R_i)^{1/2} + p^2 \qquad (27)$$

where A is the reflectivity of the monolayer, R_i is the reflectivity of the water surface in the absence of the monolayer and p^2 is the absorption of the monolayer. In addition, the shifts of the absorption maximum are correlated with the presence of aggregation at the interface [292].

The UV-Vis spectroscopy was performed in order to confirm the presence of the chromophore RFB at the air-water interface and in addition to quantify its amount during the compression and expansion of the monolayer [317].

8. Computer Simulations

The scientific method has been brought to science in the 17th centuary by Galileo, being further refined by Francis Bacon. Traditionally, the scientific method involves an observation, a formulation of a hypothesis, the test of the hypothesis and the achievement of a conclusion or the refinement of the initial hypothesis. The computer models and simulation studies may be integrated into the scientific method to test ideas before the execution of the experiments or in the other hand, to corroborate the experimental results. Therefore, the computer simulations may be used as an intermediate tool in the scientific method [318].

During this thesis two major computational chemistry softwares were used, namely, HyperChem® and MarvinView from ChemAxon®.

HyperChem® is a versatile molecular modeler and editor that offers many types of molecular and quantum mechanics calculations. Several may be used, as the well known Monte Carlo simulations. In this thesis, was applied the molecular mechanism method to complement the experimental information that pointed to a strong interaction between RFB and the polar head groups of DPPC. The computer simulations pointed to the production of a inclusion complex between the drug RFB and the polar head groups of DPPC phospholipids, which corroborate the experimental results [319].

MarvinView from ChemAxon® is chemical viewer software for single and multiple chemical structures, queries and reactions . In this thesis it was used to predict the pKa, microespecies according to the pH, log *P* and log *D* of RFB and analogs [320].

Chapter IV

Progress Beyond the State-of-the Art

This chapter presents all the manuscripts that this thesis originated, namely:

1 – Liposomes as drug delivery systems for the treatment of TB.

2 – Molecular interaction of Rifabutin on model lung surfactant monolayers.

3 – Interplay of mycolic acids, antimycobacterial compounds and pulmonary surfactant membrane: a biophysical approach to disease.

4 – Differential interactions of rifabutin with human and bacterial membranes: implication for its therapeutic and toxic effects.

5 – Drug-membrane interaction studies applied to *N′*-acetyl-rifabutin.

6 – Effects of a novel antimycobacterial compound on the biophysical properties of a pulmonary surfactant model membrane.

7 – Evaluation of the structure-activity relationship of rifabutin and analogs: a drug-membrane study.

8 – The Influence of Rifabutin on Human and Bacterial Membrane Models: Implications for Its Mechanism of Action.

9 – Interactions of *N′*-acetyl-rifabutin and *N′*-butanoyl-rifabutin with lipid bilayers: A synchrotron X-ray study.

1. Liposomes as drug delivery systems for the treatment of TB.

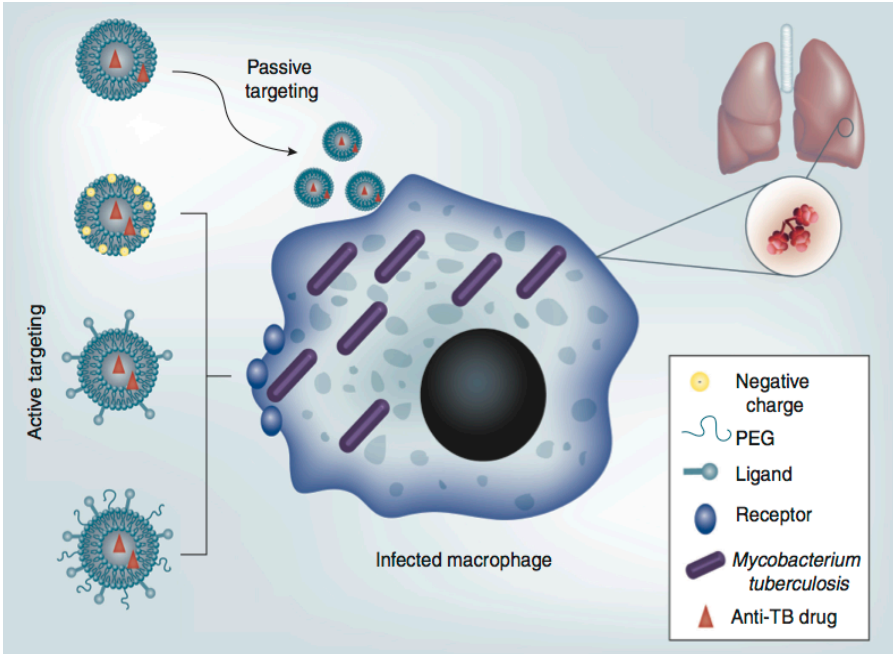

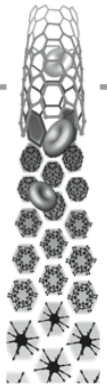

REVIEW

Liposomes as drug delivery systems for the treatment of TB

TB is an infectious disease that is far from being eradicated and controlled. The treatment for TB is associated with noncompliance to therapy because it consists of a long-term treatment with a multidrug combination and is associated with the appearance of several side effects. Liposomal formulations are being developed with first- and second-line antibiotics, and might be an extremely useful alternative to current therapies. This article will thus focus on the role of liposomes as nanodelivery systems for the treatment of TB. Among several advantages, these nanocarriers allow an increase in the bioavailability of antibiotics, which may lead to a reduction in the time of treatment. Results obtained with such nanosystems, although preliminary, are promising and are perspective of the use of inhalation for TB treatment.

KEYWORDS: anti-TB drugs • liposomes • macrophages • nanomedicine • targeting

Marina Pinheiro[1], Marlene Lúcio[1], José LFC Lima[1] & Salette Reis[†1]

[1]REQUIMTE, Departamento de Química, Faculdade de Farmácia, Universidade do Porto Rua Aníbal Cunha, 164, 4099-030 Porto, Portugal
[†]Author for correspondence:
Tel.: +351 222 078 966
Fax: +351 222 004 427
shreis@ff.up.pt

Despite being an ancient disease, TB continues to be a major health concern around the world. In fact, according to the WHO, 9 million cases of active TB emerge annually, resulting in 2 million deaths every year [1,2]. Besides representing a more severe health problem in developing countries, TB has become a renewed threat in the Western world since the mid 1980s. In view of this situation, in 1993 the WHO declared TB as a global public health emergency [3]. In fact, worldwide, it is the second most common infectious disease after HIV [4,5]. Furthermore, there is a relationship between TB and HIV infection that has significantly aggravated morbidity and death in developed and developing nations [3,6]. HIV infection is the highest risk factor identified, so far, for progression of latent TB to an active disease state, with coinfected people having a higher 5–15% risk of early development of active TB [6]. Ultimately, TB represents a major cause of death in HIV coinfected individuals [7].

Pulmonary TB is the most common manifestation of TB and the development of controlled release formulations of anti-TB drugs that are either inhaled or intravenously administrated and directly delivered to the lungs seems a possible approach in the development of novel and more efficient therapeutic alternatives. The intravenous route has particular interest in extrapulmonary TB, whereas the inhalation route is interesting for targeting drugs to the primary organ of pulmonary TB, the lung and can also be used in extrapulmonary TB [8].

Liposomes are nanobiotechnological systems with great potential to be applied in drug delivery for the treatment of TB. Their use increases the therapeutic index of anti-TB drugs, and they are safe and biocompatible. Various properties of these carriers, including size, surface charge, composition and the presence of ligands, significantly alter the specificity to alveolar macrophages. Therefore, liposomes represent appealing nanocarrier systems for anti-TB drugs and possess large potential for the treatment of pulmonary TB [9,10].

This article will focus on the role of liposomes as nanodelivery systems of anti-TB drugs targeting the alveolar macrophages (AMs) by intravenous administration. Particular emphasis will also be given to the inhalation route due to all the advantages it offers in TB treatment.

TB etiology & physiopathology

TB is initiated by the infection of a host with *Mycobacterium tuberculosis* following the inhalation of droplets (aerosols) containing the bacilli. Once in the lung, the bacilli are internalized through phagocytosis by the resident macrophages of the lung – the AMs. Belonging to the mononuclear phagocytic system (MPS), AMs are of extreme importance in lung defense, keeping the alveoli clean and sterile [11]. AMs activated by the appropriate stimuli can effectively transfer the phagocytosed *M. tuberculosis* to the destructive environment of lysosomes. However, some bacilli are able to escape lysosomal delivery and survive and multiply inside AMs [12,13]. Then, the infected AMs can remain in the lung, where the number of pathogens increases exponentially by killing host cells and by spreading through lymphatic circulation to regional lymph nodes.

10.2217/NNM.11.122 © 2011 Future Medicine Ltd

This stage occurs 3–8 weeks after infection and is termed pulmonary TB, for which the lung is the main organ infected, and the MPS, particularly the AMs, are the major targets. Later on (3 months after infection) infected AMs can be disseminated to distant highly irrigated organs (e.g., CNS, spongy bone, liver, kidneys and genitalia) [11,14,15]. At this stage of extrapulmonary TB, acute TB meningitis or disseminated TB can sometimes result in death (FIGURE 1). Finally, extrapulmonary manifestations (e.g., lesion in bones and joints) can appear [16].

The success of *M. tuberculosis* as a pathogen can be attributed to its extraordinary stealth and capacity to adapt to environmental changes throughout the course of infection. These changes include: nutrient deprivation, hypoxia, various exogenous stress conditions and, in the case of the pathogenic species, the intraphagosomal environment. Moreover, *M. tuberculosis* is a bacillus shielded by a unique thick cell wall composed of abundant glycolipids, mycolic acids, cord factor, peptidoglycans, and other carbohydrate, lipid and protein molecules [17]. The mycobacterial cell wall differs from that of most other bacteria and forms a diffusion barrier, which is 100–1000-fold less permeable to hydrophilic molecules than that of *Escherichia coli* [5,18]. Therefore, due to the highly hydrophobic waxy cell wall, bacilli are resistant to digestion by lysosomal enzymes and also resistant to the killing effects of macrophages [19].

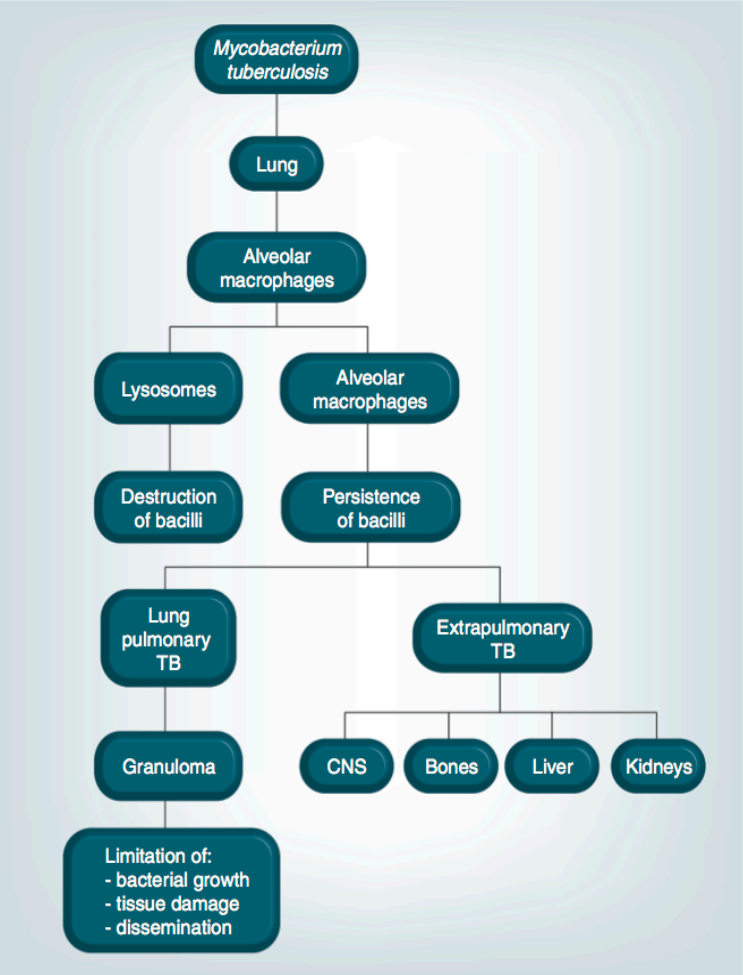

Figure 1. TB etiology and pathophysiology.

The result from the endurance of mycobacterium is the latent TB infection that persists for the lifetime of the host and reactivates with sufficient frequency to maintain a worldwide epidemic [20]. Indeed, disease caused by *M. tuberculosis* is most commonly caused, not by primary infection, but by the reactivation of a latent infection that the patient may have carried for many years [21]. During latency, bacterial growth is controlled and bacteria are confined to granulomas [20,22–24]. Granulomas are classically defined as organized collections of macrophages and lymphocytes that form to circumscribe the toxic environment, which is required to control mycobacteria, such that the delicate alveolar tissue is protected [20,21]. Thus, these cellular accumulations are crucial to limiting not only bacterial growth but also tissue damage and dissemination of the infection from the lungs, two key components of mycobacterial disease [20,21].

While the granuloma is critical for protection against disease, it can also act as a double-edged sword [25]. On the one hand, it isolates infectious organisms, preventing dissemination to peripheral organs; yet on the other hand, within these cellular aggregates, the bacilli do not replicate but remain alive and seem to internalize host lipids [22,24,25].

From the internalization of host lipids results the formation of macrophages with large numbers of lipid-free vacuoles, as well as macrophages filled with lipid-containing bodies, also termed foamy macrophages (FMs). The FMs might thus constitute a reservoir for persisting bacilli within their human host. The presence of FMs, explains not only the kinetics of the drainage of dead bacilli, debris and surfactant, but also how latent bacilli can escape from the granuloma and re-grow in the periphery, particularly in the alveolar spaces where they can disseminate easily [22,24]. In this sense, granulomas also result in localized tissue damage, which may ultimately lead to disease transmission [25].

Classical TB therapy

Clinical management of TB poses several serious questions (FIGURE 2).

The first obstacle is due to the reduction of the efficacy of chemotherapy. This may be attributed to degradation of the drug before reaching the target, the low levels of cell permeability to drugs or primary drug resistance. Other reasons for the failure of chemotherapy may be the difficulty in achieving adequately high drug concentrations at the infection site, inadequate penetration into macrophages, as well as inadequate penetration into the granulomas, which are as stated, reservoirs of latent bacteria in the host alveolar tissue [13,24]. The treatment of mycobacterial infections is also difficult because, as mentioned, mycobacteria are highly resistant intracellular pathogens [26].

The TB treatment requires a long period of chemotherapy (6–9 months) with combinations of agents to minimize the emergence of antimicrobial resistance [24,27]. The necessity of an extended period of treatment is a direct result of the lifecycle of the bacilli, some of which may enter into a 'latent' or 'persistent' phase after the initial infections [28]. Hence, the long period of chemotherapy is first to destroy the population of actively multiplying bacilli that can be found initially, and secondly, to prevent reactivation of any latent bacillus present in granulomas that attempts to multiply. Finally, an option that is not usually considered is that the macrophages themselves, following their normal dynamics, drain the bacilli from granulomas towards the outside. Thus, by reducing inflammation and preventing multiplication of the bacilli, antibiotic treatment is also highly recommendable to prevent the continuous formation of FMs and their accumulation or movement through the alveolar spaces [29].

The most effective pharmacotherapy in TB treatment is a multidrug combination of isoniazid, pyrazinamide and rifampicin. During the initial intensive stage (2 months), these three agents are administered together with ethambutol. The second phase (4 months) comprises exclusively rifampicin and isoniazid. These four drugs, together with streptomycin, make up the so-called first-line therapy. Other drugs (e.g., rifabutin, ethionamide, amikacin, kanamycin A and levofloxacin) have been used in the treatment of TB; however, these are considered as a second-line therapy since these are more toxic, more expensive and less active than first-line agents [12].

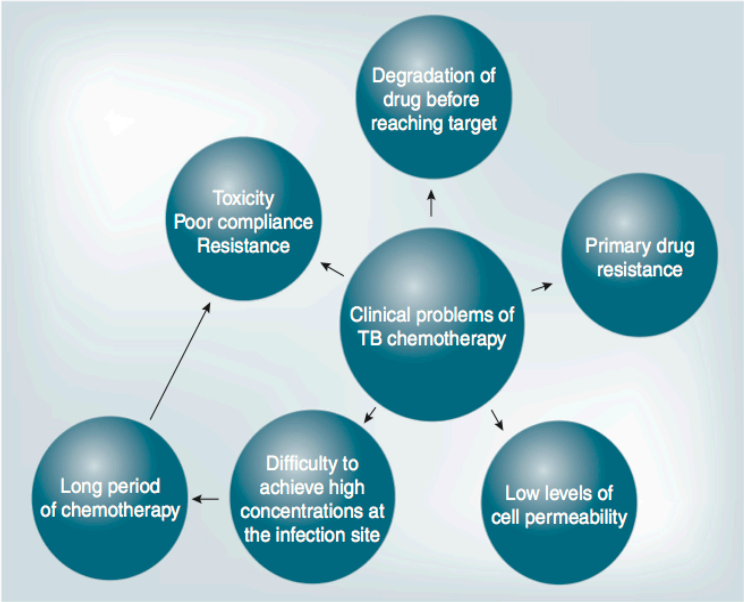

Figure 2. The clinical problems associated with TB chemotherapy.

Besides the abovementioned classical therapeutic regimes, new drugs with interest for TB treatment are being developed and they are presently in different steps of preclinical or clinical trials. This issue is out of the scope of this article, but additional information can be found in the following references [28,30–41].

Although the development of new anti-TB drugs is an obvious approach to fight TB, mechanisms to improve the efficacy of existing drugs can represent a faster strategy. The long and necessary treatment schedules of classical chemotherapy are associated with severe toxic side effects, including hepatotoxicity, and result in poor compliance, one of the main reasons for the emergence of multidrug-resistant pathogens [15,42]. In this regard, improvement of the therapeutic index of existing anti-TB drugs, namely by their encapsulation into nanodelivery systems, should be considered, aiming at maximization of the drug concentration at infected sites, reduction of toxic effects and reduction of treatment duration [15]. Furthermore, the development of nanodelivery systems will provide an opportunity to exploit the inhalatory route, which will be of particular interest in the case of pediatric patients for which most of the first-line drugs are not available [12].

According to the mentioned disadvantages of classical chemotherapy and to the hope that has been put in a nanotherapeutic approach, this article will provide a state of art in the use of liposomes as nanodelivery systems for the treatment of TB.

Liposome-based drug delivery therapy

Liposomes: definition, classification & methods of preparation

Liposomes are self-closed vesicular structures composed of phospholipids that entrap water in their interior. These structures result from self-assembly of the amphiphiles in an aqueous medium forming single or multiple concentric bilayers, where the polar headgroups are in contact with the aqueous media and the fatty acids form the hydrophobic core of the bilayers that are shielded from the water [43].

Liposomes are commonly prepared by hydration of a dry phospholipid film above the main phase transition temperature of the lipid. The diameter of liposomes ranges from 20 nm to several hundreds of nanometers, whereas the thickness of the phospholipid bilayer membrane is approximately 4–7 nm [44]. The classification of liposomes is generally based upon their size and number of lipidic bilayers. Liposomes resultant from the thin film hydration method are multilamellar vesicles (MLVs), which consist of many concentric bilayers in a single particle with diameters that vary between a few hundred to thousands of nanometers. MLVs can be processed by sonication or by extrusion, through a filter, to form unilamellar vesicles (ULVs), which are liposomes with a single membrane bilayer [45–47]. ULVs can be further classified, regarding their size, into small unilamellar vesicles (SUVs) and large unilamellar vesicles (LUVs) [48]. Accordingly, SUVs show a diameter inferior to 100 nm while LUVs present a diameter superior to 100 nm (FIGURE 3) [45,49].

Advantages of the application of liposomes as drug delivery systems

Since their discovery in 1965 by Bangham and coworkers, liposomes have attracted considerable interest owing to their organization and the versatility of their physicochemical properties [43,50]. The discovery of self-assembly phospholipids confirmed earlier studies that claimed that all plasma and intracellular membranes are based on phospholipid bilayers, and encouraged the use of liposomes as the main model systems to study physicochemical and other properties of biological membranes [51]. However, given the chemical dual nature of liposomes, consisting of both hydrophilic and hydrophobic regions, their use has soon expanded from merely membrane mimetic systems to attractive vehicles for both lipophilic and hydrophilic drugs. Hence, the employment of liposomes as nanocarriers for drug delivery started in 1970, only 5 years after their discovery [43,52]. Moreover, liposomes belonged to the first generation of nanocarriers approved by the US FDA (1995) and were used as doxorubicin delivery systems for the treatment of Kaposi's sarcoma related with acquired

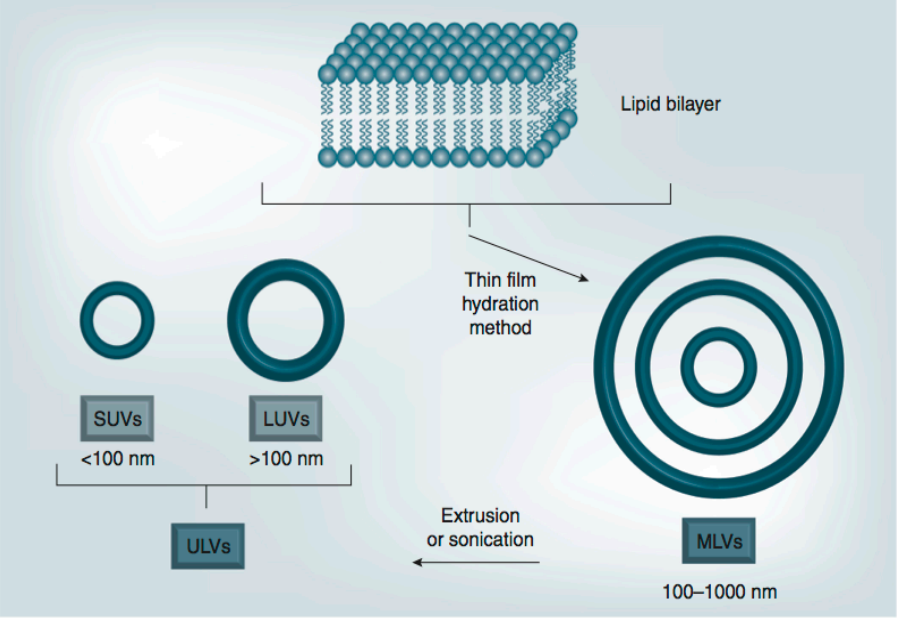

Figure 3. Liposomes of different size and number of lamellae.
SUV: Small unilamellar vesicle; LUV: Large unilamellar vesicle; MLV: Multilamellar vesicle; ULV: Unilamellar vesicle.

immunodeficiency syndrome [53,54]. Currently, liposomes are still among the most widely used nanoparticles as drug delivery systems and the most commonly used as antimicrobial delivery systems [48,55].

Despite the advantages of liposomes, which include being safe and biocompatible, their main drawback as nanocarriers is their instability in plasma [56]. When liposomes reach the blood circulation, selective serum proteins (opsonins) bind to their surface, signaling their presence. This signal is recognized by the MPS that captures liposomes and removes them from the bloodstream. In general, larger liposomes are eliminated from the blood circulation more rapidly than smaller ones and negatively charged liposomes have a shorter half-life in the bloodstream than neutral liposomes, although the contrary has also been reported [57]. However, this apparent limitation of liposomes has been exploited for the efficient delivery of antimicrobial drugs, used to treat infections localized in the MPS, such as TB [13]. Nevertheless, when the target site is beyond the MPS, the use of liposomes that are able to evade from this system is justified to reach longer circulation times. The search for liposomes with longer circulation times has started with the development of certain lipid compositions [58,59] and culminated in the development of polyethylene glycol (PEG) coated, sterically stabilized liposomes (Stealth® liposomes). Although the detailed mechanism of the enhanced stability of Stealth liposomes is not yet fully understood, there is no doubt about the efficacy of PEGs that constitute a steric barrier against the attacks of the MPS [57].

The surface of liposomes can be further decorated by the addition of ligands, such as antibodies and other molecules, which increase specificity of these drug delivery systems to recognize and bind to target cells (see more details in the 'Active targeting description' section) [19,53,60,61]. As a consequence to the increase in the specificity of liposomes for a given target cell, these nanocarriers will suffer preferential accumulation at pathological tissues and will reach lower concentrations in healthy tissues saving them from an eventual toxic effect of the drug carried [56].

In conclusion, there are many potential benefits of choosing liposomes as nanocarriers for drug delivery [51,62,63]. Figure 4 provides a schematic representation of the benefits of using liposomes as drug nanocarriers, in particular as nanocarriers for anti-TB drugs (Figure 4).

Figure 4. Advantages of liposome as drug delivery systems.

Routes of administration of liposomes as drug delivery systems for the treatment of TB

Liposomes can be used as anti-TB nanocarriers for the treatment of both pulmonary and extrapulmonary TB; however, the success of therapy is highly dependent on the administration route of these nanoparticles [64]. Since liposomes are vulnerable to intestinal lipases, their administration needs to be performed by other routes different from the oral route [65]. The intravenous administration for TB treatment is compromised by several factors, such as leakage of liposome contents in the plasma compartment before reaching the target tissue, rapid clearance from the bloodstream and liposome uptake by macrophages of the liver and the spleen [19]. Some authors, such as Gaspar *et al.* have demonstrated that after intravenous administration of liposomes with anti-TB drugs, their preferential accumulation occurs at the liver and spleen, instead of being accumulated at the lung, enabling a feasible approach to extrapulmonary TB treatment [15]. On the other hand, the intravenous administration may be of interest in pulmonary TB control, if the lung specificity is accomplished by the addition of ligands to liposomes [13,66]. Besides the invasive intravenous route, noninvasive routes, such as the inhalatory route, should, however, be considered

given the convenience to the patient and the possibility to administrate antibiotics that will be delivered to the lungs, thus enabling a very attractive approach to pulmonary TB treatment [64,67]. Hence, the inhalatory administration of liposomes as anti-TB drugs nanocarriers can also be explored in the treatment of TB; however, the liposomal size must be tuned, since the area in the respiratory tract for where the deposition of these nanoparticles will occur primarily depends on their size [68]. For 1 nm particles, deposition will primarily occur within the upper airways, including the nose, pharynx and larynx. Optimal deposition into the tracheal and bronchi regions requires the use of 5 nm particles, and 20 nm particles are optimal for deposition into the deeper alveolar regions of the lungs. Particles larger than 15 µm should be avoided as they will be retained in the throat and swallowed [68].

Once inhaled and deposited, liposomes can translocate to extrapulmonary sites and reach other target organs. To accomplish this, they need to cross the epithelia of the respiratory tract into the interstitium, accessing the bloodstream and having a consequent systemic distribution directly or via the lymphatic pathways [9,69,70].

Passive & active targeting of liposomes as drug delivery systems for the treatment of TB

Liposomes can be targeted to specific organs or tissues by passive and active methods (FIGURE 5) [71].

Passive targeting

Passive targeting corresponds to transport in the organism according to the normal distribution pattern of the liposomes that, in this type of targeting, are merely composed of phospholipids or phospholipids and sterols [10]. Passive targeting in pulmonary TB has particular interest when combined with the inhalatory route, since the particles possess an adequate size to access the alveoli and reach the AMs, being phagocytosed if their size is inferior to 5 µm in diameter. This passive targeting is thus possible due to the natural propensity of the macrophages to engulf particles. Passive targeting in extrapulmonary TB is of interest when combined with the intravenous and inhalatory routes. Once in the blood circulation, the liposomes are easily taken up by phagocytic cells of the MPS, finding access to the lysosomes [72,73].

Intravenous administration

The passive targeting strategy has been used in several studies, where the development of liposomes as nanocarriers of anti-TB drugs takes advantage of their natural tendency to reach the AMs. Gaspar *et al.* developed several formulations of liposomes with rifabutin encapsulated. These MLV formulations, after intravenous administration every 3 days over a 2-week period in mice with disseminated TB, were compared against the free drug administrated by the same route. The formulation constituted by lipids with higher phase transition temperatures, namely

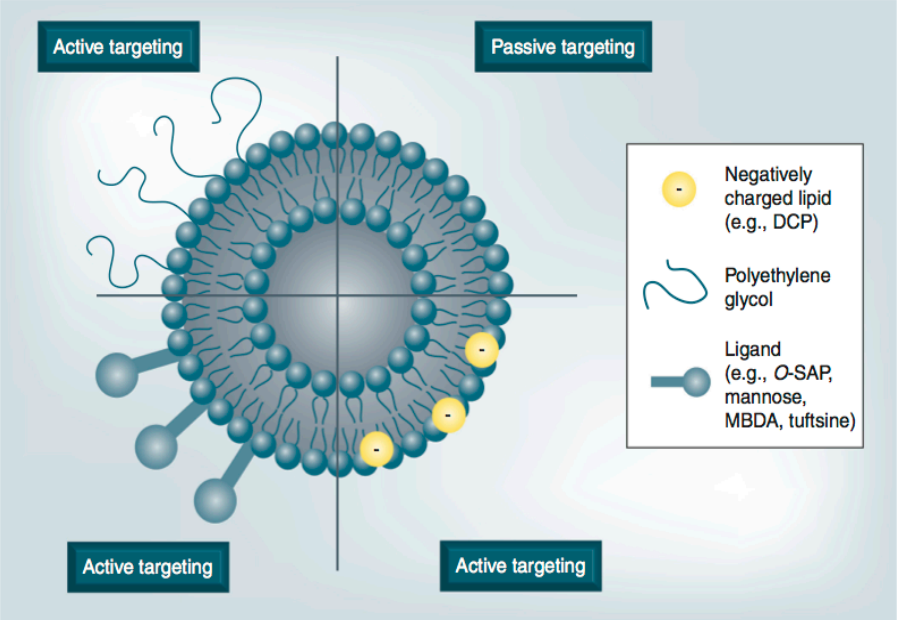

Figure 5. Different types of targeting.

phosphatidylcholine (PC)/dipalmitoylphosphatidylglycerol (DPPG; 7:3 molar ratio), turned out to be the most effective. As expected, the levels of drug in the lungs were lower than that observed for either liver or spleen. As such, this formulation seems interesting mainly for extrapulmonary TB treatment, particularly in patients coinfected with HIV/TB, as the combination of highly active antiretroviral therapy with rifampicin has been described to lead to subtherapeutic concentration of antiretroviral drugs. Indeed, the induction effect of cytochrome P450–3A is weaker with rifabutin than with rifampicin, allowing it to be an alternative due to the minimization of the interaction with the antiretroviral drugs (TABLE 1) [15,28].

Using a passive targeting strategy also, amikacin was encapsulated with great efficacy by Dhillon *et al.* into SUVs made of PC/cholesterol(Chol)/distearoylphosphatidylglycerol (DSPG; 2:1:0.1 molar ratio). The formulation was intravenously administered for 3 days a week over 4 weeks in mice with disseminated TB and the efficacy of the formulation was evaluated by colony-forming unit (CFU) counts in lungs and spleen. The results showed an increased activity against *M. tuberculosis* and higher half-life time towards the free drug, sustaining the possibility that the formulation developed will lead to a reduction in the administration frequency of anti-TB drugs [74].

In a study developed by El-Ridy *et al.* a formulation of MLVs made of dipalmitoylphosphatidylcholine(DPPC)/Chol (7:2 molar ratio) with incorporation of pirazinamide was administrated via the intravenous route in mice with disseminated TB. Efficacy was evidenced when administrated 2 days a week in a total of seven treatment doses, reducing the *M. tuberculosis* bacilli numbers in the lungs to lower levels than the free drug administrated with the same frequency (however, the levels were higher than the free drug administrated 6 days/week). In this work, a more favorable histopathologic examination of the lung was also established, compared with the free drug liposome (but less favorable than the free drug administered for 6 days/week). Results have shown that the drug-encapsulated liposomes were more effective than the free drug [72].

Inhalatory administration

A liposome-based formulation of encapsulated rifampicin and isoniazid was developed by Pandey *et al.* This formulation consisted in MLVs composed of PC/Chol (2:1.5 molar ratio) and was tested in guinea pigs via the inhalation route. Results have shown that both drugs were present in the lungs as well as in the AMs until day 5 postnebulization, and that a single nebulization of liposomal drugs could maintain therapeutic drug levels in the plasma 45 min onwards for up to 48 h (against unencapsulated drugs that were cleared after 24 h). Hence, the results obtained by this group suggest a possible reduction of the daily administration frequency of the two first-line anti-TB drugs [75].

Active targeting

In active targeting, the normal distribution patterns are modified through changes in liposome structure and composition [10]. These changes involve the use of charged lipids or the attachment of a ligand (including proteins, peptides, polysaccharides, glycolipids, glycoproteins and monoclonal antibodies) to deliver the drug to pathologic sites or to cross biological barriers based on molecular recognition processes. In addition, the already mentioned process of liposomal surface coating with PEG is also part of the active targeting strategies, prolonging the half-life of the developed liposome-based formulations (FIGURE 6) [19,76].

The modification of the liposomal surface by incorporating negatively charged lipids (e.g., by dicetylphosphate [DCP] incorporation), seems to increase the AM affinity to capture anionic liposomes via scavenger receptors. These receptors do not seem to have mechanisms of ligand-induced downregulation and exhibit rapid clearance of the ligand-bound drug from the extracellular medium to the macrophage phagolysosome [19].

The ligand-anchored liposomes are also an effective and fast way to deliver a high drug concentration to lungs with a high AM population. The AM-specific ligands are maleylated bovine serum albumin (MBSA) and *O*-steroyl amylopectin (*O*-SAP). While MBSA shows specific affinity for macrophages scavenger receptors, the *O*-SAP ligand has greater affinity towards AM, having already been identified to selectively uptake *O*-SAP-coated liposomes [19,61].

The tetrapeptide tuftsin (Thr-Lys-Pro-Arg) is another example of a liposome ligand used as a natural macrophage activator. This peptide is part of the leukophilic IgG (residues 289–292) and binds specifically to macrophages, monocytes and polymorphonuclear leukocytes. As a result, tuftsin possesses a broad spectrum of activities primarily related to the immune system function, which includes potentiation of

Table 1. Liposomes for anti-TB delivery.

Drug(s)	Liposome type and composition	Type of targeting	Animal model (route of administration)	Therapeutic effect and toxicity	Conclusion	Ref.
Rifabutin	MLVs PC/DPPG	Passive	Mice (intravenously)	Significant reduction of bacilli present at the spleen and liver compared with the free drug group; no significant differences were observed in the lungs	Good approach for extrapulmonary TB. Could be a good approach for pulmonary TB through inhalatory administration	[15]
Amikacin	SUVs PC/Chol/DSPG	Passive	Mice (intravenously)	Increased activity against *Mycobacterium tuberculosis* and improved half-life of the drug encapsulated liposomes compared with the free drug ones	Reduction in frequency of administration	[74]
Pyrazinamide	MLVs DPPC/Chol	Passive	Mice (intravenously)	Increased efficiency compared with free drug: increased reduction in *M. tuberculosis* bacilli in the lungs; more effective histopathological examination	High therapeutic efficacy of pyrazinamide liposomes	[72]
Rifampicin and Isoniazid	MLVs PC/Chol	Passive	Guinea pigs (inhalatory)	Increased therapeutic drug levels in plasma with a single dose; drugs are present in the lungs and AMs	Reduction in frequency of administration	[75]
Rifampicin and Isoniazid	MLVs PC/Chol/*O*-SAP/ DCP/DSPC-PEG 2000	Active (*O*-SAP, PEG and DCP)	Mice (intravenously)	Superior efficacy of the formulation: increased reduction of the liver, kidneys and lungs CFUs and normal lung weight; hepatotoxicity reduction and normal lung morphology, compared with the free drugs	Less toxic and more effective formulation than the free drugs	[13,66]
Rifampicin and Isoniazid	MLVs PC/Chol/DCP/ DSPE-PEG 2000 and *O*-SAP	Active (*O*-SAP, PEG and DCP)	Mice (intravenously)	Superior efficacy of the formulation: reduction of the bacilli at the lungs, liver and spleen; no toxic effects found at the liver; maintenance of bilirubin, serum alanine transaminase and alkaline phosphatase levels	More effective and nonhepatotoxic formulation than the free drugs	[78]
Rifampicin	MLVs PC/Chol and *O*-SAP, MBSA or DCP	Active (*O*-SAP, MBSA or DCP)	Rats (inhalatory)	Formulations that carry ligands (*O*-SAP, MBSA) or DCP showed a preferential lung accumulation	The inhalatory route is liable in pulmonary TB having the AM as a target	[19]
Rifampicin	SUVs PC and tuftsin	Active (tuftsin)	Mice (intravenously)	Increased efficiency compared to free drug and control formulation without tuftsin: lung bacillus load and lung weight were significantly reduced	More effective formulation than the free drug and liposomes loaded with rifampicin	[60]
Not shown	MLVs Man-LIPO	Active (mannose)	Rats (inhalatory)	More efficiently delivered to AMs after pulmonary aerosolization; the formulation did not harm lung tissues	Man-LIPO are useful for efficient aerosolized liposomal delivery to AMs	[79]
Not shown	LUVs Man-LIPO	Active (mannose)	Rats (intratracheally)	Significantly high internalization and selective targeting to AMs *in vivo* for the liposomes with higher percentage of mannose	Efficient targeting to AMs	[80]

AM: Alveolar macrophage; CFU: Colony-forming unit; Chol: Cholesterol; DCP: Dicetylphosphate; DPPC: Dipalmitoylphosphatidylcholine; DPPG: Dipalmitoylphosphatidylglycerol; DSPC: Distearoyloglycerophosphatidylcholine; DSPE: Distearoylphosphatidylethanolamine; DSPG: Distearoylphosphatidylglycerol; LUV: Large unilamellar vesicle; Man-LIPO: Mannosylated liposomes; MBSA: Maleylated bovine serum albumin; MLV: Multilamellar vesicle; O-SAP: O-steroyl amylopectin; PC: Phosphatidylcholine; PEG: Polyethylene glycol; SUV: Small unilamellar vesicle.

Table 1. Liposomes for anti-TB delivery (cont.).

Drug(s)	Liposome type and composition	Type of targeting	Animal model (route of administration)	Therapeutic effect and toxicity	Conclusion	Ref.
Rifampicin	MLVs DSPC/Chol	Not shown	*In vitro* (A549 cells)	Inferior toxicity compared with the free drug	Less toxic formulation to alveolar epithelial cell line comparing to the free drug	[81]
Isoniazid and Pyrazinamid	MLVs PC/Chol	Not shown	Not shown	Not shown	Formulation with a satisfactory drug loading (isoniazid, pyrazinamide)	[9]
Amikacin	MLVs PC/DCP/Chol	Not shown	Not shown	Not shown	The negatively charged MLVs exhibited efficacy for amikacin encapsulation	[82]

AM: Alveolar macrophage; CFU: Colony-forming unit; Chol: Cholesterol; DCP: Dicetylphosphate; DPPC: Dipalmitoylphosphatidylcholine; DPPG: Dipalmitoylphosphatidylglycerol; DSPC: Distearoyloglycerophosphatidylcholine; DSPE: Distearoylphosphatidylethanolamine; DSPG: Distearoylphosphatidylglycerol; LUV: Large unilamellar vesicle; Man-LIPO: Mannosylated liposomes; MBSA: Maleylated bovine serum albumin; MLV: Multilamellar vesicle; O-SAP: O-steroyl amylopectin; PC: Phosphatidylcholine; PEG: Polyethylene glycol; SUV: Small unilamellar vesicle.

phagocytosis, immunogenic response and bactericidal activity. Grafting of tuftsin on the liposome surface provides specific transport to the macrophage and stimulates the nonspecific cells against infections [6].

Moreover, the mannose receptors are highly expressed in cells of the immune system, such as macrophages. Hence, there is a great potential of mannose-targeted drug delivery systems for the treatment of macrophage-related diseases. Therefore, the treatment of pulmonary TB can also benefit from the use of mannose ligands in liposomes constituting the so-called mannosylated liposomes (Man-LIPO) [77].

Intravenous administration

Deol *et al.* demonstrated that coencapsulation of isoniazid and rifampicin is possible in lung-specific stealth liposomes (MLVs) containing PC, Chol, *O*-SAP, DCP and distearoylphosphatidylethanolamine-PEG 2000 (DSPE-PEG 2000). The formulation given intravenously, twice a week for 6 weeks, showed 40% accumulation in the lungs of normal and tuberculous mice. Therefore, the active targeting strategy achieved by the use of PEG 2000, *O*-SAP and DCP has proved to be successful in prolonging the blood circulation time, reducing the opsonization by avoiding the preferential accumulation at the liver and spleen macrophages, and preferentially accumulating at the lungs. The two drugs encapsulated in these stealth liposomes have also proved to be less toxic, manifesting a hepatotoxicity reduction, as the total bilirubin and hepatic enzymes (serum glutamic pyruvic transaminase and alkaline phosphatase) levels were significantly lower when compared with the free drug. The efficacy of the formulation also proved to be superior, compared to the free drugs, since it exhibited normal lung morphology, an increased reduction of liver, kidney and lung CFUs, and also a reduction in organ weight when compared with the free drugs [13,66].

Labana *et al.* developed MLVs made of PC, Chol, DCP and DSPE-PEG 2000 (2:1.5:0.2:0.2 molar ratio) containing an active targeting ligand *O*-SAP. The formulation encapsulating rifampicin and isoniazid was administered once a week for 6 weeks and its efficacy evaluated by CFU counting. A significant reduction in the number of bacilli was observed at the lungs, liver and spleen, when compared with the free drugs. The formulation also exhibited a sustained drug release for over 120 h, comparing with the 10 h observed for the free drugs. The liposomal formulation developed reduced the daily administration to only once a week. In addition, the formulation did not cause toxic effects to the liver, as proven by the bilirubin, alanine transaminase and alkaline phosphatase seric levels [78].

Inhalatory administration

Rifampicin loaded liposomes containing ligands (*O*-SAP and MBSA) and negatively charged lipids were conceived by Vyas *et al.* to directly target an aerosol formulation to the infected AMs. The developed formulations consisted of MLVs of PC/Chol (7:3 molar ratio) coated with AM-specific ligands, MBSA or *O*-SAP, in a 5:1 weight ratio of lipid: ligand. The negatively charged formulation was developed by DCP incorporation at a 0.1:10 molar ratio regarding the total lipids. The two ligand formulations had shown a higher accumulation in rat lungs, compared with the control formulation (PC/Chol 7:3 molar ratio) and with the negatively charged formulation. This latter formulation

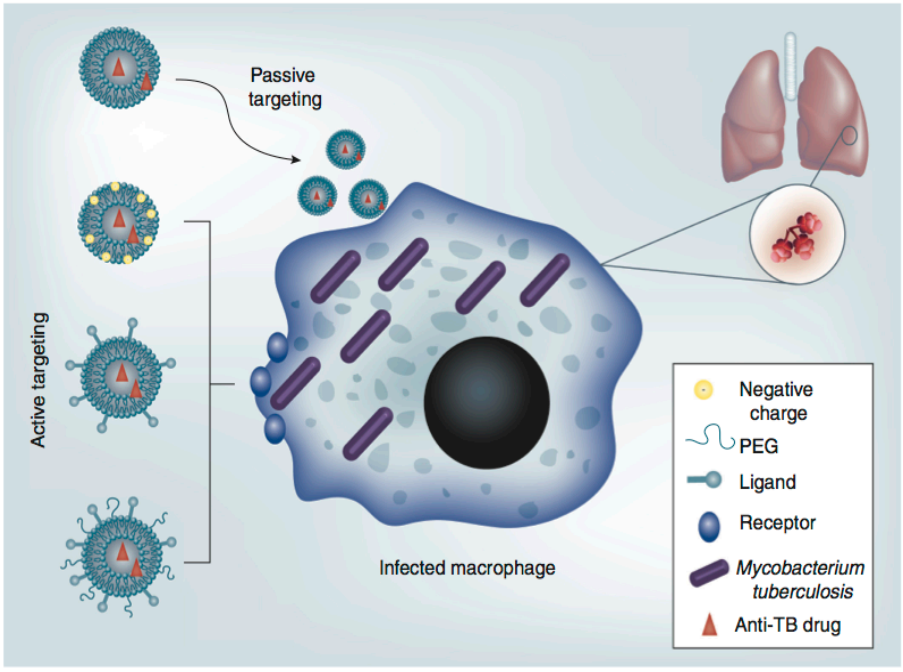

Figure 6. Liposomes as drug delivery systems to alveolar macrophage.
PEG: Polyethylene glycol.

has shown higher lung accumulation than the control. In comparison to the treatment with free drug, the developed formulations were able to maintain a higher drug concentration for a prolonged period of time, and the best results were obtained with the formulations containing ligands. Although this work has not been focused on the *M. tuberculosis* infection eradication, the results are interesting since they proved that an aerosol formulation is capable of efficiently targeting the AMs, opening a way to further explore this approach in the treatment of pulmonary TB [19].

In 1994 Agarwal *et al.* developed a tuftsin-bearing liposome formulation for the encapsulation of rifampicin. The efficacy of this formulation, consisting of SUVs of PC and tuftsin, was evaluated on mice, by intravenous administration twice a week for 2 weeks. Results have shown that the developed formulation was at least 2000-times more effective at lowering the load of lung bacilli in TB-infected mice than the free drug. Moreover, the developed tuftsin-bearing liposome formulation exhibited higher efficacy given the reduced CFU counting in lung, spleen and liver compared with free drug and to drug-loaded liposomes without tuftsin [60].

Other authors, such as Chono *et al.* and Wijagkanalan *et al.*, studied the efficiency of Man-LIPO in rats by inhalatory and intratracheal routes, respectively. Both formulations were more efficiently delivered to AMs than the liposomes without mannose [79,80].

Additional liposomal formulations with interest in TB

In some other studies, formulations of anti-TB drugs were effectively incorporated into liposomes; however, *in vivo* studies about their efficacy and toxicity are still lacking. Nevertheless, they shall be mentioned in this article since they may be an advantageous tool in TB treatment. Several MLV formulations made of PC, DPPC or DSPC with or without Chol, were developed by Zaru *et al.* The formulation composed of DSPC/Chol at a 2:1 molar ratio presented a good encapsulation efficacy of rifampicin, the highest nebulization efficiency, and membrane integrity after the use of a cryoprotectant. The toxicity and mucoadhesive properties of this formulation were further tested in A549 cell lines (representative of the alveolar epithelia), and were revealed to have less toxicity compared with the free drug; however, the developed formulation presented reduced mucoadhesive properties (compared with chitosan particles). This later observation constituted a shortcoming aspect of the developed formulation since the mucoadhesive properties are of extreme importance to promote retention and to slow down the drug release *in situ* [81].

Justo *et al.* proposed a formulation to be administrated by inhalation of LUVs made of PC/Chol (6:4 molar ratio) with several anti-TB drugs incorporated. This formulation showed a satisfactory drug loading for isoniazid and pyrazinamid, but the incorporation of ethionamide, streptomycin and rifampicin was not successful [9].

Ravaoarinoro *et al.* developed MLVs and SUV formulations aiming the encapsulation of a second-line anti-TB drug, amikacin. Results obtained indicate that the negatively charged MLV formulation made of PC/DCP/Chol was better in terms of encapsulation efficiency [82].

The described examples of liposomes as nanocarriers for the delivery of anti-TB drugs using passive and active targeting, as well as some anti-TB drugs efficiently incorporated in liposomes, are summarized in TABLE 1. The table also includes two examples of active targeting strategy applied to liposomes where mannose was included as a ligand. These studies are worth mentioning because even though the formulations developed were drug-free, they still can, in future works, be used to carry anti-TB drugs.

Many of the formulations presented are very similar to others that reach the market with regard to the size of the liposome and its constitution. However, the active strategies used in these formulations are specifically indicated for accumulation in the lung, thus being adequate for pulmonary TB treatment [83].

Liposomal formulations with immunostimulatory activity

As mentioned before, the treatment of latent TB infection requires a long period of chemotherapy, which makes treatment compliance extremely difficult. Current knowledge of latent bacilli and of the lesions with which they are associated suggests that these bacilli survive in granulomas with a central necrotic core and an outermost layer of FMs that represent an important immunosuppressive barrier [24]. According to this, it is of particular interest to undertake an immunotherapy treatment following chemotherapy in order to prevent reactivation of the bacillus as a consequence of the presence of latent bacilli in the tissues (after undertaking short-course chemotherapy) and the induction of local specific immunodepression. In this context the use of cationic liposomes to deliver synthetic analogs of mycolic acids represents a promising new strategy for exploiting the immunostimulatory activity of components derived from the mycobacterial cell wall without the associated toxicity issues observed with complex mycobacterial preparations [84,85].

Following the same reasoning of providing immunostimulation, liposomes as delivery systems have also shown interest in the development of vaccines designed for the treatment and prevention of TB. RUTI is a vaccine with fragmented *M. tuberculosis* cells delivered in liposomes with demonstrated efficacy in TB treatment following chemotherapy in experimental models of mice and guinea pigs [24,29,86]. Furthermore, vaccines with cytokines, IL-2, granulocyte macrophage-colony stimulating factor, tumor necrosis factor and vaccines with antigens from plasmid DNA can be very useful to elicit humoral and cellular immune responses, essential for TB protection. DNA vaccine combination expressing mycobacterial heat shock protein 65 (HSP 65) and IL-12 by using the hemagglutinating virus of Japan (HVJ) and tuberculosis subunit vaccine, Ag85B-ESAT-6/CAF01 (where ESAT-6 is early secreted antigenic target of 6 kDa and CAF01 is cationic adjuvant formulation 01) are examples of a vaccine liposomal-based technology with results that show a strong possibility to be a very promising candidate for a new TB DNA vaccine with interest in humans [87–90].

Conclusion

The high mortality and morbidity in pulmonary TB and the emergence of drug-resistant mycobacterial infection are extremely concerning. A more efficient treatment and a significant reduction of the treatment duration are urgently needed. Unfortunately, no new anti-TB agents have been introduced in the past 40 years. There are potential anti-TB drugs in various stages of development with the expectation that they will offer treatment options against TB and multidrug-resistant TB, but they need to be approved before reaching the market, and this can take several years [91].

Nanotechnology offers great opportunities to improve the treatment of several diseases, including TB. In this sense, a major step forward would be the development of targeted drug delivery systems that are capable of improving the effectiveness of existing medicines. Thus, treatment of TB can be revolutionized through the development of new therapeutic strategies, including the design of anti-TB carriers, such as liposomes, which are one of the most popular and successful drug delivery systems currently used to increase the effectiveness of antibiotics [12,92].

Liposomes are already beginning to make a big impact in chemotherapy, since the toxicity of drugs encapsulated in these nanocarriers is reduced as a consequence of preferential accumulation at target sites and lower concentrations in healthy tissues. Besides the success of liposomes in chemotherapy, their use seems to be able to increase efficiency of treatment and to diminish the toxicity of conventional anti-TB drugs. Furthermore, liposomes also have the advantage of being biocompatible, since it is possible to use endogenous compounds (such as the constituents of lung surfactant) in their preparation [47,75]. Furthermore, liposomes offer great flexibility to be modified and adapted against several pathological conditions, particularly in the case of TB for which the inclusion of ligands at the liposomal surface will enhance targeting to the major organ of this pathology, the lung. Liposome composition can also be tuned to select the most favorable route of administration. For instance, in the case of pulmonary TB, the use of inhalation instead of the intravenous route would certainly enhance patients' compliance to therapy, a major factor for withdrawal of treatment and emergence of resistance. Moreover, the inhalatory administration of liposomes loaded with anti-TB drugs has the advantage to: achieve high local concentrations of drugs in AMs; reduce the adverse systemic effects, as well as to reduce the frequency of administration [2,93–98]. The intravenous administration is considered to be an invasive route as it requires health-care assistance [99]. However, this route can be a reliable alternative when the other routes are committed as in the case of multidrug-resistant TB. Furthermore, the association of this route with drug delivery systems has provided a reduction in treatment duration.

In conclusion, the use of liposomes as anti-TB nanocarriers has a great potential for the treatment of TB that needs to be further explored to reach high efficiency through alternative routes of administration, such as inhalation.

Future perspective

A concerning fact in the treatment of TB antibiotic-sensitive strains is the significant lower cure rate owing to a nonadherence to therapy, mostly motivated by the combination of several drugs and their long intake period (6–9 months). The

Executive summary

TB etiology, physiopathology & current therapies

- TB is the second most prevalent infectious disease after HIV, with which it is strongly associated. It accounts for a large number of worldwide deaths, but especially in developing countries.
- Two of the major problems associated with TB, and which are closely related, are the lack of adherence to therapy and the emergence of multidrug-resistant strains to antibiotics.
- No new anti-TB agents have been introduced in the market, thus it is urgent to improve the existent drugs to reduce the duration of treatment and promote adherence to therapy.

Liposome-based drug delivery therapy

- The use of liposomes as drug delivery systems increases protection against degradation of anti-TB drugs, allowing the coencapsulation of hydrophilic and hydrophobic drugs in the same formulation, as well as the increase in the therapeutic index of drugs. Furthermore, liposomes are biocompatible, which is of extreme importance concerning their use in clinical practice.

Routes of administration that can be exploited in the treatment of TB having the alveolar macrophage as the drug target

- The intravenous route using liposomes with anti-TB drugs is useful in the treatment of extrapulmonary TB. For the treatment of pulmonary TB using the same route of administration, it is necessary to add ligands to liposomes in order to enhance the selectivity for alveolar macrophages.
- Inhalation is the most promising route for the treatment of TB. It is a noninvasive route and can be useful for both pulmonary TB and extrapulmonary TB.

Passive & active targeting of liposomes used in the treatment of TB

- The passive targeting is useful in pulmonary TB if the formulations are administered by inhalation. It is also interesting in extrapulmonary TB if the formulations are administered intravenously or by inhalation.
- The active targeting improves the specificity and selectivity for the target in pulmonary TB. The addition of ligands to liposomes increases the concentration of drug that reaches the alveolar macrophage, where the etiologic agent of TB is housed. It may be a useful approach by inhalation and an essential approach by intravenous administration, as this allows a reduction in uptake by macrophages of the liver and spleen.

Liposomal formulations with immunostimulatory activity

- Therapeutic vaccines made of detoxified, fragmented *Mycobacterium tuberculosis* cells (e.g., RUTI) delivered in liposomes were developed to reduce the period of chemotherapy. The rationale of this therapy is first to take advantage of the bactericidal properties of chemotherapy to kill active growing bacilli, eliminate the outermost layer of foamy macrophages and reduce local inflammatory responses so as to avoid the predictable reaction phenomenon caused by *M. tuberculosis* antigens when given therapeutically. After chemotherapy, vaccines can be used for inoculation to reduce the probability of regrowth of the remaining latent bacilli.

investment in the search for new drugs for TB is increasing, with 11 candidates currently in clinical trials. It is estimated that over the next 5 years two of them may be marketed. In the near future, a large investment in nanotechnology and the development of drug delivery systems to increase the therapeutic index of several drugs is also expected to occur. Besides all the advantages demonstrated as drug nanocarriers, liposomes, as drug delivery systems of the existing anti-TB drugs and the upcoming ones, add the possibility of exploring the inhalatory route of administration. This route has the potential to reduce the duration of TB treatment, to increase therapy compliance and to reduce the administration of more than one anti-TB drug to a single formulation. Moreover, although the use of liposomes as anti-TB drug delivery systems does not guarantee the absence of resistance, it will certainly decrease the probability of their appearance. Indeed, liposomes are able to increase therapy adherence and compliance (due to more efficient treatments applied in shorter periods). Consequently, less antibiotic resistance will occur. If liposomes are able to increase adherence to therapy (due to more efficient treatments that are more effective in shorter periods), then they are also able to decrease resistance. Finally, liposomes have provided the development of therapeutic vaccines made from detoxified fragments of *M. tuberculosis*. These vaccines are expected to reduce the period of chemotherapy by preventing reactivation of the latent bacillus present in granulomas. With this approach, it is expected that in the future patients must complete a short stage of chemotherapy, of no more than a month, and then be vaccinated in order to destroy the latent bacilli that they carry.

Overall, the combined strategy of using liposomes as more efficient anti-TB drug delivery systems and as immunostimulators could instigate the objectives of the WHO for 2015, which are the dramatic reduction of the prevalence of TB and the number of deaths, as well as a shortening of treatment to 1–2 months.

Financial & competing interests disclosure

M Pinheiro thanks FCT (Lisbon) for the fellowship (SFRH/BD/63318/2009). The authors have no other relevant affiliations or financial involvement with any organization or entity with a financial interest in or financial conflict with the subject matter or materials discussed in the manuscript apart from those disclosed.

No writing assistance was utilized in the production of this manuscript.

Bibliography

Papers of special note have been highlighted as:
- ▪ of interest
- ▪▪ of considerable interest

1 Sutherland JS, de Jong BC, Jeffries DJ, Adetifa IM, Ota MO. Production of TNF-α, IL-12(p40) and IL-17 can discriminate between active TB disease and latent infection in a west African cohort. *PLoS ONE* 5(8), E12365 (2010).

2 Hall G, Leff D, Gumbo T. Treatment of active pulmonary tuberculosis in adults: current standards and recent advances. Insights from the Society of Infectious Diseases Pharmacists. *Pharmacotherapy* 29, 1468–1481 (2009).

3 Raviglione MC, Snider DE Jr, Kochi A. Global epidemiology of tuberculosis. Morbidity and mortality of a worldwide epidemic. *JAMA* 273, 220–226 (1995).

4 Tiwari RP, Tiwari D, Garg SK, Chandra R, Bisen PS. Glycolipids of *Mycobacterium tuberculosis* strain H37Rv are potencial serological markers for diagnosis of active tuberculosis. *Clin. Diagn. Lab. Immunol.* 12, 465–473 (2005).

5 Chimote G, Banerjee R. Evaluation of antitubercular drug-loaded surfactants as inhalable drug-delivery systems for pulmonary tuberculosis. *J. Biomed. Mater. Res. A.* 89, 281–292 (2009).

6 Agrawal AK, Gupta CM. Tuftsin-bearing liposomes in treatment of macrophage-based infections. *Adv. Drug Deliver. Rev.* 41, 135–146 (2000).

7 Thanyani ST, Roberts V, Siko DGR, Vrey P, Verschoor JA. A novel application of affinity biosensor technology to detect antibodies to mycolic acid in tuberculosis patients. *J. Immunol. Methods.* 332, 61–72 (2008).

8 Kurmi BD, Kayat J, Gajbhiye V, Tekade RK, Jain NK. Micro- and nanocarrier-mediated lung targeting. *Expert Opin. Drug Deliv.* 7, 781–794 (2010).

9 Justo OR, Moraes AM. Incorporation of antibiotics in liposomes designed for tuberculosis therapy by inhalation. *Drug Deliv.* 10, 201–207 (2003).

10 Santos N, Castanho M. Liposomes: has the magic bullet hit the target? *Quim. Nova.* 25, 1181–1185 (2002).

11 Bowden DH. The alveolar macrophage. *Environ. Health Persp.* 55, 327–341 (1984).

12 Sosnik A, Carcaboso AM, Glisoni RJ, Moretton MA, Chiappetta D. New old challenges in tuberculosis: potentially effective nanotechnologies in drug delivery. *Adv. Drug Deliver. Rev.* 62, 547–559 (2010).

13 Deol P, Khuller G, Joshi K. Therapeutic efficacies of isoniazid and rifampin encapsulated in lung-specific stealth liposomes against *Mycobacterium tuberculosis* infection induced in mice. *Antimicrob. Agents Chemother.* 41(6), 1211–1214 (1997).

14 Pieters J. *Mycobacterium tuberculosis* and the macrophage: maintaining a balance. *Cell Host Microbe* 3, 399–407 (2008).

15 Gaspar MM, Cruz A, Penha AF *et al.* Rifabutin encapsulated in liposomes exhibits increased therapeutic activity in a model of disseminated tuberculosis. *Int. J. Antimicrob. Agents* 31, 37–45 (2008).

▪▪ **Good example of a liposome formulation with anti-TB drugs developed to the extrapulmonary TB using the passive targeting and administrated by the intravenous route.**

16 Krishnan N, Robertson BD, Thwaites G. The mechanisms and consequences of the extra-pulmonary dissemination of *Mycobacterium tuberculosis*. *Tuberculosis* 90, 361–366 (2010).

17 Kaufmann SHE. Tuberculosis: back on commentary the immunologists' agenda. *Immunity* 24, 351–357 (2006).

18 Kartmann B, Stenger S, Niederweis M. Porins in the cell wall of *Mycobacterium tuberculosis*. *J. Bacteriol.* 181, 6543–6546 (1999).

19 Vyas SP, Kannan ME, Jain S, Mishra V, Singh P. Design of liposomal aerosols for improved delivery of rifampicin to alveolar macrophages. *Int. J. Pharm.* 269, 37–49 (2004).

▪▪ **Good example of a liposome formulation with anti-TB drugs developed to pulmonary TB using active targeting and administrated by the inhalatory route.**

20 Bold TD, Ernst JD. Who benefits from granulomas, mycobacteria or host? *Cell* 136, 17–19 (2009).

21 Saunders BM, Cooper AM. Restraining mycobacteria: role of granulomas in mycobacterial infections. *Immunol. Cell Biology* 78, 334–341 (2000).

22 Peyron P, Vaubourgeix J, Poquet Y *et al.* Foamy macrophages from tuberculous patients' granulomas constitute a nutrient-rich reservoir for *M. tuberculosis* persistence. *PLoS Pathog.* 4, e1000204 (2008).

23 Co DO, Hogan LH, Kim SI, Sandor M. Mycobacterial granulomas: keys to a long-lasting host-pathogen relationship. *Clin. Immunol.* 113, 130–136 (2004).

24 Cardona PJ. RUTI: a new chance to shorten the treatment of latent tuberculosis infection. *Tuberculosis* 86, 273–289 (2006).

▪▪ **Describes a liposome-based vaccine as a new chance to shorten the treatment of latent TB infection.**

25 Guidry TV, Hunter RL Jr, Actor JK. Mycobacterial glycolipid trehalose 6,6′-dimycolate-induced hypersensitive granulomas: contribution of CD4+ lymphocytes. *Microbiology* 153, 3360–3369 (2007).

26 Sundaramurthy V, Pieters J. Interactions of pathogenic mycobacteria with host macrophages. *Microbes. Infect.* 9, 1671–1679 (2007).

27 Steenwinkel JEM, Vianen W, Kate MT *et al.* Targeted drug delivery to enhance efficacy and shorten treatament duration in disseminated *Mycobacterium avium* infection in mice. *J. Antimicrob. Chemoth.* 60, 1064–1073 (2007).

28 Figueiredo R, Moiteiro C, Medeiros MA *et al.* Synthesis and evaluation of rifabutin analogs aganist *Mycobacterium avium* and H37Rv, MDR, and NRP *Mycobacterium tuberculosis*. *Bioorg. Med. Chem.* 17, 503–511 (2009).

29 Cardona PJ, Amat I. Origin and development of RUTI, a new therapeutic vaccine against *Mycobacterium tuberculosis* infection. *Arch. Bronconeumol.* 42, 25–32 (2006).

30 Ahsan MJ, Samy JG, Dutt KR *et al.* Design, synthesis and antimycobacterial evaluation of novel 3-substituted-*N*-aryl-6,7-dimethoxy-3a,4-dihydro-3H-indeno[1,2-c]pyrazole-2 -carboxamide analogues. *Bioorg. Med. Chem. Lett.* 21, 4451–4453 (2011).

31 Barry CE, 3rd Blanchard JS. The chemical biology of new drugs in the development for tuberculosis. *Curr. Opin. Chem. Biol.* 14, 456–466 (2010).

32 Chauhan PM, Sunduru N, Sharma M. Recent advances in the design and synthesis of heterocycles as anti-tubercular agents. *Fut. Med. Chem.* 2, 1469–1500 (2011).

33 Kantevari S, Yempala T, Surineni G, Sridhar B, Yogeeswari P, Sriram D. Synthesis and antitubercular evaluation of novel dibenzo[b,d]furan and 9-methyl-9H-carbazole derived hexahydro-2H-pyrano[3,2-c]quinolines via Povarov reaction. *Eur. J. Med. Chem.* (2011).

34 Leibert E, Rom WN. New drugs and regimens for treatment of TB. *Expert Rev. Anti Infect. Ther.* 8, 801–813 (2010).

35 Li Y, Zhou Y, Ma Y, Li X. Design and synthesis of novel cell wall inhibitors of *Mycobacterium tuberculosis* GlmM and GlmU. *Carbohydr. Res.* 346(13), 1714–1720 (2011).

36 Lounis N, Guillemont J, Veziris N, Koul A, Jarlier V, Andries K. [R207910 (TMC207): a new antibiotic for the treatment of tuberculosis]. *Med. Mal. Infect.* 40, 383–390 (2010).

37 Moraski GC, Markley LD, Hipskind PA *et al.* Advent of Imidazo[1,2-a]pyridine-3-carboxamides with potent multi- and extended drug resistant antituberculosis activity. *ACS Med. Chem. Lett.* 2, 466–470 (2011).

38 Mugunthan G, Sriram D, Yogeeswari P, Ravindranathan Kartha KP. Synthesis and biological evaluation of sugar-derived chiral nitroimidazoles as potential antimycobacterial agents. *Carbohydr. Res.* 346(13), 1760–1766. (2011).

39 Sala C, Hartkoorn RC. Tuberculosis drugs: new candidates and how to find more. *Fut. Microbiol.* 6, 617–633 (2011).

40 Shi R, Sugawara I. Development of new anti-tuberculosis drug candidates. *Tohoku. J. Exp. Med.* 221, 97–106 (2010).

41 Speck-Planche A, Scotti MT, de Paulo-Emerenciano V. Current pharmaceutical design of antituberculosis drugs: future perspectives. *Curr. Pharm. Des.* 16, 2656–2665 (2010).

42 Rodrigues C, Gameiro P, Prieto M, Castro B. Interaction of rifampicin and isoniazid with large unilamellar liposomes: spectroscopic location studies. *Biochim. Biophys. Acta.* 1620, 151–159 (2003).

43 Owen R, Strasters J, Breyer ED. Lipid vesicles in capillary electrophoretic techniques: characterization of structural properties and associated membrane-molecule interactions. *Electrophoresis* 26, 735–751 (2005).

44 Balen GP, Martinet CM, Caron G *et al.* Liposome/water lipophilicity: methods, information content, and pharmaceutical applications. *Med. Res. Rev.* 24, 299–324 (2004).

45 Moghimi SM, Hunter AC, Murray JC. Nanomedicine: current status and future prospects. *FASEB J.* 19, 311–330 (2005).

46 Dean AS. Liposomal drug delivery. *J. Infus. Nurs.* 30, 89–95 (2007).

47 Malam Y, Loizidou M, Seifalian AM. Liposomes and nanoparticles: nanosized vehicles for drug delivery in cancer. *Trends Pharmacol. Sci.* 30, 592–599 (2009).

48 Zhang L, Pornpattananangku D, Hu CM, Huang CM. Development of nanoparticles for antimicrobial drug delivery. *Curr. Med. Chem.* 17, 585–594 (2010).

49 Sanvicens N, Marco MP. Multifunctional nanoparticles – properties and prospects for their use in human medicine. *Trends Biotechnol.* 26, 425–433 (2008).

50 Bangham AD, Standish MM, Watkins JC. Diffusion of univalent ions across lamellae of swollen phospholipids. *J. Mol. Biol.* 13, 238–252 (1965).

51 Schroeder A, Kost J, Barenholz Y. Ultrasound, liposomes, and drug delivery: principles for using ultrasound to control the release of drugs from liposomes. *Chem. Phys. Lipids* 162, 1–16 (2009).

52 Lindner LH, Hossann M. Factors affecting drug release from liposomes. *Curr. Opin. Drug Discov. Devel.* 13, 111–123 (2010).

53 Farokhzad OC, Langer R. Nanomedicine: developing smarter therapeutic and diagnostic modalities. *Adv. Drug Deliver. Rev.* 58, 1456–1459 (2006).

54 Bawarski WE, Chidlowsky E, Bharali DJ, Mousa SA. Emerging nanopharmaceuticals. *Nanomed-Nanotechnol.* 4, 273–282 (2008).

55 Huang YZ, Gao JQ, Liang WQ, Nakagawa S. Preparation and characterization of liposomes encapsulating chitosan nanoparticles. *Biol. Pharm. Bull.* 28, 387–390 (2005).

56 Koo OM, Rubinstein I, Onyuksel H. Role of nanotechnology in targeted drug delivery and imaging: a concise review. *Nanomed-Nanotechnol.* 1, 193–212 (2005).

57 Immordino ML, Dosio F, Cattel L. Stealth liposomes: review of the basic science, rationale, and clinical applications, existing and potential. *Int. J. Nanomed.* 1, 297–315 (2006).

58 Williams DF. On the nature of biomaterials. *Biomaterials* 30, 5897–5909 (2009).

59 Barratt G, Bretagne S. Optimizing efficacy of amphotericin B through nanomodification. *Int. J. Nanomed.* 2, 301–313 (2007).

60 Agarwal A, Kandpal H, Gupta H, Singh N, Gupta C. Tuftsin-bearing liposomes as rifampin vehicles in treatment of tuberculosis in mice. *Antimicrob. Agents Chemother.* 38, 588–593 (1994).

▪ **Demonstrated that the addition of a ligand (tuftsin) to a liposome formulation with anti-TB drugs can be a good strategy combined with the intravenous route for the treatment of pulmonary TB.**

61 Vyas SP, Khatri K. Liposome-based drug delivery to alveolar macrophages. *Expert Opin. Drug Deliv.* 4, 95–99 (2007).

62 Pandey R, Khuller GK. Antitubercular inhaled therapy: opportunities, progress and challenges. *J. Antimicrob. Chemoth.* 55, 430–435 (2005).

63 Resnik DB, Tinkle SS. Ethics in nanomedicine. *Nanomedicine (Lond.)* 2, 345–350 (2007).

64 Hoet P, Legiest B, Geys J, Nemery B. Do nanomedicines require novel safety assessments to ensure their safety for long-term human use? *Drug Safety* 32, 625–636 (2009).

65 Pandey R, Khuller GK. Nanotechnology based drug delivery system(s) for the management of tuberculosis. *Indian J. Exp. Biol.* 44, 357–366 (2006).

66 Deol P, Khuller GK. Lung specific stealth liposomes: stability, biodistribution and toxicity of liposomal antitubercular drugs in mice. *Biochim. Biophys. Acta.* 1334, 161–172 (1997).

67 Pison U, Welte T, Giersing M, Groneberg DA. Nanomedicine for respiratoy diseases. *Eur. J. Pharmacol.* 533, 341–350 (2006).

68 Gill S, Löbenberg R, Ku T, Azarmi S, Roa W, Prenner EJ. Nanoparticles: characteristics, mechanisms of action, and toxicity in pulmonary drug delivery – a review. *J. Biomed. Nanotechnol.* 3, 107–119 (2007).

69 Andrade F, Videira M, Ferreira D, Sarmento B. Nanocarriers for pulmonary administration of peptides and therapeutic proteins. *Nanomedicine (Lond.)* 6, 123–141 (2011).

70 Medina C, Santos-Martinez MJ, Radomski A, Corrigan OI, Radomski MW. Nanoparticles: pharmacological and toxicological significance. *Brit. J. Pharmacol.* 150, 552–558 (2007).

71 Surendiran A, Sandhiya S, Pradhan SC, Adithan C. Novel applications of nanotechnology in medicine. *Indian. J. Med. Res.* 130, 689–701 (2009).

72 El-Ridy MS, Mostafa DM, Shehab A, Nasr EA, Abd ES. Biological evaluation of pyrazinamide liposomes for treatment of *Mycobacterium tuberculosis*. *Int. J. Pharm.* 330, 82–88 (2007).

73 Mobley C, Hochhaus G. Pharmacokinetic considerations in the design of pulmonary drug delivery systems for glucocorticoids. In: *Drug Targeting Technology: Physical, Chemical, Biological Methods. Volume 115 (1st Edition)*. Schreier H (Ed.). New York, Informa Healthcare 72–73 (2001).

74 Dhillon J, Fielding R, Adler-Moore J, Goodael RL, Mitchison D. The activity of low-clearance liposomal amikacin in experimental murine tuberculosis. *J. Antimicrob. Chemoth.* 48, 869–876 (2001).

75 Pandey R, Sharma S, Khuller GK. Nebulization of liposome encapsulated antitubercular drugs in guinea pigs. *Int. J. Antimicrob. Ag.* 24, 93–94 (2004).

▪▪ **Good example of a liposome formulation with anti-TB drugs developed for pulmonary TB using the passive targeting and administrated by the inhalatory route.**

76 Huynh NT, Passirani C, Saulnier P, Benoit JP. Lipid nanocapsules: a new platform for nanomedicine. *Int. J. Pharm.* 379, 201–209 (2009).

77 Irache JM, Salman HH, Gamazo C, Espuelas S. Mannose-targeted systems for the delivery of therapeutics. *Expert Opin. Drug Deliv.* 5, 703–724 (2008).

78 Labana S, Pandey R, Sharma S, Khuller GK. Chemotherapeutic activity against murine tuberculosis of once weekly administered drugs (isoniazid and rifampicin) encapsulated in liposomes. *Int. J. Antimicrob. Ag.* 20, 301–304 (2002).

▪▪ **Good example of a liposome formulation with anti-TB drugs developed for extrapulmonary TB using active targeting and administrated by the intravenous route.**

79 Chono S, Kaneko K, Yamamoto E, Togami K, Morimoto K. Effect of surface-mannose modification on aerosolized liposomal delivery to alveolar macrophages. *Drug. Dev. Ind. Pharm.* (2009).

▪ **In this study a mannosylated liposome was shown to be more efficiently delivered to alveolar macrophages than the liposomes without mannose, suggesting that active targeting combined with the inhalatory route is more efficient than passive targeting.**

80 Wijagkanalan W, Kawakami S, Takenaga M, Igarashi R, Yamashita F, Hashida M. Efficient targeting to alveolar macrophages by intratracheal administration of mannosylated liposomes in rats. *J. Control. Release* 125, 121–130 (2008).

81 Zaru M, Mourtas S, Klepetsanis P, Fadda AM, Antimisiaris SG. Liposomes for drug delivery to the lungs by nebulization. *Eur. J. Pharm. Biopharm.* 67, 655–666 (2007).

82 Ravaoarinoro M, Toma E, Agbaba O, Morisset R. Efficient entrapment of amikacin and teicoplanin in liposomes. *J. Drug Target.* 1, 191–195 (1993).

83 Maurer N, Fenske DB, Cullis PR. Developments in liposomal drug delivery systems. *Expert Opin. Biol. Ther.* 1, 923–947 (2001).

84 Korf J, Stoltz A, Verschoor J, De Baetselier P, Grooten J. The *Mycobacterium tuberculosis* cell wall component mycolic acid elicits pathogen-associated host innate immune responses. *Eur. J. Immunol.* 35, 890–900 (2005).

85 Andersen CA, Rosenkrands I, Olsen AW *et al.* Novel generation mycobacterial adjuvant based on liposome-encapsulated monomycoloyl glycerol from *Mycobacterium bovis* bacillus Calmette-Guerin. *J. Immunol.* 183, 2294–2302 (2009).

86 Dascher CC, Hiromatsu K, Xiong X *et al.* Immunization with a mycobacterial lipid vaccine improves pulmonary pathology in the guinea pig model of tuberculosis. *Int. Immunol.* 15, 915–925 (2003).

87 Christensen D, Agger EM, Andreasen LV, Kirby D, Andersen P, Perrie Y. Liposome-based cationic adjuvant formulations (CAF): past, present, and future. *J. Liposome Res.* 19, 2–11 (2009).

88 Cui Z, Mumper RJ. Microparticles and nanoparticles as delivery systems for DNA vaccines. *Crit. Rev. Ther. Drug Carrier Syst.* 20, 103–137 (2003).

89 Koga H, Miyazaki Y, Kohno S, Hara K. A drug delivery system and biological response modifiers for the treatment of mycobacterial infection. *Kekkaku* 69, 113–118 (1994).

90 Okada M. Novel vaccines against tuberculosis. *Kekkaku* 81, 745–751 (2006).

91 Lalloo UG, Ambaram A. New antituberculous drugs in development. *Curr. HIV/AIDS Rep.* 7, 143–151 (2010).

92 Jain KK. Nanomedicine: application of nanobiotechnology in medical practice. *Med. Princ. Pract.* 17, 89–101 (2008).

93 Azarmi S, Roa W, Loebenberg R. Targeted delivery of nanoparticles for the treatment of lung diseases. *Adv. Drug Deliver. Rev.* 60, 863–875 (2008).

94 Comas I, Gagneux S. The past and the future of tuberculosis research. *PLoS Pathog.* 5, (2009).

95 Ginsberg AM. Tuberculosis drug development: progress, challenges, and the road ahead. *Tuberculosis* 90, 162–167 (2010).

96 Nuermberger EL, Spigelman MK, Yew WW. Current development and future prospects in chemotherapy of tuberculosis. *Respirology* 15, 764–778 (2010).

97 Pai M, Minion J, Steingart K, Ramsay A. New and improved tuberculosis diagnostics: evidence, policy, practice, and impact. *Curr. Opin. Pulm. Med.* 16, 271–284 (2010).

98 Traini D, Young PM. Delivery of antibiotics to the respiratory tract: an update. *Expert Opin. Drug Deliv.* 6, 897–905 (2009).

99 Craven DE, Steger KA, Hirschorn LR. Nosocomial colonization and infection in persons infected with human immunodeficiency virus. *Infect. Control Hosp. Epidemiol.* 17, 304–318 (1996).

2. Molecular interaction of Rifabutin on model lung surfactant monolayers.

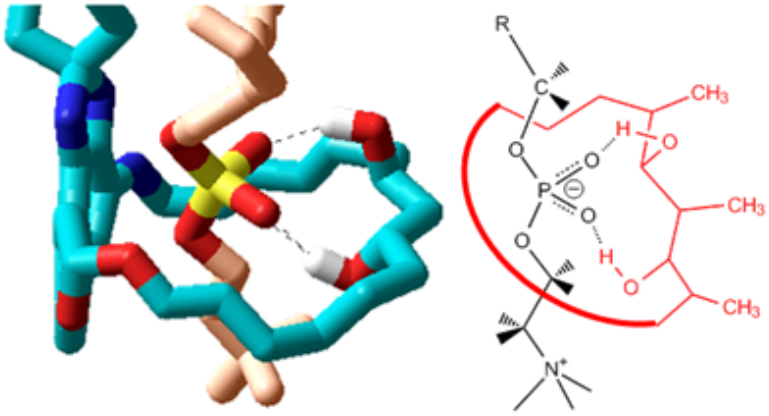

THE JOURNAL OF PHYSICAL CHEMISTRY B

Article

pubs.acs.org/JPCB

Molecular Interaction of Rifabutin on Model Lung Surfactant Monolayers

Marina Pinheiro,[†] Marlene Lúcio,[†,*] Salette Reis,[†] José L. F. C. Lima,[†] João M. Caio,[∥] Cristina Moiteiro,[∥] María T. Martín-Romero,[‡] Luis Camacho,[‡] and Juan J. Giner-Casares*[,‡,§]

[†]REQUIMTE, Departamento de Ciências Químicas, Faculdade de Farmácia, Universidade do Porto, Portugal

[‡]Department of Physical Chemistry and Applied Thermodynamics, University of Córdoba, Campus de Rabanales, Edificio Marie Curie, Córdoba, Spain E-14014

[§]Department of Interfaces, Max Planck Institute of Colloids and Interfaces, Science Park Golm, 14476 Potsdam, Germany

[∥]CQB, Departamento de Química e Bioquímica, Faculdade de Ciências, Universidade de Lisboa, Portugal

ABSTRACT: Tuberculosis is one of the most relevant problems for global health care. The design of new drugs against tuberculosis is aimed at maximizing impact against the disease, as well as minimizing the toxicological effect on the lung surfactant. In this work, the antituberculosis drug Rifabutin is studied in combination with phospholipid Langmuir monolayers as models of the lung surfactant monolayer. The zwitterionic 1,2-dipalmitoyl-*sn*-glycero-3-phosphocholine (DPPC) and the anionic 1,2-dipalmitoyl-*sn*-glycero-3-phospho-(1′-rac-glycerol) (DPPG) were used as model phospholipids. A combination of in situ experimental techniques of Brewster angle microscopy, polarization-modulated infrared reflection−absorption spectroscopy, and UV−vis reflection spectroscopy with computer simulations has been used. The interactions between Rifabutin and the DPPC and DPPG Langmuir monolayers were described as the formation of an inclusion complex. The phospholipid−Rifabutin inclusion complex prevents the penetration of the Rifabutin into the alkyl chain region of the phospholipids, leading to a disruption of the monolayer structure and a possible toxicological effect.

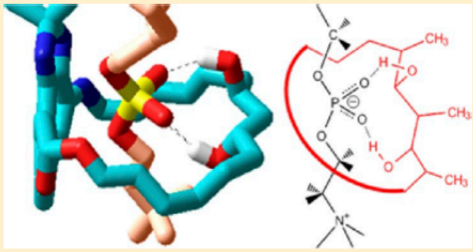

INTRODUCTION

Tuberculosis (TB) is a major problem for current global health care. TB is an infectious disease caused by the bacillus *Mycobacterium tuberculosis* (MTB). TB typically affects the lungs (pulmonary TB) but can affect other sites as well (extrapulmonary TB). TB affects mostly adults in the economically productive age groups; around two-thirds of cases are estimated to occur among people aged between the age of 15 and 59. In 2010, there were ca. 8.8 million incident cases of TB, ca. 1.1 million deaths from TB among HIV-negative people, and an additional 0.35 million deaths from HIV-associated TB.[1,2]

Intensive research is devoted to the development of new drugs against TB. Rifabutin (RBT) is an antituberculosis drug in current use, with a widespread use in the clinical practice.[3] RBT has been used as the starting structure for new derivatives as promising molecules against TB.[4] The rationale design of more efficient derivatives of RBT against TB would benefit from a deeper understanding of the molecular mechanism of action of RBT in the lung surfactant monolayer. Indeed, the lung surfactant monolayer presents several important functions by contributing to the small airway permeability, improving the mucocilliary depuration, and protecting against inhaled pathogens and injury, avoiding inflammation and oxidation.[5,6] Furthermore, due to its role in decreasing alveoli surface tension, the lung surfactant facilitates respiratory work and prevents alveoli collapse.[7,8] Hence, a low level of toxicity, i.e., low impact of the drug on the biophysical integrity of lung surfactant monolayer, is most desirable. Beyond evidence that indicates the importance of assuring the biophysical integrity of lung surfactant, the knowledge of interactions of drugs with this physiological barrier is scarce. Literature is particularly poor in information related to drugs accessibility and interaction with the lipid content of this barrier. Previous studies deal with the interactions of RBT with 3D models, such as multilamellar and unilamellar phospholipid vesicles.[9,10] However, the first steps in the interaction of RBT with the components of the lung surfactants occur at the monolayer/drug interface.

To this end, the study presented herein aims at the understanding of the interactions of RBT with a mimetic model of the lung surfactant, i.e., Langmuir monolayers formed by the most abundant lipid components in the inner interface of the lungs: 1,2-dipalmitoyl-*sn*-glycero-3-phosphocholine (DPPC) and 1,2-dipalmitoyl-*sn*-glycero-3-phospho-(1′-rac-glycerol) (DPPG) phospholipids.[11] At physiological pH, DPPC is in zwitterionic form, bearing no net charge, whereas DPPG is in

Received: April 18, 2012
Revised: August 17, 2012
Published: August 29, 2012

dx.doi.org/10.1021/jp303725j | *J. Phys. Chem. B* 2012, 116, 11635−11645

anionic form, bearing one negative charge per DPPG molecule. In bulk solution, the RBT molecule is mostly in the zwitterionic form at physiological pH, with no net charge. There is a certain contribution of the cationic form of RBT, appointed to be ca. 10% of the total RBT molecules due to the piperidine ring.[9] The molecular structures of the mentioned compounds are shown in Figure 1.

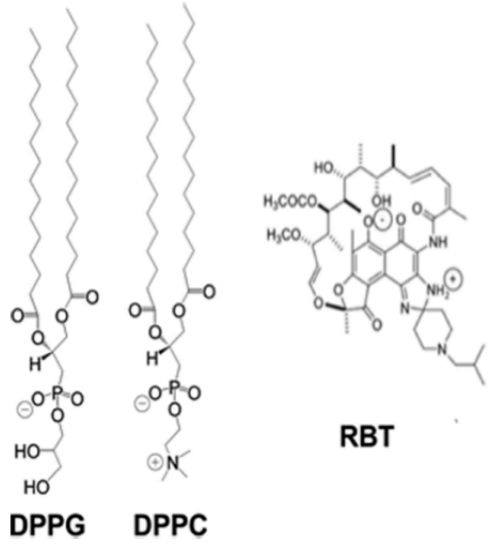

Figure 1. Molecular structures of anionic DPPG, zwitterionic DPPC, and Rifabutin RBT.

To achieve the proposed aim, the effect of the RBT on the phospholipid Langmuir monolayers was studied by a combination of experimental techniques in situ at the air/solution interface. Thermodynamic information was obtained by surface pressure-molecular area isotherms that when associated with Brewster angle microscopy (BAM) allowed recorded images of the monolayer on the micrometer scale. Moreover, UV–vis spectroscopy at the air/solution interface was used for quantifying the amount of RBT at the interface whereas polarization-modulated infrared reflection–absorption spectroscopy (PM-IRRAS) provided information on the methylene and phosphate groups. Computer simulations using a molecular mechanics method were performed to attain additional insight into the interaction between DPPC and RBT molecules with atomic details.

■ EXPERIMENTAL SECTION

Materials. DPPC and DPPG were purchased as sodium salts from Avanti Lipids, and used as received. RBT was isolated from Mycobutin and purified by column chromatography on silica and was compared with an authentic sample supplied by UpJohn & Pharmacy. The molecular structures of the phospholipids and the RBT are depicted in Figure 1. Chloroform was used as the spreading solvent for dissolving both components. The pure solvents were obtained from Aldrich and used without further purification. Phosphate buffer with a total phosphate concentration of 100 mM at a pH of 7.4 plus 100 mM NaCl was used as a subphase. The subphase containing RBT was composed by the mentioned phosphate buffer with RBT in a final concentration of 0.118 μM. This concentration of the RBT drug was used according to the concentration that has proved to be efficient in vitro, against *M. tuberculosis* and *M. avium*. Moreover, this concentration has proven to be nontoxic against Vero cells, as described in a previous study.[4] Ultrapure water was produced by a Millipore Milli-Q unit, pretreated by a Millipore reverse osmosis system (>18.2 MΩ cm). The subphase temperature was 21 °C. All experiments were performed in a large class 100 clean room.

Methods. Two different models of Nima troughs (Nima Technology, Coventry, England) were used. A Wilhelmy-type dynamometric system using a strip of filter paper was used to monitor the surface pressure. A NIMA 611D Langmuir trough with one moving barrier was used for the measurement of the UV–vis reflection spectra. A NIMA 601 Langmuir trough equipped with two symmetrical barriers was used to record the BAM images. A KSV Langmuir trough was used for measuring the PM-IRRAS spectra. The monolayers were compressed at a speed of ca. 0.1 $nm^2\ min^{-1}$ lipid $molecule^{-1}$. UV–visible reflection spectra at normal incidence as the difference in reflectivity (ΔR) of the dye film-covered water surface and the bare surface were obtained with a Nanofilm Surface Analysis Spectrometer (RefSpec[2] supplied by Accurion GmbH, Goettingen, Germany). Images of the film morphology were obtained by Brewster angle microscopy (BAM) with a I-Elli2000 (Accurion GmbH), using a 50 mW Nd:YAG diode laser with a wavelength of 532 nm. The recorded images had a lateral resolution of 2 μm. The image processing procedure included a geometrical correction of the image, as well as a filtering operation to reduce interference fringes and noise. The microscope and the film balance were located on a table with vibration isolation (antivibration system MOD-2 S, Accurion, Goettingen, Germany). PM-IRRAS spectra were recorded using a KSV PMI 550 (KSV NIMA, Espoo, Finland) equipped with an MCT detector. The setup consists of an IR source, a Michelson interferometer and an external reflection unit. The infrared radiation intensity was modulated by the interferometer and polarized with a ZnSe polarizer. The beam was then passed through a ZnSe photoelastic modulator, which modulated it between polarization in the plane of incidence (p) and polarization perpendicular to this plane (s) with a fixed frequency of 100 kHz. The angle of incidence of the infrared beam with respect to the surface normal was 80°. Spectra were recorded with a spectral resolution of 8 cm^{-1} and collected using 3000–6000 scans during 5–10 min. HyperChem 7.51 was used for the molecular mechanics simulations.[12]

Computer Simulations. The un-ionized form of the RBT molecule has been used for the complete set of calculations. The geometry of the DPPC and RBT molecules were optimized using classical molecular mechanics, i.e., MM+ force field, with no partial charges prior to the study of the interactions between those molecules. After the MM+ optimization, the charges were assigned using the PM3 semiempirical method in a single-point fashion. The following step was a second optimization of the molecular geometry using MM+. This procedure was repeated until convergence was achieved. The convergence criteria for geometrical optimization was 0.001 kcal/(Å·mol). A similar method of assigning partial charges was used elsewhere.[13,14] The procedure for studying the interactions between the DPPC and RBT molecules is described as follows: the position of the RBT and DPPC molecules were fixed. The complex geometry was optimized using the MM + force field with electrostatic atomic charge, including no cutoffs. The Polak–Robiere

dx.doi.org/10.1021/jp303725j | J. Phys. Chem. B 2012, 116, 11635–11645

method was used for minimizing the energy by varying the geometry of the complex. The convergence criteria was 0.002 kcal/(Å mol).

RESULTS AND DISCUSSION

Surface Pressure–Molecular Area (π–A) Isotherms. The surface pressure-molecular area (π–A) isotherms of the DPPC monolayer, both with and without Rifabutin (RBT) on the phosphate buffer subphase, are shown in Figure 2. A clear

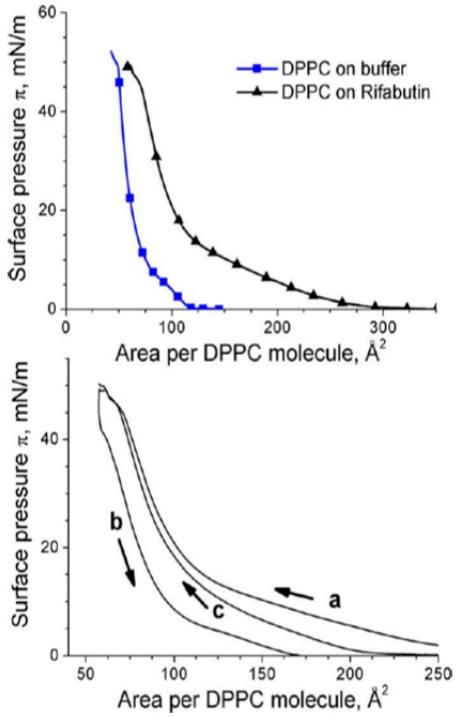

Figure 2. Top: Surface pressure-molecular area (π–A) isotherms for the DPPC monolayer on phosphate buffer (blue squares) and on phosphate buffer containing 0.12 μM of RBT (black triangles). The sampling of the surface pressure was continuous. Symbols are included for clarity. Bottom: surface pressure-molecular area isotherm cycles of the DPPC monolayer on the subphase containing RBT. a: first compression, b: decompression, and c: second compression.

expansion of the π-A isotherm is observed when RBT is present in the subphase, indicating the presence of the drug molecules at the DPPC monolayer. This expansion is still significant even at later stages of compression of the DPPC monolayer, i.e., at low values of molecular area. The liquid expanded-liquid condensed (LE-LC) transition might take place simultaneously with a certain rearrangement of RBT and DPPC molecules in the region of molecular areas between 125 and 250 Å^2 per DPPC molecule, although the detailed physical phenomenon can not be deduced from the π–A isotherm. The expansion of the molecular area in the DPPC monolayer provoked by the presence of RBT is ca. 160 Å^2 per DPPC molecule at low stages of compression of ca. 2 mN/m. The expansion of the π–A isotherm of DPPC at a surface pressure of 30 mN/m is reduced to ca. 30 Å^2 per DPPC molecule.

The stability of the RBT molecules attached to the DPPC monolayer has been tested by performing two subsequent compression π–A isotherms of the DPPC monolayer with Rifabutin in the subphase (Figure 2). A certain degree of hysteresis is observed with the decompression of the DPPC monolayer. This hysteresis might be ascribed to either an irreversible conformational change of the DPPC and RBT molecules or to a loss of RBT molecules from the DPPC monolayer. The second compression π–A isotherm shows a slight deviation from the first π–A isotherm at high values of surface area (Figure 2). However, with compression of the DPPC monolayer, the π–A isotherms for the first and second compressions overlap, indicating the similarity of the final state of the DPPC monolayer in both compressions. Quantitative insight into the amount of RBT present at the DPPC monolayer with the compression and decompression processes are attained with UV–vis reflection spectroscopy, as discussed below.

A mixed monolayer formed by the zwitterionic DPPC and the anionic DPPG phospholipids in a molar ratio DPPC:DPPG 9:1 has been used as a model for the lung surfactant monolayer. This molar ratio has been chosen to mimic the pulmonary surfactant, in which ca. 5–10% of the total content of lipids are anionic PG lipids.[5] Moreover, the incorporation of a certain degree of negative charge in the mixed phospholipid monolayer might offer information on the relevance of electrostatic interactions between RBT and phospholipids. The π–A isotherms of the mixed monolayer DPPC:DPPG on the phosphate buffer subphase, both with and without RBT, are shown in the Figure 3. Note that in this case of a mixed monolayer, the molecular area is expressed as the mean molecular area per phospholipid molecule, i.e., the DPPC and DPPG molecules are considered equivalent.

A similar situation to the one previously observed for the pure DPPC monolayer is achieved in the case of a mixed monolayer. The expansion in the molecular area when comparing the mixed monolayer DPPC:DPPG 9:1 in the presence and absence of RBT is ca. 160 Å^2 per lipid molecule at low stages of compression, as in the previous case of a pure DPPC monolayer. The expansion of the π–A isotherm of the mixed monolayer DPPC:DPPG at a surface pressure of 30 mN/m is slightly larger than for the DPPC case, reaching a value of ca. 40 Å^2 per phospholipid molecule.

The stability of the attachment of the RBT molecules to the lipids composing the mixed monolayer has been tested by two-cycle compression π–A isotherms of the mixed monolayer DPPC:DPPG 9:1 with Rifabutin in the subphase, as shown in Figure 3. A certain hysteresis is observed during the decompression process. An almost complete recovery of the π–A isotherm for the second compression is observed for high values of surface pressure, pointing to a persistent presence of the RBT in the mixed monolayer DPPC:DPPG 9:1. Additional information concerning the amount of RBT is provided by UV–vis reflection spectroscopy, as discussed below.

Brewster Angle Microscopy. Brewster angle microscopy (BAM) allows the direct visualization of the Langmuir monolayer at micrometer dimensions.[15] Figure 4 shows BAM images acquired during the compression of a DPPC monolayer on a phosphate buffer subphase, both with and without RBT. The morphology of the DPPC monolayer is described in the literature with deeper detail.[16] Briefly, during the first-order transition in the π–A isotherm the formation and growth of bright domains is observed. These bright domains correspond to aggregates of phospholipid molecules in a more condensed state (LC) than the phospholipid molecules in the surrounding media (LE). With further compression of the DPPC

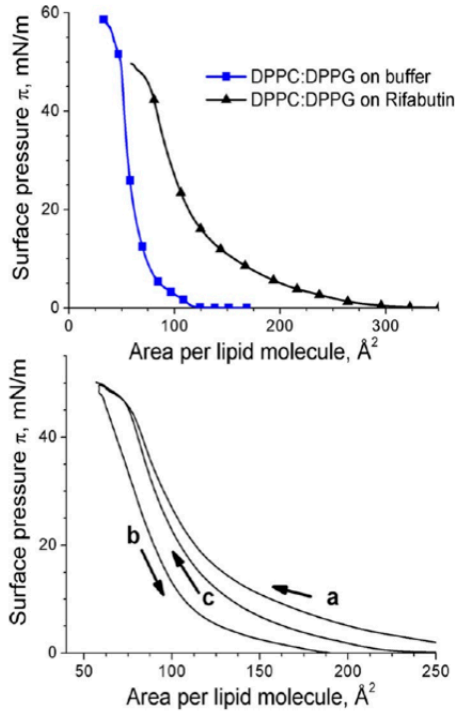

Figure 3. Top: Surface pressure-molecular area (π–A) isotherms for the mixed monolayer DPPC:DPPG 9:1 on phosphate buffer (blue squares) and on phosphate buffer containing 0.12 μM of RBT (black triangles). The sampling of the surface pressure was continuous. Symbols are included for clarity. Bottom: Surface pressure-molecular area isotherm cycles of the mixed monolayer DPPC:DPPG 9:1 on the subphase containing Rifabutin. a: first compression, b: decompression, and c: second compression.

monolayer, the domains grow and coalesce. In the final stage of compression, a bright homogeneous monolayer is observed.

When RBT is incorporated in the subphase, clear changes in the morphology of the DPPC monolayer are observed. At large values of molecular area, i.e., a highly expanded state of the DPPC monolayer small bright points, a few micrometers in size, are observed. These bright points might correspond to aggregates of RBT, although the chemical composition can not be unambiguously deduced from the BAM images. With compression of the DPPC monolayer, the domains corresponding to DPPC molecules in the LC phase appear. However, in this case almost all the LC domains are formed around the bright domains in a yolk-egg white fashion. The bright domains are already present at large values of molecular area. It is tempting to ascribe this phenomenon to the growth of DPPC domains in the LC state around aggregates formed mainly by DPPC/RBT complexes. In this scenario, the DPPC/RBT complex aggregates would serve as nuclei. A similar phenomenon has been described by Deng et al., in which an inorganic/organic hybrid molecule, i.e., a oligomeric silsesquioxane formed well-defined mono and multilayer at the air/water interface.[17−19] In the case of the silsesquioxane, the origin of the domains is related with the formation of multilayers. Remarkably, the authors use different spreading conditions, e.g., spreading on hot water and then cooling, to avoid the aggregation of the silsesquioxane molecules prior to compression.

This possibility is examined in deeper detail below, where computational simulations show that the DPPC molecule can interact with the RBT molecule forming a noncovalent inclusion complex. With further compression of the DPPC monolayer, the domains become closer to each other. In contrast to the pure DPPC monolayer, there is no total coalescence of the LC domains in the presence of RBT. When the drug RBT is present in the subphase, the bright domains in the DPPC monolayer form an inhomogeneous monolayer at high values of surface pressure. The nonhomogeneity of the monolayer might be provoked by an interfering effect of the RBT against the intermolecular DPPC attractive interactions, which would agree with the hypothesis of an inclusion complex RBT-DPPC. In this highly compressed state, the brightness of the picture is quite high, indicating a thick monolayer.

The BAM pictures recorded during compression of the mixed monolayer DPPC:DPPG 9:1 with RBT in the phosphate buffer subphase are shown in Figure 4. The domains appear smaller and with slightly rounder shapes than in the pure DPPC monolayer. This modification of the domains indicates a more significant effect of the line tension.[20] There is also a fraction of the monolayer displaying short quasiellipsoidal bright structures, which might correspond to DPPG lipid, as observed in the pure DPPG monolayer.[21]

Bright small domains and large fiber-like structures appear in the LE phase of the monolayer at ca. 7 mN/m. The bright domains show the same yolk-egg white appearance as in the pure DPPC monolayer. These domains exist along the entire isotherm. The domains display a small growth with compression of the monolayer. There is no coalescence of the domains even at a large degree of compression. The fiber-like structures grow in size with compression of the monolayer, reaching the form of elongated strips with a length of ca. 10–100 μm. There is apparently no interaction between the two types of domains. We hypothesize that the stripes might be composed of aggregates of lipids and RBT with a nondefined stoichiometry.

A magnified view of selected BAM pictures is shown in Figure 5. The coexistence of the brighter regions with the domains usually observed for lipids in a LC phase indicates the occurrence of aggregates of RBT in the polar head region of the phospholipids.[22] On the other hand, the domains are due to the arrangement of the alkyl chains of the phospholipids. The aggregation of the RBT molecules might be mediated by the polar head of the phospholipids. The interaction of RBT molecules with the polar head groups of the phospholipids is consistent with the absence of perturbation of the alkyl chains by RBT, as shown hereafter by PM-IRRAS.

UV–vis Reflection Spectroscopy. The expansion of the π–A isotherms and the BAM pictures offer direct proof for the existence of RBT in the phospholipid monolayer. Quantitative insight into the actual amount of RBT at the air/solution interface is highly desirable as is monitoring the impact of compression and decompression on the presence of RBT at the air/solution interface. To this end, UV–vis reflection spectroscopy at the air/solution interface is a highly valuable tool. The UV–vis reflection spectroscopy is exclusively sensitive to the chromophores located at the air/water interface, therefore being most useful for the in situ characterization of the Langmuir monolayers.[23]

The UV–vis reflection spectra of the DPPC monolayer at different stages of compression of the DPPC monolayer with RBT in the subphase are shown in Figure 6. The bulk UV–vis

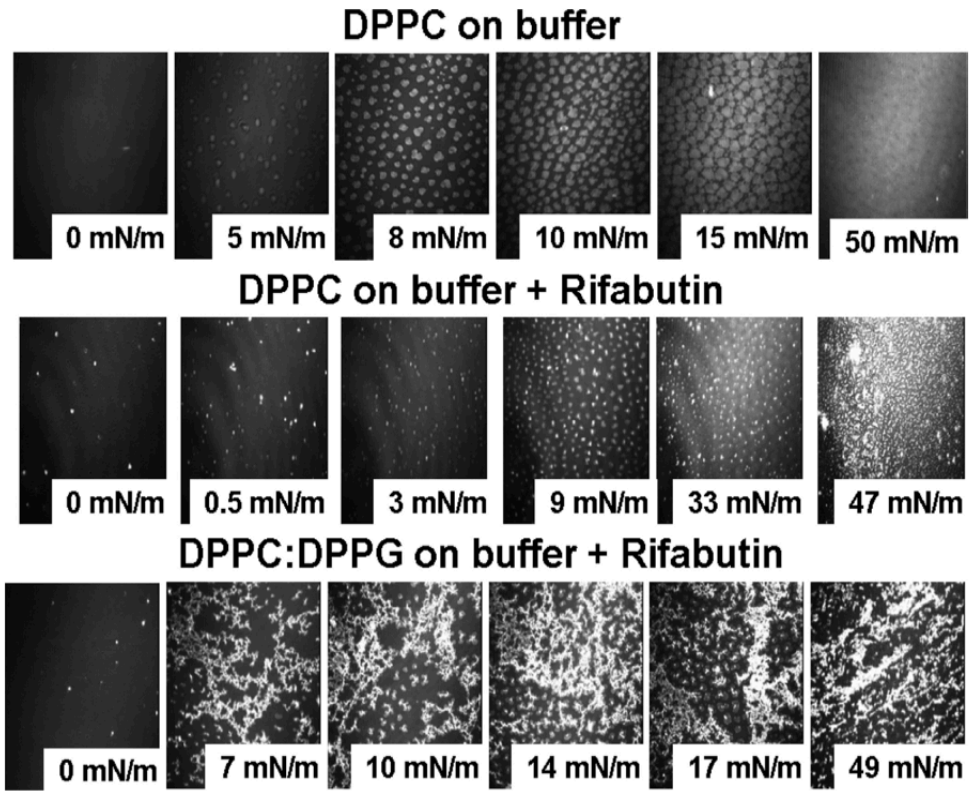

Figure 4. Brewster angle microscopy pictures of (top) a DPPC monolayer on a phosphate buffer subphase, (middle) a DPPC monolayer on a phosphate buffer containing 0.12 μM of RBT subphase, and (bottom) and a mixed DPPC:DPPG 9:1 monolayer on a phosphate buffer containing 0.12 μM of RBT subphase. Surface pressures for each image are indicated on the images, which have widths of 430 μm.

spectrum of RBT is included for comparison. The bulk UV–vis spectrum shows two main peaks centered at ca. 280 and 325 nm, as well as a shoulder at ca. 530 nm. The position of the peaks in the reflection spectra are clearly modified, indicating the presence of different states of aggregation of the RBT molecules at the air/solution interface than that of the bulk solution. Therefore, the maxima and minima of the UV–vis spectra are not clearly displayed. The intensity of the reflection signal increases with the compression of the DPPC monolayer. This increase indicates that the air/solution interface is enriched in RBT with compression of the lipid monolayer. The intensity of reflection is proportional to the relative amount of RBT located at the air/solution interface. The UV–vis reflection spectra have been integrated, and the integral values of the UV–vis reflection spectra obtained during the two π–A compression isotherms are shown in Figure 6. Note that the reference spectrum is acquired using the RBT subphase with no monolayer of phospholipid. Therefore, the UV–vis reflection signal from adsorbed molecules of RBT at the interface is neglected. Almost all of the integral coming from surface molecules comes from wavelengths below 300 nm. Control experiments with pure DPPC, pure DPPG, and DPPC:DPPG monolayers on phosphate buffer subphase without RBT were performed, showing the absence of a significant UV–vis reflection signal in all cases. The integral values are displayed as a function of the molecular area of the DPPC for direct comparison of the UV–vis reflection signal with the π–A isotherms in Figure 2. The amount of RBT in contact with the DPPC monolayer at the air/solution interface increases almost linearly with compression of the monolayer. The surface concentration of RBT molecules reaches the maximum value for the most compressed state of the DPPC monolayer. Remarkably, with the second compression of the DPPC monolayer a certain degree of hysteresis appears. The hysteresis is observed only at large values of molecular areas. The amount of RBT molecules at the air/solution interface is fully recovered at high stages of compression of the DPPC monolayer. The total recovery of RBT might indicate the reversibility of the maximum amount of the RBT molecules at the DPPC monolayer after the "squeezing-out" of the excess RBT molecules after compression of the monolayer. This reversible state of as maximum surface concentration of RBT in contact with the polar heads of the lung surfactants might occur at the lungs, where the successive breathing cycles expand and compress the lung surfactant monolayer.

The UV–vis spectra of the mixed monolayer DPPC:DPPG 9:1 in the presence of RBT are shown in Figure 7. The UV–vis reflection spectra for the DPPC/DPPG monolayer appear slightly noisier than those of the pure DPPC monolayer. The drift of the UV–vis reflection signal is a common experimental feature, especially when considering a broad range of wavelength, i.e., 250 to 700 nm. This drift is usually related with a certain mismatch between the reference and the sample spectra, i.e., the bare air/solution interface and the Langmuir monolayer, respectively. In the case of the UV–vis reflection spectra presented in the Figure 7, the drift in the long wavelength region is not considered significant for the spectral region of interest that is mainly the UV region. The significant

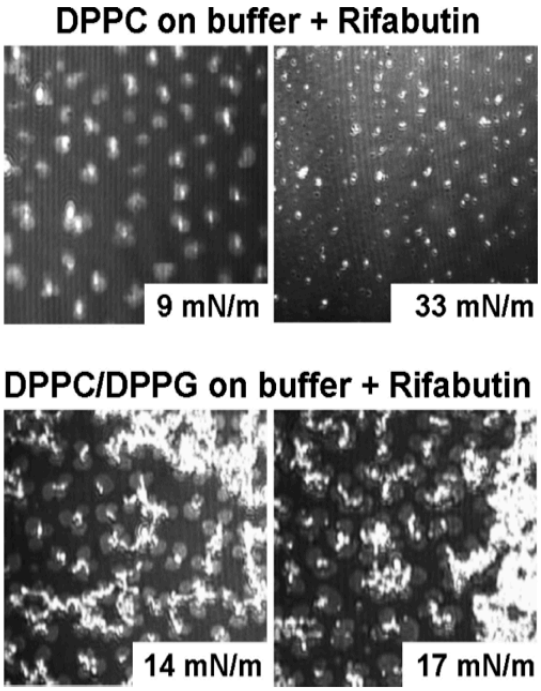

Figure 5. Magnified Brewster angle microscopy pictures. (Top) A DPPC monolayer and (bottom) a mixed DPPC:DPPG 9:1 monolayer on a phosphate buffer subphase containing 0.12 μM of RBT subphase. Surface pressures for each image are indicated on the images, which have widths of ca. 200 μm.

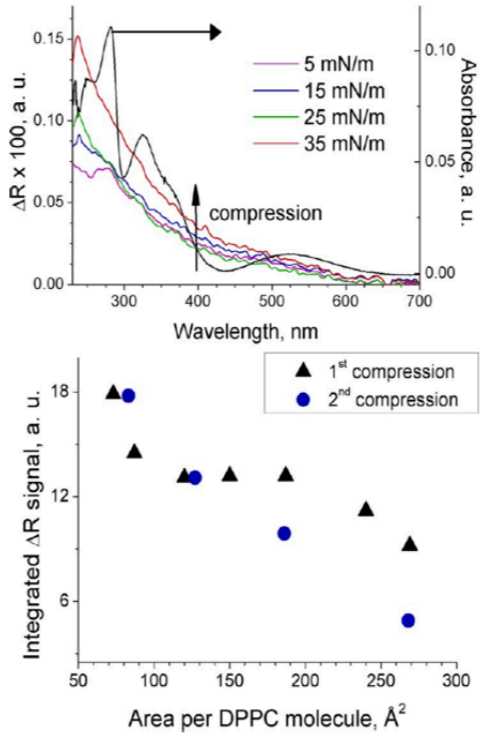

Figure 6. Top: UV–vis reflection spectra of the DPPC monolayer on a phosphate buffer containing 0.12 μM of RBT subphase at different values of surface pressure. The UV–vis spectrum of RBT in bulk solution (2×10^{-6} M in phosphate buffer solution) is included for comparison. Bottom: Integral values of the complete UV–vis reflection spectra at different values of molecular area of DPPC obtained during two successive compression π–A isotherms. Error is within experimental deviation of ca. 10%.

UV–vis reflection signal at 0 mN/m indicates the adsorption of a given amount of RBT molecules at the DPPC:DPPG 9:1 mixed monolayer prior to compression of the monolayer.

The introduction of the anionic DPPG phospholipid into the mixed monolayer leads to a reduced amount of RBT molecules at the air/solution interface, as shown by the smaller integral values of the UV–vis reflection spectra than those of the DPPC case. In the case of a mixed monolayer DPPC:DPPG 9:1, the saturation state is almost reached since ca. 250 Å^2 per phospholipid molecule. Further compression of the mixed DPPC:DPPG 9:1 monolayer leads to a small albeit significant increase of the amount of RBT at the air/solution interface. The reversible state of the maximum amount of RBT at the mixed DPPC:DPPG 9:1 monolayer for the two compression cycles are almost equivalent. Thus, the UV–vis reflection spectroscopy data might point to a slightly less favorable interaction between the anionic DPPG and the RBT molecules than between the zwitterionic DPPC and the RBT molecules for a highly compressed monolayer, taking into account exclusively the absolute values of UV–vis reflection signal. The RBT molecule is mostly in zwitterionic form with a slight contribution of cations, ca. 10%, at a pH value of 7.4 as used in the subphase.[9] Therefore, the electrostatic interactions do not contribute to a large extent to the RBT-phospholipid interactions. On the contrary, the polar headgroup of the phospholipids seems to play a significant role in the interactions between the phospholipid and RBT molecules via the formation of a noncovalent complex. Computer simulations confirm the relevance of the polar headgroup of the lipids, as described below.

The numerical values of the integral of the UV–vis reflection spectra are normalized using $\Delta R_{norm} = \Delta R \times$ lipid area,[24] so that the value of lipid area in this case is not fixed, i.e., each ΔR value is multiplied by the value of lipid area at which the UV–vis reflection spectrum was recorded. The variation of the normalized value of the integral with the compression of the monolayer is indicative of the relative changes of the surface concentration of the chromophore per lipid molecule, i.e., the variation of the surface concentration of the RBT molecules with the area per lipid. For the case of the presence of RBT at the air/solution interface exclusively forming a stable DPPC/RBT complex no variation of the normalized integral of the UV–vis reflection signal with the compression of the monolayer is expected. In other words, the intensity of the signal ΔR would vary in the same magnitude as the area per lipid molecule, thereby ΔR_{norm} being constant. On the other hand, for a "squeezing-out" of the RBT molecules from the air/solution interface to the bulk solution, a diminution of the normalized integral of the UV–vis reflection signal with the compression of the monolayer is expected. Figure 8 shows the normalized integral of the UV–vis reflection signal for the two compression isotherms of the DPPC and DPPC:DPPG monolayers on a RBT solution subphase. The results for both lipid monolayers are similar, indicating a similar mechanism of adsorption of RBT molecules at the lipid monolayer/solution interface. For the first compression, the

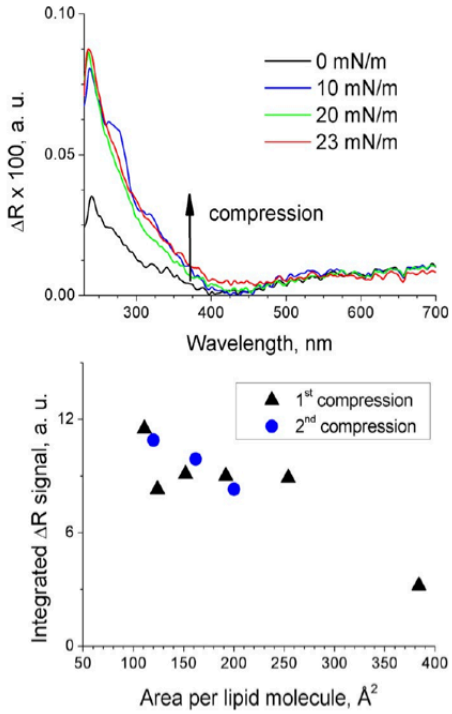

Figure 7. Top: UV–vis reflection spectra of the DPPC:DPPG 9:1 mixed monolayer on a phosphate buffer containing 0.12 μM of RBT subphase at different values of surface pressure. Bottom: Integral values of the complete UV–vis reflection spectra at different values of mean molecular area of phospholipid obtained during two successive compression π–A isotherms. Error is within experimental deviation of ca. 10%.

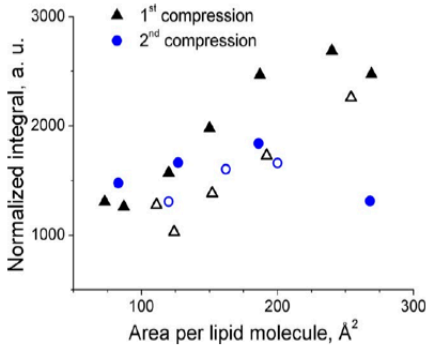

Figure 8. Normalized integral value of the UV–vis reflection spectra of both DPPC monolayer and DPPC:DPPG 9:1 mixed monolayer on a phosphate buffer containing 0.12 μM of RBT subphase. Full symbols: DPPC monolayer. Empty symbols: Mixed DPPC:DPPG mixed monolayer. Triangles: First compression. Circles: Second compression. The UV–vis reflection spectra were obtained during two compression π–A isotherms.

normalized integral diminishes with the compression of the lipid monolayer, indicating the loss of a significant amount of RBT per lipid molecule from the lipid monolayer/solution interface. On the contrary, during the second compression the normalized integral is approximately constant. Therefore, the ratio between the RBT and DPPC molecules at the air/solution interface is constant. This behavior is indicative of the formation of a noncovalent complex comprising RBT and lipid molecules during the first compression isotherm. This complex is stable, thus leading to a constant amount of RBT molecules at the lipid monolayer/solution interface in the second compression isotherm. As previously commented, this complex is attributed to an inclusion complex. This possibility is discussed in detail hereafter with respect to computer simulations and PM-IRRAS measurements.

Computer Simulations. The experimental data presented above suggest an interaction between the RBT and the phospholipids concerning mainly the polar headgroup of the phospholipids. Computer simulations have been performed using a simple model of one DPPC molecule and one RBT molecule in vacuo. In spite of the simplicity of the model, the simulated structures are consistent with the experimental results; therefore the simulations performed herein are viewed as complementary to the experimental findings. We should remark that we use the computational simulations to test the feasibility of the formation of the DPPC/RBT inclusion complex. The simulations performed herein are not intended to offer a direct proof of the formation of the DPPC/RBT inclusion complex.

In the seminal work of Casey and Whitlock, the different conformations of the Rifamycin molecule, an analogue to the RBT molecule, were analyzed.[25] The Rifamycin molecule is assumed to form an inclusion complex with a hydrophobic group, e.g., a tyrosine residue in bulk solution using water as a solvent. However, no direct experimental proof of the formation of an inclusion complex was described in the cited paper.

The situation described for Rifamycin in bulk water can not be directly extrapolated to RBT at the air/solution interface due to the spatial constraints. On the other hand, given the similarities between the molecular structures of Rifamycin and Rifabutin molecules, the formation of an inclusion complex with RBT as a host is worthy to be examined.

The computational procedure for analyzing the feasibility of the formation of the DPPC/RBT inclusion complex is as follows: The position of the DPPC lipid molecule was fixed. The DPPC polar group is considered for simplicity as the group of atoms N–C–C–O–P. The main axis of the polar headgroup is defined as the line connecting the N and P atoms. The RBT molecule is placed at different positions around the polar headgroup, therefore generating different starting configurations. The central position of the RBT cavity is located around the polar headgroup of the DPPC lipid in all cases.

A systematic study on the effect of the initial position of the RBT molecule in the optimized molecular geometry of the inclusion complex has been carried out. The initial displacement of the RBT molecule is defined as the distance between the central part of the RBT cavity and the N atom of the DPPC polar headgroup. The initial displacement was varied over a range of 5 Å, in steps of 1 Å for generating the different starting configurations. The total energy of the DPPC/RBT system was then evaluated. Please note that this method is not a molecular dynamics procedure, and water molecules are not included, therefore the effect of solvation of the DPPC headgroups is not studied. The molecular dynamics simulations of the DPPC/RBT inclusion complex lead to a significant change in the geometry of the alkyl chains of the lipids. The alkyl chains collapse on themselves after a few picoseconds. Remarkably, in no case of collapse of the alkyl chains the breakup of the

dx.doi.org/10.1021/jp303725j | J. Phys. Chem. B 2012, 116, 11635–11645

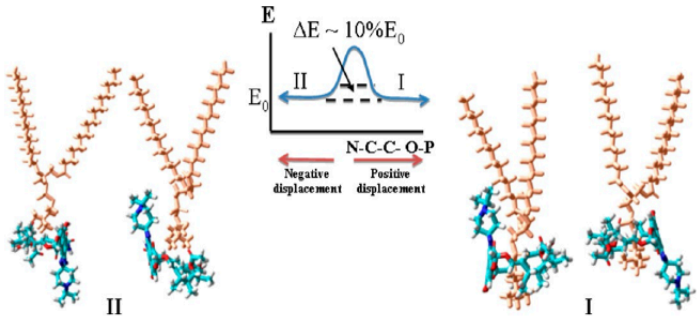

Figure 9. Left and right: Snapshots of the computer simulations of the DPPC and RBT molecules, and the change of the calculated total energy as a function of the initial configuration. Center: Scheme depicting the relative energy of stabilization gained by forming the DPPC/RBT inclusion complex. *Y* axis is energy. Brown: DPPC phospholipid molecule. The RBT molecules are displayed in white (hydrogen), light blue (carbon), red (oxygen), and deep blue (nitrogen).

inclusion complex has been observed. On the other hand, the molecular mechanics method used herein is able to find the closest minimum of energy to the starting point. Two trends of the calculated energy with the relative initial position of the RBT molecule around the DPPC molecule have been observed: for a positive value of the initial position of the RBT molecule, i.e., the RBT molecule moving deeper into the DPPC headgroup, the optimization procedure results in the formation of a DPPC/RBT inclusion complex. The RBT ring plane is displaced from the initial position of the O atom of the DPPC polar headgroup by a distance of ca. 3.6 Å from the N atom in the minimum of energy. The N atom of the DPPC headgroup is used as a reference position, i.e., zero position. The positive displacement is defined as the displacement of the ring plane of the RBT molecule displaced toward the P atom. On the other hand, the negative displacement consists in a movement of the ring plane of the RBT molecule displaced toward the alkyl chain region. For a negative value of the initial position of the RBT molecule, the optimization procedure leads to the formation of a DPPC/RBT pair, in which the interaction between the DPPC and RBT molecules is non specific. For both cases, the calculated energy of the system comprising the DPPC and RBT molecules is approximately the same, i.e., less than a 10% difference. Remarkably, both interacting combinations of DPPC and RBT, with and without forming the inclusion complex, are more stable than the DPPC and RBT molecules with no interaction by a factor of ca. 4. In other words, the computed energy for the set of one DPPC molecule and one RBT molecule is ca. 4 times lower in the case of an interaction between the DPPC and RBT molecules.

These computational results point to the formation of the two types of DPPC/RBT pairs at the air/water interface: inclusion complex and non specific interaction. The computational results are in agreement with the experimental results, in which we observe the enrichment of the air/solution interface in RBT molecules. Remarkably, a certain fraction of the RBT molecules is expelled out from the DPPC lipid monolayer after the first compression. The RBT molecules expelled out in this way might be those with a non specific interaction DPPC/RBT, whereas those RBT molecules forming the DPPC/RBT inclusion complex stay attached to the DPPC lipid monolayer even after the compression of the Langmuir monolayer.

Therefore, there is a stabilization of the global system by the interaction between the DPPC and RBT molecules. The driving force, as well as the stabilization mechanism, for the DPPC/RBT inclusion complex, is discussed below. There is certain energy of activation for modifying the interaction mode of the DPPC and RBT molecules. The DPPC/RBT inclusion complex might be formed during the spreading of the DPPC lipid layer, or during the compression. The stabilization of the DPPC/RBT system by the formation of the inclusion complex is summarized in the Figure 9.

The formation of two intermolecular hydrogen bonds with an average length of 2.2 ± 0.2 Å is observed in the DPPC/RBT complex. The H-bonds are formed between the two −OH groups of the ansa bridge for the RBT molecule, and the negatively charged oxygen of the phosphate group for the DPPC molecule. The driving force for the formation of the DPPC/RBT inclusion complex is ascribed to the formation of the intermolecular H-bonds. The formation of these H-bonds is exclusive for the DPPC/RBT inclusion complex, not being detected in the case of alternative configurations. The intermolecular H-bonds are shown in the Figure 10.

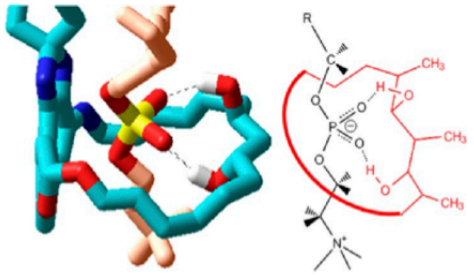

Figure 10. Left: Snapshots of the simulation of the DPPC:RBT inclusion complexes. The intermolecular H-bonds are displayed as dashed black lines. Methyl groups are not displayed for clarity. Right: Scheme depicting the atoms involved in the intermolecular H-bonds. Brown: DPPC phospholipid molecule, with red (oxygen) and yellow (phosphorus). The RBT molecule is displayed in white (hydrogen), light blue (carbon), red (oxygen), and deep blue (nitrogen).

Additionally, the conformational configuration of the RBT molecule in the DPPC/RBT inclusion complex might be relevant. In the case of the DPPC/RBT inclusion complex, the central cavity of the RBT molecule is located around the oxygen atoms of the DPPC headgroup. Given the sequence of atoms $-N-CH_2-CH_2-O-P-$, the smaller volume of the headgroup is found around the oxygen connecting the phosphorus atom with the methylene groups. The steric

hindrance is minimized at this point, and the coupling of the RBT cavity with the DPPC lipid is favored.

The formation of the DPPC/RBT inclusion complex is feasible. The formation of the DPPC/RBT inclusion complex requires a certain value of activation energy. The formation of a nonspecific coupling, i.e., noninclusion complex, between the DPPC and the RBT molecules does not require such an energy, thereby being more labile.

These two types of conformations for the pair formed by the DPPC and RBT molecules are consistent with the experimental results at the air/solution interface presented herein. As commented, a significant loss of RBT molecules from the air/solution interface is observed during the first compression cycle. On the contrary, the number of RBT molecules is approximately constant during the second compression cycle. This behavior might be interpreted as follows. Initially, the DPPC lipid monolayer is spread over the air/solution interface. A certain number of RBT molecules are then adsorbed from the bulk solution onto the DPPC lipid monolayer. Two main types of interactions between the DPPC and RBT molecules are expected: the DPPC/RBT inclusion complex and a nonspecific interaction between the DPPC polar headgroup and the RBT molecule. With the first compression cycle, the adsorbed RBT molecules that do not form inclusion complexes are likely to be expelled from the air/solution interface due to molecular crowding, given that the area occupied per DPPC molecule is smaller than that of the RBT molecule. On the other hand, the adsorbed RBT molecules included in the DPPC/RBT inclusion complex are less likely to be expelled from the air/solution interface, given that the breaking of the DPPC/RBT inclusion complex requires a certain activation energy. Moreover, the area occupied per unit of DPPC/RBT inclusion complex is only slightly larger than the area per DPPC lipid molecule. This small increase of the DPPC lipid area by the presence of RBT in the DPPC/RBT inclusion complex should not disturb to a large extent the arrangement of the DPPC lipids in the Langmuir monolayer. A semi-quantitative calculation on the increment of molecular area per DPPC molecule provoked by the RBT can be performed, considering the RBT a 2D disk. According to the simulations, the diameter of the RBT molecule can reach a value of ca. 7 Å. Thus, the expansion of the π–A isotherm of DPPC in case of the formation of an inclusion complex with RBT might lead to an expansion of ca. 50 Å^2. As commented previously (Figure 2), the experimental value of expansion of the π–A isotherm of DPPC at high stages of compression is ca. 40 Å^2, in approximate agreement with the previously calculated value. The interaction between the alkyl chains of the DPPC lipids and the formation of the domains would occur in the case of a DPPC/RBT inclusion complex, as experimentally observed.

Therefore, the formation of an inclusion complex with stoichiometry DPPC:RBT 1:1 is plausible, given the good agreement of the computational and experimental data. However, we would like to remark that we could not find direct proof of the existence of the DPPC/RBT inclusion complex rather than the proposed model and the consistency between the computational model and the experimental findings.

Polarization-Modulated Infrared Reflection Absorption Spectroscopy. PM-IRRAS allows monitoring of the vibrational spectra of the molecules present at the air/solution interface during the compression process of the π–A isotherm. The methylene vibrations are of special interest, being the symmetric $\nu_s(CH_2)$ and antisymmetric $\nu_{as}(CH_2)$ stretching modes for monitoring the aggregation state of the hydrocarbon chains.[26] The PM-IRRAS spectra for the DPPC and the DPPC:DPPG 9:1 monolayers in the presence of RBT in the subphase are shown in Figure 11. A control experiment of a pure DPPC monolayer on a pure water subphase has been included for comparison. The DPPC:DPPG 9:1 mixed monolayer does not show any significant variation with respect to the pure DPPC monolayer, probably due to the relatively small amount of DPPG present in the mixture.

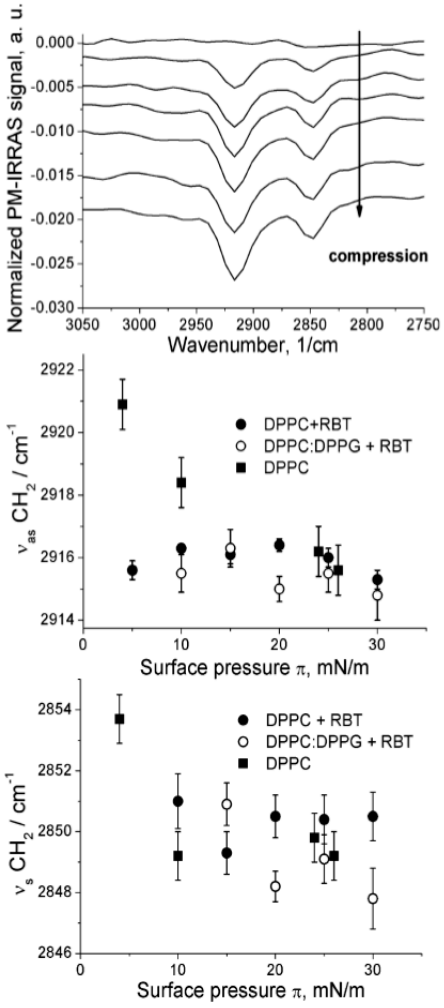

Figure 11. PM-IRRAS spectra of the methylene stretching region of a DPPC (black circles) and DPPC:DPPG 9:1 (empty circles) monolayers on a phosphate buffer containing 0.12 μM of RBT subphase recorded at different surface pressures. A control experiment of a pure DPPC monolayer (black squares) on pure water subphase is included for comparison. (Top) Evolution of the spectra of a DPPC monolayer on a phosphate buffer containing 0.12 μM of RBT subphase with the compression of the monolayer. The spectra are shifted 0.004 each for clarity. (Middle) Wavenumber values of the asymmetric methylene stretching mode with the applied surface pressure. (Bottom) Wavenumber values of the symmetric methylene stretching mode with the applied surface pressure.

dx.doi.org/10.1021/jp303725j | J. Phys. Chem. B 2012, 116, 11635–11645

The $\nu_s(CH_2)$ and $\nu_{as}(CH_2)$ bands are located at ca. 2850 and ca. 2916 cm^{-1}, respectively. These wavenumbers are characteristic from a condensed state of the alkyl chains, therefore indicating a tight packing of the hydrocarbon chains of the DPPC phospholipid molecules. The variation of the methylene stretching modes to lower values with compression of the monolayer is expected, as the alkyl chains become arranged in a more tight state, indicating a phase change.[27] Herein, the wavenumber of the methylene stretching modes are almost constant with the increase of surface pressure for both DPPC and DPPC:DPPG monolayers in presence of RBT. Therefore, we conclude the formation of a DPPC/RBT inclusion complex, as the existence of this complex leads to the observed experimental results, given that the RBT molecule adds eight methylene groups to the complex. The signal arising exclusively from the methylene groups of the phospholipids can not be distinguished from the PM-IRRAS spectra. According to the surface selection rules, the negative sign of the bands indicates a parallel orientation of the transition moment of the methylene groups with respect to the air/solution interface plane, which is consistent with an upright orientation of the alkyl chains.[28] Given a negative contribution of the methylene groups of the RBT molecule, this contribution would indicate an upright orientation of most of these methylene groups. Therefore, the impact of the formation of the inclusion complex in the physical state of the alkyl chain of the phospholipids could not be followed. On the other hand, these results support the idea of the formation of an inclusion complex DPPC:RBT, thus enriching the air/solution interface in methylene content.

In the case of the formation of an inclusion complex between the DPPC and the RBT molecules, a significant impact on the infrared spectrum of the phosphate moiety corresponding to the DPPC lipid is expected. Figure 12 shows the phosphate region of the PM-IRRAS of a DPPC monolayer on a phosphate buffer in presence and absence of RBT. The main band corresponds to the asymmetric stretching mode of PO_2^- group, located at 1252 cm^{-1} in the absence of RBT, and located at 1257 cm^{-1} in presence of RBT.[29] Remarkably, there is an inversion of the sign of this phosphate band, indicating a change in the orientation of the transition moment of the PO_2^- group with respect to the air/solution interface.[30] The phosphate band changes from a negative to a positive sign in the case of the absence and presence of RBT in the subphase, respectively. The change of sign for the PM-IRRAS signal indicates a relative change of orientation of the transition moment with respect to the air/solution interface. This change in conformation is induced by the RBT molecule. The RBT molecule in the DPPC/RBT inclusion complex constrains the conformational freedom of the phosphate group, restraining the orientation of the polar headgroup to a perpendicular arrangement with respect to the air/solution interface. The smaller bands located at 1173 and 1170 cm^{-1} in the absence and presence of RBT, respectively, are ascribed to the asymmetric stretching mode of the C−O−C group of the DPPC phospholipid, i.e., carbon atoms above the polar headgroup, as the bands appear in both cases. Therefore, the contribution of the C−O−C group of the RBT molecule to the PM-IRRAS signal can be considered not significant.[29] This band is also reversed upon interaction of the DPPC with the RBT, indicating a large conformational change of the polar headgroup.

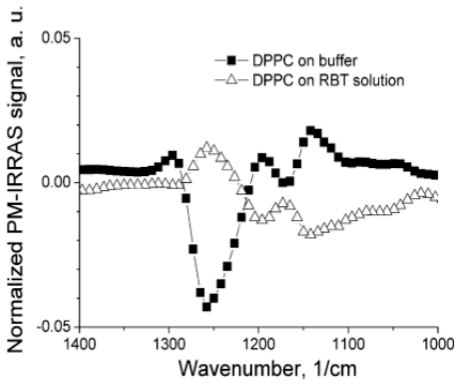

Figure 12. PM-IRRAS spectra of the phosphate and the C−O−C group vibrations region of a DPPC monolayer on a phosphate buffer subphase (black squares) and on a phosphate buffer containing 0.12 μM of RBT subphase (empty triangles) recorded at a surface pressure of 30 mN/m.

■ CONCLUSIONS

Although some data can be found in the literature about the interaction of RBT with lipid membranes, less attention has been paid to the possible effect of this drug on a physiological protective barrier: the lung surfactant. To our knowledge, this is the first report toward the study of RBT with monolayers of the zwitterionic DPPC and the anionic DPPG phospholipids used as mimetic models for the phospholipid content of lung surfactants. The presence of the RBT molecule at the phospholipid Langmuir monolayer was revealed by a significant expansion in the π−A isotherms. Results also pointed to a total recovery of the amount of RBT at the phospholipid monolayer after two subsequent compressions cycles of the monolayer. Finally, computer simulations suggest that the interactions between RBT and the DPPC and DPPG Langmuir monolayers can be described as the formation of an inclusion complex. This formed complex has an important implication preventing the penetration of the RBT into the alkyl chain region of the phospholipids, leading to a disruption of the monolayer structure and a possible toxicological effect.

■ AUTHOR INFORMATION

Corresponding Author

*E-mail: mlucio@ff.up.pt, jjginer@uco.es. Fax/Tel: +34 957 218 618.

Notes

The authors declare no competing financial interest.

■ ACKNOWLEDGMENTS

The authors thank the Spanish CICYT for financial support of this research in the framework of Projects CTQ2010-17481 and also thank the Junta de Andalucía (Consejería de Innovacion, Ciencia y Empresa) for special financial support (P08-FQM-4011 and P10-FQM-6703). Authors are also grateful to the FCT for financial support under Project PTDC/QUI-QUI/101022/2008 with coparticipation European Community funds from the FEDER, QREN, and COMPET. We thank Carlos Rubia-Paya for invaluable help with the experiments. J.J.G.-C. acknowledges Alexander von Humboldt foundation for a postdoctoral fellowship. M.P. and J.M.C. thank

FCT (Lisbon) for the fellowships (SFRH/BD/63318/2009 and SFRH/BD/66789/2009, respectively).

REFERENCES

(1) Global tuberculosis control: WHO report 2011; World Health Organization: France, 2011.
(2) Corbett, E. L.; Watt, C. J.; Walker, N.; Maher, D.; Williams, B. G.; Raviglione, M. C.; Dye, C. *Arch. Intern. Med.* **2003**, *163*, 1009−1021.
(3) DeJong, C. B.; Israelski, D. M.; Corbett, E. L.; Small, P. M. *Ann. Rev. Med.* **2004**, *55*, 283−301.
(4) Figueiredo, R.; Moiteiro, C.; Medeiros, M. A.; Almeida da Silva, P.; Ramos, D.; Spies, F.; Ribeiro, M. O.; Lourenço, M. C. S.; Júnior, I. N.; Gaspar, M. M.; et al. *Bioorg. Med. Chem.* **2009**, *17*, 503−511.
(5) King, R. J.; Clements, J. A. *Am. J. Physiol.* **1972**, *223*, 715−726.
(6) Harwood, J. L. *Prog. Lipid Res.* **1987**, *26*, 211−256.
(7) Cochrane, C. G.; Revak, S. D. *Science* **1991**, *254*, 566−568.
(8) Schurch, S.; Goerke, J.; Clements, J. A. *Proc. Natl. Acad. Sci. U.S.A.* **1976**, *73*, 4698−4702.
(9) Vostrikov, V. V.; Selishcheva, A. A.; Sorokoumova, G. M.; Shakina, Y. N.; Shvets, V. I.; Savel'ev, O. Y.; Polshakov, V. I. *Eur. J. Pharm. Biopharm.* **2008**, *68*, 400−405.
(10) Shakina, Y. N.; Vostrikov, V. V.; Sorokoumova, G. M.; Selishcheva, A. A.; Shvets, V. I. *Bull. Exp. Biol. Med.* **2005**, *140*, 711−713.
(11) Shelly, S., A.; Balis, J. U.; Paciga, J. E.; Espinoza, C. G.; Richman, A. V. *Lung* **1982**, *160*, 195−206.
(12) HyperChem 7.51; Hypercube, Inc.: Gainesville, FL.
(13) Van der Heyden, A.; Regnouf-de-Vains, J.-B.; Warszynski, P.; Dalbavie, J.-O.; Zywocinski, A.; Rogalska, E. *Langmuir* **2002**, *18*, 8854−8861.
(14) Kane, P.; Fayne, D.; Diamond, D.; Bell, S. E. J.; McKervey, M. A. *J. Mol. Model.* **1998**, *4*, 259−267.
(15) Hönig, D.; Möbius, D. *J. Phys. Chem.* **1991**, *95*, 4590−4592.
(16) Fainerman, V. B.; Zhao, J.; Vollhardt, D.; Makievski, A. V.; Li, J. B. *J. Phys. Chem. B* **1999**, *103*, 8998−9007.
(17) Deng, J.; Hottle, J. R.; Polidan, J. T.; Kim, H.-J.; Farmer-Creely, C. E.; Viers, B. D.; Esker, A. R. *Langmuir* **2004**, *20*, 109−115.
(18) Deng, J.; Polidan, J. T.; Hottle, J. R.; Farmer-Creely, C. E.; Viers, B. D.; Esker, A. R. *J. Am. Chem. Soc.* **2002**, *124*, 15194−15195.
(19) Deng, J.; Viers, B. D.; Esker, A. R.; Anseth, J. W.; Fuller, G. G. *Langmuir* **2005**, *21*, 2375−2385.
(20) Thirumoorthy, K.; Nandi, N.; Vollhardt, D. *Langmuir* **2007**, *23*, 6991−6996.
(21) Chen, X.; Huang, Z.; Hua, W.; Castada, H.; Allen, H. C. *Langmuir* **2010**, *26*, 18902−18908.
(22) Roldán-Carmona, C.; Giner-Casares, J. J.; Pérez-Morales, M.; Martín-Romero, M. T.; Camacho, L. *Adv. Colloid Interface Sci.* **2012**, *173*, 12−22.
(23) Grüniger, H.; Möbius, D.; Meyer, H. *J. Chem. Phys.* **1983**, *79*, 3701−3710.
(24) Giner-Casares, J. J.; Pérez-Morales, M.; Bolink, H. J.; Muñoz, E.; de Miguel, G.; Martín-Romero, M. T.; Camacho, L. *J. Colloid Interface Sci.* **2007**, *315*, 278−286.
(25) Casey, M. L.; Whitlock, H. W. *J. Am. Chem. Soc.* **1975**, *97*, 6231−6236.
(26) Mendelsohn, R.; Brauner, J. W.; Gericke, A. *Annu. Rev. Phys. Chem.* **1995**, *46*, 305−334.
(27) Aroti, A.; Leontidis, E.; Maltseva, E.; Brezesinski, G. *J. Phys. Chem. B* **2004**, *108*, 15238−15245.
(28) Blaudez, D.; Turlet, J. M.; Dufourcq, J.; Bard, D.; Buffeteau, T.; Desbat, B. *J . Chem. Soc., Faraday Trans.* **1996**, *92*, 525−530.
(29) Zawisza, I.; Wittstock, G.; Boukherroub, R.; Szunerits, S. *Langmuir* **2008**, *24*, 3922−3929.
(30) Blaudez, D.; Buffeteau, T.; Cornut, J. C.; Desbat, B.; Escafre, N.; Pezolet, M.; Turlet, J. M. *Appl. Spectrosc.* **1993**, *47*, 869−874.

3. Interplay of mycolic acids, antimycobacterial compounds and pulmonary surfactant membrane: a biophysical approach to disease.

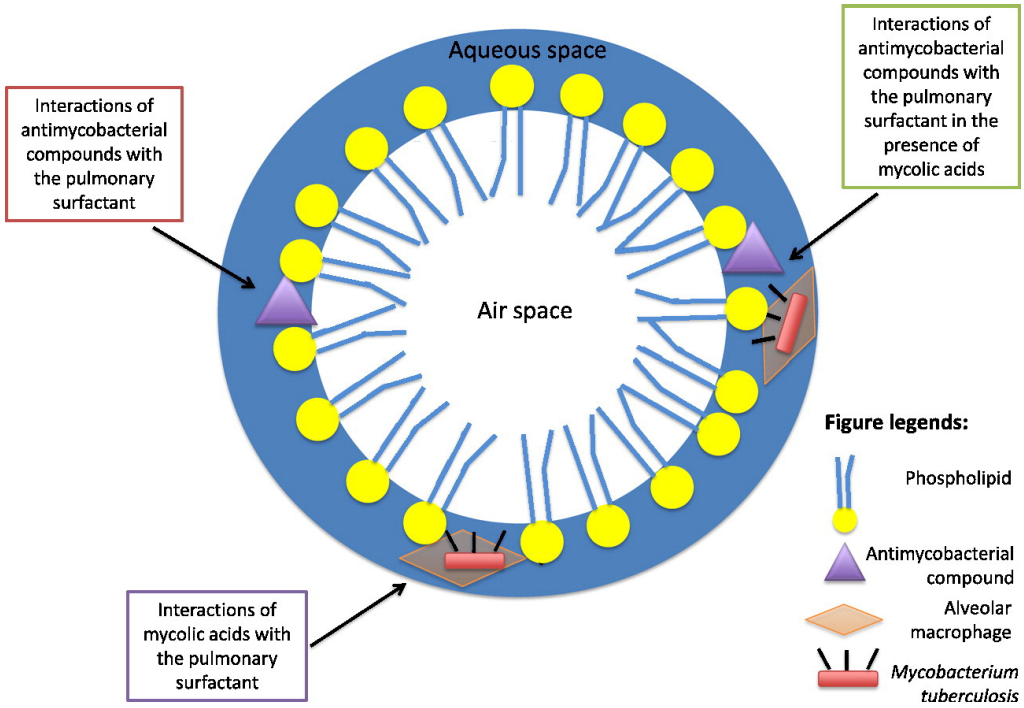

Biochimica et Biophysica Acta 1828 (2013) 896–905

Contents lists available at SciVerse ScienceDirect

Biochimica et Biophysica Acta

journal homepage: www.elsevier.com/locate/bbamem

Interplay of mycolic acids, antimycobacterial compounds and pulmonary surfactant membrane: A biophysical approach to disease

Marina Pinheiro [a], Juan J. Giner-Casares [b], Marlene Lúcio [a], João M. Caio [c], Cristina Moiteiro [c], José L.F.C. Lima [a], Salette Reis [a,*], Luis Camacho [b]

[a] REQUIMTE, Departamento de Ciências Químicas, Faculdade de Farmácia, Universidade do Porto, Portugal
[b] Departamento de Química Física y Termodinámica, Universidad de Córdoba, Spain
[c] Centro de Química e Bioquímica, Departamento de Química e Bioquímica, Faculdade de Ciências, Universidade de Lisboa, Portugal

ARTICLE INFO

Article history:
Received 26 April 2012
Received in revised form 14 September 2012
Accepted 19 September 2012
Available online 26 September 2012

Keywords:
Anti-tuberculosis drug
Brewster angle microscopy
Langmuir monolayer
Mycolic acid
Polarization-modulation infrared reflection spectroscopy
Pulmonary surfactant

ABSTRACT

This work focuses on the interaction of mycolic acids (MAs) and two antimycobacterial compounds (Rifabutin and *N*′-acetyl-Rifabutin) at the pulmonary membrane level to convey a biophysical perspective of their role in disease. For this purpose, accurate biophysical techniques (Langmuir isotherms, Brewster angle microscopy, and polarization-modulation infrared reflection spectroscopy) and lipid model systems were used to mimic biomembranes: MAs mimic bacterial lipids of the *Mycobacterium tuberculosis* (MTb) membrane, whereas Curosurf® was used as the human pulmonary surfactant (PS) membrane model. The results obtained show that high quantities of MAs are responsible for significant changes on PS biophysical properties. At the dynamic inspiratory surface tension, high amounts of MAs decrease the order of the lipid monolayer, which appears to be a concentration dependent effect. These results suggest that the amount of MAs might play a critical role in the initial access of the bacteria to their targets. Both molecules also interact with the PS monolayer at the dynamic inspiratory surface. However, in the presence of higher amounts of MAs, both compounds improve the phospholipid packing and, therefore, the order of the lipid surfactant monolayer. In summary, this work discloses the putative protective effects of antimycobacterial compounds against the MAs induced biophysical impairment of PS lipid monolayers. These protective effects are most of the times overlooked, but can constitute an additional therapeutic value in the treatment of pulmonary tuberculosis (Tb) and may provide significant insights for the design of new and more efficient anti-Tb drugs based on their behavior as membrane ordering agents.

1. Introduction

Tuberculosis (Tb) is an infectious disease caused by *Mycobacterium tuberculosis* (MTb) and represents a major health concern around the world [1]. Nearly nine million new cases are estimated each year, two million of them being fatal due to the increment of multidrug resistant Tb [2,3]. The eradication of Tb is difficult since MTb lipidic envelope confers impermeability to antibiotics and ability to withstand unfavorable conditions [1,3,4]. For this reason, the treatment of Tb is associated to a multidrug combination therapy for at least 6 months [1]. Therefore, to improve the therapeutic compliance, new and more effective drugs are urgently needed [1,5], requiring their development new approaches to understand the mechanism of action of classical therapies.

In pulmonary Tb, which is the most common manifestation of Tb, the inhaled MTb encounters the pulmonary surfactant (PS) before reaching its target (the alveolar macrophage) [6]. Besides being a physiological barrier to the entrance of bacteria in the body, PS is from a biophysical point of view, a lipid monolayer containing hydrophobic and hydrophilic proteins. This compressible monolayer possesses a fundamental role in decreasing alveoli surface tension, which has proved to be essential to facilitate respiratory work and prevent alveoli collapse [7,8]. The recent accepted mechanism for this latter crucial function states that, during expiration, the fluid lipids and proteins with less ability to sustain high surface pressures are squeezed out from the PS monolayer, leading to an enrichment of the film with less fluid lipids [9]. During respiratory movements the lost lipids and proteins are stored in surface-associated "reservoirs" at the adjacent interface being available for further re-adsorption [10–12].

The MTb cell wall is extremely rich in lipids, and this high lipid content is consistent with the bacteria primary location nearby the air/water interface of PS monolayers. The lipids from MTb cell wall have

Abbreviations: BAM, Brewster angle microscopy; DPPC, Dipalmitoylphosphatidylcholine; DPPG, Dipalmitoylphosphatidylglycerol; LC, Liquid-condensed; LE, Liquid-expanded; LUVs, Large unilamellar vesicles; LPC, Lysophosphatidylcholine; MAs, Mycolic acids; MTb, *Mycobacterium tuberculosis*; RFB, Rifabutin; RFB2, *N*′-acetyl-rifabutin; PE, Phosphatildylethanolamine; PG, Phosphatidylglycerol; PhS, Phosphatildylserine; PI, Phosphatildylinositol; PM-IRRAS, Polarization-modulation infrared reflection spectroscopy; PS, Pulmonary surfactant; SM, Sphingomyelin; SP, Surfactant protein; Tb, Tuberculosis

* Corresponding author at: REQUIMTE, Departamento de Ciências Químicas, Faculdade de Farmácia, Universidade do Porto, Rua de Jorge Viterbo Ferreira no 228, 4050–313 Porto, Portugal. Tel.: +351 220428672; fax: +351 226093483.
E-mail address: shreis@ff.up.pt (S. Reis).

0005-2736/$ – see front matter © 2012 Elsevier B.V. All rights reserved.
http://dx.doi.org/10.1016/j.bbamem.2012.09.015

been further implicated in the PS dysfunction that causes the typical symptoms of pulmonary Tb, namely the decrease of pulmonary compliance manifested as breathing difficulty and, consequently, as an increased respiratory work [1,13]. In this regard, Chimote and coworkers have previously proposed a biophysical explanation to some of the symptoms observed in pulmonary Tb. According to these authors, the pulmonary symptoms might be due to the biophysical impairment of the lung surfactant function due to the interfacial presence of mycobacterial lipids [14]. In another study performed by the same authors, it was demonstrated by atomic force microscopy (AFM) that mycobacterial lipids could aggregate within PS monolayers, resulting in a disturbed monolayer surface activity. The authors also suggested that this could be a mechanism of lung surfactant dysfunction in pulmonary Tb [13]. Wang et al. also studied the inhibitory effects of mycobacterial lipids in bovine and calf lung surfactant models and concluded that the bacterial lipids inhibited the monolayer surface activity in both PS models [15].

Besides the importance of PS as a lung reservoir for MTb, the lungs are also organs of anti-Tb drugs bioaccumulation, possibly due to their distribution at the PS lipid level. In this context, it is important to pursue biophysical studies to unveil the interplay of antimycobacterial compounds and MTb with PS lipid monolayers, as these studies might provide additional and important insights about the therapeutic role of the drugs protecting PS monolayers from the impairment effects of the mycobacterial lipid [1,16].

To our knowledge, there is only one experimental study reported in the literature concerning the interaction of anti-Tb drugs and PS. This study performed by Chimote et al. evaluates the interactions between DPPC, the main compound of the PS, and the anti-Tb drugs (isoniazid, rifampicin and ethambutol). The results of this study have shown that the antimycobacterial compounds improve the surface parameters of the PS model, which correlates with a putative protective role of these antimycobacterial compounds of the PS biophysical integrity *in vivo* [17].

Beyond the abovementioned studies, the knowledge of the biophysical effects of both MTb membrane lipids and anti-Tb drugs is still scarce, particularly the information related with their accessibility to the PS lipid monolayer. In this context, our study provides the first comprehensive survey of the implications caused by different amounts of mycobacterial lipids in a natural lung surfactant that mimics the human PS, and it is also the first study on the interaction of RFB (RFB) and *N*′-acetyl-Rifabutin (RFB2) with PS monolayer in the presence and absence of mycobacterial lipids.

RFB is a second-line drug used in Tb treatment [1,5]. Despite being a second-line drug, RFB has shown to be more efficient than first-line drugs, such as rifampicin [18]. Moreover, RFB therapeutic value is increasing due to its beneficial effect on the newly diagnosed multidrug resistant Tb and in the prevention of the disseminated *Mycobacterium avium* complex infection in HIV positive cases [18,19]. For these mentioned reasons, and given the excellent penetration capacity of RFB in cells, as well as the accumulation of this drug in the pulmonary tissue, the biophysical study proposed herein may prove important to broaden the knowledge of this drug mechanism of action or to conduct the design of more effective derivates. In this context, our newly synthesized RFB derivate is also object of the current study (Fig. 1). In comparison to RFB, RFB2 shows better *in vitro* and *in vivo* therapeutic index, thereby being a promising drug for the clinical application in Tb treatment [5]. RFB and RFB2 were both used in this work at concentrations that were reported as effective against MTb and *Mycobacterium avium* complex and as non-toxic against Vero cells [5].

The biophysical approach of our study required not only a rational choice of the anti-Tb drugs, but also a careful choice of lipids and lipid models to mimic the biological environment encountered by these drugs. In this regard, the mycolic acids (MAs) have been chosen to mimic the MTb membrane since they are the main components of the MTb cell wall, being indispensable for its structural integrity [20,21]. MAs are α-alkyl-β-hydroxyl high molecular weight fatty acids. Each molecule consists of a hydrophobic long saturated 2-alkyl branch and a hydrophilic head group (containing the groups COOH and OH) as shown in Fig. 1 [20,22,23]. MAs occur in the cell wall of MTb as variable mixtures of different classes (α-MA, methoxy-MA and keto-MA) that exhibit different conformations in the PS monolayers [24–26]. Both keto- and methoxy-MA produce the so-called "W" conformation, with the alkyl chains folded to give four parallel arms with the carbonyl and methoxy groups hydrated by water molecules in the surface layer [22]. However, independently of the surface pressures applied, keto-MA retains the compact W-shape, while methoxy-MA adopts extended structures [22]. In the case of α-MA, the most abundant form of MAs, as the surface pressure is increased by compression, the molecules apparently change from the compact W-shape to extended conformations with two hydrocarbon chains [22,27,28]. Curosurf®, a PS porcine extract, was elected as the PS model because it presents a composition and biophysical properties similar to the human PS, being used as replacement therapy in several human disorders related to lung's injury, such as the respiratory distress syndrome [9,29]. Despite the similarities with the human PS, Curosurf® possesses a different amount of components and lacks neutral lipids and hydrophilic proteins [29]. The main component of Curosurf® is dipalmitoylphosphatidylcholine (DPPC) (Fig. 1) (47% w/w). The other prevailing lipids are zwitterionic such as lysophosphatidylcholine (LPC), sphingomyelin (SM), phosphatildylethanolamine (PE), and a significant amount of negatively charged lipids (5.7–9.6% w/w) namely phosphatidylglycerol (PG), phosphatildylinositol (PI) and phosphatilserine (PhS) [29,30]. The hydrophobic proteins present in Curosurf® are surfactant protein B (SP-B) (0.4% w/w) and SP-C (0.7% w/w), which extensively interact with the surfactant phospholipids and increase their ability to efficiently decrease the surface tension [9,29]. These proteins are cationic due to the positively charged arginine and lysine amino acids present in their composition [31,32].

In summary, besides unveiling the mechanisms of interaction of antimycobacterial compounds (RFB and RFB2) with PS (Curosurf®), this work can contribute to identify novel biophysical mechanisms that explain the therapeutic effect of these antimycobacterial compounds, hence allowing the future development of more effective drugs that are able to protect the PS monolayer from the biophysical impairment effect induced by the MAs. Additionally, and besides many studies have proven the importance of SP-B and SP-C on the function of the lung activity [10,11,31,33–35], this is the first report of the effects of MAs and antimycobacterial compounds in SP-B and SP-C studied *in situ*.

2. Materials and methods

2.1. Materials

RFB was isolated from Mycobutin® and further purified as described previously [5]. RFB2 was obtained from RFB, using a selective acylation of the secondary amine [5]. MAs were purchased from BioClot GmbH, Germany, and used without any further purification. Curosurf® was purchased from Angelini Farmacêutica Lda, Portugal, and was used as originally supplied. Sodium chloride, monopotassium phosphate and dipotassium phosphate (99% pure) were purchased from Panreac®. Chloroform and methanol were used as co-spreading solvents. The subphase used, phosphate buffer 100 mM (pH 7.4; 100 mM of sodium chloride), was prepared from ultrapure water, produced by Millipore Milli-Q unit (resistivity = 18.2 MΩ cm).

2.2. Methods

2.2.1. Langmuir trough

Two different troughs models, a KN-1005 (KSV Instruments Ltd, Helsinki, Finland) and NIMA 601(Nima Technology, Coventry, England) were equipped with two symmetrical barriers and a Wilhelmy type dynamometric system using a strip of filter paper. KN-1005 is

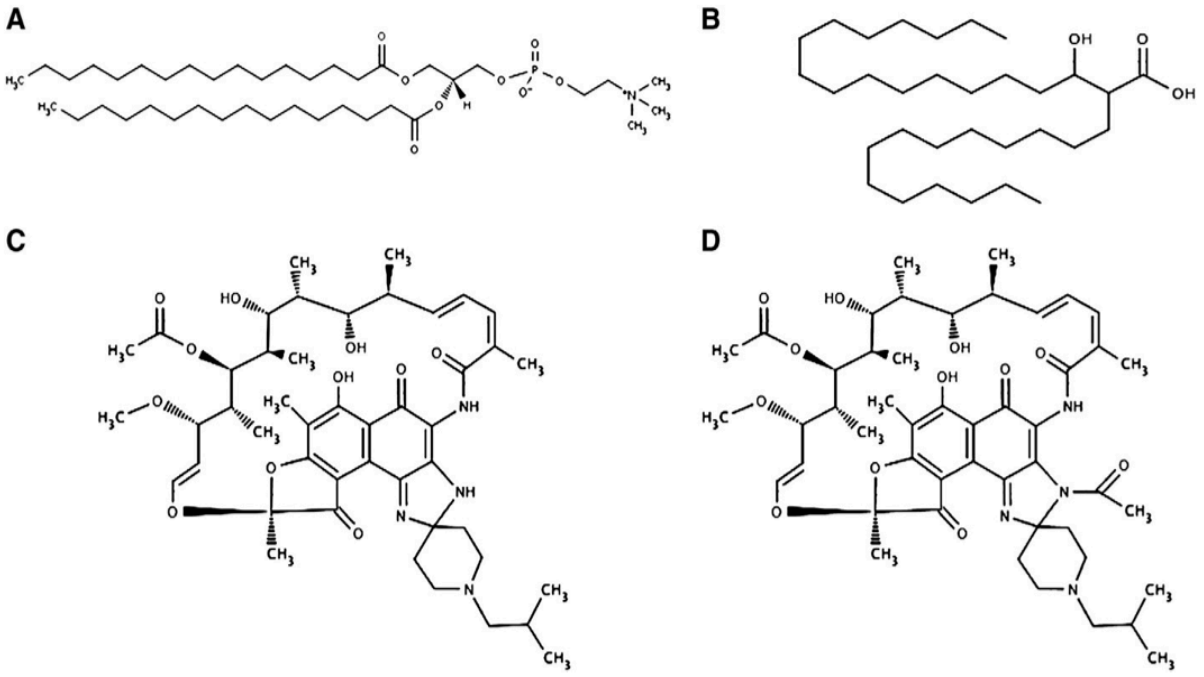

Fig. 1. Chemical structures of DPPC (A), MAs (B), RFB (C) and RFB2 (D).

nearly 325 mL in subphase volume and close to 587 cm^2 total area. NIMA 601 is about 400 mL in subphase volume with a total area close to 600 cm^2. KN-1005 was used in PM-IRRAS experiments. Due to its larger capacity and area, that allows the compensation of pressure restrictions imposed by the smaller trough [29], NIMA 601 was used to obtain the represented isotherms.

2.2.2. Film spreading

All films were prepared by spreading samples on the phosphate buffer subphase. Films were spread by deposition of tiny droplets of samples uniformly on the air–water interface, using a 250 μL microsyringe. Curosurf® was spread from 0.2 mg/mL chloroform-extracted solutions. MAs were spread from 0.2 mg/mL chloroform: methanol-extracted solutions (9:1 v/v). After spreading, solvent was allowed to evaporate for 15 min prior to film compression. The effect of antimycobacterial compounds was evaluated by spreading Curosurf®, Curosurf®:MAs (9:1 w/w) and Curosurf®:MAs (1:1 w/w) monolayers on a phosphate buffer with a known concentration of RFB and RFB2 (0.118 μM and 0.225 μM respectively).

2.2.3. Film compression

All spread films were compressed at a rate of 20 cm^2/min (at a much slower rate than the respiratory movements, due to experimental limitations). During compression, surface pressure–area isotherms (π/A) were recorded until the maximum compression possible in our trough (*i.e.* at the maximum value of ≈50 mN/m of compression). The absolute molecular area ($Å^2$/molecule) of DPPC was used to express the compression isotherms. All experiments were performed in an atmosphere with 100% relative humidity at 21 °C.

2.2.4. Brewster angle microscopy

Brewster angle microscopy (BAM) images were obtained from a I-Elli 2000 apparatus (supplied by Nanofilm Technologies, Goettingen, Germany) using a Nd:YAG diode laser, which can be recorded with a lateral resolution of 2 μm. The image processing procedure included a geometrical correction of the image, as well as a filtering operation to reduce interference fringes and noise. Furthermore, the brightness of each image was scaled to improve contrast.

2.2.5. Polarization-modulation infrared reflection spectroscopy

Polarization-modulation infrared reflection spectroscopy (PM-IRRAS) was performed using a KSV PMI 550 instrument (KSV Instruments Ltd, Helsinki, Finland) recording the spectra every 2 mN/m from 0 to 40 mN/m. The Langmuir trough was set up so that the light beam reached the monolayer at a fixed angle of incidence of 80°. The incoming light was continuously modulated between s and p polarization at a high frequency. This allowed the simultaneous measurements of spectra for the two polarizations, and their difference provides surface-specific information, while their sum provides the reference spectrum (buffer with or without antimycobacterial compound). In this work, PM-IRRAS was elected due to the advantages over the conventional IRRAS mode, namely the independence of modulated reflectivity of the isotropic adsorption from the vapor or bulk water, overcoming the problem of the surrounding water vapor [36,37].

2.2.6. Parameters studied from the surface pressure–area Langmuir isotherms

A variety of systems have been used for determining the surface activity of surfactant materials derived from the lungs, including Langmuir trough and captive bubble surfactometer [38–41]. In comparison to the Langmuir trough, the captive bubble surfactometer reveals a much lower compressibility, extremely low surface tensions and a moderated hysteresis if the film collapse is avoided [42]. However, over the past few years, the evolution of Langmuir trough designs allowed it to sustain high surface pressures which, coupled with spectroscopy and image techniques such as BAM and IRRAS, constitutes a valuable system to visualize the morphology and the characterization of the PS monolayers [9,40]. Langmuir isotherms give information about the lipid phases and the phase transitions, which are both dependent on the temperature, the pressure, and the pH [43,44]. The parameters studied from the surface pressure–area (π/A) Langmuir isotherms were: the minimum area per molecule; the hysteresis and the

compressibility. The minimum area per molecule (A_{min}) is the mean area occupied for one molecule in the surface layer and it indicates the molecular packing and the interactions between the monolayer components. This parameter was determined by extrapolation of a line tangent to the condensed region. Hysteresis was acquired by the monolayer compression/decompression isotherms and corresponds to the difference between compression and decompression areas [32]. The cycle of compression/decompression was performed to mimic the expiration/inspiration movements, respectively. Elastic modulus (C_s^{-1}) was calculated from the π/A isotherms by the following equation: $C_s^{-1} = -A\,(d\pi/dA)$, where A is the area per lipid molecule, and π is the surface pressure. C_s^{-1} describes the relationship between the surface pressure increase and the area per molecule decrease. A higher value of C_s^{-1} is indicative of a less compressible monolayer [44,45].

3. Results and discussion

3.1. Comparison of compression isotherms

Fig. 2 represents the pressure–area (π/A) isotherm of Curosurf®. In the recorded isotherm three biophysical states of the PS monolayer can be identified: zone A, zone B and zone C [43]. The molecular nature of these three regions is further discussed in the BAM and IRRAS measurements. The zone A of the Curosurf® isotherm, between 0 and 5 mN/m, represents a less ordered region with high compressibility, typical of a liquid-expanded (LE) phase of the monolayer [12]. In the LE phase, phospholipid acyl chains have a considerable degree of rotational freedom. The zone B, between 5 and 40 mN/m, corresponds to a less compressible film and represents the coexistence of two phases: liquid-condensed (LC) and LE phase. The Curosurf® isotherm did not show an apparent phase transition plateau but the appearance of a plateau region (zone C) starting at ≈43 mN/m is noticeable. In this region, before and after reaching the plateau, natural surfactant films have lower compressibility due to the removal of the LE phase from the film by the "squeezing-out" of the proteins and fluid lipids like PGs, that leave the interface and consequently lead to the monolayer enrichment with DPPC [12,46]. In this plateau region the isotherm undergoes a monolayer-to-multilayer transition plateau, in which π only increases slowly with significant film compression [9]. The appearance of the plateau region in the 40–50 mN/m range is controversially discussed. Some authors pointed this plateau region as the film collapse [47,48]. However, other authors report a first plateau region within this pressure range and describe it as the transition of monolayer-to-multilayers [9,49]. They showed that this characteristic plateau is followed by a rapid increase in the surface pressure that leads to a second plateau (the film collapse) [9]. Indeed, in Fig. 2 it is possible to observe that after the plateau region (π above 47 mN/m) a pressure increment starts to happen, possibly leading to the monolayer collapse, which was not reached due to the maximum compression possible in our trough. *In vivo*, during the inhalation–expiration cycle, the lung surfactant monolayer experiences surface tension values between 30 and 0 mN/m [50]. However since TB starts with the inhalation of MTb, the equilibrium inspiratory surface tension (correspondent to a surface pressure of 40 mN/m) is the most relevant in this work. Additionally, in the pulmonary TB, due to surfactant deficiency and/or dysfunction, a pronounced elevated alveolar surface tension might occur [51].

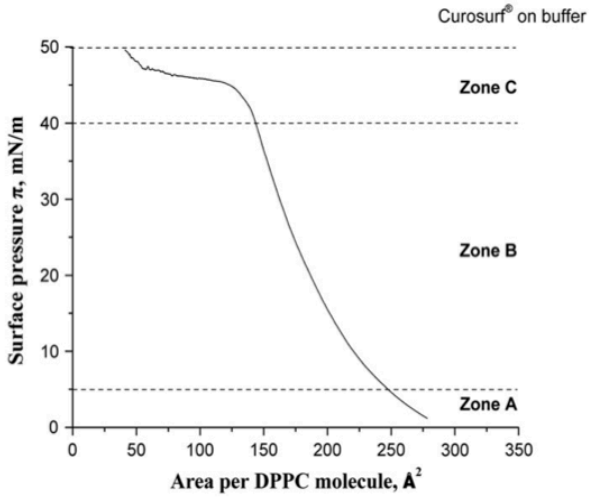

Fig. 2. Surface pressure (π/A) isotherm of Curosurf®.

The comparison between the Curosurf®:MAs (9:1 w/w) and Curosurf®:MAs (1:1 w/w) isotherms (Fig. 3) indicates that the effect of MAs on the biophysical properties of Curosurf® is concentration dependent. For lower concentrations of MAs, the biophysical effects are negligible as the isotherms Curosurf®:MAs (9:1 w/w) and Curosurf® are almost superimposed. The interactions of the Curosurf® monolayer with higher amounts of MAs are pronounced and occur at all the different regions of the isotherm. Higher amounts of MAs shift the isotherm to larger molecular areas, *i.e.* causing a monolayer expansion. At the zone C, the transition of monolayer-to-multilayer happens at the same pressure as for lower amounts of MAs, and occurs at slightly lower pressures when compared to the Curosurf® monolayer in the absence of MAs, meaning that in the presence of MAs the PS monolayer is less stable. Moreover the MAs contain negatively charged carboxyl groups at the physiological pH (predicted using MarvinView® 5.4.1.1 software from ChemAxon), and thus electrostatic repulsions with the PS head groups might happen, contributing to the monolayer expansion. Van der Waals interactions may also take place, between the mycolate alkyl chains and the PS acyl chains. Furthermore, the MAs chain-length asymmetry might create spaces through part of the lipid film thickness into which alkyl chains of associated PS phospholipids may fit, justifying the earlier transition of the PS to a more condensed phase when the MAs are present [27,52].

The antimycobacterial compounds (RFB and RFB2) clearly change the isotherm of Curosurf® (Fig. 3). The interactions with the antimycobacterial compounds are higher at the LE region (zone A) since the lower lipid density in this region facilitates the drug interaction and insertion in comparison to the LC region (zone C). Despite the very

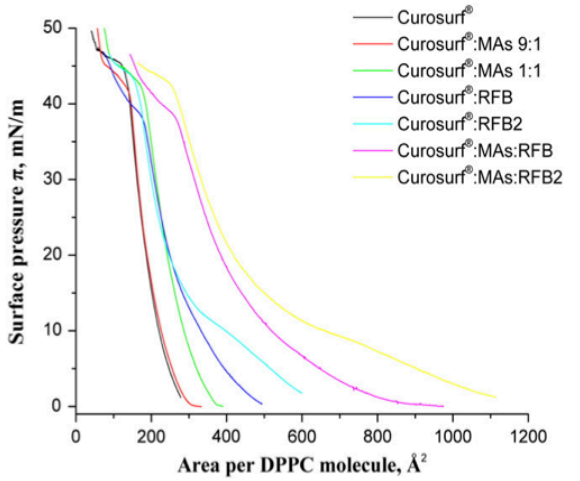

Fig. 3. Surface pressure (π/A) isotherms of Curosurf® (black line), Curosurf®:MAs 9:1 w/w (red line), Curosurf®:MAs 1:1 w/w (green line), Curosurf®:RFB (0.118 μM) (dark blue line), Curosurf®:RFB2 (0.225 μM) (light blue line), Curosurf®:MAs (1:1 w/w):RFB (0.118 μM) (purple line) and Curosurf®:MAs (1:1 w/w):RFB2 (0.225 μM) (yellow line).

similar interactions of both antimycobacterial compounds in the zones A and B, it can be observed that RFB2 interacts more extensively with the PS model. This might be due not only to the higher concentration of RFB2 used, but also to the presence of an acetyl group that confers a bulkier and an extra lipophilic group that is more prone to interact with the lipids/proteins of the PS. Moreover, the isotherm of Curosurf®:RFB2 presents a smaller plateau region at $\pi \approx 5$–10 mN/m, that is not observed in the case of Curosurf®:RFB, which represents the LE and LC phase coexistence and a more visible phase transition. The extra acetyl group of RFB2 must be once more a reason for this difference, conferring a higher surface activity that for this reason demonstrates increased ability to spread at the interface. The higher interaction of RFB2 with the PS model, comparing with RFB, might justify its previously reported higher *in vivo* efficacy [5]. This was further confirmed by the second compression isotherm of the PS model after the decompression, which has revealed to be more similar to the first compression when in presence of RFB2 than in presence of RFB (data not shown). It is possible to recognize that in the zone C the antimycobacterial compounds interact differently with the Curosurf®. In the case of RFB, the transition of monolayer-to-multilayer starts at $\pi \approx 38$ mN/m. For RFB2 the transition begins at $\pi \approx 42$ mN/m, which is slightly lower compared to the Curosurf® but higher than RFB. Since this transition occurs when the proteins and the PG lipids are "squeezed out" from the monolayer to form the multilayers [53] and at smaller pressures when in the presence of RFB, it is predictable that, in comparison to RFB2, RFB's interactions with PG and proteins are higher. According to the distribution of the charged species, predicted by MarvinView® 5.4.1.1 software from ChemAxon, at the physiological pH RFB has a higher contribution of the positively charged species (due to the ionization of the piperidine nitrogen with a pKa 9.5) [54], possibly promoting stronger electrostatic interactions with the negatively charged phospholipids (like PG).

The effect of the antimycobacterial compounds in the presence of both Curosurf® and MAs was also tested (Fig. 3). The presence of the antimycobacterial compounds and the higher quantities of MAs shifted the Curosurf® isotherm to higher areas, these changes occur in all the different regions and especially at the lower pressures for the same reasons already described. Furthermore, the transition of monolayer-to-multilayers occurs at the same pressures previously described in the isotherms of Curosurf® with the antimycobacterial compounds and in the absence of MAs.

The A_{min} determined for Curosurf® was 101 Å^2/molecule. The difference between compression and expansion isotherms is small, considering that it was only performed at the first cycle, which is essential for an efficient PS [32,43]. The maximum C_s^{-1} calculated for Curosurf® was 439 mN/m (Table 1), close to the value for pure DPPC [44,55]. As expected, the C_s^{-1} maximum values were found for surface pressures ranging from 20 to 30 mN/m, as well in the plateau region from 40 to 50 mN/m (data not shown) [55]. The A_{min} of the Curosurf® in the presence of the MAs is clearly higher. This denotes that MAs remain at the interface, probably within the PS components, under compression. The integration of MAs in the PS monolayer can occur as a result of the interactions of the MAs with the head groups or with the phospholipid tails of the lipid PS components. The interactions of the MAs with the PS head groups possibly happen by means of hydrogen bonds and electrostatic interactions, and explain the increase of the A_{min} of the Curosurf® in the presence of the MAs, as these interactions cause a large area requirement of the head group and, to optimize their van der Waals interactions, force the chains to be tilted in the condensed phase [44]. If the interactions with the phospholipid tails also take place, they would be more pronounced in the case of higher amounts of MAs. However, the value of the A_{min} is very similar in the presence of the two different proportions of the MAs studied. The intercalation of the MAs residues within the components of the PS, in order to compensate the chain-length differences and to produce higher packing density, may be the responsible for the very similar values of the A_{min} observed by higher amounts of MAs [52]. Additionally, a non-mixed monolayer may also be formed due to the lack of correlation between the MAs amount and the A_{min} and also due to the collapse pressure obtained, which is the same independently of the MAs concentration. Besides analyzing the changes induced by the MAs in the A_{min} of the PS monolayer, it is also important to study the effect of the MAs in other parameters, such as the hysteresis behavior of the PS monolayer. A good hysteresis behavior results from a small difference between the compression and expansion isotherms of the monolayer [32]. In the opposite case of higher hysteresis the interfacial work of breathing is increased [43]. MAs increase the hysteresis value of the PS monolayer and this increase reaches significantly higher values ($\approx$46%) with the higher amount of MAs. This finding is consistent with the deleterious effect caused by the MTb in the interfacial work of breathing. Regarding the effects of MAs in the C_s^{-1} of the PS monolayer, a biphasic behavior is observed. Lower amounts of MAs did not change the C_s^{-1} whereas higher amounts of MAs are responsible for a more compressible monolayer with a C_s^{-1} value lower than that obtained for the PS model in the absence of MAs. Consistent with our work, previous studies of mixed monolayers of MAs and phospholipids having a choline head group (the main phospholipids present in our PS model) reported a monolayer expansion effect (*i.e.* monolayer becomes more compressible) [14,52]. The C_s^{-1} values suggest that the MAs are integrated within the phospholipids of the monolayer, consequently causing a monolayer expansion that seems to be dependent of the MAs amount. The increase in the compressibility of the PS monolayer, as observed in the presence of MAs, has a negative connotation for the PS surface activity, as it indicates the sudden destabilization of the PS film that is related to a poorly packed surfactant and leads to an increased breathing work [51].

Table 1
Minimum area per lipid molecule, elastic Modulus and hysteresis of the Langmuir Curosurf®, Curosurf®:MAs 9:1 w/w, Curosurf®:MAs 1:1 w/w, Curosurf®:RFB (0.118 μM), Curosurf®:RFB2 (0.225 μM), Curosurf®:MAs (1:1 w/w):RFB (0.118 μM) and Curosurf®:MAs (1:1 w/w):RFB2 (0.225 μM) monolayers on the phosphate buffer.

	A_{min} (Å^2/molecule)	C_s^{-1} (mN/m)	Hysteresis ((Å^2/molecule)·mN/m)
Curosurf®	101 ± 5	439 ± 10	4013 ± 100
Curosurf®:MAs9:1	135 ± 5	441 ± 10	4698 ± 100
Curosurf®:MAs1:1	138 ± 5	398 ± 10	7470 ± 100
Curosurf®:RFB	198 ± 5	877 ± 10	6278 ± 100
Curosurf®:RFB2	183 ± 5	735 ± 10	4955 ± 100
Curosurf®:MAs:RFB	424 ± 5	1350 ± 100	8182 ± 100
Curosurf®:MAs:RFB2	481 ± 5	1330 ± 100	8348 ± 100

Both antimycobacterial compounds shift the A_{min} of Curosurf® to higher values, indicating a strong interaction of the antimycobacterial compounds with the PS. The A_{min} is higher in the presence of RFB comparing to RFB2. Although RFB2 is bulkier, this antimycobacterial compound might be located nearer to the phospholipids tails due to the presence of one extra acetyl group. RFB shallower location at the head groups of PS phospholipids is consistent with the higher A_{min}, given the large area requirement of the head groups. Both antimycobacterial compounds increase the hysteresis of the PS, being the hysteresis increase caused by RFB2 smaller ($\approx$19%) compared to the hysteresis increase caused by RFB ($\approx$36%). Overall, both RFB and RFB2 interact extensively with Curosurf® forming less compressible monolayers as observed by the increase of C_s^{-1} values. Furthermore, the interaction of the antimycobacterial compounds with "squeezed-out" components of the PS (lipids like PG and proteins) seems to happen especially for RFB, due to the lower values of the pressure of transition from monolayers to multilayers in the presence of this antimycobacterial compounds.

In the presence of MAs both antimycobacterial compounds shift the A_{min} of Curosurf® to even higher values than that observed when the

MAs were not present. The interactions of the antimycobacterial compounds with the MAs might form a bulky complex that then interacts with the negatively charged head groups of the PS justifying the great changes observed in the A_{min}. Contrastingly to the effect of the antimycobacterial compounds on Curosurf®, observed in the absence of MAs, in the presence of higher amounts of MAs, RFB2 elevates the A_{min} to higher values than RFB. This might be attributed to a closer interaction of the complex MAs and RFB2 with the head groups of the PS and consequently the greater area requirements at the head group region of the PS monolayer translate into higher A_{min} values. Both antimycobacterial compounds, in the MAs presence, increase the hysteresis of the PS (≈51%), with no noticeable differences between the effects of each antimycobacterial compound. Although in the presence of MAs the antimycobacterial compounds form less compressible PS monolayers, the increase in the C_s^{-1} values was similar to that observed when the antimycobacterial compounds were interacting with the PS monolayer in the absence of MAs.

3.2. BAM

BAM is a powerful tool that enables the visualization of the morphological changes that occur during the compression of the monolayers. Moreover, BAM also gives some information on the fluidity of the film in relation to the geometry of the domains observed at the water interface [56]. The contrast in BAM images is due to local differences in the monolayer refractivity index, caused by differences in local molecular density or packing [10,12,57].

The morphologies of Curosurf®, Curosurf®:MAs (9:1 w/w), Curosurf®:MAs (1:1 w/w), Curosurf®:RFB, Curosurf®:RFB2, Curosurf®:RFB:MAs (1:1 w/w) and Curosurf®:RFB2:MAs (1:1 w/w) at constant π of about 4, 24 and 40 mN/m (zones A, B and C) of the first compression are shown and were directly observed by BAM (Fig. 4).

The domains of Curosurf® appear at pressures above ≈24 mN/m (transition from LE to LC) and become larger with the compression, as it can be confirmed by the image obtained at 47 mN/m (Fig. 4B). For intermediate pressures (24≤π≤40 mN/m) the BAM images show a homogenous size distribution of circular shape lipid domains (see inset of ≈24 mN/m in Fig. 4A). For π>40 mN/m the lipid domains are noncircular and have ramified shape domains (see inset of 47 mN/m in Fig. 4A). These lipid domains with a starry aspect are very characteristic of this natural PS [29]. Furthermore, the BAM image obtained in the plateau region (Fig. 4A) confirms that the monolayer collapse was not reached since the domains' coalescence was not observed. The BAM image appears mainly gray, which is consistent with a high fraction of solid phase. The white spots that appear on the top are attributed to the fluid phase material that is pushed out of the interface when the transition of monolayer-to-multilayer occurs and a DPPC enriched film is formed [12,57]. The presence of low amounts of MAs is enough to promote a significant change in the PS lipid domains. The transition of LE to LC occurs at π≈3 mN/m (data not shown), and for π≈4 mN/m, small elliptical domains with a very small size can be observed (Fig. 4C). The size and number of these lipid domains increase with the pressure. For all the different regions, the domains have an elliptical shape. Higher amounts of MAs promote higher differences in the lipid domains' size and morphology. For π≈4 mN/m some brighter points appear with a heterogeneous distribution along the predominant LE region (Fig. 4D). These brighter points might be aggregates of MAs with phospholipids, such as PI [14]. Although being more pronounced for lower pressures, the brighter points are present at all the different pressures evaluated. For intermediate pressures (24≤π≤40 mN/m) the lipid domains are not as visible, but it is possible to recognize the presence of some small and elliptical domains. The brighter points are also present, but in a smaller amount and with a more homogenous distribution (data not shown). For higher pressures, the presence of smaller aggregates can be observed. In the plateau region there is an enrichment of the monolayer in DPPC and the few aggregates are probably due to MAs' collapse [22,23,27,52]. Furthermore, the BAM image, for π≈40 mN/m (Fig. 4D), confirms the MAs' collapse, probably because MAs are less surface active in comparison to the Curosurf® components, and thus the PS and MAs mixed monolayer reaches the collapse earlier at smaller surface pressures [14].

The BAM images of Curosurf® in the presence of antimycobacterial compounds reveal the existence of very bright regions that can be associated with RFB and RFB2 local clusters with high refractive index, indicating the formation of the antimycobacterial compound at the interface (Fig. 4E and F). In the case of RFB, the antimycobacterial

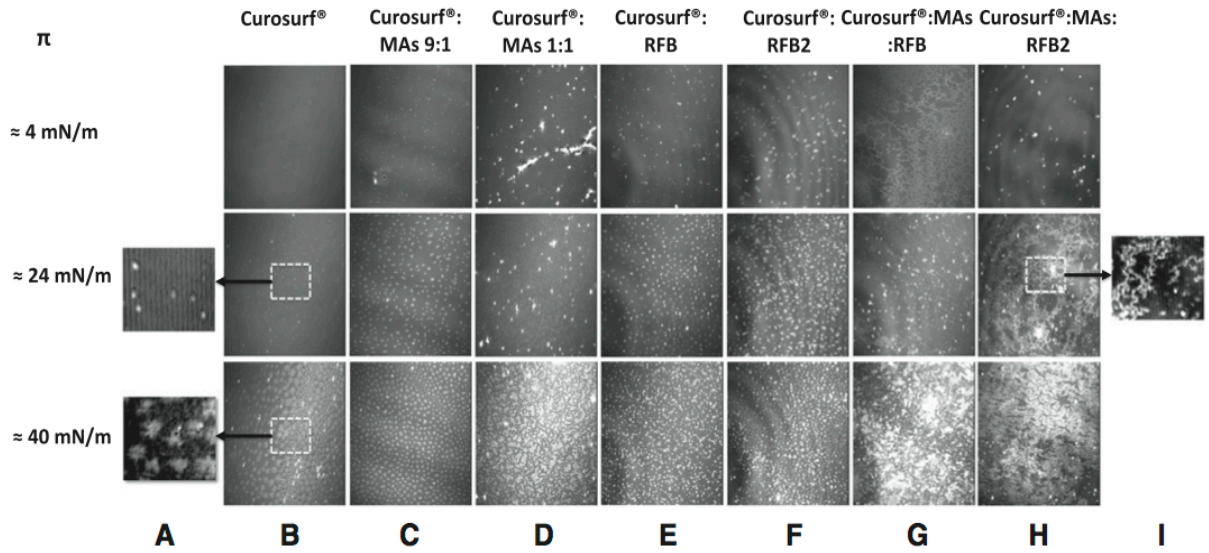

Fig. 4. BAM images of Langmuir monolayers of Curosurf® (5.3 mN/m–221 Å²/molecule; 23 mN/m–179 Å²/molecule; 47 mN/m–64 Å²/molecule), Curosurf®:MAs 9:1 w/w (6.1 mN/m–248 Å²/molecule; 25 mN/m–173 Å²/molecule; 45 mN/m–80 Å²/molecule), Curosurf®:MAs 1:1 w/w (3.7 mN/m–332 Å²/molecule; 25.6 mN/m–225 Å²/molecule; 45 mN/m–115 Å²/molecule), Curosurf®:RFB (0.118 μM) (4.4 mN/m–404 Å²/molecule; 26.5 mN/m–220 Å²/molecule; 47 mN/m–74 Å²/molecule, Curosurf®:RFB2 (0.225 μM) (6.1 mN/m–488 Å²/molecule; 24.4 mN/m–220 Å²/molecule; 43.6 mN/m–152 Å²/molecule, Curosurf®:MAs (1:1 w/w):RFB (0.118 μM) (6.6 mN/m-600 Å²/molecule; 24.7 mN/m-346 Å²/molecule; 45.4 mN/m-143 Å²/molecule) and Curosurf®:MAs (1:1 w/w):RFB2 (0.225 μM) (6.4 mN/m–804 Å²/molecule; 24 mN/m–378 Å²/molecule; 45 mN/m–164 Å²/molecule).

aggregate can be observed at π≈4 mN/m. With the rise of the pressure, while the number of lipid domains increases there is a decrease in their size, emerging bright regions inside the domains. Therefore, at intermediate and higher pressures, spherical domains presenting inner small bright points that correspond to the antimycobacterial compound (RFB or RFB2) can be observed. Moreover, in the case of Curosurf® in the presence of RFB2, and especially at higher pressures, it is possible to identify domains without the antimycobacterial compound, possibly due to a "squeezing-out" of the RFB2. This is consistent with the smaller value of the A_{min} obtained for RFB2 in comparison to RFB.

The presence of the antimycobacterial compounds and higher amounts of MAs showed the occurrence of irregular and small lipid domains at intermediate and higher pressures (Fig. 4G and H). The BAM domains do not contain the characteristic bright spots of antimycobacterial compound clusters possibly due to the binding of the RFB or RFB2 to MAs when higher amounts of MAs are present at the PS monolayer. However, some filamentary structures that are possible aggregates could be observed, particularly in the presence of RFB2 (see inset of ≈24 mN/m in Fig. 4I). The appearance of these structures confirms the occurrence of immiscibility between the different components of the monolayer [14]. At lower pressures (π≈4 mN/m), and in the presence of RFB, the monolayer seems so have some condensed structures with filamentary morphology, whereas in the presence of RFB2, the monolayer is still in the LE phase. Therefore, in the presence of RFB2, the condensed domains of the monolayer occur only at intermediate and higher pressures and occupy larger areas than the obtained in the presence of RFB. However, upon compression (π≈40 mN/m), RFB seems to be present at the interface in higher proportions, as observed from the brighter domains of the monolayer (Fig. 4G).

3.3. PM-IRRAS

The PM-IRRAS of lipid/protein monolayers films, *in situ* at the air/water interface, provides unique information about the molecular structure and orientation of the film's constituents [36,58]. The results in three different regions of the isotherm (4 mN/m, 24 mN/m and 40 mN/m) are presented in Table 2.

When analyzing the PM-IRRAS band characteristic of the lipidic portion of the PS monolayer (Curosurf®), the frequency of the bands C=O and PO_2^- were, as expected, higher for π=40 mN/m than for smaller pressures (4 mN/m). Higher wavenumbers, of the carbonyl υ(C=O) stretching band (1734 cm^{-1} at π=4 mN/m and 1736 cm^{-1} at π=40 mN/m, Table 2) and the asymmetric phosphate $\upsilon_{as}(PO_2^-)$ stretching vibration (1223 cm^{-1} at π=4 mN/m and an additional band at 1249 cm^{-1} at π=40 mN/m, Table 2), correspond to the less-hydrated head groups characteristic of the LC phase that occurs at higher pressures [59]. Moreover, the dehydration of the head groups occurs not only by the compression and expulsion of water molecules at π≈40 mN/m, but also by the transition of monolayers-to-multilayers that starts roughly at this pressure, leading to the "squeezing-out" of negative lipids of the monolayer and promotion of the dehydration process. Contrastingly, at an intermediate pressure (24 mN/m), the value of $\upsilon_{as}(PO_2^-)$ stretching vibration appears to be rather low (1216 cm^{-1}) and one would expect that the compression from 4 to 24 mN/m would increase the frequency of these bands as a consequence of water molecules being expelled from the head groups upon compression. However, it has been reported that this rather unexpected low values of $\upsilon_{as}(PO_2^-)$ may occur because the phosphate moiety of the phospholipid molecules, is thought to be involved in a strong intermolecular hydrogen bonding with the glycerol hydroxyl group of neighboring molecules and these hydroxyl groups may partially mimic the solvation properties of water [59]. With the compression from π≈4 mN/m to 40 mN/m, the CH_2 asymmetrical stretching band shifts from 2926 cm^{-1} to 2915 cm^{-1} (Table 2). Hence, the decrease in the asymmetric CH_2 stretching frequency, as the monolayer is compressed, indicates the formation of *all-trans* conformation (characteristic of LC phase) and the loss of *gauche* conformers (characteristic of LE phase) [36,60,61].

The PM-IRRAS results endorse that the interaction of the MAs with the PS model is dependent of the bacterial lipid concentrations. Lower amounts of MAs do not seem to significantly interact with the head groups of the phospholipids. Independently of the amount of MAs and comparing with the PS model, the CH_2 stretching frequencies are lower at low pressures, suggesting a more ordered lipid state which might be due to the MAs residues that may be positioned within the phospholipids chains, thereby increasing the lipid packing. The CH_2 stretching is especially affected for lower concentrations of MAs, being the monolayer, in agreement to the BAM observations, condensed at all the three pressures studied. Although being more ordered at lower pressures, when the pressure increases (π≈24 and ≈40 mN/m), the monolayer of the PS model containing higher amounts of MAs is less ordered comparing to Curosurf® in the absence of MAs. Furthermore, higher frequency values obtained for the PO_2^- and C=O stretching indicate that higher amounts of MAs are responsible for the production of a less hydrated monolayer.

Both antimycobacterial compounds interact with the phospholipid head groups of the PS model, as can be confirmed by the shift induced in the PO_2^- and in the C=O bands. For RFB, at the lower surface pressures, the band contour of PO_2^- consists of at least two overlapped features, at 1211 and at 1247 cm^{-1}, probably corresponding to dihydrated and monohydrated phosphate groups, respectively. The band position

Table 2
Vibrational wavenumbers (asymmetric phosphate, carbonyl, asymmetric methylene) of the Langmuir Curosurf®, Curosurf®:MAs 9:1 w/w, Curosurf®:MAs 1:1 w/w, Curosurf®:RFB (0.118 μM), Curosurf®:RFB2 (0.225 μM), Curosurf®:MAs (1:1 w/w):RFB (0.118 μM) and Curosurf®:MAs (1:1 w/w):RFB2 (0.225 μM) monolayers on the phosphate buffer, for lower (π=4 mN/m), intermediate (π=24 mN/m) and higher pressure (π=40 mN/m).

	π=4 mN/m			π=24 mN/m			π=40 mN/m		
	$\nu(PO_2^-)$ (cm^{-1})	ν(C=O) (cm^{-1})	$\nu_{as}(CH_2)$ (cm^{-1})	$\nu(PO_2^-)$ (cm^{-1})	ν(C=O) (cm^{-1})	$\nu_{as}(CH_2)$ (cm^{-1})	$\nu(PO_2^-)$ (cm^{-1})	ν(C=O) (cm^{-1})	$\nu_{as}(CH_2)$ (cm^{-1})
Curosurf®	1223	1734	2926	1216	1730	2916	1223 1249	1736	2915
Curosurf®:MAs9:1	1220	1729	2916	1232	1728	2916	1236 1262	1731	2916
Curosurf®:MAs1:1	1259	1745	2920	1245 1263	1746	2920	1259	1744	2920
Curosurf®:RFB	1211 1247	1735	2923	1222 1250	1731	2918	1255	1741	2916
Curosurf®:RFB2	1249	1717	2921	1229	1741	2916	1253	1739	2915
Curosurf®:MAs:RFB	1213	1744	2914	1216 1242	1744	2918	1260	1744	2918
Curosurf®:MAs:RFB2	1226	1736	2919	1231	1733	2918	1237	1740	2917

at lower wavenumber suggests a high degree of hydrogen bonding between the drug and the negative lipids, containing a large number of OH groups (*e.g.* PG and possibly PI) that may mimic the solvation properties of water. The pressure increment shifts the PO_2^- band to higher wavenumbers, which is consistent with the drug being "squeezed out" from the monolayer. The interactions of the antimycobacterial compounds with the PS monolayer also occur at the fatty acid tail level, as suggested by the shift in the CH_2 wavenumbers. At lower pressures the interaction with the fatty acid tails seems to be less pronounced for RFB than for RFB2. However, both antimycobacterial compounds produce a more ordered monolayer on account of the lower wavenumbers of the CH_2 stretching obtained in the presence of the antimycobacterial compounds. The increase in the lipid order might be due to a higher packing effect by the formation of antimycobacterial compound aggregates at the interface. For intermediate and higher pressures the interactions between the antimycobacterial compounds and the PS monolayer are not so pronounced and RFB forms a less ordered monolayer than the obtained with Curosurf® alone or Curosurf® with RFB2.

Regarding the effect of RFB on PS monolayers containing MAs, it is possible to observe from PM-IRRAS data that the drug interacts with the phospholipid head groups at all the assayed pressures. At lower pressures the small frequency value of PO_2^- stretching, points to a high degree of hydrogen bonding between the drug and the negatively charged lipids, and possibly with the carboxyl and hydroxyl groups of MAs. With the pressure increase, the vibration wavenumbers of the PO_2^- are shifted to higher values. This indicates that the established hydrogen bonds are reduced, possible due to the fact of RFB being "squeezed out" from the monolayer. The resulting monolayer is condensed at all pressures but is less ordered at intermediate and higher pressures in comparison with the PS model in the absence of drug and mycolic acids. The effect of RFB2 on the PS monolayer containing high amounts of MAs is very similar to that observed for RFB. The main difference is that the frequency value of PO_2^- stretching for pressures of ≈4 mN/m is not so low, being the electrostatic interactions with the PS negatively charged lipids not so pronounced. The resultant monolayer is also condensed at the different pressures; however at smaller pressures and in the presence of higher amounts of MAs, RFB seems to form an even more ordered monolayer.

It is well known that the secondary structure of the SP-B and SP-C is related with the normal functions of these hydrophobic proteins, and changes in their structure might have a negative implication by inducing changes in the PS surface activity [62]. Accordingly, besides analyzing the lipidic portion of the PS monolayer, we have also used PM-IRRAS to study the secondary structure of the SP-B and SP-C at the dynamic inspiratory tension. In this regard we have focused on the analysis of the amide I band (1650 cm^{-1}), which is described as more sensitive to estimate the conformation and orientation of the protein compared to the amide II band (1550 cm^{-1}) [56,63]. The amide I band can therefore give information regarding the secondary structure of the proteins and according to the band position allows the identification of β-turns (1662–1682 cm^{-1}), α-helices (1645–1662 cm^{-1}), and β-sheets (1613–1637 cm^{-1}). If the band appears as two components: one at the β-sheet position and another as a shoulder at 1682–1710 cm^{-1} it is indicative of an antiparallel β-sheet. The parallel β-sheet is predicted to have higher frequency for the lower component [62,64,65]. The disorder of random coils (unstructured) occurs at the same wavenumbers of the α-helices (1637–1650 cm^{-1}), originating from the former broader and less intense bands compared to the α-helices [62,64,66]. Fig. 5 shows the effects of antimycobacterial compounds and MAs in the secondary structure of the PS proteins given by the IRRAS amide I band for π≈40 mN/m.

For the PS model, the amide I band exhibits for this pressure two overlapping bands attributed to the α-helices and β-sheet. Although the native SP-B and SP-C have α-helical segments, the secondary

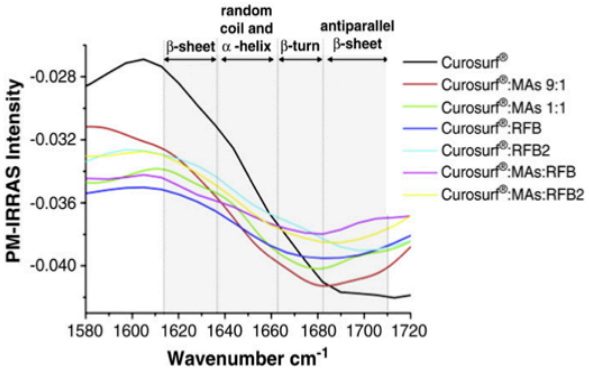

Fig. 5. PM-IRRAS spectra of Curosurf® (black line), Curosurf®:MAs 9:1 w/w (red line), Curosurf®:MAs 1:1 w/w (green line), Curosurf®:RFB (0.118 μM) (dark blue line), Curosurf®:RFB2 (0.225 μM) (light blue line), Curosurf®:MAs (1:1 w/w):RFB (0.118 μM) (purple line) and Curosurf®:MAs (1:1 w/w):RFB2 (0.225 μM) at π= 40 mN/ (yellow line).

structure is dependent of the isolation and purification procedures. Therefore, in order to conclude about the influences of other compounds in the secondary structure of the PS proteins, it is important to determine the conformation of the proteins in the conditions studied [43]. For this pressure, MAs decrease the amount of proteins at the interface, as stated by the lower intensity values of their amide I band. Higher amounts of MAs showed a more pronounced change in the secondary structure of the PS proteins. Electrostatic interactions with the proteins seem to happen, especially in the case of the presence of higher amounts of MAs as more pronounced changes are observed in the amide I stretching band. Moreover, for lower and higher amounts of MAs a decrease in absorbance centered around the α-helices region was observed. The β-turn conformation is confirmed by the presence of one peak at the 1681 cm^{-1} for lower amounts of MAs and 1678 cm^{-1} for higher amounts of MAs. Additionally, β-sheets are also formed but their amount is inferior comparing to the PS model. The interactions between RFB and the proteins of the PS model also seem to be less pronounced than the interactions between RFB2 and the proteins, probably due to the higher electrostatic repulsions verified in the former case. Although a decrease in the protein amount at the interface is confirmed in the RFB's presence, the secondary structure of the proteins does not seem to suffer a significant change as the amide I peaks assigned are similar to the ones of the Curosurf®. In the case of RFB2 interacting with the PS monolayer, the absorbance for amide I is centered around 1631, 1675 and 1700 cm^{-1} for all pressures, which is indicative of antiparallel β-sheet and β-turn conformations. When both antimycobacterial compounds and MAs are present, the PS proteins exhibit β-turns and antiparallel β-sheets. In the case of RFB, the antiparallel β-sheet has a perpendicular orientation to the air/water interface.

4. Conclusions

The PS is one of the first barriers of the lung and interacts with inhaled agents as the etiologic agent of Tb. The initial interactions of the surfactant components with the MTb may contribute to the uptake of the bacteria in alveolar epithelial cells and macrophages and subsequent initiation of adaptive immunity in the lung [43,67]. In this work, the biophysical interactions of the MTb and the antimycobacterial compounds with a PS model were evaluated, using an *in vitro* model of Langmuir monolayers. The results allowed to conclude that the amount of the MAs plays an important role in the impairment of the PS control

functions. At the dynamic inspiratory tension, with the increase of the amount of these deleterious lipids the lipid order of the PS monolayer is reduced. Since the monolayer molecular aggregation is related to the function of permeability control *via* the molecular packing [32,68], this phenomenon might be the first step in providing to the bacteria an easier access to the target, the alveolar macrophage. Hence, the lipid order decrease triggered by the high amount of MAs may contribute to the biophysical impairment of the protective PS monolayer with the consequent entrance of the bacteria into the cells due to a higher facility in reaching the alveolar macrophages. Moreover, the order decrease of the PS model is prejudicial to the lung activity, and larger quantities of MAs might largely contribute to the respiratory failure observed in chronic steps of the disease. The compounds also cause changes in the biophysical parameters of the PS, contributing RFB and RFB2 to a less compressible and more ordered monolayer. Moreover, both antimycobacterial compounds protect the PS from the lipid disordering effect caused by the higher amounts of MAs. The antimycobacterial compounds increase the order of the PS in the presence of higher amounts of MAs, and this packing increment might protect the lungs from the entry of the bacteria, being this a possible alternative explanation for the therapeutic efficiency of these antimycobacterial compounds. RFB2 also contributes to the appearance of condensed domains on the PS monolayer at very low pressures, which is indicative of an increment of the lipid order. This compound might aggregate and form monolayers, which, concerning the use of this antimycobacterial compound as a replacement therapy of atelectasis areas, could be very interesting in the future. Additionally, it is well known that a PS in normal conditions has selected properties such as high surface pressure, no hysteresis, and high compressibility of the monolayer [32,43]. The influence of the MAs and the antimycobacterial compounds in these parameters were established in order to understand the negative effects of the MAs in these parameters as well as the influence of both compounds. The MAs seem to increase the respiratory work, especially when they are present in higher quantities. The higher increment of the hysteresis associated with the lipid order decrease suggests that the bacteria could escape into the water phase, and once in the alveolar systems, be able to reach the alveolar macrophages and the bloodstream [1,53]. The secondary structure of the proteins changes upon interaction with: MAs, RFB, RFB2 and with both compounds when MAs are present. Since the antimycobacterial compounds and the MAs alter the structure of the proteins in the plateau region, the way how the material is removed from the interface also changes and this could have negative effects in the lung function and alter the normal breathing process [53,62]. Moreover, the hysteresis of the PS monolayer when both antimycobacterial compounds and MAs are present does not increase relatively to the hysteresis of the PS monolayer when MAs are present in the absence of the antimycobacterial compounds, suggesting that the RFB and its derivate might reduce the amount of bacteria that is able to reach the alveolar macrophages and the bloodstream.

Acknowledgements

Marina Pinheiro and João M. Caio thank FCT (Lisbon) for the fellowships (SFRH/BD/63318/2009 and SFRH/BD/66789/2009, respectively). Juan J. Giner-Casares acknowledges Alexander von-Humboldt foundation for a postdoctoral fellowship. Carlos Rubia-Paya is acknowledged for most valuable help during experiments. The authors thank the Spanish CICYT for financial support of this research in the framework of Projects CTQ2010-17481 and also the Junta de Andalucía (Consejería de Innovacion, Ciencia y Empresa) for special financial support (P08-FQM-4011 and P10-FQM-6703). Authors are also grateful to the FCT for financial support under projects PEst-OE/QUI/UI0612/2011 and PTDC/QUI-QUI/101022/2008 with co-participation European Community funds from the FEDER, QREN and COMPET.

References

[1] M. Pinheiro, M. Lucio, J.L. Lima, S. Reis, Liposomes as drug delivery systems for the treatment of TB, Nanomedicine (Lond) 6 (2011) 1413–1428.
[2] L.G. Dover, G.D. Coxon, Current status and research strategies in tuberculosis drug development, J. Med. Chem. 54 (2011) 6157–6165.
[3] N.R. Gandhi, P. Nunn, K. Dheda, H.S. Schaaf, M. Zignol, D. van Soolingen, P. Jensen, J. Bayona, Multidrug-resistant and extensively drug-resistant tuberculosis: a threat to global control of tuberculosis, Lancet 375 (2010) 1830–1843.
[4] A. Koul, E. Arnoult, N. Lounis, J. Guillemont, K. Andries, The challenge of new drug discovery for tuberculosis, Nature 469 (2011) 483–490.
[5] R. Figueiredo, C. Moiteiro, M.A. Medeiros, P.A. da Silva, D. Ramos, F. Spies, M.O. Ribeiro, M.C. Lourenco, I.N. Junior, M.M. Gaspar, M.E. Cruz, M.J. Curto, S.G. Franzblau, H. Orozco, D. Aguilar, R. Hernandez-Pando, M.C. Costa, Synthesis and evaluation of rifabutin analogs against Mycobacterium avium and H(37)Rv, MDR and NRP Mycobacterium tuberculosis, Bioorg. Med. Chem. 17 (2009) 503–511.
[6] Z.C. Chroneos, K. Midde, Z. Sever-Chroneos, C. Jagannath, Pulmonary surfactant and tuberculosis, Tuberculosis (Edinb) 89 (Suppl. 1) (2009) S10–S14.
[7] A.K. Agrawal, C.M. Gupta, Tuftsin-bearing liposomes in treatment of macrophage-based infections, Adv. Drug Deliv. Rev. 41 (2000) 135–146.
[8] S.M. Saad, Z. Policova, E.J. Acosta, A.W. Neumann, Effect of surfactant concentration, compression ratio and compression rate on the surface activity and dynamic properties of a lung surfactant, Biochim. Biophys. Acta 1818 (2012) 103–116.
[9] H. Zhang, Y.E. Wang, Q. Fan, Y.Y. Zuo, On the low surface tension of lung surfactant, Langmuir 27 (2011) 8351–8358.
[10] F. Bringezu, J. Ding, G. Brezesinski, A.J. Waring, J.A. Zasadzinski, Influence of pulmonary surfactant protein B on model lung surfactant monolayers, Langmuir 18 (2002) 2319–2325.
[11] U. Klenz, M. Saleem, M.C. Meyer, H.J. Galla, Influence of lipid saturation grade and headgroup charge: a refined lung surfactant adsorption model, Biophys. J. 95 (2008) 699–709.
[12] C. Alonso, T. Alig, J. Yoon, F. Bringezu, H. Warriner, J.A. Zasadzinski, More than a monolayer: relating lung surfactant structure and mechanics to composition, Biophys. J. 87 (2004) 4188–4202.
[13] G. Chimote, R. Banerjee, Effect of mycolic acid on surface activity of binary surfactant lipid monolayers, J. Colloid Interface Sci. 328 (2008) 288–298.
[14] G. Chimote, R. Banerjee, Effect of mycobacterial lipids on surface properties of Curosurf: implications for lung surfactant dysfunction in tuberculosis, Respir. Physiol. Neurobiol. 162 (2008) 73–79.
[15] Z. Wang, U. Schwab, E. Rhoades, P.R. Chess, D.G. Russell, R.H. Notter, Peripheral cell wall lipids of Mycobacterium tuberculosis are inhibitory to surfactant function, Tuberculosis (Edinb) 88 (2008) 178–186.
[16] G. Chimote, R. Banerjee, *In vitro* evaluation of inhalable isoniazid-loaded surfactant liposomes as an adjunct therapy in pulmonary tuberculosis, J. Biomed. Mater. Res. B Appl. Biomater. 94 (2010) 1–10.
[17] G. Chimote, R. Banerjee, Effect of antitubercular drugs on dipalmitoylphosphatidylcholine monolayers: implications for drug loaded surfactants, Respir. Physiol. Neurobiol. 145 (2005) 65–77.
[18] A. Kurashima, T. Mori, Y. Tomono, S. Abe, M. Nagaoka, M. Abe, A new anti-mycobacterial agent, rifabutin, Kekkaku 85 (2010) 743–756.
[19] P.A. Aristoff, G.A. Garcia, P.D. Kirchhoff, H.D. Hollis Showalter, Rifamycins – obstacles and opportunities, Tuberculosis (Edinb) 90 (2010) 94–118.
[20] Z. Zhang, Y. Pen, R.G. Edyvean, S.A. Banwart, R.M. Dalgliesh, M. Geoghegan, Adhesive and conformational behaviour of mycolic acid monolayers, Biochim. Biophys. Acta 1798 (2010) 1829–1839.
[21] P. Draper, The outer parts of the mycobacterial envelope as permeability barriers, Front. Biosci. 3 (1998) D1253–D1261.
[22] M. Villeneuve, M. Kawai, M. Watanabe, Y. Aoyagi, Y. Hitotsuyanagi, K. Takeya, H. Gouda, S. Hirono, D.E. Minnikin, H. Nakahara, Differential conformational behaviors of alpha-mycolic acids in Langmuir monolayers and computer simulations, Chem. Phys. Lipids 163 (2010) 569–579.
[23] M. Villeneuve, M. Kawai, M. Watanabe, Y. Aoyagi, Y. Hitotsuyanagi, K. Takeya, H. Gouda, S. Hirono, D.E. Minnikin, H. Nakahara, Conformational behavior of oxygenated mycobacterial mycolic acids from Mycobacterium bovis BCG, Biochim. Biophys. Acta 1768 (2007) 1717–1726.
[24] K. Takayama, C. Wang, G.S. Besra, Pathway to synthesis and processing of mycolic acids in Mycobacterium tuberculosis, Clin. Microbiol. Rev. 18 (2005) 81–101.
[25] Y.Y. Zuo, R.A. Veldhuizen, A.W. Neumann, N.O. Petersen, F. Possmayer, Current perspectives in pulmonary surfactant – inhibition, enhancement and evaluation, Biochim. Biophys. Acta 1778 (2008) 1947–1977.
[26] P. Ludwiczak, M. Gilleron, Y. Bordat, C. Martin, B. Gicquel, G. Puzo, Mycobacterium tuberculosis phoP mutant: lipoarabinomannan molecular structure, Microbiology 148 (2002) 3029–3037.
[27] Y. Benadie, M. Deysel, D.G. Siko, V.V. Roberts, S. Van Wyngaardt, S.T. Thanyani, G. Sekanka, A.M. Ten Bokum, L.A. Collett, J. Grooten, M.S. Baird, J.A. Verschoor, Cholesteroid nature of free mycolic acids from M. tuberculosis, Chem. Phys. Lipids 152 (2008) 95–103.
[28] Y.Y. Zuo, M. Ding, D. Li, A.W. Neumann, Further development of Axisymmetric Drop Shape Analysis-captive bubble for pulmonary surfactant related studies, Biochim. Biophys. Acta 1675 (2004) 12–20.
[29] H. Zhang, Q. Fan, Y.E. Wang, C.R. Neal, Y.Y. Zuo, Comparative study of clinical pulmonary surfactants using atomic force microscopy, Biochim. Biophys. Acta 1808 (2011) 1832–1842.
[30] X. Chen, Z. Huang, W. Hua, H. Castada, H.C. Allen, Reorganization and caging of DPPC, DPPE, DPPG, and DPPS monolayers caused by dimethylsulfoxide observed using Brewster angle microscopy, Langmuir 26 (2010) 18902–18908.

[31] L.A. Creuwels, E.H. Boer, R.A. Demel, L.M. van Golde, H.P. Haagsman, Neutralization of the positive charges of surfactant protein C. Effects on structure and function, J. Biol. Chem. 270 (1995) 16225–16229.
[32] N. Aydogan, B. Uslu, H. Tanaci, Biophysical investigation of the interfacial properties of cationic fluorocarbon/hydrocarbon hybrid surfactant: mimicking the lung surfactant protein C, J. Colloid Interface Sci. 360 (2011) 163–174.
[33] M. Ross, S. Krol, A. Janshoff, H.J. Galla, Kinetics of phospholipid insertion into monolayers containing the lung surfactant proteins SP-B or SP-C, Eur. Biophys. J. 31 (2002) 52–61.
[34] S.G. Taneva, K.M. Keough, Calcium ions and interactions of pulmonary surfactant proteins SP-B and SP-C with phospholipids in spread monolayers at the air/water interface, Biochim. Biophys. Acta 1236 (1995) 185–195.
[35] J. Perez-Gil, C. Casals, D. Marsh, Interactions of hydrophobic lung surfactant proteins SP-B and SP-C with dipalmitoylphosphatidylcholine and dipalmitoylphosphatidylglycerol bilayers studied by electron spin resonance spectroscopy, Biochemistry 34 (1995) 3964–3971.
[36] R. Mendelsohn, G. Mao, C.R. Flach, Infrared reflection-absorption spectroscopy: principles and applications to lipid–protein interaction in Langmuir films, Biochim. Biophys. Acta 1798 (2010) 788–800.
[37] R.M. de Oliveira, J. Ferreira, M.J. Santos, R.M. Faria, O.N. Oliveira Jr., Probing the functionalization of gold surfaces and protein adsorption by PM-IRRAS, Chemphyschem 12 (2011) 1736–1740.
[38] S. Schurch, H. Bachofen, F. Possmayer, Surface activity *in situ*, *in vivo*, and in the captive bubble surfactometer, Comp. Biochem. Physiol. A Mol. Integr. Physiol. 129 (2001) 195–207.
[39] S.M. Saad, Z. Policova, E.J. Acosta, M.L. Hair, A.W. Neumann, Mixed DPPC/DPPG monolayers at very high film compression, Langmuir 25 (2009) 10907–10912.
[40] K.Y. Lee, Collapse mechanisms of Langmuir monolayers, Annu. Rev. Phys. Chem. 59 (2008) 771–791.
[41] S. Schurch, H. Bachofen, J. Goerke, F. Possmayer, A captive bubble method reproduces the *in situ* behavior of lung surfactant monolayers, J. Appl. Physiol. 67 (1989) 2389–2396.
[42] H. Bachofen, S. Schurch, Alveolar surface forces and lung architecture, Comp. Biochem. Physiol. A Mol. Integr. Physiol. 129 (2001) 183–193.
[43] R. Wustneck, J. Perez-Gil, N. Wustneck, A. Cruz, V.B. Fainerman, U. Pison, Interfacial properties of pulmonary surfactant layers, Adv. Colloid Interface Sci. 117 (2005) 33–58.
[44] C. Nunes, G. Brezesinski, C. Pereira-Leite, J.L. Lima, S. Reis, M. Lucio, NSAIDs interactions with membranes: a biophysical approach, Langmuir 27 (2011) 10847–10858.
[45] Z. Wang, S. Yang, Effects of fullerenes on phospholipid membranes: a Langmuir monolayer study, Chemphyschem 10 (2009) 2284–2289.
[46] J. Perez-Gil, T.E. Weaver, Pulmonary surfactant pathophysiology: current models and open questions, Physiology (Bethesda) 25 (2010) 132–141.
[47] T. Ivanova, I. Minkov, I. Panaiotov, P. Saulnier, J.E. Proust, Dilatational properties and morphology of surface films spread from clinically used lung surfactants, Colloid Polym. Sci. 282 (2004) 1258–1267.
[48] T. Gross, E. Zmora, Y. Levi-Kalisman, O. Regev, A. Berman, Lung-surfactant–meconium interaction: *in vitro* study in bulk and at the air-solution interface, Langmuir 22 (2006) 3243–3250.
[49] H. Zhang, Y.E. Wang, C.R. Neal, Y.Y. Zuo, Differential effects of cholesterol and budesonide on biophysical properties of clinical surfactant, Pediatr. Res. 71 (2012) 316–323.
[50] C. Alonso, A. Waring, J.A. Zasadzinski, Keeping lung surfactant where it belongs: protein regulation of two-dimensional viscosity, Biophys. J. 89 (2005) 266–273.
[51] G. Chimote, R. Banerjee, Lung surfactant dysfunction in tuberculosis: effect of mycobacterial tubercular lipids on dipalmitoylphosphatidylcholine surface activity, Colloids Surf. B Biointerfaces 45 (2005) 215–223.
[52] R. Almog, C.A. Mannella, Molecular packing of cord factor and its interaction with phosphatidylinositol in mixed monolayers, Biophys. J. 71 (1996) 3311–3319.
[53] R.K. Harishchandra, M. Saleem, H.J. Galla, Nanoparticle interaction with model lung surfactant monolayers, J. R. Soc. Interface 7 (Suppl. 1) (2010) S15–S26.
[54] V.V. Vostrikov, A.A. Selishcheva, G.M. Sorokoumova, Y.N. Shakina, V.I. Shvets, O.Y. Savel'ev, V.I. Polshakov, Distribution coefficient of rifabutin in liposome/water system as measured by different methods, Eur. J. Pharm. Biopharm. 68 (2008) 400–405.
[55] T. Schmidt, L. Caseli, T. Nobre, M. Zaniquelli, O. Oliveira Jr., Interaction of horseradish peroxidase with Langmuir monolayers of phospholipids, Colloids Surf. A Physicochem. Eng. Asp. 321 (2008) 206–210.
[56] M. Allouche, S. Castano, D. Colin, B. Desbat, B. Kerfelec, Structure and orientation of pancreatic colipase in a lipid environment: PM-IRRAS and Brewster angle microscopy studies, Biochemistry 46 (2007) 15188–15197.
[57] A.M. Goncalves da Silva, R.I. Romao, Mixed monolayers involving DPPC, DODAB and oleic acid and their interaction with nicotinic acid at the air–water interface, Chem. Phys. Lipids 137 (2005) 62–76.
[58] C.R. Flach, A. Gericke, R. Mendelsohn, Quantitative determination of molecular chain tilt angles in monolayer films at the air/water interface: infrared reflection/absorption spectroscopy of behenic acid methyl ester, J. Phys. Chem. B 101 (1997) 58–65.
[59] A. Dicko, H. Bourque, M. Pézolet, Study by infrared spectroscopy of the conformation of dipalmitoylphosphatidylglycerol monolayers at the air–water interface and transferred on solid substrates, Chem. Phys. Lipids 96 (1998) 125–139.
[60] K. Czapla, B. Korchowiec, E. Rogalska, Differentiating oxicam nonsteroidal anti-inflammatory drugs in phosphoglyceride monolayers, Langmuir 26 (2010) 3485–3492.
[61] D.G. Cameron, E.F. Gudgin, H.H. Mantsch, Dependence of acyl chain packing of phospholipids on the head group and acyl chain length, Biochemistry 20 (1981) 4496–4500.
[62] P.C. Stenger, C. Alonso, J.A. Zasadzinski, A.J. Waring, C.L. Jung, K.E. Pinkerton, Environmental tobacco smoke effects on lung surfactant film organization, Biochim. Biophys. Acta 1788 (2009) 358–370.
[63] O.G. Travkova, J. Andra, H. Mohwald, G. Brezesinski, Conformational properties of arenicins: from the bulk to the air–water interface, Chemphyschem 11 (2010) 3262–3268.
[64] A. Banc, B. Desbat, D. Renard, Y. Popineau, C. Mangavel, L. Navailles, Structure and orientation changes of omega- and gamma-gliadins at the air-water interface: a PM-IRRAS spectroscopy and Brewster angle microscopy study, Langmuir 23 (2007) 13066–13075.
[65] J. Kubelka, T.A. Keiderling, Differentiation of beta-sheet-forming structures: *ab initio*-based simulations of IR absorption and vibrational CD for model peptide and protein beta-sheets, J. Am. Chem. Soc. 123 (2001) 12048–12058.
[66] S. Venyaminov, N.N. Kalnin, Quantitative IR spectrophotometry of peptide compounds in water (H2O) solutions. I. Spectral parameters of amino acid residue absorption bands, Biopolymers 30 (1990) 1243–1257.
[67] Z.C. Chroneos, K. Midde, Z. Sever-Chroneos, C. Jagannath, Pulmonary surfactant and tuberculosis, Tuberculosis (Edinb) 89 (2009) 10–14.
[68] T. Hasegawa, R.M. Leblanc, Aggregation properties of mycolic acid molecules in monolayer films: a comparative study of compounds from various acid-fast bacterial species, Biochim. Biophys. Acta 1617 (2003) 89–95.

4. Differential interactions of rifabutin with human and bacterial membranes: implication for its therapeutic and toxic effects.

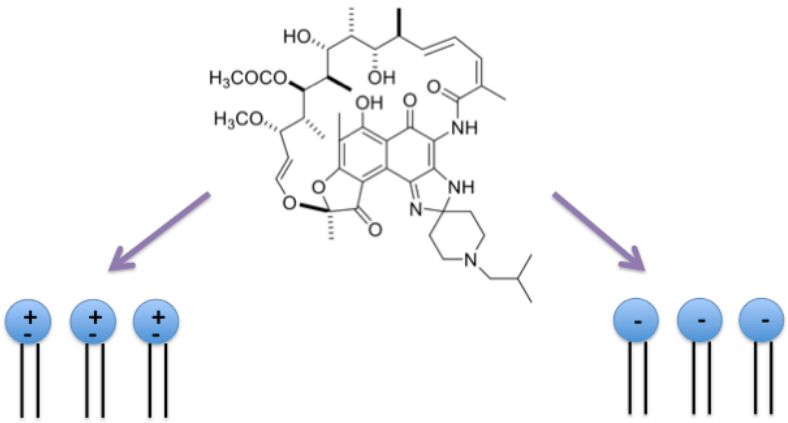

Journal of Medicinal Chemistry

Article

pubs.acs.org/jmc

Differential Interactions of Rifabutin with Human and Bacterial Membranes: Implication for Its Therapeutic and Toxic Effects

Marina Pinheiro,[†] Mariana Arêde,[†] Cláudia Nunes,[†] João M. Caio,[‡] Cristina Moiteiro,[‡] Marlene Lúcio,[†] and Salette Reis*,[†]

[†]REQUIMTE, Departamento de Ciências Químicas, Faculdade de Farmácia, Universidade do Porto, Rua de Jorge Viterbo Ferreira no. 228, Porto 4050-313, Portugal

[‡]Centro de Química e Bioquímica, Departamento de Química e Bioquímica, Faculdade de Ciências, Universidade de Lisboa, Lisboa, Portugal

ABSTRACT: This work focuses on the interaction of rifabutin (RFB), a naphthalenic ansamycin, with membrane models. Since the therapeutic and toxic effects of this class of drugs are strongly influenced by their lipid affinity, we concerned specifically on the ability of this antibiotic to affect the membrane biophysical properties. The extent of the interaction between RFB and membrane phospholipids was quantified by the partition coefficient (K_p), using membrane model systems that mimic the human (liposomes of 1,2-dimyristoyl-*sn*-glycero-phosphocholine, DMPC) and the bacterial (liposomes of 1,2-dimyristoyl-*sn*-glycero-3-phosphoglycerol, DMPG) plasma membranes. To predict the drug location in the membranes, fluorescence quenching and lifetime measurements were carried out using the above-mentioned membrane models labeled with fluorescent probes. Steady-state anisotropy measurements were also performed to evaluate the effect of RFB on the microviscosity of the membranes. Overall, the results support that RFB has higher affinity for the bacterial membrane mediated by electrostatic interactions with the phospholipid head groups.

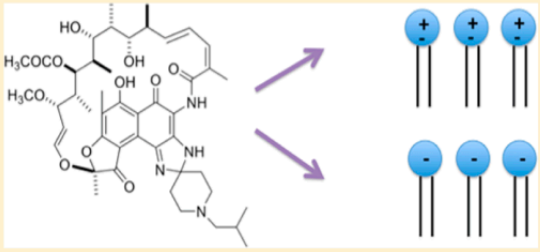

INTRODUCTION

Rifabutin (RFB, Figure 1), a naphthalenic ansamycin, is commonly used for the treatment of mycobacterial infectious diseases.[1] This semisynthetic derivate of rifamycin, which was approved in 1992 by the FDA, represents one of the most efficient antibiotics used in the tuberculosis (TB) treatment, being frequently used in HIV coinfected patients because of the fewer drug interactions with antiretroviral agents compared with rifampicin (a rifamycin first-line anti-TB drug).[2] Additionally, RFB is also used to treat atypical mycobacterial infections and, in some cases, it has shown to be active when resistance to rifampicin is found.[3,4] Although RFB is generally well-tolerated, there are some problematic side effects which include uveitis, rash, nausea, vomiting, neutropenia, anemia, discoloration of the skin and body fluids (tears, saliva, urine and perspiration), and, rarely, clinically important impairment of the liver function.[5] The accepted mechanism of action of RFB involves the binding to the β-subunit of the RNA polymerase, causing the inhibition of the RNA transcription and consequently the inhibition of the bacterial protein synthesis.[2] The binding constants for prokaryotic RNA polymerases are 10000-fold higher than those for eukaryotic enzymes, which in part might explain the higher selectivity of this drug to the bacteria and its usefulness in the TB therapy. Nevertheless, a lack of correlation has been found between the RFB inhibitory activity on the RNA polymerase and the antibiotic efficacy. Recently, it has been established that the drug's penetration through the bacteria cells explains the higher activity against Gram-positive compared to the Gram-negative despite the quite similar RNA polymerase inhibitory activities.[1] Indeed, the efficiency of the interactions of the antibiotics with the membranes constitutes one of the most important pharmacological features, playing an essential role on its biological activity.[6] RFB has an intracellular target, and hence it must pass across phospholipid bilayers to reach the RNA polymerase and elicit its pharmacological effect. There are several analogues of RFB described in the literature that were designed taking into consideration the binding to the RNA polymerase and which, despite being promising candidates, do not pass the preclinical trials.[2,7,8] In fact, the rational design of more efficient analogues of RFB against TB would benefit from a deeper understanding of the interactions of RFB with the human and bacterial membranes. Therefore, RFB was chosen in this study as a lead compound for new molecules as promising molecules against TB. For the purpose of this study, large unilamellar vesicles (LUVs) were used as lipid bilayer membrane models. As membrane models, liposomes take into account the RFB's passive diffusion across the bilayers. Nevertheless, the drugs permeation through the membranes involves other processes,

Received: July 30, 2012
Published: December 10, 2012

dx.doi.org/10.1021/jm301116j | J. Med. Chem. 2013, 56, 417−426

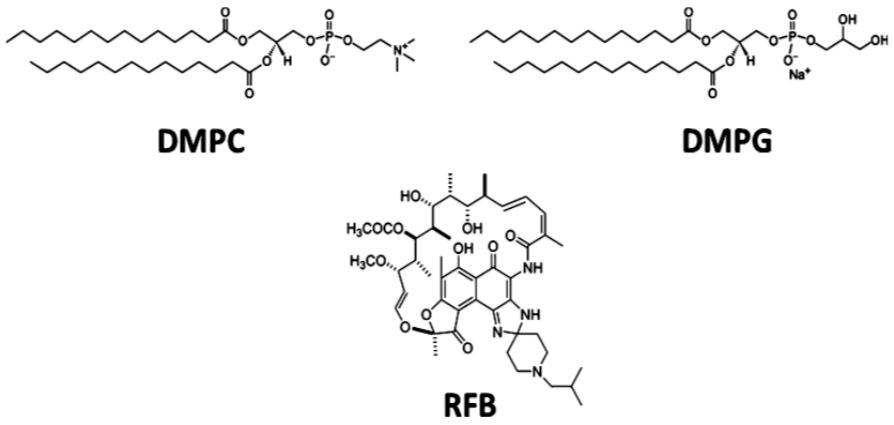

Figure 1. Molecular structures of 1,2-dimyristoyl-*sn*-glycero-phosphocholine (DMPC), 1,2-dimyristoyl-*sn*-glycero-3-phosphoglycerol (DMPG), and Rifabutin (RFB).

namely the paracellular diffusion through the cell junctions and the active transport that leads to the influx and efflux of drugs facilitated by transport proteins.[9] Because of its high lipophilicity, the passive diffusion is probably the most relevant process of the RFB's permeation through the membranes. Regarding the lipophilicity of RFB, its plasma concentrations do not reflect the concentrations that can be achieved in target organs and infected cells. Therefore, RFB penetrates well into polymorphonuclear leukocytes, lymphocytes, and macrophages, and it is well-known that it accumulates in organs as the lungs at levels six times higher compared with the plasma concentrations. Additionally, RFB is commonly used during prolonged periods and has a long half-life in the circulation.[10] Thus, because of the above-mentioned reasons the concentrations used in this work were significantly higher (approximately 25 times) compared with the plasma concentrations after a daily dose. Moreover, the range of RFB used was similar or even lower than that used in other similar studies when assessing the RFB−membrane models interactions.[11,12] Because phosphatidylcholines are practically absent in bacterial plasma membranes and are generally the most abundant phospholipids in eukaryotic plasma membranes, DMPC (Figure 1), a zwitterionic lipid, was chosen to mimic the human plasma membrane.[13,14] For these reasons, DMPC constitutes a suitable model for the surface membrane of mammalian cells and mimics the neutral charge of the host human plasma membrane. On the other hand, phosphatidylglycerols are almost absent in eukaryotic plasma membranes but are ubiquitous and often abundant in bacterial plasma membranes. Hence, DMPG (Figure 1), a negatively charged lipid, may be considered an adequate model for the mycobacterial membrane by mimicking the phospholipid negative charge of the inner plasma membrane of the Gram-positive bacteria (that includes the *Mycobacterium* spp.).[13,15] In fact, one of the main differences between Gram-positive and Gram-negative bacteria is the lipid composition of its membranes. Despite the wide variation in the phospholipid composition, while plasma membranes of Gram-positive bacteria predominantly contain anionic lipids, plasma membranes of Gram-negative bacteria contain both anionic and zwitterionic lipids.[16]

The knowledge concerning the biophysical interactions of RFB with the membrane lipid bilayer is scarce, in particular the information regarding the penetration into membranes of different phospholipid constitution. Previous works reported the higher preference of RFB for negatively charged membrane models.[11,12,17] Vostrikov and co-workers[12] determined the distribution coefficient of RFB by fluorescence quenching using LUVs of PC and PC:cardiolipin (CL) and concluded that RFB might establish electrostatic interactions with the membranes due to the higher distribution obtained in the negatively charged model. Using phase separation and fluorescence quenching, Vostrikov and colleagues determined the distribution coefficient of RFB and proved that the insertion of a CL in PC multilamellar liposomes (MLVs) increases the binding of RFB to the lipid bilayer. Results obtained by ^{31}P NMR spectroscopy have shown that despite RFB penetrating the membrane, it does not alter the bilayer structure of the membrane models studied.[11]

The main purpose of this work is to study the effect of RFB on the different nature head group phospholipids, evaluate the putative differential RFB interactions with human and bacterial membrane models, gain a higher knowledge about the RFB's location and transport through the human and bacterial biomembranes, and understand if the drug induces changes in the biophysical properties of the lipid bilayer membranes. To assess the interaction between RFB and the membranes, several biophysical techniques were used. The partition of RFB between DMPC:aqueous and DMPG:aqueous phases was determined using derivative UV−Vis spectrophotometry. The fluorescence determinations were executed by monitoring the quenching of two probes, 1,6-diphenyl-1,3,5-hexatriene (DPH) and (2-carboxyethyl)-1,6-diphenyl-1,3,5-hexatriene (DPH-PA) in the RFB's presence. Fluorescence quenching was performed in order to obtain the drug location within the membrane lipid bilayers. Because the probe's location is well-known and the extent of the drug quenching is inversely proportional to its distance to the fluorophore, it is possible to estimate the drug's location within the membrane models.[18] To understand the biophysical modifications in the membrane's lipid bilayer induced by RFB molecules, steady-state anisotropy measurements were also employed. To our knowledge, this is the first report with the prevision of the RFB's location and its influence in the biophysical parameters of the human and bacterial membrane model systems.

The overall results allow us to conclude that RFB is able to permeate both membrane models. Notwithstanding, the ionic bonds are responsible for a higher affinity of RFB to the

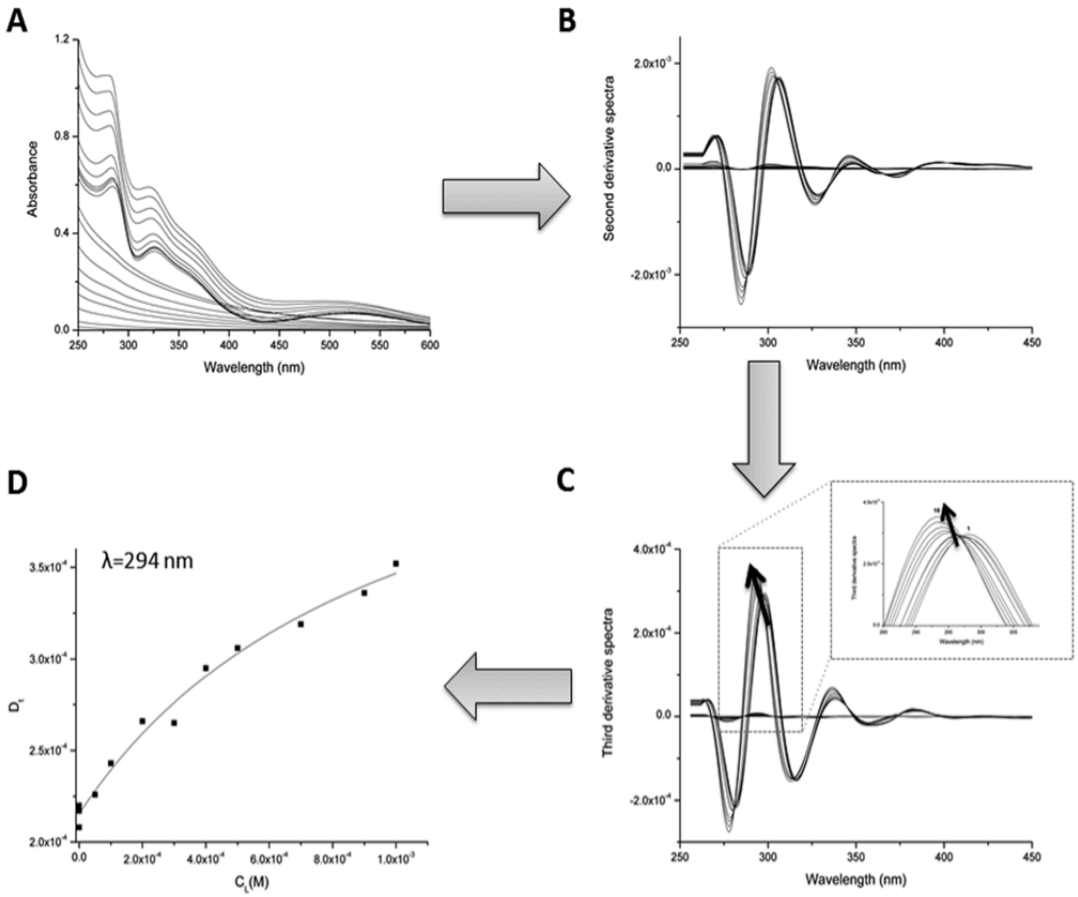

Figure 2. Absorption spectra (A), second derivative spectra (B), and third derivative spectra (C) of RFB (25 μM) incubated in LUVs of DMPC liposomes (black lines) and LUVs of DMPC liposomes without drug (gray lines) with different concentrations (M): (1) 0, (2) 5×10^{-5}, (3) 1×10^{-4}, (4) 2×10^{-4}, (5) 3×10^{-4}, (6) 4×10^{-4}, (7) 5×10^{-4}, (8) 7×10^{-4}, (9) 9×10^{-4}, (10) 1×10^{-3}. The curve (D) represents the best fit by eq 1 to experimental third derivative spectrophotometric data (D_t vs $[L]$) using a nonlinear least-squares regression method at wavelength 294 nm where the scattering is eliminated.

negatively charged membrane model. Regarding this, the mechanism by which this antibiotic permeates through the phospholipid bilayers might include an electrostatic adsorption at the interface region, followed by its permeation and induction of pronounced changes into the bacterial membrane biophysics.

In summary, this work contributes to identify novel biophysical mechanisms that may permit to explain the toxic and therapeutic effects of RFB and that might allow the future development of more effective anti-TB drugs.

RESULTS AND DISCUSSION

Partition of RFB on DMPC and DPMG Liposome-Based Membrane Mimetic Systems. The lipophilicity of drug molecules (normally represented as the logarithm of the *n*-octanol:water partition coefficient, log *P*) often strongly correlates with their pharmacological activity.[19] Thus, the lipophilicity is an important property of an antibacterial agent and should increase its efficacy, especially in the *Mycobacterium* spp. Indeed, the intrinsic permeability of the lipid domain of the mycobacterial cell wall is so low that an increment in the lipophilicity is expected to increase the extent of penetration and hence the efficacy of the antibiotics.[20]

The determination of the lipophilicity of ionizable compounds, which is normally represented by the distribution coefficient (log *D*), is often misleading, with some variability in the results according to the different techniques. The RFB molecule contains some groups that can undergo protonation (piperidine nitrogen, pK_a 9.5 and imidazole nitrogen, pK_a 3.5) and deprotonation (naphthol oxygen, pK_a 6.5). At the physiological pH, while zwitterionic species predominate (83.4%), cations make up 16.6% (predicted using a chemical software).[11] Because of the RFB ionization at the physiological pH and in order to evaluate the different interactions that occur between the drug and the bacterial plasma membrane and between the drug and host plasma membrane, we have chosen a liposome:aqueous system instead of the classical biphasic *n*-octanol:aqueous system. In fact, because of their structural and anisotropic environment similar to the biomembranes, liposomes constitute a more realistic analytical system and can better mimic the cell membranes, providing additional information to that obtained with the *n*-octanol:aqueous system.[14] The K_p, expressed in terms of log *D*, was obtained by derivative UV−Vis spectrophotometry. This spectroscopic technique, due to its sensitivity, allows straightforward procedures and the possibility to analyze signals originated

dx.doi.org/10.1021/jm301116j | J. Med. Chem. 2013, 56, 417−426

from both lipid and aqueous phases without the need to apply separation procedures.[14] Derivative spectrophotometry eliminates the intense background signals arising from the light scattered by lipid vesicles and improves the resolution of overlapping bands, features that have been reported by several authors.[18,21] The partition coefficients were calculated from the second and third derivative spectra (determined from the recorded absorption spectra after blank subtraction) at the wavelengths where the scattering is eliminated, by fitting eq 1 to the experimental data (D_t versus $[L]$) using a nonlinear least-squares regression method where the adjustable parameter is the partition constant, K_p:[14,21]

$$D_T = D_w + \frac{(D_m - D_w)K_p[L]V_m}{1 + K_p[L]V_m} \quad (1)$$

In this equation, D is the second or the third derivative intensity ($D = (d^n Abs)/(d\lambda^n)$) obtained from the absorbance values of the total concentration of RFB (D_T), RFB distributed on the lipid membrane phase (D_m), and RFB distributed in the aqueous phase (D_w); $[L]$ is the lipid concentration and V_m is the lipid molar volume. For DMPC and DMPG, the values of V_m are respectively 0.66 and 0.67 L mol^{-1} (calculated from the mean molecular weight and the reported specific volume of lipids).[14]

The absorption and the second and the third derivative spectra for RFB containing different concentrations of LUVs composed of DMPC are shown in Figure 2. The λ of the maximum absorption of RFB in DMPC (Figure 2D) and DMPG (not shown) exhibits a hypsochromic shift (of 4 nm) in accordance to the increase in the lipids concentration, indicating the partition of the drug to the lipid bilayers.[21] Figure 2D shows, as an example, the best fit of the eq 1 to the third derivative spectrophotometric data collected at λ = 294 nm for RFB with different concentrations of DMPC liposomes.

The values of the K_p of RFB, expressed as log D, between lipids (LUVs of DMPC and DMPG) and the buffer system are listed in the Table 1.

Table 1. Partition Coefficients (log D) (Dimensionless) for RFB in DMPC and DMPG Liposomes (500 μM, T = 37.0 ± 0.1 °C pH 7.4) Obtained in the Fluid Phase[a]

	DMPC:aqueous	DMPG:aqueous
log D	3.0 ± 0.1	3.6 ± 0.1

[a]Results present the mean and standard deviation of at least three independent assays.

The analysis of the obtained log D values reveals that RFB exhibits a higher partition for the DMPG liposomes. At the physiological pH, the contribution of the positively charged molecules (due to the ionization of the piperidine nitrogen) might be responsible for this higher partition due to the electrostatic interactions with the polar head groups of DMPG liposomes.

The predicted log P and log D, obtained using the chemical software, were respectively 4.57 and 3.06. The predicted log P is clearly higher because it does not account the occurrence of modifications in the hydrophobicity of ionizable compounds at varying pH. Contrastingly, the predicted log D is in close agreement with the experimental partition of RFB obtained for DMPC liposomes. Therefore, hydrophobic interactions are expected to be the main interactions occurring with the zwitterionic lipid membranes. Furthermore, the higher log D obtained for DMPG confirms that not only hydrophobic intermolecular forces drive the drug's partition. Therefore, the RFB's interaction with DMPG also encodes ionic bonds between the protonated imidazole and piperidine nitrogen and the deprotonated phosphate from the phospholipid head groups.[22]

Studies of RFB Location in the Lipid Bilayer of Membrane Mimetic Systems. Fluorescence quenching is a sensitive method that has long been used to study the location of specific ligands within liposomes and biological membranes.[23] The membrane location of RFB was assessed by fluorescence quenching measurements using two fluorescent probes (DPH and DPH-PA). When the probes are included in the lipid bilayer, the precise fluorophore positions along the membrane depth plane are well-established and documented.[24,25] While DPH-PA probe is anchored to the surface of the membrane in the phospholipids polar head groups,[24,26,27] the DPH probe has a deeper location and a parallel alignment to the acyl chains.[24−26] A huge variety of molecular interactions can result in the decrease of the fluorescence intensity of a sample (process called quenching). Because it is the most appropriate method to distinguish the type of quenching (static or dynamic), not only the intensity of the fluorescence emission was measured but also the fluorescence lifetimes.[23] Moreover, to definitely prove the type of fluorescence quenching the studies were performed at several temperatures.[28] The collisional quenching of fluorescence is described by the Stern−Volmer equation (eq 2):[23]

$$\frac{I_0}{I} = 1 + K_{SV}[Q]_m = \frac{\tau_0}{\tau} \quad (2)$$

In this equation, I_0 and I are respectively the fluorescence intensities in the absence and presence of the quencher; K_{SV} is the quenching constant, called the Stern−Volmer constant; τ_0 and τ are the lifetime of the fluorophore in the absence and presence of the quencher; $[Q]_m$ is the concentration of the quencher that is able to partition the membrane, which is calculated from the total drug concentration ($[Q]_T$) and from the drug's partition coefficient (K_p), as described by the following equation:[23]

$$[Q]_m = \frac{K_p[Q]_T}{K_p\alpha_m + (1 - \alpha_m)} \quad (3)$$

where α_m is the volume fraction of the membrane phase ($\alpha_m = V_m/V_T$; V_m and V_T represent respectively the volumes of the membrane and water phases). The Stern−Volmer equation (eq 2) illustrates an important characteristic of the collisional quenching, which is an equivalent decrease in the fluorescence intensity and lifetime. If the quenching is purely collisional, $I_0/I - 1$ is expected to be linearly dependent upon the concentration of the quencher. In several instances, the fluorophore can be quenched both by collisions and by complex formation with the same quencher, being an upward curvature of the Stern−Volmer plot a characteristic feature in these circumstances. The dynamic portion of the observed quenching is determined by lifetime measurements using the following equation, $\tau_0/\tau = 1 + K_D[Q]$. So, by knowing the dynamic component, the static contribution may be found by linearization of the following equation (eq 4):

dx.doi.org/10.1021/jm301116j | J. Med. Chem. 2013, 56, 417−426

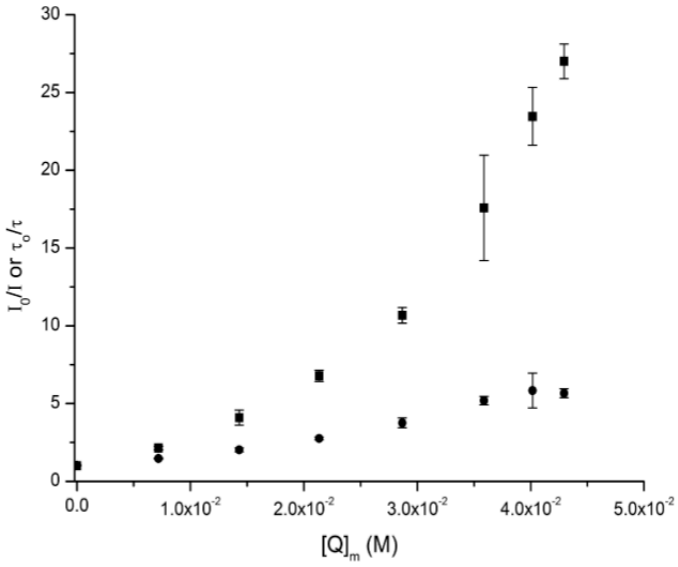

Figure 3. Stern–Volmer plots of the probe DPH-PA in LUVs of DMPG (500 μM, T = 37.0 ± 0.1 °C pH 7.4) by increasing concentrations (M) of the quencher RFB. The squares (■) represent Stern–Volmer plot obtained by steady-state fluorescence measurements (I_0/I), and circles (●) represent Stern–Volmer plot obtained by lifetime fluorescence measurements (τ_0/τ).

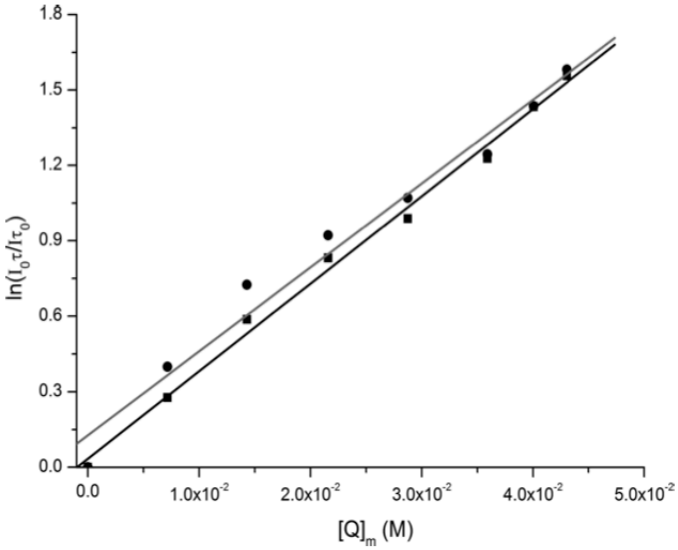

Figure 4. Fluorescence quenching of DPH (■) and DPH-PA (●) probes in LUVs of DMPG (500 μM, T = 37.0 ± 0.1 °C pH 7.4) by increasing concentrations of RFB and respective application of the mathematical model "sphere of action". Lines represent fits to eq 5.

$$\frac{I_0}{I} \times \frac{1}{1 + K_D[Q]_m} = 1 + K_S[Q]_m \quad (4)$$

This modified form of the Stern–Volmer equation is second order in $[Q]_m$, which accounts for the upward curvature observed when both static and dynamic quenching occur for the same fluorophore. In the Figure 3, the Stern–Volmer plots of I_0/I against $[Q]_m$ and τ_0/τ against $[Q]_m$ are depicted. From the Figure 3, it may be concluded that the quenching is not purely collisional and might also be due to the formation of a static quenching process. As a result, RFB must diffuse to the fluorophore during the lifetime of the excited state. After the contact, the fluorescent probe returns to the ground state without the photon emission. Moreover the static quenching is also present and the fluorophore and RFB form a non-fluorescent complex.[23,28]

Nevertheless, the positive deviation of the Stern–Volmer plots can also be interpreted in terms of a "sphere of action" static quenching model. According to this model, instantaneous quenching occurs if the quencher molecule is adjacent to the fluorophore at the moment of excitation. When the fluorophore and quencher are in such proximity, there is a high probability that quenching will occur before these molecules diffuse apart. As the quencher concentration increases this probability also increases because the quencher is within the "sphere of action" of the fluorophore at the moment of excitation. Hence, only a

dx.doi.org/10.1021/jm301116j | J. Med. Chem. 2013, 56, 417–426

Table 2. Values of Stern–Volmer Constant at T = 37.0 ± 0.1 °C (K_{SV}) and 42.0 ± 0.1 °C (K_{SV}*) and Bimolecular Quenching Constant (K_q) Obtained for RFB in DMPC and DMPG Liposomes (500 μM, T = 37.0 ± 0.1 °C pH 7.4) Labeled with DPH or DPH-PA Probes

	K_{SV} (M^{-1})		K_{SV}* (M^{-1})		K_q (M^{-1} s^{-1})	
	DPH	DPH-PA	DPH	DPH-PA	DPH	DPH-PA
DMPC	216 ± 10	165 ± 10	156 ± 14	76 ± 9	27 ± 1	29 ± 2
DMPG	167 ± 13	181 ± 10	132 ± 8	121 ± 9	19 ± 1	26 ± 1

certain fraction of the excited fluorophore is quenched by the Stern–Volmer collisional mechanism. Moreover, this model assumes that if the quencher is located inside a spherical volume (V) adjacent to the fluorophore, the probability for the quencher to be inside this volume at the time of excitation depends on the volume itself and on the quencher concentration ($[Q]_m$), as it is described by the modified Stern–Volmer equation (eq 5):[23]

$$\ln\left(\frac{I_0\tau}{I\tau_0}\right) = V[Q]_m \tag{5}$$

For both membrane models, the data was treated according to the "sphere of action" quenching model and is represented in the Figure 4. The analyses of the Figure 4 permit the conclusion that the results obtained in this work are in good agreement with the "sphere of action" quenching model.

The bimolecular quenching constant (K_q) is a fundamental parameter that reflects the efficiency of quenching or the accessibility of the probes to the drug and is calculated as follows (eq 6):[23]

$$K_q = \frac{K_{SV}}{\tau_0} \tag{6}$$

The K_{SV} values at two different temperatures and the K_q as the sum of both contributions (static and dynamic) are listed in the Table 2. The results suggest that for both membrane models the quenching process is the result of dynamic and static interactions with a dominant static component. The K_{SV} values decrease with the increase of temperature (from 37.0 to 42.0 °C), which is indicative of a nonfluorescence complex dissociation and a confirmation that the static quenching is present. The location studies have shown that in DMPG liposomes, the quenching efficiency of the DPH-PA is higher than that of DPH. This is in accordance with the preferential location of RFB near the polar region of the negatively charged phospholipids. The similar K_q values obtained for DPH and DPH-PA in the DMPC suggest that RFB does not have a preferential location in phospholipid membranes with no net charge. Hence, RFB in the zwitterionic membrane model is located in the surface as well as inside of the membrane hydrocarbon core. Moreover, the high values obtained for the DPH indicate that the drug is able to penetrate the bilayer in both lipids and especially in the DMPC. The molecules of RFB with no net charge should be inserted in the phospholipid bilayers according to their hydrophobicity gradient. The hydrophilic part of RFB, namely imidazole and piperidine moieties (Figure 1), should therefore be located near the head groups of the phospholipids and the hydrophobic naphthol must be embedded within the membrane, establishing van der Waals interactions with the phospholipid tails.[11] Moreover, the positively charged RFB seems to establish electrostatic interactions with the deprotonated phosphate group of the DMPG phospholipids. The electrostatic interactions appear to be less pronounced in the case of DMPC due to the presence of a protonated choline group in the head groups of the phospholipids that may cause electrostatic repulsions that hinder the partition of the positively charged drug.

Effects of RFB on the Microviscosity of the Membrane Mimetic Systems. Steady-state fluorescence anisotropy measurements have been widely used to quantify the fluidity gradient across bilayer structures and the results obtained have proven to be consistent with a variety of other physical techniques.[13] To study the influence of the RFB on the fluidity of the membranes, cell-based assays and the parallel artificial membrane permeability assay (PAMPA) could also have been performed. However, these techniques do not allow to fully understanding how RFB affects the biophysical parameters of the membrane models used.[29] Furthermore, to complement the information provided by the quenching data, steady-state fluorescence anisotropy was carried out to study the effect of RFB on the membrane lipids main phase transition temperature (T_m) and, accordingly, extrapolate the influence of this compound on the bacterial and human host plasma membrane microviscosity. The fluorescence steady-state anisotropy (r_s) is defined by the following equation (eq 7):[21,30]

$$r_s = \frac{I_{VV} - I_{VH}G}{I_{VV} + 2I_{VH}G} \tag{7}$$

where I_{VV} and I_{VH} are the polarized intensities measured in directions parallel and perpendicular to the excitation beam. The correction factor ($G = I_{HV}/I_{HH}$) is the ratio of the detection system sensitivity for vertically and horizontally polarized light, which is given by the ratio of vertical to horizontal components when the excitation light is polarized in the horizontal direction.[30] The temperature dependence of the DPH fluorescence anisotropy in the absence and presence of RFB is shown for DMPC and DMPG liposomes, respectively, in Figure 5A and 5B. From the experimental data displayed, it is possible to calculate the cooperativity (B) and the T_m, which corresponds to the temperature of the gel-to-fluid phase transition of DMPC and DMPG and is calculated from the inflection point of the data fitted to sigmoid curves of steady-state anisotropy (r_s) versus temperature (T) (eq 8):

$$r_s = r_{s1} + p_1T + \frac{r_{s2} - r_{s1} + p_2T - p_1T}{1 + 10^{B(1/T - 1/T_m)}} \tag{8}$$

where p_1 and p_2 correspond to the slopes of the straight lines at the beginning and at the end of the plot and r_{s1} and r_{s2} are the respective steady-state anisotropy intercepting values at the y axis. The order parameter can also be calculated $s = (r_\infty/r_0)^{1/2}$, where r_0 (fundamental anisotropy) is the fluorescence anisotropy in absence of any rotational motion of the probe and r_∞ (limiting anisotropy) reflects the restriction of the probe motion.[21]

Besides analyzing the differences of RFB in its ability to disturb the DMPC and DMPG liposomes, it is important to

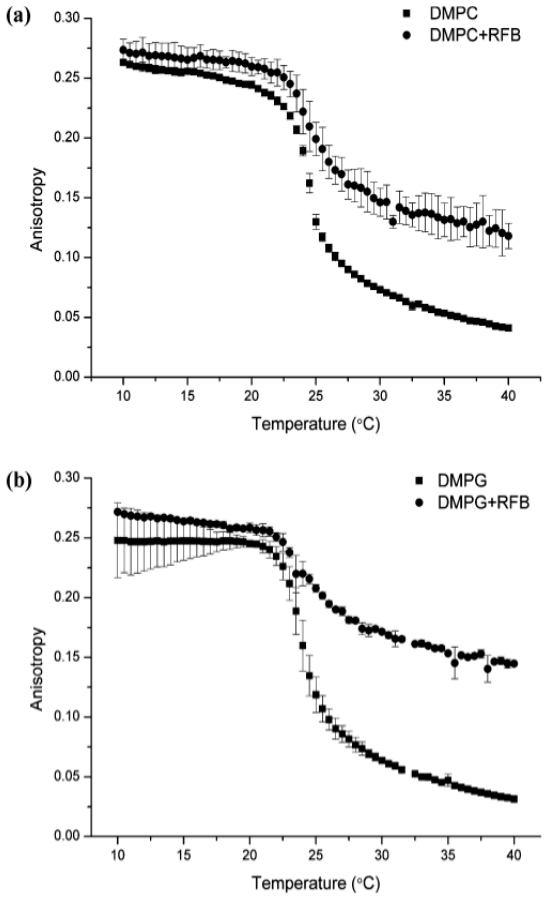

Figure 5. (A) Steady-state anisotropy of DPH in absence (■) and in the presence (●) of RFB (30 μM) in DMPC liposomes at pH = 7.4 as a function of temperature. Each point corresponds to the mean value of three experiments. Continuous lines are the best-fit curves using eq 8. (B) Steady-state anisotropy of DPH in absence (■) and in the presence (●) of RFB (30 μM) in DMPG liposomes at pH = 7.4 as a function of temperature. Each point corresponds to the mean value of three experiments. Continuous lines are the best-fit curves using eq 8.

compare the results obtained for DPH and DPH-PA, as they are located in different sites of the lipid bilayer and therefore report the microfluidity of those regions.[31] Moreover, regarding the previous results, RFB has already shown capacity to quench DPH and DPH-PA. The results presented in Table 3 for DMPC and DMPG using both probes show that the T_m values of DMPC and DMPG are consistent with the literature.[32,33] Independently of the probe, the T_m is not affected by the drug's presence in both models (Table 3). RFB penetrate both membrane models at temperatures above the T_m, taking into consideration the changes in the anisotropy when compared to the liposomes without drug (Figure 5). This is in accordance with the bulky structure of RFB and its relative rigid structure, being the highly ordered state of the lipids a hindrance to the drug's penetration.[11,12] Additionally, at temperatures above the T_m, RFB is responsible for higher values of anisotropy in both models compared to the liposomes alone. The higher values of anisotropy indicate that the drug decreases the fluidity of the membrane models (Figure 5). The decrease in the membrane fluidity due to the RFB's presence is more pronounced for the DMPG liposomes. In contrast to the T_m, at the fluid phase the cooperativity and the degree of molecular packing (order) significantly change with the drug's presence (Table 3). The drug decreases the cooperativity of the phase transitions and increases the order of both lipids, which confirms that RFB penetrates both membrane models. Moreover, RFB changed the cooperativity and the order (Table 3), especially in the DMPG, meaning that in this model, the drug must be located closer to the more ordered region, namely in the vicinity of the head groups of the phospholipids (correspondent to the acyl chains from C1 to C8 region).[34,35] Therefore, the increment in the DMPG order may be caused by the electrostatic interactions between RFB and the phospholipid head groups, with a consequent screening of the negative surface charge that might decrease the repulsive forces between the phospholipid head groups. Again, these results are consistent with the above-mentioned prevision of the drug's location.

■ CONCLUSION

Antibiotic-mediated bacterial cell death is a complex process that begins with the biophysical interaction between the drugs and the biomembranes.[36,37] Thus, to reach its intracellular target (bacterial RNA polymerase), RFB must pass across the human plasma membranes (absorption/distribution) and thereafter the mycobacterial plasma membranes (generally inside the human macrophages). Notwithstanding the binding to the RNA polymerase, the mechanism of action of RFB seems to be much more multifaceted and might be related to the drug's lipid affinity. The results revealed that the surface charge of the phospholipids played a major role in the differential interactions of RFB with membranes. The determination of the partition coefficient showed a higher value for the DMPG:aqueous compared to the DMPC:aqueous liposomes, suggesting that the partition of the drug depends on the lipid's charge and it is regulated by electrostatic interactions. The higher partition of the drug for the mycobacterial membrane model is in agreement with the higher affinity of RFB to the membranes with negatively charged lipids, which result in a higher selectivity and higher RFB concentrations that reach the

Table 3. Values of Main Phase Transition Temperature (T_m), Cooperativity (B), and Order Parameter (S) Obtained for DMPC and DMPG Liposomes (500 μM, T = 37.0 ± 0.1 °C pH 7.4) Labeled with DPH or DPH-PA Probes in the Absence and in the Presence of RFB (30 μM)

	DPH			DPH-PA		
	T_m (°C)	cooperativity (B)	order (S)	T_m (°C)	cooperativity (B)	order (S)
DMPC	24.4 ± 0.2	347 ± 34	0.39 ± 0.04	24.6 ± 0.3	246 ± 27	0.66 ± 0.02
DMPC+RFB	24.5 ± 0.8	254 ± 35	0.63 ± 0.03	24.5 ± 0.4	214 ± 23	0.73 ± 0.03
DMPG	24.1 ± 0.5	233 ± 5	0.34 ± 0.03	23.9 ± 0.3	354 ± 37	0.75 ± 0.02
DMPG+RFB	24.4 ± 0.3	182 ± 34	0.66 ± 0.02	24.2 ± 0.7	209 ± 28	0.85 ± 0.02

dx.doi.org/10.1021/jm301116j | J. Med. Chem. 2013, 56, 417−426

pharmacological target. Additionally, this differential affinity for biomembranes with different charge might contribute to understanding the higher activity and higher drug's penetration in Gram-positive bacteria compared with Gram-negative bacteria. The membrane location studies revealed that RFB is able to penetrate both membrane models. Indeed, the high partition and the deep location of RFB into the DMPC bilayer are suggestive of the drug's potential in vivo penetration into biological membranes.[38] The results obtained support the drug's wide distribution through the human body. Moreover, they contribute to our understanding of some of the toxicological effects, which are related to the RFB−membrane tropism and the ability to reach the body fluids and some of the most ordered membranes in the human body such as the epiretinal membrane.[39] The drug affects the biophysical parameters of membranes, namely the cooperativity, the lipid's order, and the fluid phase of both models. In particular, the drug causes a higher perturbation of these biophysical parameters in the negatively charged membrane model, with a noticeable increase of the order parameter in the fluid phase. The lipid's order increment indicates that the presence of the drug is responsible for higher phospholipid packing. This is consistent with the higher partition of RFB and its preferential location in the region nearer to the membrane surface, which might be translated in more pronounced effects in the biophysical parameters of the bacterial membrane. These data provide evidence that after the adsorption to the membrane interface via electrostatic interactions, RFB molecules undergo full immersion into the hydrophobic core. The zwitterionic contribution of RFB should be inserted according to its hydrophobicity gradient. In the human membrane, the hydrophilic part of RFB, namely imidazole and piperidine moieties, should therefore be located in the glycerol backbone and the hydrophobic naphthol should be incorporated at the phospholipid tails.[11] In the bacterial membrane model and because the positively charged contribution of RFB molecules are due to the protonated piperidine, the drug molecules establish stronger electrostatic interactions with the phosphate group of the DMPG, which explain the higher partition and the preferential surface location of RFB in the negatively charged model.

The results gathered suggest that the interactions of RFB with the bacterial membranes are mediated by electrostatic interactions, which might be a key to understand and to complement the knowledge about its mechanism of action. In fact, the mechanism by which RFB permeates through the bacterial membrane bilayer may include electrostatic adsorption. As the drug permeates through the membrane in direction to the RNA polymerase located inside of the bacterial cell, the location of the drug in the phospholipid membrane is responsible for a differential destabilization of the membranes. The RFB anchored to the head groups in the ordered region of the phospholipid membrane perturbs the phospholipid packing in the bacteria membrane. This closer lipid packing and therefore more restricted lateral movement might increase the susceptibility of the bacterial membrane to the oxidation of the membrane due to the action of the free radicals inside the macrophages, leading to the inhibition/killing of the bacteria.[40−42] Moreover, the influx/efflux of ions and nutrients trough the bacterial membrane might be compromised. Nevertheless, the human plasma membrane is much less disturbed due to a deeper insertion of the drug within the bilayer.

In conclusion, these findings represent a contribution to the medicinal chemistry field and permit to understand the differential interaction of RFB with membranes of different charge, which are putatively related to the therapeutic and toxic effects of this antibiotic and should therefore be taken into consideration when developing new RFB analogues for anti-TB therapy.

■ EXPERIMENTAL SECTION

Reagents and Equipment. The lipids (DMPC and DMPG) and *N*-(2-hydroxyethyl)piperazine-*N*′-(2-ethanesulfonic acid) (HEPES) were purchased from Sigma-Aldrich Co. (St. Louis, MO, USA). The probes, DPH and DPH-PA,were obtained from Molecular Probes (Invitrogen, Paisley, UK) and all were used as supplied. RFB was isolated from Mycobutin (Pfizer, Inc., New York) and further purified as described previously.[2] All other chemicals were supplied from Merck (Darmstadt, Germany). RFB's stock solutions were prepared in buffer:ethanol (9:1, v/v). The buffer HEPES 0.01 M (pH 7.4) was prepared with double-deionized water (conductivity less than 0.1 μS cm^{-1}) from a Millipore system, and the ionic strength (I = 0.1 M) was adjusted with NaCl.

Spectrophotometric measurements: the absorption spectra were recorded using a Perkin−Elmer Lambda 45 UV−Vis spectrophotometer, using quartz cells with a 1 cm^{-1} path length and a spectral range from 250 to 600 at 1 nm intervals.

Fluorescence measurements: fluorimetric data were collected using a Perkin−Elmer LS 50 B steady-state fluorescence spectrometer equipped with a constant-temperature cell holder. All data were recorded with excitation and emission slits between 2.5 and 3.0 nm. The excitation wavelength was set to 357 nm for DPH and 360 nm for DPH-PA. The emission wavelength was set to 427 nm for DPH and 430 nm for DPH-PA. All fluorescence intensity data were corrected for the quencher absorbance at the excitation wavelength.[43]

Fluorescence lifetime measurements: modulation frequencies were acquired between 10 and 200 MHz in a Fluorolog Tau-3 Lifetime spectrofluorimeter. Integration time was 10 s. Manual slits were of 0.5 mm, slits for monochromator excitation were of 7 mm (side entrance) and 0.7 mm (side exit) and for monochromator emission of 7 mm (side entrance) and 7 mm (side exit). The fluorescence emission was detected with a 90° scattering geometry. All measurements were made using Ludox as a reference standard (τ = 0.00 ns).

Anisotropy measurements: the fluorescence anisotropy was measured with a Jasco FP-6500 spectrofluorometer (Jasco, Great Dunmow, UK) equipped with two polarizers in the paths for excitation and emission using the L-format method. Samples with DPH and DPH-PA were heated in a range of 10 to 40 °C at the same wavelengths used for the fluorescence measurements.

Experimental Methods. *Preparation of Liposomes.* A lipid film was formed from a chloroform solution of lipids, dried under a stream of nitrogen, and left under reduced pressure for a minimum of 45 min to remove all traces of the organic solvent. Liposomes were prepared by the addition of the buffer system, followed by vortexing to yield multilamellar vesicles (MLVs). Lipid suspensions were equilibrated at 37.0 ± 0.1 °C for 30 min and extruded 10 times through polycarbonate filters with a pore diameter of 100 nm to form LUVs.[14] To prepare the fluorescence labeled liposomes, the probes (DPH or DPH-PA) were dissolved in chloroform/methanol and added to the lipid to give a probe:lipid molar ratio of 1:300, followed by a 30 min incubation period in the dark.[21,44,45]

Determination of Partition Coefficients by Derivative Spectrophotometry. The partition coefficient (K_p) of RFB between LUVs suspensions of DMPC or DMPG and aqueous solution (HEPES: 0.01 M, I = 0.1 M, pH 7.4) was determined by derivative spectrophotometry. In the derivative spectrophotometric studies, a series of buffered suspensions containing a fixed concentration of RFB (25 μM) and increasing concentrations of DMPC or DMPG (50, 100, 200, 300, 400, 500, 700, 900, 1000 μM) were prepared. The corresponding reference solutions were identically prepared but without the drug. All

dx.doi.org/10.1021/jm301116j | J. Med. Chem. 2013, 56, 417−426

suspensions were then vortexed and incubated in the dark at 37.0 ± 0.1 °C for 30 min.

Membrane Location Studies by Fluorescence Quenching. The drug's location within the membrane models were performed using steady-state fluorescence and lifetime fluorescence measurements of DPH and DPH-PA fluorophore probes in liposome buffered suspensions prepared with DMPC and DMPG at pH 7.4 (HEPES: 0.01 M, I = 0.1 M, pH 7.4). Buffer solutions of RFB were added to liposomes labeled with the probes, and the resulting suspensions were incubated in the dark at 37.0 ± 0.1 °C for 30 min. The studies were made according to an already described method[21] and consisted of the incubation of increasing amounts of drug (0−27 μM) with DMPC and DMPG liposomes at 37.0 ± 0.1 °C for 30 min while maintaining the total lipid concentration constant (500 μM).

Membrane Fluidity Studies. The effect of RFB (30 μM) on membrane microviscosity was evaluated by steady-state anisotropy measurements using LUVs of DMPC and DMPG (500 μM) labeled with DPH and DPH-PA probes as previously described.[21] The anisotropy values were recorded at several temperatures between 10 and 40 °C, with an accuracy of 0.1 °C. The order parameter was calculated in the fluid phase for both lipids.

Computational Methods. The chemical software used to predict the charge of RFB in bulk solution (pH 7.4) and to the octanol/water log P and log D was the MarvinView 5.4.1.1 software from ChemAxon.

■ AUTHOR INFORMATION

Corresponding Author

*Phone: +351-220428672. Fax: +351-226093483. E-mail: shreis@ff.up.pt.

Notes

The authors declare no competing financial interest.

■ ACKNOWLEDGMENTS

Marina Pinheiro and João M. Caio thank FCT (Lisbon) for the doctoral fellowships (SFRH/BD/63318/2009 and SFRH/BD/66789/2009, respectively). Cláudia Nunes thanks FCT (Lisbon) for the postdoctoral fellowship (SFRH/BPD/81963/2011). We are also grateful to the FCT for financial support under projects PEst-OE/QUI/UI0612/2011 and PTDC/QUI-QUI/101022/2008 with coparticipation European Community funds from the FEDER, QREN, and COMPET.

■ ABBREVIATIONS USED

CL, cardiolipin; DMPC, 1,2-dimyristoyl-*sn*-glycero-phosphocholine; DMPG, 1,2-dimyristoyl-*sn*-glycero-3-phosphoglycerol; DPH, 1,6-diphenyl-1,3,5-hexatriene; DPH-PA, (2-carboxyethyl)-1,6-diphenyl-1,3,5-hexatriene; HEPES, *N*-(2-hydroxyethyl) piperazine-*N*′-(2-ethanesulfonic acid); LUVs, Large unilamellar vesicles; MLVs, multilamellar vesicles; RFB, Rifabutin; TB, tuberculosis; T_m, main phase transition temperature

■ REFERENCES

(1) Aristoff, P. A.; Garcia, G. A.; Kirchhoff, P. D.; Hollis Showalter, H. D. Rifamycins—obstacles and opportunities. *Tuberculosis* **2010**, *90*, 94−118.

(2) Figueiredo, R.; Moiteiro, C.; Medeiros, M. A.; da Silva, P. A.; Ramos, D.; Spies, F.; Ribeiro, M. O.; Lourenco, M. C.; Junior, I. N.; Gaspar, M. M.; Cruz, M. E.; Curto, M. J.; Franzblau, S. G.; Orozco, H.; Aguilar, D.; Hernandez-Pando, R.; Costa, M. C. Synthesis and evaluation of rifabutin analogs against *Mycobacterium avium* and H(37)Rv, MDR, and NRP *Mycobacterium tuberculosis*. *Bioorg. Med. Chem.* **2009**, *17*, 503−511.

(3) Gaspar, M.; Neves, S.; Portaels, F.; Pedrosa, J.; Silva, M.; Cruz, M. Therapeutic efficacy of lipossomal rifabutin in a *Mycobacterium avium* model of infection. *Antimicrob. Agents Chemother.* **2000**, *44*, 2424−2430.

(4) Sousa, M.; Pozniak, A.; Boffito, M. Pharmacokinetics and pharmacodynamics of drug interactions involving rifampicin, rifabutin, and antimalarial drugs. *J Antimicrob Chemother.* **2008**, *62*, 872−878.

(5) Gisbert, J. P.; Calvet, X. Review article: rifabutin in the treatment of refractory *Helicobacter pylori* infection. *Aliment. Pharmacol. Ther.* **2012**, *35*, 209−221.

(6) Lucio, M.; Lima, J. L.; Reis, S. Drug−membrane interactions: significance for medicinal chemistry. *Curr. Med. Chem.* **2010**, *17*, 1795−1809.

(7) Vollhardt, D.; Fainerman, V. B. Characterisation of phase transition in adsorbed monolayers at the air/water interface. *Adv. Colloid Interface Sci.* **2010**, *154*, 1−19.

(8) Lintker, K. B.; Kpere-Daibo, P.; Fliesler, S. J.; Serfis, A. B. A comparison of the packing behavior of egg phosphatidylcholine with cholesterol and biogenically related sterols in Langmuir monolayer films. *Chem. Phys. Lipids* **2009**, *161*, 22−31.

(9) Bernardo, M. A.; Pina, F.; Garcia-Espana, E.; Latorre, J.; Luis, S. V.; Llinares, J. M.; Ramirez, J. A.; Soriano, C. Thermodynamic and Steady-State Fluorescence Emission Studies on Metal Complexes of Receptors Containing Benzene Subunits. *Inorg Chem.* **1998**, *37*, 3935−3942.

(10) Komath, S. S.; Kenoth, R.; Swamy, M. J. Thermodynamic analysis of saccharide binding to snake gourd (*Trichosanthes anguina*) seed lectin. Fluorescence and absorption spectroscopic studies. *Eur. J. Biochem.* **2001**, *268*, 111−119.

(11) Vostrikov, V. V.; Selishcheva, A. A.; Sorokoumova, G. M.; Shakina, Y. N.; Shvets, V. I.; Savel'ev, O. Y.; Polshakov, V. I. Distribution coefficient of rifabutin in liposome/water system as measured by different methods. *Eur. J. Pharm. Biopharm.* **2008**, *68*, 400−405.

(12) Vostrikov, V. V.; Selishcheva, A. A.; Sorokoumova, G. M.; Shvets, V. I. Determination of the distribution coefficient of rifabutin by the fluorescence study in the system liposome−water. *Biofizika.* **2007**, *52*, 521−526.

(13) Merino, S.; Vazquez, J. L.; Domènech, Ò.; Berlanga, M.; Vinãs, M.; Montero, M. T.; Hernández-Borrell, J. Fluoroquinolone−Biomembrane Interaction at the DPPC/PG Lipid−Bilayer Interface. *Langmuir* **2002**, *18*, 3288−3292.

(14) Pereira-Leite, C.; Nunes, C.; Lima, J. L.; Reis, S.; Lucio, M. Interaction of celecoxib with membranes: the role of membrane biophysics on its therapeutic and toxic effects. *J. Phys. Chem. B* **2012**, *116*, 13608−13617.

(15) Alves, I. D.; Goasdoue, N.; Correia, I.; Aubry, S.; Galanth, C.; Sagan, S.; Lavielle, S.; Chassaing, G. Membrane interaction and perturbation mechanisms induced by two cationic cell penetrating peptides with distinct charge distribution. *Biochim. Biophys. Acta* **2008**, *1780*, 948−959.

(16) Raquel, E.; Richard, E. Functional Consequences of the Lateral Organization of Biological Membranes. In *The Structure of Biological Membranes*, 3rd ed.; Yeagle, L. P., Ed.; CRC Press: New York, 2011; pp 133−152.

(17) Shakina, Y. N.; Vostrikov, V. V.; Sorokoumova, G. M.; Selishcheva, A. A.; Shvets, V. I. Interaction of rifabutin with model membranes. *Bull. Exp. Biol. Med.* **2005**, *140*, 711−713.

(18) Ferreira, H.; Lucio, M.; de Castro, B.; Gameiro, P.; Lima, J. L.; Reis, S. Partition and location of nimesulide in EPC liposomes: a spectrophotometric and fluorescence study. *Anal. Bioanal. Chem.* **2003**, *377*, 293−298.

(19) Henzing, A. J.; Dodson, H.; Reid, J. M.; Kaufmann, S. H.; Baxter, R. L.; Earnshaw, W. C. Synthesis of novel caspase inhibitors for characterization of the active caspase proteome in vitro and in vivo. *J. Med. Chem.* **2006**, *49*, 7636−7645.

(20) Connell, N. D.; Nikaido, H. Membrane Permeability and Transport in *Mycobacterium tuberculosis*. In *The Tuberculosis: Pathogenesis, Protection, and Control*, 1st ed.; Bloom, B., Ed.; ASM Press: Washington DC, 1994; pp 340.

(21) Brittes, J.; Lucio, M.; Nunes, C.; Lima, J. L.; Reis, S. Effects of resveratrol on membrane biophysical properties: relevance for its pharmacological effects. *Chem. Phys. Lipids* **2010**, *163*, 747−754.

(22) Grumetto, L.; Carpentiero, C.; Barbato, F. Lipophilic and electrostatic forces encoded in IAM-HPLC indexes of basic drugs: Their role in membrane partition and their relationships with BBB passage data. *Eur. J. Pharm. Sci.* **2012**, *45*, 685−692.
(23) Eftink, R. M. Fluorescence Quenching: Theory and Applications. In *The Principles of Fluorescence Spectroscopy*, 3rd ed.; Lakowicz, J. R., Ed.; Springer: New York, 2006; pp 53−120.
(24) Cardoso, A. M. S.; Faneca, H.; Almeida, J. o. A. S.; Pais, A. A. C. C.; Marques, E. F.; de Lima, M. C. P.; Jurado, A. l. S. Gemini surfactant dimethylene-1,2-bis(tetradecyldimethylammonium bromide)-based gene vectors: a biophysical approach to transfection efficiency. *Biochim. Biophys. Acta, Biomembr.* **2011**, *1808*, 341−351.
(25) Kaiser, R. D.; London, E. Location of Diphenylhexatriene (DPH) and Its Derivatives within Membranes: A Comparison of Different Fluorescence Quenching Analyses of Membrane Depth. *Biochemistry* **1998**, *37*, 8180−8190.
(26) Monteiro, J.; Videira, R.; Matos, M.; Dinis, A.; Jurado, A. Non-Selective Toxicological Effects of the Insect Juvenile Hormone Analogue Methoprene. A Membrane Biophysical Approach. *Appl. Biochem. Biotechnol.* **2008**, *150*, 243−257.
(27) Lucio, M.; Ferreira, H.; Lima, J. L.; Reis, S. Use of liposomes to evaluate the role of membrane interactions on antioxidant activity. *Anal. Chim. Acta* **2007**, *597*, 163−170.
(28) Castanho, M. A.; Prieto, M. J. Fluorescence quenching data interpretation in biological systems. The use of microscopic models for data analysis and interpretation of complex systems. *Biochim. Biophys. Acta* **1998**, *1373*, 1−16.
(29) Weeraman, C.; Chen, M.; Moffatt, D. J.; Lausten, R.; Stolow, A.; Johnston, L. J. A combined vibrational sum frequency generation spectroscopy and atomic force microscopy study of sphingomyelin-cholesterol monolayers. *Langmuir* **2012**, *28*, 12999−13007.
(30) Grancelli, A.; Morros, A.; Cabanas, M. E.; Domenech, O.; Merino, S.; Vazquez, J. L.; Montero, M. T.; Vinas, M.; Hernandez-Borrell, J. Interaction of 6-fluoroquinolones with dipalmitoylphosphatidylcholine monolayers and liposomes. *Langmuir* **2002**, *18*, 9177−9182.
(31) Lucio, M.; Ferreira, H.; Lima, J. L.; Reis, S. Interactions between oxicams and membrane bilayers: an explanation for their different COX selectivity. *Med Chem.* **2006**, *2*, 447−456.
(32) John, K.; Kubelt, J.; Muller, P.; Wustner, D.; Herrmann, A. Rapid transbilayer movement of the fluorescent sterol dehydroergosterol in lipid membranes. *Biophys. J.* **2002**, *83*, 1525−1534.
(33) Riske, K. A.; Fernandez, R. M.; Nascimento, O. R.; Bales, B. L.; Lamy-Freund, M. T. DMPG gel−fluid thermal transition monitored by a phospholipid spin labeled at the acyl chain end. *Chem. Phys. Lipids* **2003**, *124*, 69−80.
(34) Lipp, M. M.; Lee, K. Y.; Waring, A.; Zasadzinski, J. A. Fluorescence, polarized fluorescence, and Brewster angle microscopy of palmitic acid and lung surfactant protein B monolayers. *Biophys. J.* **1997**, *72*, 2783−2804.
(35) Nunes, C.; Brezesinski, G.; Pereira-Leite, C.; Lima, J. L.; Reis, S.; Lucio, M. NSAIDs interactions with membranes: a biophysical approach. *Langmuir* **2011**, *27*, 10847−10858.
(36) Rodrigues, C.; Gameiro, P.; Prieto, M.; Castro, B. Interaction of rifampicin and isoniazid with large unilamellar liposomes: spectroscopic location studies. *Biochim. Biophys. Acta* **2003**, *1620*, 151−159.
(37) Kohanski, M. A.; Dwyer, D. J.; Collins, J. J. How antibiotics kill bacteria: from targets to networks. *Nature Rev. Microbiol.* **2010**, *8*, 423−435.
(38) Pinheiro, M.; Lucio, M.; Reis, S.; Lima, J. L.; Caio, J. M.; Moiteiro, C.; Martin-Romero, M. T.; Camacho, L.; Giner-Casares, J. J. Molecular interaction of rifabutin on model lung surfactant monolayers. *J. Phys. Chem. B* **2012**, *116*, 11635−11645.
(39) Borchman, D.; Yappert, M. C. Lipids and the ocular lens. *J. Lipid Res.* **2010**, *51*, 2473−2488.
(40) Mowri, H.; Nojima, S.; Inoue, K. Effect of lipid composition of liposomes on their sensitivity to peroxidation. *J. Biochem.* **1984**, *95*, 551−558.
(41) Parker, A.; Miles, K.; Cheng, K. H.; Huang, J. Lateral distribution of cholesterol in dioleoylphosphatidylcholine lipid bilayers: cholesterol−phospholipid interactions at high cholesterol limit. *Biophys. J.* **2004**, *86*, 1532−1544.
(42) Huang, J. Model membrane thermodynamics and lateral distribution of cholesterol: from experimental data to Monte Carlo simulation. *Methods Enzymol.* **2009**, *455*, 329−364.
(43) Sweeney, L. G.; Wang, Z.; Loebenberg, R.; Wong, J. P.; Lange, C. F.; Finlay, W. H. Spray-freeze-dried liposomal ciprofloxacin powder for inhaled aerosol drug delivery. *Int. J. Pharm.* **2005**, *305*, 180−185.
(44) Lúcio, M.; Nunes, C.; Gaspar, D.; Golebska, K.; Wisniewski, M.; Lima, J. L. F. C.; Brezesinski, G.; Reis, S. Effect of anti-inflammatory drugs in phosphatidylcholine membranes: a fluorescence and calorimetric study. *Chem. Phys. Lett.* **2009**, *471*, 300−309.
(45) Nunes, C.; Brezesinski, G.; Lopes, D.; Lima, J. L.; Reis, S.; Lucio, M. Lipid−drug interaction: biophysical effects of tolmetin on membrane mimetic systems of different dimensionality. *J. Phys. Chem. B* **2011**, *115*, 12615−12623.

5. Drug-membrane interaction studies applied to *N'*-acetyl-rifabutin.

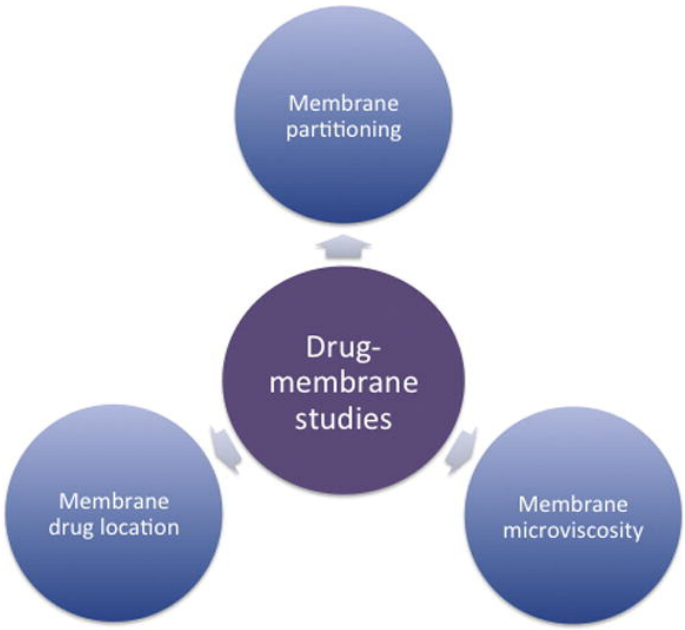

ARTICLE IN PRESS

European Journal of Pharmaceutics and Biopharmaceutics xxx (2013) xxx–xxx

Contents lists available at SciVerse ScienceDirect

European Journal of Pharmaceutics and Biopharmaceutics

journal homepage: www.elsevier.com/locate/ejpb

Research paper

Drug–membrane interaction studies applied to N′-acetyl-rifabutin

Marina Pinheiro [a], Mariana Arêde [a], João M. Caio [b], Cristina Moiteiro [b], Marlene Lúcio [a], Salette Reis [a,*]

[a] REQUIMTE, Departamento de Ciências Química, Universidade do Porto, Portugal
[b] Departamento de Química e Bioquímica, Universidade de Lisboa, Portugal

ARTICLE INFO

Article history:
Received 13 September 2012
Accepted in revised form 28 February 2013
Available online xxxx

Keywords:
Dynamic light scattering
Fluorescence quenching
Lifetime measurements
Partition coefficient
Steady-state anisotropy
Tuberculosis

ABSTRACT

This work aims the systematic study of the biophysical interactions of a novel antimycobacterial compound (N′-acetyl-rifabutin, RFB2) with membrane models of different lipid composition and surface charge. Membrane mimetic models were used to evaluate the RFB2's membrane partition, its preferential location across the membrane, and the effect of RFB2 on the biophysical properties of the membrane, which ultimately might be related with the antimycobacterial compound bioavailability and the membrane toxicity. According to the aforementioned, liposomes of dimyristoyl-sn-glycero-phosphocholine (DMPC) and 1,2-dimyristoyl-sn-glycero-3-phosphoglycerol (DMPG) were, respectively, used as mimetic models of human and bacterial cell membranes.

The antimycobacterial compound lipophilicity was evaluated by spectroscopic methods, which enabled the determination of the partition coefficient (K_p). To study the RFB2 membrane's location, fluorescence quenching studies and lifetime measurements were executed in liposomes labeled with fluorescent probes. In order to evaluate the changes induced by RFB2 on the membrane biophysical properties, dynamic light scattering (DLS) and steady-state anisotropy were performed.

The overall results reveal a strong interaction between RFB2 and the membrane models and allowed the evaluation of its lipophilicity, which is a key molecular descriptor in the characterization of novel potential drugs. Moreover, the higher partition of RFB2 and the more pronounced changes in the biophysical parameters of the negatively charged membrane model suggest that RFB2 has more affinity to the bacterial membrane. For the above-mentioned reasons, this work supports that RFB2 has a potential value as a drug in pharmaceutical formulations used to treat mycobacterial infections.

1. Introduction

Tuberculosis (TB) is an infectious disease caused by the bacillus *Mycobacterium tuberculosis* (MTB). Despite being an ancient disease, TB is nowadays more prevalent than at any other time in the human history [1]. In 2011, there were 8.7 million incident cases of TB, almost 1.0 million deaths due to TB among HIV-negative people and an additional 0.43 million deaths from HIV-associated TB [2]. Generally, only a relatively small proportion of people infected with MTb will develop TB disease; however, the probability of developing TB is markedly higher among people with impairment of their immune system such as that caused by the human immunodeficiency virus (HIV) [2,3]. In fact, the strong relationship between TB and HIV infection has significantly aggravated the worldwide morbidity and death. HIV co-infection is the most severe risk factor for the progression of the infection to active disease, increasing by 20-fold the risk of latent TB reactivation [4]. Ultimately, TB represents a major cause of death in HIV co-infected individuals [1]. According to the above-mentioned concerns about TB persistence, mortality and the emergence of multidrug-resistant (MDR) strains, the prospect of finding newer and more effective drugs motivates the synthesis of new antibiotic molecules [5]. In this context, RFB2 (Fig. 1) is a novel synthesized antimycobacterial compound and a derivative of rifabutin, with *in vitro* and *in vivo* efficacy and security proven [6]. Rifabutin is an antibiotic currently used in the prevention of *Mycobacterium avium* complex in immunocompromised patients and a second-line agent for the treatment of TB. In TB/HIV co-infected patients, it represents a useful alternative to the use of the first-line drug, rifampicin, which is a more potent cytochrome P450 (CYP) inducer resulting in numerous drug–drug interactions that complicate therapy. On the other hand,

Abbreviations: DMPC, 1,2-dimyristoyl-sn-glycero-phosphocholine; DMPG, 1,2-dimyristoyl-sn-glycero-3-phosphoglycerol; DPH, 1,6-diphenyl-1,3,5-hexatriene; DPH-PA, (2-carboxyethyl)-1,6-diphenyl-1,3,5-hexatriene; DLS, dynamic light scattering; HIV, human immunodeficiency virus; LUVs, large unilamellar vesicles; T_m, main phase transition temperature; MTB, *Mycobacterium tuberculosis*; MDR-TB, multidrug-resistant TB; MLVs, multilamellar vesicles; K_p, partition coefficients; RFB2, N′-acetyl-rifabutin; K_{SV}, Stern–Volmer constant; TB, tuberculosis.

* Corresponding author. REQUIMTE, Departamento de Ciências Químicas, Faculdade de Farmácia, Universidade do Porto, Rua de Jorge Viterbo Ferreira no. 228, 4050-313 Porto, Portugal. Tel.: +351 220428672; fax: +351 226093483.
E-mail address: shreis@ff.up.pt (S. Reis).

0939-6411/$ - see front matter © 2013 Elsevier B.V. All rights reserved.
http://dx.doi.org/10.1016/j.ejpb.2013.02.015

Please cite this article in press as: M. Pinheiro et al., Drug–membrane interaction studies applied to N′-acetyl-rifabutin, Eur. J. Pharm. Biopharm. (2013), http://dx.doi.org/10.1016/j.ejpb.2013.02.015

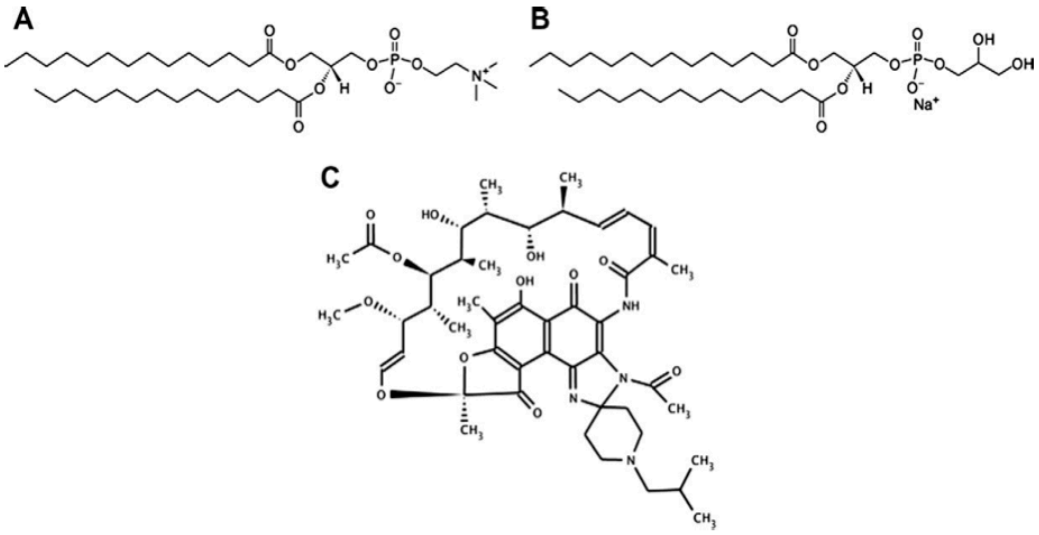

Fig. 1. Chemical structures of DMPC (A), DMPG (B) and N′-acetyl-rifabutin, RFB2 (B).

RFB2 may be able to be used as a prodrug, since it has an acetyl group that allows a longer half-life in circulation [6]. Therefore, studies of the RFB2-cell membrane interactions are needed since antibiotic–cell membrane interactions play a crucial role for the understanding of the drugs bioavailability, the drugs entrance into the cellular compartments, and the drugs-induced toxicity [7].

To achieve the purpose of this study, liposomes were used to mimic the human and bacteria cell membranes. Liposomes are widely used as membrane models due to their similar membrane chemical and physical constitution, having a bilayer of phospholipids and an anisotropic environment [8,9]. Moreover, these systems taken into account the electrostatic interactions, which are of particular importance in molecules with charge, as in the case of RFB2. The phospholipids chosen were 1,2-dimyristoyl-sn-glycero-phosphocholine (DMPC) (Fig. 1), a zwitterionic lipid and 1,2-dimyristoyl-sn-glycero-3-phosphoglycerol (DMPG) (Fig. 1), a negatively charged lipid. Phosphatidylcholines (PCs) are almost absent in bacterial membranes but are generally the most abundant phospholipids in eukaryotic plasma membranes. For these reasons, DMPC constitutes a suitable model for the surface membrane of mammalian cells and mimics the neutral charge of the human membrane host. Because phosphatidylglycerols (PGs) are less frequent in eukaryotic plasma membranes but ubiquitous and often abundant in bacterial membranes, DMPG can serve as a simple but appropriate model for the bacterial membrane, mimicking the phospholipid electrical charge of the inner plasma membrane of the MTB [10,11].

This study assessed important biophysical parameters such as the partition coefficient (K_p), being its determination of utmost importance during the early stage of the drug design process. The K_p was determined by UV–Vis derivative spectrophotometry. The fluorescence quenching studies were performed using two probes, 1,6-diphenyl-1,3,5-hexatriene (DPH) and (2-carboxyethyl)-1,6-diphenyl-1,3,5-hexatriene (DPH-PA) with different location within the lipid bilayer [12]. A higher proximity of RFB2 to the probes will decrease the fluorescence intensity, which will be reflected in a higher Stern–Volmer constant (K_{SV}) value. The influence of RFB2 on the membrane biophysical parameters such as cooperativity, the lipid's order, and the main phase transition temperature (T_m) were also evaluated using two different techniques (steady-state anisotropy and dynamic light scattering studies).

The biophysical results obtained in this work, associated with the proven *in vitro* and *in vivo* efficacy and safety, support the potential benefit of this new molecule for the treatment of TB and prevention of the *M. avium* complex. Additionally, the results obtained indicate that the RFB2 interaction is not restricted to the human cell membrane model and occurs more widely with the bacterial cell membrane model. This is important for a higher antibiotic selectivity and consequently a favorable therapeutic index. Although further studies are needed, this novel antimycobacterial compound seems to be very promising to reach the market.

2. Materials and methods

2.1. Reagents

RFB2 was obtained from rifabutin (isolated from Mycobutin®) as previously described [6]. DMPC and DMPG were purchased from Avanti Polar Lipids (Alabaster, AL, USA). HEPES was obtained from Sigma–Aldrich Co. (St. Louis, MO, USA). The probes, DPH and DPH-PA, were obtained from Molecular Probes (Invitrogen, Paisley, UK), and all were used as supplied. All other chemicals were from Merck. The buffer solution consisted on 10 mM N-(2-hydroxyethyl) piperazine-N′-(2-ethanesulfonic acid) (HEPES) adjusted under physiological conditions, that is, the ionic strength to 100 mM with NaCl and the pH to 7.4. The solutions were prepared with double-deionized water (conductivity less than 0.1 Scm^{-1}).

2.2. Experimental

2.2.1. Preparation of liposomes

Large unilamellar vesicles (LUVs) were prepared by hydration of the lipid filmes as previously described [9,13,14]. To prepare the fluorescence labeled liposomes, the probes (DPH and DPH-PA) were dissolved in chloroform/methanol and added to the preformed liposome suspension as small aliquots. Incorporation of the probes was always in a ratio of 1:300 (probe:lipid) [13].

2.2.2. Determination of RFB2's partition coefficients by derivative spectrophotometry

The partition coefficient (K_p) of RFB2 between LUVs suspensions of DMPC or DMPG and buffer solution was determined by derivative spectrophotometry, as described in previous works [13–15]. Briefly, buffered suspensions of LUVs with increasing concentra-

Please cite this article in press as: M. Pinheiro et al., Drug–membrane interaction studies applied to N′-acetyl-rifabutin, Eur. J. Pharm. Biopharm. (2013), http://dx.doi.org/10.1016/j.ejpb.2013.02.015

tions of DMPC or DMPG (100, 200, 300, 400, 500, 600, 700, 800, 900, 1000 μM) containing a fixed concentration of RFB2 (40 μM) were prepared. The absorption spectra were recorded using a Perkin–Elmer Lambda 45 UV–Vis spectrophotometer, using quartz cells with a 1 cm^{-1} path length and a spectral range from 250 to 600 nm at 1 nm intervals. The mathematical treatment of the results was performed using a developed routine, K_p calculator [15].

2.2.3. Membrane location studies by fluorescence quenching

The RFB2's membrane location studies were performed by steady-state fluorescence and fluorescence lifetime measurements using DPH and DPH-PA fluorescence probes in liposomes buffered suspensions prepared with DMPC and DMPG. The studies were made according to an already described method [13,16–18] and consisted on the incubation of increasing amounts of RFB2 (0–27 μM) with DMPC and DMPG liposomes at 37.0 °C for 1 h, while maintaining the total lipid concentration constant (500 μM). Fluorimetric data were collected using a Perkin–Elmer LS 50 B steady-state fluorescence spectrometer equipped with a constant-temperature cell holder. All data were recorded with excitation and emission slits between 2.5 and 3.0 nm. The excitation wavelength was set to 357 nm for DPH and 360 nm for DPH-PA. The emission wavelengths were set to 427 nm for DPH and 430 nm for DPH-PA [9,19].

2.2.4. Membrane fluidity studies

The effect of RFB2 (40 μM) on the biophysical parameters (T_m and cooperativity) of DMPC and DMPG liposomes (500 μM) was determined by DLS, as elsewhere described [20]. The count rate was obtained using a BI-MAS DLS instrument (Brookhaven Instruments, USA), containing a controlled temperature cell holder. The samples were heated from 10.0 to 40.0 °C with intervals of 1.0 °C with an equilibration period of 2 min. At each temperature, 6 runs of 2 min were performed.

The influence of RFB2 (40 μM) on the biophysical parameters (T_m, cooperativity and lipid's order) was also evaluated by steady-state anisotropy measurements, using LUVs of DMPC and DMPG (500 μM), labeled with the DPH probe as previously described. The anisotropy was recorded at several temperatures between 10.0 and 40.0 °C, with an accuracy of 0.1 °C. The fluorescence anisotropy was measured with a Jasco FP-6500 spectrofluorometer (Jasco, Great Dunmow, UK) equipped with two polarizers in the paths for excitation and emission using the L-format method.

3. Results and discussion

3.1. Partition coefficients of RFB2 in membranes with lipids of varying surface charges

The drug's pharmacokinetics is affected by the lipophilicity and generally the higher the lipophilicity the greater is the drug's distribution through the body [21]. In addition, the lipophilicity of an antimycobacterial agent should increase their efficacy since the entry into the hydrophobic mycobacterial membranes is positively affected by an increment in the lipophilicity [22]. In fact, the lipophilicity of chemical compounds is very often described as partition coefficient (log$P$) in the octanol/water system. It was established that a desirable antimycobacterial candidate should have a preferred value for log$P$ between 1.3 and 4.1 [23]. For ionizable compounds as RFB2, the lipophilicity is normally represented by the distribution coefficient (log$D$). In this work, the partition coefficient (K_p) of this novel compound, expressed in term of log$D$, has been determined in a liposomes/buffer system using derivative UV–Vis spectroscopy, since there might be a huge discrepancy between the partition coefficient estimated in a octanol/buffer system and in the biological membranes [9,24]. Derivative spectrophotometry eliminates the intense background signals arising from light scattering caused by the lipid vesicles and improves the resolution of overlapping bands, features that have been reported by several authors [13,15,25]. Following equilibration, the absorption spectra were recorded. Derivative intensities can be related to the partition coefficient by the following equation (Eq. (1)) [13]:

$$D_T = D_w + \frac{(D_m - D_w)K_p[L]V_m}{1 + K_p[L]V_m} \quad (1)$$

In this equation, D is the second or third derivative intensity ($D = (d^n\text{Abs})/(d\lambda^n)$) obtained from the absorbance values of the total amount of RFB2 (D_T); RFB2 distributed on the lipid membrane phase (D_m); RFB2 distributed in the aqueous phase (D_w); lipid concentration ($[L]$); and the lipid molar volume (V_m). For DMPC, the mean molecular weight was considered to be 677.93 g/mol and V_ϕ to be 0.66 M. For DMPG, the mean molecular weight was considered to be 688.85 g/mol and V_ϕ to be 0.67 M [14]. The Eq. (1) was fitted to the experimental second and third derivate spectrophotometric data (D_T versus $[L]$) using a nonlinear least-squares regression method at wavelengths where the scattering is eliminated [13,14]. Fig. 2 shows the second derivate spectra of RFB2 in DMPC and DMPG liposomes. The isosbestic points and the hypsochromic shift observed with increasing lipid concentrations provide a clear indication that the partition happens and RFB2 exists in two forms: compound in polar bulk water and in DMPC or DMPG bilayers [13]. Fig. 3 shows, as an example, the best fit of the Eq. (1) to the second derivative spectrophotometric data collected at λ = 324 nm for RFB2 with different concentrations of DMPG liposomes.

The K_p obtained for RFB2 in DMPC was 1413 ± 132 and in DMPG was 2486 ± 221 (Table 1). These results show that the K_p of RFB2 is dependent of the phospholipids head group composition. RFB2 molecule contains groups that can undergo protonation (piperidine, pK_a = 7.59 and imidazole nitrogen atoms, pK_a = 0.74) and deprotonation (napthol oxygen, pK_a = 8.15). As in the case of rifabutin, at the physiological pH, zwitterionic species predominate but a significant contribution of cations coexist (predicted using MarvinView® 5.4.1.1 software from ChemAxon). The more pronounced electrostatic and hydrogen bonds between RFB2 and the polar head groups of DMPG might contribute for the higher K_p. Additionally in DMPG, the absence of the ammonium and the presence of two additional OH groups might explain, respectively, less electrostatic repulsions and the occurrence of hydrogen bonds. In a previous work, the predicted log$P$ for RFB2 was 4.35 [6]. This value was slightly higher comparing with the predicted log$P$ for rifabutin (4.25), as the substitution of a hydrogen atom at the nitrogen of an imidazole ring by an acetyl group causes an increase in the molecule hydrophobicity [6]. In this work, the experimental log$D$ obtained in the DMPC:aqueous for RFB2 was 3.33 (being in account the V_ϕ of DMPC). The computational predicted log$P$ is higher since it accounts only for the neutral forms of the compound. As the neutral species are more hydrophobic than the charged ones, the partition considering only the zwitterion contribution of RFB2 is higher. Moreover, the lack of correlation between log$D$ and the predicted log$P$, as well as the different log$D$ for the two membrane models, confirms that not only hydrophobic intermolecular forces drive the drug's partition. This is especially true in the biomembranes, where due to the electrostatic interactions between electrically charged species and phospholipids with different head groups, the partition in phospholipids also encodes ionic bonds. Thus, the higher log$D$ obtained for RFB2 in DMPG, 3.57 (being in account the V_ϕ of DMPG) might be explained by stronger interactions with the negatively charged group of DMPG liposomes mediated by electrostatic interactions and possibly by hydrogen bonds.

Please cite this article in press as: M. Pinheiro et al., Drug–membrane interaction studies applied to N′-acetyl-rifabutin, Eur. J. Pharm. Biopharm. (2013), http://dx.doi.org/10.1016/j.ejpb.2013.02.015

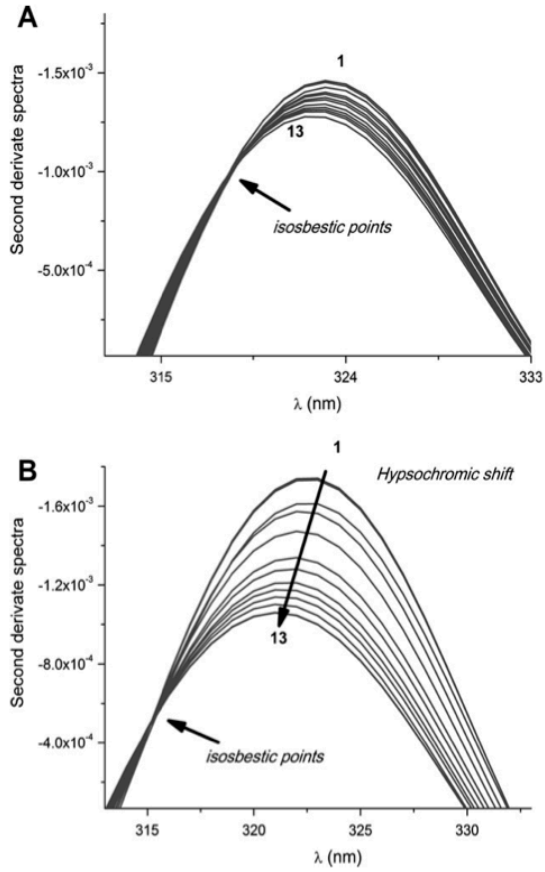

Fig. 2. Second derivate spectra of RFB2 (40 μM) incubated in LUVs of DMPC (A) and DMPG (B) with different concentrations (M): (1) 0; (2) 1×10^{-4}; (3) 2×10^{-4}; (4) 3×10^{-4}; (5) 4×10^{-4}; (6) 5×10^{-4}; (7) 6×10^{-4}; (8) 7×10^{-4}; (9) 8×10^{-4}; (10) 9×10^{-4}; (11) 1×10^{-3}.

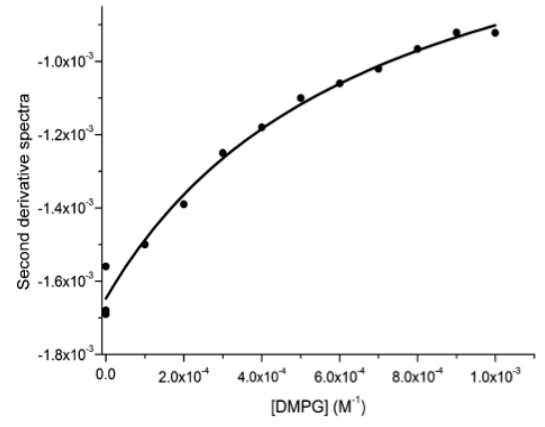

Fig. 3. Second derivate spectra for RFB2 at different concentrations of LUVs of DMPG. The curve represents the best fit by Eq. (1) using a nonlinear least-squares regression method at wavelength 324 nm where the scattering is eliminated.

3.2. Location studies of RFB2 in membranes with lipids of varying surface charges

The membrane location of RFB2 within the lipid bilayer was assessed by fluorescence quenching measurements using two fluorescent probes (DPH and DPH-PA). When the probes are included in the lipid bilayer, the precise fluorophore positions along the membrane depth plane of these probes are known [26]. While the DPH-PA probe is anchored to the surface of the membrane near the phospholipids polar heads groups, DPH has a deeper location and is aligned parallel to the acyl chains [9,27].

Table 1
Partition coefficients (K_p) (M) for RFB2 in DMPC and DMPG liposomes (500 μM, T = 37.0 °C pH 7.4) obtained in the fluid phase. Results present the mean and standard deviation of at least three independent assays.

	DMPC:aqueous	DMPG:aqueous
K_p (M^{-1})	1413 ± 132	2486 ± 221

In this work, not only the intensity of the fluorescence emission was measured but also the fluorescence lifetimes, which is the most definitive method to distinguish static from dynamic quenching. To definitely prove the type of fluorescence quenching, studies at two different temperatures were performed [28]. The fluorescence spectrum obtained clearly indicates that the presence of RFB2 induces a decrease in the fluorescence intensity of DPH-PA at around 460 nm, at an excitation wavelength of 360 nm (Fig. 4A). Moreover, the fluorescence intensity decreases linearly with the increase of the RFB2 concentration, indicating an absence of changes in the fluorophore environment [29]. The same is also verified for the DPH (data not shown). In order to confirm the quenching mechanism, the fluorescence quenching data were analyzed by the Stern–Volmer equation (Eq. (2)) [30]:

$$\frac{I_0}{I} = 1 + K_{SV}[Q]_m = \frac{\tau_0}{\tau} \quad (2)$$

In this equation, I_0 and I are the fluorescence intensities in the absence and presence of the quencher, respectively; K_{SV} is the quenching constant, called the Stern–Volmer constant; τ_0 and τ are the lifetime of the fluorophore in the absence and presence of the quencher; $[Q]_m$ is the concentration of the quencher that is able to partition the membrane, which is calculated from the total drug concentration ($[Q]_T$) and from the drug's partition coefficient (K_p), as described by the following equation [30]:

$$[Q]_m = \frac{K_p[Q]_T}{K_p\alpha_m + (1 - \alpha_m)} \quad (3)$$

where α_m is the volume fraction of membrane phase ($\alpha_m = V_m/V_T$; V_m and V_T represents, respectively, the volumes of the membrane and water phases). The Stern–Volmer (Eq. (2)) illustrates an important characteristic of collisional quenching, which is an equivalent decrease in the fluorescence intensity and lifetime. The dynamic component of the observed quenching was determined by lifetime measurements using the equation $\tau_0/\tau = 1 + K_D[Q]$. Therefore, after knowing the dynamic component, the static contribution was determined by linearization of the following equation (Eq. (4)) [30]:

$$\frac{I_0}{I} \times \frac{1}{1 + K_D[Q]_m} = 1 + K_S[Q]_m \quad (4)$$

Fig. 4B is represented the Stern–Volmer plots of the probe DPH-PA in LUVs of DMPC by increasing concentrations of RFB2. This modified form of the Stern–Volmer equation is second order in $[Q]_m$, which accounts for the upward curvature observed when both static and dynamic quenching occur for the same fluorophore.

The observed positive deviation of the Stern–Volmer plots may also be interpreted in terms of a "sphere of action" static quenching model. According to this model, if the quencher is located inside a spherical volume (V) adjacent to the fluorophore, the probability for the quencher to be inside this volume at the time of excitation depends on the volume itself and on the quencher

Please cite this article in press as: M. Pinheiro et al., Drug–membrane interaction studies applied to N′-acetyl-rifabutin, Eur. J. Pharm. Biopharm. (2013), http://dx.doi.org/10.1016/j.ejpb.2013.02.015

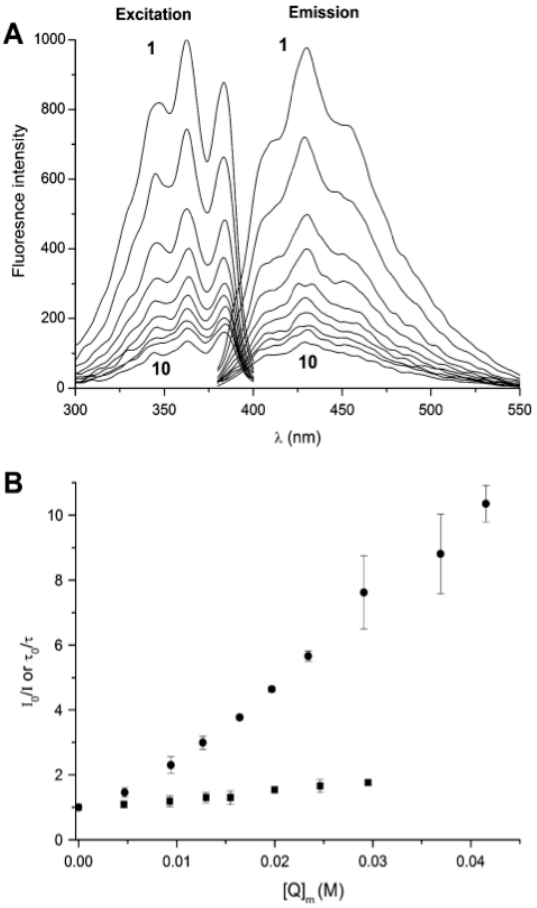

Fig. 4. Excitation and emission spectra of fluorescence quenching (A) and Stern–Volmer plots (B) of the probe DPH-PA in LUVs of DMPC (500 μM, T = 37.0 °C pH 7.4) by increasing concentrations (M) of the quencher RFB2. The circular symbols (•) represent Stern–Volmer plot obtained by steady-state fluorescence measurements (I_0/I) and square symbols (■) represent Stern–Volmer plot obtained by lifetime fluorescence measurements (τ_0/τ).

concentration ($[Q]_m$), as it is described by the modified Stern–Volmer equation (Eq. (5)) [30]:

$$\ln\left(\frac{I_0\tau}{I\tau_0}\right) = V[Q]_m \tag{5}$$

In the Fig. 5, it is possible to notice that the "sphere of action" model adjusts to the experimental data.

The bimolecular quenching constant (K_q) that reflects the efficiency of quenching or the accessibility of the probes to RFB2 was calculated by the Eq. (6) [30,31]:

$$K_q = \frac{K_{SV}}{\tau_0} \tag{6}$$

The values of the apparent Stern–Volmer constant obtained for RFB2 in DMPC and DMPG are included in Table 2. The results suggest that for both models, the quenching process is the result of dynamic and static interactions with a dominant static component; hence, the values decrease with the increase in the temperature (from 37.0 °C to 42.0 °C), which are due to a non-fluorescence complex dissociation. Indeed, in the static quenching, the increment in the temperature is likely to result in a decreased complex stability and consequent lower values of the static quenching constants [30].

At the physiological temperature (37 °C), the similar K_{SV} values obtained for DPH and DPH-PA in the DMPC liposomes suggest that

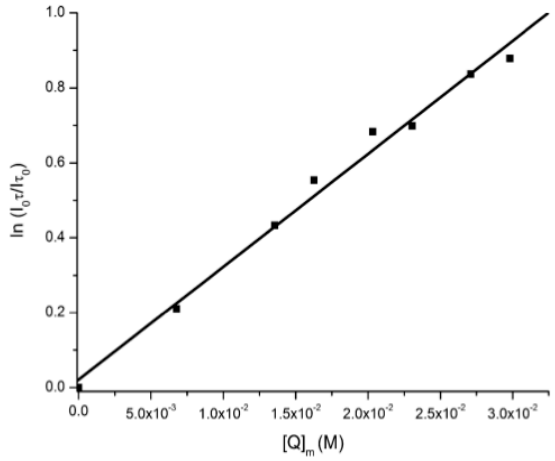

Fig. 5. Fluorescence quenching of DPH-PA probe in LUVs of DMPG (500 μM, T = 37.0 °C pH 7.4) by increasing concentrations of RFB2 and respective application of the mathematical model "sphere of action". Line represents fits to Eq. (6).

Table 2
Values of Stern–Volmer constant at T = 37 °C (K_{SV}) and 42 °C (K^*_{SV}), and bimolecular quenching constant (K_q) obtained for RFB2 in DMPC and DMPG liposomes (500 μM, T = 37 °C pH 7.4) labeled with DPH or DPH-PA probes.

	K_{SV} (M^{-1})		K^*_{SV} (M^{-1})		$K_q \times 10^{10}$ (M^{-1} s^{-1})	
	DPH	DPH-PA	DPH	DPH-PA	DPH	DPH-PA
DMPC	125 ± 3	124 ± 4	86 ± 5	58 ± 3	1.5 ± 0.2	2.1 ± 0.1
DMPG	111 ± 7	133 ± 6	132 ± 8	92 ± 8	1.3 ± 0.2	1.9 ± 0.1

in the zwitterionic membrane model, RFB2 does not have a preferential location within the lipid bilayer. Contrastingly, in DMPG liposomes, the quenching efficiency of DPH-PA is higher than that of DPH. Indeed, in these liposomes, RFB2 has a more superficial location and must be preferentially located near the polar region of the bilayer. Nevertheless, the high K_{SV} values obtained for the DPH indicate that RFB2 is able to penetrate both membrane models. For the above-mentioned reasons, the representative contribution of positively charged RFB2 molecules might be responsible for more pronounced interactions with the negatively charged.

3.3. Studies of the effect of RFB2 on the fluidity of membranes with lipids of varying surface charges

Dynamic light scattering (DLS) technique using the count rate is considered a reliable, simple, and reproducible technique to determinate the T_m of the. Data as the normalized mean count rate versus temperature were collected and fitted using the Eq. (7) [20]:

$$r_s = r_{s1} + p_1 T + \frac{r_{s2} - r_{s1} + p_2 T - p_1 T}{1 + 10^{B(1/T - 1/T_m)}} \tag{7}$$

where r_s is the average count rate, T is the temperature (°C), p_1 and p_2 correspond to the slopes of the straight lines at the beginning and at the end of the plot, and r_{s1} and r_{s2} are the respective count rate intercepting values at the y axis. From the experimental data displayed, it was possible to calculate the cooperativity (B) and the midpoint of the phase transition, which corresponds to the temperature of the gel-to-fluid phase transition of DMPC and DMPG (T_m). The T_m was calculated from the slope and the inflection point of the data fitted to sigmoid curves of count rate (r_s) versus temperature (T). The analysis of the Table 3 reveals that although RFB2 did not change the T_m of both lipids, a perturbation of the lipid alkyl chain cooperativity (i.e., the number of chains that change simulta-

Please cite this article in press as: M. Pinheiro et al., Drug–membrane interaction studies applied to N′-acetyl-rifabutin, Eur. J. Pharm. Biopharm. (2013), http://dx.doi.org/10.1016/j.ejpb.2013.02.015

Table 3
Values of main phase transition temperature (T_m) and cooperativity (B) obtained for DMPC and DMPG liposomes (500 μM, T = 37.0 °C pH 7.4) in the absence and in the presence of RFB2 (40 μM).

	T_m (°C)	Cooperativity (B)
DMPC	23.9 ± 0.3	228 ± 33
DMPC + RFB2	23.7 ± 0.1	170 ± 30
DMPG	22.5 ± 0.2	342 ± 121
DMPG + RFB2	21.4 ± 0.2	360 ± 204

Table 4
Values of main phase transition temperature (T_m), cooperativity (B) and order parameter (S) obtained for DMPC and DMPG liposomes (500 μM, T = 37.0 °C pH 7.4) labeled with DPH in the absence and in the presence of RFB2 (40 μM).

	T_m (°C)	Cooperativity (B)	Order (S)
DMPC	24.5 ± 0.1	234 ± 34	0.46 ± 0.02
DMPC + RFB2	23.6 ± 0.1	219 ± 7	0.48 ± 0.02
DMPG	23.9 ± 0.1	341 ± 11	0.36 ± 0.02
DMPG + RFB2	23.5 ± 0.1	183 ± 15	0.67 ± 0.03

neously) during the T_m happens [32]. Thus, RFB2 decrease the cooperativity of the phase transition in both lipids and especially in the DMPG, which confirms a differential perturbation in the membrane models induced by RFB2 molecules [33].

In order to complement the information provided by DLS, steady-state fluorescence anisotropy was used to evaluate the effect of RFB2 on the T_m, cooperativity and on the lipid's order. The presence of DPH at the hydrocarbon tails allowed the observation of the lipid chain fluidity effects induced by RFB2 molecules [34]. From the experimental data displayed, it was possible to obtain the cooperativity (B) and the T_m, calculated from the slope and the inflection point of the data fitted to sigmoid curves of steady-state anisotropy (r_s) versus temperature (T) data (Eq. (7)). The r_{s1} and r_{s2} are the respective steady-state anisotropy intercepting values at the y axis. The order parameter can be also calculated from $S = \sqrt{r_\infty / r_0}$, where r_0 (fundamental anisotropy) is the fluorescence anisotropy in the absence of any rotational motion of the probe and r_∞ (limiting anisotropy) reflects the restriction of the probe motion [13]. As the bilayer phase transition occurs from gel-to-fluid, the fluorescence polarization drops due to the increase in the rotational freedom of the probe.

The results presented in Table 4 show that the T_m for DMPC and DMPG, as reported by the anisotropy of DPH, were found to be in good agreement with the values reported in the literature [35,36]. Fig. 6 listed the temperature dependence of DPH fluorescence anisotropy for DMPC and DMPG liposomes in the absence and in the presence of RFB2. As it can be observed, the incorporation of RFB2 does not greatly modify the DMPC and DMPG lamellar gel state. Nevertheless, at temperatures above T_m, RFB2 is responsible for an increase in the anisotropy values, especially in DMPG. This is consistent with the higher lipid packing of the membrane models due to the RFB2 intercalation. Furthermore, the obtained results of the biophysical parameters are consistent, independently of the chosen technique. The T_m, the degree of molecular packing (order) at the fluid phase and the cooperativity of the lipids suffer significant changes in the presence of RFB2. Thus, RFB2 is responsible in both lipids, for a decrease in the cooperativity and for an increment in the order. This is consistent with the partition and fluorescence quenching results, supporting RFB2 penetration in both membrane models. Moreover, RFB2 seems to be responsible for a more pronounced effect in the order and in the cooperativity of the DMPG model. Nevertheless, a more superficial location of RFB2 in the DMPG vesicles is expected, since this antimycobacterial compound must be located nearer the highly ordered region and closer to the head groups (C1–C9) [33], which is in close agreement with the quenching results.

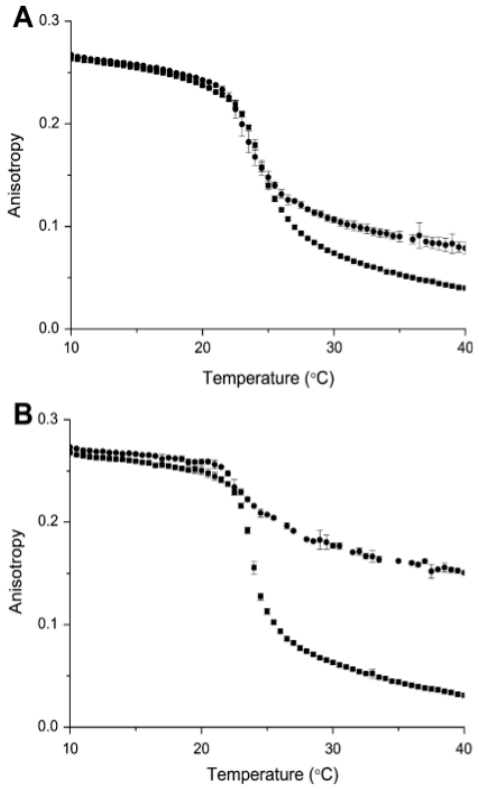

Fig. 6. Steady-state anisotropy of DPH in absence (■) and in the presence (•) of RFB2 (40 μM) in DMPC (A) and in DMPG (B) liposomes at pH = 7.4 as a function of temperature. Each point corresponds to the mean value of three experiments. Continuous lines are the best-fit curves using Eq. (7).

4. Conclusions

The global resurgence of TB and the rapid emergence of MDR-TB underscore the importance of the development of new anti-TB drugs [1,2]. In this regard, RFB2 is a new antimycobacterial compound synthesized from a series of rifabutin analogs that showed to be one of the best preclinical candidate drugs [6]. Moreover, due to the acetyl group, it shall present a greater bioavailability. The higher bioavailability allows the maintenance of constant concentrations of antibiotics and the use of a less frequent dosing, which would certainly be helpful in increasing the adherence to therapy, one of the major drawbacks in the TB treatment failure [5,37]. For the above-mentioned reasons, RFB2 has not only the potential to shorten the treatment for drug-susceptible TB but also to improve the treatment for multidrug-resistant TB (MDR-TB) and to allow the simultaneous administration of anti-TB and antiretroviral drugs in people co-infected with TB/HIV [2].

The study of the interactions of this novel bioactive compound with the biomembranes constitutes a preliminary step to the biological (and toxic) study, as it can affect the rate of penetration of RFB2's molecules in human and bacterial membranes in order to reach its pharmacological target [38]. In this context, to understand the bioavailability and toxicity of RFB2, some important biophysical techniques were performed, such as the K_p, fluorescence quenching, lifetime measurements, steady-state anisotropy and DLS. The overall results reveal that the partition of RFB2 is higher in the negatively charged model, probably due to the electrostatic

Please cite this article in press as: M. Pinheiro et al., Drug–membrane interaction studies applied to N′-acetyl-rifabutin, Eur. J. Pharm. Biopharm. (2013), http://dx.doi.org/10.1016/j.ejpb.2013.02.015

interactions and/or hydrogen bonds. The RFB2 membrane location studies support that RFB2 is able to penetrate both membrane models. Additionally, in the zwitterionic membrane model, RFB2 did not significantly alter membrane biophysical parameters as the T_m, cooperativity and order, demonstrating significant changes in the negatively charged model. For these reasons, it is expected that RFB2 shows more affinity to the bacterial membrane, when compared with the host membrane, which is suitable for a favorable efficacy/toxicity relationship. The biophysical assays of our study support the favorable physicochemical properties of this antimycobacterial compound, reinforcing the potential to reach the market and to constitute a powerful tool for the clinical practice.

Acknowledgments

Marina Pinheiro and João M. Caio thank FCT (Lisbon) for the doctoral fellowships (SFRH/BD/63318/2009 and SFRH/BD/66789/2009, respectively). Authors are grateful to the FCT for financial support under Projects PEst-OE/QUI/UI0612/2011 and PTDC/QUI-QUI/101022/2008 with co-participation European Community funds from the FEDER, QREN and COMPET.

References

[1] M. Pinheiro, M. Lucio, J.L. Lima, S. Reis, Liposomes as drug delivery systems for the treatment of TB, Nanomedicine (Lond.) 6 (2011) 1413–1428.
[2] World Health Organization: Global Tuberculosis Control 2012 Report. <http://apps.who.int/iris/bitstream/10665/75938/1/9789241564502_eng.pdf> (accessed 01.01.13).
[3] S. Ahmad, New approaches in the diagnosis and treatment of latent tuberculosis infection, Respir. Res. 11 (2010) 169.
[4] A. Pawlowski, M. Jansson, M. Skold, M.E. Rottenberg, G. Kallenius, Tuberculosis and HIV co-infection, PLoS Pathog. 8 (2012) e1002464.
[5] N.R. Gandhi, P. Nunn, K. Dheda, H.S. Schaaf, M. Zignol, D. van Soolingen, P. Jensen, J. Bayona, Multidrug-resistant and extensively drug-resistant tuberculosis: a threat to global control of tuberculosis, Lancet 375 (2010) 1830–1843.
[6] R. Figueiredo, C. Moiteiro, M.A. Medeiros, P.A. da Silva, D. Ramos, F. Spies, M.O. Ribeiro, M.C. Lourenco, I.N. Junior, M.M. Gaspar, M.E. Cruz, M.J. Curto, S.G. Franzblau, H. Orozco, D. Aguilar, R. Hernandez-Pando, M.C. Costa, Synthesis and evaluation of rifabutin analogs against *Mycobacterium avium* and H(37)Rv, MDR and NRP *Mycobacterium tuberculosis*, Bioorg. Med. Chem. 17 (2009) 503–511.
[7] M. Pinheiro, J.J. Giner-Casares, M. Lucio, J.M. Caio, C. Moiteiro, J.L. Lima, S. Reis, L. Camacho, Interplay of mycolic acids, antimycobacterial compounds and pulmonary surfactant membrane: a biophysical approach to disease, Biochim. Biophys. Acta 2013 (1828) 896–905.
[8] M. Lucio, H. Ferreira, J.L. Lima, S. Reis, Interactions between oxicams and membrane bilayers: an explanation for their different COX selectivity, Med. Chem. 2 (2006) 447–456.
[9] M. Lucio, H. Ferreira, J.L. Lima, S. Reis, Use of liposomes to evaluate the role of membrane interactions on antioxidant activity, Anal. Chim. Acta 597 (2007) 163–170.
[10] C. Paradis-Bleau, I. Cloutier, L. Lemieux, F. Sanschagrin, J. Laroche, M. Auger, A. Garnier, R.C. Levesque, Peptidoglycan lytic activity of the *Pseudomonas aeruginosa* phage phiKZ gp144 lytic transglycosylase, FEMS Microbiol. Lett. 266 (2007) 201–209.
[11] I.D. Alves, N. Goasdoue, I. Correia, S. Aubry, C. Galanth, S. Sagan, S. Lavielle, G. Chassaing, Membrane interaction and perturbation mechanisms induced by two cationic cell penetrating peptides with distinct charge distribution, Biochim. Biophys. Acta 1780 (2008) 948–959.
[12] S. Jaikishan, A. Bjorkbom, J.P. Slotte, Phosphatidyl alcohols: effect of head group size on domain forming properties and interactions with sterols, Biochim. Biophys. Acta 1798 (2010) 1615–1622.
[13] J. Brittes, M. Lucio, C. Nunes, J.L. Lima, S. Reis, Effects of resveratrol on membrane biophysical properties: relevance for its pharmacological effects, Chem. Phys. Lipids 163 (2010) 747–754.
[14] C. Pereira-Leite, C. Carneiro, J.X. Soares, C. Afonso, C. Nunes, M. Lucio, S. Reis, Biophysical characterization of the drugs–membrane interaction. The case of propranolol and acebutolol, Eur. J. Pharm. Biopharm. (2013).
[15] L.M. Magalhaes, C. Nunes, M. Lucio, M.A. Segundo, S. Reis, J.L. Lima, High-throughput microplate assay for the determination of drug partition coefficients, Nat. Protoc. 5 (2010) 1823–1830.
[16] C. Nunes, G. Brezesinski, D. Lopes, J.L. Lima, S. Reis, M. Lucio, Lipid–drug interaction: biophysical effects of tolmetin on membrane mimetic systems of different dimensionality, J. Phys. Chem. B 115 (2011) 12615–12623.
[17] C. Sousa, C. Nunes, M. Lucio, H. Ferreira, J.L. Lima, J. Tavares, A. Cordeiro-da-Silva, S. Reis, Effect of nonsteroidal anti-inflammatory drugs on the cellular membrane fluidity, J. Pharm. Sci. 97 (2008) 3195–3206.
[18] A.M. Cardoso, S. Trabulo, A.L. Cardoso, A. Lorents, C.M. Morais, P. Gomes, C. Nunes, M. Lucio, S. Reis, K. Padari, M. Pooga, M.C. Pedroso de Lima, A.S. Jurado, S4(13)-PV cell-penetrating peptide induces physical and morphological changes in membrane-mimetic lipid systems and cell membranes: implications for cell internalization, Biochim. Biophys. Acta 2012 (1818) 877–888.
[19] E.W. Mosmuller, E.H. Pap, A.J. Visser, J.F. Engbersen, Steady-state fluorescence studies on lipase–vesicle interactions, Biochim. Biophys. Acta 1189 (1994) 45–51.
[20] N. Michel, A.S. Fabiano, A. Polidori, R. Jack, B. Pucci, Determination of phase transition temperatures of lipids by light scattering, Chem. Phys. Lipids 139 (2006) 11–19.
[21] J.H. Lin, A.Y. Lu, Role of pharmacokinetics and metabolism in drug discovery and development, Pharmacol. Rev. 49 (1997) 403–449.
[22] B.R. Bloom, Tuberculosis: Pathogenesis, Protection, and Control, ASM Press, 1994.
[23] C.E. Barry Iii, R.A. Slayden, A.E. Sampson, R.E. Lee, Use of genomics and combinatorial chemistry in the development of new antimycobacterial drugs, Biochem. Pharmacol. 59 (2000) 221–231.
[24] A. Pola, K. Michalak, A. Burliga, N. Motohashi, M. Kawase, Determination of lipid bilayer/water partition coefficient of new phenothiazines using the second derivative of absorption spectra method, Eur. J. Pharm. Sci. 21 (2004) 421–427.
[25] H. Ferreira, M. Lucio, J.L. Lima, C. Matos, S. Reis, Interaction of clonixin with EPC liposomes used as membrane models, J. Pharm. Sci. 94 (2005) 1277–1287.
[26] A.P. Demchenko, Y. Mely, G. Duportail, A.S. Klymchenko, Monitoring biophysical properties of lipid membranes by environment-sensitive fluorescent probes, Biophys. J. 96 (2009) 3461–3470.
[27] J. Repakova, J.M. Holopainen, M.R. Morrow, M.C. McDonald, P. Capkova, I. Vattulainen, Influence of DPH on the structure and dynamics of a DPPC bilayer, Biophys. J. 88 (2005) 3398–3410.
[28] M.A. Castanho, M.J. Prieto, Fluorescence quenching data interpretation in biological systems. The use of microscopic models for data analysis and interpretation of complex systems, Biochim. Biophys. Acta 1373 (1998) 1–16.
[29] N. Alminana, M.A. Alsina, F. Reig, New GHK hydrophobic derivatives: interaction with phospholipid bilayers, Colloids Surf. B: Biointerf. 57 (2007) 243–249.
[30] R.M. Eftink, Fluorescence Quenching: Theory and Applications. In the Principles of Fluorescence Spectroscopy, Springer ed., New York, 2006.
[31] M. Meissner, D. Varwig, C. Beier, V. Jacobi, R. Kaufmann, J. Gille, Dystrophic calcinosis cutis after subcutaneous administration of para-aminosalicylic acid for treatment of pulmonary tuberculosis, J. Dtsch. Dermatol. Ges. 4 (2006) 489–491.
[32] M. Lúcio, C. Nunes, D. Gaspar, K. Golebska, M. Wisniewski, J.L.F.C. Lima, G. Brezesinski, S. Reis, Effect of anti-inflammatory drugs in phosphatidylcholine membranes: a fluorescence and calorimetric study, Chem. Phys. Lett. 471 (2009) 300–309.
[33] C. Nunes, G. Brezesinski, C. Pereira-Leite, J.L. Lima, S. Reis, M. Lucio, NSAIDs interactions with membranes: a biophysical approach, Langmuir 27 (2011) 10847–10858.
[34] J.L. Vázquez, M.T. Montero, S. Merino, Ò. Domènech, M. Berlanga, M. Viñas, J. Hernández-Borrell, Location and nature of the surface membrane binding site of ciprofloxacin: a fluorescence study, Langmuir 17 (2001) 1009–1014.
[35] K. John, J. Kubelt, P. Muller, D. Wustner, A. Herrmann, Rapid transbilayer movement of the fluorescent sterol dehydroergosterol in lipid membranes, Biophys. J. 83 (2002) 1525–1534.
[36] K.A. Riske, R.M. Fernandez, O.R. Nascimento, B.L. Bales, M.T. Lamy-Freund, DMPG gel–fluid thermal transition monitored by a phospholipid spin labeled at the acyl chain end, Chem. Phys. Lipids 124 (2003) 69–80.
[37] A. Koul, E. Arnoult, N. Lounis, J. Guillemont, K. Andries, The challenge of new drug discovery for tuberculosis, Nature 469 (2011) 483–490.
[38] R. Pignatello, T. Musumeci, L. Basile, C. Carbone, G. Puglisi, Biomembrane models and drug–biomembrane interaction studies: involvement in drug design and development, J. Pharm. Bioallied Sci. 3 (2011) 4–14.

Please cite this article in press as: M. Pinheiro et al., Drug–membrane interaction studies applied to N′-acetyl-rifabutin, Eur. J. Pharm. Biopharm. (2013), http://dx.doi.org/10.1016/j.ejpb.2013.02.015

6. Effects of a novel antimycobacterial compound on the biophysical properties of a pulmonary surfactant model membrane.

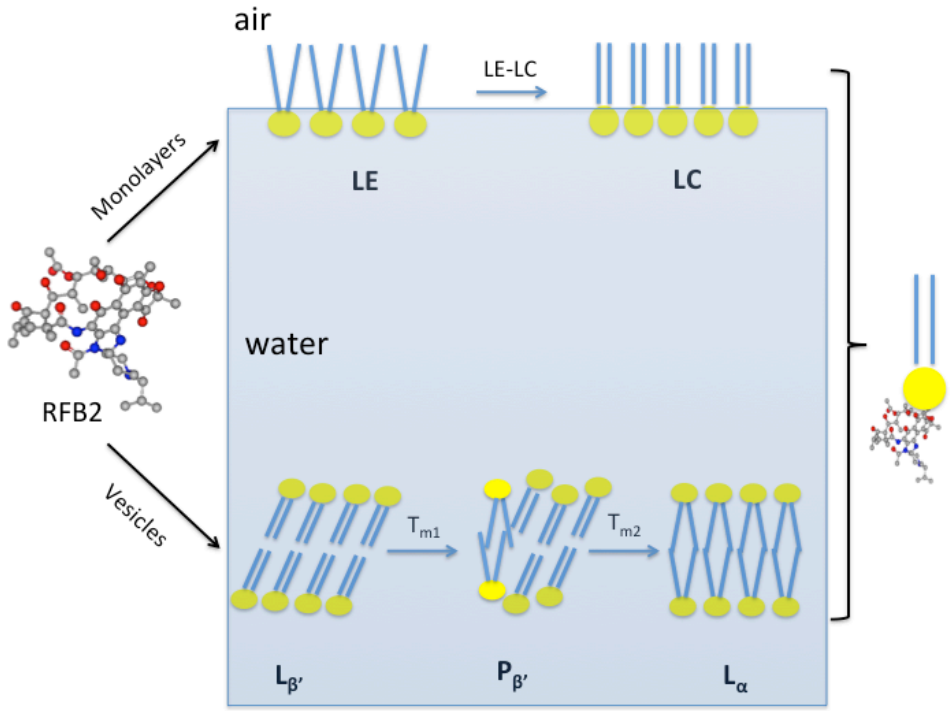

International Journal of Pharmaceutics 450 (2013) 268–277

Contents lists available at SciVerse ScienceDirect

International Journal of Pharmaceutics

journal homepage: www.elsevier.com/locate/ijpharm

Effects of a novel antimycobacterial compound on the biophysical properties of a pulmonary surfactant model membrane

Marina Pinheiro[a], Mariana Arêde[a], Juan J. Giner-Casares[b,c], Cláudia Nunes[a], João M. Caio[d], Cristina Moiteiro[d], Marlene Lúcio[a], Luis Camacho[b], Salette Reis[a,*]

[a] REQUIMTE, Departamento de Ciências Químicas, Faculdade de Farmácia, Universidade do Porto, Portugal
[b] Departamento de Química Física y Termodinámica, Universidad de Córdoba, Spain
[c] Department of Interfaces, Max Planck Institute of Colloids and Interfaces, Science Park Golm, 14476 Potsdam, Germany
[d] Centro de Química e Bioquímica, Departamento de Química e Bioquímica, Faculdade de Ciências, Universidade de Lisboa, Portugal

ARTICLE INFO

Article history:
Received 23 February 2013
Received in revised form 21 March 2013
Accepted 23 March 2013
Available online 18 April 2013

Keywords:
Langmuir monolayers
Lipid–drug interaction
Liposomes
Pulmonary surfactant
Rifabutin
Tuberculosis

ABSTRACT

In this work, the interactions of a novel rifabutin's analogue (*N*′-acetyl-rifabutin, RFB2) with two-dimensional (Langmuir monolayers) and three-dimensional (large unilamellar and multilamellar vesicles) membrane models of the pulmonary surfactant (PS) were evaluated. The main purpose of this study is to obtain detailed information at the molecular level between the interactions of RFB2 with the phospholipids of the PS, under physiological conditions. Therefore, the effects of RFB2 in the monolayer phase behaviour at the air–water interface and in the lipid bilayer of membrane models composed of 1,2-dipalmitoyl-*sn*-glycero-3-phosphocholine (DPPC) have been systematically compared. In this context, several biophysical techniques were carried out to establish the interactions of RFB2 with the two-dimensional membrane models of the PS: Langmuir isotherms, Brewster angle microscopy (BAM), and polarization-modulation infrared reflection–absorption spectroscopy (PM-IRRAS); and with three-dimensional membrane models of the PS: derivate spectrophotometry partition coefficient (K_p), dynamic light scattering (DLS), small and wide angle X-ray scattering (SAXS and WAXS).

The results gathered by the different biophysical techniques and the PS membrane model used provide detailed information about the strong interactions of RFB2 with the polar head groups of the PS phospholipids and permit to establish the impact of the RFB2-PS membrane interactions, justifying an often unexplored biophysical approach to the drug's pharmacokinetics and toxicological effect.

1. Introduction

Tuberculosis (TB) is still one of the major infectious diseases affecting the humankind (Koul et al., 2011; Pinheiro et al., 2011). TB infection is commonly initiated by the entry of the *Mycobacterium tuberculosis* (MTb) into to the respiratory system through aerosol droplets, being the pulmonary TB as a consequence, the most commonly manifestation of TB (Pinheiro et al., 2011). Clinically, pulmonary TB is characterized by widespread lung damage in the form of areas of pulmonary atelectasis, fibrosis and scarring, resulting in decreased pulmonary compliance and impaired gas exchange (Rugonyi et al., 2008b; Stevens and Sinkin, 2007). Despite the significant progress that has been made to reduce global incidence of drug-susceptible TB, the emergence of multidrug-resistant (MDR) TB during the past decade threatens to undetermined these advances. Hence, the discovery of new molecules is a strategic priority, requiring the current situation a re-engineering of some old drug families to achieve effective control (Gandhi et al., 2010; Koul et al., 2011). In this context, *N*′-acetyl-rifabutin (RFB2) (Fig. 1) is a novel synthetized antimycobacterial compound and a derivate of rifabutin that showed to be the best candidate from a series of analogues synthetized and evaluated *in vitro* and *in vivo* against *Mycobacterium avium* and MTb susceptible and resistant strains. Furthermore, RFB2 was synthetized from rifabutin, adding an acetyl group with the major goal to improve the pharmacokinetics properties as anti-TB drug candidate and overcome the biological barriers (Figueiredo et al., 2009). Since the lungs are the main organs of anti-TB drugs bioaccumulation it is

Abbreviations: BAM, Brewster angle microscopy; DPPC, dipalmitoylphosphatidylcholine; HEPES, N-(2-hydroxyethyl) piperazine-*N*′-(2-ethanesulfonic acid); LC, liquid-condensed; LE, liquid-expanded; LUVs, large unilamellar vesicles; MDR, multidrug-resistant; MLVs, multilamellar vesicles; MTb, *Mycobacterium tuberculosis*; RFB2, *N*′-acetyl-rifabutin; PM-IRRAS, polarization-modulation infrared reflection-absorption spectroscopy; PS, pulmonary surfactant; SP, surfactant protein; T_m, main phase transition temperature; TB, tuberculosis.

* Corresponding author at: REQUIMTE, Departamento de Ciências Químicas, Faculdade de Farmácia, Universidade do Porto, Rua de Jorge Viterbo Ferreira n.° 228, 4050-313 Porto, Portugal. Tel.: +351 220428672.
E-mail address: shreis@ff.up.pt (S. Reis).

0378-5173/$ – see front matter © 2013 Elsevier B.V. All rights reserved.
http://dx.doi.org/10.1016/j.ijpharm.2013.03.062

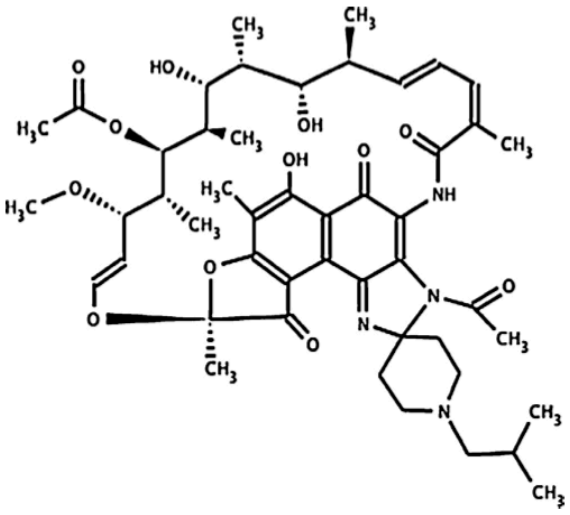

Fig. 1. Chemical structure of *N*′-acetyl-rifabutin (RFB2).

essential to perform biophysical studies to clarify the interactions of this antimycobacterial compound with the PS lipid membrane model (Chimote and Banerjee, 2010; Pinheiro et al., 2011) and understand where RFB2 preferentially locates and what are the membrane biophysical consequences of the antimycobacterial compound (namely how the packing of the lipids is affected), which can be ultimately related with the compound bioavailability and the membrane induced toxicity (Brogden and Fitton, 1994).

The PS is produced in the lungs by type II alveolar cells and is composed by 80% phospholipids, 8% neutral lipids, and 12% proteins (Poulain and Clements, 1995; Stevens and Sinkin, 2007). The PS main role is the reduction of the alveoli surface tension, allowing the decrease of the respiratory work and the prevention of the alveoli collapse (Agrawal and Gupta, 2000; Calkovská, 2000). In this work, Langmuir monolayers and liposomes (multilamellar vesicles, MLVs and large unilamellar vesicles, LUVs) were selected owing to the PS *in vivo* assumption of a configuration of both monolayers or vesicles formed from the bilayers fusion (Rugonyi et al., 2008b). Herein, the major compound of the PS, namely 1,2-dipalmitoyl-*sn*-glycero-3-phosphocholine (DPPC) phospholipid, was chosen in order to mimic the PS (Brogden and Fitton, 1994; Kaviratna and Banerjee, 2009). In addition, the phosphatidylcholines are also the most abundant lipids in the human cell membrane, being the DPPC commonly used by several authors to mimic the cell membranes (Merino et al., 2002; Nunes et al., 2011b; Pereira-Leite et al., 2013). At the physiological pH (7.4), DPPC is in zwitterionic form with no net charge and at the physiological temperature (37.0 °C) is in the gel phase (Chen et al., 2010; Chimote and Banerjee, 2008; Rugonyi et al., 2008a; Zuo et al., 2008).

To achieve the aim of this study, several biophysical techniques were performed. The partition coefficient (K_p) of RFB2 between DPPC:aqueous was determined using derivate UV–Vis spectrophotometry (Brittes et al., 2010; Lucio et al., 2006; Nunes et al., 2011c). Dynamic light scattering (DLS) was executed to understand the putative biophysical modifications (Michel et al., 2006) induced by RFB2 molecules on the PS membrane model. The structural information of the effect of RFB2 on the DPPC bilayer was obtained by using small and wide-angle X-ray scattering techniques (SAXS and WAXS) (Cosimati et al., 2013). Additionally, thermodynamic information was obtained by surface pressure-molecular area Langmuir isotherms associated with Brewster angle microscopy (BAM) to record images of the monolayer on the micrometre scale (Amado et al., 2008). Furthermore, polarization-modulated infrared reflections-absorption spectroscopy (PM-IRRAS) provided information of the phospholipids characteristic groups (Mendelsohn et al., 2010).

The overall results point to a strong interaction of RFB2 with the PS membrane models. Regarding the partition results it is expected that, *in vivo* this antimycobacterial compound, exhibit a high affinity and bioaccumulation in the lungs. Nevertheless, the interactions of RFB2 with the major phospholipids present in the PS membrane happen at the head groups level, which prevent the intercalation of the compound into the alkyl chain region of the phospholipids, leading to a possible disturbance of the PS organization with potential toxicological consequences. Moreover, the knowledge about drug–membrane interactions may provide significant insights for the design of more efficient and safe anti-TB drugs as well as novel liposome-based drug delivery systems.

2. Materials and methods

2.1. Materials

1,2-dipalmitoyl-sn-glycero-3-phosphocholine (DPPC) was purchased from Avanti Polar Lipids, and used as received. RFB2 was obtained from rifabutin (isolated from Mycobutin®), using a selective acylation of the secondary amine (Figueiredo et al., 2009). Chloroform was used as the spreading solvent in the monolayers experiments. A mixture of chloroform:methanol (3:1, v/v) was used as the organic solvents in the vesicles preparation. Phosphate buffer with a total phosphate concentration of 0.1 M at a pH of 7.4 plus 0.1 M of NaCl was used as the subphase in the monolayers experiments. In the experiments using the vesicles as membrane models, the buffer solution consisted of 0.01 M N-(2-hydroxyethyl) piperazine-*N*′-(2-ethanesulfonic acid) (HEPES) and adjusted the ionic strength to 0.1 M with NaCl and the pH to 7.4. The pure solvents were obtained from Sigma–Aldrich Co. (St. Louis, MO, USA) and used without further purification. Solutions were prepared with double-deionized water (conductivity less than 0.1 S cm^{-1}).

2.2. Methods

2.2.1. Preparation of the PS membrane models

2.2.1.1. Large unilamellar vesicles. A lipid film was formed from a chloroform solution of DPPC, dried under a stream of nitrogen and left under reduced pressure to remove all traces of the organic solvent. Vesicles with a concentration of 1800 μM were prepared by the addition of the buffer solution, followed by vortexing to obtain multilamellar vesicles (MLVs). Lipid suspensions were equilibrated at 50.0 ± 0.1 °C for 30 min and extruded 10 times through polycarbonate filters with a pore diameter of 100 nm to form large unilamellar vesicles (LUVs). In the experiments using LUVs the final concentration of RFB2 was 40 μM.

2.2.1.2. Mutilamellar vesicles. Different amounts of RFB2 were mixed with DPPC (136 mM) in a chloroform/methanol mixture (3:1, v/v) according to the required 5% and 10% molar fraction of RFB2, with a final concentration of the antimycobacterial compound of 15 and 35 mM, respectively. Lipid films were formed from these solutions, dried at 50.0 ± 0.1 °C under a stream of N_2 and left overnight under reduced pressure to remove all traces of the organic solvents. The lipid films were hydrated by adding HEPES buffer and then alternately heated above the lipid phase transition in a water bath at a temperature above the main phase transition (T_m), namely at 50.0 ± 0.1 °C, mixed by vortexing for about 5 min and centrifuged for 30 s at 2000 × *g*. This procedure was repeated three times to ensure that all lipid film was hydrated. Finally, the samples were aged overnight at 4.0 ± 0.1 °C and shaken by vortex at room temperature for 5 min. Thereafter, the dispersions were transferred into glass capillaries of 1.5 mm diameter

(Hilgenberg, Malsfeld, Germany), which are transparent to X-rays. The flame-sealed capillaries were stored at 4.0 ± 0.1 °C until the measurements.

2.2.1.3. Langmuir monolayers. The monolayers were prepared by spreading samples on the phosphate buffer subphase. Monolayers were spread by deposition of tiny droplets of samples uniformly through the air–water interface, using a 250 μL microsyringe. DPPC was spread from 0.2 mM chloroform solutions. After spreading, solvent was allowed to evaporate for 15 min prior to monolayer compression. The effect of RFB2 was evaluated by spreading DPPC monolayers on a phosphate buffer with a known concentration (0.118 μM) of this antimycobacterial compound. All experiments were performed at a room temperature of 21.0 ± 0.1 °C in a large class 100 clean room.

2.2.2. Partition coefficients by derivative spectrophotometry

The partition coefficient (K_p) of RFB2 between LUVs suspensions of DPPC and the HEPES buffer solution was determined by derivative spectrophotometry (Ferreira et al., 2005). In the derivative spectrophotometry a series of buffered suspensions containing a fixed concentration of RFB2 (40 μM) and increasing concentrations of DPPC (100, 200, 300, 400, 500, 600, 700, 800, 900, and 1000 μM) were prepared. The corresponding reference suspensions were identically prepared, but without RFB2. All suspensions were then vortexed and incubated in the dark for 30 min at several temperatures, below the T_m (20.0 and 37.0 ± 0.1 °C) and above the T_m (50.0 ± 0.1 °C). The absorption spectra were recorded using a Perkin-Elmer Lambda 45 UV–Vis spectrophotometer, using quartz cells with a 1 cm^{-1} path length and a spectral range from 250 to 600 nm at 1 nm intervals. The mathematical treatment of the results was performed using a developed routine, K_p calculater (Magalhaes et al., 2010).

2.2.3. Dynamic light scattering

The effect of RFB2 (40 μM) on the biophysical parameters (T_m and cooperativity) of DPPC liposomes (500 μM) were determined by DLS, as elsewhere described (Michel et al., 2006). The count rate was obtained using a BI-MAS DLS instrument (Brookhaven Instruments, USA), containing a controlled temperature cell holder. The samples were heated from 30.0 ± 0.1 °C to 60.0 ± 0.1 °C with intervals of 1.0 ± 0.1 °C and with an equilibration period of 2 min. At each temperature 6 runs of 2 min were performed.

2.2.4. Small and wide angle X-ray scattering

SAXS and WAXS experiments were executed at beamline A2 at Doris III of HASYLAB (DESY, Hamburg, Germany) with a monochromatic radiation of wavelength 0.15 nm. The SAXS detector was calibrated with rat-tail tendon and the WAXS detector with polyethylene terephthalate (PET) The samples were exposed to static measurements at different temperatures, below (20.0 and 37.0 ± 0.1 °C) and above (50.0 ± 0.1 °C) the T_m. After each temperature step, the sample was allowed to equilibrate for 5 min before the diffraction pattern was recorded. In order to minimize the X-ray exposure to the sample, a shutter mounted before the sample was kept closed when no data was acquired. The lamellar repeat distance d was calculated from the small-angle Bragg reflections using Bragg's equation $s = n/d$; where $s = \lambda/2 \sin \Theta$ is the scattering vector and n the order of the reflection ($n = 1, 2, \ldots$). To obtain more precise position of the s, the diffraction peaks were fitted with Lorentzians and the positions of maximum intensities and half widths of peaks at one half of their intensity were determined (Cosimati et al., 2013).

2.2.5. Langmuir isotherms

Two different troughs models (KN-1005 and NIMA 601) (Nima Technology, Coventry, England) were equipped with two symmetrical barriers and a Wilhelmy type dynamometric system using a strip of filter paper. KN-1005 has nearly 325 mL subphase volume and close to 587 cm^2 total area. NIMA 601 has about 400 mL in subphase volume with a total area close to 600 cm^2. KN-1005 was used in the PM-IRRAS experiments. Due to its larger capacity and area, NIMA 601 was used to obtain the represented isotherms. The monolayers prepared as above-mentioned were compressed at a rate of 20 cm^2/min. During compression, surface pressure-molecular area isotherms (π/A) were recorded.

2.2.6. Brewster angle microscopy

Brewster angle microscopy (BAM) images were obtained from a I-Elli 2000 apparatus (supplied by Nanofilm Technologies, Göttingen, Germany) using a Nd:YAG diode laser, which can be recorded with a lateral resolution of 2 μm. The image processing procedure included a geometrical correction of the image, as well as a filtering operation to reduce interference fringes and noise. Furthermore, the brightness of each image was scaled to improve contrast. For BAM experiments and isotherms recorded, the model NIMA 601 (Nima Technology, Coventry, England) equipped with two symmetrical barriers and a Wilhelmy type dynamometric system using a strip of filter paper was applied.

2.2.7. Polarization-modulation infrared reflection-absorption spectroscopy

PM-IRRAS spectra were recorded using a KSV PMI 550 (KSV NIMA, Espoo, Finland) equipped with an MCT detector and a KN-1005 trough (Nima Technology, Coventry, England). The setup consists of an IR source, a Michelson interferometer and an external reflection unit. The infrared radiation intensity was modulated by the interferometer and polarized with a ZnSe polarizer. The beam was then passed through a ZnSe photoelastic modulator, which modulated it between polarization in the plane of incidence (p) and polarization perpendicular to this plane (s) with a fixed frequency of 100 kHz. This allowed the simultaneous measurements of spectra for the two polarizations, and their difference provides surface-specific information, while their sum provides the reference spectrum (buffer or buffer with RFB2). The angle of incidence of the infrared beam with respect to the surface normal was 80°. Spectra were recorded with a spectral resolution of 8 cm^{-1} and collected using 3000–6000 scans during 5–10 min.

3. Results and discussion

3.1. Derivative spectrophotometry

The lipophilicity is a very important molecular descriptor that often correlates with the drug's biological activity (Demchenko et al., 2009; Mattow et al., 2006). Indeed, the transport and distribution of the antibiotics are strongly related with their pharmacological effect (Vostrikov et al., 2007, 2008). Specifically, in the case of an anti-TB, it must be a compound well-distributed thought the body in order to reach the lung tissues infected by the MTb (Vostrikov et al., 2008). Therefore, the lipophilicity, expressed by the logarithm of lipid:water partition coefficient log P or distribution coefficient log D (in the case of ionizable compounds), constitutes a valuable predictor of membrane transport properties of drugs. In addition, it was established that a desirable antimycobacterial candidate should have a preferred value for Log P between 1.3 and 4.1 (Barry et al., 2000). In this work, the partition coefficient (K_p) expressed in terms of log D has been determined in a liposomes/buffer system using derivative UV–vis spectrophotometry, since there might be a pronounced discrepancy between the partition coefficient estimated in a octanol/buffer system and in the biological membranes (Lucio et al., 2007; Pola et al., 2004). Derivative spectrophotometry eliminates the intense background signals

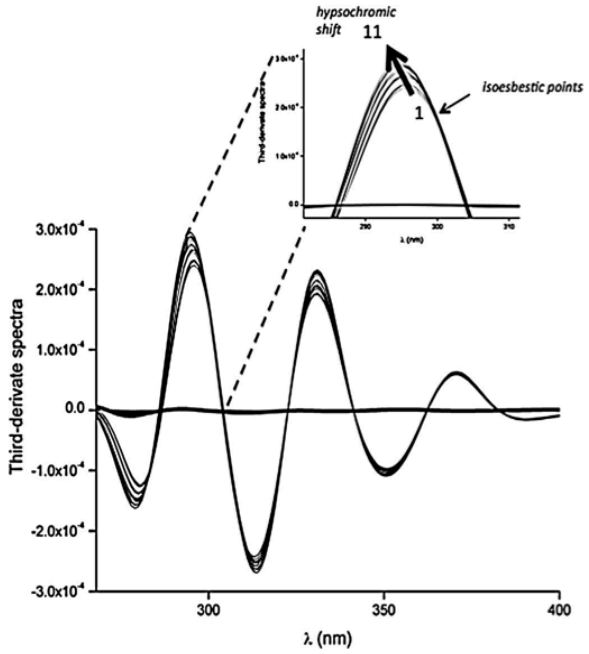

Fig. 2. Third-derivate spectra of RFB2 (40 μM) incubated in LUVs of DPPC with different concentrations (M): (1) 0; (2) 1×10^{-4}; (3) 2×10^{-4}; (4) 3×10^{-4}; (5) 4×10^{-4}; (6) 5×10^{-4}; (7) 6×10^{-4}; (8) 7×10^{-4}; (9) 8×10^{-4}; (10) 9×10^{-4}; (11) 1×10^{-3}.

arising from light scattered by lipid vesicles, and improves the resolution of overlapping bands, features that have been reported by several authors (Brittes et al., 2010; Ferreira et al., 2005; Pinheiro et al., 2013). Following equilibration, the absorption spectra were recorded. Derivative intensities can be related to the partition coefficient by the following equation (Eq. (1)):

$$D_T = D_w + \frac{(D_m - D_w)K_p[L]V_m}{1 + K_p[L]V_m} \quad (1)$$

In this equation, D is the first, second or third derivative intensity ($D = (d^n Abs)/(d\lambda^n)$) obtained from the absorbance values of the total amount of RFB2 (D_T); RFB2 distributed on the lipid membrane phase (D_m); RFB2 distributed in the aqueous phase (D_w); lipid concentration ([L]) and the lipid molar volume (V_m). For DPPC, the mean molecular weight was considered to be 734.04 g/mol^{-1} and the V_m 0.701 M. The Eq. (1) was fitted to the experimental second and third derivate spectrophotometric data (D_T *versus* [L]) using a non-linear least-squares regression method at wavelengths where the scattering is eliminated (Lucio et al., 2006). The third-derivate spectrum of RFB2 in DPPC liposomes is presented in Fig. 2. It is possible to observe the isosbestic points and the hypsocromic shift with increasing lipid concentrations, which provide significant insights that the partition happens and RFB2 exists in two forms: compound in polar bulk water and in DPPC bilayers (Brittes et al., 2010). Fig. 3 shows, as an example, the best fit of Eq. (1) to the third-derivative spectrophotometric data collected at λ = 296 nm for RFB2 with different concentrations of DPPC liposomes at the temperature of 20.0 ± 0.1 °C.

The RFB2's partition coefficients in DPPC:water liposomes were performed at different temperatures at which the lipids are expected to be in the gel phase (20.0 ± 0.1 °C), rippled-gel (37.0 ± 0.1 °C) and fluid phase (50.0 ± 0.1 °C) and are listed in Table 1. The analysis of the obtained values presented in Table 1, demonstrates that the partition of RFB2 in the DPPC liposomes is independent of the temperature. This suggests that the partition is independent of the phospholipid packing. However, RFB2 changes

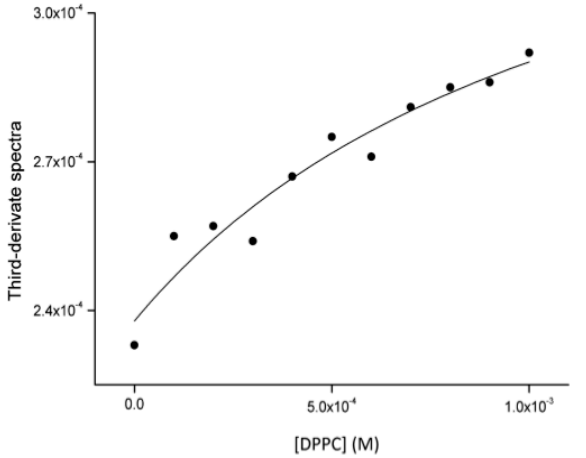

Fig. 3. Third-derivate spectra for RFB2 (40 μM) at different concentrations of LUVs of DPPC in the gel phase (T = 20 °C). The curve represents the best fit by Eq. (1) using a non-linear least squares regression method at wavelength 296 nm where the scattering is eliminated.

the expected phospholipid packing, which was confirmed by the further studies.

3.2. DLS

The dynamic light scattering (DLS) exploiting the count rate is a reliable, simple and reproducible technique to determinate the T_m (Michel et al., 2006). The alteration in the measured scattering intensity reflects changes in the optical properties of the material. Thus, discontinuity in the mean count rate (average number of photons detected per second) as the temperature changes, corresponds to an alteration in the optical properties of the material studied (*i.e.* transition from initial state to another one) (Michel et al., 2006). Data as the normalized mean count rate *versus* temperature were collected and fitted using Eq. (2):

$$r_s = r_{s1} + p_1 T + \frac{r_{s2} - r_{s1} + p_2 T - p_1 T}{1 + 10^{B(1/T - 1/Tm)}} \quad (2)$$

where r_s is the average count rate, T is the temperature (°C), p_1 and p_2 correspond to the slopes of the straight lines at the beginning and at the end of the plot, and r_{s1} and r_{s2} are the respective count rate intercepting values at the y-axis. From the experimental data displayed, it was possible to calculate the cooperativity (B) and the midpoint of the phase transition, which corresponds to the T_m. The T_m was calculated from the slope and the inflection point of the data fitted to sigmoid curves of count rate (r_s) *versus* temperature (T) (Michel et al., 2006).

The normalized count rate dependence for DPPC liposomes in the absence and in the presence of RFB2, according to the temperature, is shown in Fig. 4.

In Table 2 are depicted the obtained values for the biophysical parameters: T_m and cooperativity of DPPC in the absence and in the presence of RFB2. The analysis of Table 2, reveals that for DPPC the obtained T_m is consistent with previous studies (Michel et al., 2006). RFB2 lowered roughly 1.6 ± 0.1 °C the T_m of the DPPC

Table 1
Partition coefficients (log D) (dimensionless) of RFB2 (40 μM) in LUVs of DPPC at pH 7.4 and at 20 °C (gel phase), 37 °C (rippled-gel) and 50 °C (fluid phase).

T (°C)/expected lipid phase	log D
20 ($L_{\beta'}$)	3.29 ± 0.20
37 ($P_{\beta'}$)	3.25 ± 0.05
50 (L_α)	3.24 ± 0.10

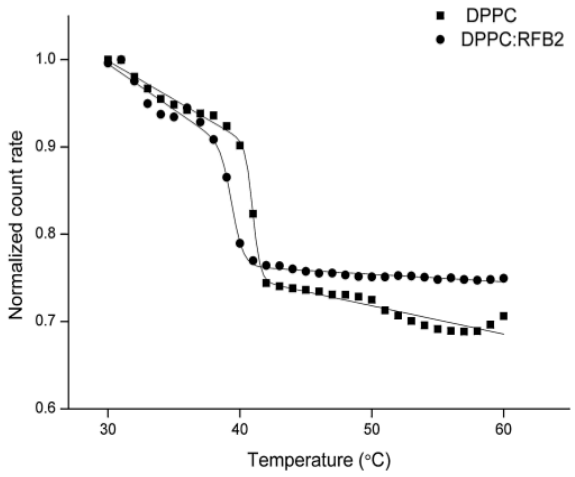

Fig. 4. Average count rate of DPPC liposomes in the absence (square symbols) and presence (circular symbols) of RFB2 (40 μM) at pH 7.4 as a function of temperature. Continuous lines are the best-fit curves using Eq. (2).

Table 2
Values of main phase transition temperature (T_m) and cooperativity (B) obtained for DPPC liposomes (500 μM, T = 37.0 °C, pH 7.4) in the absence and in the presence of RFB2 (40 μM).

	T_m (°C)	Cooperativity (B)	Order (S)
DPPC	40.8 ± 0.2	2408 ± 164	0.457 ± 0.02
DPPC + RFB2	39.2 ± 0.3	1192 ± 276	0.479 ± 0.02

liposomes and decreased the cooperativity (*i.e.* the number of chains that change simultaneously) of the phase transition (B). In fact, the changes in the biophysical parameters of the lipids normally give an indication for the drug's location (Nunes et al., 2011c). Therefore, RFB2 may be located in the chain region near the head groups of the phospholipids (C1–C9) since its intercalation in the phospholipid bilayer affects the phospholipid packing (Dynarowicz-Latka et al., 2001; Nunes et al., 2011c).

3.3. SAXS and WAXS

The influence of RFB2 in DPPC bilayers was investigated using X-ray diffraction patterns at small and wide angles, which provide information, respectively, on long range bilayer organization and hydrocarbon chain packing (Liu et al., 2001). The SAXS and WAXS studies were carried out according to the thermotropic behaviour of DPPC, namely at 20, 37, and 50 °C, corresponding respectively to the gel phase ($L_{\beta'}$), ripple gel phase ($P_{\beta'}$) and fluid phase (L_α). Additionally, the Bragg reflections detected were decomposed and

Table 4
Short distances (d) and correlation length (ξ) determined from WAXS diffraction patterns at pH 7.4 and at 20, 37 and 50 °C. The data are presented in Å as a function of the mol% of RFB2.

Sample	T (°C)/expected lipid phase	d_{WAXS} (Å)		ξ_1 (Å)
		d_1	d_2	
DPPC	20 ($L_{\beta'}$)	4.10	4.04	228 ± 10
	37 ($P_{\beta'}$)	4.11	–	432 ± 10
DPPC + RFB2 (5%)	20 ($L_{\beta'}$)	4.04	–	52 ± 10
	37 ($P_{\beta'}$)	4.09	–	27 ± 10
DPPC + RFB2 (10%)	20 ($L_{\beta'}$)	4.07	–	45 ± 10
	37 ($P_{\beta'}$)	4.13	–	31 ± 10

their profiles fitted as a sum of Lorentzian functions. For DPPC, the SAXS pattern (Table 3) depicted the first order Bragg reflection peaks on the scattering curves, which appear at 1/64.5 $Å^{-1}$ ($L_{\beta'}$), 1/64.2 and 1/71.7 $Å^{-1}$ ($P_{\beta'}$), and 1/67.4 $Å^{-1}$ (L_α), and are in close agreement with the literature (Nunes et al., 2011a; Winter, 2005). The deconvolution of the WAXS patterns (Table 4) displays a sharp reflection at 1/4.10 $Å^{-1}$, with a shoulder located at 1/4.04 $Å^{-1}$, which reflects the orthorhombic, pseudo-hexagonal lattice of the chain packing arrangement in the bilayers, characteristic of the $L_{\beta'}$ phase (Sachan et al., 2012). At 37 °C, the only one diffraction peak presents a symmetric profile, indicating a hexagonal chain packing characteristic of the $P_{\beta'}$ in phosphatidylcholines (Kunin, 1996). At 50 °C, in the L_α, a very diffuse reflection appears (data not shown), corresponding to melted chain states.

The SAXS diffraction patterns of DPPC in the absence and in the presence of 5 and 10 mol% of RFB2 are shown in Fig. 5.

At 20 °C and for low angle spectra, the positions of the first Bragg reflection were detected at 1/72.2; 1/59.9 for 5% and 1/72.6; 1/59.8 $Å^{-1}$ for 10% molar fraction of RFB2. These profiles are similar to the $P_{\beta'}$ of pure DPPC. This suggests that the RFB2 molecules induced the rippled gel phase at lower temperatures than those typical for the pure DPPC [48]. Moreover, the wide angle spectrum displays a single, symmetrical peak that points to a hexagonal hydrocarbon chain packing (Cosimati et al., 2013; Nunes et al., 2011a), evidencing a change in the orientational direction of the chains with respect to the normal bilayer. This indicates that the interaction of RFB2 with DPPC modifies the lateral hydrocarbon chain packing of the membrane. The formation of a $P_{\beta'}$ phase at temperatures at which a more packed gel phase was expected reveals that RFB2 has a disordering effect on the DPPC lipid bilayers, and this might be related with orientation of the polar head groups. The degree of the increase in the d-spacing and the pre-transition removal can provide evidence that the DPPC hydrocarbon chains are oriented normal to the bilayer plane when RFB2 is added since pre-transitions do not occur in bilayers with chains perpendicular to the bilayer plane (Peetla et al., 2009). For higher temperatures

Table 3
Long distances (d) and correlation length (ξ) determined from SAXS diffraction patterns at pH 7.4 and at 20, 37 and 50 °C. The data are presented in Å as a function of the mol% of RFB2.

Sample	T (°C)/expected lipid phase	d_{SAXS}					
		d_1 (Å)	ξ_1 (Å)	d_2 (Å)	ξ_2 (Å)	d_3 (Å)	ξ_3 (Å)
DPPC	20 ($L_{\beta'}$)	64.5 ± 0.5	381 ± 10	–	–	–	–
	37 ($P_{\beta'}$)	64.2 ± 0.5	561 ± 10	71.7 ± 0.5	372 ± 10	–	–
	50 (L_α)	67.4 ± 0.5	779 ± 10	–	–	–	–
DPPC + RFB2 (5%)	20 ($L_{\beta'}$)	59.9 ± 0.5	577 ± 10	72.2 ± 0.5	518 ± 10	–	–
	37 ($P_{\beta'}$)	61.4 ± 0.5	302 ± 10	71.8 ± 0.5	709 ± 10	76.3 ± 0.5	956 ± 10
	50 (L_α)	69.6 ± 0.5	735 ± 10	–	–	–	–
DPPC + RFB2 (10%)	20 ($L_{\beta'}$)	59.8 ± 0.5	131 ± 10	72.6 ± 0.5	391 ± 10	–	–
	37 ($P_{\beta'}$)	61.0 ± 0.5	294 ± 10	71.9 ± 0.5	611 ± 10	76.4 ± 0.5	743 ± 10
	50 (L_α)	71.0 ± 0.5	665 ± 10	–	–	–	–

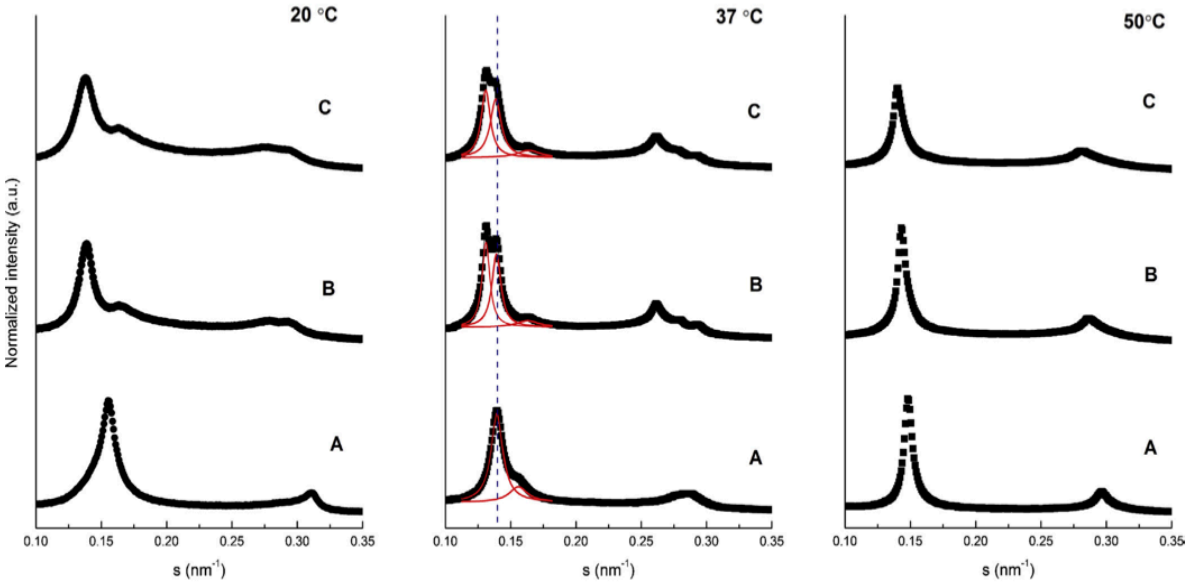

Fig. 5. Small angle X-ray diffraction profiles at 20, 37 and 50 °C for DPPC (A) and mixtures of DPPC with RFB2 at 5 mol% (B) and 10 mol% (C) at pH 7.4.

(37 °C), the asymmetric Bragg peak obtained in the SAXS experiments for DPPC with both molar fractions of RFB2 is indicative of a lipid phase separation, a $P_{\beta'}$ non-influenced DPPC phase and a DPPC phase influenced by RFB2 (Fig. 5). Additionally, the Bragg peaks obtained in the presence of RFB2 show a reduced full width half maximum than the diffraction peak correspondent to the pure DPPC (Fig. 5), indicating that the correlation (ξ) between the bilayers increases in the antimycobacterial presence and pointing to an increase in the lipid's order. The interaction between RFB2 and the DPPC choline group may cause the choline group to adopt a more extended position. In fact, this mixed DPPC phase leads to a *d*-spacing increment until a maximum of ~4 Å (Table 3). This increase in the long spacing could be the result of a change in the hydration behaviour of DPPC due to the interaction with the RFB2 molecules (Cosimati et al., 2013; Nunes et al., 2011a). In addition, the WAXS profile for DPPC in the presence of RFB2 reveals that, the correlation length (ξ) between the bilayers was also significantly affected by the presence of this antimycobacterial compound. Above the transition, the lamellar reflections correspond to the existence of a homogeneous phase. At 50 °C, the repeat distance slightly increases from 67.4 Å for the L_α phase of DPPC to 69.6 Å in the presence of 5 mol% of RFB2 and to 71.0 Å in the presence of 10 mol% of RFB2 (Table 3). The increase of approximately 3 Å may result from an increase in the water layer between the bilayers or an increase in the phospholipid bilayer thickness. These hypothesis points to a location of the RFB2 molecules near the lipid polar head group-water interface. In addition, the ξ is lower than the observed for pure DPPC, which might be due to the existence of flatness defects in the polar head groups surface as a consequence of the insertion of RFB2.

Overall, the SAXS and WAXS results endorse that the location of RFB2 is mainly close to the head groups and near the whole water shells.

3.4. Surface pressure-molecular area (π/A) isotherms

Isotherms give valuable information about the lipid phases and the phase transitions, which are both dependent on the temperature, the pressure, and the pH (Jiménez-Millan et al., 2011; Giner-Casares et al., 2008a,b; Wustneck et al., 2005). In this work, the studied parameters from the pressure-molecular area (π/A) isotherms were the hysteresis and the elastic modulus. The hysteresis was acquired by consecutive measurements of monolayer compression/decompression isotherms and corresponds to the difference between compression and decompression areas (Aydogan et al., 2011; Wüstneck et al., 2002). The cycle of compression/decompression was performed in order to mimic the breathing movements (with a much slower rate due to the experimental limitations). Elastic modulus (C_s^{-1}) was calculated from the π/A isotherms by the following Eq. (3):

$$C_s^{-1} = -A\left(\frac{d\pi}{dA}\right), \tag{3}$$

where A is the area per lipid molecule, and π is the surface pressure. C_s^{-1} describes the relationship between the surface pressure increase and the area per molecule decrease. A higher value of C_s^{-1}

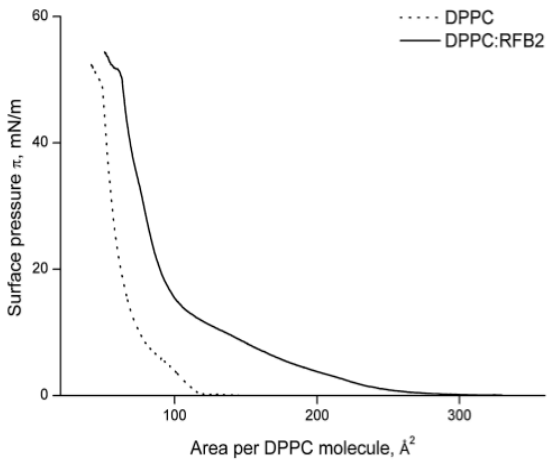

Fig. 6. Surface/pressure (π/A) isotherm of DPPC and on the subphase containing RFB2 (0.118 μM).

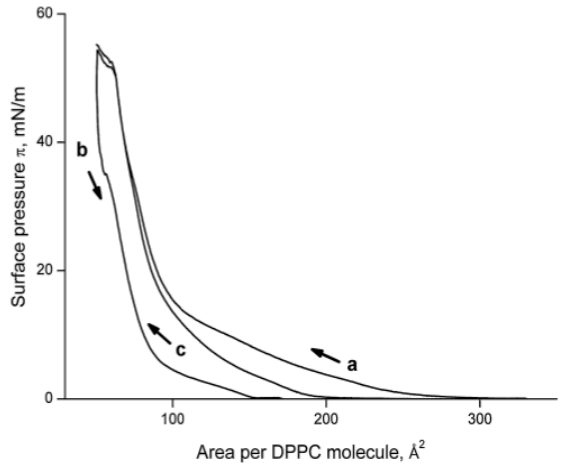

Fig. 7. Cyclic surface/pressure (π/A) isotherm of the DPPC monolayer on the subphase containing RFB2 (0.118 μM). (a) First compression, (b) decompression, and (c) second compression.

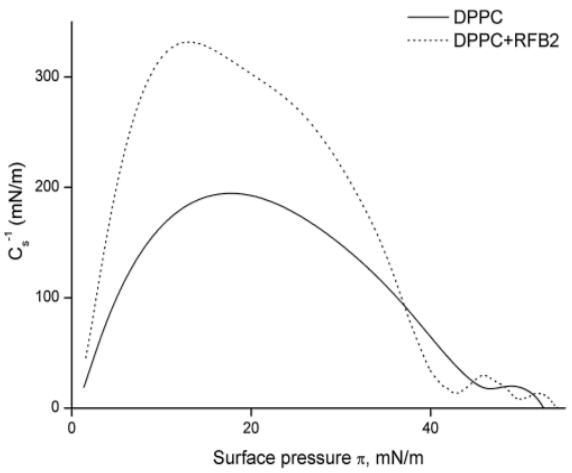

Fig. 8. C_s^{-1} diagrams of DPPC in the absence (straight-line) and in the presence of RFB2 (0.118 μM) (dashed line).

is indicative of a less compressible monolayer (Nunes et al., 2011c; Wang and Yang, 2009)

The surface pressure–molecular area (π/A) isotherms of the DPPC monolayer, both with and without RFB2 are shown in Fig. 6.

The π/A isotherm of pure DPPC is in good agreement with the literature (Foglia et al., 2011; Nunes et al., 2011c). Upon compression, the DPPC monolayer proceeds from the gas phase to the liquid-expanded (LE) (Harishchandra et al., 2010). Thereafter, the first order transition from LE–liquid-condensed (LC) happens with a plateau at a pressure ranging from ~4 to 8 mN/m. After the first plateau region, the condensed region appears, corresponding the second plateau to the monolayer collapse, which for the experimental conditions mentioned was at a pressure of ~52 mN/m (Foglia et al., 2011; Nunes et al., 2011c). The expansion of the isotherm indicates that RFB2 is present at the interface air/water, interacting with the DPPC phospholipids. These interactions occur at the LE as well as at the LC regions. The transition from LE–LC seems to take place simultaneously at the interval 2–15 mN/m. This is consistent with the DLS results and confirms that, although RFB2 is responsible for an earlier transition from the gel to the fluid phase, once the transition process is initiated, it is less cooperative when comparing to the lipid without RFB2. The two subsequent

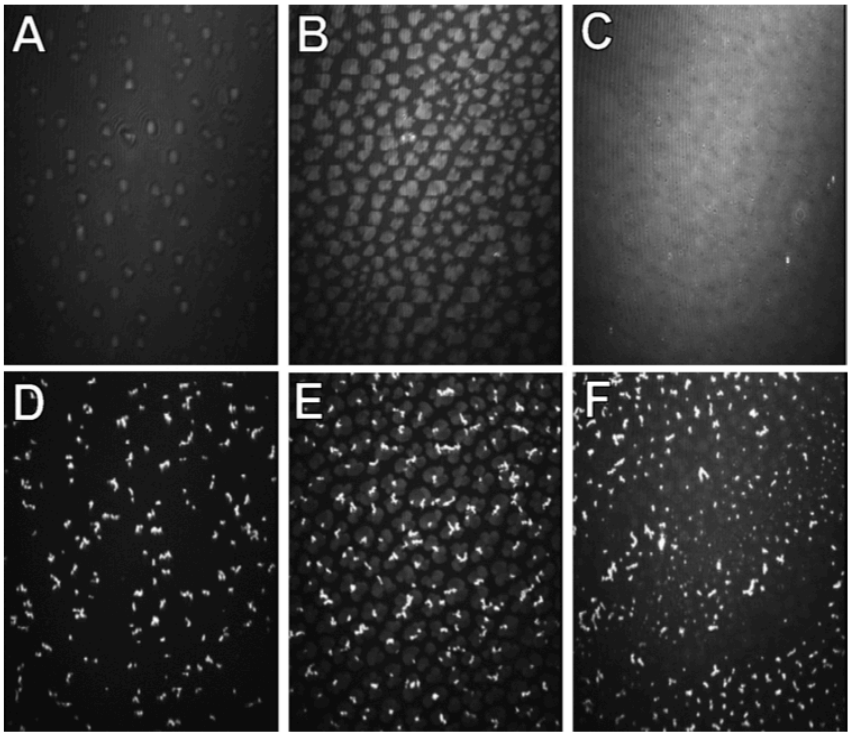

Fig. 9. BAM images of Langmuir monolayers of: (Top) DPPC monolayer on a phosphate buffer subphase; A (5 mN/m–82 Å²/molecule), B (10 mN/m–64 Å²/molecule), C (56 mN/m–37 Å²/molecule). (Bottom) DPPC monolayer on a phosphate buffer containing 0.118 μM of RFB2 subphase; D (5 mN/m–134 Å²/molecule), E (10 mN/m–93 Å²/molecule), F (40 mN/m–54 Å²/molecule).

Table 5
Vibrational wavenumber (phosphate, carbonyl, and asymmetric methylene) of the DPPC monolayers in the absence and in the presence of RFB2 (0.118 μM), for π = 4 mN/m, 24 mN/m and 40 mN/m.

	π = 4 mN/m			π = 24 mN/m			π = 40 mN/m		
	$\nu(PO_2^-)$ (cm^{-1})	ν(C=O) (cm^{-1})	$\nu_{as}(CH_2)$ (cm^{-1})	$\nu(PO_2^-)$ (cm^{-1})	ν(C=O) (cm^{-1})	$\nu_{as}(CH_2)$ (cm^{-1})	$\nu(PO_2^-)$ (cm^{-1})	ν(C=O) (cm^{-1})	$\nu_{as}(CH_2)$ (cm^{-1})
DPPC	1244 1259 1269	1734	2921	1244 1267	1738	2918	1245 1268	1736	2917
DPPC + RFB2	1228 1256	1728	2918	1238 1265	1729	2917	1237 1257	1731	2919

compression π/A isotherms of DPPC in the presence of RFB2 molecules are represented in Fig. 7. A certain degree of hysteresis is observed with decompression of the DPPC monolayer and is attributed to a loss of RFB2 molecules to the subphase (Fig. 7). Nevertheless, an almost full recovery of RFB2 molecules at the air–water interface is achieved due to the second isotherm obtained, which was very similar to the first one (Fig. 7). The C_s^{-1}-π of DPPC in the absence and in the presence of RFB2 are depicted in Fig. 8, being possible to observe that RFB2 forms a less compressible monolayer, as detected by the increase in the C_s^{-1} values. Additionally, the analysis of this Fig. 8 allows inferring that for pressures of 40 mM/m, RFB2 increases the compressibility of the monolayer. The expansion of the isotherms to larger areas and the production of a more compressible monolayer for higher surface pressures are consistent with the lower phospholipd packing induced by the RFB2 presence at the air–water interface.

3.5. BAM

BAM is a powerful technique that enables the visualization of the two-dimensional organization of monolayers materials, including the size and the shape of the domains and the heterogeneity in Langmuir films (Dynarowicz-Latka et al., 2001).

Fig. 9 shows, respectively, the BAM pictures acquired during the first compression of DPPC monolayers on the subphase, both without and with RFB2. For pure DPPC, the micrograph 9A shows the beginning of the transition from LE–LC, and the appearance of the circular condensed domains of DPPC (Chen et al., 2010; Harishchandra et al., 2010). With further compression of the DPPC monolayer, the domains grow in size and acquire irregular shapes (9B) and coalesce, leading to a bright homogeneous monolayer at high values of surface pressure (9C) (Chen et al., 2010; Wang et al., 2009). The incorporation of RFB2 in the subphase clearly changes the morphology of the DPPC monolayer. Therefore, the bright regions are associated with RFB2 molecules present in the form of relatively thick local aggregates and so with a high refractive index (9D) as previously described (Wang et al., 2009). Remarkably, the lipid domains are higher in size and assume a more irregular shape (9E), presenting inner small bright points that correspond to RFB2. With the monolayer compression the aggregates increase inside the lipid's domains, even though for higher pressures and due to a possible "squeezing-out" of RFB2, the number of aggregates is reduced (9F). Hence, the pronounced changes induced by RFB2 in the morphology and of the DPPC domains do not be related with the alkyl chain arrangement. Thus, the coexistence of the brighter regions with the LC lipid domains usually strongly suggests the occurrence of aggregates of RFB2 in the polar head region of the DPPC phospholipids (Roldan-Carmona et al., 2012).

3.6. PM-IRRAS

The polarization-modulated infrared reflection-absorption spectroscopy (PM-IRRAS) of lipid/protein monolayers films *in situ* at the air/water interface provides information about the molecular structure and orientation of the films constituents (Flach et al., 1997; Mendelsohn et al., 2010).

In Table 5 are summarize the vibrational wavenumbers of the asymmetric methylene, the carbonyl and the asymmetric phosphate groups for DPPC monolayers in the absence and in the presence of RFB2, at constant π of about 4, 24 and 40 mN/m of the first compression.

For DPPC, with the pressure increment, the decrease in the wavenumber of the methylene is observed due to the tight packing of the monolayer and consequent increase in the film's order. In the case of DPPC, the CH_2 asymmetrical stretching modes shift from 2921 from to approximately 2918 cm^{-1}, from 4 mN/m to 24 mN/m respectively, representing a transition from the LE to the LC state (Czapla et al., 2010; Mendelsohn et al., 2010). Thus, the decrease in the asymmetric CH_2 stretching frequency as the monolayer is compressed indicates the formation of *all-trans* conformation (characteristic of LC phase) and the loss of *gauche* conformers (characteristic of LE phase) (Cameron et al., 1981; Czapla et al., 2010; Mendelsohn et al., 2010). When RFB2 is incorporated in the subphase and for lower pressures, the monolayer is more ordered as suggested by the shift for lower values in the CH_2 wavenumbers. For high pressure the contrary happens, and a less ordered monolayer seems to take place regarding the higher value obtained for the methylene wavenumbers and in comparison with the DPPC monolayer. Nevertheless, RFB2 interactions are more evident with the phospholipid head groups, regarding the more pronounced changes in the wavenumbers of the PO_2^- and C=O in comparison with the CH_2. Hence in the presence of RFB2, a shift for lowers wavenumbers of the PO_2^- and the C=O stretching bands is observed for all the surface pressures studied. On the other side, the interactions of RFB2 with the head groups of the phospholipids seem to be more marked for lower surface pressures. For pressures of 4 mN/m, the band contour of PO_2^- consists at two overlapped features, namely at 1228 and at 1256 cm^{-1}, corresponding respectively to dehydrated and unhydrated phosphate groups, respectively. For the C=O group, intensities bellow 1730 cm^{-1} indicate the production of hydrogen bonds (Wagner et al., 2008). Moreover, the stronger hydration of the head groups suggests a high degree of hydrogen bonding between RFB2 and the head groups of DPPC. Nevertheless, the shift for higher values of the PO_2^- and for the C=O wavenumbers occurring with the pressure increment, being consistent with the "squeezed out" of RFB2 molecules from the air/water interface.

4. Conclusion

In order to gain further insights of the effects of RFB2 on the biophysical properties of the PS, two-dimensional and three-dimensional membrane models composed of DPPC were used. The overall results confirmed that, RFB2 molecules change the packing of the PS membrane constituent phospholipids. Particularly, the results obtained by the Langmuir isotherms, PM-IRRAS and the DLS,

are in full agreement and suggest a decrease of the phospholipid T_m in the presence of RFB2 molecules. Herein, DPPC, the main component of the PS, has a transition temperature of around 41 °C, being at the physiological temperature (37 °C) in the gel phase (Chimote and Banerjee, 2008). The gel phase is essential for its main properties in reducing the surface tension to near-zero values, but results in poor adsorption ability at the air/water interface. Therefore, other biological compounds help DPPC in this task, fluidizing DPPC below its gel to fluid transition temperature. In this work, we demonstrate by several accurate biophysical techniques, that RFB2 might contribute *in vivo* for the dynamic respreading of the surfactant film by fluidizing the DPPC and thus facilitating the normal breathing process (Chimote and Banerjee, 2008; Harishchandra et al., 2010; Sachan et al., 2012). Moreover, the high partition obtained suggest that RFB2 has a desirable log *D* to be used as an anti-TB drug (Harishchandra et al., 2010). The high partition values obtained, associated with the almost full recovery of the amphiphilic RFB2 to the interface air/water in the second compression, predicts a higher distribution of this compound through the biological membranes and probably accumulation at the PS lipid level during the breathing process. The mechanism of interaction of the RFB2 with the DPPC was qualitatively the same and independent of the molecular orientation (two-dimensional and three-dimensional) of the PS membrane model.

Furthermore, RFB2 decrease the phospholipid packing of DPPC in the more ordered phases, which may be an advantage in the future development of DPPC liposomal controlled release formulations exploiting the inhalatory delivery directly to lungs. Therefore, the encapsulation of RFB2 in liposomes made of DPPC (a replacement of the PS), featured a faster opening and release of the liposomes content (Pinheiro et al., 2011).

In conclusion, the obtained results provide a motivation for further studies involving more complex models with other lipids and the PS proteins, as well as natural PS surfactants. We expect that the analogues of rifabutin and specifically RFB2 have an impact in the TB treatment. Moreover, the knowledge of the consequences of the antimycobacterial compounds on the biophysical properties of the PS membrane may be useful to understand their bioavailability and toxicity, allowing the design of more effective and less toxic anti-TB drugs.

Acknowledgements

Marina Pinheiro, João M. Caio and Cláudia Nunes thank FCT (Lisbon) for the fellowships (SFRH/BD/63318/2009, SFRH/BD/66789/2009 and SFRH/BPD/81963/2011), respectively. Juan J. Giner-Casares acknowledges Alexander von-Humboldt foundation for a postdoctoral fellowship. The authors thank the Spanish CICYT for financial support of this research in the framework of Projects CTQ2010-17481 and also the Junta de Andalucía (Consejería de Innovacion, Ciencia y Empresa) for special financial support (P08-FQM-4011 and P10-FQM-6703). Authors are grateful to the FCT for financial support under projects PEst-OE/QUI/UI0612/2011 and PTDC/QUI-QUI/101022/2008 with co-participation European Community funds from the FEDER, QREN and COMPET. The authors thank HASYLAB at DESY, Hamburg, Germany, for beam time and support through the project II-20100139 EC.

References

Agrawal, A.K., Gupta, C.M., 2000. Tuftsin-bearing liposomes in treatment of macrophage-based infections. Adv. Drug Deliv. Rev. 41, 135–146.

Amado, E., Kerth, A., Blume, A., Kressler, J., 2008. Infrared reflection absorption spectroscopy coupled with Brewster angle microscopy for studying interactions of amphiphilic triblock copolymers with phospholipid monolayers. Langmuir 24, 10041–10053.

Aydogan, N., Uslu, B., Tanaci, H., 2011. Biophysical investigation of the interfacial properties of cationic fluorocarbon/hydrocarbon hybrid surfactant: mimicking the lung surfactant protein C. J. Colloid Interface Sci. 360, 163–174.

Barry 3rd, C.E., Slayden, R.A., Sampson, A.E., Lee, R.E., 2000. Use of genomics and combinatorial chemistry in the development of new antimycobacterial drugs. Biochem. Pharmacol. 59, 221–231.

Brittes, J., Lucio, M., Nunes, C., Lima, J.L., Reis, S., 2010. Effects of resveratrol on membrane biophysical properties: relevance for its pharmacological effects. Chem. Phys. Lipids 163, 747–754.

Brogden, R.N., Fitton, A., 1994. Rifabutin. A review of its antimicrobial activity, pharmacokinetic properties and therapeutic efficacy. Drugs 47, 983–1009.

Calkovská, A., 2000. Pulmonary surfactant in the respiratory tract. Cesk. Fysiol. 49, 145–151.

Cameron, D.G., Gudgin, E.F., Mantsch, H.H., 1981. Dependence of acyl chain packing of phospholipids on the head group and acyl chain length. Biochemistry 20, 4496–4500.

Chen, X., Huang, Z., Hua, W., Castada, H., Allen, H.C., 2010. Reorganization and caging of DPPC, DPPE DPPG, and DPPS monolayers caused by dimethylsulfoxide observed using Brewster angle microscopy. Langmuir 26, 18902–18908.

Chimote, G., Banerjee, R., 2008. Effect of mycolic acid on surface activity of binary surfactant lipid monolayers. J. Colloid Interface Sci. 328, 288–298.

Chimote, G., Banerjee, R., 2010. In vitro evaluation of inhalable isoniazid-loaded surfactant liposomes as an adjunct therapy in pulmonary tuberculosis. J. Biomed. Mater. Res. B Appl. Biomater. 94, 1–10.

Cosimati, R., Milardi, G.L., Bombelli, C., Bonincontro, A., Bordi, F., Mancini, G., Risuleo, G., 2013. Interactions of DMPC and DMPC/gemini liposomes with the cell membrane investigated by electrorotation. Biochim. Biophys. Acta 1828, 352–356.

Czapla, K., Korchowiec, B., Rogalska, E., 2010. Differentiating oxicam nonsteroidal anti-inflammatory drugs in phosphoglyceride monolayers. Langmuir 26, 3485–3492.

Demchenko, A.P., Mely, Y., Duportail, G., Klymchenko, A.S., 2009. Monitoring biophysical properties of lipid membranes by environment-sensitive fluorescent probes. Biophys. J. 96, 3461–3470.

Dynarowicz-Latka, P., Dhanabalan, A., Oliveira Jr., O.N., 2001. Modern physicochemical research on Langmuir monolayers. Adv. Colloid Interface Sci. 91, 221–293.

Ferreira, H., Lucio, M., Lima, J.L., Matos, C., Reis, S., 2005. Interaction of clonixin with EPC liposomes used as membrane models. J. Pharm. Sci. 94, 1277–1287.

Figueiredo, R., Moiteiro, C., Medeiros, M.A., da Silva, P.A., Ramos, D., Spies, F., Ribeiro, M.O., Lourenco, M.C., Junior, I.N., Gaspar, M.M., Cruz, M.E., Curto, M.J., Franzblau, S.G., Orozco, H., Aguilar, D., Hernandez-Pando, R., Costa, M.C., 2009. Synthesis and evaluation of rifabutin analogs against *Mycobacterium avium* and H(37)Rv MDR and NRP *Mycobacterium tuberculosis*. Bioorg. Med. Chem. 17, 503–511.

Flach, C.R., Gericke, A., Mendelsohn, R., 1997. Quantitative determination of molecular chain tilt angles in monolayer films at the air/water interface: infrared reflection/absorption spectroscopy of behenic acid methyl ester. J. Phys. Chem. B 101, 58–65.

Foglia, F., Barlow, D.J., Szoka, F.C., Huang, Z., Rogers, S.E., Lawrence, M.J., 2011. Structural studies of the monolayers and bilayers formed by a novel cholesterol-phospholipid chimera. Langmuir 27, 8275–8281.

Gandhi, N.R., Nunn, P., Dheda, K., Schaaf, H.S., Zignol, M., van Soolingen, D., Jensen, P., Bayona, J., 2010. Multidrug-resistant and extensively drug-resistant tuberculosis: a threat to global control of tuberculosis. Lancet 375, 1830–1843.

Giner-Casares, J.J., Camacho, L., Martin-Romero, M.T., Cascales, J.J., 2008a. A DMPA Langmuir monolayer study: from gas to solid phase. An atomistic description by molecular dynamics simulation. Langmuir 24, 1823–1828.

Giner Casares, J.J., Camacho, L., Martin-Romero, M.T., Lopez Cascales, J.J., 2008b. Effect of Na^+ and Ca^{2+} ions on a lipid Langmuir monolayer: an atomistic description by molecular dynamics simulations. Chemphyschem 9, 2538–2543.

Harishchandra, R.K., Saleem, M., Galla, H.J., 2010. Nanoparticle interaction with model lung surfactant monolayers. J. R. Soc. Interface 7 (Suppl. 1), S15–S26.

Jiménez-Millan, E., Giner-Casares, J.J., Martín-Romero, M.T., Brezesinski, G., Camacho, L., 2011. Chiral textures inside 2D achiral domains. J. Am. Chem. Soc. 133, 19028–19031.

Kaviratna, A.S., Banerjee, R., 2009. The effect of acids on dipalmitoyl phosphatidylcholine (DPPC) monolayers and liposomes. Colloids Surf. A: Physicochem. Eng. Aspects 345, 155–162.

Koul, A., Arnoult, E., Lounis, N., Guillemont, J., Andries, K., 2011. The challenge of new drug discovery for tuberculosis. Nature 469, 483–490.

Kunin, C.M., 1996. Antimicrobial activity of rifabutin. Clin. Infect. Dis. 22 (Suppl. 1), S3–S13, discussion S13-14.

Liu, X.Y., Yang, Q., Kamo, N., Miyake, J., 2001. Effect of liposome type and membrane fluidity on drug–membrane partitioning analyzed by immobilized liposome chromatography. J. Chromatogr. A 913, 123–131.

Lucio, M., Ferreira, H., Lima, J.L., Reis, S., 2006. Interactions between oxicams and membrane bilayers: an explanation for their different COX selectivity. Med. Chem. 2, 447–456.

Lucio, M., Ferreira, H., Lima, J.L., Reis, S., 2007. Use of liposomes to evaluate the role of membrane interactions on antioxidant activity. Anal. Chim. Acta 597, 163–170.

Magalhaes, L.M., Nunes, C., Lucio, M., Segundo, M.A., Reis, S., Lima, J.L., 2010. High-throughput microplate assay for the determination of drug partition coefficients. Nat. Protocol 5, 1823–1830.

Mattow, J., Siejak, F., Hagens, K., Becher, D., Albrecht, D., Krah, A., Schmidt, F., Jungblut, P.R., Kaufmann, S.H., Schaible, U.E., 2006. Proteins unique to intraphagosomally grown *Mycobacterium tuberculosis*. Proteomics 6, 2485–2494.

Mendelsohn, R., Mao, G., Flach, C.R., 2010. Infrared reflection–absorption spectroscopy: principles and applications to lipid–protein interaction in Langmuir films. Biochim. Biophys. Acta 1798, 788–800.
Merino, S., Vázquez, J.L., Domènech, Ò., Berlanga, M., Viñas, M., Montero, M.T., Hernández-Borrell, J., 2002. Fluoroquinolone–biomembrane interaction at the DPPC/PG lipid–bilayer interface. Langmuir 18, 3288–3292.
Michel, N., Fabiano, A.S., Polidori, A., Jack, R., Pucci, B., 2006. Determination of phase transition temperatures of lipids by light scattering. Chem. Phys. Lipids 139, 11–19.
Nunes, C., Brezesinski, G., Lima, J.L.F.C., Reis, S., Lucio, M., 2011a. Effects of non-steroidal anti-inflammatory drugs on the structure of lipid bilayers: therapeutical aspects. Soft Matter 7, 3002–3010.
Nunes, C., Brezesinski, G., Lopes, D., Lima, J.L., Reis, S., Lucio, M., 2011b. Lipid–drug interaction: biophysical effects of tolmetin on membrane mimetic systems of different dimensionality. J. Phys. Chem. B 115, 12615–12623.
Nunes, C., Brezesinski, G., Pereira-Leite, C., Lima, J.L., Reis, S., Lucio, M., 2011c. NSAIDs interactions with membranes: a biophysical approach. Langmuir 27, 10847–10858.
Peetla, C., Stine, A., Labhasetwar, V., 2009. Biophysical interactions with model lipid membranes: applications in drug discovery and drug delivery. Mol. Pharm. 6, 1264–1276.
Pereira-Leite, C., Carneiro, C., Soares, J.X., Afonso, C., Nunes, C., Lucio, M., Reis, S., 2013. Biophysical characterization of the drugs-membrane interaction: the case of propranolol and acebutolol. Eur. J. Pharm. Biopharm..
Pinheiro, M., Arede, M., Nunes, C., Caio, J.M., Moiteiro, C., Lucio, M., Reis, S., 2013. Differential interactions of rifabutin with human and bacterial membranes: implication for its therapeutic and toxic effects. J. Med. Chem. 56, 417–426.
Pinheiro, M., Lucio, M., Lima, J.L., Reis, S., 2011. Liposomes as drug delivery systems for the treatment of TB. Nanomedicine (London) 6, 1413–1428.
Pola, A., Michalak, K., Burliga, A., Motohashi, N., Kawase, M., 2004. Determination of lipid bilayer/water partition coefficient of new phenothiazines using the second derivative of absorption spectra method. Eur. J. Pharm. Sci. 21, 421–427.
Poulain, F.R., Clements, J.A., 1995. Pulmonary surfactant therapy. West. J. Med. 162, 43–50.
Roldan-Carmona, C., Giner-Casares, J.J., Perez-Morales, M., Martin-Romero, M.T., Camacho, L., 2012. Revisiting the Brewster angle microscopy: the relevance of the polar headgroup. Adv. Colloid Interface Sci. 173, 12–22.
Rugonyi, S., Biswas, S., Hall, S.B., 2008a. The biophysical function of pulmonary surfactant. Respir. Physiol. Neurobiol. 163, 244–255.
Rugonyi, S., Biswas, S.C., Hall, S.B., 2008b. The biophysical function of pulmonary surfactant. Respir. Physiol. Neurobiol. 163, 244–255.
Sachan, A.K., Harishchandra, R.K., Bantz, C., Maskos, M., Reichelt, R., Galla, H.J., 2012. High-resolution investigation of nanoparticle interaction with a model pulmonary surfactant monolayer. ACS Nano 6, 1677–1687.
Stevens, T.P., Sinkin, R.A., 2007. Surfactant replacement therapy. Chest 131, 1577–1582.
Vostrikov, V.V., Selishcheva, A.A., Sorokoumova, G.M., Shakina, Y.N., Shvets, V.I., Savel'ev, O.Y., Polshakov, V.I., 2008. Distribution coefficient of rifabutin in liposome/water system as measured by different methods. Eur. J. Pharm. Biopharm. 68, 400–405.
Vostrikov, V.V., Selishcheva, A.A., Sorokoumova, G.M., Shvets, V.I., 2007. Determination of the distribution coefficient of rifabutin by the fluorescence study in the system liposome–water. Biofizika 52, 521–526.
Wagner, K., Desbat, B., Brezesinski, G., 2008. Liquid–liquid immiscibility in model membranes activates secretory phospholipase A2. Biochim. Biophys. Acta 1778, 166–174.
Wang, Z., Li, X., Yang, S., 2009. Studies of dipalmitoylphosphatidylcholine (DPPC) monolayers embedded with endohedral metallofullerene (Dy@C82). Langmuir 25, 12968–12973.
Wang, Z., Yang, S., 2009. Effects of fullerenes on phospholipid membranes: a langmuir monolayer study. Chemphyschem 10, 2284–2289.
Winter, R., 2005. Chapter 2 – High Pressure Effects in Molecular Bioscience, Chemistry at Extreme Conditions. Elsevier, Amsterdam, pp. 29–82.
Wustneck, R., Perez-Gil, J., Wustneck, N., Cruz, A., Fainerman, V.B., Pison, U., 2005. Interfacial properties of pulmonary surfactant layers. Adv. Colloid Interface Sci. 117, 33–58.
Wüstneck, R., Wüstneck, N., Moser, B., Pison, U., 2002. Surface dilatational behavior of pulmonary surfactant components spread on the surface of a pendant drop 2. Dipalmitoyl phosphatidylcholine and surfactant protein B. Langmuir 18, 1125–1130.
Zuo, Y.Y., Keating, E., Zhao, L., Tadayyon, S.M., Veldhuizen, R.A., Petersen, N.O., Possmayer, F., 2008. Atomic force microscopy studies of functional and dysfunctional pulmonary surfactant films I. Micro- and nanostructures of functional pulmonary surfactant films and the effect of SP-A. Biophys. J. 94, 3549–3564.

7. Evaluation of the structure-activity relationship of rifabutin and analogs: a drug-membrane study.

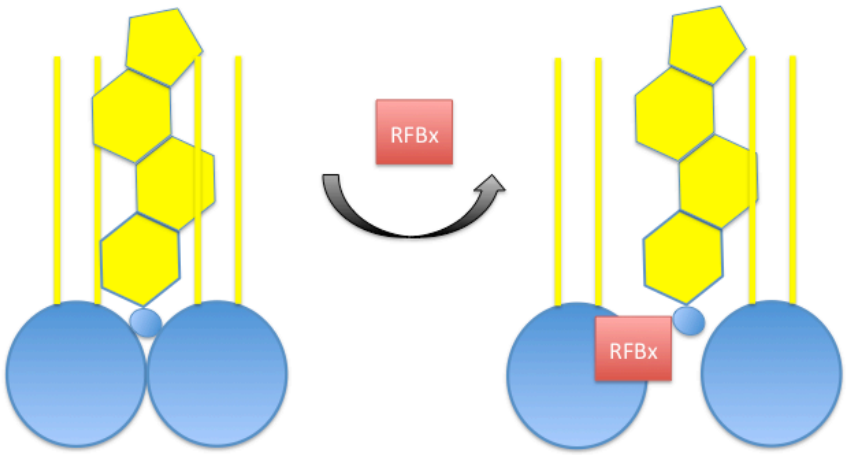

CHEMPHYSCHEM
ARTICLES
www.chemphyschem.org

DOI: 10.1002/cphc.201300262

Evaluation of the Structure–Activity Relationship of Rifabutin and Analogs: A Drug–Membrane Study

Marina Pinheiro,[a] Catarina Pereira-Leite,[a] Mariana Arêde,[a] Cláudia Nunes,[a] João M. Caio,[b] Cristina Moiteiro,[b] Juan J. Giner-Casares,[c, d] Marlene Lúcio,[a] Gerald Brezesinski,[d] Luis Camacho,[c] and Salette Reis*[a]

This work focuses on the influence of rifabutin and two novel analogs, namely, *N*′-acetyl-rifabutin and *N*′-butanoyl-rifabutin, on the biophysical properties of lipid membranes. Monolayers and multilamellar vesicles composed of egg L-α-phosphatidylcholine:cholesterol in a molar ratio of 4:1 are chosen to mimic biological membranes. Several accurate biophysical techniques are used to establish a putative relationship between the chemical structure of the antimycobacterial compounds and their activity on the membranes. A combination of in situ experimental techniques, such as Langmuir isotherms, Brewster angle microscopy, polarization-modulated infrared reflection–absorption spectroscopy, and small-angle X-ray scattering, is used to assess the drug–membrane interaction. A relationship between the effect of a drug on the organization of the membranes and their chemical structure is found and may be useful in the development of new drugs with higher efficacy and fewer toxic effects.

1. Introduction

Tuberculosis (TB), an ancient disease affecting humans, remains far from being eradicated.[1,2] In 2011 there were 8.7×10^6 incident cases of TB, 10^6 deaths from TB among HIV-negative people, and an additional 0.43×10^6 deaths from HIV-associated TB.[3] The re-emergence of and the concerns about TB have intensified the interest in finding newer and more effective drugs and stimulated the synthesis of new antibiotics.[4,5] Rifabutin (RFB, Figure 1), one of the most efficient antibiotics used in TB/HIV co-infection, was chosen in this study as the lead compound for new analogues showing promise against TB.[6,7] In this context, *N*′-acetyl-rifabutin (RFB2, Figure 1) was obtained from RFB by selective acylation of the secondary amino group, as previously described.[8] In addition, *N*′-butanoyl-rifabutin (RFB3, Figure 1) was obtained from RFB as described in the Experimental Section. In comparison to RFB, RFB2 has an extra acetyl group, has shown better in vitro and in vivo therapeutic indices, and is thus a promising drug for clinical application in TB treatment.[8] RFB3 bears a bulkier butanoyl group (COC_3H_7), which was added with the major goal of improving the pharmacokinetic properties as an anti-TB drug candidate. In addition, the partition coefficient log*P* predicted for RFB by using MarvinView 5.11.5 from Chemaxon was 4.53. The log*P* values predicted for the analogs were 5.53 for RFB2 and 5.68 for RFB3. Therefore, substitution of a hydrogen atom in the imidazole ring by an acetyl or a butanoyl group increases the hydrophobicity.

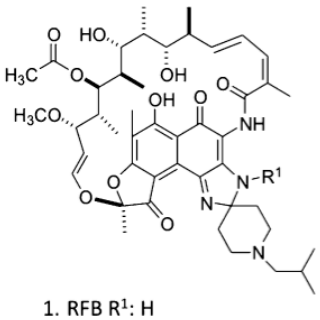

1. RFB R^1: H
2. RFB2 R^1:$COCH_3$
3. RFB3 R^1: COC_3H_7

Figure 1. Chemical structures of rifabutin (RFB), *N*′-acetyl-rifabutin (RFB2), and *N*′-butanoyl-rifabutin (RFB3).

Since the efficacy of antibiotics depends on complex drug–membrane interactions, antibiotic–cell membrane interactions play a crucial role in understanding the bioavailability of drugs, their entry into the cellular compartments, and drug-induced toxicity.[9–11] In this regard, a systematic comparison of the degree of penetration of RFB and two recently synthesized an-

[a] *M. Pinheiro, C. Pereira-Leite, M. Arêde, Dr. C. Nunes, Dr. M. Lúcio, Dr. S. Reis*
REQUIMTE
Departamento de Ciências Químicas
Faculdade de Farmácia, Universidade do Porto
Rua de Jorge Viterbo Ferreira n.° 228
4050-313 Porto (Portugal)
E-mail: shreis@ff.up.pt

[b] *J. M. Caio, Dr. C. Moiteiro*
Centro de Química e Bioquímica
Departamento de Química e Bioquímica
Faculdade de Ciências, Universidade de Lisboa (Portugal)

[c] *Dr. J. J. Giner-Casares, Dr. L. Camacho*
Departamento de Química Física y Termodinámica
Universidad de Córdoba, España (Spain)

[d] *Dr. J. J. Giner-Casares, Dr. G. Brezesinski*
Department of Interfaces
Max Planck Institute of Colloids and Interfaces
Science Park Golm, 14476 Potsdam (Germany)

alogs into membrane models, and their ability to induce changes in the biophysical properties of the membrane lipid bilayers was established, since their therapeutic and toxic effects seem to be strongly dependent on their lipid affinity. If any correlation is found, it will give useful indications for understanding the influence of different structural interdependencies between the chemical composition of an antimycobacterial compound and its expected effects.

In this study, two-dimensional (Langmuir monolayers) and three-dimensional [multilamellar vesicles (MLVs)] model systems that mimic the behavior of eukaryotic plasma membranes were chosen. Egg L-α-phosphatidylcholine (EPC) and cholesterol (CHOL) in a molar ratio of 4:1 were selected to elucidate the influence of the antimycobacterial compounds on the structure-packing behavior and molecular organization of the model membranes. Such lipids are major components of the outer layer of human membranes.[12] Phosphatidylcholines are the most abundant lipids in human cell membranes,[13] and EPC is a natural phosphatidylcholine obtained from egg yolk. Moreover, EPC comprises a mixture of zwitterionic phospholipids with the phosphatidylcholine head group but different saturated and unsaturated acyl chains, mostly 16:0 (sn1) and 18:1 or 18:2 (sn2).[14,15] Besides phospholipids, CHOL is also a major component of the human cell membrane,[9] and is fundamental not only to maintaining cell membrane structures,[10,11] such as lipid rafts,[12] but also to the physiology and function of the membrane.[16] Furthermore, CHOL has the ability to modulate the fluidity of the membranes and consequently their permeability.[17] Therefore, a 20 mol% fraction of CHOL was chosen in the binary mixture, since it has physiological relevance in mammalian cell membranes.[18]

Several accurate biophysical techniques were employed as potent tools to perform the above-mentioned investigations in the different membrane model systems. The effect of the antimycobacterial compounds on the phospholipid Langmuir monolayers was studied by a combination of experimental in situ techniques at the air/water interface.[19,20] Thermodynamic information was obtained from surface pressure–molecular area isotherms, which in association with Brewster angle microscopy (BAM) allowed images of the monolayer to be recorded on the micrometer scale.[13] Polarization-modulated infrared reflection–absorption spectroscopy (PM-IRRAS) provided important information about the molecular structure and orientation of the constituents of the monolayer.[21] The effect of the antimycobacterial compounds on the structure of EPC:CHOL (4:1) bilayer was investigated by small-angle X-ray scattering (SAXS).[22]

The results presented herein, besides unraveling the mechanism by which these antimycobacterial compounds diffuse across the membranes, demonstrate that the interactions of the antimycobacterial compounds with the membranes are dependent on small changes in their chemical structure. Additionally, a possible relationship between the modifications in the lead structure and the effects on the membranes was established, which allows prediction of their putative bioavailability and toxic effects.

2. Results and Discussion

2.1. Surface Pressure–Molecular Area Isotherms

Langmuir isotherms allow one to study the interactions between drugs and lipid monolayers, that is, their ability to penetrate into the lipid layer and the changes in the fluidity and permeability of the monolayer due to their incorporation.[24] In this work, the analyzed parameters from the surface pressure–molecular area (π–A) isotherms were the elastic modulus C_s^{-1}, the limiting area per EPC molecule in the compressed state A_{min}, and the collapse pressure $\pi_{collapse}$. The C_s^{-1} values were calculated from the π–A isotherms according to Equation (1):

$$C_s^{-1} = -A(d\pi/dA)$$

where A is the area per lipid molecule and π the surface pressure. The C_s^{-1} value describes the relationship between the increase in surface pressure and the decrease in area per molecule. A higher value of C_s^{-1} is indicative of a less compressible monolayer.[25,26] The A_{min} value corresponds to the mean area occupied by one molecule of EPC in the surface layer just before collapse. It is indicative of both the molecular packing and the interactions between the monolayer components.[27–29] The $\pi_{collapse}$ value corresponds to the beginning of a plateau region in the isotherm in which the surface pressure remains constant even with decreasing area, and is indicative of the stability of the monolayer.[30]

The π–A isotherms of EPC:CHOL (4:1) on phosphate buffer in the absence and in the presence of the antimycobacterial compounds are shown in Figure 2. The EPC:CHOL monolayers exhibited a well-defined lift-off point at 120 Å^2 per EPC molecule. This point indicates the end of the transition region between the gaseous and liquid-expanded phases. Moreover, the C_s^{-1} value obtained for the EPC:CHOL monolayer lies in the typical range of liquid-condensed states (100–250 mN m^{-1}). Thus, and as previously reported by several authors, the pres-

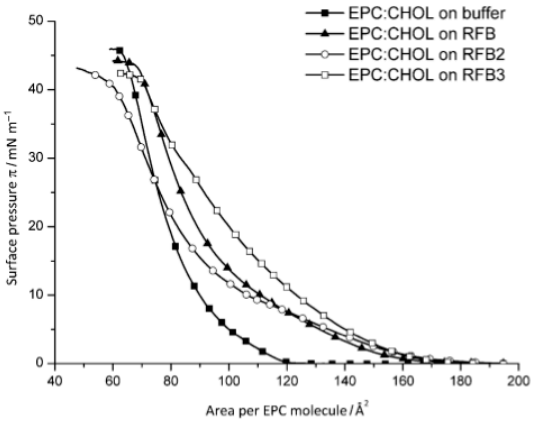

Figure 2. Surface pressure–molecular area (π–A) isotherms of EPC:CHOL (4:1 molar ratio) and EPC:CHOL (4:1) on a subphase containing RFB, RFB2, or RFB3 (0.118 μM).

CHEMPHYSCHEM
ARTICLES
www.chemphyschem.org

ence of 20 mol% of CHOL molecules at the air/water interface was enough to promote significant condensation of the fluid EPC monolayer through hydrogen bonds and van der Waals forces.[17,31–34]

According to the C_s^{-1} values obtained for EPC monolayers, described in previous works, the CHOL molecules, as expected, decrease the fluidity of the EPC monolayer.[15,35,36] The collapse pressure of 46 mN m^{-1} obtained for EPC:CHOL (4:1) (Table 1) is slightly lower than that reported for pure EPC

Table 1. Elastic modulus C_s^{-1}, limiting area per EPC molecule in the compressed state A_{min}, and collapse pressure $\pi_{collapse}$ of Langmuir monolayers of EPC:CHOL (4:1 molar ratio) on a phosphate buffer subphase and a subphase containing 0.118 μM of RFB, RFB2, or RFB3, respectively.

	A_{min} [Å^2 molecule^{-1}]	$\pi_{collapse}$ [mN m^{-1}]	C_s^{-1}
EPC:CHOL	60 ± 1	46 ± 1	221 ± 10
EPC:CHOL:RFB	66 ± 1	44 ± 1	136 ± 10
EPC:CHOL:RFB2	59 ± 1	42 ± 1	96 ± 10
EPC:CHOL:RFB3	68 ± 1	43 ± 1	97 ± 10

(≈50 mN m^{-1}).[15] The isotherms of EPC:CHOL in the presence of the antimycobacterial compounds have different shapes to that of EPC:CHOL. The most notable distinct feature is the expansion of the monolayer to clearly larger areas at low surface pressures (Figure 2).[37] The expansions of the molecular area in the EPC:CHOL monolayer caused by the presence of RFB, RFB2, and RFB3 are similar (ca. 50 Å^2 per EPC molecule) for surface pressures close to 0 mN m^{-1}. The expansion of the π–A isotherm of EPC:CHOL at a surface pressure of 30 mN m^{-1} decreases to about 10 and 6 Å^2 per EPC molecule in the presence of RFB3 and RFB, respectively. In the case of RFB2, the expansion to larger areas is not observed for surface pressures above 25 mN m^{-1}. The presence of a crossover shows that the monolayer can be compressed to smaller areas in the presence of RFB2. Thus, the interactions of the antimycobacterial compounds with the EPC:CHOL monolayer are more pronounced for lower pressures, as revealed by expansion to larger areas, which suggests that penetration of the antimycobacterial molecules into less-compressed lipid monolayers is easier. Nevertheless, additional processes may occur: "squeezing out" of existing antimycobacterial molecules at the air/solution interface on compression, rearrangement of the molecules/aggregates, and conformational changes of the molecules.[15] The maximum expansion occurred for RFB3 and was less pronounced for RFB2. The presence of the antimycobacterial compounds is responsible for the decay of C_s^{-1}, that is, addition of the antimycobacterial compounds leads to a more compressible monolayer. Hence, the maximum value of C_s^{-1} subsequently decreased with increasing lipophilicity in the sequence RFB3 ≈ RFB2 < RFB. The higher A_{min} values obtained for RFB and RFB3 reveal that the antimycobacterial compounds are still incorporated at pressures above the monolayer–bilayer equivalence surface pressure of about 30 mN m^{-1} and act as spacers between the lipid molecules. On the other hand, the lower A_{min} values obtained for RFB2 suggest that it can reduce the steric and/or dipolar repulsions between the polar regions of the lipids. This may be due to a change in the orientation and/or hydration of the lipids provoked by RFB2.[26] Additionally, the collapse pressure was not significantly affected by the presence of the antimycobacterial compounds, especially in the case of RFB, which is an indication of maintenance of the monolayer stability.[38] This may be interpreted in terms of complete "squeezing-out" of the antimycobacterial compounds from the monolayer to the subphase. Furthermore, analysis of the isotherms in terms of the area expansion and C_s^{-1} revealed a strong interaction of the antimycobacterial compounds with the lipid membrane model. Therefore, this interaction is more pronounced in the case of RFB3 as this compound is the bulkiest and the most lipophilic.

2.2. Brewster Angle Microscopy

Brewster angle microscopy (BAM) is a powerful technique that allows one to visualize domains in the two-phase coexistence region between fluid and condensed phase and enables direct visualization of the domain shape and inner texture.[39,40] Additionally, BAM gives information about the fluidity of the monolayer in relation to the geometry of the domains observed at the air/water interface.[41] Thus, the contrast in BAM images is due to local differences in the refractive index of the monolayer, caused by differences in the local molecular density or packing.[42] In BAM images, the dark background corresponds to the fluid phase, and the light gray areas to the condensed domains at the interface.[43,44]

The BAM images acquired during the first compression of the EPC:CHOL monolayer on a phosphate buffer subphase are depicted in Figure 3. To the best of our knowledge, this was the first time that this lipid mixture (EPC:CHOL, 4:1 molar ratio) was characterized by BAM. The morphology of the EPC monolayer is described in the literature in terms of the formation of noncircular-shaped domains at low pressures and a homogenous condensed phase for pressures above 25 mN m^{-1}.[35] On the other hand, the monolayers of CHOL are characterized by the appearance of small brighter spots on a fluid background.[45,46] It is well-known that CHOL molecules can undergo tight packing with phosphatidylcholines, which results in the formation of domains in the membranes and liquid-ordered phases in artificial systems.[34] Therefore, before compression of the monolayer it is possible to observe the existence of "elliptic vacuoles", which are attributed to the coexistence of two phases (Figure 3, marked with arrows).[36,38] On compression, small circular nuclei of a presumably liquid-condensed phase are seen on the black background of a liquid-disordered phase. These liquid-condensed lipid domains exhibit a homogenous distribution. During compression the nuclei gradually increase in size until the monolayer collapses. This regular distribution may occur to maximize the CHOL–CHOL separation, and according to the "umbrella model" the polar head groups of the phospholipids act as a shield for the large hydrophobic CHOL molecules with only a small hydroxyl group making contact with water.[18] Therefore, these lipid aggregates may result from the interaction between CHOL and phosphatidylcholine

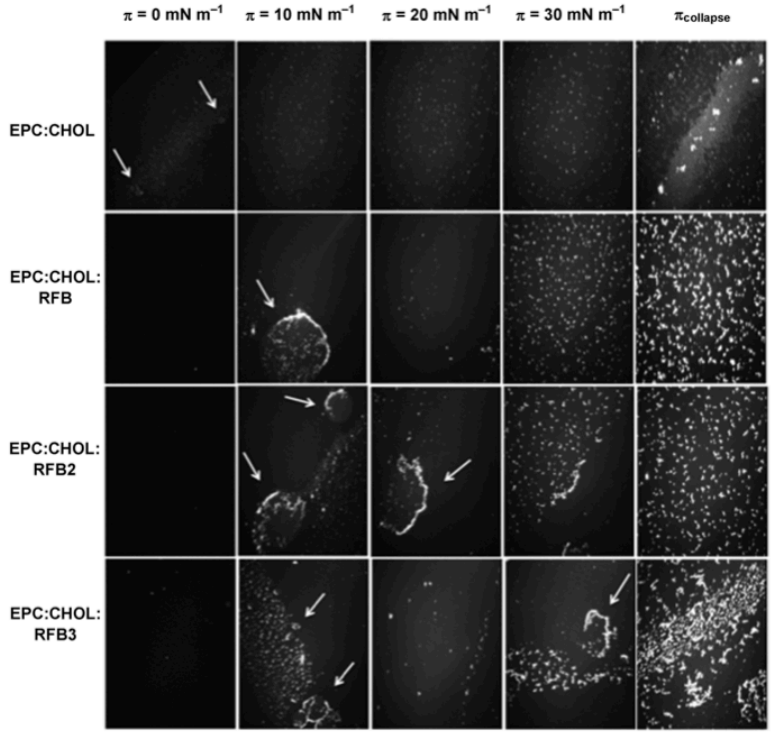

Figure 3. BAM images of Langmuir monolayers of EPC:CHOL (4:1 molar ratio) on a phosphate buffer subphase and on a subphase containing 0.118 μM of RFB, RFB2, or RFB3 for $\pi = 0$, 10, 20, 30 mN m^{-1}, and $\pi_{collapse}$.

molecules.[45] The observed condensed domains are probably due to the formation of aggregates of CHOL with saturated PC, since CHOL selectively interacts with saturated chains even in a mixed-chain environment.

The BAM images recorded in the presence of the antimycobacterial compounds are in good agreement with the lower lipid packing density and consequent fluidization of the EPC:CHOL monolayer. Therefore, the antimycobacterial compounds suppress the formation of the monodisperse condensed domains up to lateral pressures of 20 mN m^{-1} in the case of RFB and 30 mN m^{-1} for the analogs. Moreover, the brighter regions observed are due to the presence of antimycobacterial molecules at the air/solution interface, recognizable in the form of relatively thick local aggregates with a high refractive index, as previously described.[10] Additionally, these bright spots emerging for pressures above 0 mN m^{-1} are in an localized pattern and appear to be associated with larger islands, which result from the phase separation (Figure 3, marked with arrows). Thus, the segregation of the monolayer takes place in the presence of the antimycobacterial compounds, which suggest that RFB and its analogs are responsible for changes in the molecular packing of the lipid mixture at the air/solution interface. This is in accordance with intercalation of the molecules of the antimycobacterial compounds between EPC and CHOL molecules, which possibly promotes an excess of free CHOL molecules by hindering their binding to EPC molecules.

2.3. Polarization-Modulated Infrared Reflection–Absorption Spectroscopy

Polarization-modulated infrared reflection–absorption spectroscopy (PM-IRRAS) of lipid/protein monolayers in situ at the air/water interface provides information about the molecular structure and orientation of the constituents of the monolayers.[21,47] Moreover, PM-IRRAS allows monitoring of the vibrational spectra of the characteristic head groups of the phospholipids, such as phosphate and carbonyl present at the air/solution interface during compression of the monolayer.[21,23] The band positions of the asymmetric phosphate and carbonyl stretching vibrations in the EPC:CHOL monolayer in the absence and presence of the antimycobacterial compounds are listed in Table 2. Analysis of the phosphate and carbonyl bands is of special interest and allowed the interactions of the antimycobacterial compounds with the polar phospholipid head groups to be monitored. On the other hand, these groups are sensitive to the hydration state of the monolayer. A shift to lower wavenumbers indicates an increase in hydration of the phosphate and carbonyl moieties on interaction with the antimycobacterial compounds.[26] Thus, the systematic comparison of the interactions of the antimycobacterial compounds with the lipid monolayer was undertaken at three different surface pressures: 10, 20, and 30 mN m^{-1} (with more biological relevance).[15] For the

Table 2. Vibrational wavenumbers (asymmetric phosphate and carbonyl) of the EPC:CHOL (4:1 molar ratio) monolayers in the absence and in the presence of RFB, RFB2, or RFB3 (0.118 μM) for $\pi = 10$, 20, and 30 mN m^{-1}.

	$\pi = 10$ mN m^{-1}		$\pi = 20$ mN m^{-1}		$\pi = 30$ mN m^{-1}	
	$\tilde{\nu}(PO_2^-)$ [cm^{-1}]	$\tilde{\nu}$(C=O) [cm^{-1}]	$\tilde{\nu}(PO_2^-)$ [cm^{-1}]	$\tilde{\nu}$(C=O) [cm^{-1}]	$\tilde{\nu}(PO_2^-)$ [cm^{-1}]	$\tilde{\nu}$(C=O) [cm^{-1}]
EPC:CHOL	1230	1762	1261	1745	1219, 1256	1763
EPC:CHOL:RFB	1224, 1249	1732	1242	1742	1250	1733
EPC:CHOL:RFB2	1241, 1261	1725	1259	1745	1258	1735
EPC:CHOL:RFB3	1221, 1258	1729	1240, 1259	1707 1743	1255	1763

EPC:CHOL mixture, the $\nu(PO_2^-)$ stretching band shifts to higher wavenumbers on compression (from 10 to 20 mN m^{-1}), and this indicates decreased hydration of the phosphate groups. However, the opposite happens with the ν(C=O) stretching band, and the shift to lower wavenumbers during compression is possibly attributable to hydrogen bonding between the hydroxyl group of the CHOL molecule and the carbonyl group of EPC.[48]

Significant changes of the $\nu(PO_2^-)$ and ν(C=O) stretching bands in the presence of the antimycobacterial compounds suggest strong interactions with the polar head groups of the phospholipid, possibly by formation of hydrogen bonds. Thereby, extended hydrogen bonding between the hydroxyl groups of the antimycobacterial compounds and the phospholipids is expected to take place. Table 2 indicates that, independent of the surface pressure, the interactions with the phosphate groups of EPC are more pronounced with RFB, as indicated by the larger shifts in the positions of the stretching bands in comparison with the analogues. Moreover, at physiological pH, in comparison with its analogues, RFB has a higher contribution of the positively charged species. Substitution of the imidazole moiety ($pK_a = 3.5$; Figure 1) probably leads to weaker electrostatic interactions with the negatively charged phosphate group of EPC.[49] On the other hand, RFB2 and RFB3 are bulkier than RFB and, due to their extra lipophilic groups, they may be located closer to the phospholipid tails. In the presence of RFB and at a surface pressure of 10 mN m^{-1}, the contour of the $\nu(PO_2^-)$ band consists of two overlapping contributions that correspond to dihydrated and monohydrated phosphate groups. The ν(CO) stretching band at 1730 cm^{-1} arises from hydrated C=O bonds. At higher surface pressures, the monolayer is more hydrated, and this suggests a high degree of hydrogen bonding between the drug and the phospholipids. Regarding the effect of RFB2 in the EPC:CHOL monolayer, at lower surface pressure, the phosphate band consists of at least two overlapping contributions, at 1241 and at 1261 cm^{-1}, which probably correspond to monohydrated and unhydrated phosphate groups, respectively. Nevertheless, the shift to lower values of the ν(C=O) stretching band is indicative of the establishment of hydrogen bounds at this surface pressure. Thus, considering its lipophilic group, even at lower surface pressures RFB2 is probably located near the hydrophobic tails. With increasing pressure, the wavenumbers of the $\nu(PO_2^-)$ and ν(C=O) vibrations are shifted to lower values in comparison with EPC:CHOL, which is suggestive of a more hydrated monolayer. RFB3 also interacts with the phospholipid head groups of the EPC:CHOL monolayer, as is confirmed by the shift induced in the $\nu(PO_2^-)$ and ν(C=O) bands for pressures of 10 and 20 mN m^{-1}. At higher pressures (30 mN m^{-1}), the wavenumbers are very similar to those observed in the EPC:CHOL monolayer, which together with the higher A_{min} value attained, suggests deeper penetration into the acyl chain region, possibly with establishment of hydrophobic interactions with the phospholipid tails.

2.4. Small-Angle X-ray Scattering

Small-angle X-ray scattering (SAXS) is one of the most powerful techniques for characterization of the structure and dynamics of biomimetic systems. Regarding membranes, SAXS is useful to study the insertion of biomolecules or xenobiotics into bilayers and accurately determine the structural alterations induced by that interaction.[38,48]

The interaction of the antimycobacterial compounds with EPC:CHOL (4:1) bilayers was assessed by SAXS at 20, 37, and 45 °C and pH 7.4 to evaluate the effect of the drugs on the long-range bilayer order. The long-range distances d_1 and correlation lengths ξ of the first-order Bragg peak determined from SAXS diffraction patterns are listed in Table 3. Figure 4 displays the SAXS diffraction patterns obtained at physiological temperature (37 °C).

Table 3. Long-range repeat distances d_1 and correlation lengths ξ determined from SAXS patterns at pH 7.4 and 20, 37, and 45 °C.

	c_{drug} [mol%]	20 °C		37 °C		45 °C	
		d_1 [Å]	ξ_1 [Å]	d_1 [Å]	ξ_1 [Å]	d_1 [Å]	ξ_1 [Å]
EPC:CHOL	0	65.7±0.5	1390±10	65.8±0.5	1296±10	65.7±0.5	1069±10
EPC:CHOL:RFB	5	68.2±0.5	1252±10	68.5±0.5	988±10	68.9±0.5	853±10
	20	70.6±0.5	867±10	70.5±0.5	847±10	70.7±0.5	812±10
EPC:CHOL:RFB2	5	67.2±0.5	1222±10	67.7±0.5	1051±10	67.8±0.5	974±10
	20	68.3±0.5	1780±10	68.9±0.5	1603±10	69.6±0.5	1482±10
EPC:CHOL:RFB3	5	68.1±0.5	544±10	68.2±0.5	455±10	68.3±0.5	410±10
	20	67.6±0.5	486±10	68.6±0.5	339±10	69.2±0.5	313±10

The results obtained indicate that at all temperatures studied the EPC:CHOL mixture self-assembles into a lamellar phase, which is in agreement with the previously reported results.[50] Compared to the reported d_1 value for pure EPC bilayers ($\approx$57 Å),[51] the incorporation of 20 mol% of CHOL leads to a pronounced increase in bilayer thickness at all temperatures studied (Table 3), which may result from a decrease in tilt angle of the EPC acyl chains and/or increase in the thickness of hydration layer between the EPC:CHOL bilayers. Indeed, it was already proposed that CHOL induces reorientation of the hydrocarbon chains of phospholipids that become fully extended with a vertical orientation within the bilayer, which results in a more ordered bilayer, as discussed above. Furthermore, it was also reported that the presence of CHOL within phosphatidylcholine bilayers leads to an increase of the hydration layer, likely due to the effect of CHOL as a spacer molecule, which allows the water to further penetrate into the head-group region.[50,52] The data in Table 3 reveal that the long-range distances of the EPC:CHOL bilayer are practically temperature independent, whereas its correlation length decreases with increasing temperature. Indeed, it was already reported that the

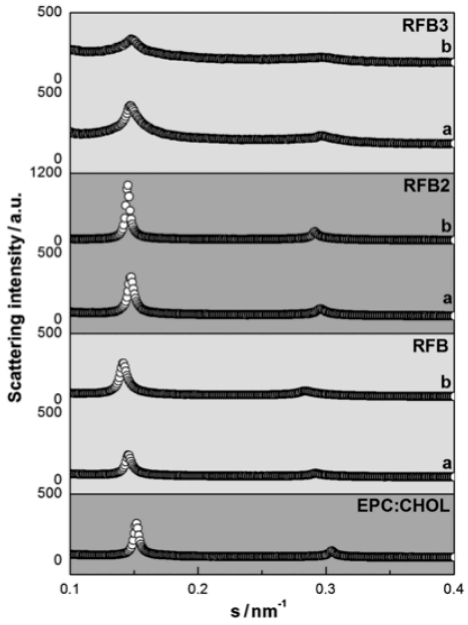

Figure 4. SAXS profiles at 37 °C for EPC:CHOL (4:1 molar ratio) and mixtures of EPC:CHOL with 5 (a) and 20 mol% (b) RFB, RFB2, or RFB3 at pH 7.4.

bilayer order decreases with increasing temperature.[53] The disordering effect of the temperature may be correlated with a gradual increase in the spaces between the phospholipid and CHOL molecules, which leads to a decrease in bilayer cooperativity.

At all temperatures studied, the insertion of RFB and its analogs into the EPC:CHOL bilayers leads to an increase of their repeat distance and a decrease of their correlation length (Table 3). Since EPC:CHOL bilayers are in the L_o (liquid-ordered) phase, the increase of the d_1 values in the presence of the antimycobacterial compounds is due to a change in hydration of the phospholipid head groups, which leads to an increase in the thickness of the water layer between the bilayers. Additionally, the decrease in peak correlation length demonstrates that RFB and its analogs have a disordering effect on the bilayer structure. The peak correlation length is an indication of the bilayer cooperativity, and its decrease on insertion of the antimycobacterial compounds into the EPC:CHOL bilayers is revealed by the broadening of the peaks in Figure 4. Table 3 reveals that RFB and its analogs have different effects on the order of the EPC:CHOL bilayer. Although all the antimycobacterial compounds generally increase the d_1 value as a function of concentration at all temperatures studied, RFB has the most pronounced effect on this parameter, increasing the d_1 value by 5 Å for the EPC:CHOL system with 20 mol% of drug. This is in close agreement with the above results from the isotherms concerning the larger area requirement per EPC molecule in the presence of RFB at all studied pressures and the pronounced shifts of the $\nu(PO_2^-)$ and $\nu(CO)$ peaks, and endorses the strong interactions of these compounds with the polar head groups of EPC, mediated by hydrogen bonds and probably by more pronounced electrostatic interactions in comparison to the analogs. In contrast to the other antimycobacterial compounds, which decrease the peak correlation length with increasing concentration, 5 mol% of RFB2 decreases the cooperativity of the EPC:CHOL bilayer, whereas 20 mol% of RFB2 leads to an increase of the first-order peak correlation length at all temperatures studied. This difference in behavior may be ascribable to the higher RFB2 concentrations being able to screen the negative charges of the phosphate groups in the phospholipid EPC, which reduces the electrostatic interactions between the phosphatidylcholine dipoles.[26] Regarding the correlation length, RFB3 has the most prominent effect on the cooperativity of the EPC:CHOL bilayers at all temperatures, which is demonstrated by the low ξ_1 values obtained (Table 3) and the existence of very broad peaks in the SAXS patterns (see Figure 4). This may be due to its higher lipophilicity and deeper penetration into the phospholipid tail region, which compromises the close packing of EPC with CHOL molecules and results in a less ordered bilayer.

3. Conclusions

The effect of antimycobacterial compounds (RFB, RFB2, and RF3) on the physicochemical properties of two- and three-dimensional models of cell membranes was investigated by means of Langmuir isotherms, BAM, PM-IRRAS, and SAXS. These techniques allow one to study the influence of RFB and its synthetic analogs on membrane structure and fluidity and thus to understand how these compounds diffuse across cell membranes. The results support modification of the molecular packing in the surfaces of EPC:CHOL membrane models due to interaction of the antimycobacterial compounds with the polar head group of the phospholipids, which is essential for closer packing of the membrane phospholipids with the CHOL molecules. Therefore, antimycobacterial compounds inserted in the monolayer seem to be intercalated between CHOL:EPC, and this leads to phase separation of the lipid mixture.[38] Moreover, it is well-known that CHOL is a key compound for understanding the pathogenesis of TB. Indeed, the presence of CHOL is essential for uptake of the etiological agent of TB by macrophages, and it has been found to accumulate at the site of entrance of bacteria. Thus, these antimycobacterial compounds seem to decrease the acyl-chain order by interacting with the phospholipid head groups and hindering coverage of the polar phospholipid head groups by the nonpolar bodies of CHOL. In vivo this effect is expected to promote an increase in membrane permeability, which will enable a higher concentration of the antibiotic to reach the target.[18] Although incorporation of all of the antimycobacterial compounds into membranes induces less ordered packing, they exhibit quantitatively distinctive effects which are ascribed to their location in the membrane. The obtained results pointed to different interactions with the membranes, which are attributed to the differences in the chemical structures of the antimycobacterial compounds. Therefore, the increase in the lipophilicity of the antimycobacterial compound and addition of a bulky moiety

(RFB2 and RFB3 versus RFB) are responsible for pronounced changes in lipid packing. Thus, in comparison with RFB, the acetyl and butanoyl groups of the analogs are responsible for deeper interactions with the membranes. Hereby, the less pronounced ionic bonds and the extra lipophilic groups permit the establishment of marked van der Waals forces, which were found to be related to the penetration abilities of these analogs. Consequently, in vivo, RFB2 and RFB3 are expected to promote more pronounced membrane fluidization and greater diffusion across biological cell membranes compared to RFB. Moreover, the results of our study support deeper and more pronounced changes in the biophysical properties of the membranes for the RFB analogs, since substitution of the secondary amino group with additional lipophilic groups was responsible for marked interactions with the membranes. These higher lipid affinities should increase access of the antibiotic to the cells in which the bacteria are located and its entry into the extremely lipophilic mycobacterial membranes.[54] On the other hand, it is well known that the toxic effects of this class of drugs are strongly influenced by their affinity to biological membranes.[55] Therefore, the RFB analogs may exhibit more pronounced side effects as the discoloration of the skin, eyes, and body fluids, and further studies are needed to ensure their safety before they can reach the market.[55]

In summary, we have provided a comprehensive study of the interaction of RFB and its analogs with lipids, providing useful information about the relationship between the chemical structures of the antimycobacterial compound and changes in the biophysical properties of the membrane. The knowledge about the structure–activity relationship of the drugs in the membranes and the lipid–drug interaction is crucial to understanding the mechanism of action at the molecular level, which is essential to develop more effective and safer antibiotics to effectively fight TB.

Experimental Section

Materials

EPC and CHOL were purchased from Avanti Polar Lipids and used as received. The mixture of EPC contains approximately 46% of saturated phosphatidylcholines, of which dipalmitoylphosphatidylcholine is the predominant compound (32.7%). RFB was isolated from Mycobutin and further purified as previously described.[8] RFB2 was obtained from RFB by selective acylation of the secondary amino group, as previously described.[8] RFB3 was also synthesized from RFB, as described below. Sodium chloride, monopotassium phosphate, and dipotassium phosphate (99% pure) were purchased from Panreac. *N*-(2-Hydroxyethyethyl)piperazine-*N*′-(2-ethanesulfonic acid) (HEPES) was purchased from Sigma-Aldrich Co. Chloroform and methanol were used as co-spreading solvents in the monolayer experiments. Chloroform/methanol (3/1 v/v) was used as the organic solvents in vesicle preparation. The 100 mM phosphate buffer (pH 7.4; 100 mM of sodium chloride) and 10 mM HEPES buffer (pH 7.4; 100 mM of sodium chloride) subphases were prepared from Millipore Milli-Q ultrapure water (resistivity: 18.2 MΩ cm^{-1}).

Synthesis

N′-Butanoyl-rifabutin (RFB3): Triethylamine (96 μL, 0.74 mmol) was added dropwise to a solution of rifabutin (200 mg; 0.23 mmol) in THF (5.9 mL) at −10 °C with stirring, followed by a solution of butanoyl chloride (52 μL, 0.74 mmol) in THF (3.9 mL), and the resulting mixture was left to stir till it reached room temperature (ca. 5 min). The resulting precipitate of triethylamine hydrochloride was removed by filtration and the solvent removed under reduced pressure. Then the product was extracted with ethyl acetate (3×20 mL) and the extract washed with water (3×10 mL), dried with $MgSO_4$, filtered, and evaporated to dryness. The product was purified by flash chromatography with ethyl acetate:hexane:methanol (3:4:0.2) as eluent to afford RFB3 as a homogeneous orange solid in 43% yield. ^{1}H NMR ($CDCl_3$): $\delta = -0.02$ (3H, brs, CH_3-34), 0.58 (3H, brs, CH_3-33), 0.68-1.15 (15H, m, CH_3-31, CH_3-11′, CH3-12′, CH_3-32, CH_3-41), 1.55-1.86 (9H, m, H-24, H-26, CH_3-13, H-22, CH_2-40), 1.88-2.19 (11H, m, H-10′, CH_2-6′, CH_2-4′, CH_3-36, CH_3-30), 2.14-2.40 (m, 5H, CH_2-39, CH_2-9′, H-20), 2.48 (3H, s, CH_3-14), 2.91-3.22 (m, 9H, CH_2-5′, CH_2-7′, H-23, H-21, CH_3-37), 3.37-3.42 (1H, m, H-27), 3.75 (1H, s, 23-OH), 3.87 (1H, s, 21-OH), 4.73-5.32 (2H, m, H-25, H-28), 5.82-6.35 (3H,m, H-19, H-29, H-17, H-18), 8.19 (1H, s, NH), 13.81 ppm (1H, s, 8-OH); ^{13}C NMR ($CDCl_3$): $\delta = 7.5$ (C-14), 8.5 (C-33), 10.7 (C-34, C-41), 10.8 (C-32), 13.7 (C-31), 20.6 (C-30, C-36), 21.0 (C-11′, C-12′, C-13), 25.6 (C-39, C10′), 32.9 (C-22), 36.3 (C-4′, C-8′), 37.2 (C-24), 38.1 (C-26, C-20), 39.3 (C-40), 51.1 (C-7′), 51.2, 51.2, 51.2 (C-5′, C-37), 65.7 (C-9′), 72.8 (C-21), 73.8 (C-25), 77.1 (C-23), 90.2 (C-27), 96.5 (C-2′), 106.0 (C-3), 108.8 (C-12), 111.0 (C-10), 113.6 (C-9), 114.4 (C-7, C-28), 128.8 (C-18), 130.6 (C-5), 136.2 (C-16, C-17), 141.2 (C-19), 141.5 (C-2), 142.2 (C-29), 153.1 (C-4), 166.6 (C-8), 166.7 (C-38, C-15) 172.4 (C-6, C-35), 186.1 (C-1), 191.4 ppm (C-11); TOF-MS: *m/z* 918 $[M+1]^+$, 917 $[M]^+$.

Langmuir Isotherms

Langmuir Troughs: Two different troughs (KN-1005 and NIMA 601, Nima Technology, Coventry, England) were equipped with two symmetrical barriers and a Wilhelmy-type dynamometric system by using a strip of filter paper. KN-1005 has nearly 325 mL subphase volume and close to 587 cm^2 total area. NIMA 601 has about 400 mL subphase volume with a total area close to 600 cm^2. KN-1005 was used in the PM-IRRAS experiments. Due to its larger capacity and area, NIMA 601 was used to obtain the isotherms.

Monolayer Spreading: The monolayers were prepared by spreading the lipid mixture (EPC:CHOL, 4:1 molar ratio) on the phosphate buffer subphase. The monolayers were spread by the deposition of tiny droplets of samples uniformly on the buffer surface by using a 250 μL microsyringe. After spreading, the solvent was allowed to evaporate for 15 min prior to monolayer compression. The effect of the antimycobacterial compounds was evaluated by spreading EPC:CHOL (4:1 molar ratio) monolayers on a phosphate buffer with a known concentration of RFB, RFB2, and RFB3 (0.118 μM).

Monolayer Compression: The monolayers were compressed at a rate of 20 cm^2 min^{-1}. During compression, surface pressure–molecular area (π–A) isotherms were recorded. All experiments were performed at 21 °C in an atmosphere with 100% relative humidity.

Brewster Angle Microscopy: Brewster angle microscopy (BAM) images were obtained from a I-Elli 2000 apparatus (supplied by Nanofilm Technologies, Göttingen, Germany) with an Nd:YAG diode laser. The lateral resolution was 2 μm. The image processing procedure included geometrical correction of the image and a filtering operation to reduce interference fringes and noise. Further-

more, the brightness of each image was scaled to improve contrast.

Polarization-Modulation Infrared Reflection–Absorption Spectroscopy: Polarization-modulation infrared reflection-absorption spectroscopy (PM-IRRAS) was performed with a KSV PMI 550 instrument (KSV Instruments Ltd, Helsinki, Finland) recording the spectra at 10, 20, and 30 mN m^{-1}. The Langmuir trough was set up so that the IR beam reached the monolayer at a fixed angle of incidence of 80°. The incoming light was continuously modulated between s and p polarization at a high frequency. This allowed simultaneous measurement of spectra for the two polarizations, whereby their difference provided surface-specific information, and their sum the reference spectrum (buffer or buffer with the antimycobacterial compound). PM-IRRAS was used due its advantages over the conventional IRRAS mode, namely, the independence of the modulated reflectivity of the isotropic adsorption from bulk water or water vapor, which allows the problem of the surrounding water vapor to be overcome.[21,23]

Multilamellar Vesicles

Different amounts of the antimycobacterial compounds were mixed with EPC:CHOL in chloroform:methanol (3:1 v:v) to give the required molar fraction of the antimycobacterial compound (5 and 20 mol%). The lipid films formed from these solutions were dried under a stream of N_2 at 50.0±0.1 °C and left overnight under reduced pressure to remove all traces of the organic solvents. The lipid films were hydrated by adding HEPES buffer and then alternately heated to 50.0±0.1 °C, mixed by vortexing for about 5 min, and centrifuged for 30 s at 2000 *g*. This procedure was repeated three times. Finally, the samples were aged overnight at 4.0± 0.1 °C and shaken by vortex at room temperature for 5 min. Thereafter, the dispersions were transferred into X-ray-transparent glass capillaries of 1.5 mm diameter (Hilgenberg, Malsfeld, Germany). The flame-sealed capillaries were stored at 4.0±0.1 °C until the measurements.

Small-angle X-ray scattering experiments were performed at the Soft Condensed Matter beamline A2 at Doris III of HASYLAB (DESY, Hamburg, Germany) with monochromatic radiation having a wavelength of 0.15 nm. The detector was calibrated with rat-tail tendon. The samples were measured at different temperatures (20.0±0.1, 37.0±0.1, and 45.0±0.1 °C). After each temperature step, the sample was allowed to equilibrate for 5 min before the diffraction pattern was recorded. To minimize the X-ray exposure of the sample, a shutter mounted before the sample was kept closed when no data were being acquired. The lamellar repeat distance *d* was calculated from the small-angle Bragg reflections by using Bragg's equation $s=n/d$, where $s=\lambda/2\sin\Theta$ is the scattering vector and n the order of the reflection ($n=1, 2, \ldots$). The diffraction peaks were fitted with Lorentzians and the positions of the maximum intensities and the full-widths of the peaks at half-height were determined.[22]

Acknowledgements

M.P., J.M.C., and C. N. thank FCT (Lisbon) for the fellowships SFRH/BD/63318/2009, SFRH/BD/66789/2009, and SFRH/BPD/81963/2011, respectively. J.J.G.-C. acknowledges Alexander von-Humboldt Foundation for a postdoctoral fellowship. The authors thank the Spanish CICYT for financial support of this research in the framework of Projects CTQ2010-17481 and also the Junta de Andalucía (Consejería de Innovacion, Ciencia y Empresa) for special financial support (P08-FQM-4011 and P10-FQM-6703). The authors are also grateful to the FCT for financial support under projects PEst-OE/QUI/UI0612/2011 and PTDC/QUI-QUI/101022/2008 with co-participation European Community funds from FEDER, QREN, and COMPETE. The authors thank HASYLAB at DESY, Hamburg, Germany, for beam time and support through the project II-20100139 EC. The authors are grateful to Dr. Sérgio Funari for help at beamline A2.

Keywords: antibiotics · monolayers · phospholipids · structure–activity relationships · vesicles

[1] M. Pinheiro, M. Lucio, J. L. Lima, S. Reis, *Nanomedicine* **2011**, *6*, 1413–1428.
[2] A. Koul, E. Arnoult, N. Lounis, J. Guillemont, K. Andries, *Nature* **2011**, *469*, 483–490.
[3] World Health Organization: Global Tuberculosis Control 2012 Report (last accessed on Jan. 1, **2013**. Available from: http://apps.who.int/iris/bitstream/10665/75938/1/9789241564502_eng.pdf.
[4] N. R. Gandhi, P. Nunn, K. Dheda, H. S. Schaaf, M. Zignol, D. van Soolingen, P. Jensen, J. Bayona, *Lancet* **2010**, *375*, 1830–1843.
[5] Y. Benadie, M. Deysel, D. G. Siko, V. V. Roberts, S. Van Wyngaardt, S. T. Thanyani, G. Sekanka, A. M. Ten Bokum, L. A. Collett, J. Grooten, M. S. Baird, J. A. Verschoor, *Chem. Phys. Lipids* **2008**, *152*, 95–103.
[6] M. Sousa, A. Pozniak, M. Boffito, *J. Antimicrob. Chemother.* **2008**, *62*, 872–878.
[7] M. Gaspar, S. Neves, F. Portaels, J. Pedrosa, M. Silva, M. Cruz, *Antimicrob. Agents Chemother.* **2000**, *44*, 2424–2430.
[8] R. Figueiredo, C. Moiteiro, M. A. Medeiros, P. A. da Silva, D. Ramos, F. Spies, M. O. Ribeiro, M. C. Lourenco, I. N. Junior, M. M. Gaspar, M. E. Cruz, M. J. Curto, S. G. Franzblau, H. Orozco, D. Aguilar, R. Hernandez-Pando, M. C. Costa, *Bioorg. Med. Chem.* **2009**, *17*, 503–511.
[9] M. Lucio, J. L. Lima, S. Reis, *Curr. Med. Chem.* **2010**, *17*, 1795–1809.
[10] M. Pinheiro, M. Lucio, S. Reis, J. L. Lima, J. M. Caio, C. Moiteiro, M. T. Martin-Romero, L. Camacho, J. J. Giner-Casares, *J. Phys. Chem. B* **2012**, *116*, 11635–11645.
[11] M. Pinheiro, J. J. Giner-Casares, M. Lucio, J. M. Caio, C. Moiteiro, J. L. Lima, S. Reis, L. Camacho, *Biochim. Biophys. Acta Biomembr.* **2013**, *1828*, 896–905.
[12] P. Wydro, *Colloids Surf. B* **2012**, *93*, 174–179.
[13] E. Amado, A. Kerth, A. Blume, J. Kressler, *Langmuir* **2008**, *24*, 10041–10053.
[14] P. Tauc, C. R. Mateo, J. C. Brochon, *Biophys. J.* **1998**, *74*, 1864–1870.
[15] G. S. Lorite, T. M. Nobre, M. E. Zaniquelli, E. de Paula, M. A. Cotta, *Biophys. Chem.* **2009**, *139*, 75–83.
[16] J. B. Massey, H. S. She, A. M. Gotto, Jr., H. J. Pownall, *Biochemistry* **1985**, *24*, 7110–7116.
[17] A. K. Panda, P. Wojciechowski, K. Nag, F. Possmayer, N. Petersen, *J. Dispersion Sci. Technol.* **2009**, *30*, 1255–1261.
[18] A. Parker, K. Miles, K. H. Cheng, J. Huang, *Biophys. J.* **2004**, *86*, 1532–1544.
[19] J. J. G. Casares, L. Camacho, M. T. Martin-Romero, J. J. L. Cascales, *ChemPhysChem* **2008**, *9*, 2538–2543.
[20] J. J. Giner-Casares, L. Camacho, M. T. Martin-Romero, J. J. Cascales, *Langmuir* **2008**, *24*, 1823–1828.
[21] R. Mendelsohn, G. Mao, C. R. Flach, *Biochim. Biophys. Acta Biomembr.* **2010**, *1798*, 788–800.
[22] C. Nunes, G. Brezesinski, J. L. Lima, S. Reis, M. Lucio, *J. Phys. Chem. B* **2011**, *115*, 8024–8032.
[23] R. Marques de Oliveira, J. Ferreira, M. J. Santos, R. M. Faria, O. N. Oliveira, Jr., *ChemPhysChem* **2011**, *12*, 1736–1740.
[24] T. S. F. Schmidt, L. Caseli, T. M. Nobre, M. E. D. Zaniquelli, O. N. Oliveira, Jr., *Colloids Surf. A* **2008**, *321*, 206–210.
[25] Z. Wang, S. Yang, *ChemPhysChem* **2009**, *10*, 2284–2289.
[26] C. Nunes, G. Brezesinski, C. Pereira-Leite, J. L. Lima, S. Reis, M. Lucio, *Langmuir* **2011**, *27*, 10847–10858.

[27] T. Gross, E. Zmora, Y. Levi-Kalisman, O. Regev, A. Berman, *Langmuir* **2006**, *22*, 3243 – 3250.
[28] N. Aydogan, B. Uslu, H. Tanaci, *J. Colloid Interface Sci.* **2011**, *360*, 163 – 174.
[29] B. Lagane, S. Mazeres, C. Le Grimellec, L. Cezanne, A. Lopez, *Biophys. Chem.* **2002**, *95*, 7 – 22.
[30] P. D. Łatka, M. Pérez-Morales, E. Muñoz, M. Broniatowski, M. T. Martín-Romero, L. Camacho, *J. Phys. Chem. B* **2006**, *110*, 6095 – 6100.
[31] W. Y. Gao, P. J. Quinn, Z. W. Yu, *Mol. Membr. Biol.* **2008**, *25*, 485 – 497.
[32] C. Weeraman, M. Chen, D. J. Moffatt, R. Lausten, A. Stolow, L. J. Johnston, *Langmuir* **2012**, *28*, 12999 – 13007.
[33] I. Brzozowska, Z. A. Figaszewski, *Colloids Surf. B* **2002**, *23*, 51 – 58.
[34] K. B. Lintker, P. Kpere-Daibo, S. J. Fliesler, A. B. Serfis, *Chem. Phys. Lipids* **2009**, *161*, 22 – 31.
[35] D. Risović, S. Frka, Z. Kozarac, *J. Chem. Phys.* **2011**, *134*, 024701.
[36] M. M. Conde, O. Conde, J. M. Trillo, J. Minones, *J. Phys. Chem. B* **2010**, *114*, 10774 – 10781.
[37] M. A. Mitsche, L. Wang, D. M. Small, *J. Phys. Chem. B* **2010**, *114*, 3276 – 3284.
[38] B. W. Walker, N. Manhanke, K. J. Stine, *Biochim. Biophys. Acta Biomembr.* **2008**, *1778*, 2244 – 2257.
[39] R. Bartucci, N. Gulfo, L. Sportelli, *Biochim. Biophys. Acta* **1990**, *1025*, 117 – 121.
[40] D. Vollhardt, V. B. Fainerman, *Adv. Colloid Interface Sci.* **2010**, *154*, 1 – 19.
[41] M. Allouche, S. Castano, D. Colin, B. Desbat, B. Kerfelec, *Biochemistry* **2007**, *46*, 15188 – 15197.
[42] F. Bringezu, J. Ding, G. Brezesinski, A. J. Waring, J. A. Zasadzinski, *Langmuir* **2002**, *18*, 2319 – 2325.
[43] A. M. Gonçalves da Silva, R. I. Romão, *Chem. Phys. Lipids* **2005**, *137*, 62 – 76.
[44] C. Alonso, T. Alig, J. Yoon, F. Bringezu, H. Warriner, J. A. Zasadzinski, *Biophys. J.* **2004**, *87*, 4188 – 4202.
[45] K. J. Stine, R. K. Hercules, J. D. Duff, B. W. Walker, *J. Phys. Chem. B* **2006**, *110*, 22220 – 22229.
[46] M. M. Lipp, K. Y. Lee, A. Waring, J. A. Zasadzinski, *Biophys. J.* **1997**, *72*, 2783 – 2804.
[47] C. R. Flach, A. Gericke, R. Mendelsohn, *J. Phys. Chem. B* **1997**, *101*, 58 – 65.
[48] J. M. Berg, J. L. Tymoczko, L. Stryer, *Biochemistry, 5th ed.*, W. H. Freeman, New York, **2002**.
[49] V. V. Vostrikov, A. A. Selishcheva, G. M. Sorokoumova, Y. N. Shakina, V. I. Shvets, O. Y. Savel'ev, V. I. Polshakov, *Eur. J. Pharm. Biopharm.* **2008**, *68*, 400 – 405.
[50] E. Raquel, E. Richard in *The Structure of Biological Membranes, 3rd ed.*, CRC, New York, **2011**, pp. 133 – 152.
[51] P. J. Quinn, C. Wolf, *FEBS J.* **2010**, *277*, 4685 – 4698.
[52] C. Pereira-Leite, C. Nunes, J. L. Lima, S. Reis, M. Lucio, *J. Phys. Chem. B* **2012**, *116*, 13608 – 13617.
[53] J. A. Clarke, A. J. Heron, J. M. Seddon, R. V. Law, *Biophys. J.* **2006**, *90*, 2383 – 2393.
[54] B. R. Bloom, *Tuberculosis: Pathogenesis, Protection, and Control*, ASM Press, Washington D.C., **1994**.
[55] M. Pinheiro, M. Arêde, C. Nunes, J. M. Caio, C. Moiteiro, M. Lúcio, S. Reis, *J. Med. Chem.* **2013**, *56*, 417 – 426.

Received: March 15, 2013
Published online on ■■ ▮▮, 2013

8. The Influence of Rifabutin on Human and Bacterial Membrane Models: Implications for Its Mechanism of Action.

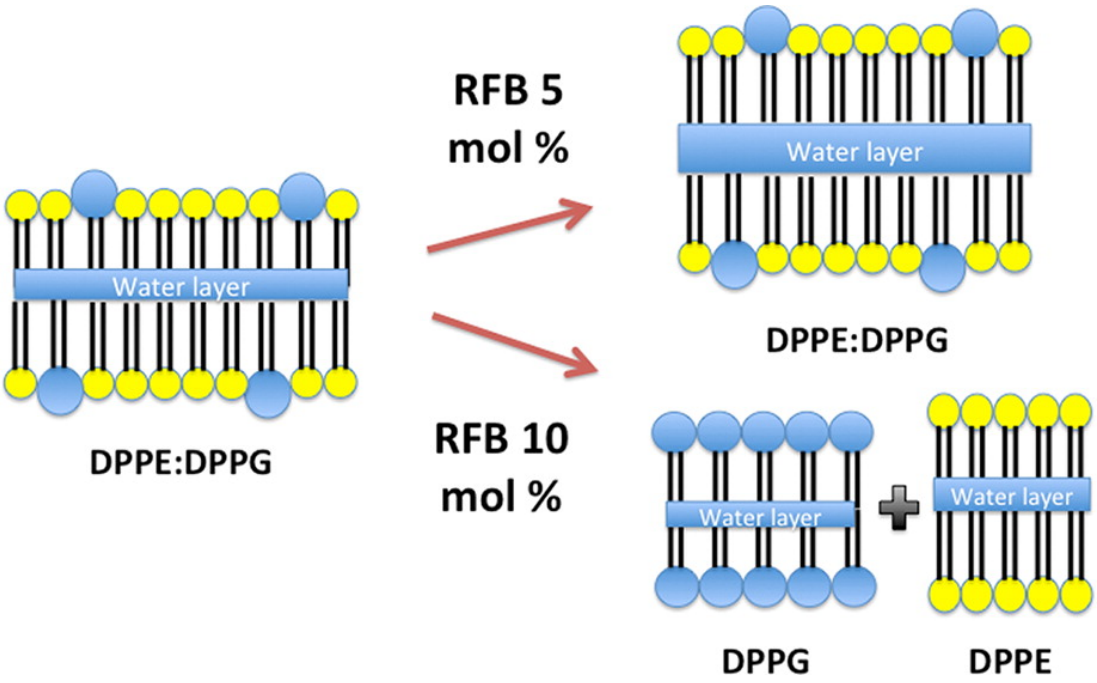

THE JOURNAL OF PHYSICAL CHEMISTRY B

Article

pubs.acs.org/JPCB

The Influence of Rifabutin on Human and Bacterial Membrane Models: Implications for Its Mechanism of Action

Marina Pinheiro,[†] Cláudia Nunes,[†] João M. Caio,[‡] Cristina Moiteiro,[‡] Marlene Lúcio,[†] Gerald Brezesinski,[§] and Salette Reis*,[†]

[†]REQUIMTE, Departamento de Ciências Químicas, Faculdade de Farmácia, Universidade do Porto, Portugal

[‡]Centro de Química e Bioquímica, Departamento de Química e Bioquímica, Faculdade de Ciências, Universidade de Lisboa, Portugal

[§]Department of Interfaces, Max Planck Institute of Colloids and Interfaces, Science Park Golm, 14476 Potsdam, Germany

ABSTRACT: This work focuses on the interaction of the antibiotic Rifabutin (RFB) with phospholipid membrane models using small- and wide-angle X-ray scattering (SAXS and WAXS) to assess drug–membrane interactions. The effect of different concentrations of RFB on human and bacterial cell membrane models was studied using multilamellar vesicles (MLVs) at the physiological pH (7.4). In this context, MLVs of 1,2-dimyristoyl-*rac*-glycero-3-phosphocholine (DMPC) were chosen to mimic the human cell membrane. To mimic the bacterial cell membrane, 1,2-dimyristoyl-*sn*-glycero-3-phospho-*rac*-(1-glycerol) (DMPG) and a mixture of 1,2-dipalmitoyl-*sn*-glycero-3-phosphoethanolamine (DPPE) and 1,2-dipalmitoyl-*sn*-glycero-3-phospho-*rac*-(1-glycerol) (DPPG) (8:2 molar ratio) were used. The results support a perturbation of the lipid bilayers caused by RFB, especially in the bacterial membrane model, inducing phase separation that might compromise the integrity of the bacterial membrane. Therefore, the different effects of this antibiotic depending on the concentration, the charge of the phospholipid headgroup, and the membrane organization may be related with the RFB antibiotic activity and the side effects, and should be accounted for during the anti-tuberculosis (anti-TB) drug design.

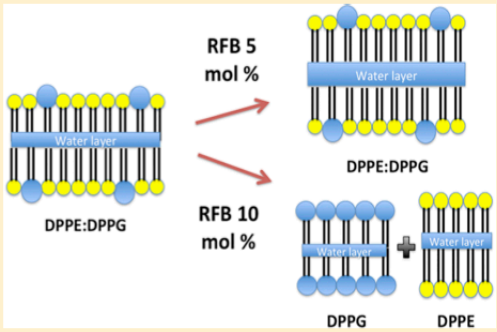

1. INTRODUCTION

Rifabutin (RFB, Figure 1) is a wide spectrum antibiotic used in the treatment of mycobacterial infectious diseases.[1] It is used as a second-line anti-tuberculosis (anti-TB) drug regarding its high activity against *Mycobacterium tuberculosis* (MTB), the etiological agent of tuberculosis (TB). This semisynthetic derivate of ryfamicin is less prone to the interactions with the antiretroviral drugs than the first-line-drug rifampicin (also a derivate of ryfamicin), being therefore mostly used as the first choice in the HIV (human immunodeficiency virus)-TB coinfected patients.[2] RFB has an intracellular target, namely, the enzyme RNA polymerase, and therefore, it must pass across the human and mycobacterial membranes to reach the pharmacological target. Nevertheless, a lack of correlation exists between the inhibitory activity of ryfamicins on the RNA polymerase and the antibiotic efficacy, with the efficacy mainly being attributed to the drug's penetration into the cells.[3] In fact, it is well-known that part of the success of RFB as an antimycobacterial compound is related with its high membrane lipid tropism and high penetration into the infected cells such as the alveolar macrophages in the lungs. For instance, RFB accumulates in the lungs at levels 6 times higher when compared with the plasma concentrations. The high lipid affinity of RFB seems to be responsible for the discrepancy between the plasma concentrations and the much higher concentrations achieved in the tissues and infected cells.[2] Additionally, our previous work contributes to the elucidation of the higher drug accumulation in the lungs due to a distribution at the pulmonary surfactant lipid level, evidenced by the inclusion complex formed between the drug and the polar head groups of the phospholipids. On the other hand, the inclusion complex formed by the drug is restricted to the polar head groups of the phospholipids, which might explain the low toxicity to the lungs despite the high drug concentrations reaching this organ.[3] In addition, the side effects of RFB, such as uveitis and discoloration of the skin, seem to be related to its affinity and ability to cross the biological membranes.[3]

To mimic the cell membranes, multilamellar vesicles (MLVs) were used as reliable cell membrane models, which allow one to study the drug–membrane interactions, since they account for the most relevant process of the drug's permeation across the bilayers (i.e., the diffusion).[3] The phosphatidylcholines represent the major components of the outer layer of the human membranes and are practically absent in bacterial membranes.[4] Hence, DMPC (Figure 1), a zwitterionic phospholipid, was chosen as a simple but suitable membrane model of the human cell membrane for mimicking the neutral charge of the surface membrane of eukaryotic plasma membranes.[4] On the other side, DMPG (Figure 1), a negatively

Received: March 28, 2013
Published: April 25, 2013

dx.doi.org/10.1021/jp403073v | J. Phys. Chem. B 2013, 117, 6187–6193

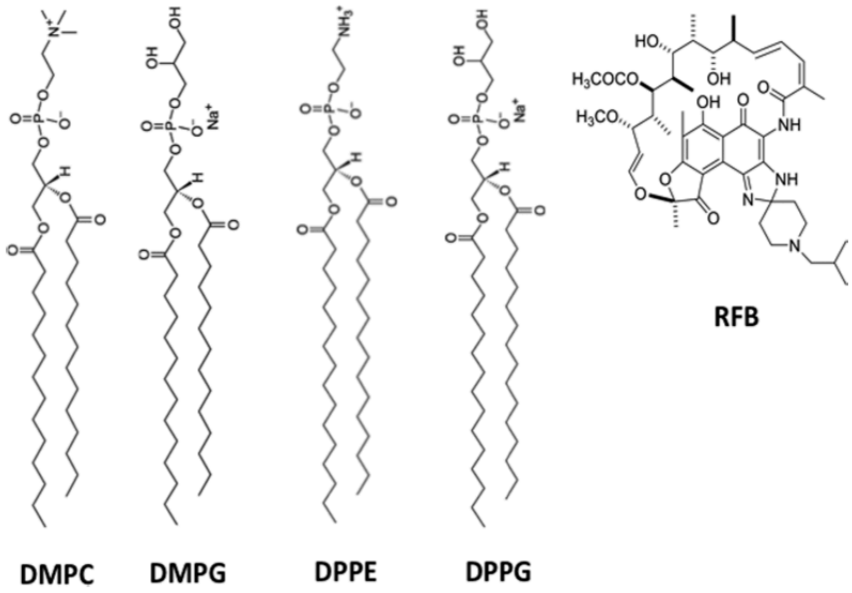

Figure 1. Chemical structure of 1,2-dimyristoyl-*rac*-glycero-3-phosphocholine (DMPC), 1,2-dimyristoyl-*sn*-glycero-3-phospho-*rac*-(1-glycerol) (DMPG), 1,2-dipalmitoyl-*sn*-glycero-3-phospho-*rac*-(1-glycerol), 1,2-dipalmitoyl-*sn*-glycero-3-phosphoethanolamine (DPPE), and rifabutin (RFB).

charged lipid, was chosen as the bacterial cell membrane model, mimicking the negative charge of the inner plasma membrane.[3] In addition, DPPE:DPPG (Figure 1) 8:2 (molar ratio) was the selected composition of a more complex bacterial membrane model, with the phosphatidylethanolamines also being one of the major constituents of the bacterial membranes.[5,6]

Small-angle X-ray scattering (SAXS) and wide-angle X-ray scattering (WAXS), two powerful X-ray techniques, were used in this study to assess the drug−membrane model interaction.

The experimental results point to a more pronounced interaction of RFB with the bacterial membrane models, which is ascribed for the electrostatic interactions between RFB and the polar head groups of the phospholipids, which may promote the disturbance of the bacterial membrane and consequently the bacterial cell death.

2. MATERIALS AND METHODS

2.1. Materials. DMPC and DMPG were purchased from Sigma-Aldrich Co. DPPG and DPPE were purchased from Avanti Polar Lipids. RFB was isolated from Mycobutin and further purified as previously described.[2] *N*-(2-Hydroxyethyethyl)piperazine-*N*′-(2-ethanesulfonic acid) (HEPES) and sodium chloride (NaCl) were purchased from Sigma-Aldrich Co. The buffer system (HEPES 0.01 M, pH 7.4, I = 0.1 M) was prepared with ultrapure water produced by Millipore Milli-Q (resistivity = 18.2 MΩ cm), and the ionic strength was adjusted with NaCl.

2.2. Methods. *2.2.1. Mutilamellar Vesicles.* Different amounts of RFB were mixed with DMPC, DMPG, and DPPE:DPPG (8:2 molar ratio) in a chloroform:methanol mixture (3:1 v/v) according to the required molar fraction of the drug (5 and 10 mol %). Lipid films were formed from these solutions, dried at 65.0 ± 0.1 °C under a stream of N_2, and left overnight under reduced pressure to remove all traces of the organic solvents. The lipid films were hydrated by adding the buffer system and then alternately heated to 65.0 ± 0.1 °C, mixed by vortexing for about 5 min, and centrifuged for 30 s at 2000*g*. This procedure was repeated three times. Finally, the samples were aged overnight at 4.0 ± 0.1 °C and shaken by vortex at room temperature for 5 min. Thereafter, the dispersions were transferred into glass capillaries of 1.5 mm diameter (Hilgenberg, Malsfeld, Germany), which are transparent to X-rays. The flame-sealed capillaries were stored at 4.0 ± 0.1 °C until the measurements.

2.2.2. Small Angle X-ray Scattering and Wide Angle X-ray Scattering. SAXS and WAXS experiments were executed at beamline A2 at Doris III of HASYLAB (DESY, Hamburg, Germany) using monochromatic radiation with a wavelength of 0.15 nm. The SAXS detector was calibrated with rat-tail tendon and the WAXS detector with polyethyleneterephthalat (PET). Heating scans from 8 to 70 °C were performed at a rate of 1 K min^{-1}. Data was recorded for 10 s every minute. The samples were also exposed to static measurements according to the thermotropic behavior of the lipids. After each temperature step, the sample was allowed to equilibrate for 5 min before the diffraction pattern was recorded. In order to minimize the X-ray exposure to the sample, a shutter mounted before the sample was kept closed when no data was acquired. The lamellar repeat distance d was calculated from the diffraction patterns using Bragg's equation $s = n/d$, where $s = (2 \sin \Theta)/\lambda$ is the scattering vector and n the order of the reflection (n = 1, 2, ...). To obtain the precise position of the Bragg peaks, Lorentzian curves were fitted to the diffraction peaks, and the positions of maximum intensities as well as the full width at half-maximum (fwhm) were determined.[4]

3. RESULTS AND DISCUSSION

The interaction of RFB with DMPC, DMPG, and DPPE:DPPG was investigated using X-ray diffraction patterns at small and wide angles, yielding information, respectively, on long-range bilayer organization and hydrocarbon chain packing.[7] The SAXS and WAXS studies were carried out in a range of temperature from 8 to 70 °C, with the purpose of elucidating the different lipid phases and assessing the

Table 1. Long Distances (d) of DMPC Bilayers and Correlation Lengths (ξ) Determined from SAXS Diffraction Patterns at pH 7.4 and at 10, 18, and 40 °C[a]

		d_{SAXS} (Å)			
sample (mol % RFB)	T (°C)	d_1	d_2	ξ_1 (Å)	ξ_2 (Å)
DMPC:RFB 0	10	61.2 ± 0.5		678 ± 10	
	18	66.8 ± 0.5		604 ± 10	
	40	62.6 ± 0.5		629 ± 10	
DMPC:RFB 5	10	62.4 ± 0.5		968 ± 10	
	18	71.9 ± 0.5		789 ± 10	
	40	63.4 ± 0.5		590 ± 10	
DMPC:RFB 10	10	64.4 ± 0.5		825 ± 10	
	18	70.7 ± 0.5		866 ± 10	
	40	64.7 ± 0.5	61.7 ± 0.5	498 ± 10	797 ± 10

[a]The data are presented in Å as a function of the 5 and 10 mol % RFB.

transition temperatures between these phases. Additionally, static measurements were also performed, according to the thermotropic behavior of the lipids to the Lβ', Pβ', and Lα phases and specifically at 10, 18, and 40 °C for DMPC and 8, 18, and 40 °C for DMPG, respectively. For the lipid mixture DPPE:DPPG, the investigated temperatures were 37, 56, and 65 °C in order to study the structures of the gel and fluid phases. In the presence of excess water, the mentioned lipids form lyotropic lamellar phases whose structure and organization are dependent on the temperature. DMPC and DMPG form three different phases, namely, Lβ', Pβ', and Lα, depending on the temperature. The lipid mixture DPPE:DPPG (8:2 molar ratio) seems to have only two different phases (Lβ' and Lα). The Lβ' corresponds to the gel phase in which the acyl chains are in an all-*trans* conformation and tilted. The temperature increase leads to the pretransition from Lβ' to Pβ' (in the case of DMPC and DMPG), in which the lipid bilayers are distorted by a periodic ripple in the lamellae plane. Further temperature increase leads to the main lipid phase transition to the liquid-crystalline Lα phase: in the case of DMPC and DMPG (Pβ' → Lα) or in the case of the lipid mixture DPPE:DPPG (Lβ' → Lα). In the liquid-crystalline Lα phase, the acyl chains are disordered (*trans*–*gauche* isomerization).[8]

3.1. Effects of RFB on the Structure of DMPC Bilayers.

The repeat distances d deduced from the SAXS patterns of DMPC in the absence and presence of RFB are depicted in Table 1. For DMPC, the Bragg peaks appear at 1/61.2 Å^{-1} (Lβ'), 1/66.8 Å^{-1} (Pβ'), and 1/62.6 Å^{-1} (Lα), and are in close agreement with the literature data.[9] In addition, the repeat distances d, deduced from the WAXS patterns of DMPC in the absence and in the presence of RFB, are represented in Table 2. Analyzing Table 2, the diffraction pattern of DMPC at 10 °C displays a sharp reflection at 1/4.13 Å^{-1} with a shoulder located at 1/3.96 Å^{-1}, which reflects the orthorhombic (pseudohexagonal) lattice of the chains in the bilayers, characteristic of the Lβ' phase.[10] At 18 °C, only one diffraction peak is observed at 1/4.15 Å^{-1} with a symmetric profile, indicating a hexagonal chain packing characteristic of the Pβ' phase.[10,11] At 40 °C, in the Lα phase, a broad halo appears, which corresponds to the disordered molten chains (data not shown).[9] Furthermore, the main transition occurs at 22–24 °C, connected with the disappearance of the well-defined WAXS peaks (data not shown).[12]

Table 2. Short Distances (d) of DMPC Bilayers and Correlation Lengths (ξ) Determined from WAXS Diffraction Patterns at pH 7.4 and at 10, 18, and 40 °C[a]

sample (mol % RFB)	T (°C)	d_{WAXS} (Å)		ξ_1 (Å)	ξ_2 (Å)
DMPC 0	10	4.13	3.96	49 ± 10	82 ± 10
	18	4.15		80 ± 10	
DMPC:RFB 5	10	4.13		40 ± 10	
	18	4.18		30 ± 10	
DMPC:RFB 10	10	4.14		41 ± 10	
	18	4.19		31 ± 10	

[a]The data are presented in Å as a function of the 5 and 10 mol % RFB.

The incorporation of RFB into the DMPC MLVs is responsible for pronounced changes in the SAXS patterns with a d-spacing increase in the gel phases (Table 1). Therefore, in both gel phases (Lβ' and Pβ'), the bilayer thickness, including the water layer between the bilayers, increases up to approximately 5 Å. Moreover, this effect seems to be dependent on the drug concentration in the Lβ' phase. In the Lα phase, considered to be the most biologically relevant mesophase, 5 mol % RFB does not change the d-spacing (within the experimental error) (Figure 2). However, two lamellar phases with different d-spacings are observed in samples with 10 mol % RFB (Figure 2). Therefore, a noninfluenced DMPC phase (since the d values are not relevantly changed in comparison with pure DMPC) and a mixed DMPC phase with a higher d value coexist. The correlation length between the bilayers (ξ) increases in the gel phase due to the incorporation of RFB, whereas in the fluid phase a decrease of the correlation length is observed.

The evaluation of the WAXS pattern in the gel phases (Lβ' and Pβ') (Table 2) confirms that RFB changes the lattice constants and the correlation length ξ in a non-concentration-dependent manner, which is consistent with the pronounced interactions with the phospholipid head groups and with the membrane disordering effect in the most organized and tightly packed phospholipid phases. The WAXS diffraction pattern of DMPC in the absence and in the presence of 10 mol % RFB at 10 °C is shown in Figure 3. The WAXS spectrum of DMPC in the presence of 10 mol % RFB displays a single, symmetrical but quite broad peak, which points to a hexagonal hydrocarbon chain packing induced by RFB (Figure 3).[10]

Furthermore, RFB is a bulky and amphiphilic molecule, which contains some groups that can be protonated (piperidine nitrogen and imidazole nitrogen) and deprotonated (naphthol oxygen) depending on the pH value. At a pH of 7.4, while the zwitterionic species predominate (83.4%), a significant contribution of positively charged molecules (roughly 16.6%) (predicted using MarvinView 5.4.1.1 software from ChemAx-

dx.doi.org/10.1021/jp403073v | J. Phys. Chem. B 2013, 117, 6187–6193

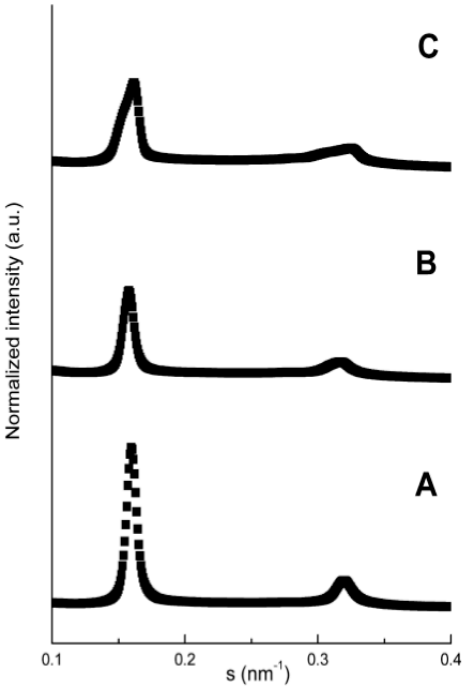

Figure 2. Small-angle X-ray diffraction profiles of DMPC (A) and mixtures of DMPC with RFB at 5 mol % (B) and 10 mol % (C) at 40 °C.

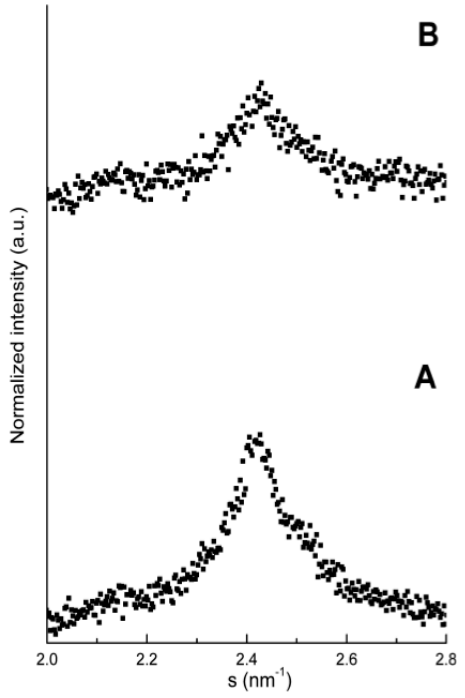

Figure 3. Wide-angle X-ray diffraction patterns of DMPC (A) and mixtures of DMPC with RFB at 10 mol % (B) at 10 °C.

on) exists. The zwitterionic species are more lipophilic in comparison to the charged ones.[3] Therefore, the zwitterionic species of RFB are expected to be inserted into the DMPC phospholipid bilayers according to their hydrophobicity gradient.[3] The hydrophilic imidazole and piperidine moieties should be inserted near the polar head groups of the phospholipids and hydrophobic naphthol should be embedded within the membranes, establishing van der Waals interactions with the hydrophobic tails.[13] This interaction is expected to cause a pronounced destabilization of the gel phases, which are characterized by a high degree of order and tight hydrocarbon chain packing in comparison with the fluid phase. Therefore, in the DMPC vesicles, the RFB location close to the head groups (C1−C9) is expected to produce an enhanced membrane perturbation.[14] In order to explore the influence of RFB on the T_m, SAXS and WAXS diffraction patterns of DMPC were taken on heating the sample. The results point to a marginal decrease of the DMPC main-transition temperature (T_m) even for high concentrations of RFB (data not shown).

3.2. Effects of RFB on the Structure of DMPG Bilayers.

Table 3 displays the long-range repeat distances (d) and the correlation length (ξ) between the DMPG bilayers in the absence and in the presence of RFB. The SAXS diffraction pattern (Figure 4A) of DMPG exhibits only a single broad peak, especially for higher temperatures. Thus, it was previously described that in charged phospholipids, due to the electrostatic repulsions, instead of the formation of MLVs, the formation of large unilamellar vesicles or of noncorrelated bilayers takes place. We did not analyze the broad peak in terms of a form factor of the DMPG bilayer. We only determined the d-spacings associated with a larger error bar (see Table 3).[11] The Bragg reflection peaks for DMPG appear at 1/47.9 Å^{-1} (Lβ'), 1/51.1 Å^{-1} (Pβ'), and 1/48.4 Å^{-1} (Lα), being in good agreement with literature data.[15]

Table 3. Long Distances (d) of DMPG Bilayers and Correlation Lengths (ξ) Determined from SAXS Diffraction Patterns at pH 7.4 and at 8, 18, and 40 °C[a]

sample (mol % RFB)	T (°C)	d_{SAXS} (Å)	ξ_1 (Å)
DMPG 0	8	47.9 ± 0.7	396 ± 10
	18	51.1 ± 0.7	421 ± 10
	40	48.4 ± 0.7	36 ± 10
DMPG:RFB 5	8	51.2 ± 0.7	324 ± 10
	18	48.1 ± 0.7	336 ± 10
	40	46.7 ± 0.7	23 ± 10
DMPG:RFB 10	8	51.5 ± 0.7	221 ± 10
	18	48.0 ± 0.7	171 ± 10
	40	45.9 ± 0.7	17 ± 10

[a]The data are presented in Å as a function of the 5 and 10 mol % RFB.

The WAXS patterns show an asymmetric Bragg peak centered around 1/4.03 and 1/3.86 Å^{-1}, typical of the pseudohexagonal lattice of the DMPG chains. Upon heating, one symmetric Bragg peak appears, centered around 1/4.04 Å^{-1}, indicating the formation of a hexagonal chain lattice with an unexpected small cross-sectional area of the chains (19 Å^2). Finally, at 40 °C, the characteristic broad band appears in the Lα phase (data not shown).[16] In addition, the expected melting transition at 22−24 °C was verified by SAXS and WAXS heating scans (data not shown). In fact, the ionic strength used (similar to the physiological conditions) is reported to preserve the narrow temperature interval of the phase transition from the gel to the liquid-crystalline phase similar to DMPC.[15] The analysis of the effect of RFB on the repeat distance of DMPG bilayers reveals that significant differences are observed for all

dx.doi.org/10.1021/jp403073v | J. Phys. Chem. B 2013, 117, 6187−6193

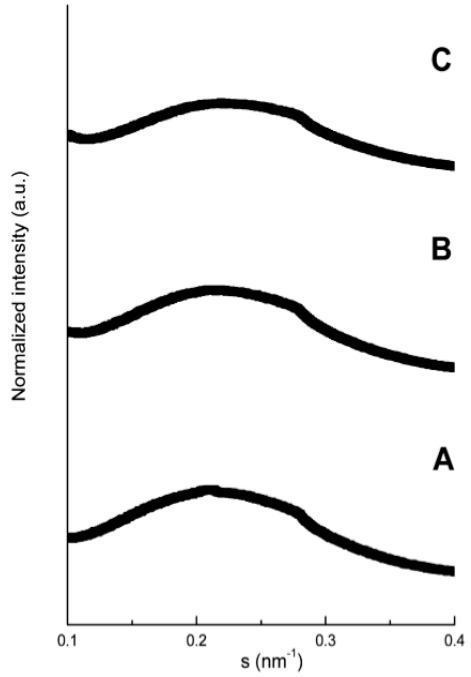

Figure 4. Small-angle X-ray diffraction patterns of DMPG (A) and mixtures of DMPG with RFB at 5 mol % (B) and 10 mol % (C) at 40 °C.

the phases of DMPG (Table 3). While the *d*-spacings increase in the Lβ' phase, they decrease both in the Pβ' and in the Lα phases with increasing RFB concentration. In addition, the correlation length (ξ) supports the observation that RFB disturbs the bilayer correlation in a concentration-dependent manner. On the other hand, the WAXS diffraction patterns (Table 4) indicate that RFB has a pronounced effect on the

Table 4. Short Distances (d) of DMPG Bilayers and Correlation Lengths (ξ) Determined from WAXS Diffraction Patterns at pH 7.4 and at 8, 18, and 40 °C[a]

		d_{WAXS} (Å)			
sample (mol % RFB)	T (°C)	d_1	d_2	ξ_1 (Å)	ξ_2 (Å)
DMPG 0	8	4.03	3.86	132 ± 10	14 ± 10
	18	4.04		177 ± 10	
DMPG:RFB 5	8	3.99		28 ± 10	
	18	3.98		24 ± 10	
DMPG:RFB 10	8	3.97		43 ± 10	
	18	3.97		31 ± 10	

[a]The data are presented in Å as a function of the 5 and 10 mol % RFB.

phospholipid chain packing. The single and symmetrical peak obtained in the presence of RFB is indicative of hexagonal hydrocarbon chain packing (data not shown). Surprisingly, the chain cross-sectional area decreases by incorporating RFB. This shows that RFB changes the effective area requirement of the phospholipid head groups, allowing a tighter packing of the chains.

On the other hand, the low correlation length (ξ) obtained (for both SAXS and WAXS measurements) may be attributed to the RFB ability to induce a marked disturbance in the DMPG bilayers. As mentioned above, at pH 7.4, RFB has a significant contribution of positively charged molecules that may establish electrostatic interactions with the deprotonated phosphate of DMPG. This effect could change the orientation of the phospholipid head groups and consequently allow the observed change in the chain packing. Moreover, the RFB interactions with the charged headgroup of DMPG might also be responsible for the observed decrease of the correlation length between the bilayers by a decrease of the stabilizing electrostatic repulsion.[11,16] The analysis of the heating scans shows that the T_m reported for DMPG, i.e., 22−24 °C, remains unchanged even for high drug concentrations (data not shown).

3.3. Effects of RFB on the Structure of DPPE:DPPG Bilayers. The SAXS diffraction patterns obtained for the DPPE:DPPG mixture in the gel phase at 37 °C in the absence and in the presence of RFB are presented in Figure 5. The

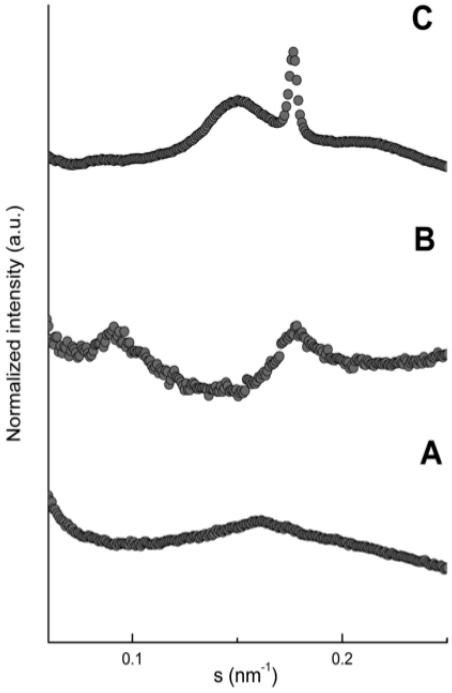

Figure 5. Small-angle X-ray diffraction patterns for DPPE:DPPG (A) and mixtures of DPPE:DPPG with RFB at 5 mol % (B) and 10 mol % (C) at 37 °C.

diffraction pattern with only one broad peak is clearly dominated by the 20% DPPG in this mixture. The broad peak observed in aqueous dispersions of anionic DPPG indicates the formation of noncorrelated bilayers in contrast to DPPE, which forms well-correlated bilayers characterized by a sharp Bragg peak.

The temperature of the main phase transition, determined using WAXS measurements, was 61−63 °C (data not shown) in accordance with the previously reported one for this lipid mixture.[17] Taking into account the phase transition temperatures of DPPE (63 °C) and DPPG (41 °C), the transition temperature is in contrast to the structure dominated by the 80% DPPE. DPPG and DPPE have the same chain pattern but completely different head groups. The headgroup of DPPG is negatively charged, while that of DPPE is zwitterionic but has a

dx.doi.org/10.1021/jp403073v | J. Phys. Chem. B 2013, 117, 6187−6193

Table 5. Long Distances (d) of DPPE:DPPG Bilayers and Correlation Lengths (ξ) Determined from SAXS Diffraction Patterns at pH 7.4 and at 37, 56, and 65 °C[a]

		d_{WAXS} (Å)			
sample (mol % RFB)	T (°C)	d_1	d_2	ξ_1 (Å)	ξ_2 (Å)
DPPE:DPPG 0	37	62.8 ± 0.5		137 ± 10	
	56	61.2 ± 0.5		317 ± 10	
	65	64.4 ± 0.5		202 ± 10	
DPPE:DPPG:RFB 5	37	117 ± 0.5		113 ± 10	
	56	110 ± 0.5		64 ± 10	
	65	114 ± 0.5		98 ± 10	
DPPE:DPPG:RFB 10	37	65.8 ± 0.5	56.6 ± 0.5	33 ± 10	1418 ± 10
	56	65.1 ± 0.5	56.1 ± 0.5	197 ± 10	1636 ± 10
	65	66.4 ± 0.5	56.1 ± 0.5	228 ± 10	1267 ± 10

[a]The data are presented in Å as a function of the 5 and 10 mol % RFB.

pronounced ability for hydrogen bond formation, being the main reason for the high T_m value.[8,18] In an ideal mixture, one would expect a transition temperature around 59 °C. The observed higher T_m indicates stronger interactions between the molecules in the mixture compared to the pure lipid systems. As shown in Figure 5, and as previously described, this lipid mixture exhibits only the broad scattering feature of MLVs or noncorrelated bilayers.[8,19] Nevertheless, we used the maximum of the broad peak to determine d-values: 1/62.8 $Å^{-1}$ at 37 °C (gel phase), 1/61.2 $Å^{-1}$ at 56 °C (gel phase), and 1/64.4 $Å^{-1}$ at 65 °C (fluid phase), being concordant with literature data.[8] The WAXS pattern (Table 6) shows a single Bragg reflection at 1/4.07 $Å^{-1}$ at 37 °C and 1/4.12 $Å^{-1}$ at 56 °C, corresponding to the hexagonal chain packing in the gel phase. The cross-sectional area of the alkyl chains increases with increasing temperature in the gel phase from 19.1 to 19.6 $Å^2$. At 65 °C, the broad halo obtained is consistent with the chain melting (data not shown).[8]

The SAXS and to a moderate extent the WAXS patterns of DPPE:DPPG are influenced by the addition of RFB. The effect depends on the drug concentration. As shown in Figure 5 and Table 5, the addition of 5 mol % RFB is responsible for the appearance of two Bragg peaks in the s-ratio of 1:2 at all temperatures studied, characteristic of correlated bilayers. The interaction with RFB leads to a much better correlation between the bilayers but at a much larger distance of 110 Å. This larger d-value can only be explained by a much larger water layer between the bilayers. On the other side, 10 mol % RFB (Figure 5C) leads to a phase separation into DPPE-rich and DPPE-poor domains. The first ones are characterized by a sharp Bragg peak, as observed for pure DPPE, the second ones show the broad diffraction pattern typical for noncorrelated bilayers of DPPG. The WAXS diffraction pattern obtained for DPPG:DPPE in the presence of RFB (Table 6) exhibits also only one Bragg peak, independently of the drug concentration. Above 65 °C, the WAXS peak disappears, which is connected with the chain melting in the liquid crystalline phase (data not shown).[8] The correlation length (ξ) in the DPPE:DPPG bilayer (obtained by WAXS measurements) is not considerably influenced by RFB. In fact, RFB is an amphiphilic charged molecule with the ability to interact with charged phospholipid head groups. Therefore, it might be preferentially located at the hydrophilic/hydrophobic interface of a lipid bilayer stabilized by electrostatic interactions as well as hydrophobic interactions. Above a certain threshold concentration of RFB, the electrostatic interactions with DPPG lead to a phase separation in the lipid mixture.

Table 6. Short Distances (d) of DPPE:DPPG Bilayers and Correlation Lengths (ξ) Determined from WAXS Diffraction Patterns at pH 7.4 and at 37, 56, and 65 °C[a]

sample (mol % RFB)	T (°C)	d_{SAXS} (Å)	ξ_1 (Å)
DPPE:DPPG 0	37	4.07	132 ± 10
	56	4.12	177 ± 10
DPPE:DPPG:RFB 5	37	4.07	114 ± 10
	56	4.16	56 ± 10
DPPE:DPPG:RFB 10	37	4.07	175 ± 10
	56	4.17	176 ± 10

[a]The data are presented in Å as a function of the 5 and 10 mol % RFB.

4. CONCLUSIONS

In this work, the effect of RFB on human and bacterial membrane mimetic models (DMPC and DMPG, DPPE:DPPG) was evaluated using X-ray diffraction techniques. The overall results show that the interaction of the antimycobacterial drug RFB with the used membrane models is putatively related with the drug's mechanism of action. Therefore, the interaction of the drug with the membrane models is strongly dependent on the phospholipid head groups, the hydrocarbon chains, and the concentrations of the drug.

The effects of RFB on the DMPC bilayer are pronounced only in the gel phases. In the fluid Lα phase, the effects on the bilayer repeat distance are negligible. Therefore, the pronounced disordering effect of RFB on the gel phases of the DMPC bilayer might be related to some adverse effects caused by its ability to interact with some of the most ordered membranes of the human body, causing uveitis and the discoloration of the skin.[3] In fact, despite that most cell membranes exist in the fluid phase, the gel lamellar phase of lipid bilayers has biological relevance for specialized membranes such as stractum corneum.[20,21] Contrastingly to the effects of the antimycobacterial compound on the human membrane model (with a large amount of zwitterionic phosphatidylcholines), RFB has pronounced effects in the fluid phase (with most biological relevance) on the bacterial membrane model. In addition, RFB might exert a direct effect in the bacterial membrane. In fact, RFB (above a certain threshold) induces phase separation in the DPPG:DPPE mixture that can promote the membrane dysfunction due to increased permeability of the lipid bilayer.[8]

In summary, these results represent a contribution to the knowledge of the mechanism of action of RFB and might be

useful for the development of more potent antibiotics with fewer side effects.

AUTHOR INFORMATION

Corresponding Author

*Address: REQUIMTE, Departamento de Ciências Químicas, Faculdade de Farmácia, Universidade do Porto Rua de Jorge Viterbo Ferreira n.° 228 4050-313 Porto, Portugal. E-mail: shreis@ff.up.pt. Phone: +351-220428672. Fax: +351-226093483.

Notes

The authors declare no competing financial interest.

ACKNOWLEDGMENTS

M.P., J.M.C., and C.N. thank FCT (Lisbon) for the fellowships (SFRH/BD/63318/2009, SFRH/BD/66789/2009, and SFRH/BPD/81963/2011, respectively). The authors are also grateful to the FCT for financial support under projects PEst-OE/QUI/UI0612/2011 and PTDC/QUI-QUI/101022/2008 with coparticipation European Community funds from the FEDER, QREN, and COMPET. The authors thank HASYLAB at DESY, Hamburg, Germany, for beam time and support through the project II-20100139 EC. The authors are grateful to Dr. Sérgio Funari for help at beamline A2.

REFERENCES

(1) Aristoff, P. A.; Garcia, G. A.; Kirchhoff, P. D.; Hollis Showalter, H. D. Rifamycins–Obstacles and Opportunities. *Tuberculosis* **2010**, *90* (2), 94−118.

(2) Figueiredo, R.; Moiteiro, C.; Medeiros, M. A.; da Silva, P. A.; Ramos, D.; Spies, F.; Ribeiro, M. O.; Lourenco, M. C.; Junior, I. N.; Gaspar, M. M.; Cruz, M. E.; Curto, M. J.; Franzblau, S. G.; Orozco, H.; Aguilar, D.; Hernandez-Pando, R.; Costa, M. C. Synthesis and Evaluation of Rifabutin Analogs against Mycobacterium avium and H(37)Rv, MDR and NRP Mycobacterium tuberculosis. *Bioorg. Med. Chem.* **2009**, *17* (2), 503−511.

(3) Pinheiro, M.; Arede, M.; Nunes, C.; Caio, J. M.; Moiteiro, C.; Lucio, M.; Reis, S. Differential Interactions of Rifabutin with Human and Bacterial Membranes: Implication for Its Therapeutic and Toxic Effects. *J. Med. Chem.* **2013**, *56* (2), 417−426.

(4) Pereira-Leite, C.; Carneiro, C.; Soares, J. X.; Afonso, C.; Nunes, C.; Lucio, M.; Reis, S. Biophysical Characterization of the Drugs-Membrane Interaction: The Case of Propranolol and Acebutolol. *Eur. J. Pharm. Biopharm.* **2013**, *84*, 183−191.

(5) Maloney, E.; Stankowska, D.; Zhang, J.; Fol, M.; Cheng, Q. J.; Lun, S.; Bishai, W. R.; Rajagopalan, M.; Chatterjee, D.; Madiraju, M. V. The Two-Domain LysX Protein of Mycobacterium tuberculosis Is Required for Production of Lysinylated Phosphatidylglycerol and Resistance to Cationic Antimicrobial Peptides. *PLoS Pathog.* **2009**, *5* (7), e1000534.

(6) Rappolt, M.; Hickel, A.; Bringezu, F.; Lohner, K. Mechanism of the Lamellar/Inverse Hexagonal Phase Transition Examined by High Resolution X-ray Diffraction. *Biophys. J.* **2003**, *84* (5), 3111−3122.

(7) Pili, B.; Bourgaux, C.; Meneau, F.; Couvreur, P.; Ollivon, M. Interaction of an Anticancer Drug, Gemcitabine, with Phospholipid Bilayers. *J. Therm. Anal. Calorim.* **2009**, *98* (1), 19−28.

(8) Oszlanczi, A.; Bota, A.; Klumpp, E. Influence of Aminoglycoside Antibiotics on the Thermal Behaviour and Structural Features of DPPE-DPPG Model Membranes. *Colloids Surf., B* **2010**, *75* (1), 141−148.

(9) Eisenblatter, J.; Winter, R. Pressure Effects on the Structure and Phase Behavior of DMPC-Gramicidin Lipid Bilayers: a Synchrotron SAXS and 2H-NMR Spectroscopy Study. *Biophys. J.* **2006**, *90* (3), 956−966.

(10) Nunes, C.; Brezesinski, G.; Lima, J. L.; Reis, S.; Lucio, M. Synchrotron SAXS and WAXS Study of the Interactions of NSAIDs with Lipid Membranes. *J. Phys. Chem. B* **2011**, *115* (24), 8024−8032.

(11) Cardoso, A. M.; Trabulo, S.; Cardoso, A. L.; Lorents, A.; Morais, C. M.; Gomes, P.; Nunes, C.; Lucio, M.; Reis, S.; Padari, K.; Pooga, M.; Pedroso de Lima, M. C.; Jurado, A. S. S4(13)-PV Cell-Penetrating Peptide Induces Physical and Morphological Changes in Membrane-Mimetic Lipid Systems and Cell Membranes: Implications for Cell Internalization. *Biochim. Biophys. Acta* **2012**, *1818* (3), 877−888.

(12) Grabielle-Madelmont, C.; Hochapfel, A.; Ollivon, M. Antibiotic−Phospholipid Interactions as Studied by DSC and X-ray Diffraction. *J. Phys. Chem. B* **1999**, *103* (21), 4534−4548.

(13) Vostrikov, V. V.; Selishcheva, A. A.; Sorokoumova, G. M.; Shakina, Y. N.; Shvets, V. I.; Savel'ev, O. Y.; Polshakov, V. I. Distribution Coefficient of Rifabutin in Liposome/Water System as Measured by Different Methods. *Eur. J. Pharm. Biopharm.* **2008**, *68* (2), 400−405.

(14) Nunes, C.; Brezesinski, G.; Pereira-Leite, C.; Lima, J. L. F. C.; Reis, S.; Lúcio, M. NSAIDs Interactions with Membranes: A Biophysical Approach. *Langmuir* **2011**, *27* (17), 10847−10858.

(15) Duarte, E. L.; Oliveira, T. R.; Alves, D. S.; Micol, V.; Lamy, M. T. On the Interaction of the Anthraquinone Barbaloin with Negatively Charged DMPG Bilayers. *Langmuir* **2008**, *24* (8), 4041−4049.

(16) Spinozzi, F.; Paccamiccio, L.; Mariani, P.; Amaral, L. Q. Melting Regime of the Anionic Phospholipid DMPG: New Lamellar Phase and Porous Bilayer Model. *Langmuir* **2010**, *26* (9), 6484−6493.

(17) Sevcsik, E.; Pabst, G.; Richter, W.; Danner, S.; Amenitsch, H.; Lohner, K. Interaction of LL-37 with Model Membrane Systems of Different Complexity: Influence of the Lipid Matrix. *Biophys. J.* **2008**, *94* (12), 4688−4699.

(18) Chen, X.; Huang, Z.; Hua, W.; Castada, H.; Allen, H. C. Reorganization and Caging of DPPC, DPPE, DPPG, and DPPS Monolayers Caused by Dimethylsulfoxide Observed Using Brewster Angle Microscopy. *Langmuir* **2010**, *26* (24), 18902−18908.

(19) Urbán, E.; Bóta, A.; Kocsis, B. Non-Bilayer Formation in the DPPE−DPPG Vesicle System Induced by Deep Rough Mutant of Salmonella minnesota R595 Lipopolysaccharide. *Colloids Surf., B* **2006**, *48* (2), 106−111.

(20) Norlen, L. Skin Barrier Structure and Function: the Single Gel Phase Model. *J. Invest. Dermatol.* **2001**, *117* (4), 830−836.

(21) Tristram-Nagle, S.; Liu, Y.; Legleiter, J.; Nagle, J. F. Structure of Gel Phase DMPC Determined by X-ray Diffraction. *Biophys. J.* **2002**, *83* (6), 3324−3335.

9. Interactions of *N'*-acetyl-rifabutin and *N'*-butanoyl-rifabutin with lipid bilayers: A synchrotron X-ray study.

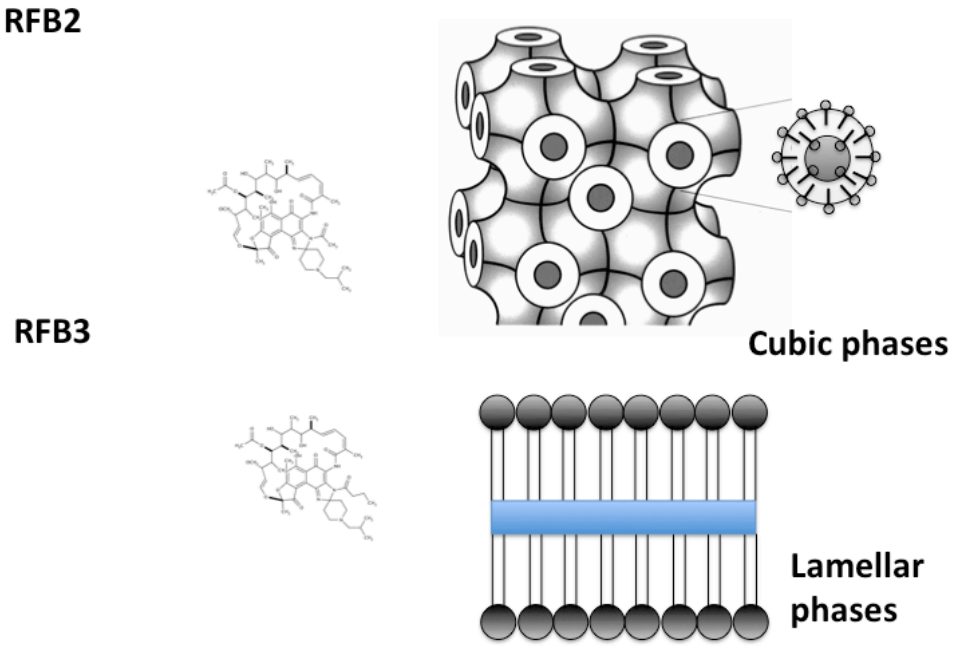

G Model
IJP-13406; No. of Pages 9
ARTICLE IN PRESS
International Journal of Pharmaceutics xxx (2013) xxx–xxx
Contents lists available at SciVerse ScienceDirect
International Journal of Pharmaceutics
journal homepage: www.elsevier.com/locate/ijpharm

Pharmaceutical Nanotechnology

Interactions of *N*′-acetyl-rifabutin and *N*′-butanoyl-rifabutin with lipid bilayers: A synchrotron X-ray study

Marina Pinheiro [a], Cláudia Nunes [a], João M. Caio [b], Cristina Moiteiro [b], Gerald Brezesinski [c], Salette Reis [a,*]

[a] REQUIMTE, Departamento de Ciências Químicas, Faculdade de Farmácia, Universidade do Porto, Portugal
[b] Centro de Química e Bioquímica, Departamento de Química e Bioquímica, Faculdade de Ciências, Universidade de Lisboa, Portugal
[c] Department of Interfaces, Max Planck Institute of Colloids and Interfaces, Science Park Golm, 14476 Potsdam, Germany

ARTICLE INFO

Article history:
Received 22 April 2013
Received in revised form 8 June 2013
Accepted 11 June 2013
Available online xxx

Keywords:
Cubic phases
Membrane models
Rifabutin
Small-angle X-ray scattering
Tuberculosis
Wide-angle X-ray scattering

ABSTRACT

This work focuses on the interaction of *N*′-acetyl-rifabutin (RFB2) and *N*′-butanoyl-rifabutin (RFB3) with human and bacterial cell membrane models under physiological conditions. The effect of RFB2 and RFB3 on human cell membrane models was assessed using multilamellar vesicles (MLVs) composed of 1,2-dimyristoyl-*rac*-glycero-3-phosphocholine (DMPC). In order to mimic the bacterial cell membrane, MLVs of 1,2-dimyristoyl-*sn*-glycero-3-phospho-*rac*-(1-glycerol) (DMPG) and a mixture of 1,2-dipalmitoyl-*sn*-glycero-3-phosphoethanolamine (DPPE) and 1,2-dipalmitoyl-*sn*-glycero-3-phospho-*rac*-(1-glycerol) (DPPG) (8:2 molar ratio) were chosen. Small and wide-angle X-ray scattering (SAXS and WAXS) were used to study the effect of these antimycobacterial compounds on the structure formed in aqueous lipid dispersions. This study contributes to understanding the molecular mechanisms of the drugs delivery through the human and bacterial cells and the effect of these antimycobacterial compounds on the membrane lipids organization, which is related with their antibiotic efficacy and toxic effects.

1. Introduction

Tuberculosis (TB) is still one of the major infectious diseases affecting the developing countries, being also re-emerging in industrialized nations mainly due to the HIV/AIDS pandemic (Pinheiro et al., 2011). In 2011 there were 8.7 million incident cases of TB, resulting in 1.43 million deaths (WHO, 2012). Notwithstanding the significant progress that has been made to reduce the global impact of TB, the emergence of multidrug-resistant (MDR) TB during the past decade threatens these advancements. In fact, the emergence of MDR strains of the etiological agent of TB (i.e. *Mycobacterium tuberculosis*) makes the discovery of new drug molecules a strategic priority, requiring the current situation an upgrading of old drug families to achieve successful control (Gandhi et al., 2010). Herein, two novel analogs of the anti-TB drug rifabutin (RFB), *N*′-acetyl-rifabutin (RFB2) and *N*′-butanoyl-rifabutin (RFB3) (Fig. 1) were synthetized in order to improve the pharmacokinetics and pharmacodynamics of the lead compound (Figueiredo et al., 2009). Additionally, RFB2 already shows better in vitro and in vivo therapeutic index than RFB, being a promising anti-TB drug for the clinical application (Figueiredo et al., 2009).

Multilamellar vesciles (MLVs) of different phospholipid composition were used to mimic the human and bacterial cell membranes (Wesolowska et al., 2009). The zwitterionic phospholipid, 1,2-dimyristoyl-*rac*-glycero-3-phosphocholine (DMPC) was chosen as a simple but suitable membrane model of the human cell membrane, mimicking the neutral charge of the surface membrane of eukaryotic plasma membrane and the composition of the mammalian membranes, mainly composed of phosphatidylcholines (Pereira-Leite et al., 2012). The negatively charged phospholipid, 1,2-dimyristoyl-*sn*-glycero-3-phospho-*rac*-(1-glycerol) (DMPG) was selected because the bacterial cell membranes are predominantly negatively charged, being the phosphatidylglycerols one of the main components of the prokaryotic membranes (Pinheiro et al., 2013a). In addition, a mixture of DPPE:DPPG 8:2 (molar ratio) was chosen as a more complex bacterial membrane model, being the phosphatidylethanolamines in addition to the phosphatidylglycerols one of the main constituents of the bacterial membranes (Maloney et al., 2009). Moreover, this lipid mixture permits to study if the antimycobacterial compounds induce non-lamellar phases, one of the mechanisms of action of some antibiotics (Oszlanczi et al., 2010a).

Small-angle X-ray scattering (SAXS) and wide-angle X-ray scattering (WAXS) measurements were performed to assess the

* Corresponding author at: REQUIMTE, Departamento de Ciências Químicas, Faculdade de Farmácia, Universidade do Porto, Rua de Jorge Viterbo Ferreira n.º 228, 4050-313 Porto, Portugal. Tel.: +351 220428672; fax: +351 226093483.
E-mail address: shreis@ff.up.pt (S. Reis).

0378-5173/$ – see front matter © 2013 Elsevier B.V. All rights reserved.
http://dx.doi.org/10.1016/j.ijpharm.2013.06.018

Please cite this article in press as: Pinheiro, M., et al., Interactions of *N*′-acetyl-rifabutin and *N*′-butanoyl-rifabutin with lipid bilayers: A synchrotron X-ray study. Int J Pharmaceut (2013), http://dx.doi.org/10.1016/j.ijpharm.2013.06.018

G Model
IJP-13406; No. of Pages 9
ARTICLE IN PRESS

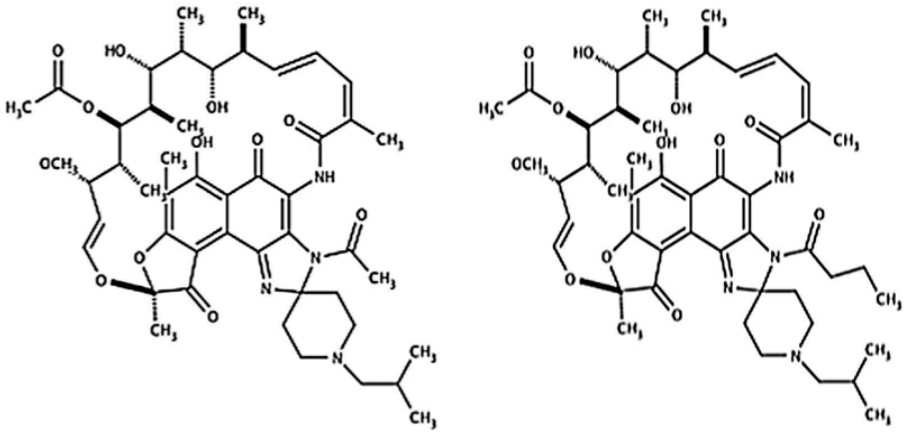

RFB2 RFB3

Fig. 1. Chemical structure of *N′*-acetyl-rifabutin (RFB2) and *N′*-butanoyl-rifabutin (RFB3).

interaction of RFB2 and RFB3 with the membrane models, providing detailed information of the influence of these compounds on the structural organization of the membrane models at the molecular level (Cardoso et al., 2012).

In summary, this study besides highlighting the molecular mechanisms of the cell entrance of these antimycobacterial compounds through the biological membranes contributes to the design of more effective anti-TB drugs.

Overall, the results suggest that RFB2 and RFB3 show a pronounced disordering effect on the bacterial membrane models, while the human membrane model with large fractions of neutral phospholipids remains less affected. Moreover, RFB2 and RFB3 induce the formation of isotropic phases in the bacterial membrane model, which may be related with a mechanism of disruption or impairment of the bacterial membrane and consequently cell death (Cardoso et al., 2012).

1.1. Materials

DMPC and DMPG were purchased from Sigma–Aldrich Co®. DPPG and DPPE were purchased from Avanti Polar Lipids®. RFB was isolated from Mycobutin®. RFB2 was obtained from RFB, using a selective acylation of the secondary amine (Figueiredo et al., 2009). RFB3 was synthetized from RFB as described below. N-(2-hydroxyethyethyl)piperazine-*N′*-(2-ethanesulfonic acid) (HEPES) and sodium chloride (NaCl) were purchased from Sigma–Aldrich Co®. The buffer system (HEPES 0.01 M, pH = 7.4, I = 0.1 M) was prepared with ultrapure water produced by Millipore Milli-Q (resistivity = 18.2 MΩcm), being the ionic strength adjusted with NaCl.

1.2. Methods

1.2.1. General

^{1}H and ^{13}C NMR (APT) spectra (Appendices, Figs. A.1 and A.2) were registered in a Bruker spectrometer CXP400 with a proton frequency of 400.13 MHz and a carbon-13 frequency of 100.61 MHz. All the reagents and the solvents used were analytical pure products. The reaction was followed by thin layer chromatography (TLC) on Merck 60 F254 (0.2 mm), silica gel pre-prepared plates. The isolation of the product was performed by column chromatography using silica gel Merck 60 (230–400 mesh, 0.04–0.063 mm), at normal atmospheric pressure or flash with nitrogen pressure, or also by preparative thin layer chromatography on silica gel Merck 60 F254 (0.5 mm) plates. Drug RFB was isolated from Micobutin® and purified by column chromatography on silica and was compared with an authentic sample supplied by UpJohn & and Pharmacia. All samples were dissolved in 99% deuterated chloroform, with tetramethylsilane as internal standard. The obtained results are presented in the following order: solvent, chemical shift (δ in ppm); relative intensity (as number of protons, H); multiplicity (s-singlet, br s-broad singlet, d-duplet, dd-double duplet, br d-broad duplet, t-triplet, q-quartet, m-multiplet); coupling constant J in Hz; and location in the molecule structure. MS spectrum was obtained in a Q-TOF2 mass spectrometer (Appendices, Fig. A.3) (Micromass, Manchester, UK) operated in the positive mode (flow rate, 10 μL min^{-1}; cone voltage, 30 V; capillary voltage, 3 kV, source temperature, 80 °C; desolvation temperature, 150 °C).

1.2.2. Synthesis of *N′*-butanoyl-rifabutin (RFB3)

To a round-bottomed flask containing a solution of RFB (200 mg; 0.23 mmol) in tetrahydrofuran (5.9 mL), triethylamine (96 μL; 0.74 mmol) was added dropwise, at −10 °C, with stirring, followed by a solution of butanoyl chloride (52 μL; 0.74 mmol) in tetrahydrofuran (3.9 mL), and the resulting mixture was left with stirring till it reached room temperature (~5 min). The resulting precipitate, the triethylamine hydrochloride, was filtered and the solvent was removed under reduced pressure. Then the product was extracted with ethyl acetate (3 × 20 mL) and the ethyl acetate was washed with water (3 × 10 mL), dried with $MgSO_4$, filtered, and evaporated to dryness. The product was purified by flash chromatography using a eluent mixture of ethyl acetate:hexane:methanol (3:4:0.2) to afford RFB3 as a homogeneous orange-colored solid in 43% yield. ^{1}H NMR ($CDCl_3$) δ −0.20 (3H, br s, CH_3-34), 0.58 (3H, br s, CH_3-33), 0.68–1.15 (15H, m, CH_3-31, CH_3-11′, CH3-12′, CH_3-32, CH_3-41), 1.55–1.86 (9H, m, H-24, H-26, CH_3-13, H-22, CH_2-40), 1.88–2.19 (11H, m, H-10′, CH_2-6′, CH_2-4′, CH_3-36, CH_3-30), 2.14–2.40 (m, 5H, CH_2-39, CH_2-9′, H-20), 2.48 (3H, s, CH_3-14), 2.91–3.22 (m, 9H, CH_2-5′, CH_2-7′, H-23, H-21, CH_3-37), 3.37–3.42 (1H, m, H-27), 3.75 (1H,s, 23-OH), 3.87 (1H, s, 21-OH), 4.73–5.32 (2H, m, H-25, H-28), 5.82–6.35 (3H,m, H-19, H-29, H-17, H-18), 8.19 (1H, s, NH), 13.81 (1H, s, 8-OH). ^{13}C NMR ($CDCl_3$) δ 7.5 (C-14), 8.5 (C-33), 10.7 (C-34, C-41), 10.8 (C-32), 13.7 (C-31), 20.6 (C-30, C-36), 21.0 (C-11′, C-12′, C-13), 25.6 (C-39, C10′), 32.9 (C-22), 36.3 (C-4′, C-8′), 37.2

Please cite this article in press as: Pinheiro, M., et al., Interactions of *N′*-acetyl-rifabutin and *N′*-butanoyl-rifabutin with lipid bilayers: A synchrotron X-ray study. Int J Pharmaceut (2013), http://dx.doi.org/10.1016/j.ijpharm.2013.06.018

G Model
IJP-13406; No. of Pages 9
ARTICLE IN PRESS
M. Pinheiro et al. / International Journal of Pharmaceutics xxx (2013) xxx–xxx

Table 1
Long distances (d) of DMPC bilayers and correlation length (ξ) determined from SAXS diffraction patterns at pH 7.4 and at 10, 18 and 40 °C. The data are presented in Å as a function of the concentration of RFB2 and RFB3.

Sample (mol %)	T (°C)	d_{SAXS} (Å)	ξ_1 (Å)
DMPC	10	61.3 ± 0.5	678 ± 10
	18	66.8 ± 0.5	604 ± 10
	40	62.6 ± 0.5	629 ± 10
DMPC:RFB2 5	10	63.6 ± 0.5	609 ± 10
	18	70.2 ± 0.5	873 ± 10
	40	63.1 ± 0.5	562 ± 10
DMPC:RFB2 10	10	64.3 ± 0.5	774 ± 10
	18	73.0 ± 0.5	765 ± 10
	40	66.7 ± 0.5	716 ± 10
DMPC:RFB3 5	10	63.8 ± 0.5	371 ± 10
	18	71.6 ± 0.5	1104 ± 10
	40	64.5 ± 0.5	1095 ± 10
DMPC:RFB3 10	10	63.7 ± 0.5	1105 ± 10
	18	74.6 ± 0.5	1061 ± 10
	40	66.0 ± 0.5	537 ± 10

Table 2
Short distances (d) of DMPC bilayers and correlation length (ξ) determined from WAXS diffraction patterns at pH 7.4 and at 10, 18 °C. The data are presented in Å as a function of the concentration of RFB2 and RFB3.

Sample (mol %)	T (°C)	d_{WAXS} (Å)		ξ_1 (Å)	ξ_2 (Å)
		1st Peak	2nd Peak		
DMPC	10	4.13	3.96	49 ± 10	82 ± 10
	18	4.15		80 ± 10	
DMPC:RFB2 5	10	4.13	3.92	47 ± 10	115 ± 10
	18	4.17		30 ± 10	
DMPC:RFB2 10	10	4.13	3.92	48 ± 10	
	18	4.16		42 ± 10	
DMPC:RFB3 5	10	4.07	3.83	22 ± 10	63 ± 10
	18	4.09		37 ± 10	
DMPC:RFB3 10	10	4.09	3.81	22 ± 10	24 ± 10
	18	4.09		36 ± 10	

(C-24), 38.1 (C-26, C-20), 39.3 (C-40), 51.1 (C-7′), 51.2, 51.2, 51.2 (C-5′, C-37), 65.7 (C-9′), 72.8 (C-21), 73.8 (C-25), 77.1 (C-23), 90.2 (C-27), 96.5 (C-2′), 106.0 (C-3), 108.8 (C-12), 111.0 (C-10), 113.6 (C-9), 114.4 (C-7, C-28), 128.8 (C-18), 130.6 (C-5), 136.2 (C-16, C-17), 141.2 (C-19), 141.5 (C-2), 142.2 (C-29), 153.1 (C-4), 166.6 (C-8), 166.7 (C-38, C-15) 172.4 (C-6, C-35), 186.1 (C-1), 191.4 (C-11); TOF-MS m/z 918 $[M+1]^+$, 917 $[M]^+$.

1.2.3. Multilamellar vesicles (MLVs)

Different amounts of RFB2 and RFB3 were mixed with DMPC (147 mM), DMPG (145 mM) and DPPE:DPPG 8:2 molar ratio (82:19 mM) in chloroform:methanol mixture (3:1, v/v) according to the required molar fraction of the antimycobacterial compound 5 and 10 mol%, with the final concentration of the antimycobacterial compounds (i.e. RFB2 and RFB3) respectively, 7.4 and 14.7 mM (in the DMPC vesicles), 7.3 and 14.5 mM (in the DMPG vesicles) and 5.1 and 10.1 mM (in the DPPE:DPPG vesicles). Lipid films were formed from these solutions, dried at 70.0 ± 0.1 °C under a stream of N_2 and left overnight under reduced pressure to remove all traces of the organic solvents. The lipid films were hydrated by adding the buffer system and then alternately heated at 70.0 ± 0.1 °C, mixed by vortexing for about 5 min and centrifuged for 30 s at 2000 × g. This procedure was repeated three times to ensure that all lipid film was hydrated. Finally, the samples were aged overnight at 4.0 ± 0.1 °C and shaken by vortex at room temperature for 5 min. Thereafter, the dispersions were transferred into glass capillaries of 1.5 mm diameter (Hilgenberg, Malsfeld, Germany), which are transparent to X-rays. The flame-sealed capillaries were stored at 4.0 ± 0.1 °C until the measurements.

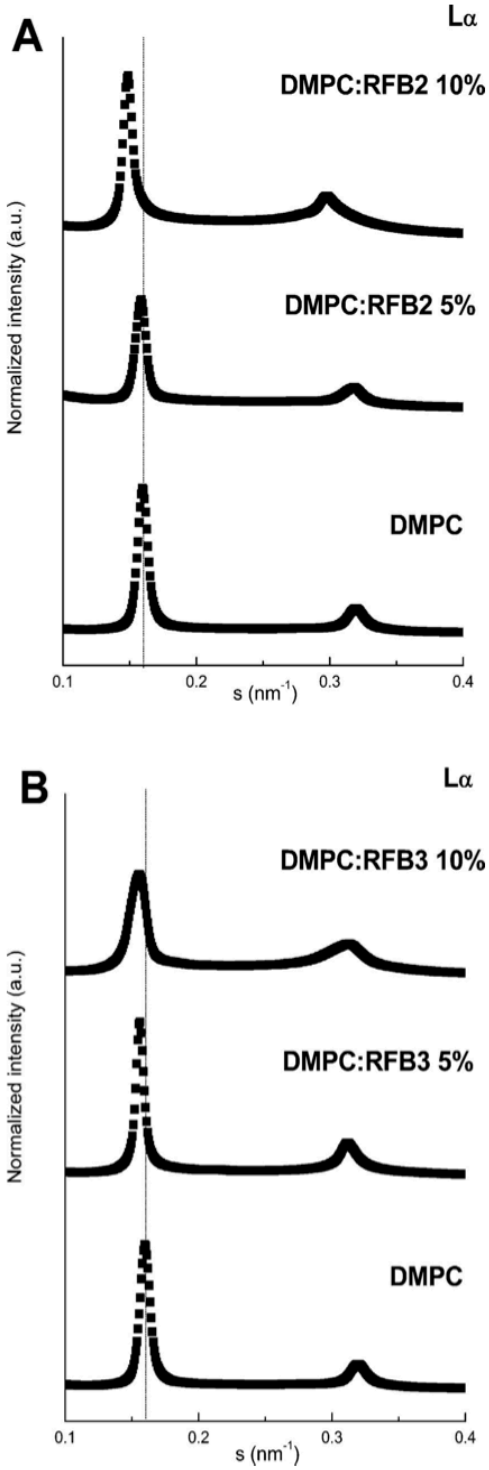

Fig. 2. Small-angle X-ray diffraction profiles of DMPC with 5 mol% and 10 mol% RFB2 (A) and DMPC with 5 mol% and 10 mol% RFB3 (B) at 40 °C.

1.2.4. Small-angle X-ray scattering and wide-angle X-ray scattering

SAXS and WAXS experiments were executed at beamline A2 at Doris III of HASYLAB (DESY, Hamburg, Germany) with a monochromatic radiation wavelength of 0.15 nm. The SAXS detector was

Please cite this article in press as: Pinheiro, M., et al., Interactions of N′-acetyl-rifabutin and N′-butanoyl-rifabutin with lipid bilayers: A synchrotron X-ray study. Int J Pharmaceut (2013), http://dx.doi.org/10.1016/j.ijpharm.2013.06.018

G Model
IJP-13406; No. of Pages 9
ARTICLE IN PRESS
4 M. Pinheiro et al. / International Journal of Pharmaceutics xxx (2013) xxx–xxx

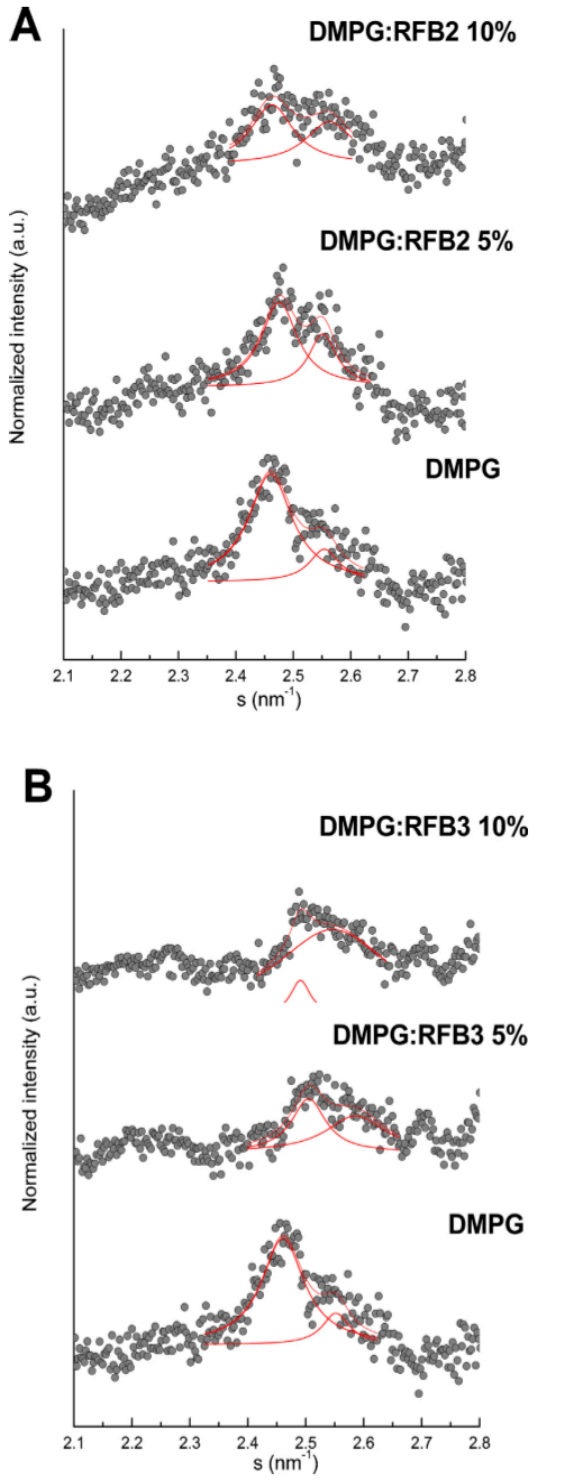

Fig. 3. Wide-angle X-ray diffraction patterns of DMPG with 5 mol% and 10 mol% RFB2 (A) and DMPG with 5 mol% and 10 mol% RFB3 (B) at 10 °C.

calibrated with rat-tail tendon and the WAXS detector with polyethylene terephthalate (PET). The samples were exposed to static measurements at different temperatures according the thermotropic behavior of the lipids. After each temperature step, the sample was allowed to equilibrate for 5 min before the diffraction pattern was recorded. In order to minimize the X-ray exposure of the sample, a shutter, mounted in front of the sample, was kept closed when no data was acquired. The lamellar repeat distance d was calculated from the diffraction patterns using Bragg's equation $s = n/d$; where $s = \lambda/2 \sin\Theta$ is the scattering vector and n the order of the reflection ($n = 1, 2, \ldots$). To obtain more s values, the diffraction peaks were fitted with Lorentzians and the positions of maximum intensities and full-width at half-maximum (fwhm) of the peaks were determined (Nunes et al., 2011a).

Table 3
Long distances (d) of DMPG bilayers and correlation length (ξ) determined from SAXS diffraction patterns at pH 7.4 and at 8, 18 and 40 °C. The data are presented in Å as a function of the concentration of RFB2 and RFB3.

Sample (mol %)	T (°C)	d_{SAXS} (Å)	ξ_1 (Å)
DMPG	8	47.9 ± 0.7	396 ± 10
	18	51.1 ± 0.7	421 ± 10
	40	48.4 ± 0.7	36 ± 10
DMPG:RFB2 5	8	48.4 ± 0.7	261 ± 10
	18	48.1 ± 0.7	272 ± 10
	40	46.6 ± 0.7	10 ± 10
DMPG:RFB2 10	8	48.2 ± 0.7	137 ± 10
	18	48.0 ± 0.7	131 ± 10
	40	45.9 ± 0.7	10 ± 10
DMPG:RFB3 5	8	48.1 ± 0.7	346 ± 10
	18	48.1 ± 0.7	272 ± 10
	40	46.6 ± 0.7	10 ± 10
DMPG:RFB3 10	8	48.0 ± 0.7	190 ± 10
	18	48.0 ± 0.7	130 ± 10
	40	45.9 ± 0.7	10 ± 10

Table 4
Short distances (d) of DMPG bilayers and correlation length (ξ) determined from WAXS diffraction patterns at pH 7.4 and at 8, 18 °C. The data are presented in Å as a function of the concentration of RFB2 and RFB3.

Sample (mol %)	T (°C)	d_{WAXS} (Å)		ξ_1 (Å)	ξ_2 (Å)
		1st Peak	2nd Peak		
DMPG	8	4.03	3.86	132 ± 10	14 ± 10
	18	4.04		177 ± 10	
DMPG:RFB2 5	8	4.04	3.93	206 ± 10	15 ± 10
	18	3.96		10 ± 10	
DMPG:RFB2 10	8	4.06	3.89	60 ± 10	45 ± 10
	18	3.97		10 ± 10	
DMPG:RFB3 5	8	3.99	3.85	87 ± 10	31 ± 10
	18	4.00		31 ± 10	
DMPG:RFB3 10	8	4.00		13 ± 10	13 ± 10
	18	3.99		62 ± 10	

2. Results and discussion

2.1. Effects of RFB2 and RFB3 on the structure of DMPC bilayers

The zwitterionic phospholipid DMPC as other phosphatidylcholines spontaneously forms lamellar phases in excess of water, whose structure and long-range organization are dependent of the temperature (Eisenblatter and Winter, 2006). Static measurements at several temperatures (10, 18 and 40 °C) were carried out by simultaneous SAXS and WAXS, yielding information on long range bilayer organization and hydrocarbon chain packing, respectively. Moreover, the SAXS measurements allow to obtain the distances between the thickness of the bilayer plus the water layer, whereas the WAXS measurements permit to determine the distances between the phospholipids head groups (Pili et al., 2009). The investigated temperatures 10, 18 and 40 °C were chosen to cover respectively, the thermal ranges of the gel (Lβ′), ripple gel (Pβ′) and lamellar fluid (Lα) phases (Eisenblatter and Winter, 2006). In the Lβ′ the acyl chains are fully extended, tilted and packed in a distorted hexagonal lattice. Temperature increase leads to the

Please cite this article in press as: Pinheiro, M., et al., Interactions of N′-acetyl-rifabutin and N′-butanoyl-rifabutin with lipid bilayers: A synchrotron X-ray study. Int J Pharmaceut (2013), http://dx.doi.org/10.1016/j.ijpharm.2013.06.018

G Model
IJP-13406; No. of Pages 9
ARTICLE IN PRESS
M. Pinheiro et al. / International Journal of Pharmaceutics xxx (2013) xxx–xxx

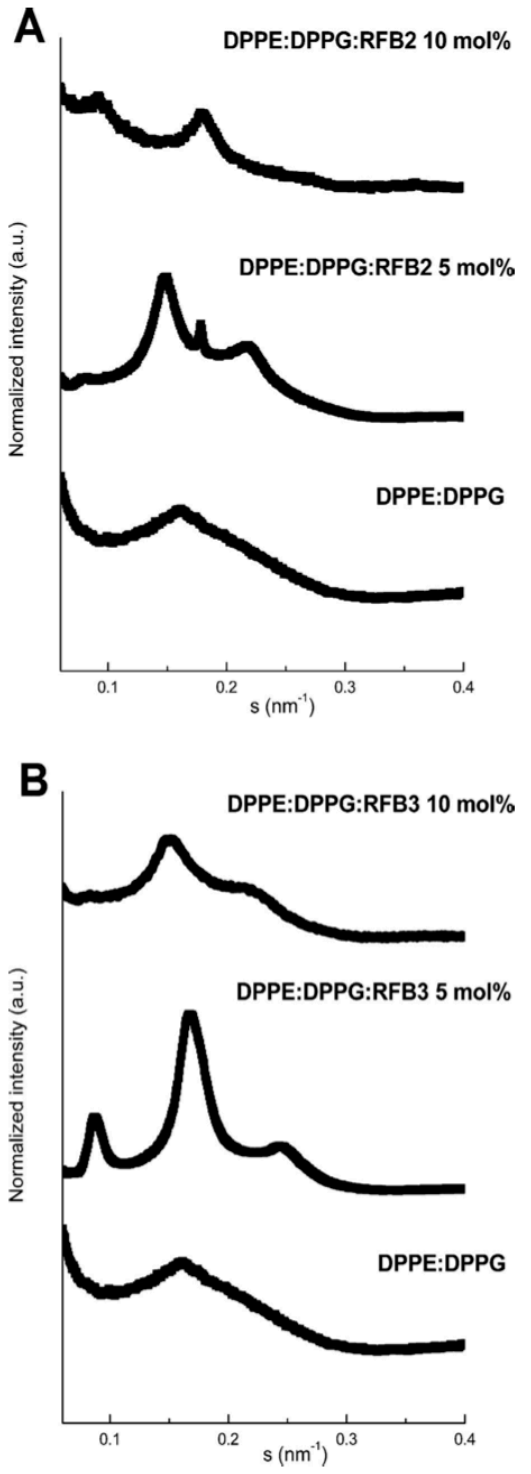

Fig. 4. Small-angle X-ray diffraction profiles of DPPE:DPPG with 5 mol% and 10 mol% RFB2 (A) and DPPE:DPPG with 5 mol% and 10 mol% RFB3 (B) at 37 °C.

pre-transition from Lβ′ to Pβ′, in which the lipid bilayers are distorted by a periodic ripple in the lamellae plane. The Lα phase is formed above the main transition temperature (T_m), being the acyl chains disordered (*trans-gauche* isomerization) (Nunes et al., 2011b). The repeat distance, *d* deduced from the SAXS patterns of DMPC as well as the correlation between the bilayers (ξ) are listed in Table 1. For DMPC, the first order Bragg peaks in the scattering curves appear at 1/61.3 Å^{-1} (Lβ′), 1/66.8 Å^{-1} (Pβ′), and 1/62.6 Å^{-1} (Lα) in good agreement with the literature (Eisenblatter and Winter, 2006). The *d*-values of the chain lattice of DMPC obtained by WAXS measurements and the corresponding correlation lengths (ξ) are listed in Table 2. Analyzing these shows that DMPC displays a sharp reflection at 1/4.13 Å^{-1} with a shoulder located at 1/3.96 Å^{-1}, which indicates the orthorhombic (pseudo-hexagonal) lattice of the chains in the DMPC bilayers (Nunes et al., 2011a; Eisenblatter and Winter, 2006). At 18 °C, only one diffraction peak is observed at 1/4.15 Å^{-1} with a symmetric profile, which indicates the hexagonal chain packing characteristic of the Pβ′ phase (Nunes et al., 2011b). At 40 °C, in the Lα, a diffuse reflection appears corresponding to the disordered molten chains (Fig. 2A) (Cardoso et al., 2012; Eisenblatter and Winter, 2006).

The incorporation of RFB2 and RFB3 in DMPC bilayers leads to a change of the SAXS and WAXS diffraction patterns depending on the chemical structure and concentration of the antimycobacterial compound. In the presence of RFB2, the first order Bragg reflection peaks on the scattering curves appear at 1/63.6 (Lβ′), 1/70.2 (Pβ′), 1/63.1 Å^{-1} (Lα) for 5 mol% and at 1/64.3 (Lβ′), 1/73.0 (Pβ′), 1/66.7 (Lα) Å^{-1} for 10 mol%(Table 1). Thus, RFB2 increases the bilayer thickness and/or the adjacent water layer of the DMPC bilayers in a concentration-dependent manner and especially in the gel Pβ′ phase. In addition, the SAXS diffraction spectra obtained for DMPC in the Lα phase in the absence and in the presence of RFB2 and RFB3 are represented in Fig. 2. In the most biological relevant mesophase (i.e. Lα phase), 5 mol% of RFB2 produce only a slight increase of the *d*-spacing (Fig. 2A). The observed bigger increase of the *d*-spacings for higher concentrations may be mainly due to an increase of the hydration of the phospholipids head groups (Cardoso et al., 2012).

The *d*-spacing increases by approximately 3 Å in the Lβ′, 6 Å in the Pβ′ and 4 Å in the Lα phase. Furthermore, the correlation between the lipid bilayers (ξ) is increased in the presence of 10 mol% RFB2. Similar to the SAXS features, no significant changes in the WAXS profile were obtained (Table 2). This shows that the in-plane structure of DMPC bilayers is preserved, and the effect of RFB2 is mainly restricted to the water layer (Nunes et al., 2011b). Regarding the effect of RFB3, the first order Bragg reflection peaks in the scattering curves of DMPC bilayers are located at 1/63.8 (Lβ′), 1/71.6 (Pβ′), 64.5 Å^{-1} (Lα) for 5 mol% and at 1/63.7 (Lβ′), 1/74.6 (Pβ′), 1/66.0 (Lα) Å^{-1} for 10 mol% (Table 1). Thus, the effects of RFB3 on the DMPC lipid bilayers seem to be similar to the ones described for RFB2. Thus, the *d*-spacings increase by roughly 3 Å in the Lβ′ and Lα phases, and 8 Å in the Pβ′. The more pronounced changes in the WAXS diffraction patterns (Table 2) suggest a stronger interaction of RFB3 with the phospholipids in comparison with RFB2. The changes to larger *d*-spacings obtained may be due to the reduction of the chain tilt in the gel phases caused by the RFB3 molecules penetrating the lipid bilayers (Nunes et al., 2011a,b). The more pronounced disordering effect on the in-plane structure of DMPC bilayers caused by RFB3 in comparison to RFB2 may be due to the different location of the antimycobacterial compounds within the DMPC lipid bilayer (Pereira-Leite et al., 2013). In fact, RFB3 is a bulkier and more lipophilic molecule than RFB2, being the presence of a more hydrophobic group, i.e. butanoyl in comparison to the acetyl, probably responsible for a deeper penetration into the hydrophobic region of the lipid bilayers (Figueiredo et al., 2009).

2.2. *Effects of RFB2 and RFB3 on the structure of DMPG bilayers*

The negatively charged phospholipid DMPG exhibits at high salt concentrations a similar thermotropic behavior as the phosphatidylcholines (Lamy-Freund and Riske, 2003). Nonetheless, the

Please cite this article in press as: Pinheiro, M., et al., Interactions of *N*′-acetyl-rifabutin and *N*′-butanoyl-rifabutin with lipid bilayers: A synchrotron X-ray study. Int J Pharmaceut (2013), http://dx.doi.org/10.1016/j.ijpharm.2013.06.018

G Model
IJP-13406; No. of Pages 9
ARTICLE IN PRESS

Table 5
Long distances (d) of DPPE:DPPG bilayers and correlation length (ξ) determined from SAXS diffraction patterns at pH 7.4 and at 37, 56 and 65 °C. The data are presented in Å as a function of the concentration of RFB2 and RFB3.

Sample (mol %)	T (°C)	d_{SAXS} (Å)				ξ_1 (Å)	ξ_2 (Å)	ξ_3 (Å)	ξ_4 (Å)
		$d1$	$d2$	$d3$	$d4$				
DPPE:DPPG	37	62.8 ± 0.5				137 ± 10			
	56	61.2 ± 0.5				317 ± 10			
	65	64.4 ± 0.5				202 ± 10			
DPPE:DPPG:RFB2 5	37	118.0 ± 0.5	68.5 ± 0.5	56.6 ± 0.5	47.2 ± 0.5	20 ± 10	246 ± 10	942 ± 10	158 ± 10
	56	125.0 ± 0.5	66.7 ± 0.5	55.9 ± 0.5	47.7 ± 0.5	96 ± 10	273 ± 10	1662 ± 10	18 ± 10
	65	124.3 ± 0.5	67.3 ± 0.5	56.2 ± 0.5	47.2 ± 0.5	14 ± 10	274 ± 10	1694 ± 10	20 ± 10
DPPE:DPPG:RFB2 10	37	115.6 ± 0.5	56.0 ± 0.5			83 ± 10	321 ± 10		
	56	109.7 ± 0.5	54.9 ± 0.5			174 ± 10	326 ± 10		
	65	112.2 ± 0.5	53.8 ± 0.5			23 ± 10	389 ± 10		
DPPE:DPPG:RFB3 5	37	110.6 ± 0.5	58.9 ± 0.5	43.3 ± 0.5		319 ± 10	155 ± 10	34 ± 10	
	56	110.2 ± 0.5	58.0 ± 0.5	41.3 ± 0.5		362 ± 10	186 ± 10	50 ± 10	
	65	113.3 ± 0.5	59.1 ± 0.5	41.9 ± 0.5		405 ± 10	227 ± 10	59 ± 10	
DPPE:DPPG:RFB3 10	37	120.9 ± 0.5	65.5 ± 0.5	49.9 ± 0.5		20 ± 10	160 ± 10	13 ± 10	
	56	117.6 ± 0.5	64.9 ± 0.5	48.5 ± 0.5		34 ± 10	198 ± 10	26 ± 10	
	65	120.9 ± 0.5	66.5 ± 0.5	48.0 ± 0.5		10 ± 10	219 ± 10	31 ± 10	

Table 6
Short distances (d) of DPPE:DPPG bilayers and correlation length (ξ) determined from WAXS diffraction patterns at pH 7.4 and at 37, 56 °C. The data are presented in Å as a function of the concentration of RFB2 and RFB3.

Sample (mol %)	T (°C)	d_{WAXS} (Å)	ξ_1 (Å)
DPPE:DPPG	37	4.07	93 ± 10
	56	4.16	10 ± 10
DPPE:DPPG:RFB2 5	37	4.08	322 ± 10
	56	4.17	284 ± 10
DPPE:DPPG:RFB2 10	37	4.05	101 ± 10
	56	4.16	86 ± 10
DPPE:DPPG:RFB2 10	37	4.06	92 ± 10
	56	4.16	79 ± 10
DPPE:DPPG:RFB3 10	37	4.05	113 ± 10
	56	4.17	233 ± 10

SAXS diffraction patterns of DMPG had shown a very diffuse and broad scattering, which points to a much lower correlation between bilayers as previously reported (Cardoso et al., 2012; Spinozzi et al., 2010). In aqueous dispersions of charged phospholipids, due to the electrostatic repulsions, the formation of large unilamellar vesicles or of non-correlated bilayers takes place. The broad peaks obtained were not analyzed in terms of a form factor of the DMPG bilayer but the intensity maximum was used to obtain the d-spacings associated with a larger error bar (see Table 3). Table 3 displays the long-range repeat distances (d) and the correlation length (ξ) between the DMPG bilayers. The Bragg reflection peaks on the scattering curves for DMPG appear at 1/47.9 (Lβ′), 1/51.1 (Pβ′), 1/48.4 $Å^{-1}$ (Lα). The d-spacing values obtained are in accordance with the values described in the literature using similar conditions (Duarte et al., 2008). The WAXS diffraction patterns of DMPG (Fig. 3) show an asymmetric Bragg peak centered around 1/4.03 $Å^{-1}$ and 1/3.86 $Å^{-1}$ (Table 4), corresponding to the pseudo-hexagonal lattice of the DMPG chains. Upon heating, one symmetric Bragg peak appears, centered around 1/4.04 $Å^{-1}$, indicating the formation of a hexagonal chain lattice with an unusual small cross-sectional area (19 $Å^2$) of the chains (Nunes et al., 2011b). Finally, at 40 °C the characteristic broad profile of molten chains appears in the Lα phase (data not shown) (Spinozzi et al., 2010).

From the SAXS and WAXS profiles obtained one can conclude that both antimycobacterial compounds have a pronounced disordering effect on the structure of DMPG bilayers. Overall, the incorporation of RFB2 and RFB3 in the DMPG bilayers leads to a decrease in the bilayer and/or water layer thickness as well as in the correlation length (ξ) between the negatively charged bilayers (Table 3). In the case of RFB2, the Bragg peaks in the scattering curves are centered at 1/48.4 (Lβ′), 1/48.1 (Pβ′), 1/46.6 $Å^{-1}$ (Lα) for 5 mol% and at 1/48.2 (Lβ′), 1/48.0 (Pβ′), 1/45.9 (Lα) $Å^{-1}$ for 10 mol% (Table 3). In addition, the decrease in the correlation length (ξ) (Table 3) between the bilayers supports a high disturbance effect of RFB2, being especially observed for high concentrations. On the other hand, the changes in the WAXS diffraction patterns at 8 °C as a function of the RFB2 concentration prove the marked electrostatic interaction of RFB2 with the negatively charged phospholipids. Thus, the Bragg peaks become less asymmetric with increasing RFB2 concentration, indicating the reduction of the chain lattice distortion connected with a decrease of the chain tilt, and the alteration of the phospholipid packing from orthorhombic to hexagonal (Fig. 3A) (Pereira-Leite et al., 2012; Nunes et al., 2011b). RFB2 and RFB3 at the physiological pH (7.4) are charged molecules (predicted using MarvinView® 5.4.1.1 software from ChemAxon). These molecules are predominantly in the zwitterionic form having also a significant contribution of positively charged groups. Thus, electrostatic interactions between the protonated imidazole and/or piperidine (Fig. 1) with the deprotonated phosphate of DMPG may contribute to the pronounced interactions of RFB2 with the negatively charged phospholipids (Cardoso et al., 2012; Spinozzi et al., 2010). Therefore, the positively charged antimycobacterial compounds seem to screen the repulsive effect of the negatively charged phospholipid head groups, leading to the observed changes in the chain lattice (Table 4; Cardoso et al., 2012).

In the presence of RFB3, the thicknesses of the bilayer and/or water layer of DMPG were affected in a similar way in comparison to the RFB2 (Table 3). Nevertheless, the correlation between the bilayers (ξ) is more affected in the presence of the bulkier RFB3, which suggest a more pronounced disordering effect possibly due to a different location between the negatively charged lipid bilayers. The WAXS data reinforce these observations regarding the slightly larger d-values indicating a decreased packing density in the chain region (Table 4). In contrast to DMPC, Bragg peaks in the wide-angle region become less asymmetric with the increase of the RFB2 and RFB3 concentrations (Fig. 3) indicating a drastic change of the chain packing mode. This observation is in agreement with the noticed marked interaction of the antimycobacterial compounds with the negatively charged phospholipid head groups, which seems to be connected with the establishment of electrostatic interactions between the protonated groups (piperidine and imidazole) and the polar head groups of DMPG (Nunes et al., 2011a,b).

Please cite this article in press as: Pinheiro, M., et al., Interactions of N′-acetyl-rifabutin and N′-butanoyl-rifabutin with lipid bilayers: A synchrotron X-ray study. Int J Pharmaceut (2013), http://dx.doi.org/10.1016/j.ijpharm.2013.06.018

G Model
IJP-13406; No. of Pages 9
ARTICLE IN PRESS
M. Pinheiro et al. / International Journal of Pharmaceutics xxx (2013) xxx–xxx

2.3. Effects of RFB2 and RFB3 on the structure of DPPE:DPPG bilayers

The lipid mixture DPPE:DPPG (8:2 molar ratio) in the gel phase is characterized by a SAXS diffraction pattern with only one broad peak clearly dominated by the 20 mol% of DPPG. The broad peak in aqueous dispersions of anionic DPPG indicates the formation of non-correlated bilayers in contrast to DPPE, which forms well-correlated bilayers characterized by a sharp Bragg peak usually with no higher order reflections. It is known that this mixture exhibits a non-ideal miscibility behavior and consequently forms microdomains (Oszlanczi et al., 2010b, 2007). The Lβ phase of DPPE is stable until 61 °C, and only above this temperature the Lα phase is formed (Oszlanczi et al., 2010b). The SAXS diffraction patterns obtained for the DPPE:DPPG mixture are shown in Fig. 4. The maximum position of the broad diffraction pattern is located near 1/62.8 Å^{-1} (37 °C), 1/61.2 (56 °C) (Lβ) and 1/64.4 Å^{-1} (Lα) (Table 5), being in good agreement with the literature (Oszlanczi et al., 2010a). The single Bragg peak obtained in the WAXS profile (Table 6) at 1/4.07 Å^{-1} (Lβ′) (37 °C) is consistent with the hexagonal chain packing in the Lβ phase (Oszlanczi et al., 2010b). A shift to larger values (1/4.13 Å^{-1}) is observed during heating (56 °C) and indicates the increase of the cross-sectional area of the chains from 19.2 Å^2 to 19.7 Å^2 connected with an increased chain mobility. At 65 °C, the WAXS diffraction peak becomes broad, which confirms the chain melting (data not shown), being these features in good agreement with the literature (Oszlanczi et al., 2010a, 2007).

The incorporation of the antimycobacterial compounds in the DPPE:DPPG bilayers leads to a marked alteration in the layer arrangement and chain packing. The effect of RFB2 and RFB3 on the DPPE:DPPG bilayers is shown in the SAXS diffraction patterns at several temperatures (Fig. 4). Remarkably, a clear change in the features of the SAXS profile of DPPE:DPPG can be observed even for low concentrations of the antimycobacterial compounds. Moreover, for both antimycobacterial compounds, the Bragg peaks with the higher intensity do not follow the n/d (n is integer, d is periodicity) characteristic of the lamellar phase. Therefore, the formation of a non-lamellar phase has to be assumed (i.e. cubic structure) (Oszlanczi et al., 2010a). The SAXS patterns of DPPE:DPPG in the presence of 5 mol% of RFB2 exhibit at each temperature four more or less pronounced Bragg peaks (the positions can be found in Table 5) on a broader background. The diffuse peaks indicate a small coherence length in the formed lattice. However, it is obvious that 5 mol% of RFB2 lead to much larger repeat distances. The observed four peaks are in a ratio of s_1: $\sqrt{3}\cdot s_2$: $2\cdot s_3$: $\sqrt{6}\cdot s_4$. The expected $\sqrt{2}$ peak is too weak to be observed on the broad background. Such a ratio of d-spacings is a clear indication for a cubic structure (Phan et al., 2011). Thus, the repulsions between the negatively charged head groups were minimized by the intercalation of the charged RFB2 molecules, acting as a shield of the surface net charge (Cardoso et al., 2012). The only surprising observation is that the phase structure does almost not change during heating pointing to a coexistence of a cubic (with molten chains) phase and a lamellar (with rigid chains) phase with uncorrelated bilayers. In the presence of 10 mol% of RFB2, the Bragg peaks are displaced in a ratio of 1:2, characteristic of lamellar phases (Table 5). The broad background originating from noncorrelated bilayers is almost absent, so that purely the liquid-crystalline Lα phase is formed. In the presence of 5 mol% of RFB3, a similar ratio in the spacings can bee seen as for RFB2 but with less pronounced Bragg peaks, so that the addition of RFB3 also leads to the formation of nonlamellar phases (Table 5). In the case of 10 mol% of RFB3, a similar scattering curve can be observed but with slightly larger d-values (Table 5). As observed for RFB2, the structure does almost not change during heating. In a similar way as for RFB2, the correlation length within the observed structure also increases in the presence of RFB3. Moreover, the WAXS profile obtained for both antimycobacterial compounds (Table 6) shown an overall increase of the correlation length (ξ), which is consistent with the strong interaction of the antimycobacterial compounds with DPPE:DPPG and the minimization of the electrostatic repulsions between the phospholipid head groups.

3. Conclusions

In this work, the interactions of two novel antimycobacterial compounds (RFB2 and RFB3) with the bacterial and human membrane models were assessed using two powerful biophysical techniques, SAXS and WAXS. The results obtained point to a differential interaction depending on the charge of the head groups of the phospholipids. The effects of these novel antimycobacterial compounds are scarce in the zwitterionic membrane model and are marked in the negatively charged membrane models. In addition, the interactions of the antimycobacterial compounds with the lipid bilayers are strongly influenced by the concentrations of RFB2 and RFB3 used. In fact, the effects of lower concentrations of these novel antimycobacterial compounds are negligible in the zwitterionic membrane model and more evident on the gel phases. On the other hand, the interactions are strongly dependent of the antimycobacterial compound structure. Therefore, a slight change in the chemical structure of the antimycobacterial compound (acetyl versus butanoyl group) is responsible for differential interactions with the membrane models. Herein, the addition of substituents by more lipophilic ones permits the establishment of marked van der Waals forces, which were found to be related to the higher penetration abilities of RFB3 in comparison with RFB2. Consequently, in vivo, RFB3 is expected to have a marked bioavailability and diffusion across the cell membranes when compared to RFB2. However, the toxic effects can be also pronounced since in the case of RFB are strongly dependent with its lipid affinity and ability to cross particularly ordered biological membranes, such as uveitis and discoloration of the skin (Pinheiro et al., 2013b). Herein, these antimycobacterial compounds, and especially in high concentrations, are putatively expected to induce perturbation in highly ordered membranes of the human body as stratum corneum and the retinal membrane, causing the above-mentioned side effects. On the other hand, the interactions of these compounds with the negatively charged bacterial membrane models are pronounced in all lipid phases including the fluid phase with more physiological relevance. In addition, the antibacterial activity of RFB2 and RFB3 seem to be also related with the ability to induce negative curvature in the bacterial membranes, which may be related with their selectivity for the bacterial cells in comparison to the human cell. Moreover, the mechanism of action of the antimicrobial peptides related with their ability to destabilize the lamellar phases was already described in the literature (Cardoso et al., 2012; Rappolt et al., 2003). In fact, the transition from lamellar to cubic phases constitutes an important route of membrane fusion (Rappolt et al., 2003). The electrostatic interaction between these compounds with the negatively charged bacterial membrane, associated with the ability of these drugs to induce cubic phases may contribute to the bacterial cell death through pores production in the membrane (Hickel et al., 2008).

In summary, both antimycobacterial compounds exhibit a differential interaction with the membrane models studied, which may be translated in a higher selectivity to the bacterial cell. Nevertheless, in comparison to RFB3, RFB2 had shown a pronounced disordering effect in the bacterial membrane models and a less pronounced effect in the human membrane model. Therefore, this might be related with less adverse effects and higher antibiotic efficacy of RFB2, reinforcing its high potential interest for the clinical

Please cite this article in press as: Pinheiro, M., et al., Interactions of N′-acetyl-rifabutin and N′-butanoyl-rifabutin with lipid bilayers: A synchrotron X-ray study. Int J Pharmaceut (2013), http://dx.doi.org/10.1016/j.ijpharm.2013.06.018

G Model
IJP-13406; No. of Pages 9
ARTICLE IN PRESS

practice and management of TB. On the other side, the lipid mixture DPPE:DPPG 8:2 (molar ratio) may be further exploited to produce liposomes as drug delivery systems of RFB2 and RFB3 because of the great interest in the use of cubic phases in the lipid-based liquid crystalline materials as drug delivery systems, since they provide a diffusion controlled release of the drugs (Phan et al., 2011).

Acknowledgments

Marina Pinheiro, João M. Caio and Cláudia Nunes thank FCT (Lisbon) for the fellowships (SFRH/BD/63318/2009, SFRH/BD/66789/2009 and SFRH/BPD/81963/2011), respectively. Authors are also grateful to the FCT for financial support under projects PEst-OE/QUI/UI0612/2013 and PTDC/QUI-QUI/101022/2008 with co-participation European Community funds from the FEDER, QREN and COMPET. The authors thank HASYLAB at DESY, Hamburg, Germany, for beam time and support through the project II-20100139 EC. The authors are grateful to Dr. Sérgio Funari for help at beamline A2.

Appendix A.

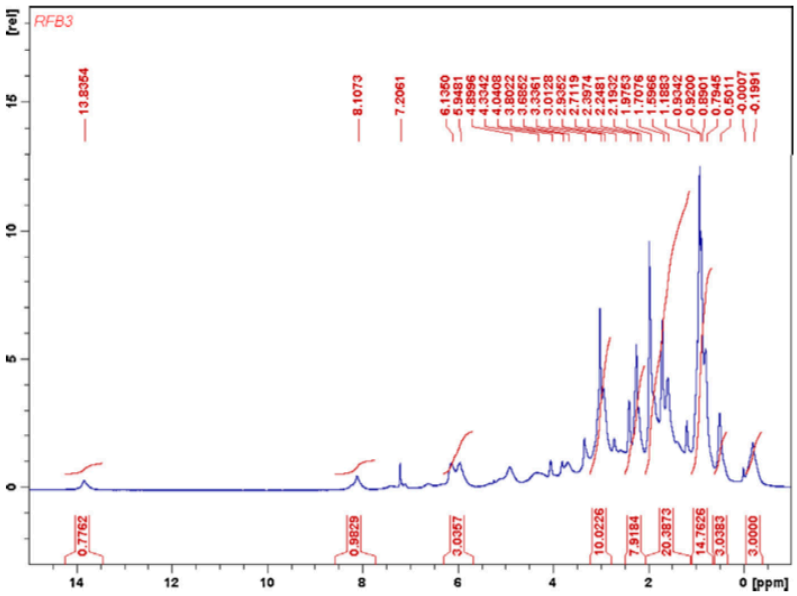

Fig. A.1. ^{1}H NMR spectrum of RFB3.

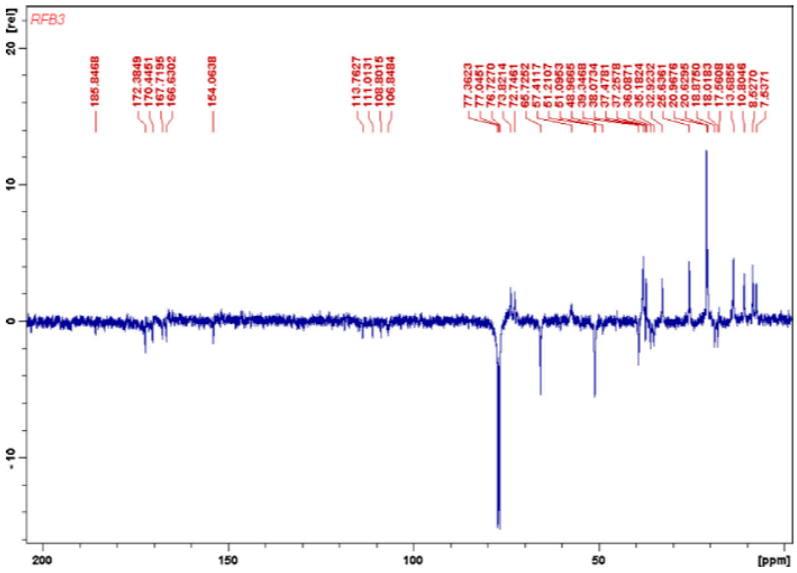

Fig. A.2. ^{13}C NMR (APT) spectrum of RFB3.

Please cite this article in press as: Pinheiro, M., et al., Interactions of *N*′-acetyl-rifabutin and *N*′-butanoyl-rifabutin with lipid bilayers: A synchrotron X-ray study. Int J Pharmaceut (2013), http://dx.doi.org/10.1016/j.ijpharm.2013.06.018

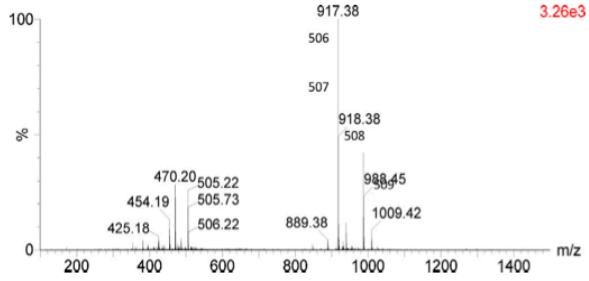

Fig. A.3. TOF-MS spectrum of RFB3.

References

Cardoso, A.M., Trabulo, S., Cardoso, A.L., Lorents, A., Morais, C.M., Gomes, P., Nunes, C., Lucio, M., Reis, S., Padari, K., Pooga, M., Pedroso de Lima, M.C., Jurado, A.S., 2012. S4(13)-PV cell-penetrating peptide induces physical and morphological changes in membrane-mimetic lipid systems and cell membranes: implications for cell internalization. Biochim. Biophys. Acta 1818, 877–888.

Duarte, E.L., Oliveira, T.R., Alves, D.S., Micol, V., Lamy, M.T., 2008. On the interaction of the anthraquinone barbaloin with negatively charged DMPG bilayers. Langmuir 24, 4041–4049.

Eisenblatter, J., Winter, R., 2006. Pressure effects on the structure and phase behavior of DMPC-gramicidin lipid bilayers: a synchrotron SAXS and 2H-NMR spectroscopy study. Biophys. J. 90, 956–966.

Figueiredo, R., Moiteiro, C., Medeiros, M.A., da Silva, P.A., Ramos, D., Spies, F., Ribeiro, M.O., Lourenco, M.C., Junior, I.N., Gaspar, M.M., Cruz, M.E., Curto, M.J., Franzblau, S.G., Orozco, H., Aguilar, D., Hernandez-Pando, R., Costa, M.C., 2009. Synthesis and evaluation of rifabutin analogs against Mycobacterium avium and H(37)Rv, MDR and NRP *Mycobacterium tuberculosis*. Bioorg. Med. Chem. 17, 503–511.

Gandhi, N.R., Nunn, P., Dheda, K., Schaaf, H.S., Zignol, M., van Soolingen, D., Jensen, P., Bayona, J., 2010. Multidrug-resistant and extensively drug-resistant tuberculosis: a threat to global control of tuberculosis. Lancet 375, 1830–1843.

Hickel, A., Danner-Pongratz, S., Amenitsch, H., Degovics, G., Rappolt, M., Lohner, K., Pabst, G., 2008. Influence of antimicrobial peptides on the formation of non-lamellar lipid mesophases. Biochim. Biophys. Acta 1778, 2325–2333.

Lamy-Freund, M.T., Riske, K.A., 2003. The peculiar thermo-structural behavior of the anionic lipid DMPG. Chem. Phys. Lipids 122, 19–32.

Maloney, E., Stankowska, D., Zhang, J., Fol, M., Cheng, Q.J., Lun, S., Bishai, W.R., Rajagopalan, M., Chatterjee, D., Madiraju, M.V., 2009. The two-domain LysX protein of Mycobacterium tuberculosis is required for production of lysinylated phosphatidylglycerol and resistance to cationic antimicrobial peptides. PLoS Pathog. 5, e1000534.

Nunes, C., Brezesinski, G., Lima, J.L.F.C., Reis, S., Lucio, M., 2011a. Effects of non-steroidal anti-inflammatory drugs on the structure of lipid bilayers: theraputical aspects. Soft Matter. 7, 3002–3010.

Nunes, C., Brezesinski, G., Lima, J.L., Reis, S., Lucio, M., 2011b. Synchrotron SAXS and WAXS study of the interactions of NSAIDs with lipid membranes. J. Phys. Chem. B 115, 8024–8032.

Oszlanczi, A., Bota, A., Klumpp, E., 2007. Layer formations in the bacteria membrane mimetic DPPE-DPPG/water system induced by sulfadiazine. Biophys. Chem. 125, 334–340.

Oszlanczi, A., Bota, A., Klumpp, E., 2010a. Influence of aminoglycoside antibiotics on the thermal behaviour and structural features of DPPE-DPPG model membranes. Colloids Surf. B. Biointerfaces 75, 141–148.

Oszlanczi, A., Bota, A., Berenyi, S., Klumpp, E., 2010b. Structural and morphological changes in bacteria-membrane mimetic DPPE/DPPG/water systems induced by sulfadiazine. Colloids Surf. B. Biointerfaces 76, 519–528.

Pereira-Leite, C., Nunes, C., Lima, J.L., Reis, S., Lucio, M., 2012. Interaction of celecoxib with membranes: the role of membrane biophysics on its therapeutic and toxic effects. J. Phys. Chem. B 116, 13608–13617.

Pereira-Leite, C., Carneiro, C., Soares, J.X., Afonso, C., Nunes, C., Lucio, M., Reis, S., 2013. Biophysical characterization of the drugs-membrane interaction: the case of propranolol and acebutolol. Eur. J. Pharm. Biopharm., http://dx.doi.org/10.1016/j.ejpb.2012.12.005.

Phan, S., Fong, W.K., Kirby, N., Hanley, T., Boyd, B.J., 2011. Evaluating the link between self-assembled mesophase structure and drug release. Int. J. Pharm. 421, 176–182.

Pili, B., Bourgaux, C., Meneau, F., Couvreur, P., Ollivon, M., 2009. Interaction of an anticancer drug, gemcitabine, with phospholipid bilayers. J. Therm. Anal. Calorim. 98, 19–28.

Pinheiro, M., Lucio, M., Lima, J.L., Reis, S., 2011. Liposomes as drug delivery systems for the treatment of TB. Nanomedicine (Lond.) 6, 1413–1428.

Pinheiro, M., Arede, M., Caio, J.M., Moiteiro, C., Lucio, M., Reis, S., 2013a. Drug–membrane interaction studies applied to *N*′-acetyl-rifabutin. Eur. J. Pharm. Biopharm., http://dx.doi.org/10.1016/j.ejpb.2013.02.015.

Pinheiro, M., Arede, M., Nunes, C., Caio, J.M., Moiteiro, C., Lucio, M., Reis, S., 2013b. Differential interactions of rifabutin with human and bacterial membranes: implication for its therapeutic and toxic effects. J. Med. Chem. 56, 417–426.

Rappolt, M., Hickel, A., Bringezu, F., Lohner, K., 2003. Mechanism of the lamellar/inverse hexagonal phase transition examined by high resolution X-ray diffraction. Biophys. J. 84, 3111–3122.

Spinozzi, F., Paccamiccio, L., Mariani, P., Amaral, L.Q., 2010. Melting regime of the anionic phospholipid DMPG: new lamellar phase and porous bilayer model. Langmuir 26, 6484–6493.

Wesolowska, O., Michalak, K., Maniewska, J., Hendrich, A.B., 2009. Giant unilamellar vesicles – a perfect tool to visualize phase separation and lipid rafts in model systems. Acta Biochim. Pol. 56, 33–39.

World Health Organization: Global Tuberculosis Control 2012. http://www.who.int/tb/publications/global_report/2011/gtbr11_full.pdf

Please cite this article in press as: Pinheiro, M., et al., Interactions of *N*′-acetyl-rifabutin and *N*′-butanoyl-rifabutin with lipid bilayers: A synchrotron X-ray study. Int J Pharmaceut (2013), http://dx.doi.org/10.1016/j.ijpharm.2013.06.018

Chapter V

Conclusions

The full picture of drug-membrane interactions is often neglected and underestimated, being the retrospective perspective beyond the biophysical studies an indubitable key to fully understand the mechanism of action and the side effects of the drugs, and consequently to develop more effective and safer medicines. The idea beyond the development of drugs considering only a specific target is overvalued and often leads to the screening of molecules that despite an optimal binding to the target (e.g. receptor, enzyme), will never reach the market due to the lack of pharmacokinetics properties or even the necessary efficacy to be useful in the clinical practice. In fact, it is undeniable that the drugs pass through the membranes, being questionable the harmless of the drug to the diverse biological membranes that cross along its track. Moreover, the perspective of the biological membranes as undamaged structures and merely passive barriers, while drug's crossing may only be interpreted in terms of a reductionist perspective of a drug as a "magic bullet" that follows a certain trajectory in the direction of a specific target. In addition, the contact of the drugs with many different biological membranes goes along the destiny of a drug after its oral administration. In the particular case of RFB, from the circulating macrophage cells to the vessel endothelium, to the more complex absorption barriers and the bacterial membrane, until reach the target sites, the interaction with these membranes largely affects its pharmacokinetics properties. Moreover, investigating the phenomena occurring on the human and bacterial plasma membranes, as well as their different interaction with drugs under physiological conditions, is important to exploit the molecular basis of TB and to identify new potential therapeutic strategies [264]. In this context, the results of the drug-membrane interaction studies support differential interactions between the human and the bacterial membrane models. In addition, the mechanism by which this antibiotic permeates through the phospholipid bilayers seems to include an electrostatic adsorption at the interface region, followed by its permeation and induction of pronounced changes into the bacterial membrane biophysics. RFB also demonstrated to induce a phase separation in the bacterial membrane models, which might compromise the integrity of that membrane. On the other hand, RFB showed marked effects in the human membrane model, especially in the gel phases, which may be related to some adverse effects caused by its ability to interact with some of the most ordered membranes of the human body, causing uveitis and with the reaching to the stratum corneum, triggering the discoloration of the skin. The study of the drug-membrane

involving RFB and their analogs allowed to establish a relationship between the chemical structures of the antimycobacterial compound and their effects in the membranes. The correlation found may be useful in the development of new drugs with more favourable pharmacokinetics properties, since the knowledge about the influence of different structural interdependencies between the antimycobacterial compound's chemical composition and the antimycobacterial compound's expected effects is fundamental to the rational development of more effective drugs with less toxic effects. Therefore, the substitution with additional lipophilic groups in the secondary amine of the RFB's analogs was responsible for more marked interactions with the biological membranes. This higher lipid-affinity seems to increase the access of the antibiotics to the cells where the bacteria is located and its entry into the extremely lipophilic mycobacterial membranes. On the other hand, since the toxic effects of this class of drugs are strongly influenced by their affinity to the biological membranes, the RFB analogs may exhibit more pronounced effects as the uveitis, discoloration of the skin and body fluids, being needed further studies to ensure their security before reaching the market. Nevertheless, the electrostatic interactions with the bacterial membrane are expected to be less pronounced than in the case of the lead compound (i.e. RFB). In fact, the affinity of RFB2 to the bacterial membrane model was proved to be less pronounced than in the case of RFB. This expected consequence is due to the above-mentioned effect of the substitution in a protonated group (secundary amine of the imidazole) that decreases the positively charged molecules able to interact by ionic bonds with the negatively charged phospholipids of the bacterial membrane. Nonetheless, both analogs seem to change the bacterial membrane curvature, promoting the formation of cubic phases that may contribute to the bacterial cell death through the production of pores in the membrane. Regarding the interest of the cubic phases in the lipid-based liquid crystalline materials as drug delivery systems, the lipid composition may be exploited to produce liposomes as drug delivery systems of RFB2 and RFB3.

The study of the interaction of RFB with the PS membrane models was useful to understand the accumulation of the drugs in the main organ affected by the TB disease drug, the lungs. In fact, the accumulation of the drug seems to be related with its distribution at the PS lipid level. Indeed, an inclusion complex formed by RFB and the polar head groups of the phospholipids was reported. In addition, the inclusion complex restricted to the polar head groups of the phospholipids prevents the penetration of the drug into the hydrophobic tails, leading to a possible disruption of the monolayer with toxicological effects to the normal function of the lungs. The interaction of RFB2 with the PS also revealed also a strong interaction with the phospholipid head groups associated with a decrease of the phospholipid packing, which may be an advantage in the future

development of liposomal controlled release formulations exploiting the inhalatory delivery of this antimycobacterial compound directly to lungs. Therefore, the encapsulation of RFB2 in liposomes made of the main phospholipid present in the PS featured a faster opening and release of the liposomes content, which is a major drawback in the use of liposomes as drug delivery systems for the inhalatory route.

Furthermore the protecting effect of RFB and RFB2, by avoiding the surfactant dysfunction promoted by compressibility changes induced by the bacterial lipids (i.e. MAs), was proven. At the dynamic inspiratory surface tension (with more biological relevance), high amounts of MAs decrease the order of the lipid monolayer. Moreover, it was proven that the amount of MAs might play a critical role in the initial access of the bacteria to their targets (AMs). In the presence of higher amounts of MAs, RFB and RFB2 increase the phospholipid packing and, therefore, the order of the lipid surfactant monolayer. In addition, the hysteresis of the PS monolayer when both antimycobacterial compounds and MAs are present does not increase in comparison to the hysteresis of the PS monolayer when MAs are present in the absence of the antimycobacterial compounds, suggesting that the RFB and RFB2 may reduce the amount of bacteria that is able to reach the AMs and the bloodstream, by acting as ordering agents.

In summary, this thesis gave a contribution regarding the drug-membrane interactions, allowing to obtain a deeper understanding beyond the therapeutic and toxic effects of RFB and analogs, which may be useful in the design of new drugs with a more limited range of toxicity.

1. Limitations of the Experimental Studies

One of the major limitations pointed to the biophysical studies of drug-membrane interactions is generally the lack of all the constituents generally present in the membranes (e.g. proteins, sugars) and/or the lipid composition chosen. However, the biophysical studies should be interpreted in the most cases as retrospectives studies. Thus, in the presence of a certain phenomena not fully explained by the conventional point of view of a drug's mechanism of action (i.e. drug that has a specific target and commonly a protein), the biophysical studies may help to get a higher knowledge about the mechanism of action, using for that simple but reliable membrane models. It is important to report that the simplification and therefore a complete control of so complex structures is critical to understand the interactions at the molecular level. For instance, in the case of the inclusion complex formed by the drug and the main lipids of the PS, it would be impossible to described it using the same techniques with a more complex PS membrane model (e.g. Curosurf®). In addition, the concentrations used are in most cases

much higher in comparison with the achieved therapeutic plasmatic concentration of RFB (can reach until ~1 μM depending of several factors). This is obviously related with the sensibility of the techniques used but more important with the interest of study the high concentrations acumulated in the tissues, much more higher than the plasmatic concentration. In fact, the plasma concentrations of RFB do not reflect the much higher concentrations that can be achieved in the infected cells and in organs as the lungs, where the levels are six times higher when compared with the plasma concentrations.

2. Future Perspectives

At the end of the thesis is undeniable that the obtained results obtained bring new answers and hypothesis that may lead to future studies, involving:

- Membrane models of different composition. In fact, in a first approach the lipid composition should be chosen as the most simplistic possible (although reliable), and then must be successively optimized and approximated to the physiological. The lipid composition has been revealed as a critical factor to the drug-membrane interactions. For instance, RFB interacts differently according to the plasma membrane model chosen (1,2-dimyristoyl-sn-glycero-3-phosphocholine (DMPC) vs. (egg-phosphocholine) EPC:CHOL). Nevertheless, this approach allowed us to understand how the drug interacts with the phospholipids and the role of CHOL in the different interactions. In addition, the interaction is dependent of the chosen PS membrane model, DPPC, DPPC:DPPC:DPPG or a natural PS (i.e. Curosurf®). The former model is the one with most biological relevance (regarding the presence of proteins and the presence of other lipids that are present in the PS). Other PS membrane models may be used with a more complex composition, more similar to the human PS (for instance Curosurf® does not have hydrophilic proteins). In addition, to mimic human plasma membrane models, proteins may be add, as well as mixtures of CHOL, sphingomyelin to mimic the lipid rafts. To better mimic the bacterium membrane, lipids as CL and PI should be used. In addition, the lipid envelop of the MTb also has in its composition the TDM and therefore it should be used in substitution of the MAs.

- Studies with other experimental conditions. In fact, all the studies were made at the physiological pH (i.e. 7.4). However, it is well know that when the MTb is inside the AMs, the pH decreases to values that depend on the macrophage activation (6.2 and 5); being the studies of the drug interactions with membrane models at a lower pH of interest, in order to understand if the drug interacts differently with the membrane according to the

pH. Moreover, RFB is a drug that eradicates the *Helicobacter pylori* located in the stomach, being non toxic to the stomach layer and therefore, lower pH's that mimic the acid pH of the stomach (range pH 2-5) may be tested.

- This study could be extended to other anti-TB drugs as other ryfamicins (e.g. RIF) and other anti-TB drugs (e.g. isoniazid), for which the mechanism of action still remains not fully understood.

- Application of other biophysical techniques to study drug-membrane interactions. Namely, the nuclear magnetic resonance (NMR) and neutron diffraction to study the location of the drugs within the membranes without the necessity of using probes. Techniques, such as the atomic force microscopy (AFM) allow to visualize the supported lipid bilayers. Techniques such as Grazing incidence X-ray diffraction (GIXD) and X-ray reflectivity may be applied to the monolayers in order to study, respectively, the changes of the phospholipids molecular order induced by the drugs or other lipids (e.g. MAs) and to study the influence in the structure of the monolayer.

- These biophysical studies may be interpreted as the preliminary studies to the further design and development of an innovative of a nano-carrier lipid based (e.g. liposomes and lipid nanoparticles) for targeted delivery of RFB and analogs. Indeed, the present thesis seeks to deepen the scientific knowledge about the biophysics underlying drug-membrane interactions, in order to chose lipid based nano-carriers systems with a rational composition selection based in the biophysical properties observed for the drug-membrane interactions. The chosen membrane models allow us to predict the type of the interactions of RFB and analogs with the drug delivery systems (e.g. liposomes and lipid nanoparticles), which could be critical for efficient drug delivery lipid-based systems. For instance, to obtain a significant incorporation of RFB and analogs and regarding their interactions, liposomes with several lipid bilayers (MLVs instead LUVs) should allow a higher incorporation. In addition, lipids with negative charge may be considered for inclusion in the formulation, avoiding mixtures that seem to permit the release of the drug (i.e. EPC:CHOL 4:1 molar ratio). Nevertheless, the release may be desirable in the delivery of the liposomes by the inhalatory route. Moreover, the analogs induce isotropic phases (i.e. cubic phases) in the lipid nano-carrier and this might be exploited to a controlled release formulation of these molecules.

List of Equations

Equation 1

$$D_T = D_w + \frac{(D_m - D_w)K_p[L]V_m}{1 + K_p[L]V_m}$$

Equation 2

$$\frac{I_0}{I} = 1 + K_{SV}[Q]_m$$

Equation 3

$$[Q]_m = \frac{K_p[Q]_T}{K_p\alpha_m + (1 - \alpha_m)}$$

Equation 4

$$I_{corr} = I\frac{A_Q}{A_F}\frac{1-10^{-A_F}}{1-10^{-A_Q}}$$

Equation 5

$$\frac{I_0}{I} = 1 + K_D[Q]_m$$

Equation 6

$$\frac{I_0}{I} = 1 + K_S[Q]_m$$

Equation 7

$$K_q = \frac{K_{SV}}{\tau_0}$$

Equation 8

$$\frac{I_0}{I} \times \frac{1}{1 + K_D[Q]_m} = 1 + K_S[Q]_m$$

Equation 9

$$ln\left(\frac{I_0\tau}{I\tau_0}\right) = V[Q]_m$$

Equation 10

$$\tan\varphi_\omega = \omega t$$

Equation 11

$$m_\omega = (1 + \omega^2\tau^2)^{-1/2}$$

Equation 12

$$\chi^2 = \frac{1}{\upsilon}\left[\sum_{1=1}^{N}\frac{\left[\Phi(\omega_i) - \Phi_c(\omega_i)\right]^2}{\sigma_\Phi(\omega_i)} + \sum_{i=1}^{N}\frac{\left[M(\omega_i) - M_c(\omega_{i)}\right]^2}{\sigma_M(\omega_i)}\right]$$

Equation 13

$$r_s = r_{s1} + p_1T + \frac{r_{s2} - r_{s1} + p_2T - p_1T}{1 + 10^{B(1/T - 1/T_m)}}$$

Equation 14

$$r_{ss} = \frac{I_{\parallel} - GI_{\perp}}{I_{\parallel} + 2GI_{\perp}}$$

Equation 15 $$G = \frac{I_{\perp}}{I_{\parallel}}$$

Equation 16 $$r_s = r_{s1} + p_1 T + \frac{r_{s2} - r_{s1} + p_2 T - p_1 T}{1 + 10^{B(1/T - 1/T_m)}}$$

Equation 17 $$r_{\infty} = 4/3 r_{ss} - 0.10$$

Equation 18 $$s = \sqrt{r_{\infty} / r_0}$$

Equation 19 $$q = \frac{4\pi sen\theta}{\lambda}$$

Equation 20 $$n\lambda = 2dsen(\theta)$$

Equation 21 $$d = \frac{2\pi}{q}$$

Equation 22 $$\xi = \frac{2\pi}{FWHM}$$

Equation 23 $C_s^{-1} = -A\,(d\pi/dA)$

Equation 24 $K = \frac{1}{Cs-1}$

Equation 25 $\tan \alpha = \frac{n2}{n1}$

Equation 26 $-\log_{10}(R/R_o)$

Equation 27 $\Delta R = A\,(R_i)^{1/2} + p^2$

References

[1]. http://www.nobelprize.org/educational/medicine/tuberculosis/readmore.html?do [cited 2013 Apr 12]. Available from: http://www.nobelprize.org/educational/medicine/tuberculosis/readmore.html?do.1.

[2]. Donoghue HD. Human tuberculosis-an ancient disease, as elucidated by ancient microbial biomolecules. Microbes Infect 2009;11(14-15):1156–62.

[3]. Long R. The Canadian lung association/canadian Thoracic Society and tuberculosis prevention and control. Can Resp J 2007;14(7):427–31.

[4]. Doherty TM, Andersen P. Vaccines for Tuberculosis : Novel concepts and recent progress.Clin Microbiol Rev 2005;18(4):687–702.

[5]. Schön T, Lerm M, Stendahl O. Shortening the “short-course” therapy- insights into host immunity may contribute to new treatment strategies for tuberculosis. J Intern Med 2013;273(4):368–82.

[6]. Khan F a, Minion J, Pai M, Royce S, Burman W, Harries AD, et al. Treatment of active tuberculosis in HIV-coinfected patients: a systematic review and meta-analysis. Clin Infect Dis 2010;50(9):1288–99.

[7]. Global Tuberculosis Report. 2012 p. 1–89 [cited 2013 May 20]. Available from: http://www.who.int/tb/publications/global_report/gtbr12_main.pdf.

[8]. Pinheiro M, Lúcio M, Lima J, Reis S. Liposomes as drug delivery systems for the treatment of TB. Nanomedicine 2011;1–16.

[9]. Silva Miranda M, Breiman A, Allain S, Deknuydt F, Altare F. The tuberculous granuloma: an unsuccessful host defence mechanism providing a safety shelter for the bacteria? Clin Dev Immunol 2012.

[10]. Dahl J. Electron microscopy analysis of Mycobacterium tuberculosis cell division. FEMS Microbiol Lett 2004;240:15–20.

[11]. Cardona PJ, Amat I. [Origin and development of RUTI, a new therapeutic vaccine against Mycobacterium tuberculosis infection]. Arch Bronconeumol 2006;42(1):25–32.

[12]. Sundaramurthy V, Pieters J. Interactions of pathogenic mycobacteria with host macrophages. Microbes Infect 2007;9(14-15):1671–9.

[13]. Gaspar MM, Cruz a, Penha a F, Reymão J, Sousa a C, Eleutério C V, et al. Rifabutin encapsulated in liposomes exhibits increased therapeutic activity in a model of disseminated tuberculosis. Int J Antimicrob Ag 2008;31(1):37–45.

[14]. Barter DM, Agboola SO, Murray MB, Bärnighausen T. Tuberculosis and poverty: the contribution of patient costs in sub-Saharan Africa-a systematic review. BMC Public Health 2012;12:980.

[15]. Walls T, Shingadia D. The epidemiology of tuberculosis in Europe. Arch Dis Childh 2007;92(8):726–9.

[16]. Direcação Geral da Saúde, Ministério da Saúde. Programa nacional de luta contra a tuberculose ponto da situação epidemiológica e de desempenho 2013.

[17]. Gandhi NR, Nunn P, Dheda K, Schaaf HS, Zignol M, Van Soolingen D, et al. Multidrug-resistant and extensively drug-resistant tuberculosis: a threat to global control of tuberculosis. Lancet 2010;375(9728):1830–43.

[18]. Tuberculosis-from ancient plague to modern-day nemesis. Lancet 2012;380(9851):1359.

[19]. Onozaki I, Raviglione M. Stopping tuberculosis in the 21st century: goals and strategies. Respirology 2010;15(1):32–43.

[20]. Niemann S, Richter E, Rüsch-Gerdes S. Differentiation among members of the Mycobacterium tuberculosis complex by molecular and biochemical features: evidence for two pyrazinamide-susceptible subtypes of M. bovis. J Clin Microbiol 2000;38(1):152–7.

[21]. Weiss CH, Glassroth J. Pulmonary disease caused by nontuberculous mycobacteria. Expert Rev Respir Med 2012;6(6):597–612.

[22]. Gagneux S. Host-pathogen coevolution in human tuberculosis. Phil Trans R Soc B 2012;367(1590):850–9.

[23]. Hershberg R, Lipatov M, Small PM, Sheffer H, Niemann S, Homolka S, et al. High functional diversity in Mycobacterium tuberculosis driven by genetic drift and human demography. PLoS Biol 2008;6(12):e311.

[24]. Escombe a R, Oeser CC, Gilman RH, Navincopa M, Ticona E, Pan W, et al. Natural ventilation for the prevention of airborne contagion. PLoS Med 2007;4(2):e68.

[25]. Munawwar A, Singh S. AIDS associated tuberculosis: a catastrophic collision to evade the host immune system. Tuberculosis 2012;92(5):384–7.

[26]. Agrawal a K, Gupta CM. Tuftsin-bearing liposomes in treatment of macrophage-based infections. Adv Drug Deliv Rev 2000;41(2):135–46.

[27]. Thanyani ST, Roberts V, Siko DGR, Vrey P, Verschoor JA. A novel application of affinity biosensor technology to detect antibodies to mycolic acid in tuberculosis patients. J Immunol Methods 2008;332:61–72.

[28]. De Steenwinkel JEM, Van Vianen W, Ten Kate MT, Verbrugh H a, Van Agtmael M a, Schiffelers RM, et al. Targeted drug delivery to enhance efficacy and shorten treatment duration in disseminated Mycobacterium avium infection in mice. J Antimicrob Chemother 2007;60(5):1064–73.

[29]. Gaspar MM, Neves S, Portaels F, Pedrosa J, Silva MT, Cruz ME. Therapeutic efficacy of liposomal rifabutin in a Mycobacterium avium model of infection. Antimicrob Agents Chemother 2000;44(9):2424–30.

[30]. Ottenhoff THM. The knowns and unknowns of the immunopathogenesis of tuberculosis. Int J Tuberc Lung D 2012;16(11):1424–32.

[31]. Sullivan T, Ben Amor Y. The co-management of tuberculosis and diabetes: challenges and opportunities in the developing world. PLoS Med 2012;9(7):e1001269.

[32]. Zuñiga J, Torres-García D, Santos-Mendoza T, Rodriguez-Reyna TS, Granados J, Yunis EJ. Cellular and humoral mechanisms involved in the control of tuberculosis. Clin Dev Immunol 2012.

[33]. Sosnik A, Carcaboso AM, Glisoni RJ, Moretton M a, Chiappetta D a. New old challenges in tuberculosis: potentially effective nanotechnologies in drug delivery. Adv Drug Deliv Rev 2010;62(4-5):547–59.

[34]. Deol P, Khuller GK, Joshi K. Therapeutic efficacies of isoniazid and rifampin encapsulated in lung-specific stealth liposomes against Mycobacterium tuberculosis infection induced in mice. Antimicrob Agents Chemother 1997;41(6):1211–4.

[35]. Chimote G, Banerjee R. Effect of mycolic acid on surface activity of binary surfactant lipid monolayers. J Colloid Interf Sci 2008;328(2):288–98.

[36]. Zhang L, Pornpattananangku D, Hu M, Huang M. Development of nanoparticles for antimicrobial drug delivery. Curr Med Chem 2010;17:585–94.

[37]. Chimote G, Banerjee R. Lung surfactant dysfunction in tuberculosis: effect of mycobacterial tubercular lipids on dipalmitoylphosphatidylcholine surface activity. Colloid Surface B 2005;45(3-4):215–23.

[38]. Urdahl KB, Shafiani S, Ernst JD. Initiation and regulation of T-cell responses in tuberculosis. Mucosal Immunol 2011;4(3):288–93.

[39]. Trajman A, Lapa E Silva JR, Dalcolmo M, Golub JE. Pulmonary tuberculosis. Pulm Med 2013;2013:645747.

[40]. Druszczyńska M, Kowalewicz-Kulbat M, Fol M, Włodarczyk M, Rudnicka W. Latent M. tuberculosis infection--pathogenesis, diagnosis, treatment and prevention strategies. Pol J Microbiol 2012;61(1):3–10.

[41]. Doherty T. Immunotherapy for TB. J Immunother 2012;4(6):629–47.

[42]. Barry C, Boshoff H, Dartois V, Dick T, Ehrt S, Flynn J, et al. The spectrum of latent tuberculosis: rethinking the biology and intervention strategies. Nat Rev Microbiol 2009;7:845–55.

[43]. Gengenbacher M, Kaufmann SHE. Mycobacterium tuberculosis: success through dormancy. FEMS Microbiol Rev 2012;36(3):514–32.

[44]. Villeneuve M, Kawai M, Horiuchi K, Watanabe M, Aoyagi Y, Hitotsuyanagi Y, et al. Conformational folding of mycobacterial methoxy and ketomycolic acids facilitated by α-methyl trans-cyclopropane groups rather than cis-cyclopropane units. Microbiology 2013.

[45]. Chimote G, Banerjee R. Evaluation of antitubercular drug-loaded surfactants as inhalable drug-delivery systems for pulmonary tuberculosis. J Biomed Mater Res A 2009;89(2):281–92.

[46]. Kartmann B, Stenger S, Niederweis M, Stengler S. Porins in the cell wall of Mycobacterium tuberculosis. J Bacteriol 1999;181(20):6543–6.

[47]. Vyas SP, Kannan ME, Jain S, Mishra V, Singh P. Design of liposomal aerosols for improved delivery of rifampicin to alveolar macrophages Int J Pharm. 2004;269:37–49.

[48]. Cook G, Berney M, Gebhard, Susanne Heinemann M, Cox R, Danilchanka O, Niederweis M. Physiology of Mycobacteria. Adv Microb Physiol 2009;55:81–182.

[49]. Kaufmann S. Tuberculosis vaccines—a new kid on the block. Nat Med 2011;17:159–60.

[50]. Aldridge B, Fernandez-Suarez M, Heller D, Ambravaneswaran V, Irimia D, Toner M, et al. Asymmetry and aging of mycobacterial cells leads to variable growth and antibiotic susceptibility. Science 2012;335(6064):100–4.

[51]. Sia IG, Wieland ML. Current concepts in the management of tuberculosis. Mayo Clin Proc 2011;86(4):348–61.

[52]. Zaman K. Tuberculosis: a global health problem. J Health Popul Nutr 2010;28(2):111–3.

[53]. Chimote G, Banerjee R. Effect of antitubercular drugs on dipalmitoylphosphatidylcholine monolayers: implications for drug loaded surfactants. Respir Physiol Neurobiol 2005;145(1):65–77.

[54]. Swick BL. Polymerase chain reaction-based molecular diagnosis of cutaneous infections in dermatopathology. Semin Cutan Med Surg 2012;31(4):241–6.

[55]. Guo S, Ao Z. Phage in the diagnosis and treatment of tuberculosis. Front Biosci 2012;17(1):2691–7.

[56]. Tsara V, Serasli E, Christaki P. Problems in diagnosis and treatment of tuberculosis infection. Hippokratia 2009;13(1):20–2.

[57]. Howard AA, Gasana M, Getahun H, Harries A, Lawn SD, Miller B, et al. PEPFAR Support for the Scaling Up of Collaborative TB / HIV Activities. J Acquir Immune Defic Syndr 2012;60:136–44.

[58]. Maertzdorf J, Iii JW, Kaufmann SHE. Enabling biomarkers for tuberculosis control. Int J Tuberc Lung D 2012;16:1140–8.

[59]. Leigh P. Infectious disease: TB's revenge. Nature 2013;493:14–6.

[60]. Imperiale BR, Zumárraga MJ, Weltman G, Zudiker R, Cataldi A a, Morcillo NS. First evaluation in Argentina of the GenoType® MTBDRplus assay for multidrug-resistant Mycobacterium tuberculosis detection from clinical isolates and specimens. Rev Argent Microbiol 2012;44(4):283–9.

[61]. Maiga M, Abaza A, William B. Current tuberculosis diagnostic tools & role of urease breath test. Indian J Med Res 2012;135:731–6.

[62]. Gowthaman U, Rai, P, Khan N, Jackson D, Javed A. Lipidated promiscuous peptides vaccine for tuberculosis-endemic regions. Trends Mol Med 2012;18:607–14.

[63]. Martín C. The dream of a vaccine against tuberculosis; new vaccines improving or replacing BCG? Eur Respir J 2005;26(1):162–7.

[64]. Rappuoli R, Aderem A. A 2020 vision for vaccines against HIV, tuberculosis and malaria. Nature 2011;473(7348):463–9.

[65]. Ottenhoff THM, Kaufmann SHE. Vaccines against tuberculosis: where are we and where do we need to go? PLoS Pathog 2012;8(5):e1002607.

[66]. Wallis RS, Kim P, Cole S, Hanna D, Andrade BB, Maeurer M, et al. Tuberculosis 2013 : 2 Tuberculosis biomarkers discovery : developments, needs, and challenges. Lancet Infect Dis 2013;13(4):362–72.

[67]. Pitt JM, Blankley S, McShane H, O'Garra A. Vaccination against tuberculosis: How can we better BCG? Microb Pathogenesis 2012;58:2–16.

[68]. Thaiss C a, Kaufmann SHE. Toward novel vaccines against tuberculosis: current hopes and obstacles. Yale J Biol Med 2010;83(4):209–15.

[69]. Rowland R, Mcshane H. Tuberculosis vaccines in clinical trials. Expert Rev Vaccines 2012;10(5):645–58.

[70. Cardona PJ. RUTI: A new chance to shorten the treatment of latent tuberculosis infection. Tuberculosis 2006;86:273–89.

[71. Tseng CL, Oxlade O, Menzies D, Aspler A, Schwartzman K. Cost-effectiveness of novel vaccines for tuberculosis control: a decision analysis study. BMC Public Health 2011;11(1):55.

[72]. Brennan MJ, Stone MR, Evans T. A rational vaccine pipeline for tuberculosis. Int J Tuberc Lung D 2012;16:1566–73.

[73]. Goldberg D, Siliciano R, Jr W. Outwitting evolution: Fighting drug resistance in the treatment of TB, Malaria and HIV. Cell 2012;148(6):1271–83.

[74]. Gomez JE, McKinney JD. M. tuberculosis persistence, latency, and drug tolerance. Tuberculosis 2004;84(1-2):29–44.

[75]. Ralph AP, Ralph AR, Lucas RM, Norval M. Vitamin D and solar ultraviolet radiation in the risk and treatment of tuberculosis. Lancet Infect Dis 2013;13(1):77–88.

[76]. Songane M, Kleinnijenhuis J, Netea MG, Van Crevel R. The role of autophagy in host defence against Mycobacterium tuberculosis infection. Tuberculosis 2012;92(5):388–96.

[77]. Guo S, Ao Z. Immunotherapy for Tuberculosis: what's the better choice? Front Biosci 2012;17:2684–90.

[78]. Panickar JR, Hoskyns W. Treatment failure in tuberculosis. Eur Respir J 2007;29(3):561–4.

[79]. Gelband H. Regimens of less than six months for treating tuberculosis. Cochrane Database Syst Rev 2000; (2):CD001362.

[80]. Figueiredo R, Moiteiro C, Medeiros MA, Da Silva PA, Ramos D, Spies F, et al. Synthesis and evaluation of rifabutin analogs against Mycobacterium avium and H(37)Rv, MDR and NRP Mycobacterium tuberculosis. Bioorg Med Chem 2009;17(2):503–11.

[81]. Palomino JC, Martin A. TMC207 becomes bedaquiline, a new anti-TB drug. Future Microbiol 2013; 1071-80.

[82]. Rodrigues C, Gameiro P, Prieto M, De Castro B. Interaction of rifampicin and isoniazid with large unilamellar liposomes: spectroscopic location studies. Biochim Biophys Acta 2003;1620(1-3):151–9.

[83]. Hingley-Wilson SM, Casey R, Connell D, Bremang S, Evans JT, Hawkey PM. Undetected multidrug-resistant tuberculosis amplified by first-line therapy in mixed infection. Emerg Infect Dis 2013;19(7):1138–41.

[84]. Schatz A, Waksman S. Streptomycin, a substance exhibiting antibiotic activity against Gram positive and Gram-negative bacteria. Proc Soc Exp Biol Med 1944;55:66–9.

[85]. Huyen MNT, Cobelens FGJ, Buu TN, Lan NTN, Dung NH, Kremer K, et al. Isoniazid resistance mutations: epidemiology and effect on tuberculosis treatment outcomes. Antimicrob Agents Chemother 2013. 57(8):3620–7.

[86]. Ahmad S, Mokaddas E. Recent advances in the diagnosis and treatment of multidrug-resistant tuberculosis. Respir Med 2009;103(12):1777–90.

[87]. Avorn J. Approval of a tuberculosis drug based on a paradoxical surrogate measure. JAMA 2013;309:1349–50.

[88]. Voelker R. MDR-TB has new drug foe after fast-track approval. JAMA 2013;309:430.

[89]. Grosset JH, Singer TG, Bishai WR. New drugs for the treatment of tuberculosis : hope and reality. Int J Tuberc Lung D 2012;16(8):1005–14.

[90]. Janssen S, Jayachandran R, Khathi L, Zinsstag J, Grobusch MP, Pieters J. Exploring prospects of novel drugs for tuberculosis. Drug Des Dev Ther 2012;6:217–24.

[91]. Sanfilippo A, Della C, Marsili L. Biological activity of a new class of rifamycins, spiropiperdyl-rifamycins. J Antibiot 1980;1193–8.

[92]. Gisbert J, Calvet X. Review article: rifabutin in the treatment of refractory Helicobacter pylori infection. Aliment Pharm Ther 2012;35:209–21.

[93]. Aristoff P, Garcia G, Kirchhoff PD, Hollis Showalter HD. Rifamycins-obstacles and opportunities. Tuberculosis 2010;90(2):94–118.

[94]. Sirgel F a., Warren RM, Böttger EC, Klopper M, Victor TC, Van Helden PD. The Rationale for Using Rifabutin in the Treatment of MDR and XDR Tuberculosis Outbreaks. PLoS One 2013;8(3):e59414.

[95]. Baciewicz AM, Chrisman CR, Finch CK, Self TH. Update on rifampin and rifabutin drug interactions. JAMA 2008;335(2):126–36.

[96] Vourvahis M, Davis J, Wang R, Layton G, Choo HW, Chong C-L, et al. Effect of rifampin and rifabutin on the pharmacokinetics of lersivirine and effect of lersivirine on the pharmacokinetics of rifabutin and 25-O-Desacetyl-rifabutin in healthy subjects. Antimicrob Agents Chemother 2012;56(8):4303–9.

[97]. Schraufnagel DE. Tuberculosis treatment for the beginning of the next century. Int J Tuberc Lung D 1999;3(8):651–62.

[98]. Loeliger A, Suthar B, Ripin D, Glaziou P, O'Brien M, Renaud-Thery F, et al. Protease inhibitor-containing antiretroviral treatment and tuberculosis: can rifabutin fill the breach? Int J Tuberc Lung D 2012;16(1):6–15.

[99]. Harold F. The vital force: a study in bioenergetics. W. H. Freeman & Co., New York, N.Y.; 1986.

[100]. Van Meer G, Voelker DR, Feigenson GW. Membrane lipids: where they are and how they behave. Nat Rev Mol Cell Biol 2008;9(2):112–24.

[101]. Cooper G. The Cell, A Molecular Approach. 2nd ed. Washington, D.C.: ASM Press; 2000.

[102]. Marsden HR, Tomatsu I, Kros A. Model systems for membrane fusion. Chem Soc Rev 2011;40(3):1572–85.

[103]. Thomas JA, Rana FR. The influence of environmental conditions, lipid composition, and phase behavior on the origin of cell membranes. Orig Life Evol Biosph 2007;37(3):267–85.

[104]. Frolov VA, Zimmerberg J. Cooperative elastic stresses, the hydrophobic effect, and lipid tilt in membrane remodeling. FEBS Lett 2010;584(9):1824–9.

[105]. Chan Y-HM, Boxer SG. Model membrane systems and their applications. Curr Opin Chem Biol 2007;11(6):581–7.

[106]. Lodish H, Berk A, Zipursky L, Matsudaira P, Baltimore D, Darnell J. Molecular Cell Biology. New York: W. H. Freeman and Company; 2000.

[107]. Olivera-Couto A, Aguilar PS. Eisosomes and plasma membrane organization. Mol Genet Genomics : MGG 2012;287(8):607–20.

[108]. Brown FLH. Elastic modeling of biomembranes and lipid bilayers. Annu Rev Phys Chem 2008;59:685–712.

[109]. Seydel J, Wiese M. Drug-Membrane Interactions: Analysis, drug distribution, modeling. Wiley-VCH; 2002.

[110]. Mouritsen OG. Model answers to lipid membrane questions. Cold Spring Harb Perspect Biol. 2011;3(9):a004622.

[111]. Peetla C, Stine A, Labhasetwar V. Biophysical interactions with model lipid membranes: applications in drug discovery and drug delivery. Mol Pharm 2009;6(5):1264–76.

[112]. Singer SJ, Nicolson GL. The fluid mosaic model of the structure of cell membranes. Science 1972;175(4023):720–31.

[113]. Helms JB, Zurzolo C. Lipids as targeting signals : Lipid rafts and intracellular trafficking. Traffic 2004;(5):247–54.

[114]. Chichili GR, Rodgers W. Cytoskeleton-Membrane interactions in membrane raft structure. Cell Mol Life Sci 2010;66(14):2319–28.

[115]. Hunte C, Richers S. Lipids and membrane protein structures. Curr Opin Struct Biol 2008;18(4):406–11.

[116]. Witkowski T, Backofen R, Voigt A. The influence of membrane bound proteins on phase separation and coarsening in cell membranes. Phys Chem Chem Phys 2012;14(42):14509–15.

[117]. Jin S, Zhou F, Katirai F, Li P-L. Lipid raft redox signaling: molecular mechanisms in health and disease. Antioxid Redox Sign 2011;15(4):1043–83.

[118]. Berg J, Tymoczko J, Stryer L. Biochemistry. New York: W. H. Freeman & Co., New York, N.Y.;

[119]. Mouritsen O. Life as a matter of fat - the emerging science of Lipidomics. Springer; 2005.

[120]. Van Meer G. Cellular lipidomics. EMBO J 2005;24(18):3159–65.

[121]. Lange Y, Steck TL. Cholesterol homeostasis and the escape tendency (activity) of plasma membrane cholesterol. Prog Lipid Res 2008;47(5):319–32.

[122]. Tierney KJ, Block DE, Longo ML. Elasticity and phase behavior of DPPC membrane modulated by cholesterol, ergosterol, and ethanol. Biophys J 2005;89(4):2481–93.

[123]. Quinn PJ. Lipid-lipid interactions in bilayer membranes: married couples and casual liaisons. Prog Lipid Res 2012;51(3):179–98.

[124]. Heimburg T. Lipid ion channels. Biophys Chem 2010;150(1–3):2–22.

[125]. Neurochemistry JOF. Division of Glycopathology, Institute of Molecular Biomembranes and Glycobiology, Tohoku Pharmaceutical University, Sendai, Miyagi, Japan 2011;756–63.

[126]. Maggio B, Borioli G a, Del Boca M, De Tullio L, Fanani ML, Oliveira RG, et al. Composition-driven surface domain structuring mediated by sphingolipids and membrane-active proteins. Above the nano- but under the micro-scale: mesoscopic biochemical/structural cross-talk in biomembranes. Cell Biochem Biophys 2008;50(2):79–109.

[127]. Waheed A, Freed E. Lipids and Membrane Microdomains in HIV-1 Replication. Virus Res 2010;143(2):162–76.

[128]. LaRocca TJ, Pathak P, Chiantia S, Toledo A, Silvius JR, Benach JL, et al. Proving lipid rafts exist: membrane domains in the prokaryotic Borrelia burgdorferi have the same properties as eukaryotic lipid rafts. PloS Pathog 2013;9(5):e1003353.

[129]. Feigenson G. Phase behavior of lipid mixtures. Nat Chem Biol 2006;2(11):560–3.

[130]. Van der Meer-Janssen YPM, Van Galen J, Batenburg JJ, Helms JB. Lipids in host-pathogen interactions: pathogens exploit the complexity of the host cell lipidome. Prog Lipid Res 2010;49(1):1–26.

[131]. Kulkarni C V. Lipid crystallization: from self-assembly to hierarchical and biological ordering. Nanoscale 2012;4(19):5779–91.

[132]. Quinn PJ, Wolf C. The liquid-ordered phase in membranes. Biochim Biophys Acta 2009;1788(1):33–46.

[133]. Lenoir G, Williamson P, Holthuis JCM. On the origin of lipid asymmetry: the flip side of ion transport. Curr Opin Chem Biol 2007;11(6):654–61.

[134]. Asegawa AYA, Sujimoto MT. Lipid dynamics and pathobiology in membrane lipid rafts asymmetric distribution of phospholipids in biomembranes 2006;29:1547–53.

[135]. Lenoir G, Joost CM, Marshall WF. The elusive flippases. Curr Biol 1973;14(21):912–3.

[136]. Sanyal S, Menon A. Flipping lipids: why an' what's the reason for? ACS Chem Biol 2010;4(11):895–909.

[137]. Roy H. Tuning the properties of the bacterial membrane with aminoacylated phosphatidylglycerol. IUBMB Life 2009;61(10):940–53.

[138]. Geiger O, González-Silva N, López-Lara IM, Sohlenkamp C. Amino acid-containing membrane lipids in bacteria. Prog Lipid Res 2010;49(1):46–60.

[139]. Huijbregts RP, De Kroon AI, De Kruijff B. Topology and transport of membrane lipids in bacteria. Biochim Biophys Acta 2000;1469(1):43–61.

[140]. Kol MA, Kruijff B De, Kroon AIPM De. Phospholipid flip-flop in biogenic membranes : what is needed to connect opposite sides. Semin Cell Dev Biol 2002;13(02):163–70.

[141]. Epand RM, Epand RF. Domains in bacterial membranes and the action of antimicrobial agents. Mol Biosyst 2009;5(6):580–7.

[142]. Pinheiro M, Arêde M, Nunes C, Caio JM, Moiteiro C, Lúcio M, et al. Differential interactions of rifabutin with human and bacterial membranes: implication for its therapeutic and toxic effects. J Med Chem 2013;56(2):417–26.

[143]. Zhang Z, Pen Y, Edyvean RG, Banwart S a, Dalgliesh RM, Geoghegan M. Adhesive and conformational behaviour of mycolic acid monolayers. Biochim Biophys Acta 2010;1798(9):1829–39.

[144]. Villeneuve M, Kawai M, Watanabe M, Aoyagi Y, Hitotsuyanagi Y, Takeya K, et al. Differential conformational behaviors of alpha-mycolic acids in Langmuir monolayers and computer simulations. Chem Phys of Lipids 2010;163(6):569–79.

[145]. Villeneuve M, Kawai M, Watanabe M, Aoyagi Y, Hitotsuyanagi Y, Takeya K, et al. Conformational behavior of oxygenated mycobacterial mycolic acids from Mycobacterium bovis BCG. Biochim Biophys Acta 2007;1768(7):1717–26.

[146]. Indrigo J. Cord factor trehalose 6,6'-dimycolate (TDM) mediates trafficking events during mycobacterial infection of murine macrophages. Microbiology 2003;149(8):2049–59.

[147]. Trifiro S, Bourgault a M, Lebel F, René P. Ghost mycobacteria on Gram stain. J Clin Microbiol 1990;28(1):146–7.

[148]. Hernick M. Mycothiol: a target for potentiation of rifampin and other antibiotics against Mycobacterium tuberculosis. Expert Rev Anti Infect Ther 2013;11:49–67.

[149]. McCulloch MWB, Haltli B, Marchbank DH, Kerr RG. Evaluation of pseudopteroxazole and pseudopterosin derivatives against Mycobacterium tuberculosis and other pathogens. Mar Drugs 2012;10(8):1711–28.

[150]. Fu L, CS F-L. Is Mycobacterium tuberculosis a closer relative to Gram-positive or Gram-negative bacterial pathogens? Tuberculosis 2002;82:85–90.

[151]. Geisel RE, Sakamoto K, Russell DG, Rhoades ER. In vivo activity of released aell wall lipids of mycobacterium bovis bacillus Calmette-Guérin is due principally to trehalose mycolates. J Immunol 2005;174:5007–15.

[152]. Haites RE, Morita YS, McConville MJ, Billman-Jacobe H. Function of phosphatidylinositol in mycobacteria. J Biol Chem 2005;280(12):10981–7.

[153]. Jackson M, Crick DC, Brennan PJ. Phosphatidylinositol is an essential phospholipid of mycobacteria. J Biol Chem 2000;275(39):30092–9.

[154]. Akira S, Uematsu S, Takeuchi O. Pathogen recognition and innate immunity. Cell 2006;124(4):783–801.

[155]. Halliday H. Controversies: synthetic or natural surfactant. The case for natural surfactant. J Perinat Med 1996;24:417–26.

[156]. Sweet D, Halliday H. The use of surfactants in 2009. Arch Dis Childh 2009;94:78-83.

[157]. Halliday H. History of Surfactant from 1980. Biol Neonate 2005;87:317–22.

[158]. Ariki S, Nishitani C, Kuroki Y. Diverse functions of pulmonary collectins in host defense of the lung. J Biomed Biotechnol 2012.

[159]. Akella A, Deshpande S. Pulmonary surfactants and their role in pathophysiology of lung disorders. Indian J Exp Biol 2013;51:5–22.

[160]. Piknova B, Schram V, Hall SB. Pulmonary surfactant: phase behavior and function. Curr Opin Struct Biol 2002;12(4):487–94.

[161]. Ikegami M, Weaver TE, Grant SN, Whitsett J a. Pulmonary surfactant surface tension influences alveolar capillary shape and oxygenation. Am J Respir Cell Mol Biol 2009;41(4):433–9.

[162]. Moses D, Holm B, Spitale P, MY L, Enhorning G. Inhibition of pulmonary surfactant function by meconium. Am J Obstet Gynecol 1991;164:477–81.

[163]. Agassandian M, Mallampalli RK. Surfactant phospholipid metabolism. Biochim Biophys Acta 2013;1831:612–25.

[164]. Stevens TP, Sinkin R a. Surfactant replacement therapy. Chest 2007;131(5):1577–82.

[165]. Casals C, Cañadas O. Role of lipid ordered/disordered phase coexistence in pulmonary surfactant function. Biochim Biophys Acta 2012;1818(11):2550–62.

[166]. Poulain FR, Clements JA, Francisco S. Conferences and reviews pulmonary Surfactant Therapy. 1995;

[167]. Rugonyia S, Biswasb S, Hallc S. The biophysical function of pulmonary surfactant. Respir Physiol Neurobiol 2009;163:244–55.

[168]. Christmann U, Witonsky SG, Hite RD. Role of lung surfactant in respiratory disease: current knowledge in large animal medicine. J Vet Intern Med 2009;23:227–42.

[169]. Hamm H, Fabel H, Bartsch W. The surfactant system of the adult lung: physiology and clinical perspectives. J Clin Invest 1992;70:637–57.

[170]. Winter R. Effects of hydrostatic pressure on lipid and surfactant phases. Curr Opin in Colloid Interface Sci 2001;6(3):303–12.

[171]. Haney EF, Nathoo S, Vogel HJ, Prenner EJ. Induction of non-lamellar lipid phases by antimicrobial peptides: a potential link to mode of action. Chem Phys of Lipids 2010;163(1):82–93.

[172]. Huang C, Li S. Calorimetric and molecular mechanics studies of the thermotropic phase behavior of membrane phospholipids. Biochim Biophys Acta. 1999;1422(3):273–307.

[173]. Tresset G. The multiple faces of self-assembled lipidic systems. PMC Biophys 2009;2(1):3.

[174]. Tristram-Nagle S, Nagle JF. Lipid bilayers: thermodynamics, structure, fluctuations, and interactions. Chem Phys of Lipids 2004;127(1):3–14.

[175]. Lindblom G, Orädd G. Lipid lateral diffusion and membrane heterogeneity. Biochim Biophys Acta 2009;1788(1):234–44.

[176]. Eeman M, Deleu M. From biological membranes to biomimetic model membranes. BASE 2010;14(4):719–36.

[177]. Dürr UHN, Gildenberg M, Ramamoorthy A. The magic of bicelles lights up membrane protein structure. Chem Rev 2012;112(11):6054–74.

[178]. Letters MB. Volume 10, (2005) pp 711 – 719. 2005;10:711–9.

[179]. Fenz S, Sengupta K. Giant vesicles as cell models. Integr Biol 2012;4:982–95.

[180]. Cebecauer M. Lipids and proteins in membranes: from in silico to in vivo. Mol Membr Biol 2012;29(5):115–7.

[181]. Zagnoni M. Miniaturised technologies for the development of artificial lipid bilayer systems. Lab Chip 2012;12(6):1026–39.

[182]. Tan S, Tan HT, Chung MCM. Membrane proteins and membrane proteomics. Proteomics 2008;8(19):3924–32.

[183]. Jackman J a, Cho N-J. Model membrane platforms for biomedicine: case study on antiviral drug development. Biointerphases 2012;7(1-4):18.

[184]. Uline MJ, Szleifer I. Mode specific elastic constants for the gel, liquid-ordered, and liquid-disordered phases of DPPC/DOPC/cholesterol model lipid bilayers. Faraday Discuss 2013;161:177–91.

[185]. Sezgin E, Schwille P. Model membrane platforms to study protein-membrane interactions. Mol Membr Biol 2012;29:144–54.

[186]. Le M, Litzenberger J, Prenner E. Biomimetic model membrane systems serve as increasingly valuable in vitro tools 2011.

[187]. Owen RL, Strasters JK, Breyer ED. Lipid vesicles in capillary electrophoretic techniques: characterization of structural properties and associated membrane-molecule interactions. Electrophoresis 2005;26(4-5):735–51.

[188]. Bangham A, Standish M, Watkins J. Diffusion of univalent ions across the lamellae of swollen phospholipids. J Mol Biol 1965;13:238–52.

[189]. Svetina S, Zeks B. Shape behavior of lipid vesicles as the basis of some cellular processes. Anat Rec 2002;268(3):215–25.

[190]. Schroeder A, Kost J, Barenholz Y. Ultrasound, liposomes, and drug delivery: principles for using ultrasound to control the release of drugs from liposomes. Chem Phys of Lipids 2009;162(1-2):1–16.

[191]. Moghimi SM, Hunter a C, Murray JC. Nanomedicine: current status and future prospects. FASEB J 2005;19(3):311–30.

[192]. Mozafari M. Liposomes: an overview of manufacturing techniques. Cell Mol Biol Lett 2005;10:711–9.

[193]. Kikuchi H, Yamauchi H, Sadao S. A Polyol dilution method for mass production of liposomes. J Liposome Res 1994;4:71–91.

[194]. Talsma H, Van Steenbergen, MJ, Borchert J, Crommelin D. A novel technique for the one-step preparation of liposomes and nonionic surfactant vesicles without the use of organic solvents. Liposome formation in a continuous gas stream: the “bubble” method. J Pharm Sci 1994;83:276–80.

[195]. Hwang SY, Kim HK, Choo J, Seong GH, Hien TBD, Lee EK. Effects of operating parameters on the efficiency of liposomal encapsulation of enzymes. Colloid Surface B 2012;94:296–303.

[196]. Sanvicens N, Marco MP. Multifunctional nanoparticles-properties and prospects for their use in human medicine. Trends Biotechnol 2008;26(8):425–33.

[197]. Moghaddam B, Ali MH, Wilkhu J, Kirby DJ, Mohammed AR, Zheng Q, et al. The application of monolayer studies in the understanding of liposomal formulations. Int J Pharm 2011;417(1-2):235–44.

[198]. Dynarowicz-Latka P, Dhanabalan a, Oliveira ON. Modern physicochemical research on Langmuir monolayers. Adv Colloid Interface Sci 2001;91(2):221–93.

[199]. Sato H, Tamura K, Yamagishi A. Application of Clay Mineral-Iridium (III) Complexes Hybrid Langmuir-Blodgett Films for Photosensing 2012.

[200]. Brezesinski G, Möhwald H. Langmuir monolayers to study interactions at model membrane surfaces. Adv Colloid Interface Sci 2003;100-102:563–84.

[201]. Ma G, Allen HC. New insights into lung surfactant monolayers using vibrational sum frequency generation spectroscopy. Photochem Photobiol 2006;1517–29.

[202]. Ariga K, Hill JP. Monolayers at air-water interfaces: from origins-of-life to nanotechnology. Chem Rec 2011;11(4):199–211.

[203]. Azevedo CMG, Afonso CMM, Sousa D, Lima RT, Helena Vasconcelos M, Pedro M, et al. Multidimensional optimization of promising antitumor xanthone derivatives. Bioorg Med Chem 2013;21(11):2941–59.

[204]. XY L, Nakamura C, Yang Q, Kamo N, Miyake J. Immobilized liposome chromatography to study drug-membrane interactions. Correlation with drug absorption in humans. J Chromatogr A 2002;961:113–8.

[205]. Michalek M, Salnikov ES, Werten S, Bechinger B. Membrane Interactions of the amphipathic amino terminus of Huntingtin. Biochemistry 2013;52(5):847-58.

[206]. Ilić N, Novković M, Guida F, Xhindoli D, Benincasa M, Tossi A, et al. Selective antimicrobial activity and mode of action of adepantins, glycine-rich peptide antibiotics based on anuran antimicrobial peptide sequences. Biochim Biophys Acta 2013;1828(3):1004–12.

[207]. Bozelli JC, Sasahara ET, Pinto MRS, Nakaie CR, Schreier S. Effect of head group and curvature on binding of the antimicrobial peptide tritrpticin to lipid membranes. Chem Phys of Lipids 2012;165(4):365–73.

[208]. Papareddy P, Mörgelin M, Walse B, Schmidtchen A, Malmsten M. Antimicrobial activity of peptides derived from human ß-amyloid precursor protein. J Pept Sci 2012;18(3):183–91.

[209]. Hite RD, Grier BL, Waite BM, Veldhuizen R a, Possmayer F, Yao L-J, et al. Surfactant protein B inhibits secretory phospholipase A2 hydrolysis of surfactant phospholipids. Am J Physiol Lung Cell Mol Physiol 2012;302(2):L257–65.

[210]. Pinheiro M, Arêde M, Giner-Casares JJ, Nunes C, Caio JM, Moiteiro C, et al. Effects of a novel antimycobacterial compound on the biophysical properties of a pulmonary surfactant model membrane. Int J Pharm 2013;1–10.

[211]. Nakahara H, Ohmine A, Kai S, Shibata O. Monolayer compression induces fluidization in binary system of partially fluorinated alcohol (F4H11OH) with DPPC. J Oleo Sci 2013;62(5):271–81.

[212]. Davies MJ, Kerry TD, Seton L, Murphy MF, Gibbons P, Khoo J, et al. The crystal engineering of salbutamol sulphate via simulated pulmonary surfactant monolayers. Int J Pharm 2013;446(1-2):34–45.

[213]. Eftaiha AF, Brunet SMK, Paige MF. Influence of film composition on the morphology, mechanical properties, and surfactant recovery of phase-separated phospholipid-perfluorinated fatty acid mixed monolayers. Langmuir 2012;28(43):15150–9.

[214]. Sosnowski T, Koliński M, Gradoń L. Alteration of surface properties of dipalmitoyl phosphatidylcholine by benzo[a]pyrene: a model of pulmonary effects of diesel exhaust inhalation. J Biomed Nanotechnol 2012;8:818–25.

[215]. Minkov I, Mircheva K, Grozev N, Tz I, Panaiotov I. Properties of mixed monolayers of clinical lung surfactant, serum albumin and hydrophilic polymers. Colloid Surface B 2013;101:135–42.

[216]. Tatur S, Badia A. Influence of hydrophobic alkylated gold nanoparticles on the phase behavior of monolayers of DPPC and clinical lung surfactant. Langmuir 2012;28(1):628–39.

[217]. Eftaiha AF, Brunet SMK, Paige MF. Thermodynamic and structural characterization of a mixed perfluorocarbon-phospholipid ternary monolayer surfactant system. J Colloid Interf Sci 2012;368(1):356–65.

[218]. Sarangi NK, Patnaik A. Unraveling tryptophan modulated 2D DPPC lattices: an approach toward stimuli responsiveness of the pulmonary surfactant. J Phys Chem B 2011;115(46):13551–62.

[219]. Davies MJ, Seton L, Tiernan N, Murphy MF, Gibbons P. Towards crystal engineering via simulated pulmonary surfactant monolayers to optimise inhaled drug delivery. Int J Pharm 2011;421(1):1–11.

[220]. Duncan SL, Dalal IS, Larson RG. Molecular dynamics simulation of phase transitions in model lung surfactant monolayers. Biochim Biophys Acta 2011;1808(10):2450–65.

[221]. Chimote G, Banerjee R. Molecular interactions of cord factor with dipalmitoylphosphatidylcholine monolayers: implications for lung surfactant dysfunction in pulmonary tuberculosis. Colloid Surface B 2008;65(1):120–5.

[222]. Pinheiro M, Giner-Casares J, Lúcio L, Caio J, Moiteiro C, Lima L, et al. Interplay of mycolic acids, antimycobacterial compounds and pulmonary surfactant membrane: a biophysical approach to disease. Biochim Biophys Acta 2013;1828:896–905.

[223]. Valeur B. Molecular Fluorescence: Principles and Applications. Wiley-VCH Verlag GmbH; 2001. p. 155–98.

[224]. Pinheiro M, Nunes C, Caio JM, Moiteiro C, Lúcio M, Brezesinski G, et al. The influence of rifabutin on human and bacterial membrane models: Implications for its mechanism of action. J Phys Chem B 2013;117(20):6187–93.

[225]. Paloncýová M, Berka K, Otyepka M. Molecular insight into affinities of drugs and their metabolites to lipid bilayers. J Phys Chem B 2013;117(8):2403–10.

[226]. Liu X, Testa B, Fahr A. Lipophilicity and its relationship with passive drug permeation. Pharm Res 2011;28(5):962–77.

[227]. Giaginis C, Tsantili-kakoulidou A. Alternative measures of lipophilicity: from octanol – water partitioning to IAM retention. J Pharm Sci 2008;97(8):2984–3004.

[228]. Lin J, Lu A. Role of Pharmacokinetics and metabolism in drug. Pharmacol Rev 1997;49(4).

[229]. Dobson P, Kell D. Carrier-mediated cellular uptake of pharmaceutical drugs: an exception or the rule? Nat Rev Drug Discov 2008;7:205–20.

[230]. Lipinski C a, Lombardo F, Dominy BW, Feeney PJ. Experimental and computational approaches to estimate solubility and permeability in drug discovery and development settings. Adv Drug Deliv Rev 2001;46(1-3):3–26.

[231]. Barry CE, Slayden R a, Sampson a E, Lee RE. Use of genomics and combinatorial chemistry in the development of new antimycobacterial drugs. Biochem Pharm 2000;59(3):221–31.

[232]. Pereira-Leite C, Nunes C, Lima JLFC, Reis S, Lúcio M. Interaction of celecoxib with membranes: the role of membrane biophysics on its therapeutic and toxic effects. J Phys Chem B 2012;116(46):13608–17.

[233]. Salminen T, Pulli a, Taskinen J. Relationship between immobilised artificial membrane chromatographic retention and the brain penetration of structurally diverse drugs. J Pharm Biomed Anal 1997;15(4):469–77.

[234]. De Castro B, Gameiro P, Lima J, Matos C, Reis S. A fast and reliable spectroscopic method for the determination of membrane-water partition coefficients of organic compounds. Lipids 2001;36:89–96.

[235]. Ferreira H, Lúcio M, De Castro B, Gameiro P, Lima JLFC, Reis S. Partition and location of nimesulide in EPC liposomes: a spectrophotometric and fluorescence study. Anal Bioanal Chem 2003;377(2):293–8.

[236]. Ferreira H, Lúcio M, Lima JLFC, Matos C, Reis S. Interaction of clonixin with EPC liposomes used as membrane models. J Pharm Sci 2005;94(6):1277–87.

[237]. Séamus H. Analytical Chemistry. Oxford: Oxford University Press; 2004. p. 105–38.

[238]. Alves F, Oliveira FS, Oder BS, Matos C, Marrucho IM. Synthesis , Characterization , and liposome partition of a novel tetracycline derivative using the ionic liquids framework. J Pharm Sci 2013;102(5):1504–12.

[239]. Manuel M, Martins J. Partitioning of 1-pyrenesulfonate into zwitterionic and mixed zwitterionic/anionic fluid phospholipid bilayers. Chem Phys of Lipids 2008;154(2):79–86.

[240]. Matos C, Moutinho C, Lobão P. Liposomes as a model for the biological membrane: studies on daunorubicin bilayer interaction. J Membr Biol 2012;245(2):69–75.

[241]. Omran AA. An in vitro spectrometric method for determining the partition coefficients of non-steroidal anti-inflammatory drugs into human erythrocyte ghost membranes. Spectrochim Acta Mol Biomol Spectros 2013;104:461–7.

[242]. Brittes J, Lúcio M, Nunes C, Lima JLFC, Reis S. Effects of resveratrol on membrane biophysical properties: relevance for its pharmacological effects. Chem Phys of Lipids 2010;163(8):747–54.

[243]. Omran AA, Kitamura K, Takegami S, Kitade T, El-Sayed A-AY, Mohamed MH, et al. Effect of phosphatidylserine content on the partition coefficients of diazepam and flurazepam between phosphatidylcholine-phosphatidylserine bilayer of small unilamellar vesicles and water studied by second derivative spectrophotometry. Chem Pharm Bull 2002;50(3):312–5.

[244]. Poła A, Michalak K, Burliga A, Motohashi N, Kawase M. Determination of lipid bilayer/water partition coefficient of new phenothiazines using the second derivative of absorption spectra method. Eur J Pharm Sci 2004;21(4):421–7.

[245]. Magalhães L, C N, M L, Segundo M, S R, Lima J. High-throughput microplate assay for the determination of drug partition coefficients. Nat Protoc 2010;5:1823–30.

[246]. Mason R, Rhodes D, Herbette L. Reevaluating equilibrium and kinetic binding parameters for lipophilic drugs based on a structural model for drug interaction with biological membranes. J Med Chem 1991;34:869–77.

[247]. Ko YT, Ludescher RD, Frost DJ, Wasserman BP. Use of cilofungin as direct fluorescent probe for monitoring antifungal drug-membrane interaction. Antimicrob Agents Chemother 1994;38(6):1378–85.

[248]. Illinger D, Kubina M, Duportail G, P P, Bartholeyns J, Kuhry J. TMA-DPH a fluorescent probe of membrane dynamics in living cells. How to use it in phagocytosis. Cell Biophys 1989;14:17–26.

[249]. Lakowicz J. Principles of Fluorescence Spectroscopy. New York: Springer; 2006.

[250]. Pinheiro M, Arêde M, Caio JM, Moiteiro C, Lúcio M, Reis S. Drug-membrane interaction studies applied to N'-acetyl-rifabutin. Eur J Pharm Biopharm 2013;450.

[251]. Nunes C, Brezesinski G, Lopes D, Lima JLFC, Reis S, Lúcio M. Lipid-drug interaction: biophysical effects of tolmetin on membrane mimetic systems of different dimensionality. J Phys Chem B 2011;115(43):12615–23.

[252]. Baumgart T, Hunt G, Farkas ER, Webb WW, Gerald W. Fluorescence probe partitioning between Lo/Ld phases in lipid membranes. Biochim Biophys Acta 2009;1768(9):2182–94.

[253]. Yeum K-J, Russell RM, Krinsky NI, Aldini G. Biomarkers of antioxidant capacity in the hydrophilic and lipophilic compartments of human plasma. Arch Biochem Biophys 2004;430(1):97–103.

[254]. Kaiser R, London E. Location of diphenylhexatriene (DPH) and its derivatives within membranes: comparison of different fluorescence quenching analyses of membrane depth. Biochemistry 1999;38(8):2610.

[255]. Franová M, Repáková J, Capková P, Holopainen JM, Vattulainen I. Effects of DPH on DPPC-cholesterol membranes with varying concentrations of cholesterol: from local perturbations to limitations in fluorescence anisotropy experiments. J Phys Chem B 2010;114(8):2704–11.

[256]. Kitagawa S, Hirotaka H. Effects of alcohols on fluorescence anisotropies of diphenylhexatriene and its derivatives in bovine blood platelets: relationships of the depth-dependent change in membrane fluidity by alcohols with their effects on platelet aggregation and adenylate cyc. Biochim Biophys Acta 1992;23:14–8.

[257]. Massol RH, Antollini SS, Barrantes FJ. Effect of organochlorine insecticides on nicotinic acetylcholine receptor-rich membranes. Neuropharmacol 2000;39(6):1095–106.

[258]. Cardoso AMS, Faneca H, Almeida J a S, Pais A a CC, Marques EF, De Lima MCP, et al. Gemini surfactant dimethylene-1,2-bis(tetradecyldimethylammonium bromide)-based gene vectors: a biophysical approach to transfection efficiency. Biochim Biophys Acta 2011;1808(1):341–51.

[259]. Paul BK, Guchhait N. Spectroscopic probing of location and dynamics of an environment-sensitive intramolecular charge transfer probe within liposome membranes. J Colloid Interf Sci 2011;363(2):529–39.

[260]. Bozkurt E, Bayraktutan T, Acar M, Toprak M. Spectroscopic studies on the interaction of fluorescein and safranine T in PC liposomes. Spectrochim Acta Mol Biomol Spectros 2013;101:31–5.

[261]. Rodrigues M, Santos A, De la Torre BG, Rádis-Baptista G, Andreu D, Santos NC. Molecular characterization of the interaction of crotamine-derived nucleolar targeting peptides with lipid membranes. Biochim Biophys Acta 2012;1818(11):2707–17.

[262]. Millar DP. Time-resolved fluorescence spectroscopy. Curr Opin Struct Biol 1996;6(5):637–42.

[263]. Lakowicz J. Principles of Fluorescence Spectroscopy. Springer; 2006. p. 157–204.

[264]. Pignatello R, Musumeci T, Basile L, Carbone C, Puglisi G. Biomembrane models and drug-biomembrane interaction studies: Involvement in drug design and development. J Pharm Bioall Sci 2011;3:4–14.

[265].Rutkowska E, Pajlk K, Józwiak K. Lipohilicity-methods of determination and its role in medicinal chemistry. Acta Pol Pharm 2013;70(1):3-18.

[266]. Monteiro JP, Martins AF, Nunes C, Morais CM, Lúcio M, Reis S, et al. A biophysical approach to menadione membrane interactions: Relevance for menadione-induced mitochondria dysfunction and related deleterious/therapeutic effects. Biochim Biophys Acta 2013;1828(8):1899–908.

[267]. Michel N, Fabiano A-S, Polidori A, Jack R, Pucci B. Determination of phase transition temperatures of lipids by light scattering. Chem Phys of Lipids 2006;139(1):11–9.

[268]. Pereira-Leite C, Nunes C, Reis S. Interaction of nonsteroidal anti-inflammatory drugs with membranes: In vitro assessment and relevance for their biological actions. Prog Lipid Res 2013.

[269]. Grancelli A, Morros A, Caban ME, Merino S, Va L, Montero MT, et al. Interaction of 6-Fluoroquinolones with dipalmitoylphosphatidylcholine monolayers and liposomes Langmuir 2002;9177–82.

[270]. Mowri H, Nojima S, Inoue K. Effect of lipid composition of liposomes on their sensitivity to peroxidation. J Biochem 1984;18(24):9177-82.

[271]. Parker A, Miles K, Cheng KH, Huang J. Lateral distribution of cholesterol in dioleoylphosphatidylcholine lipid bilayers: cholesterol-phospholipid interactions at high cholesterol limit. Biophys J 2004;86(3):1532–44.

[272]. http://www.nobelprize.org/nobel_prizes/physics/laureates/1901/rontgen-bio.html [cited 2013 May 20]. Available from: http://www.nobelprize.org/nobel_prizes/physics/laureates/1901/rontgen-bio.html.

[273]. Cullity D. Elements Of X Ray Diffraction. Addison-Wesley Publishing Company, Inc.; 1956.

[274]. http://www.nobelprize.org/nobel_prizes/physics/laureates/1914/laue-bio.html [cited 2013 May 21]. Available from: http://www.nobelprize.org/nobel_prizes/physics/laureates/1914/laue-bio.html.

[275]. Pabst G, Kucerka N, Nieh M-P, Rheinstädter MC, Katsaras J. Applications of neutron and X-ray scattering to the study of biologically relevant model membranes. Chem Phys of Lipids 2010;163(6):460–79.

[276]. Garvey CJ, Lenné T, Koster KL, Kent B, Bryant G. Phospholipid Membrane Protection by Sugar Molecules during Dehydration-Insights into Molecular Mechanisms Using Scattering Techniques. Int J Mol Sci 2013;14(4):8148–63.

[277]. Müller-Goymann CC. Physicochemical characterization of colloidal drug delivery systems such as reverse micelles, vesicles, liquid crystals and nanoparticles for topical administration. Eur J Pharm Biopharm 2004;58(2):343–56.

[278]. Nozue Y, Shinohara Y, Amemiya Y. Application of microbeam small- and wide-angle X-ray scattering to polymeric material characterization. Polym J 2007;39(12):1221–37.

[279]. Yaghmur A, Rappolt M. Structural characterization of lipidic systems under nonequilibrium conditions. Eur Biophys J 2013;41(10):831–40.

[280]. Pérez J, Nishino Y. Advances in X-ray scattering: from solution SAXS to achievements with coherent beams. Curr Opin Struct Biol 2012;22(5):670–8.

[281]. Sarangi B, Karmakar S, Raghunathan V. Chapter Seven – X-ray and neutron scattering studies of lipid–sterol model membranes. Advances in Planar Lipid Bilayers and Liposomes 2010;11:159–86.

[282]. Mills TT, Tristram-Nagle S, Heberle F a, Morales NF, Zhao J, Wu J, et al. Liquid-liquid domains in bilayers detected by wide angle X-ray scattering. Biophys J 2008;95(2):682–90.

[283]. Tenchov B, Koynova R, Rapp G. New ordered metastable phases between the gel and subgel phases in hydrated phospholipids. Biophys J 2001;80(4):1873–90.

[284]. Marsh D. Lateral order in gel, subgel and crystalline phases of lipid membranes: wide-angle X-ray scattering. Chem Phys of Lipids 2012;165(1):59–76.

[285]. Kriechbaum M, Laggner P. States of phase transitions in biological structures. Prog Surf Sci 1996;51(3):233–61.

[286]. Wang Z, Yang S. Effects of fullerenes on phospholipid membranes: a langmuir monolayer study. Chemphyschem 2009;10(13):2284–9.

[287]. Jiménez-Millan E, Giner-Casares JJ, Martín-Romero MT, Brezesinski G, Camacho L. Chiral textures inside 2D achiral domains. J Am Chem Soc 2011;133(47):19028–31.

[288]. Vollhardt D, Fainerman VB. Penetration of dissolved amphiphiles into two-dimensional aggregating lipid monolayers. Adv Colloid Interface Sci 2000;86(1-2):103–51.

[289]. Seelig A. The use of monolayers for simple and quantitative analysis of lipid-drug interactions exemplified with dibucaine and substance P. Cell Biol Int Rep 1990;14(14):369-80.

[290]. Parasuraman D, Sarker AK, Serpe MJ. Poly(N-isopropylacrylamide)-based microgels and their assemblies for organic-molecule removal from water. Chemphyschem 2012;13(10):2507-15.

[291]. Vollhardt D, Fainerman VB. Progress in characterization of Langmuir monolayers by consideration of compressibility. Adv Colloid Interface Sci 2006;127(2):83–97.

[292]. Giner Casares JJ, Camacho L, Martín-Romero, Lopéz JJ. Methylene blue adsoption on a DMPA lipid Langmuir monolayer. Chemphyschem 2010;11(10):2241–7.

[293]. Lagane B, Mazères S, Le Grimellec C, Cézanne L, Lopez a. Lateral distribution of cholesterol in membranes probed by means of a pyrene-labelled cholesterol: effects of acyl chain unsaturation. Biophys Chem 2002;95(1):7–22.

[294]. Gross T, Zmora E, Levi-Kalisman Y, Regev O, Berman A. Lung-surfactant-meconium interaction: in vitro study in bulk and at the air-solution interface. Langmuir 2006;22(7):3243–50.

[295]. Wüstneck R, Perez-Gil J, Wüstneck N, Cruz a, Fainerman VB, Pison U. Interfacial properties of pulmonary surfactant layers. Adv Colloid Interface Sci 2005;117(1-3):33–58.

[296]. Aydogan N, Uslu B, Tanaci H. Biophysical investigation of the interfacial properties of cationic fluorocarbon/hydrocarbon hybrid surfactant: mimicking the lung surfactant protein C. J Colloid Interf Sci 2011;360(1):163–74.

[297]. Roldán-Carmona C, Giner-Casares JJ, Pérez-Morales M, Martín-Romero MT, Camacho L. Revisiting the Brewster angle microscopy: the relevance of the polar headgroup. Adv Colloid Interface Sci 2012 M;173:12–22.

[298]. Volinsky R, Kolusheva S, Berman A, Jelinek R. Investigations of antimicrobial peptides in planar film systems. Biochim Biophys Acta 2006;1758(9):1393–407.

[299]. Müller PU, Akpo CC, Stöckelhuber KW, Weber E. Novel amphiphiles with preorganized functionalities-formation of Langmuir-films and efficiency in mineral flotation. Adv Colloid Interface Sci 2005;114-115:291–302.

[300]. Allouche M, Castano S, Colin D, Desbat B, Kerfelec B. Structure and orientation of pancreatic colipase in a lipid environment: PM-IRRAS and Brewster angle microscopy studies. Biochemistry 2007;46(51):15188–97.

[301]. Alonso C, Alig T, Yoon J, Bringezu F, Warriner H, Zasadzinski J a. More than a monolayer: relating lung surfactant structure and mechanics to composition. Biophys J 2004;87(6):4188–202.

[302]. Gonçalves da Silva AM, Romão RIS. Mixed monolayers involving DPPC, DODAB and oleic acid and their interaction with nicotinic acid at the air-water interface. Chem Phys of Lipids 2005;137(1-2):62–76.

[303]. Mendelsohn R, Flach CR. Infrared Reflection – Absorption Spectrometry of Monolayer Films at the Air – Water Interface. John Wiley & Sons Ltd; 2002. p. 1019–41.

[304]. Meier DM, Urakawa A, Mäder R, Baiker A. Design and performance of a flow-through polarization-modulation infrared reflection-absorption spectroscopy cell for time-resolved simultaneous surface and liquid phase detection under concentration and temperature perturbations. Rev Sci Instrum 2009;80(9):094101.

[305]. Mendelsohn R, Mao G, Flach CR. Infrared reflection-absorption spectroscopy: principles and applications to lipid-protein interaction in Langmuir films. Biochim Biophys Acta 2010;1798(4):788–800.

[306]. Bredenbeck J, Ghosh A, Nienhuys H-K, Bonn M. Interface-specific ultrafast two-dimensional vibrational spectroscopy. Acc Chem Res 2009;42(9):1332–42.

[307]. Czapla K, Korchowiec B, Rogalska E. Differentiating oxicam nonsteroidal anti-inflammatory drugs in phosphoglyceride monolayers. Langmuir 2010;26(5):3485–92.

[308]. Scherer JR. Dependence of lipid chain and head group packing of the inverted hexagonal phase on hydration. Biophys J 1989;55(5):965–71.

[309]. Kubelka J, Keiderling T a. Differentiation of beta-sheet-forming structures: ab initio-based simulations of IR absorption and vibrational CD for model peptide and protein beta-sheets. J Am Chem Soc 2001;123(48):12048–58.

[310. Banc A, Desbat B, Renard D, Popineau Y, Mangavel C, Navailles L. Structure and orientation changes of omega- and gamma-gliadins at the air-water interface: a PM-IRRAS spectroscopy and Brewster angle microscopy study. Langmuir 2007;23(26):13066–75.

[311]. Stenger PC, Alonso C, Zasadzinski J a, Waring AJ, Jung C-L, Pinkerton KE. Environmental tobacco smoke effects on lung surfactant film organization. Biochim Biophys Acta 2009;1788(2):358–70.

[312]. Johnson S, Liu W, Thakur G, Dadlani A, Patel R, Orbulescu J, et al. Surface chemistry and spectroscopy of human insulin Langmuir monolayer. J Phys Chem B 2012;116(34):10205-12.

[313]. Venyaminov S, Kalnin N. Quantitative IR spectrophotometry of peptide compounds in water (H2O) solutions. Biopolymers 1990;30:1243–57.

[314]. Blaudez D, Buffeteau T, Cornut J, Desbat B, Escafre N, Pezolet M, et al. Polarization-modulated FT-IR spectroscopy of a spread monolayer at the air/water interface. Appl Spectrosc Rev 1993;47:869–74.

[315]. Cea P, Martín S, Villares A, Möbius D, López MC. Use of UV-vis reflection spectroscopy for determining the organization of viologen and viologen tetracyanoquinodimethanide monolayers. J Phys Chem B 2006;110(2):963–70.

[316]. Rubia-Payá C, Jimenez-Millán E, Giner-Casares JJ, Brezesinski G, Martín-Romero MT, Camacho L. From two-dimensional to three-dimensional at the air/water interface: the self-aggregation of the acridine dye in mixed monolayers. Langmuir 2013;29(15):4796–805.

[317]. Pinheiro M, Lúcio M, Reis S, Lima JLFC, Caio JM, Moiteiro C, et al. Molecular interaction of Rifabutin on model lung surfactant monolayers. J Phys Chem B 2012;116(38):11635–45.

[318]. Summers RL. Computer Simulation Studies and the scientific method. J Appl Anim Welf Sci 2010;1(2):119-31.

[319]. Guide P. HyperChem® Computational chemistry. Hipercube, Inc; 1996. p. 1–49.

[320]. http://www.chemaxon.com/marvin/help/view/view-intro.html [cited 2013 May 30]. Available from: http://www.chemaxon.com/marvin/help/view/view-intro.html.